Welding, Bonding, and Fastening 1984

DISTRIBUTION STATEMENT A

Approved for public release
Distribution Unlimited

19960306 016

*Proceedings of a symposium held at
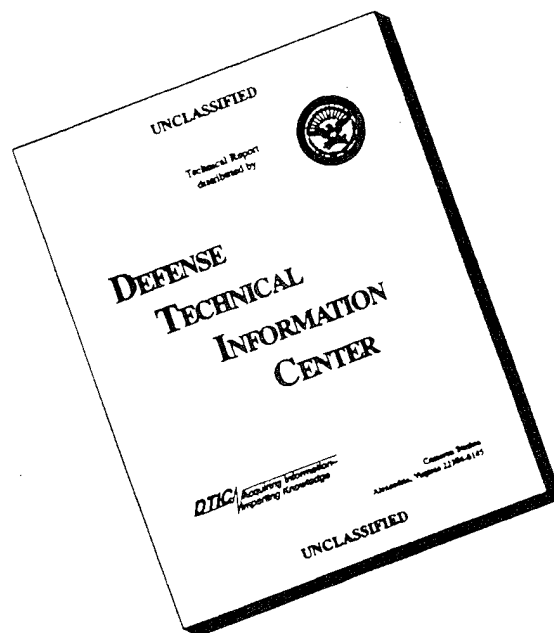Langley Research Center
Hampton, Virginia
October 23-25, 1984*

NASA

DISCLAIMER NOTICE

UNCLASSIFIED

Technical Report
distributed by

DEFENSE
TECHNICAL
INFORMATION
CENTER

DTIC Acquiring Information·
Imparting Knowledge

UNCLASSIFIED

THIS DOCUMENT IS BEST
QUALITY AVAILABLE. THE
COPY FURNISHED TO DTIC
CONTAINED A SIGNIFICANT
NUMBER OF PAGES WHICH DO
NOT REPRODUCE LEGIBLY.

Welding, Bonding, and Fastening 1984

Edited by
John D. Buckley and Bland A. Stein
Langley Research Center
Hampton, Virginia

DTIC QUALITY INSPECTED 4

NASA

PREFACE

One of the major considerations in the fabrication of any aerospace or hydrospace vehicle is safe, reliable attachment systems. This symposium provided a forum for the presentation of technical data pertinent to new equipment and innovative techniques for joining advanced materials and structures. The theme of the symposium was "1990's Joining Technology for High-Performance Aerospace and Hydrospace Structures." As this conference publication documents, the wide range of presentations concerning joining technologies includes welding, brazing, and soldering; mechanical fastening, explosive welding, and solid-state bonding; and adhesive bonding and nondestructive evaluation. The presentations were given to more than 100 attendees from government, academia, and aerospace and consumer industries.

We would like to acknowledge the contributions of the authors, attendees, and the Langley Research Center staff to the success of Welding, Bonding, and Fastening – 1984.

The use of trade names or names of manufacturers in this report does not constitute an official endorsement of such products or manufacturers, either expressed or implied, by the National Aeronautics and Space Administration.

John D. Buckley
NASA Langley Research Center

Bland A. Stein
Langley Research Center

Conference Coordinators

CONTENTS

SESSION III(B) - NONDESTRUCTIVE EVALUATION
Chairman: J. S. Heyman

SESSION IV - SELECTED JOINING TECHNIQUES
Chairman: D. M. Royster

SESSION V - ADHESIVES I - MATERIALS DEVELOPMENT
AND CHARACTERIZATION
Chairman: P. M. Hergenrother

SESSION VI – ADHESIVES II – PROGRAMS, BONDING
PROCESSES, AND ENVIRONMENTAL EFFECTS
Chairman: T. L. St. Clair

ATTENDEES

Mr. John H. Allen
NASA Johnson Space Center
Mail Stop JHA
Houston, TX 77058

Mr. Sid Allison
NASA Langley Research Center
Instrument Research Division
Mail Stop 231
Hampton, VA 23665

Mr. Steve Barhorst
Hobard Brothers Co.
Troy, OH 45373

Mr. Wayne Bartlett
NASA Lewis Research Center
Mail Stop 86-2
21000 Brookpark Road
Cleveland, OH 44111

Mr. Laurence J. Bement
NASA Langley Research Center
Systems Engineering Division
Mail Stop 433
Hampton, VA 23665

Mr. James F. Bradshaw
NASA Langley Research Center
Systems Engineering Division
Mail Stop 432
Hampton, VA 23665

Mr. J. K. Brandau
Newport News Shipbuilding
4104 Washington Avenue
Newport News, VA 23607

Mr. Hal Brinson
VPI & SU
Blacksburg, VA 24061

Dr. John D. Buckley
NASA Langley Research Center
Fabrication Division
Mail Stop 387
Hampton, VA 23665

Mr. Henry Bursion
NASA Langley Research Center
Facilities Engineering Division
Mail Stop 439
Hampton, VA 23665

Mr. M. A. Butti
Penn. Voc. Tech. Soc.
2102 Mercedes Drive
Hampton, VA 23661

Mr. James Byman
LTV Aerospace & Defense Co.
Mail Stop 49R-32
P. O. Box 225907
Dallas, TX 75265

Mr. Tom Byun
Northrop Corp.
Aircraft Division
One Northrop Avenue
Hawthorne, CA 90250

Mr. Allen Case
General Electric Co.
Bldg. 5, Room 237
1 River Road
Schenectady, NY 12345

Mr. Willard Castle
Penninsula Vo Tech. Soc.
2102 Mercedes Drive
Hampton, VA 23661

Mr. Richard Chattin
NASA Langley Research Center
Fabrication Division
Mail Stop 385
Hampton, VA 23665

Mr. Ram Darolia
General Electric Co.
Aircraft Engine Group
Mail Stop M-89
Cincinnati, OH 45069

Mr. Joseph B. Davenport
NASA Langley Research Center
Fabrication Division
Mail Stop 114
Hampton, VA 23665

Mr. Guy D. Davis
Martin Marietta Labs
1450 S. Rolling Road
Baltimore, MD 21227

Mr. Del Drier
NASA Lewis Research Center
Mail Stop 86-2
21000 Brookpark Road
Cleveland, OH 44111

Mr. Stephen J. Empert, Jr.
Peninsula Vo Tech. Soc.
2102 Mercedes Drive
Hampton, VA 23661

Mr. W. H. Eure
Newport News Shipbuilding
113 Valirey Drive
Hampton, VA 23669

Mr. William W. Fernald
NASA Langley Research Center
Systems Engineering Division
Mail Stop 432
Hampton, VA 23665

Mr. George C. Firth
NASA Langley Research Center
Systems Engineering Division
Mail Stop 432
Hampton, VA 23665

Mr. Jerome E. Fischler
Douglas Aircraft Co.
Mail Code 36-55
3855 Lakewood Boulevard
Long Beach, CA 90846

Mr. Joseph Fleck
NASA Langley Research Center
Facilities Engineering Division
Mail Stop 439
Hampton, VA 23665

Mr. James Forster
Texas Instruments, Inc.
Mail Stop 10-13
34 Forest Street
Attleboro, MA 02703

Mr. John Gaul
Dow Corning
Mail Stop C41D01

Ms. Judith Gauland
Grumman Aerospace Corp.
Mail Stop A04-12
Bethpage, NY 11714

Mr. L. R. Gentry
NASA Langley Research Center
Systems Engineering Division
Mail Stop 432
Hampton, VA 23665

Mr. Barry Gibbens
NASA Langley Research Center
Systems Engineering Division
Mail Stop 432
Hampton, VA 23665

Mr. Ross Goble
Induction Corporation
704 Gum Rock Court, Suite 400
Newport News, VA 23606

Mr. J. W. Goslee
NASA Langley Research Center
Space Systems Division
Mail Stop 364
Hampton, VA 23665

Mr. Luis E. Gutierrez
NASA Langley Research Center
Facilities Engineering Division
Mail Stop 439
Hampton, VA 23665

Mr. E. Thomas Hall
NASA Langley Research Center
Fabrication Division
Mail Stop 397
Hampton, VA 23665

Mr. Richard Hammar
G. M. Research Labs
12 Mile & Mound Roads
Warren, MI 48090

Mr. Roy Hardwick
Explosive Fabricators Inc.
1301 Courtesy Road
Louisville, CO 80027

Mr. John Harris
ADVEX Corporation
121 Floyd Thompson Drive
Hampton, VA 23666

Mr. W. Henshaw
Naval Research Lab
Washington, DC

Mr. Paul M. Hergenrother
NASA Langley Research Center
Materials Division
Mail Stop 226
Hampton, VA 23665

Dr. Joseph Heyman
NASA Langley Research Center
Instrument Research Division
Mail Stop 231
Hampton, VA 23665

Mr. Jim Hill
Martin Marietta Aerospace
P. O. Box 29304
Dept. 3573
New Orleans, LA 70189

Dr. Jeffrey Hinkley
NASA Langley Research Center
Materials Division
Mail Stop 226
Hampton, VA 23665

Mr. Todd Hodges
NASA Langley Research Center
Materials Division
Mail Stop 226C
Hampton, VA 23665

Mr. Eric Hoffman
NASA Langley Research Center
Metallic Materials Branch
Mail Stop 188A
Hampton, VA 23665

Mr. Reid Hull
NASA Langley Research Center
Mail Stop 432
Systems Engineering Division
Hampton, VA 23665

Mr. Robert Irving
Iron Age Magazine
Radnor, PA 19010

Mr. Jim Jacobs
School of Technology
Norfolk State University
Norfolk, VA 23504

Mr. Brian J. Jensen
NASA Langley Research Center
Materials Division
Mail Stop 226
Hampton, VA 23665

Mr. Theo Kattami
University of Connecticut
Storrs, CT 06268

Mr. Thomas F. Kilduff
Thomas Nelson Community College
Hampton, VA 23670

Dr. Narain S. Lalwaney
Battelle-Columbus Labs
505 King Avenue
Columbus, OH 43201

Mr. Richard C. Landt
SPS Technologies
Highland Avenue
Jenkintown, PA 19046

Mr. Jack B. Levy
General Electric Co.
10 Mayfair Drive
Scotia, NY 12302

Mr. Joseph W. Lorenzino
PD Pruden Voc-Tec. Center
4169 Pruden Boulevard
Suffolk, VA 23434

Mr. Donald Lumley
Martin Marietta Aerospace
P. O. Box 29304
New Orleans, LA 70189

Mr. David B. McNally
Newport News Shipbuilding
4104 Washington Avenue
Newport News, VA 23607

Dr. Michael Mann
NASA Langley Research Center
Transonic Aerodynamics Division
Mail Stop 294
Hampton, VA 23665

Mr. K. Masubuchi
MIT
Department of Ocean Engineering
Room 5-219
Cambridge, MA 02139

Mr. Roy Meade
Lockheed-Georgia Co.
Dept. 72-77 Z399
Marietta, GA 30063

Dr. Jimmy Mote
University of Denver
Denver, CO 80208

Mr. Brian Norris
Rohr Industries
MZ 19T
P. O. Box 878
Chula Vista, CA 92124

Mr. Marvin Parker
NASA Langley Research Center
Fabrication Division
Mail Stop 386
Hampton, VA 23665

Mr. Harry E. Pattee
Metalworking Section
Battelle-Columbus Labs
505 King Avenue
Columbus, OH 43201

Mr. Carlos S. Perez
NASA Langley Research Center
Facilities Engineering Division
Mail Stop 437
Hampton, VA 23665

Mr. Merven N. Pfeiffer
NASA Langley Research Center
Fracture Mech. Eng. Section
Mail Stop 437
Hampton, VA 23665

Mr. Roscoe A. Pike
United Technologies Research
Center Mail Stop 22
Silver Lane
East Hartford, CT 06108

Mr. Barry L. Price
NASA Langley Research Center
Systems Engineering Division
Mail Stop 432
Hampton, VA 23665

Mr. John Price
NASA Langley Research Center
Systems Engineering Division
Mail Stop 432
Hampton, VA 23665

Mr. Carl Richter
NASA Lewis Research Center
Mail Stop 86-2
21000 Brookpark Road
Cleveland, OH 44135

Mr. R. Scott Riefler
American Cyanamid
Old Post Road
Havre de Grace, MD 21078

Mr. T. A. Roach
SPS Technologies
Highland Avenue
Jenkintown, PA 19046

Mr. Nick Rodriquez
Douglas Aircraft Co.
Mail Code 1-22
3855 Lakewood Boulevard
Long Beach, CA 90846

Mr. Lester Rose
NASA Langley Research Center
Technology Utilization
Mail Stop 139A
Hampton, VA 23665

Mr. Dick Royster
NASA Langley Research Center
Materials Division
Mail Stop 224
Hampton, VA 23665

Mr. Carl E. Rucker
NASA Langley Research Center
Materials Division
Mail Stop 188E
Hampton, Virginia 23665

Mr. Homer Rush
NASA Langley Research Center
Systems Engineering Division
Mail Stop 432
Hampton, VA 23665

Dr. James. W. Sawyer
NASA Langley Research Center
Space Systems Division
Mail Stop 190
Hampton, VA 23665

Mr. J. W. Schroeder
Foster Wheeler Development Corp.
12 Peach Tree Hill Road
Livingston, NJ 07039

Mr. Bob Schwensfeir
Texas Instruments, Inc.
Mail Stop 10-13
34 Forest Street
Attleboro, MA 02703

Mr. Dana Shatts
Hughes Aircraft, EDD
3100 Lomita Boulevard
Torrance, CA 90509

Mr. W. Albert Shearin
NASA Langley Research Center
Fabrication Division
Mail Stop 222B
Hampton, VA 23665

Mr. Joseph M. Shinn, Jr.
NASA Langley Research Center
Materials Division
Mail Stop 188A
Hampton, VA 23665

Mr. Gene Smiles
615 Bland Boulevard
Newport News, VA 23602

Dr. Terry L. St. Clair
NASA Langley Research Center
Materials Division
Mail Stop 226
Hampton, VA 23665

Mr. Bland A. Stein
NASA Langley Research Center
Materials Division
Mail Stop 226
Hampton, VA 23665

Mrs. Laura Stokley
NASA Lewis Research Center
Mail Stop 86-2
21000 Brookpark Road
Cleveland, OH 44135

Mr. P. H. Stranges
NTI
4 Chittenden Lane
Owings Mills, MD 21117

Mr. Mike Sudsina
NASA Lewis Research Center
21000 Brookpark Road
Mail Stop 14-1
Cleveland, OH 44135

Mr. Steven M. Sullivan
McDonnell Aircraft
P. O. Box 516
St. Louis, MO 63166

Mr. Robert J. Swaim
NASA Langley Research Center
Fabrication Division
Mail Stop 390
Hampton, VA 23665

Mr. William Tennis
NASA Langley Research Center
Operations Support Division
Mail Stop 166B
Hampton, VA 23665

Mr. Clyde Thiele
5 Trail Lane
Hampton, VA

Ms. Diana P. Tyler
Reynolds Metals
P. O. Box 27003
Richmond, VA 23261

Mr. Robert Uhl
American Society of Metals
Metals Park, OH 44073

Mr. Ellery N. Vandenbree
NASA Langley Research Center
Fabrication Division
Mail Stop 387
Hampton, VA 23665

Mr. Roy E. Van Raden
Douglas Aircraft Co.
Mail Code 1-22
3855 Lakewood Boulevard
Long Beach, CA 90846

Mr. John Wallace
NASA Langley Research Center
Systems Engineering Division
Mail Stop 432
Hampton, VA 23665

Mr. Freddy Walter
ADVEX Corporation
121 Floyd Thompson Drive
Hampton, VA 23666

Mr. S. E. Wentworth
AMMRC
DMXMR-OP
Watertown, MA 02172

Mr. James E. Woods
Reynolds Metals
P. O. Box 27003
Richmond, VA 23261

Dr. Clarence P. Young
NASA Langley Research Center
Systems Engineering Division
Mail Stop 431
Hampton, VA 23665

The Factory of the Future

J. E. Byman
Manager, Systems Engineering
Industrial Modernization
Vought Aero Products Division
LTV Aerospace and Defense Company
Dallas, Tx.

Introduction

In the early years, aircraft were relatively simple in their design and construction. Their mission was basically to fly and land safely. The simple design shapes and nonmetal composition required little in the way of heavy equipment or special tooling to form, shape and assemble the vehicle. The entire manufacturing operation was centrally located in a relatively small facility with the equipment and tools brought to the developing structure by the builders during the fabrication process. The aircraft were constructed basically one at a time, by a team of men who shared the full gamut of skills and duties required to produce the product. This integrated operation allowed the flexibility for accommodating changes in the product configuration and manufacturing processes. Each aircraft produced varied slightly as engineering improvements and field testing refined the design. Quality was built into the product by this team of skilled craftsmen who were involved in the total process from detail fabrication through final assembly.

Paperwork required for product documentation and production control was minimal. Configuration, inventory and production records were centrally located and readily available - maintained through a simple manual system by the chief engineer/builder in this integrated operating environment. Thus, manufacturing support costs were negligible.

In this "bicycle shop" manufacturing environment, a majority of the costs of the aircraft were accrued in the construction process. Direct, hands-on labor required to fabricate and assemble the product was the largest investment, comprising some 75 percent of the total cost. Material cost accounted for 10 percent with the remaining 15 percent committed to the cost of facilities, energy, support functions and the few simple tools used by the engineer/builder.

The Maturing Years

The World Wars, World War II in particular, brought the U.S. aerospace industry into a new era of mass production and advanced manufacturing methods. The diverse, multi-mission requirements of the combat environment changed the characteristics of the product. Metallic structures, with complex shapes, were designed to meet the higher performance and durability requirements. Offensive and defensive systems were added to the aircraft along with more advanced avionics and control systems, all of which presented new manufacturing challenges to fabricate and assemble the more complex structure and to install the miles of wiring and tubing required. The aircraft became an integrated weapons system - a flying fortress of metal - strong, durable and much more difficult to configure. Field support and maintenance became critical issues necessitating tighter configuration controls. Parts had to be replaceable for quick repair, and interchangeable to assure efficient production and field support.

Product complexity coupled with high-volume, high-rate production demands and the requirements for standardized configuration ushered Henry Ford's batch-manufacturing, assembly line approach into America's aircraft factories.

With the implementation of this methodology, the "bicycle shop" environment was replaced with thousands of square feet of

factory space, dimensioned to house dozens of aerostructures in work.

The equipment and tools once brought to the single aircraft in production were now centralized at work stations. The developing aerostructures were moved to the resources, progressively located along the assemble line.

In order to facilitate batch-manufacturing, fabrication tasks were divided into numerous subtasks. This multi-level division of effort necessitated standardized fabrication and assembly methods as well as extensive production and quality control procedures, to assure proper fit and structural integrity of the subassemblies as they were joined together to produce the end item.

The number of specialized functions and the complicated logistics involved in producing an aircraft in the assembly line environment prevented the continuation of the integrated team approach, where a few skilled craftsmen performed a wide range of tasks.

The team of multi-skilled engineer/ builders was replaced with scores of specialists - machinists, welders, assemblers and technicians, each performing a minute part of the now segregated task.

With the manufacturing task divided into numerous subtasks, the step-by-step precision and quality control performed by the team of engineer/builders in the early days were impossible. With the fabrication and assembly effort fragmented, even the most conscientious worker was hard pressed to verify or even envision the final result. In this atmosphere of specialization and division of labor, the functions of post-fabrication and post-assembly quality inspection became major technical and cost issues.

Segregation of the manufacturing activities established the need for more extensive planning, scheduling, material man-agement, process control and quality assurance systems to coordinate the numerous activities and assure smooth work flow. Product complexity and logistic support needs dictated stringent configuration and data management requirements. New organizations were formed to perform the documentation and operations control functions previously handled by the team of engineer/builders.

These functions were performed by a new class of U.S. aerospace industry worker - the white collar "manufacturing support" employee. This support worker, who was not directly involved in building the product, became an "indirect" charge against the final product cost. His output, 'the paper airplane' and the mountain of paperwork required for planning, controlling and monitoring factory functions, came to be regarded as a permanent cost-of-doing-business.

The maturing years brought complication and complexity to the U.S. aerospace industry and changed the structure of product costs. Direct labor accounted for approximately 50 percent of the total cost of the aircraft.

The use of metals and the addition of complex hydraulics and electronics in aircraft designs resulted in an increase in the amount of the total product cost allotted to materials from 10 to 25 percent. The vast expanses of factory space equipped with a variety of specialized equipment, along with the new class of support workers, increased the share alloted to indirect burdens from 15 to 25 percent.

As we entered the post-world-war period, the high-rate military aircraft programs of the war years were replaced by mid- and low-rate production programs. Military philosophy shifted from an approach of assuring victory with quantities to a position of preventing conflict with sophisticated, quality weapons that posed a deterrent to the enemy. The horizon of

2

earth was replaced by the frontier of outer space. The unparalled technological advances that enabled man to travel to the moon added new capabilities and dimensions to U.S. aerospace industry products. A new level of quality was needed for these products in order to assure their success in the foreign and unforgiving environment of outer space.

The growing number and complexity of government regulations and standards imposed on the industry to assure product quality and configuration, as well as production accountability, significantly contributed to the increase in resources required to manage major aerospace programs.

The flying fortresses of the World War II Era were replaced with multimission, high performance aircraft characterized by speed and agility as well as survivability.

These high-technology aircraft featured complex electronic systems, onboard computers for navigation, control of electro/mechanical systems and special mission capabilities. Structural designs and configurations became more complex as the shapes and silhouettes became more sophisticated. The requirements for lightweight, multi-contoured configurations led the industry to apply advanced materials technologies to the space age aircraft design effort.

The heavy metals that had comprised the aircraft of the maturing years were replaced wherever possible with nonmetals and hybrid materials such as composites, plastics and honeycomb structures. The manufacturing requirements for these high technology aircraft offered new and distinct challenges to the aerospace industry. Facilities were modified to provide the environmental controls necessary for storage and processing of advanced materials and components. Advanced manufacturing techniques and equipment were developed to meet shop floor requirements such as automatic tape layers for fabricating composite

skins and structures, and automatic fastening equipment to join the complex structures.

However, while automated equipment on the shop floor worked to effectively reduce the number of man-hours required to actually fabricate these advanced aerostructures, the complexity of the above-shop-floor support functions and the volume of paperwork grew unchecked, and the number of white collar manufacturing support workers continued to increase.

Space age advances in technology and its application altered the composition of product cost significantly. The addition of automated equipment on the shop floor reduced the direct labor required to produce aerostructures. As a result, the cost of direct labor fell from 50 percent of the total in the maturing years of high-rate mass production to no more than 10 percent. The inclusion of advanced computer and electronic components along with high-technology nonmetals pushed the share of total cost for materials from 25 percent to more than 55 percent. Specialized facilities, equipment and the growing ranks of manufacturing support personnel that were required to administrate the operation and manage the volumes of paperwork caused an increase in the indirect cost burdens from 25 to 35 percent.

Economic constraints, spiraling production costs, a nation-wide decline in productivity, and concerns about quality have significantly increased the costs of weapon systems over the last 15 years. This signals an end to the era in which the aerospace industry can ignore costs for the sake of performance, even when dealing with systems at the leading edge of technology.

Throughout its history, the U.S. aerospace industry has established an unsurpassed record for developing high-performance, quality aircraft that could survive in the harshest environments. The constant demands for bigger, better, faster, smarter,

more reliable aircraft have been met by the integration of advanced materials, electronics, and structures technologies into the product designs. However, while the products have progressed technologically, the manufacturing processes employed to build these complex aircraft have not developed at the same pace, resulting in higher and higher manufacturing costs.

Rising costs, coupled with growing foreign competition, have led the U.S. aerospace industry to face the fact that to compete successfully in the rapidly changing industrial environment, they must develop new manufacturing methods that are less vulnerable to shifts in the world marketplace than standardized production methods. These new methods must allow efficient, low cost operation in an environment characterized by multiple customers, proliferating product lines and low-to-midrange production volumes. They must be responsive to variable product requirements and frequent, often unpredictable, changes in the product to meet customer needs.

Ironically, the initial efforts in modernization were, and still are, focused on the shop floor - where only 10 percent of the total cost of our aeroproducts originates. These efforts did not attack those functions that were the major contributers to cost, such as: material queues, inventory, material handling and set up, or scrap and rework. Nor did they address the integration of the above-shop-floor data management and support functions where a significant portion of indirect costs occur.

Considerable sums of money have been invested by U.S. firms on equipment and automated methods that simply served to perpetuate the old business-as-usual operation by automating the As-Is functions. This concentration on improving methods and functions that are obsolete and in some cases unnecessary for the manufacture and support of the product have not led to any significant reduction in costs. The significant capital outlays, coupled with the maintenance of status quo staffing and resourcing of isolated manufacturing functions negated any real cost benefits from these "islands of automation." This status quo cost dilemma points up the need to develop a strategy for effective modernization and to establish a clearly defined road map for achieving flexible, integrated manufacturing.

Government and industry have joined forces to develop this road map through such efforts as the U.S. Air Force sponsored Integrated Computer-Aided Manufacturing (ICAM) Program which brought leading aerospace firms, industry consultants and academia together to study and assess technologies and to organize and structure plans for cost-effective and efficient implementation of technologies to meet the manufacturing requirements of current and next generation aero-structures. Studies such as the ICAM Conceptual Design for Computer Integrated Manufacturing Project, in which the Vought Aero Products Division served as prime contractor, set about establishing a framework for effective industrial modernization and a conceptual design for factory-wide, computer-integrated-manufacturing -- The Factory of The Future.

Addressing current and future aerostructures designs and corresponding manufacturing needs, the team developed a profile of the U.S. aerospace products in the mid-1990's time frame. The general characteristics included:

o   Technology-driven design features

o   High-precision hardware and software requirements

o   Complex structures and systems

o   Dynamic configurations

o   Multimission/variable mission and military/commercial roles

4

o   Dimensional extremes

o   High-technology/exotic materials

o   Low-rate production require-
    ments.

Based on this analysis, it became apparent that there was a critical need for flexible manufacturing facilities that were responsive to changes in:

o   Product design and product mix;

o   Production quantities and
    schedules;

o   Processing sequences, equipment and
    technology;

o   Organizational structure and op-
    erating methods.

To provide that flexibility, the FOF objective became one of integrating computer and automation technologies to the fullest extent possible in not only shop-floor activities, but in those highly labor-intensive and historically costly areas of manufacturing support. The basic data management and decision support capabilities required for production are built into the computer systems that control the FMS providing a common information resource and improved visibility of operation allowing integration of all the organizational functions – finance, marketing, engineering, purchasing and manufacturing – to provide more effective management of the total production process. The use of advanced computer functions such as simulation and artifical intelligence in the decision making process will further reduce the labor requirements in the "above the shop floor" functions.

The Factory of the Future plan offers a hierarchical, functional structure based on the factory management, marketing, product definition and planning, information resourcing, provisioning and logistics act-

ivities that are necessary to produce current and next-generation aerostructures.

The coalescing agent in this concept is information. Information stored, controlled and disseminated from the management level to the shop floor will return the future factory environment to that state of integration and coordination found in the early days of the industry. Just as all the decision-making and tracking was maintained at a central point by the chief engineer/builder, the function and control of the factory will center in the factory control computer system – programmed with the management philosophy and goals, as determined by the firm's leaders.

This will allow implementation of a serial (one-ship-set-at-a-time) manufacturing philosophy to meet the needs of the future product line while reducing costs in inventory, work-in-process, scrap and rework, and labor. The single-aircraft focus of the early days will allow the FOF to accommodate a range of product envelopes, multi-program product mixes, variable/changing configuration and low yet "surgeable" rate production.

The information flow and decision-making process for serial production will all culminate in a modular, hierarchical factory environment comprised of integrated, flexible manufacturing systems that will provide a simple, efficient work flow from raw material to finished product. And this activity will be conducted with minimal human intervention, all under computer control.

Quality assurance will once again become an integral part of the fabrication process with the inspection function built into each flexible manufacturing cell leading eventually to in-process verification capability.

Flexible Manufacturing Systems (FMS) are regarded by many experts as the best way to meet the conflicting demands of low

5

volume, low cost production while improving product quality. These systems offer more than just factory automation. Flexible Manufacturing Systems provide for the physical integration of materials and equipment flowing through the factory, for shop-floor automation, wherever cost effective, and for the integration of all functions that direct, monitor and control the operation.

Flexible manufacturing systems integrate the use of hardware and software to manufacture products in the most cost-effective and efficient manner. Flexible manufacturing is the application of the "just-in-time" production philosophy to the fabrication of multiple-configuration products in mixed, small-batch (ideally one) quantities to an "only-as-needed" schedule.

The flexibility provided in the FOF environment will provide for better utilization of equipment, facilities, and labor, which are all significant contributors to the cost of the product.

We must remember in moving toward this factory of the future concept of flexible manufacturing that automation is not synonymous with flexibility in manufacturing. Conventional machines and methods, stand-alone NC machines and large transfer systems each have their place in the factory of the future depending on the volume and variety of workpieces. The key is to match operating methods and technologies to the task such that the facility most effectively satisfies its intended mission. Integration of these resources and functions in the above-shop-floor control systems will provide the management flexibility required to improve the productivity and cost effectiveness of each work cell.

Flexible, just-in-time manufacturing capabilities can reduce the cost of U.S. aerospace industry products by:

o   Reducing work-in-process, and thus reducing facility space, storage and

staging equipment, and inventory requirements

o   Reducing waste by eliminating:

- Scrap resulting from changes to finished products that are fabricated ahead of need in batch production

- Scrap resulting from errors made in batch manufacturing, due to the recovery capability between serially produced parts

- Scrap resulting from human error as a result of reduced human intervention

o   Improving utilization of equipment and facilities

o   Increasing realization of labor

o   Improving productivity above as well as on the shop floor.

o   Maximizing resource utilization and distribution by automated provisioning of materials, tools, equipment, and information on an as-needed basis.

Implementing the factory of the future is a monumental task and will require careful planning. The plan must allow for incremental implementation of the flexible manufacturing cells to meet product needs. The cells must be integrated into the existing operation so as not to interrupt work flow. These criteria can be satisfied by establishing a well defined structure for the total manufacturing system and applying systems engineering methods to the total task.

Flexible Manufacturing Today At VAPD

We have followed this approach at VAPD in our reindustrialization efforts. Our Flexible Machining Cell (FMC), which began production operations on 2 July,

1984, is a modular component of our first flexible manufacturing system. It is the initial building block in the LTV Aerospace and Defense Company multiproduct factory of the future.

The FMC is the result of study, development, design and implementation by the VAPD Industrial Modernization (IMOD) organization, which was founded in 1982 to lead the firm's drive for reindustrialization. The flexible cell was designed using the ICAM life cycle development methodology to meet the machining needs for the current B-1B-aft and aft-intermediate fuselage subcontract effort for Rockwell International.

The VAPD Flexible Machining Cell is a computer controlled system capable of performing 4-axis machining, part cleaning, dimensional inspection and material handling functions in an unmanned environment. The cell was designed to:

o   Allow processing of similar and dissimilar parts in random order without disrupting production.

o   Allow serial (one-shipset-at-a-time) manufacturing

o   Reduce work-in-process inventory

o   Maximize machine utilization through remote set-up

o   Maximize throughput, minimize labor.

The system is comprised of the following elements:

o   Eight Cincinnati-Milacron 4-axis, single spindle, Computer Numerically Controlled (CNC) machining centers to perform profile milling, drilling, boring, reaming and tapping operations. Key features include:

    –   Prismatic work area up to 32 in. x 32 in. x 36 in.

    –   3-axis and 4-axis simultaneous contouring

    –   Automatic cutting tool storage, selection and changing

    –   Part surface sensing and broken tool detection

    –   Automatic pallet shuttle system

o   Two DEA coordinate measuring machines (CMM) with direct computer control drive system; a measuring range greater than the cutting machine envelope, and an accuracy/ repeatability tolerance closer than the cutting machine

o   System computer control network with Direct Numerical Control (DNC) capability. The total FMC computing complement includes:

    –   1 – DEC PDP 11/44, the cell host computer

    –   2 – DEC PDP 11/24 for robocarrier control

    –   2 – DEC PDP 11/23 controllers for the CMMs

    –   16 – controller/processors

    –   1 – DEC PDP 11/70 for backup, batch computing and simulation

o   Two fixture buildup stations with CRT terminals for buildup instruction

o   Automated storage and retrieval system for cutting tools; CRT terminal for tool buildup instructions, and electronic gaging

o   Two carrousel storage devices. Each carrousel has two load/ unload stations, with CRT terminals for operator instructions

o   Four Eaton Kenway robocarriers for transporting pallets between work stations

o   One Taylor Gaskin wash module designed for unmanned operation providing automatic part transfer, rollover, wash and discharge equipment

o   A Henry Filter, dual-flume chip removal/coolant distribution system to support all milling machines and the wash station. The system is designed to segregate and handle ferrous and nonferrous chips.

The system functions without human intervention except for the part loading/unloading operation and support areas such as fixture buildup, and cutter loading and delivery. The functions performed by the system software include:

o   Communication with the factory production data base systems to determine work order requirements and due dates based on data from the Master Schedule and Manufacturing Planning Systems, and to download the NC part programs required to control the milling and coordinate measurement machines. Upon completion of the machining and inspection functions, the system reports order status information, resource utilization and inspection results back to the appropriate management systems, closing the loop and providing the necessary integration with conventional operations

o   Management and distribution of NC part programs as well as the management of all tools within the cell

o   Managing cell functions of scheduling, traffic coordination, communication with station controllers/processors to effect the commands necessary to initiate processing or provide operator load/unload instructions.

Operation Scenario

Part production begins when a load/unload operator loads blanks to be machined onto a pallet according to instructions displayed on a CRT. The detail instructions are supplemented by a graphic display to assure proper location and orientation on the 4-sided riser blocks. The pallet, which may contain up to 16 different parts, is then automatically shuttled onto the carrousel, which has the capacity to hold up to 10 pallets. The load/unload stations are colocated in pairs adjacent to the respective carrousels. The loaded pallets remain on the rotating storage carrousels until all resources required to machine the particular part load included on a designated pallet are available within the cell.

When a pallet is required by the cell, a robocarrier is dispatched to retrieve the pallet from the carrousel. The cart receives its commands from the PDP 11/24 controller via signals in a wire embeded in the floor. The pallet is then transported to the assigned machining center and shuttled into the input queue. Each center has a total queue capacity of five pallets, with two in the input queue, one in work and two in the output queue awaiting transport.

The machining center controller interfaces with the system computer to determine its specific task. The proper NC programs are downloaded, the proper tools are selected and changed automatically from a tool magazine containing a 90 cutter tool complement and the part is machined. The pallet is automaticall rotated to machine parts on each face of the riser.

Once part machining is completed, the pallet is transported via an assigned robocarrier to a programmed wash station where chips are removed and the parts dried in preparation for inspection. After processing through the wash station, the next available robocarrier picks up the pallet and transports it to the assigned inspection station where the CMM automatically verifies part

geometry for each configuration represented on the pallet and transmits the results to the system computer. The pallet of inspected parts is then routed to the assigned carrousel. Once returned to the carrousel, the completed pallet load is forwarded to a load/unload station where parts are removed or remounted, as required, for additional machining. When processing is complete, the parts are logged out of the system and the work order system is updated with status information.

Further enhancements are planned for FMC, including automatic storage and retrieval systems for tools and materials, blank preparation, and robotic load and unload, to further integrate the cell with factory operations and improve productivity. Additional flexible manufacturing systems are also planned in other functional areas such as sheet metal fabrication, chemical and thermal processing, nonmetals fabrication, electrical assembly and structural assembly to complete the FOF architecture.

Advanced manufacturing technologies will be needed to bring these systems to maturity. Integration of these technologies into flexible manufacturing cells will provide the industry with a truly high technology factory of the future.

In summary, I feel the opportunity exists for the American aerospace industry to re-shape its future, to improve productivity and enhance its competitive position. The pathway to reindustrialization is clear.

The window of opportunity is relatively short lived and exists today. The expanding aerospace industries of Europe and the Far East are positioned and ready to overtake the world market in commercial as well as military aircraft. Widespread U.S. industry modernization now will assure our position in the world marketplace in the next century. Our challenge is to make this third industrial revolution happen.

American industry, individually and collectively, can meet this challenge by committing to factories of the future featuring highly skilled labor, advanced manufacturing technologies, flexible manufacturing systems and functionally integrated organizations.

9

AUTOMATIC ORBITAL GTA WELDING:

HIGHEST QUALITY WELDS FOR

TOMORROW'S HIGH-PERFORMANCE SYSTEMS

Barbara K. Henon
Arc Machines, Inc.
Pacoima, California 91331

ABSTRACT

Automatic orbital GTAW (TIG) welding is certain to play an increasingly prominent role in tomorrow's technology. The welds are of the highest quality and the repeatability of automatic weldings is vastly superior to that of manual welding. Since less heat is applied to the weld during automatic welding than manual welding, there is less change in the metallurgical properties of the parent material. In stainless steel pipe and tube, this process can eliminate carbide precipitation and reduce the tendency towards IGSCC.

The possibility of accurate control and the cleanliness of the automatic GTAW welding process make it highly suitable to the welding of the more exotic and expensive materials which are now widely used in the aerospace and hydrospace industries. Titanium, stainless steel, Inconel, and Incoloy as well as aluminum can all be welded to the highest quality specifications automatically.

Automatic orbital GTAW equipment is available for the fusion butt welding of tube-to-tube as well as tube to autobuttweld fittings. The same equipment can also be used for the fusion butt welding of up to 6-inch pipe with a wall thickness of up to 0.154 inches. To weld pipe from 1-1/2 inches and up with heavier wall thicknesses requiring the use of filler wire, automatic orbital GTAW pipe welding systems with remote welding capabilities are available.

These technologies have already been widely used in various aerospace applications such as: aircraft fuel and hydraulic lines, space shuttle module lines and aircraft drop tanks. Applications for hydrospace include underwater hyperbaric welding in high pressure, mixed gas atompheres using both semiautomated and automated processes. Undoubtedly, automatic orbital GTAW will find a wider application in future systems.

Introduction and Point of View

We intend to present Automatic Orbital GTAW (TIG) welding from the point of view of a manufacturer of this type of equipment. At this time we see a tremendous broadening of the application base for automatic orbital in-place welding. There are a number of reasons for the increase in the use of automated processes. To understand these reasons it is useful to look at the origins of the applications, what the current uses for this kind of equipment are, and then to discuss how we expect this technology to be used in the 1990's.

Automatic orbital TIG welding has found a niche in certain key industries. It began in the aerospace industry in the early 1960's at Rockwell (Rocketdyne) in Los Angeles. At that time the power supplies were very large, unreliable and difficult to use. Any kind of serious welding required an engineer, a welding technician, and an electronic technician. Even then, when a good weld was achieved, there were advantages over either compression fittings or manual welding techniques. There was an increase in the strength of the weld, an improvement in the consistency of penetration, and (particularly compared to compression fittings) a decrease in the likelihood of a leak. Using autogenous welding techniques also eliminated the necessity of using a compression fitting resulting in a savings in weight which was critical for aerospace applications.

In the mid 60's, companies such as Astro-Arc and Dimentrics produced production equipment to do this type of welding. The major users were Lockheed on the C-5A and L-1011 and Bell Aerosystems on the Minuteman missile.

The next major application for automatic orbital tube welding occurred in the early 1970's. This was the welding of instrumentation tubing in nuclear plants. At this time, the Parker-Hannifin Corporation developed the autobuttweld fitting for use with 1/4, 3/8, and 1/2-inch instrumentation tubing. These fittings featured a patented locator rib which automatically aligns the joint to the tungsten. A lip on the end of the fitting helps

to   align the tube to the fitting, as well as provide filler metal for the weld.

PARKER-HANNIFIN AUTOMATIC
BUTTWELD TUBE FITTINGS
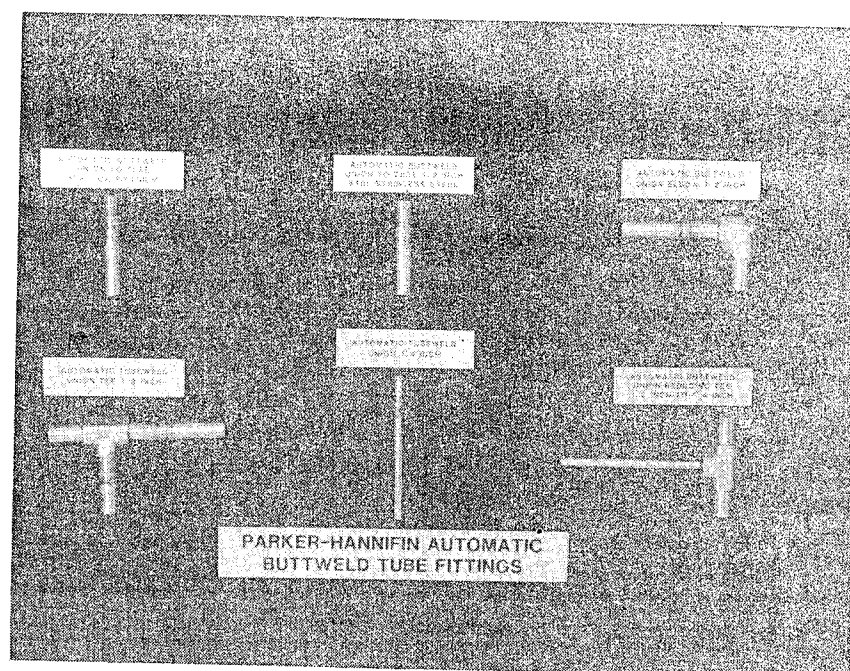
Description of Equipment and Process

Arc Machines, Inc., manufactures automatic orbital pipe welding systems, tube-to-tube sheet systems as well as orbital tube-to-tube welding equipment. The power supplies used for this type of auto-mated welding are all transistorized and programmable to the extent that the weld, from pre-purge through post-purge, is made automa-tically, without operator control.
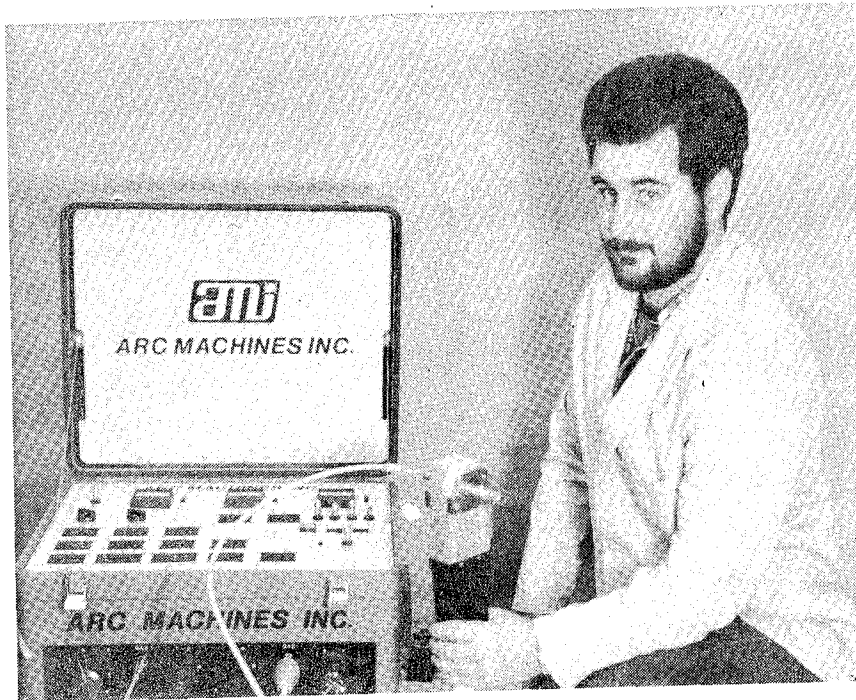
As you can see, the power supply is considerably more compact and portable than earlier models. The weld heads for fusion welding contain an internal rotor which holds the tungsten and rotates around the work. The tube, or pipe, therefore remains in place and the weld can be placed close to a wall, ceiling or bulkhead as the internal rotor is the means of moving the arc around the joint. The weld heads must provide gas shielding of the entire weld zone, and a motor to give precise rotational control. The power supply for tube-to-tube welding controls the following welding parameters automatically: pre-purge time, controlled arc strike with no overshoot, pulsation, rotation delay, four timed levels of current control, downslope and post-purge. The pipe welding equipment adds arc voltage control, oscillation and cold wire feed. All these controls must be extremely accurate and a general industry standard is that accuracy of 1% of dial reading is necessary for high-quality repeatable welds.

The process used is TIG, or more properly, GTAW. In the tube
welding equipment, the weld head forms a purge chamber which is
filled with the shield gas prior to, during, and after the welding
operation. The most common shield gas is Argon, but for some
stainless steel welds Argon/Hydrogen in the ratio of 95% Argon,
5% Hydrogen is used; for carbon steel or some relatively thick
wall stainless applications, 75% Helium/25% Argon can be utilized.
The tungsten is fixed to the rotor and the welding current is
developed in the power supply, transmitted via cables to the weld
head and finally to the rotor, the tungsten and across the arc
gap to the work. Pulsation is used both to reduce the heat input
into the material and to permit welding in the 5-G position.
Essentially, the fusion weld consists of a series of spot welds
in which the main welding current penetrates the material and the
background current chills the puddle. Metallurgically, the re-
sults are excellent welds. If there are no impurities in the
base metal, there are none in the weld. The heat input to the
material is low, the heat affected zone is small, and the strength
of the weld is greater than the tube. With this welding technique,
problems common to manual welding techniques, such as overheating
of the weld, are not a factor. While the fusion technique is most
commonly used on thin-wall tubes of 0.035", 0.065" and 0.095" wall
thickness, one of our customers is performing satisfactory produc-
tion welds on 2" Schedule 40 pipe, with a 0.154" thick wall. Those
welds have been extensively tested, and according to the customer,
"pass with flying colors!" However, as a company policy, you
should be advised that we do not recommend the use of fusion
techniques, that is without filler wire, beyond 6" Schedule 10
pipe, which is 0.134" wall thickness.

ARC MACHINES, INC.

EXAMPLES OF FUSION
BUTT WELDING
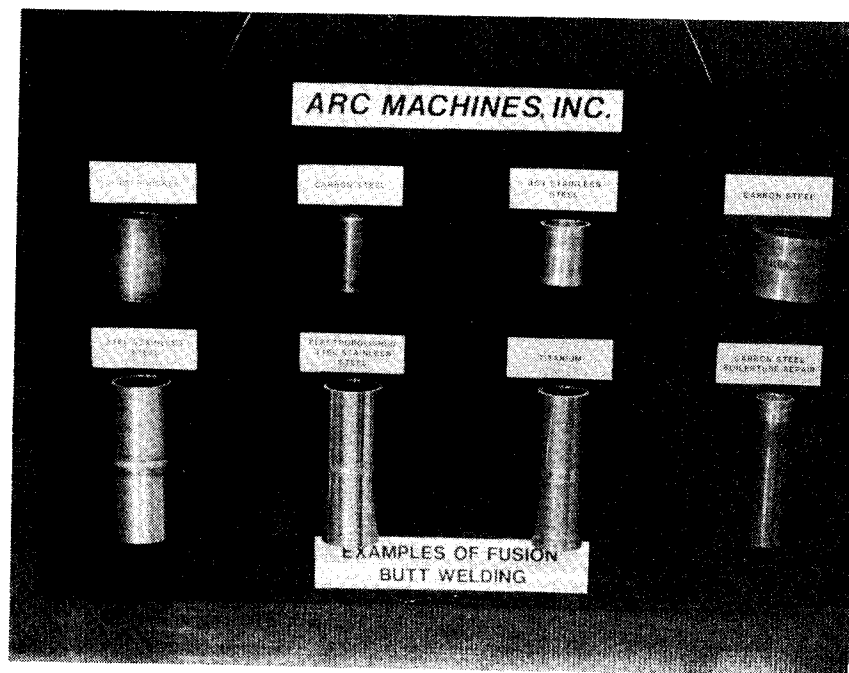
The present uses of orbital tube welding have grown beyond the initial aerospace and nuclear applications. The largest single use of orbital tube welding equipment today is in process lines for the semiconductor industry. Parker-Hannifin, Cajon and Valex fitings are used to join and terminate the process lines for the hazardous gasses (such as Arsene and Silene) and the de-ionized water used in wafer fabrication. The Cajon fitting is similar to the Parker, but lacks the locator rib for alignment. Cajon uses a shoulder which butts up against the outside of the tube clamp insert to align the tungsten to the joint on tee and elbow fittings. Pharmaceutical and bio-technology plants also commonly specify automatic orbital welding to ensure the cleanliness of their process lines for biological or pharmaceutical components and water for injection into the human body. Ladish Tri-Clover and Valex are fitting manufacturers who adapted their fittings to the requirements of automatic welding. Lastly, the final ingredient necessary to make in-place fusion butt welding really field-practical is the ready availability of portable, in-place tube prepping equipment. This is now readily available and produces the kind of machined finished square joint that is absolutely necessary for repeatable orbital fusion butt welding.

From this base, we see a general broadening of the application. Many of our mechanical contractor customers who purchased fusion butt welding equipment for semiconductor use are using the equipment on more mundane jobs - paint thinner plants and a chocolate factory are two that come to mind. In aerospace and hydrospace, the applications are also broadening. Fusion butt welding is relatively common in many aircraft, missiles, and spacecraft. Now we find that the fuel-handling facilities and many lines associated with hazardous, high-pressure or cryogenic gasses are being welded with orbital equipment. Recently we demonstrated to a manufacturer of jet engine test panels and discovered a whole new application area that could make excellent use of existing, proven fusion butt welding techniques and available fittings.

For hydrospace, we also see a broadening of the application. To date, fusion butt welding has not been accepted as readily for marine use as has been the case with aerospace. In 1984, the U.S. Navy seriously tested fusion butt weld fittings. The lip on the fitting produces a weld that is thicker than the tube wall, with both full penetration on the inside and reinforcement on the outside of the tube. These welds may well meet Navy specifications for crown, in which case their use could multiply in ship construction. Another factor is the increase in size that we have seen in autobutt weld fittings. From the initial 1/4", 3/8" and 1/2" sizes,

16

3/4" and 1" are now commonly used in semiconductor plants. The semiconductor plants are requesting the fitting manufacturers to produce even larger fittings and I can now show a prototype 2" O.D. auto butt weld fitting. If this weld becomes approved, the increase in size means that more and more tubes on board ship could be fusion butt welded. Aside from ship applications, shore facilities could benefit from fusion butt welding. It has long been the belief of our company that there is a lot of process pipe installed that could be thin wall tubing. The theoretical internal burst pressure of thin wall tubing is higher than generally realized: 1/2" 0.049" wall theoretical burst pressure is 14,700 p.s.i.; 1-1/2" 0.065 wall theoretical burst pressure is 5,800 p.s.i.; 30" 0.083" wall is 4,150 p.s.i. Many applications for fuel, oil or water are at 400 p.s.i. or less. If a facility were built using thin-wall tubing where it is appropriate, instead of thick-wall pipe, the savings could be quite large. The material is very easy to handle and prepare for welding. The welds are top quality, repeatable and are made very quickly, particularly when compared to manual thick-wall pipe welding. The support structure for tube could be lighter and possibly use smaller material than would be required for pipe. The foundations could be designed to carry less load. We are not mechanical engineers, but it would be an interesting exercise to calculate how much could be saved by using this approach.

Orbital Pipe Welding

Orbital pipe welding requires more complex equipment than the fusion tube welding equipment just described.
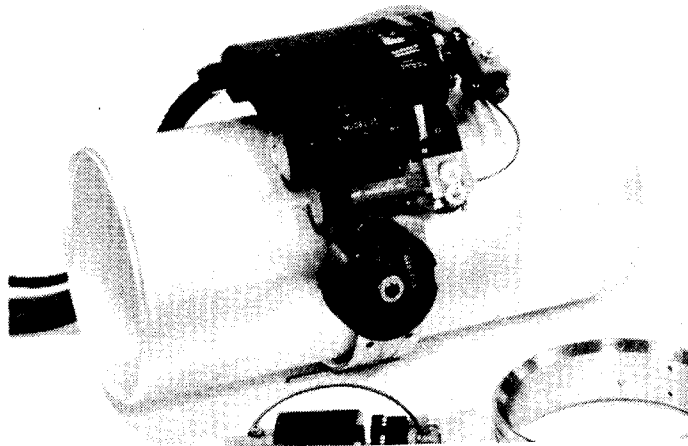
The pipe joint configurations, with a groove which must be filled with weld metal provided by filler wire, require additional electronic functions, and their mechanical equivalents. The filler wire addition requires accurate wire feed motors and mechanisms. The necessity to move the torch across the groove requires accurate control of both the rate of movement, the distance moved and the dwell on the sidewall. Accurate rotational movement around the pipe must also be provided, together with current pulsation and the ability to change parameters as this becomes necessary. Weld head radial clearance poses a real challenge for the designers, as the heads must be as small as possible, yet sturdy enough to meet their real-world requirements found on the job site. The result of this design effort is a level of control of the weld puddle that results in welds that are metallurgically and physically excellent, as well as aesthetically attractive.

Most recently, remote operation of this equipment has come into its own. Several nuclear plants have been repaired in 1983 and 1984 with remotely operable pipe welding equipment. Our system uses fiber optics to view the leading and trailing edges of the puddle and may be operated up to 200 feet from the weld joint. This remote ability can also be used on weld heads which mount inside a pipe and weld or clad the I.D.

18

The aerospace applications of this equipment are, to date, limited to fuel handling facilities. Little or no additional applications are expected in the future. Marine applications, however, are greater. Several constructors in the United States have very strong orbital pipe welding programs. Newport News Shipyard and General Dynamics Electric Boat are two that come immediately to mind. Developments of weld heads such as our miniature pipe weld head with very minimum radial clearance of 1-3/8" will no doubt increase the applications for ship construction. We expect the experience in on-board construction to carry over to the shore based support facilities involved in direct ship servicing, as well as to the refineries that produce fuel. Another application is that demonstrated by the recent completion of the first stainless steel pipeline. The cost of the material, and metallurgical considerations, dictated the use of orbital welding equipment.

A fascinating application of orbital pipe welding is the use of orbital equipment to weld pipelines under water. Not a "pipe dream", this is now a field-proven technique used by Subsea International at their base in Aberdeen, Scotland, that uses a microprocessor controlled welding power supply and programmer topside, which operates an orbital pipe welding head in a habitat up to 300 M (1,000 feet) below the surface. The current application is in the repair of underwater pipelines. In operation, the habitat, on the ocean floor, is placed over the broken or ruptured pipe and this is brought up into the habitat. The pipe is cut and prepped in place, and the repair section tacked into position. The technician doing this work need not be a skilled welder - tacking is easier than pipe welding. The welding head is placed on its guide ring and the entire weld is then performed on command from the surface. In this way, for the first time, nuclear quality repair welds can be made in place, on the ocean bottom.

CONCLUDING REMARKS

In summation, we believe that orbital in-place welding, particularly tube welding, will see a great expansion of applications in the near future, and will become, in time, a very common joining technique.

AN INTERIM REPORT ON INVESTIGATION OF LOW-TEMPERATURE

SOLDERS FOR CRYOGENIC WIND TUNNEL MODELS

George C. Firth and Vernon E. Watkins, Jr.
NASA Langley Research Center
Hampton, Virginia 23665

ABSTRACT

The advent of high Reynolds number cryogenic wind tunnels has forced alteration of manufacturing and assembly techniques and eliminated usage of many materials associated with conventional wind tunnel models. One of the techniques affected is soldering.

Solder alloys commonly used for wind tunnel models are susceptible to low-temperature embrittlement and phase transformation. The low-temperature performance of several solder alloys is being examined during research and development activities being conducted in support of design and fabrication of cryogenic wind tunnel models. Among the properties examined during these tests are shear strength, surface quality, joint stability, and durability when subjected to dynamic loading. Results of these tests and experiences with recent models are summarized in this paper.

INTRODUCTION

The wind tunnel model manufacturing community utilizes solder technology for electrical connections, structural joining, and filling of aerodynamic surface imperfections. The advent of cryogenic wind tunnels, with the associated severe test environment and aerodynamic surface quality requirements which are well beyond those which are required for conventional wind tunnel models, severely impacts usage of solders on models. The low temperatures (-300°F) encountered in cryogenic wind tunnels cause embrittlement of many materials including most of the soft solders commonly used by model builders.

High tin alloys are often the preferred solders because of their good strength, hardness, wetting capabilities, finishing characteristics and appearance. Unfortunately, tin becomes brittle at a temperature well above the potential test temperatures in cryogenic facilities. Additionally, tin is susceptible to a low-temperature initiated crystalline transformation referred to as "tin pest" which results in a nonstructural "gray tin" powder. Additions of alloying elements are known to help alleviate both tin pest and low-temperature embrittlement.

High lead alloys remain ductile at cryogenic temperatures but exhibit poor wetting and finishing characteristics. Additions of selected alloying elements will serve to alleviate these problems, but will decrease low-temperature ductility.

Indium alloys are known to possess excellent low-temperature ductility and good wetting characteristics. However, indium alloys are soft and consequently exhibit poor finishing characteristics.

The purpose of this report is to discuss the efforts that are being made to identify and characterize soft solders suitable for cryogenic wind tunnel models. The solders being investigated include those embraced by conventional wind tunnel model fabricators as well as alloys which are known to possess low-temperature ductility.

ONE-PERCENT SPACE SHUTTLE MODEL
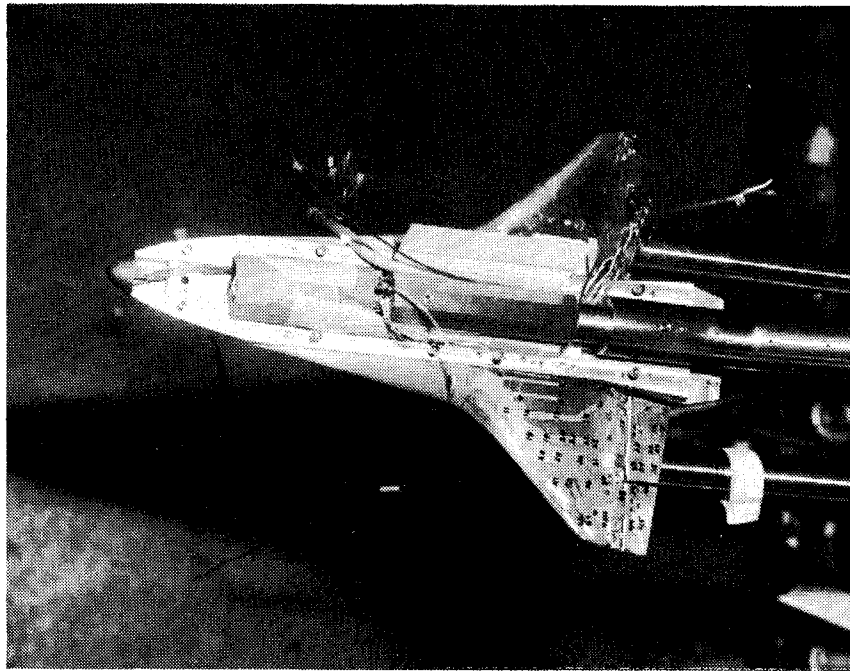
The most difficult surface imperfection to fill is created intentionally. Grooves are cut in an aerodynamic surface to facilitate routing of pressure tubing from the point on the surface point at which the static pressure is being measured to the location of the pressure transducer. Surface routing and solder filling is utilized whenever test requirements and model materials permit. The Shuttle model shown above, with upper fuselage removed, illustrates the usage of solder to fill the tubing grooves (lighter areas on wing).

FILLING MATERIALS COMPARISONS

	BRAZE ALLOYS	SOLDER ALLOYS	POLYMERIC FILLER
PLUSES	Strength Hardness Conductivity Coefficient of thermal expansion	Moderate heat Conductivity Coefficient of thermal expansion	Low heat Application
MINUSES	Heat Facilities Permanent	Corrosive fluxes Soft	Coefficient of thermal expansion Soft

The three types of materials generally considered for filling surface imperfections in wind tunnel models are braze alloys, soft solders, and polymers. A comparison of the advantages and disadvantages of each with respect to cryogenic models is tabulated above. This comparison reveals that selection of a filler is dependent on the particular application and in all likelihood will not be a clear-cut decision.

The shear strength of soldered joints should match or exceed that of bonded joints, but will not approach that of brazed joints and, therefore, should be used cautiously as a primary structural joining technique. Solders do not require heat levels high enough to cause model distortion or alteration of base metal properties. The thermal conductivity of a typical solder matches closely the conductivities of model base metals. The typical solder's coefficient of thermal expansion is approximately twice that of the base metal or less than forty percent of the typical polymer's coefficient. For most applications the contraction differential between base metal and solder will cause no structural problems but could prove to be a problem with respect to local surface "dimpling" at low temperatures. Of greater concern with regard to surface quality is dimpling caused by the difference in hardness between the solder and model base metal. This differential induces undercutting of the filled areas during hand finishing of contoured surfaces. The softness of solders falls in between that of braze alloys and polymers. The chief disadvantage associated with solders is the necessity of using corrosive fluxes for preparing most of the cryogenic model metals for soldering. The corrosion induced by flux residues and entrapped flux has been a persistent problem and can only be alleviated by exacting joint design, meticulous soldering procedures, and thorough post soldering cleaning.

PROGRAM GOALS

O   IDENTIFY SOLDER ALLOYS SUITABLE FOR
     CRYOGENIC WIND TUNNEL MODELS

O   DETERMINE LOW-TEMPERATURE PROPERTIES
     OF SUITABLE ALLOYS

As solder alloys have been determined to have some redeeming values as a wind tunnel model filler material, a program was initiated to investigate solders and their usage at cryogenic temperatures. The initial goal of the investigation is to identify solder alloys suitable for usage on cryogenic wind tunnel models. The final goal is to characterize the low-temperature mechanical properties of the suitable alloys.

HIGH TIN SOLDERS

ADVANTAGES: WETTABILITY
                WIDE USAGE
                STRENGTH

DISADVANTAGES: TIN PEST
                  LOW TEMPERATURE
                  EMBRITTLEMENT

SOLDERS CONSIDERED: 97% Sn 3% Ag
                       95% Sn 5% Sb

Solders with a high tin content are attractive because of their inherent good wetting characteristics, relatively high tensile strength, good surface finishing characteristics, and the level of experience with these alloys that is held by wind tunnel model fabricators. Offsetting these advantages is the susceptibility of tin to low-temperature embrittlement and "tin pest."

Tin-based solder alloys typically become brittle at temperatures slightly below the freezing point of water. This embrittlement dictates that usage is to be limited to components exposed to low stress levels. The tin pest problem is a low-temperature crystalline structure transformation which results in white tin being transformed to gray tin powder. This transformation can be alleviated by addition of alloying elements, most notably, antimony.

The two high tin alloys investigated in this program were 97% tin-3% silver and 95% tin-5% antimony. These two alloys were chosen because of their high strength, good wetting, and good surface finishing characteristics.

TIN/LEAD SOLDERS

ADVANTAGES: INCREASING DUCTILITY
           AVAILABILITY

DISADVANTAGES: SOFTNESS
             DECREASING WETTABILITY

SOLDERS CONSIDERED: 49.5% Pb 50% Sn .5% Sb
                              93% Pb 5.2% Sn 1.8% Ag

     The tin-lead solder alloys exhibit increasing low-temperature ductility
with increasing lead content. Alloys with over 70% lead are ductile at tem-
peratures approaching absolute zero. Tin-lead alloys containing lead in excess
of 40% are generally considered to be "wiping" solders and are frequently used
in plumbing and filling of gaps on automotive bodies. Unfortunately, solders
with a high lead content are soft, which complicates surface finishing, and
exhibit greatly reduced wetting characteristics.

     A 49.5% lead-50% tin-0.5% antimony solder alloy has been examined during
this program because of its position between high tin and high lead content
alloys according to existing mechanical property data. A high lead solder, 93%
lead-5.2% tin-1.8% silver, will be investigated in the near future.

INDIUM SOLDERS

ADVANTAGES: DUCTILITY
               LOW HEAT
               BASE MATERIALS


DISADVANTAGES: SOFTNESS
                COST
                EXPERIENCE

SOLDERS CONSIDERED: 37.5% Pb 37.5% Sn 25% In
                       50% Pb 50% In

Indium-based solder alloys offer greatly improved ductility at cryogenic temperatures, intermediate melting temperatures, and the capability to join a variety of base materials. Complicating the usage of indium solders is the extreme softness of the material with respect to the model base material. Additional considerations which may make the indium alloys less than the optimum choice are the high cost and the lack of fabrication experience with these solders.

Among the indium alloy solders to be examined in this program are a 37.5% lead-37.5% tin-25% alloy and a 50% lead-50% alloy. The lead-tin-indium alloy is expected to have a good combination of mechanical properties and the lead-indium alloy is expected to have excellent ductility and acceptable wetting characteristics.

28
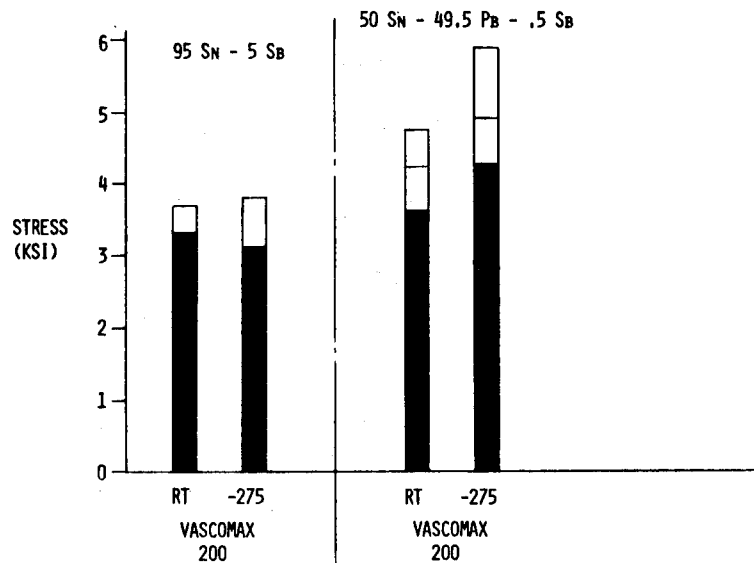
SOLDER - SHEAR TEST

A limited number of lap-shear tests involving 18% nickel maraging steel specimens (VASCOMAX) joined with 95% tin-5% antimony and 50% tin-49.5% lead-0.5% antimony solders provided some surprises. Contrary to expectations, the tin-antimony alloy shear strength was less than that of the tin-lead-antimony alloy at room temperature and did not demonstrate an increase at cryogenic temperatures. The tin-lead-antimony alloy did demonstrate an increase in shear strength at cryogenic temperatures, but not to the degree expected. A disturbing development was the scatter of data. In the bar graph above, the shaded portion of the bars represents the minimum strength, the top of the bars represents the maximum strength and the line in-between indicates the average shear strength. The data band width for the tin-antimony alloy at the cryogenic temperature tests was approximately 50% of the average value.
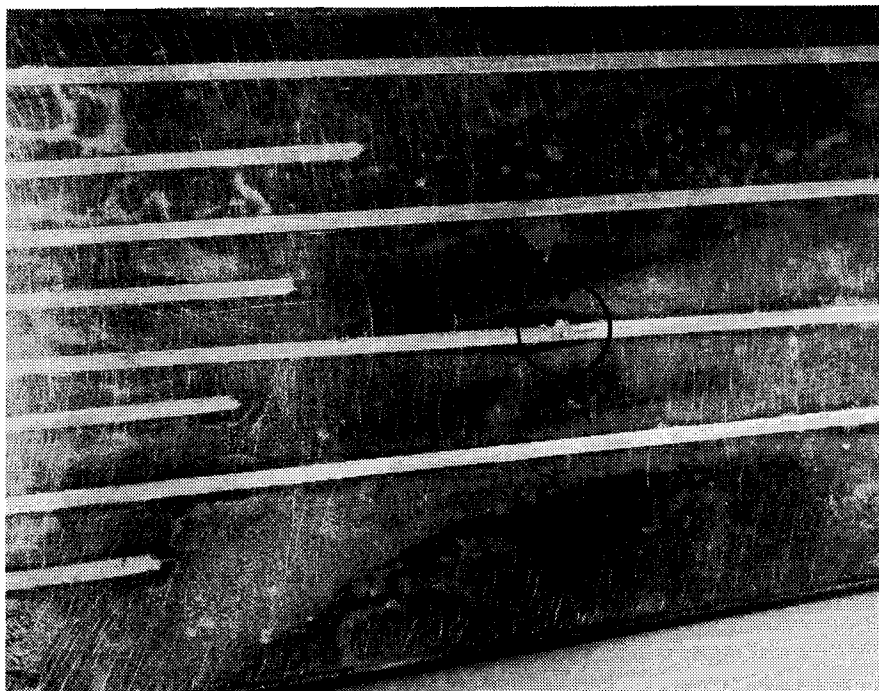
SOLDER - TENSILE TEST
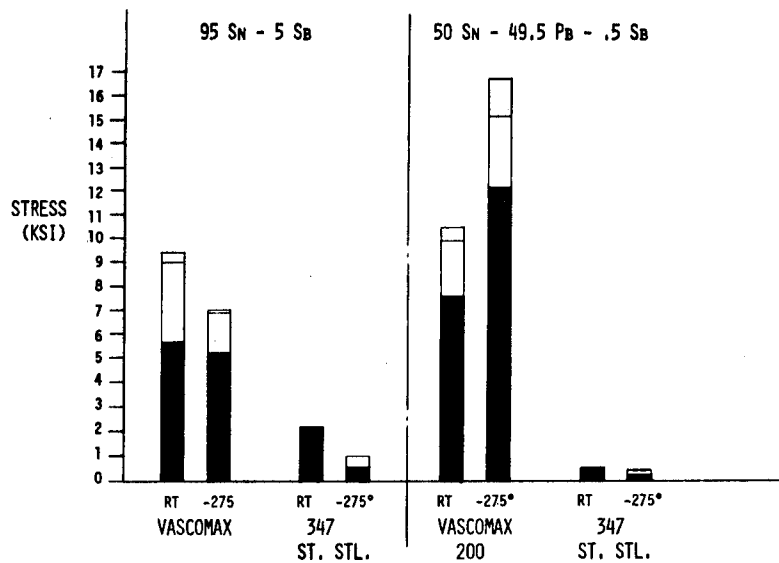
Similarly, tensile strength tests were conducted at room and cryogenic temperatures with the same solder alloys being used to join 18% nickel maraging steel specimens and 347 stainless-steel specimens. The bar graph of the test data indicates the same tendencies which were evident in the shear test data. Generally, the tin-lead-antimony alloy performed about as expected for the 18% nickel maraging steel specimens and the tin-antimony alloy did not meet expectations. Especially disappointing were the tensile strengths measured for the stainless-steel specimens. Also troubling, once again, was the scatter of data for the maraging steel specimens. Examination of the tested specimens revealed poor joint quality. The joint quality can be attributed to several factors: large joint area contributed to flux entrapment and void formation, improper surface finishing impeded solder flow, and specimen size which made uniform heating difficult. These factors are being addresed and will be minimized in future testing.

30

DYNAMIC MODEL WING SPECIMEN
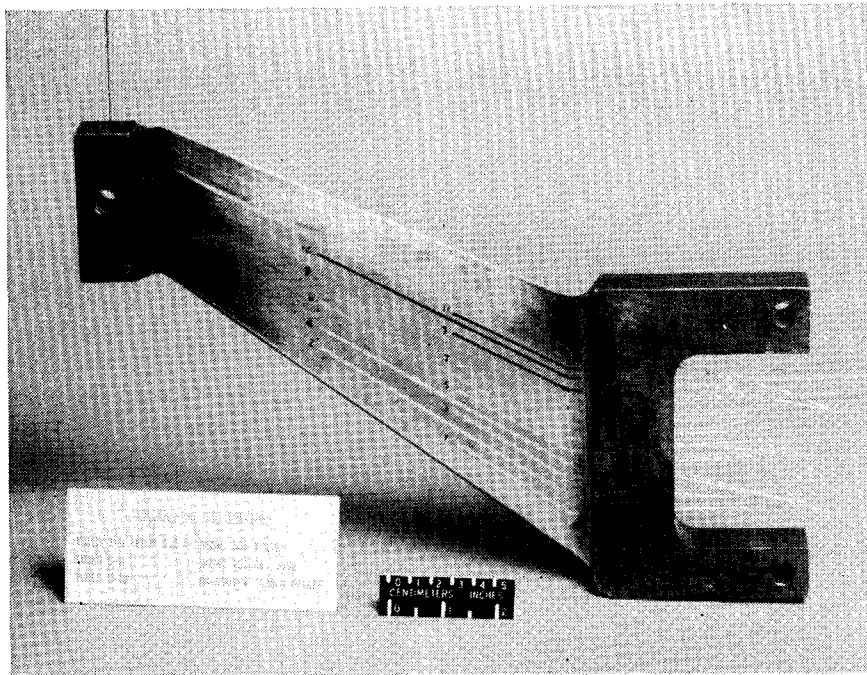
A dynamic test at cryogenic temperatures was conducted to determine suitability of the tin-antimony and tin-lead-antimony alloys for covering surface routed grooves in a wind tunnel model. A simulated model wing made with VASCOMAX, with tube grooves filled with the two solders and a modified epoxy, was used for this test. The specimen was clamped at the root end in a loading fixture. The assembly was lowered into a cryostat and allowed to reach equilibrium at approximately -300°F. A load was then applied to the block of material at the wing tip at a rate of 12 cycles per minute for 5 thousand cycles. This sequence was repeated to give 5 thousand cycles at each of 4 levels of loading. The loading levels represented specimen surface bending stress levels of 22, 44, 66, and 88 thousand pounds per square inch.

A test of the simulated wing specimen was uneventful and surprisingly suc-
cessful. There were no structural failures. No filled area separated or moved
relative to the specimen surface, nor was any cracking of the solders or epoxy
observed. However, there was formation of liquid droplets, circled in the photo-
graph, along the tin-antimony solder filled grooves. These droplets were deter-
mined to be acidic and apparently were the result of flux entrapment in the
solder joint. Under thermal cycling between room and cryogenic temperatures,
the joint apparently developed microcracks allowing moisture to migrate to
entrapped flux through capillary action. This acidic solution then gradually
seeped to the surface over an extended period of time. These droplets were evi-
dent throughout the 95% tin-5% antimony joints, but appeared in only three spots
on the 50% tin-49.5% lead-0.5% antimony soldered areas.

CONCLUSIONS

O SOLDER ALLOY SUITABLE FOR CRYOGENIC
  WIND TUNNEL MODELS HAS BEEN IDENTIFIED

O STRUCTURAL PROPERTIES DEPENDENT ON
  TECHNIQUE/EXPERIENCE

The program thus far has identified 50% tin-49.5% lead-0.5% antimony as a common solder which can be utilized for filling surface flaws and tube grooves in cryogenic wind tunnel models. Other alloys which should be suitable will be investigated as this program continues.

The program has served to reemphasize the fact that structural properties are as dependent on technique as they are on any other factor. Strict adherence to procedures to be developed for cryogenic wind tunnel model application will be required in order to achieve acceptable solder joints.

BIBLIOGRAPHY

1. Buckley, John D.; and Sandefur, Paul G., Jr.: Cryogenic Technology, NASA CP-2122, Part I, November 1979, pp 259-269.

2. Ferris, Alice T.: Cryogenic Technology, NASA CP-2122, Part II, November 1979, pp 299-315.

3. Rush, Homer F.: Cryogenic Wind Tunnel Models/Design and Fabrication, NASA CP-2262, May 1982, pp 177-186.

4. Tobler, R.L.: Materials for Cryogenic Wind Tunnel Testing, National Bureau of Standards, Boulder, CO, NBSIR 79-1624, 1980.

5. Young, C. P., Jr.; Bradshaw, J. F.; Rush, H. F.; Wallace, J.W.; and Watkins, V.E.: Cryogenic Wind-Tunnel-Model Technology Development Activities at the NASA Langley Research Center, AIAA Paper No. 84-0586, March 1984.

NTF - SOLDERING TECHNOLOGY DEVELOPMENT FOR CRYOGENICS

E. Thomas Hall, Jr.
NASA Langley Research Center
Hampton, Virginia 23665

ABSTRACT

The advent of the National Transonic Facility (NTF) brought about a new application for an old joining method, soldering. Soldering for use at cryogenic temperatures requires that solders remain ductile and free from tin-pest (grey tin), have toughness to withstand aerodynamic loads associated with flight research, and maintain their surface finishes. Solders are used to attach 347 Stainless-Steel tubing in surface grooves of models. The solder must fill up the gap and metallurgically bond to the tubing and model. Cryogenic temperatures require that only specific materials for models can be used, including: Vasco Max 200 CVM, Lescalloy A-286 Vac Arc, PH 13-8 Mo. Solders identified for testing at this time are: 50% Sn - 49.5% Pb - 0.5% Sb, 95% Sn - 5% Sb, 50% In 50% Pb, and 37.5% Sn - 37.5% Pb - 25% In. With these materials and solders, it is necessary to determine their solderability. After solderability is determined, tube/groove specimens are fabricated and stressed under cryogenic temperatures. Compatible solders are then used for actual models.

INTRODUCTION

NTF - SOLDERING TECHNOLOGY DEVELOPMENTS FOR CRYOGENICS

In an earlier presentation (ref. 1), Firth discussed objectives of the solder research program, problems associated with using solders at cryogenic temperatures, test results, and experiences with recent models.

This presentation will cover soldering methods, testing procedures, and results of solderability tests done on Vasco Max 200. Soldering techniques to install pressure tubes on cryogenic models, physical testing of the solders, surface preparation, and surface analysis will also be discussed.

BASE METALS

o   Vasco Max 200 CVM - 18% Nickel Alloy

o   347 Stainless Steel - Tubing

o   Lescalloy A-286 Vac Arc

o   PH 13-8 Mo

Various metals usable at cryogenic temperatures were selected for testing
their solderability. Vasco Max 200, Lescalloy A-286, and PH 13-8 Mo are used
in making cryogenic wind tunnel models. Pressure tubes used on these models
are made of 347 Stainless Steel. Testing is being done on the Vasco Max 200
and 347 Stainless Steel at this time. Lescalloy A-286 Vac Arc and PH 13-8 Mo
will be tested later. The rest of this presentation centers around Vasco Max
200 and 347 Stainless Steel.

SOLDERS TO BE TESTED

o INDALLOY #119 50% SN, 49.5% PB, 0.5% SB 420° F LIQUIDUS

o 95% SN, 5% SB   464° F LIQUIDUS

o INDALLOY #7 50% IN, 50% PB   480° F LIQUIDUS

o INDALLOY #5 37.5% SN, 37.5% PB, 25% IN 358° F LIQUIDUS

The solders listed above were selected for testing. At this time, 50% Sn - 49.5% Pb - 0.5% Sb and 95 Sn - 5 % Sb solders are being tested. Once tensile and lap shear specimens are completed, testing will begin on 50% In - 50% Pb and 37.5% Sn - 37.5% Pb - 25% In. The liquidus temperatures for each solder are included. This list is not intended to exclude other solders. The 93% Pb - 5.2% Ag solder has been mentioned as another possible solder for investigation (ref. 1).

FLUXES TESTED

o EUTECTIC'S EUTECTOR FLUX 157 - CONTAINS FLUORIDE

o ALL-STATE DUZALL FLUX - CONTAINS ZINC CHLORIDE

o RUBY'S STAINLESS STEEL SOLDERING FLUX - CONTAINS MURIATIC ACID

The base metals selected are considered very difficult to solder. Therefore, corrosive fluxes are needed to break the surface oxides and promote good wetting by the solders. Selection of the fluxes listed above was based upon their availability and their recommended use on the base metals mentioned earlier. Testing of these three fluxes was conducted on Vasco Max 200. Vasco Max samples were fluxed, placed on a pre-heated hot plate, and allowed to heat up to soldering temperature. Solder was then applied to the fluxed surface. After the solder finished flowing the sample was removed from the hot plate, air cooled to room temperature, and washed in water.

Visual inspection of each sample showed the fluoride flux promoted better wetting of the solder. The zinc chloride flux and muriatic acid flux had to continually be added during the heatup and soldering operation. The fluoride flux was applied to the surface before heating up and again when the solder was applied. Samples of 347 Stainless Steel tubing were tinned using each of the fluxes previously mentioned. Again the fluoride flux worked better than the other two. The fluxes will be tested on samples of the other base metals at a later date. Other fluxes are being looked at for possible use on these base metals.

SOLDERABILITY TEST

o   SPREAD SPECIMENS

o   TINNING SPECIMENS

o   TUBE/GROOVE SPECIMENS

o   WING SPECIMENS

A solderability test will be conducted on each base metal and solder. At this time only Vasco Max 200 has been tested using 50% Sn - 49.5% Pb - 0.5% Sb. Listed above are four tests to be used for evaluation. Spread/wettability specimens were done on various abraded surfaces to determine which surface gave the best wettability of the solder. Abrading the surface is necessary because Vasco Max 200 oxidizes when heat treated. Fluxes cannot remove this heavy oxide so mechanical abrading methods are used. After determining which surface finishing methods give the best percent spreading/wettability these surfaces were used in subsequent tests to evaluate their tinning qualities.

Tube/groove specimens were fabricated to determine the best method for soldering 347 Stainless-Steel tubing in the grooves of a Vasco Max specimen. Once a satisfactory method was determined, tubes were soldered in grooves on both the upper and lower surfaces of a wing specimen for the fatigue/flex test. Chemical or plated surface preparations were not considered due to the lack of practical application to the model's partial assembly and the intricate nature of hardware design.

40

FORMULAS FOR EVALUATING PERCENT SPREADING

$$D = 0.3937 \sqrt[3]{\frac{\text{WEIGHT}}{\text{SPECIFIC GRAVITY}} \left(\frac{6}{\pi}\right)}$$

$$\frac{D-H}{D} \times 100 = \text{PERCENT SPREADING}$$

D = DIAMETER OF THE HYPOTHETICAL SPHERE

H = HEIGHT OF THE SOLDER DROPLET AFTER
     SPREADING OVER THE METAL

The formulas above (ref. 2) were used to calculate the percent spreading/wettability of the solder. Calculate the diameter of the hypothetical sphere (D) using the first formula. Weight (gms) and specific gravity (gms/cm^3) of the solder are known values, and the value 0.3937 converts centimeters to inches. Measure the height of the solder droplet (H) after spreading over the metal surface. Plug the values for D and H into the second formula and calculate the percent spreading. The lower the height of the solder after spreading the higher the percent spreading. The ideal percent spreading would be one that reaches 100%.

Vasco Max 200

50% Sn, 49.5% Pb, 0.5% Sb

Specimen Number	Surface	Ra	Solders Specific Gravity (gm/cm³)	Solders Weight (grams)	H (inches)	D (inches)	% Spreading	Description
1A	Sanded w/240 Alum. Oxide	15	8.85	0.0918	0.0228	0.1065	78.6%	Adequate
1B	No. 1 Alum Oxide Powder	34	8.85	0.1095	0.0581	0.1330	48%	Very Poor
1C	Glass Bead Blasted	34	8.85	0.1175	0.0299	0.1157	74.1%	Adequate
1D	120 Grit Blasted	40	8.85	0.1044	0.0350	0.1112	68%	Poor to Fair
2A	Brown Oxide Heat Treated	13	8.85	0.1299	0.0193	0.1196	83.8%	Good
2B	Brown Oxide Wire Brushed	13	8.85	0.1206	0.0164	0.1167	85.9%	Very Good
3	Sanded with 120 Alum. Oxide	19	8.85	0.5	0.0214	0.1875	88.6%	Very Good
4	Steel Wooled Heavy Oxide	22	8.85	0.5	0.1045	0.1875	44.3%	Very Poor
5	120 Grit Blasted	51	8.85	0.5	0.0375	0.1875	80%	Adequate/Good
6	Glass Bead Blasted	34	8.85	0.5	0.0285	0.1875	84.8%	Good +
7	Machined Surface (Lathe)	16	8.85	0.5	0.0230	0.1875	88%	Very Good
8	Machined Surface (Mill)	15	8.85	0.5	0.0145	0.1875	92%	Excellent

Spread test data on Vasco Max 200, 50% Sn - 49.5% Pb - 0.5% Sb solder, and the floride flux are shown in the chart above. All Vasco Max 200 specimens have been heat treated. Solder of a known weight and flux was placed on the specimen surface. The specimen was placed on a hot plate and heated to approximately 525° F which allowed the specimen to reach the solder's flow temperature. After the solder stopped flowing the specimen was removed from the hot plate, air cooled to room temperature, and cleaned of flux residue. The height of the solder, after spreading over the specimen, was measured. Calculations were performed to determine percent spreading. This procedure was followed on each spread test specimen. Specimen #1 (see photos that follow) was divided into four areas for preliminary investigation of various surfaces. Area #1B, abraded with No. 1 Aluminum Oxide (27 microns), had the worst percent spreading of the four surfaces. Because of low percent spreading on surface 1B no more tests were done for this type of surface. Percent spreading on the other three was not as high as expected. Therefore, the surfaces of specimens #3 through #8 were prepared for soldering as shown in the chart above. Each specimen was soldered with 0.5 grams of solder using the same soldering procedures as specimen #1. Specimen #3, sanded with 120 aluminum oxide, had 88.6% spreading. Specimen #4, oxide rubbed with coarse steel wool, had 44.3% spreading. Specimen #5, grit blasted with 120 grit, had 80% spreading. Specimen #6, glass bead blasted, had 84.8% spreading. Specimens #7 and #8 were machined by lathe and milling machine, respectively, to remove oxidation.
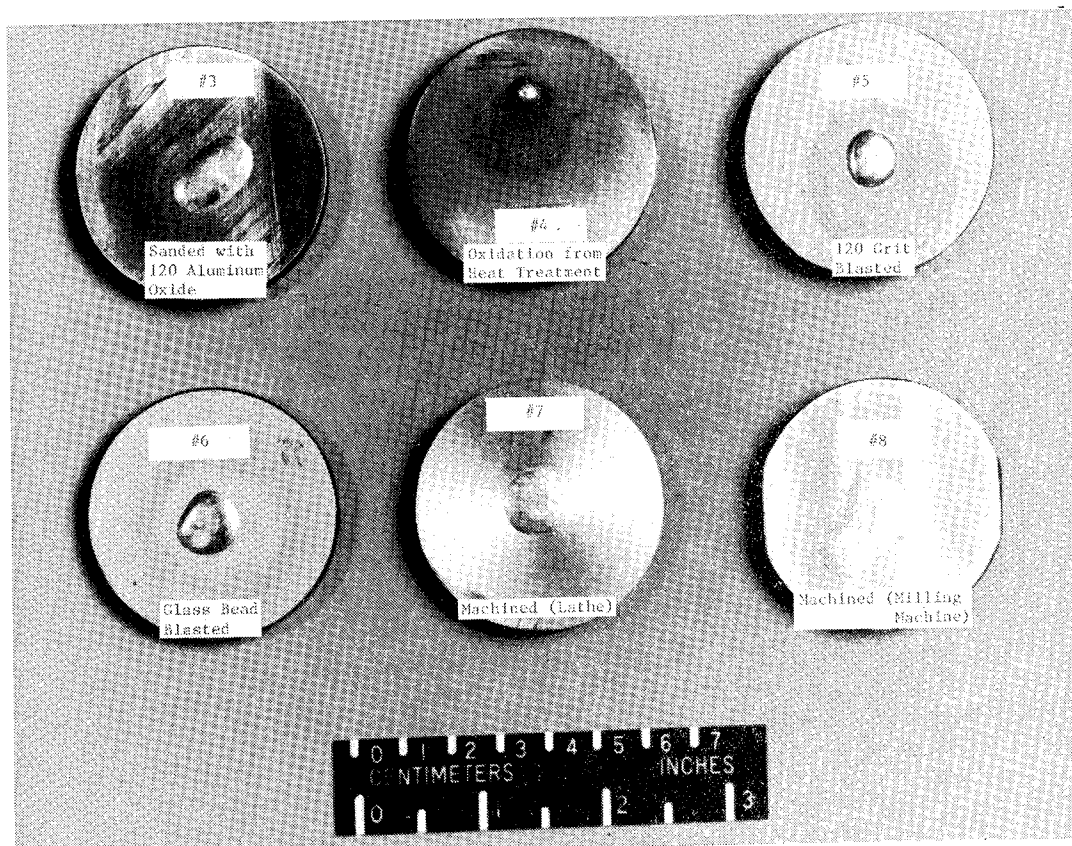
Specimen #7 had 88% spreading and specimen #8 had 92% spreading. Specimen #8 was inadvertently tilted while being removed from the hot plate which resulted in the solder flowing and wetting more of the surface. Therefore, the spreading percent is slightly higher. Surface finishes were measured for each specimen to determine if any relationship exists between it and percent spreading. There did not appear to be any distinct relationship between the two.
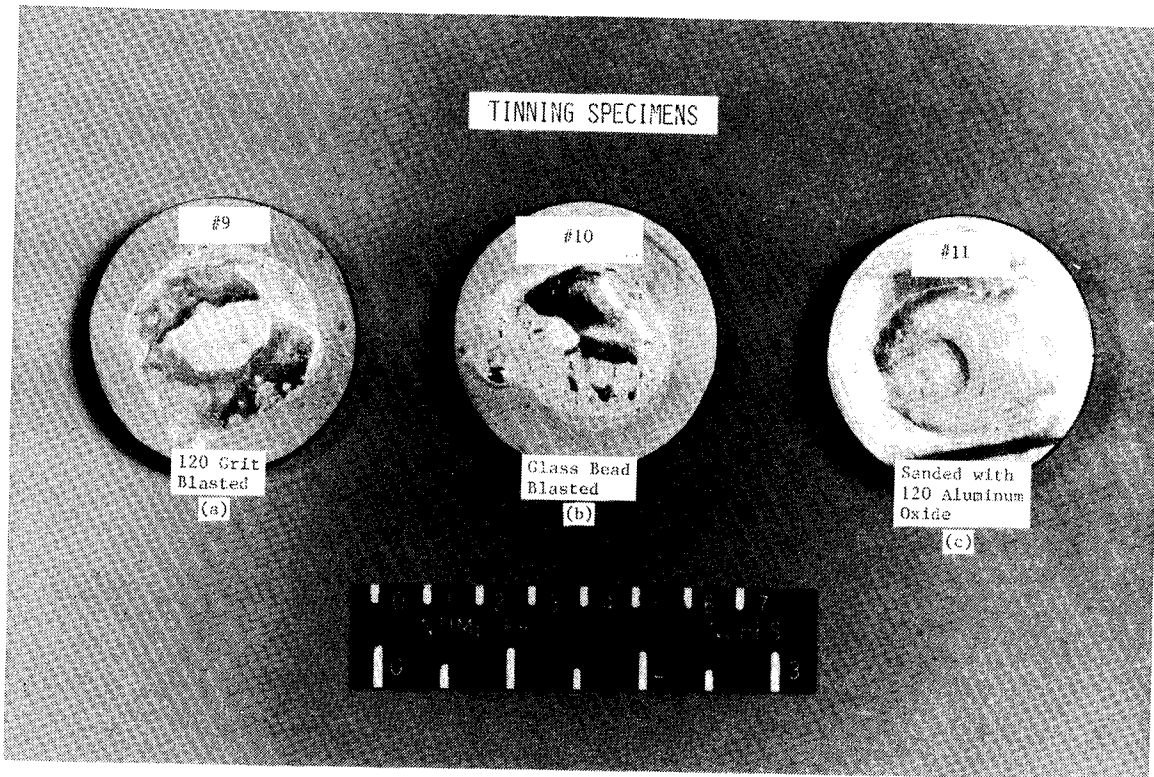
Specimen #2 was heat treated in an argon atmosphere retort to eliminate oxidation. If oxidation was eliminated there would be no need to abrade the surface. A golden brown oxide that formed on the specimen was the result of a leaky retort. Prior to spread testing, #2B was wire brushed while nothing was done to #2A. Wire brushing did not remove the oxide. The flux broke the oxide allowing the solder to spread over the surface. Surfaces #2A had 83% spreading and #2B had 85.9%.

SPREAD TEST SPECIMENS
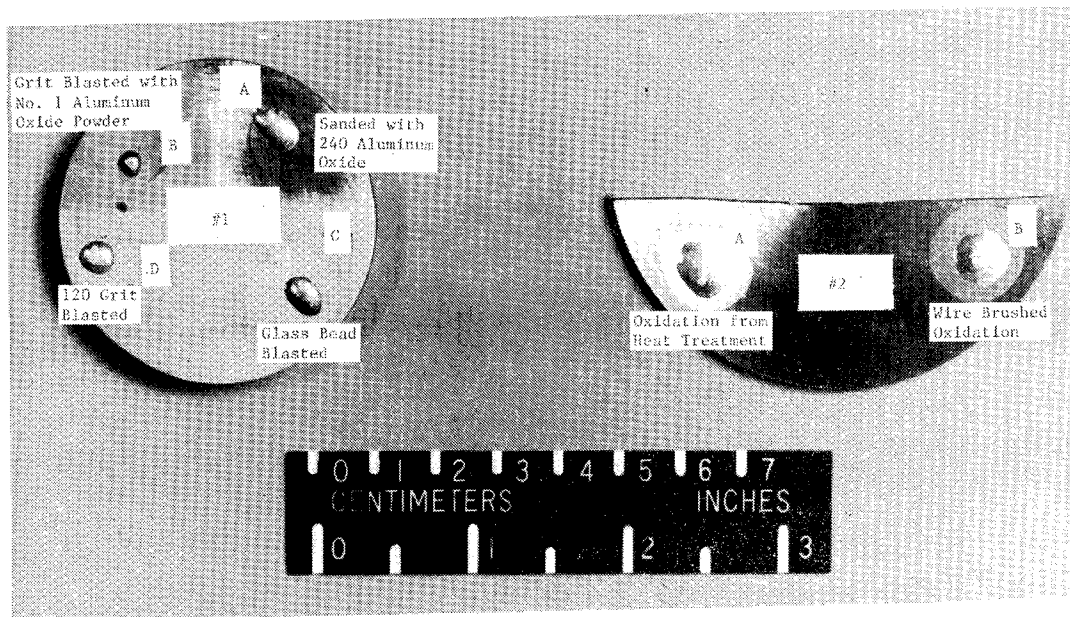
SPREAD TEST SPECIMENS

TINNING SPECIMENS

#9
120 Grit
Blasted
(a)

#10
Glass Bead
Blasted
(b)

#11
Sanded with
120 Aluminum
Oxide
(c)

Tinning specimen surfaces were prepared as shown in the picture above. These specimens were heated the same way as for spread testing. Once the specimens reached soldering temperature a soldering gun was used to tin the surface. Specimens #9 (a) and #10 (b) had areas of dewetting whereas #11 (c) tinned excellently with total wetting. A machined surface was not tinned because from past experience machined surfaces in excellently. Grit and bead blasting, which do not promote capillary action, are not recommended methods of surface preparation for soldering.

TUBE/GROOVE SPECIMEN

With Tubes
(a)

Soldered
(b)

Dye Penetrant Check
(c)

Rod
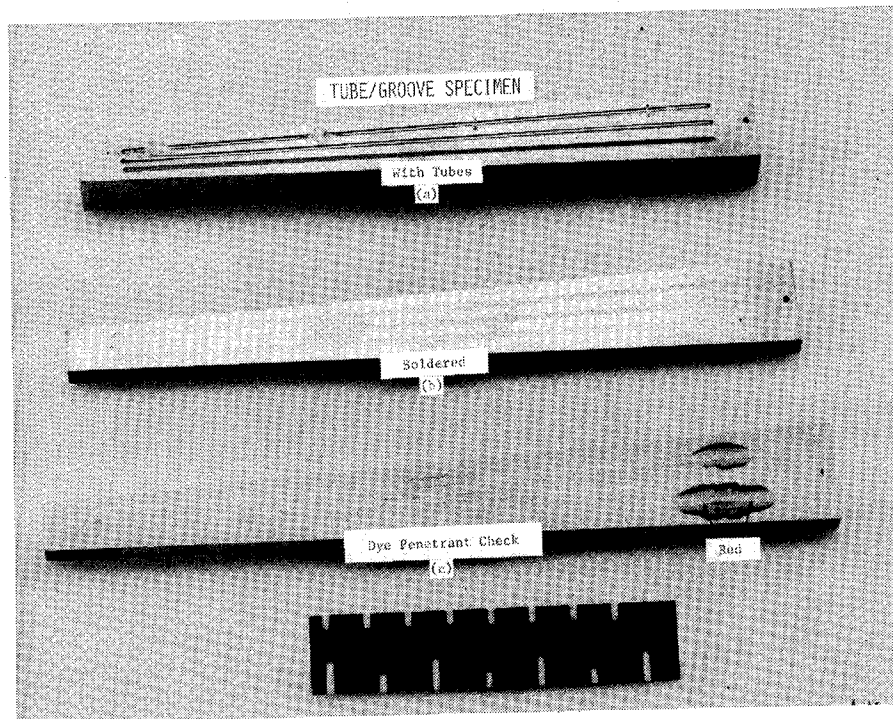
Now that a method of removing heat treatment oxides has been found, tube/groove specimens have been fabricated. The purpose of these specimens was to develop a method for soldering tubes in surface grooves. The specimens were then subjected to cryogenic temperatures.

Grooves were sanded with 120 aluminum oxide and cleaned of all contaminants. Tubes were straightened as much as possible, tinned, and placed in the groove. To insure that the tubes remain below the surface during soldering the following two methods were used: staked in place or tacked in place with solder (a). Staking the tubes in place was done before heating. Tacking in place was done at approximately 100°F below the solder's liquidus temperature. A soldering gun was used to heat the tack area to the solder's flow temperature. A small amount of flux was applied to the tube/groove prior to heating. At the high points of the tube, it was pushed to the bottom of the groove and tacked in place. Starting at one end of the groove the tube was soldered in place using a soldering gun. Solder flowed into the groove and around the tube to fill the groove so that excess solder built up above the specimen surface. When soldering was completed and the specimen cooled down, it was cleaned in soapy hot water to remove flux residue. Excess solder was machined to within .002" to .003" of the surface, then hand finished (b). Since solder is softer than the base metal there was a tendency to undercut the solder. This is normal, and care must be taken to keep undercutting to a minimum.

The finished surface was dye penetrant checked for metallurgical bonding between solder and specimen (c). Dark, wet looking areas are where flux is weeping from a debond area. Red areas also indicate debonding. Debonding may be the result of: edge contamination, specimen not being hot enough, or poor technique. After the specimens were cryo cycled they were dye penetrant checked again for any growth of debond areas. This would indicate whether flux left in the joint between solder and specimen or brittleness of the solder affected the metallurgical bond.

SURFACE ANALYSIS

		CUTOFF	.030	PROFILE ROUGHNESS AVERAGE	[X]	PROFILE ROUGHNESS AVERAGE	[X]	DATE	
100	MICRO INCHES	SKID						PART	
10,000		SKIDLESS	[X]						
100									

SIDE "A" to "B"
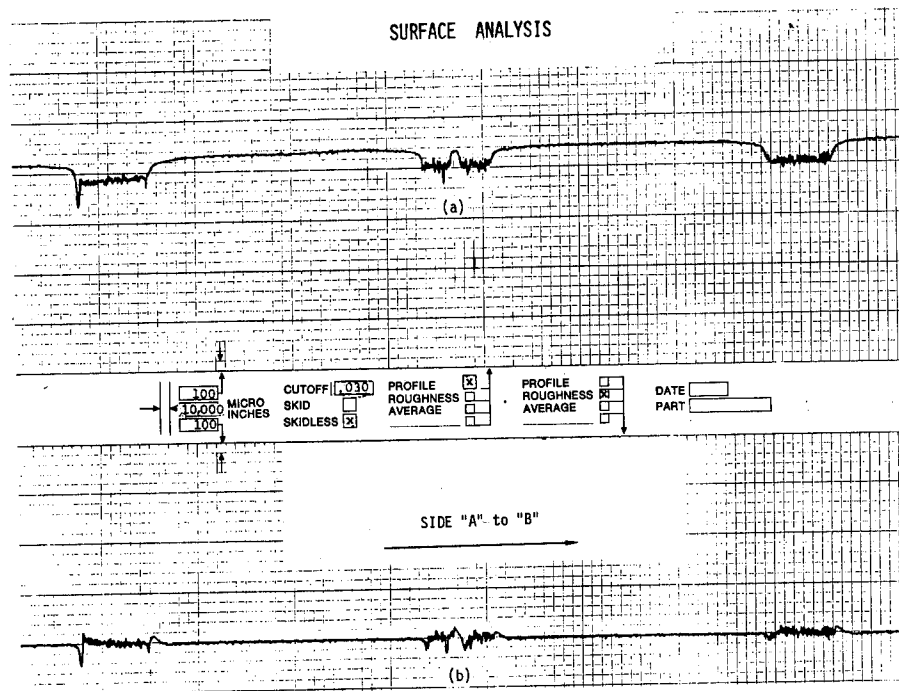
A surface analysis of the previous tube/groove specimen was done before and after cryo cycling. One cross section of the analysis is shown above. Solder at each groove has been undercut during finishing. The center groove of (a) has a raised spot in the middle because the tube was not on the groove bottom when soldered.

The surface roughness of the solder and specimen is shown above in (b). Because of the solder's softness it was rougher than the base metal surface. A surface typical of the one shown above would be usable on a conventional wind tunnel model. However, on cryogenic wind tunnel models this surface is not acceptable. Air flow over the grooves would not be smooth, resulting in lower Reynolds numbers. One way to correct this problem would be to paint the surface with a cryogenic compatible coating and finish to a uniform finish.

WING SPECIMEN
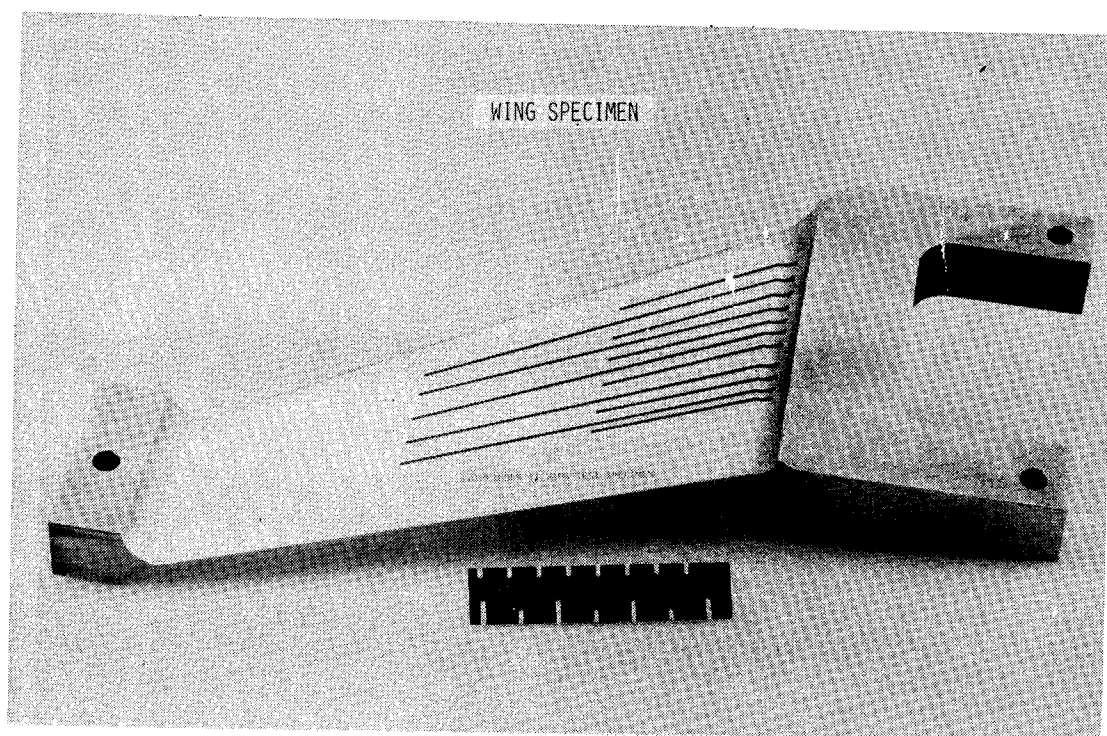
Flex tests on the Vasco Max 200 wing shown above were done to test the solder's ability to withstand aerodynamic loading in cyrogenic environments. Grooves are located on both upper and lower surfaces. Tubes tinned with 95% Sn - 5% Sb were placed in the first four grooves on the upper surface. The wing was placed on a hot plate that had been preheated to approximately 100°F below the liquidus temperature of 95% Sn - 5% Sb. The tubes/grooves were soldered and finished by the same method used for the tube/groove specimens. After the upper surface was hand finished, the first four grooves of the lower surface were tubed, soldered and hand finished. This process was repeated for the next four grooves on upper and lower surfaces using 50% Sn - 49.5% Pb - 0.5% Sb solder. The wing was cleaned in soapy, hot water and dried. A filler material was used to bond tubing and fill the groove in the last 3 grooves on upper and lower surfaces.

A surface analysis and dye penetrant check were done on both surfaces before and after testing. The 50% Sn - 49.5% Pb - 0.5% 5b solder wet and flowed better than the 95% Sn - 5% Sb solder. Test results showed 95% Sn - 5% Sb to be too brittle, whereas 50% Sn - 49.5% Pb - 0.5% Sb remained ductile. Results concerning the filler material are given in reference 1.

49

PHYSICAL TESTING OF SOLDER

o   LAP SHEAR SPECIMENS

   o   ROOM TEMPERATURE

   o   -275° F

o   TENSILE SPECIMENS

   o   ROOM TEMPERATURE

   o   -275° F

Vasco Max specimens were tested using single lap and butt joints to determine lap shear and tensile strengths. Lap shear specimens were 1" wide and with a 1" overlap at the joint and gapped to .003". Tensile specimens were 1" in diameter and gapped to .003". After soldering, the specimens were cryo cycled from room temperature to -275°F five times. Half the specimens were pulled at room temperature while the others were pulled at -275°F. Testing was done at a cross-head rate of 0.05 in/min. Lap shear specimens were tested on Vasco Max 200 using 95% Sn - 5% Sb and 50% Sn - 49%.5% Pb - 0.5% Sb solders. At the present time testing on the tensile specimens is not complete.

LAP SHEAR SPECIMENS

(a)   (b)   (c)   (d)   (e)   (f)

Pulled at Room Temperature   VASCO MAX 200   Pulled at -275°F

50% Sn, 49.5% Pb, 0.5% Sb Solder
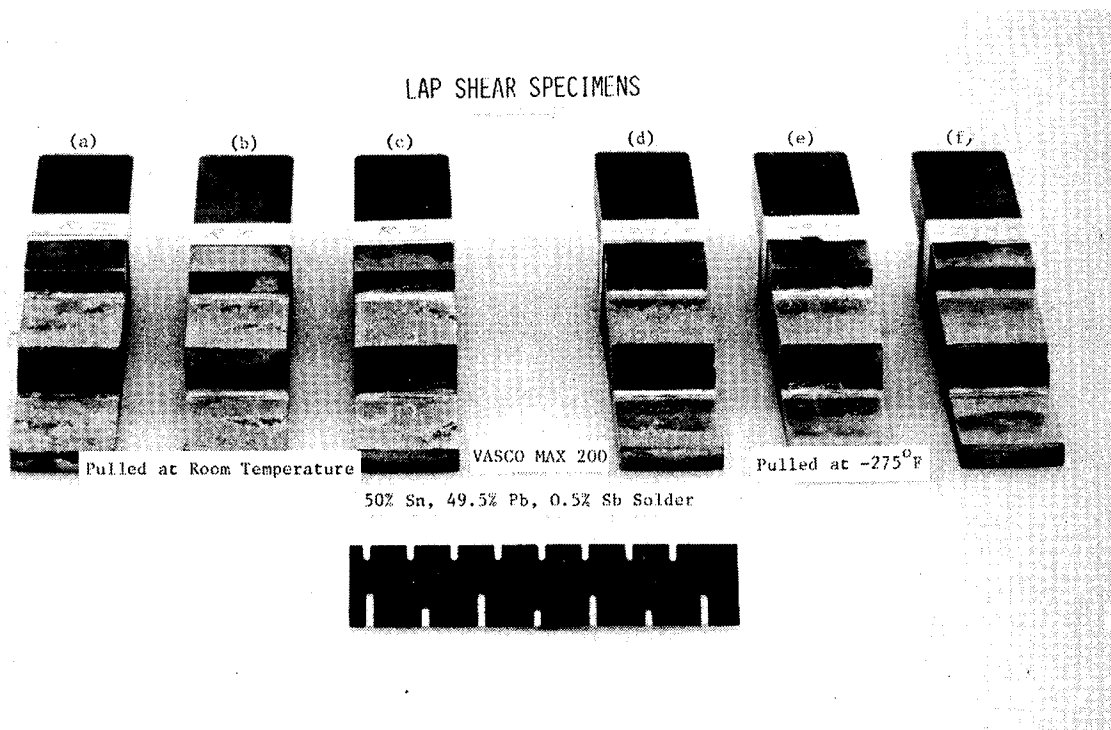
Specimens for the lap shear test are shown above. A fixture was made to hold the specimens during soldering so that the gap would be .003". Prior to soldering each mating surface was tinned and cleaned. The fluoride flux was brushed on the tinned surfaces. The specimen was then clamped in the fixture. The fixtured specimen was turned upside down so that the specimen's top rested on the hot plate. The hot plate had been preheated to approximately 100°F above the solder's liquidus temperature. After the specimen reached temperature, solder was applied to the joint. The fixtured specimen was then removed from the hot plate and air cooled to room temperature. Flux residue was washed off in hot, running water.

Specimens (a), (b), and (c) failed in the solder. Solder pulled away from the specimen surface in (d) and (e), while in specimen (f) 1/3 of the joint failed in the solder and the rest pulled away from the surface. Lap shear strengths of the specimens are listed below:

Specimen (a) - 4395 psi   Specimen (d) - 3030 psi
Specimen (b) - 4200 psi   Specimen (e) - 240 psi
Specimen (c) - 4400 psi   Specimen (f) - 4850 psi

The strengths were not as high as expected. More specimens will be fabricated and tested later. Flux inclusions were seen on all lap shear specimens. From all observations some amount of flux inclusion is normal.

51

ELEVONS FOR 1% SHUTTLE NTF MODEL
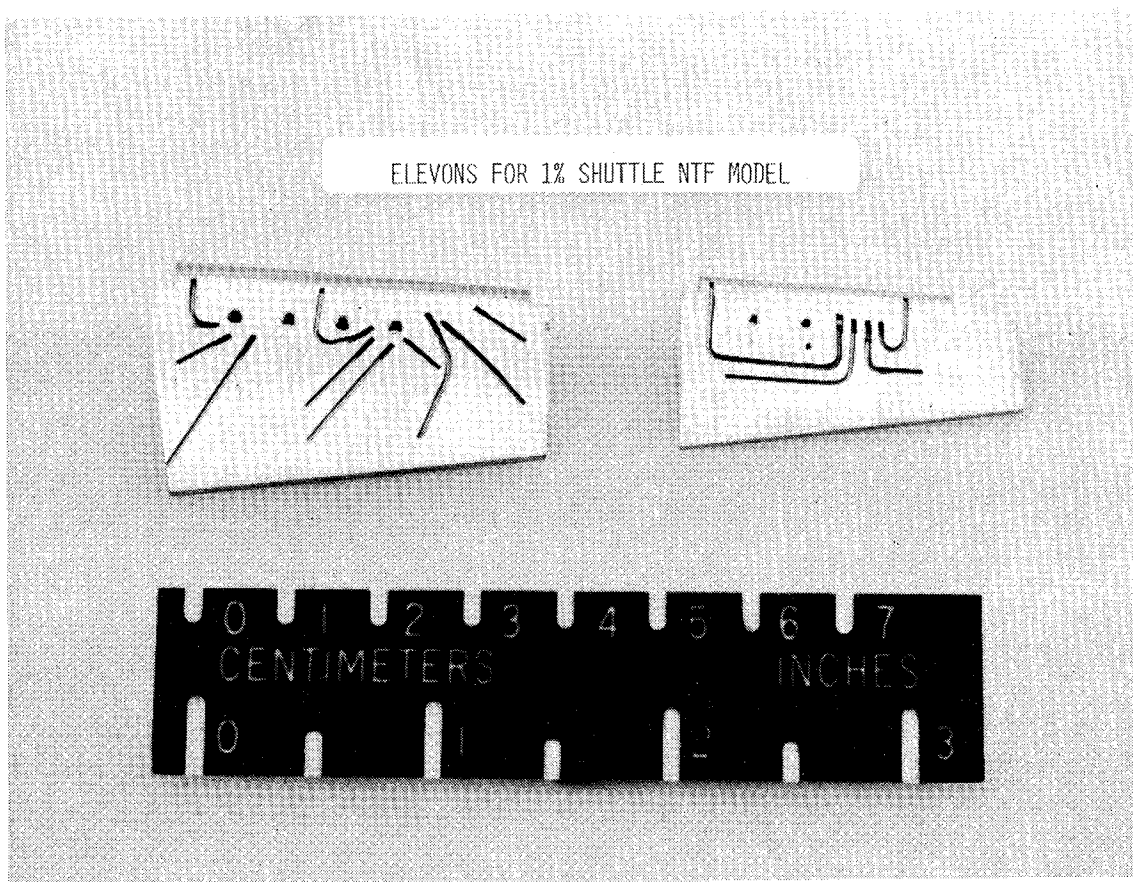
An application for soldering pressure tubes in surface grooves is found in the elevons for the 1% Shuttle Accent NTF Model. Grooves were machined on both sides to accept 0.020" O.D. Stainless-Steel tubing. Sharp edges were chamfered slightly to prevent the solder's tendency to pull away from sharp edges. After soldering is complete and the elevons surface have been finished a 0.010" diameter hole will be drilled into the tube normal to the surface. This will allow pressure readings to be gathered from the elevon's surface during tunnel test model.

Concluding Remarks

1. Testing is almost complete on Vasco Max 200.

2. A method and materials for soldering pressure tubes on both upper and lower surfaces of a Vasco Max 200 wing specimen have been determined.

3. The flux containing fluoride promotes better wetting and flow of 50% Sn - 49.5% Pb - 0.5% Sb solder on Vasco Max 200 and 347 stainless steel.

4. The ductility of 50% Sn - 49.5% Pb - 0.5% Sb solder appears to be very good at cryogenic temperatures.

5. Oxidation from heat treating Vasco Max 200 has to be removed before soldering or eliminated in the heat treatment.

6. Mechanically abrading with a course aluminum oxide paper or remachining the surface are the recommended methods of surface preparation prior to soldering or tinning.

7. Surfaces prepared by grit or glass bead blasting do not tin well and inhibit capillary action.

8. The 95% Sn - 5% Sb solder is too brittle at cryogenic temperatures to withstand aerodynamic loads.

9. Soldered surfaces when finished are rougher than the base metal; therefore, model surfaces that have had pressure tubes soldered in place will need cryogenic resistant coating to maintain a smooth, aerodynamic surface.

10. The reason for lower than expected lap shear strengths for both 50% Sn - 49.5% Pb - 0.5% Sb and 95% Sn - 5% Sb solders is not known so additional tests will be conducted.

11. Tensile specimens have been completed at this time using 50% Sn - 49.5% Pb -0.5% Sb and 95% Sn - 5% Sb solders.

Acknowledgement

Bibliography

Manko, Howard H., "Inspection and Quality of Solder Joints", Solders and Soldering. 1964, pp. 267 - 269.

American Welding Society, Inc., Soldering Manual, 2nd edition, revised, 1978.

References

1. Firth, George C. and Watkins, Vernon E., Jr.: "An Interim Report on Investigation of Low-Temperature Solders for Cryogenic Wind Tunnel Models," Welding, Bonding, and Fastening 1984, NASA CP-2387, September 1985.

2. Manko, Howard H.: "Solders and Soldering Materials, Design, Production, and Analysis for Reliable Bonding," McGraw-Hill Book Company, New York, 1964.

MECHANICAL FASTENERS FOR ADVANCED COMPOSITE MATERIALS

Richard C. Landt
SPS Technologies, Inc.
Jenkintown, PA   19046

ABSTRACT

Advanced composite materials, which are increasingly being used to build air-craft, have different properties than the metals they replace. Fasteners intended for composite-material joints must be designed and selected to allow for these differences. For example, blind fasteners (one-sided access) used to assemble composite-to-composite joints have been redesigned. to expand to larger diameters to resist pull-through and cocking failures.

This paper reviews the fastener designs needed for composite materials. Topics discussed are galvanic corrosion, pull-through resistance, fastener rotation, installation damage, fastener galling and conductivity. A blind fastener recently developed by SPS Technologies is described to show how these require-ments are incorporated.

Introduction

Commercial and military aircraft are now being built using advanced composites such as graphite-epoxy materials. Although these materials often reduce the number of structural components and offer alternative joining methods, mechanical fasteners play a vital role in aircraft assembly. In the commercial sector, composite materials are used in secondary structures; the NASA Aircraft Energy Efficiceny (ACEE) Program illustrates some typical applications (Figure 1). These ACEE structures were fabricated from separate graphite-epoxy spars, ribs and skins that were assembled with mechanical fasteners.

Composite materials differ from the metals they replace because they are not as ductile and their properties are directional. Fasteners develop clamping forces and resist joint loads which act in the through-the-thickness direction in a joint; this is also the weakest direction in a composite laminate. Experience with composite joints has identified some potential problems related to fastener design and selection.

ACEE Structures	Fasteners ?
DC10 Aft. Rudder	NO
DC10 Vert. Stabilizer	YES
737 Hor. Stabilizer	YES
737 Elevator	YES
L1011 Vert. Stabilizer	YES
L1011 Aileron	YES

Figure 1. NASA ACEE program structures.

Galvanic Compatibility

When metal fasteners are coupled with graphite-fiber composites in a corrosive environment, graphite's low electrical potential causes the fastener to act as an anode and corrode. The rate at which corrosion proceeds is measured by the current density. Figures 2 and 3 rank the electrical potentials and current densities for various metals coupled with graphite. Current density is the better indicator of compatibility; 6Al-4V titanium alloy, for example, forms a
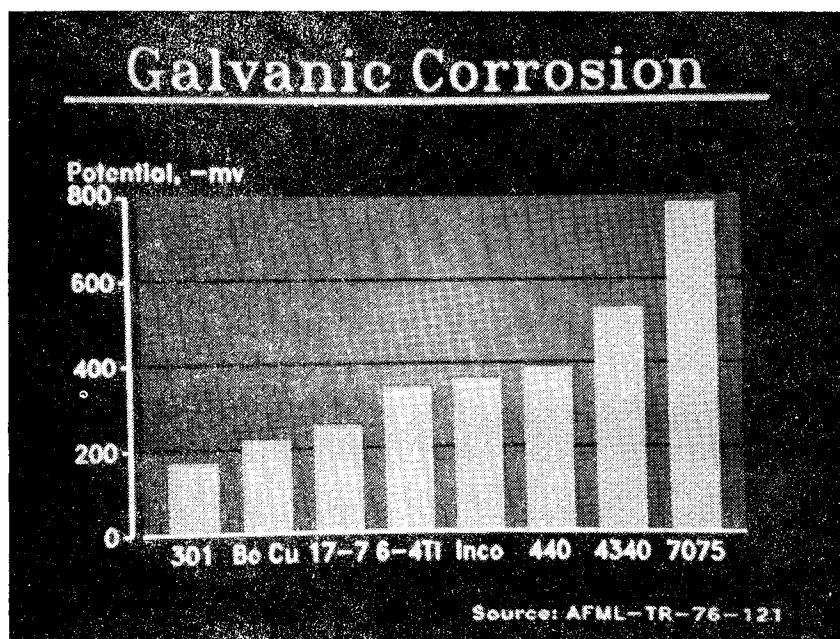
Figure 2. Potential of metals coupled with graphite (ref. 1).
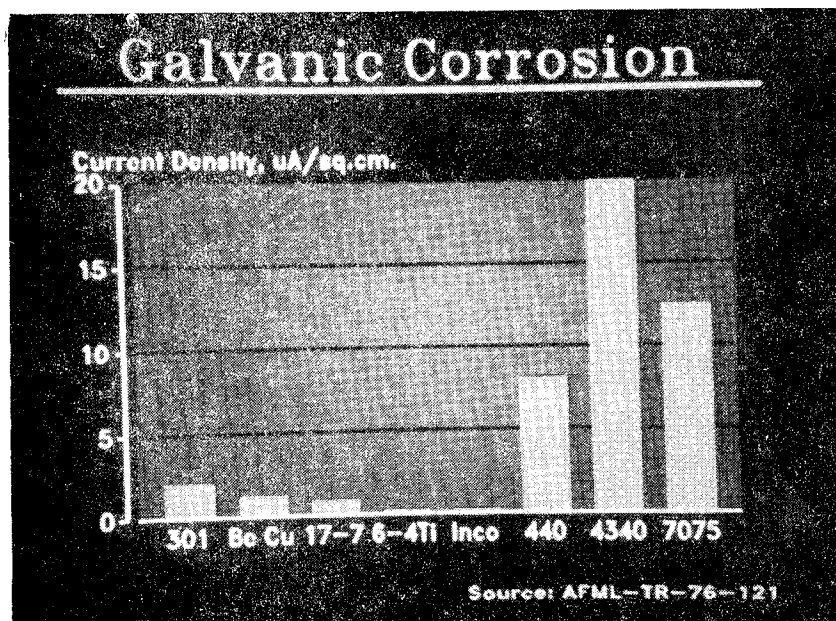
Figure 3. Current density of metals coupled with graphite (ref. 1).

tightly adhering protective oxide film which resists further corrosion. Titanium and its alloys, MULTIPHASE® alloys MP159® and MP35N®; and Inconel alloys 600 and 718 are compatible with graphite-fiber composites. These materials show no evidence of corrosion after 500 hours of 5% salt-spray testing. Corrrosion-resistant steels A-286, Ph13-8Mo, Ph17-7, 301, 304 and 316 are accepted for use with graphite-fiber composites. Occasionally these stain in salt-spray tests, therefore fasteners of these material are usually installed with sealant. Monel 400 and 405 materials will pit and rapidly corrode and are not recommended for graphite composites. Corrosion-resistant steel 440, alloy steels and aluminum alloys are not compatible with graphite. Even when fastener materials are compatible, sealants are generally applied to deny access by the corrosive environment.

Pull-Through Failures

Figure 4 illustrates the pull-through failure mode. The joint fails when through-plane shear forces pull the fastener through the laminate. The failure load is influenced by bending moments, in-plane stresses and dynamic effects that act in combination with the through-plane shear stress to lower the failure load.

Structures joined with shear, flush-head fasteners and blind fasteners are particularly susceptible to this type of failure. Pull-through strength can be improved by using fasteners with larger bearing circumferences because they develop higher through-plane shear loads. Current design practice is to use tension- rather than shear-head fasteners if pull-through strength is critical. Blind fastener applications have required washers under the blind head to provide desired strengths.
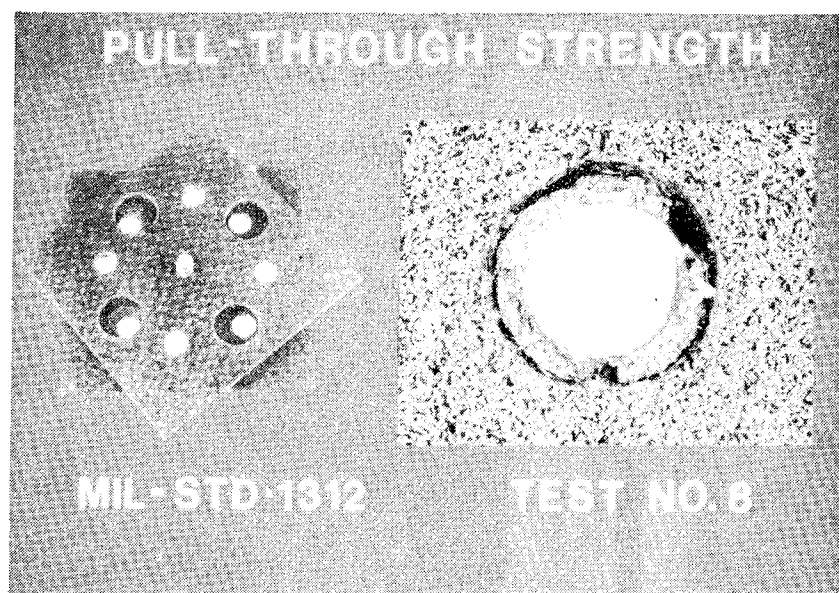
Figure 4. Pull-through failure in joint tensile strength test.

Fastener Rotation

Fastener rotation refers to a fastener cocking in the joint, not the turning action that occurs when a fastener is torqued. Shear loaded joints develop non-uniform bearing contact between the fastener shank and hole. At these highly stressed contact points, the composite structure fails and the fastener rotates into the laminate. Figure 5 illustrates a failed single-lap shear joint. Eventually, the fastener embeds or pulls through the laminate.

Fasteners with large bearing diameters resist cocking forces and retard rotation. Figure 6 summarizes joint tensile strength data for experimental 3/16" diameter, 130^0 flush-head, titanium bolts with stainless-steel nuts. By increasing the nut flange diameter from .250" to .600" (1.3 to 3.2 shank diameters), the ultimate joint strength improved 36%. However, as Figure 7 shows, increasing flange diameter limitlessly will add weight and not improve joint strength. Based on weight efficiency (ultimate load/fastener weight) a flange diameter of 2X shank diameter optimizes this joint's strength.
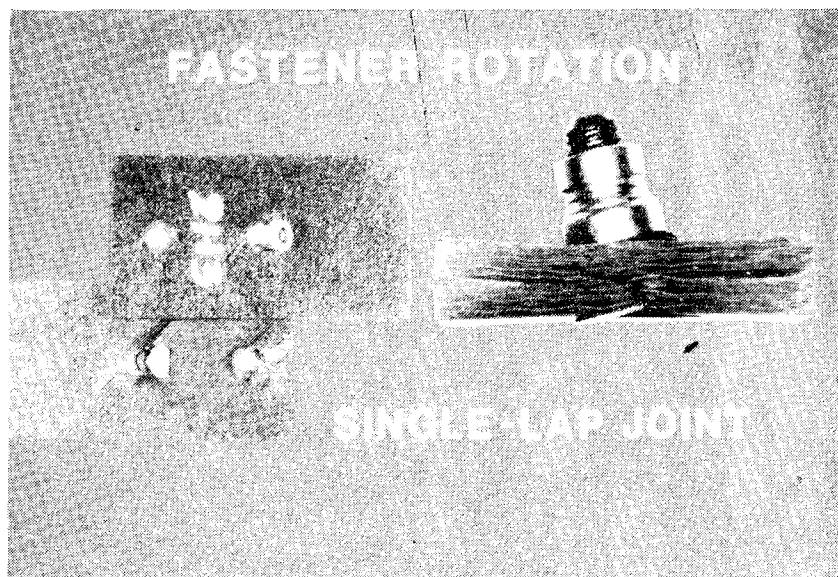
Figure 5.   Single-lap joint illustrating fastener rotation failure.

Threaded Fastener Galling

Titanium bolts are widely used with graphite-fiber composites because they are galvanically compatible and lightweight. Airframe manufacturers have reported that galling (seizing) may occur when using titanium or stainless-steel prevailing-torque nuts with these bolts. This effectively destroys the bolt and nut.

To prevent galling, A-286 and 300-series stainless nuts must be coated with a dry-film lubricant and in some cases, first plated with cadmium or coated with aluminum. These finishes are not compatible and would be consumed in service but lubricate the nut or bolt for the initial assembly operation.

An alternative to the threaded fastener is a nonthreaded lockbolt with a swaged collar.

Installation Damage

Some fasteners developed for use in metallic structures will damage composite structures. Damage occurs when the clamping stress exceeds the compressive strength of the laminate; radial expansion in the fastener hole delaminates or buckles plies, impact forces delaminate the structure, or turning fasteners abrade or splinter the composite surface.

Current design practice is to avoid interference fits without using a protective sleeve, fasteners with inadequate bearing area, or rivets and blind fasteners that expand radially, and using rivet guns to install fasteners.

Conductivity

An electrically conductive path between the fastener and the structure is needed to protect graphite-epoxy structures during lightning strikes. Damage can occur at the attachment, exit and transition points (joints), with arcing a danger near fuel cells.

Measures to prevent galvanic corrosion often isolate the fastener with nonconductive sealants, coatings and lubricants. Improved fastener-to-hole contact and conductive coatings must be developed to solve this problem.

Blind Fasteners

Blind fasteners with their special design requirements challenge the fastener designer concerned with composites. Because blind fasteners can be installed from one side of the structure, large bearing diameters are difficult to achieve. In forming the "blind head" these fasteners must not damage the composite structure. Typical applications for blind fasteners include cover-to-spar joints in closing-out stabilizers, ailerons and rudders. These applications are truly "blind" since the fastener bearing surface created inside the structure cannot be seen and inspected. Therefore a blind fastener must be reliable. More recently, airframe manufacturers are evaluating honeycomb sandwich-to-composite joints containing blind fasteners where the fastener's blind head forms inside the core material against the sandwich face sheet.

The aerospace fastener industry is offering a variety of new fasteners for composite materials. One of these is the COMP-TITE™ blind fastener. Shown in Figure 8, it is comprised of four elements: a nut, corebolt, coiled washer and sleeve. During installation (Figure 9) the coiled washer and sleeve are driven over the tapered end of the nut and expanded to their final diameters. The formed washer is then seated against the joint surface as the corebolt advances.
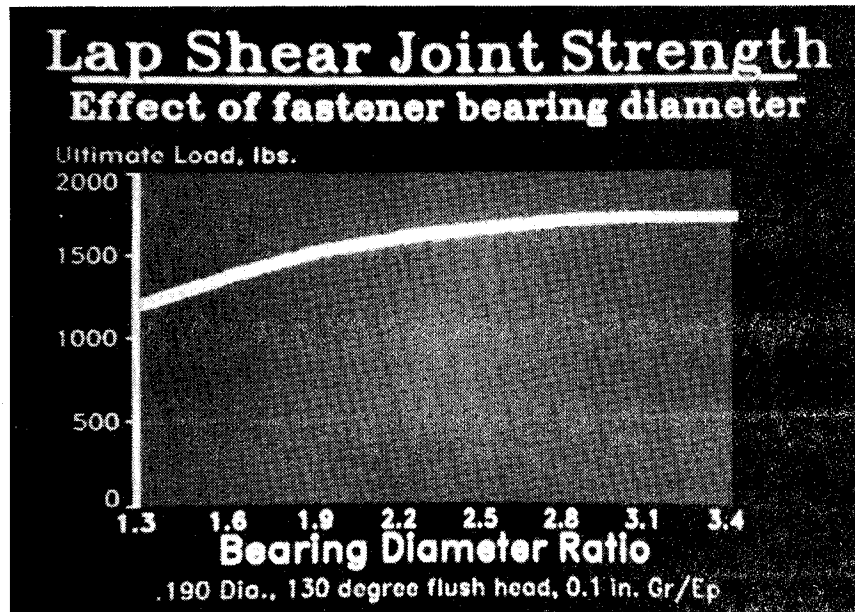
60

Figure 6. Effect of nut bearing diameter on joint strength.
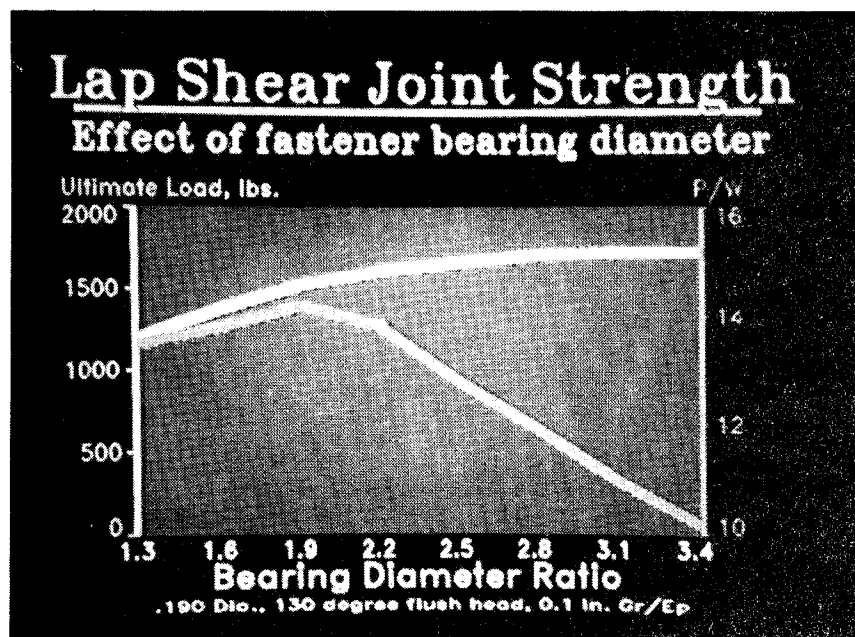

Figure 7. Effect of nut bearing diameter on joint strength versus joint efficiency.

61

The corebolt drive stem shears at a torque-limiting groove after the joint is clamped. This design approach achieves a large blind-side bearing diameter while minimizing the possibility of joint damage due to excessive bearing stress. A separate washer element also protects the composite surface should the sleeve turn during installation.

Other design advantages are a flat washer bearing surface, consistent blind-head diameters, no fastener hole expansion, and improved installation tolerance of hole condition.

The 6Al-4V titanium nut, MULTIPHASE® alloy MP159® corebolt, 304 S/S sleeve and 316 S/S washer satisfy galvanic compatibility requirements.
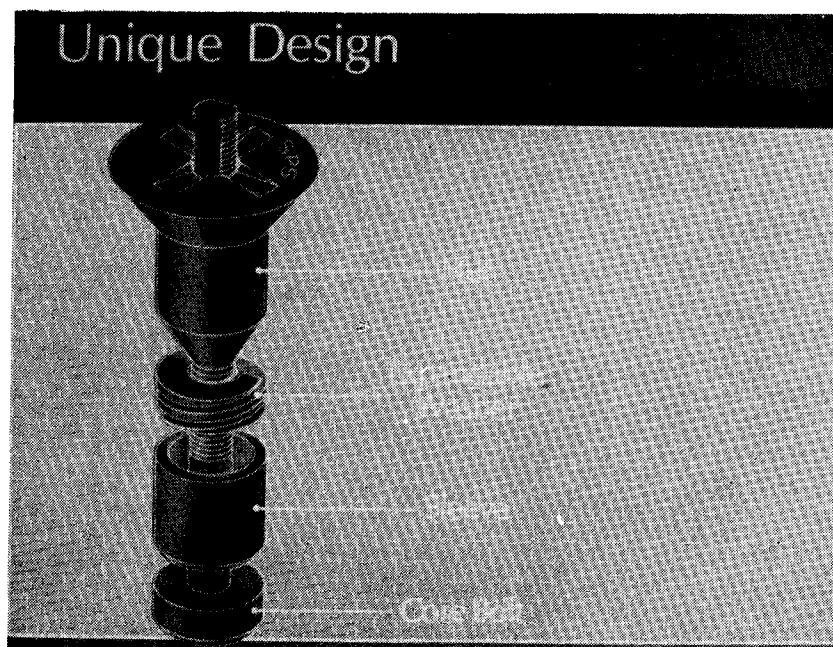
Figure 8. COMP-TITE™ blind fastener.
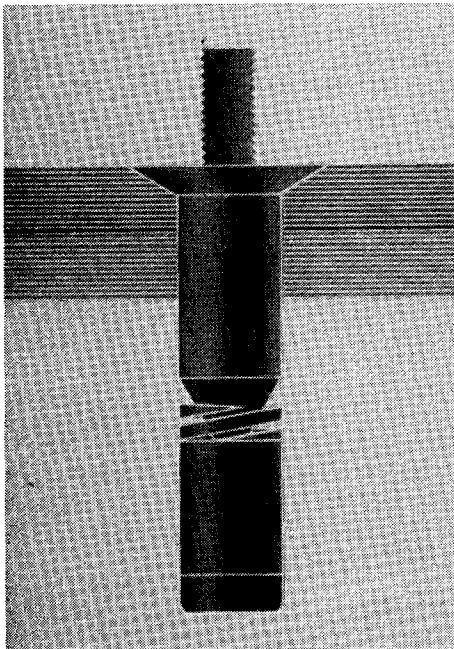
a.
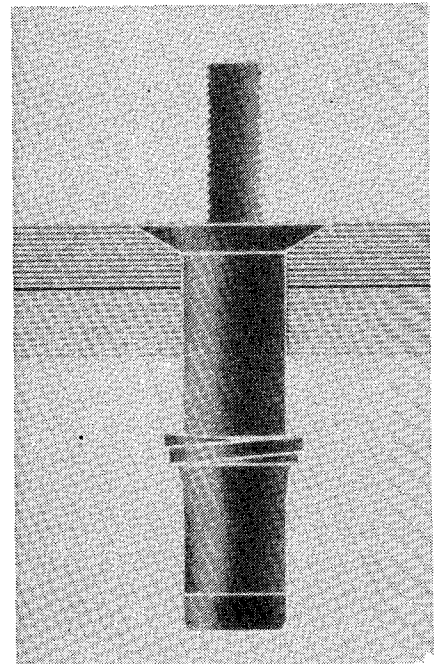
b.
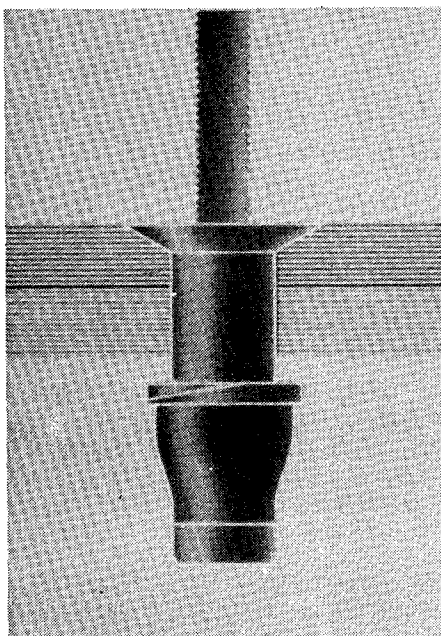
c.
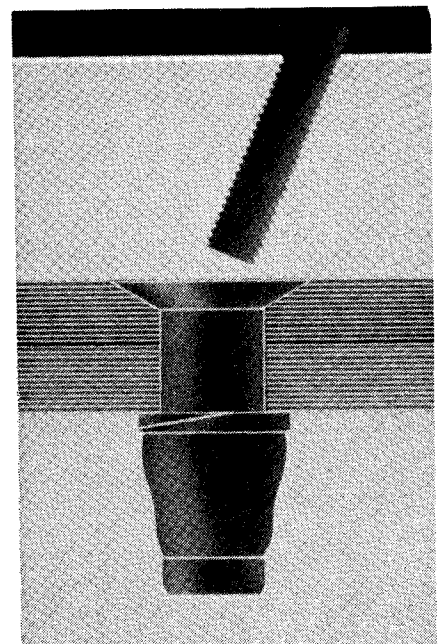
d.

Figure 9. COMP-TITE™ blind fastener installation.

63

Concluding Remarks

Fastener selection for bolted composite joints should involve a review of the considerations addressed in this paper. The fastener industry is providing new fastener designs which can improve joint strength and reduce corrosion problems. One of these is the COMP-TITE™ blind fastener which was designed for improved pull-through strength and cocking resistance.

Reference

1. B. A. Miller and S. G. Lee: "The Effect of Graphite-Epoxy Composites on the Galvanic Corrosion of Aerospace Alloys", Six Force Materials Laboratory (AFML); Wright Patterson Air Force Base, Ohio, TR-76-121, September 1976.

65

THE ALTERNATING SURFACE SEGMENTED LAP JOINT:

A DESIGN FOR THIN HIGHLY LOADED JOINTS

Vernon E. Watkins, Jr. and George C. Firth
NASA Langley Research Center
Hampton, Virginia 23665

ABSTRACT

The combination of thin airfoil sections and high aerodynamic loads on many wind tunnel models presents a major problem for attachment of flap elements. Conventional methods of attaching fixed control elements such as lap and tongue-in-groove joints are not rigid enough to provide surface continuity required in high Reynolds number research. For the extreme cases, the solution has been to fabricate separate wings for each flap setting with the flap element being an integral part of the wing.

This paper presents an attractive solution to this problem, the "Alternating Surface Segmented Lap Joint." This joint provides increased rigidity and lower stress levels than conventional joints. Additionally, attachment fastener loading is low and the joint can be designed to accommodate high shear levels due to bending without the use of dowel pins.

INTRODUCTION

One of the most formidable tasks facing a designer of high-performance aircraft wind tunnel models is the attachment of flap elements to thin wings. The simplest approach is to utilize a lap joint. This joint is easy to fabricate and assemble, and requires little design input. Unfortunately, the lap joint is often structurally inadequate. The reductions in section modulus of the joined elements lead to high stress levels and distortions. Additionally, the loading may dictate use of a fastener size which cannot be accommodated with the thickness available.

A second choice of designers is the tongue-in-groove joint. This joint requires precision fabrication but provides increased stiffness. Fasteners are not as heavily loaded, but the thickness available for the fastener head is reduced significantly.

A joint concept has been developed for attachment of the trailing-edge flap to the thin, highly loaded wing of the Pathfinder II model to be tested in the National Transonic Facility. This concept promises to be a viable design for situations where a conventional configuration is inadequate.

NTF CHARACTERISTICS IMPACT MODEL DESIGN

O HIGH REYNOLDS NUMBER RESEARCH

    o HIGH-QUALITY SURFACES

    o MINIMUM SURFACE DISCONTINUITIES

O HIGH DYNAMIC PRESSURES-HIGH MODEL LOADS

    o HIGH DISTORTIONS

    o JOINT DISCONTINUITIES

    o HIGH BENDING STRESSES

    o HIGH SHEAR LOADS

     The National Transonic Facility (NTF) at Langley Research Center, because of its unique capabilities, imposes greater structural demands upon wind tunnel models than conventional wind tunnels. The NTF has the capability to operate at higher Reynolds numbers than any other research facility in the free world. To the model designer and fabricator, the significant consequence of this capability is the requirement to provide higher quality aerodynamic surfaces than would be required for the conventional wind tunnel model. This requirement is fulfilled by better surface finish, greater contour fidelity, and minimized distortion due to aerodynamic loading.

    The capability to operate at high dynamic pressures (required for achievement of high Reynolds numbers) works against the quest to minimize surface distortion. The area most directly impacted by the requirement of minimized distortion combined with high aerodynamic loading is the attachment of flaps to thin wings.

CONVENTIONAL JOINT DISTORTION TENDENCIES

TONGUE IN GROOVE

LAP
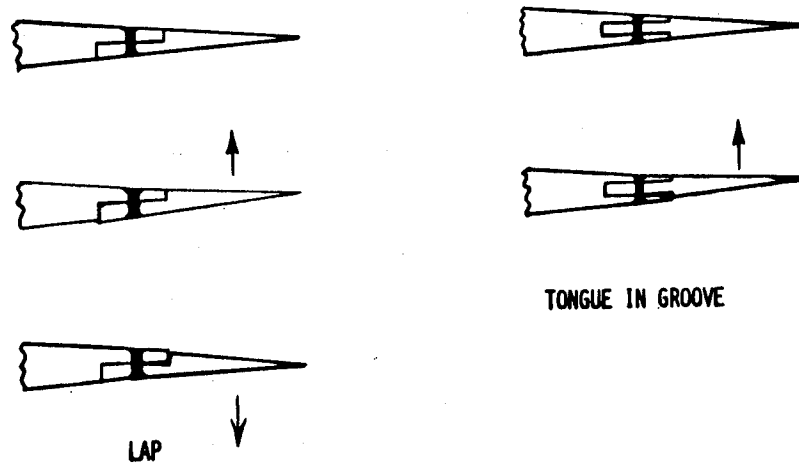
Examining the distortion tendencies of the typical lap joint as applied to a model wing's trailing-edge flap attachment reveals the potential for surface steps at the wing-flap interface. With a positive load on the flap, the upper joint element tends to deform as a cantilever beam forming a concave upper surface. The lower element aft of the fasteners deforms to match the curvature of the upper element. Forward of the fasteners, however, the lower element tends to maintain its original geometry, thus departing from the mating surface and creating a forward facing step on the lower surface. With reversed loading, the aft portion of the lower element bends while the aft portion of the upper element remains straight, thus creating an aft facing step. It is also worth noting that joint separation is resisted by tensile forces in the fasteners.

The tongue-in-groove joint adds stiffness to the portion of the joint being bent and consequently has less departure from the original contour than the lap joint. The aft portion of the flap element is assisted by the aft portion of the upper wing element in resisting distortion caused by positive loading. In this instance, an aft facing step is created on the lower surface. With reversed loading the end result is an aft facing step on the upper surface. The fasteners are subjected to tensile loading to minimize separation of the female element on the side opposite the loading direction.

70

COMPARISON: NEW DESIGN VERSUS CONVENTIONAL DESIGN

LAP JOINT

TONGUE-IN-
GROOVE JOINT
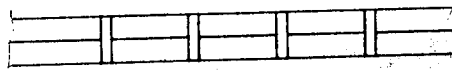
ALTERNATING SURFACE
LAP JOINT
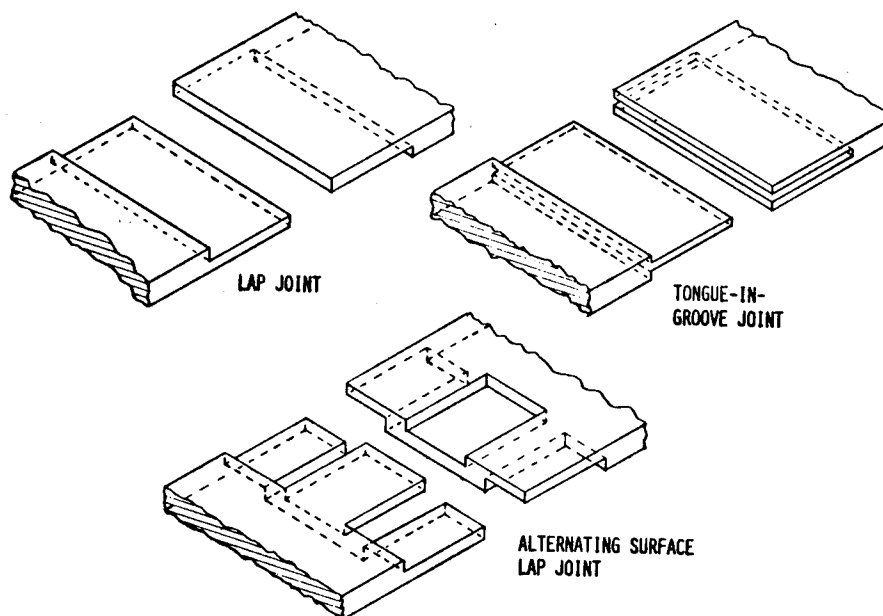
Comparing the stiffness of the two conventional joints, there is a marked decrease in the section modulus at both ends of the lap joint and at one end of the tongue-in-groove joint. Each area of marked section modulus decrease results in increased rate of distortion and an increased stress level.
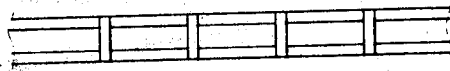
The alternating surface segmented lap joint combines features of both conventional joints. By appearance, the simplest half can be described as a series of lap joint elements which alternate from one surface to the other. The section modulus at the joint interface on this half has the element thickness as the lap joint elements and the male portion of the tongue-in-groove joint. The section modulus is greater than either of the conventional joints by virtue of the displacement of the segments about the neutral axis. The mating half has essentially the same geometry but the individual segments are joined resulting in a slightly higher section modulus. As with the tongue-in-groove joint, fasteners would be utilized to minimize separation from the mating surface of the segment on the surface opposite the loading direction.
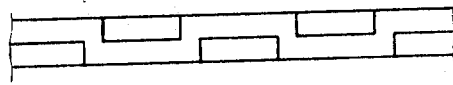
SHEAR LOADING COMPARISONS

LAP

TONGUE IN GROOVE

ALTERNATING SURFACE SEGMENTED LAP

A major consideration in flap element attachment is the shear loading due to spanwise bending. The lap joint relies on fasteners in single shear to resist the shear load. The advantage enjoyed by the tongue-in-groove joint of having the fasteners in double shear is offset by the limitations imposed by the limited bearing area. For both joints, the fastener size is restricted by the meager joint thickness and the necessity of having the head below the aerodynamic surface. The alternating surface segmented lap joint is not dependent upon fasteners to carry the shear loads. The joint segments themselves can act as shear ties provided that tolerances are controlled to maintain adequate contact between the sides of the individual segments and the mating recesses.

PATHFINDER II FLAP ATTACHMENTS

ALTERNATING SURFACE
SEGMENTED LAP JOINT
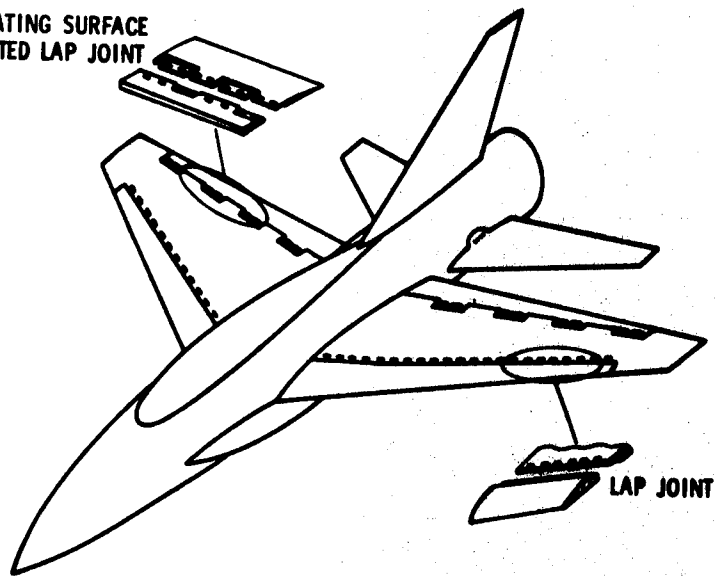
LAP JOINT

   The alternating surface segmented lap joint was developed and will be used for attachment of the trailing-edge flap to the wing of the initial configuration of the first high-performance fighter model to be designed and fabricated for testing in the National Transonic Facility. This generic model, designatd the Pathfinder II, features the capability of testing several aerodynamic configu- rations. The forebody, strakes, canopy, lower fuselage, wings, and stabilizers are all replacable, allowing incorporation of swept wings, delta wings, forward swept wings, and modified area distributions.

73

The Pathfinder II wing is thin (4% t/c) and twisted. The thickness distribution was such that a conventional lap joint was suitable for the leading-edge attachment, although the wing twist dictated that the mating surfaces had to consist of three inclined planes. The severity of the problem due to thickness of the trailing-edge flap attachment is illustrated in the drawing above. The airfoil thickness in the region for this joint ranges from a quarter of an inch at the root to less than a tenth of an inch at the tip.

A proof-of-concept specimen which will duplicate the wing geometry and trailing-edge flap attachment is being fabricated at this time. This test article will be subjected to thermal cycling between room and cryogenic temperatures, static loading, and dynamic loading at cryogenic temperatures to validate the design before final processing of the wing tunnel model component.

CONCLUSIONS

THE ALTERNATING SURFACE

SEGMENTED LAP JOINT OFFERS:

O INCREASED STIFFNESS

O DECREASED STRESS LEVELS

O REDUCED FASTENER LOADS

O ELIMINATION OF SHEAR PINS

O MODERATE COST

In conclusion, a unique joint configuration has been developed which offers a more efficient method of attaching thin highly loaded members. This joint features increased stiffness and reduced stress levels when compared to conventional lap and tongue-in-groove joints. The joint also reduces the tendency of mating elements to separate under loading thus reducing the need for fasteners. The joint elements themselves provide shear ties thus eliminating the need for shear pins. The manufacturing cost should be similar to that associated with manufacture of precision tongue-in-groove joints.

BIBLIOGRAPHY

!. Young C. P., Jr.; Bradshaw J. F.; Rush, H. F.; Wallace, J. W.; and
    Watkins, V. E.: Cryogenic Wind-Tunnel-Model Technology Development
    Activities at the NASA Langley Research Center, AIAA Paper No. 84-0586,
    March 1984.

AUTOMATIC FASTENING LARGE STRUCTURES - A NEW APPROACH

Donald F. Lumley
Senior Staff Engineer
Production Engineering
Martin Marietta Aerospace
New Orleans, LA.

ABSTRACT

The External Tank (ET) for the Space Shuttle is produced by Martin Marietta Aerospace at the NASA - Michoud Assembly Facility in New Orleans, Louisiana. The assembly of the ET Intertank Structure, a 27.5 ft. diameter 22.5 ft. long externally stiffened mechanically fastened skin-stringer-frame structure, was a labor intensive manual build on a modified Saturn tooling position.

A new approach was developed based on half-section subassemblies. The heart of this manufacturing approach will be 33 ft. high vertical automatic riveting system with a 28 ft. rotary positioner coming on-line in mid 1985.

The Automatic Riveting System incorporates many of the latest automatic riveting technologies. Key features include: vertical columns with two sets of independently operating CNC drill-riveting heads; capability to drill, insert and upset any one piece fastener up to 3/8 inch diameter including slugs without displacing the workpiece; offset bucking ram with programmable rotation and deep retraction; vision system for automatic parts program re-synchronization and part edge margin control; automatic rivet selection/handling system permits stack height sensor or parts program selection from 16 feeders; riveting cycle control by servo upset force or head height; automatic tool changer; automatic hole inspection; and printout capability for hole size, upset force, and head height.

INTRODUCTION

The Space Shuttle is America's economical and effective Space Transportation System (STS) developed by the National Aeronautics and Space Administration (NASA) to conduct space missions for projected national and international space program activities. The Space Shuttle vehicle consists of three major elements: a reusable manned Orbiter, an expendable External Tank (ET) containing the Orbiter propellant, and two reusable Solid Rocket Boosters (SRBs). The External Tank, built by Martin Marietta Aerospace at the NASA Michoud Assembly Facility in New Orleans, Figure 1, is the largest element of the Space Shuttle. It serves as the backbone structure for attachment of the Orbiter and SRBs and also contains and delivers propellants for the three Orbiter main engines. The External Tank accommodates the complex stresses created by its own weight and that of the Orbiter prior to launch, then the thrust generated by the Orbiter and the SRBs during launch. The overall Shuttle has a gross lift-off weight of 4.5 million pounds. Fuel can be supplied from the External Tank to the three main engines at the rate of 45,283 gallons of liquid hydrogen (LH2) per minute and 16,800 gallons of liquid oxygen (LO2) per minute.
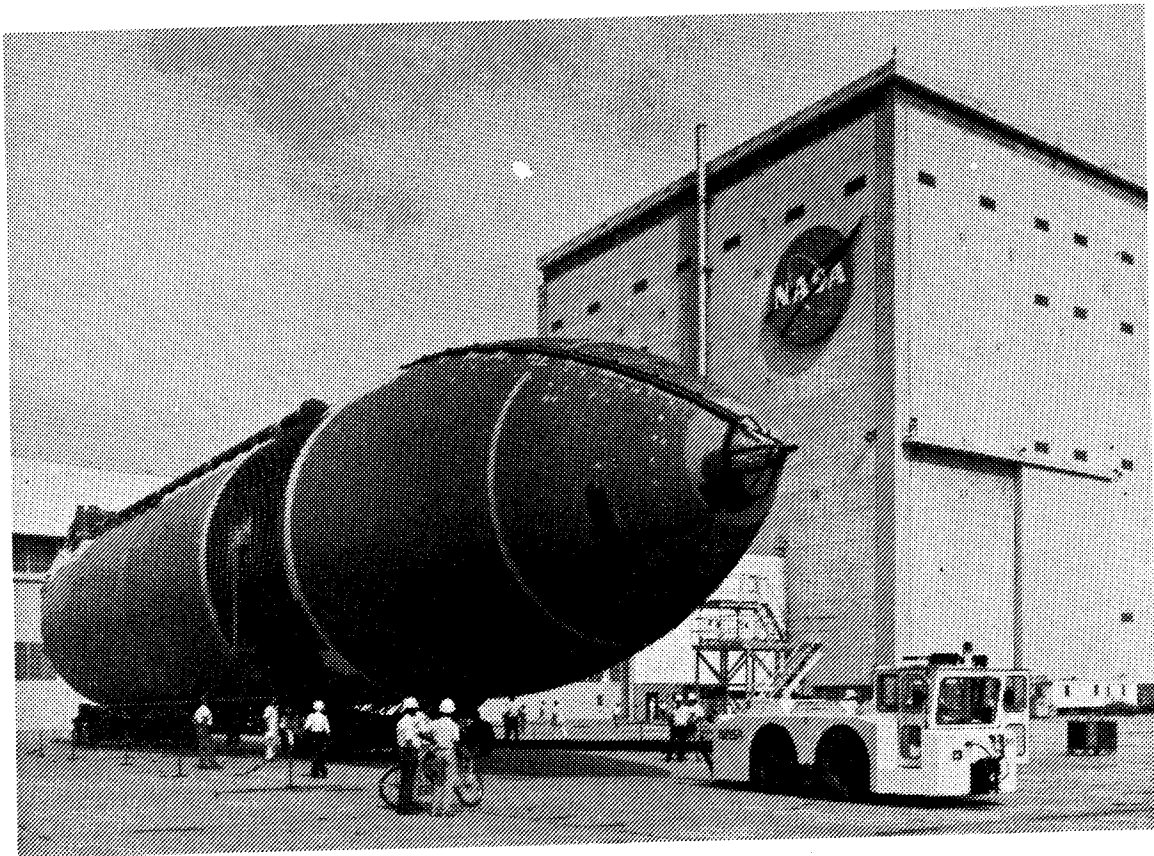
Figure 1.
Completed External Tank Being Transported From Michoud Assembly Facility.

The External Tank is 153.8 feet long
and 27.6 feet in diameter. It
weighs approximately 69,000 pounds
empty and when loaded with
propellants at launch weighs
approximately 1,660,000 pounds.
Three primary structures make up the
ET; a LO2 Tank, an Intertank, and a
LH2 Tank. Both propellant tanks are
constructed of aluminum alloy skins
with support or stability frames as
required, and their skins are butt
fusion welded to provide reliable
sealed joints. The Intertank
aluminum structure utilizes
mechanically fastened skins and
stringers with stabilizing frames.
The External Tank primary structure
is shown in Figure 2.

Figure 3.
Intertank Structure

Figure 2.
External Tank Primary Structure.

DISCUSSION

The Intertank, Figure 3, is the ET
structural connection that joins
with both the LO2 and LH2 tanks to
provide structural continuity
between these assemblies. Its
primary functions are to receive and
distribute all thrust loads from the
SRBs and transfe loads between
propellant tanks. The Intertank
also functions as a protective
compartment for housing
instrumentation, range safety
components, and other subsystems.

The Intertank cylindrical structure
consists of two integrally machined
thrust panels and six mechanically
fastened stringer stiffened panels.
It is 27.6 feet in diameter and 22.5
feet long. The two thrust panels
distribute the concentrated axial
SRB thrust loads to the LO2 and LH2
tanks and adjacent skin panels. The
thrust panels are selectively
machined with tapered skin
thicknesses and external integral
ribs. The six stringer stiffened
panels are similar to each other
except for penetrations, system

installation provisions, and an access door. Each panel is 10.8 feet wide and 22.5 feet long and includes a forward and aft chord for attachment to the LO2 and LH2 tanks.

The skin/stringer panels are each made of two aluminum skins mechanically spliced longitudinally by internal and external butt straps. Skin doublers provide necessary reinforcement for areas where the skin is penetrated and localized reinforcements to distribute thrust loads. There are 18 aluminum hat section stringers mechanically fastened to each skin/stringer panel.

The six stringer stiffened panels and two thrust panels are mechanically spliced using longitudinal butt splices to form the Intertank skin shell.

One main frame is employed to transmit the transverse SRB thrust loads and the intermediate ring frames stabilize the cylindrical shell. The main frame is constructed of machined outer and inner chords joined to webs to form an I-beam 20 inches deep. The four intermediate ring frames are constructed similar to main frame and are 12 inches deep.

The SRB beam assembly running through the middle of the Intertank is a rectangular box beam. It is 42.95 inches deep at the center, tapers to 26 inches at the ends, and is 15 inches wide. Two SRB thrust fittings, machined aluminum forgings, are attached at either end of the beam and provide for SRB attachment.

The Intertank structural assembly is performed at the NASA Michoud Assembly Facility (MAF) in New Orleans, Louisiana. Major components including thrust panels, stringer panels, frame quadrant

sections, and the SRB beam are subcontracted.

The Development and early production Intertanks were built on modified Saturn S-1C tooling remaining from the previous Saturn/Apollo program at Michoud. A new Intertank manufacturing approach was developed utilizing a half section subassembly. New tooling was designed and built and implemented in a manual mode in the fourth quarter of 1983. The heart of the half section manufacturing approach will be a new and unique Automatic Riveting System for large structures. The new riveting system is being built by GEMCOR and is currently in preliminary checkout at their facility. It will go into operation at Michoud in the third quarter 1985.

The Intertank half section, Figure 4, consists of three skin/stringer panels, 180 degree sections of the five frames, butt splices, and miscellaneous items. The components are joined using blind fasteners (under hat section stringers), 1/4 inch diameter A286 Hi-Sets, and Hi-Loc fasteners.

The first position in the half section family of tooling is the panel and frame tack fixture. In this fixture, the four 180 degree intermediate frame segments, 180 degree main frame segment, the three 45 degree skin/stringer panels are positioned and located for tack fastening. Blind fasteners located under the hat section stringers are the primary tack fasteners.

The third position is for finish, inspection, repair and bracket and subsystem support structure installation. In the current manual mode, fasteners that will be installed by the Automatic Riveting System are installed in this fixture or the tacking fixture.
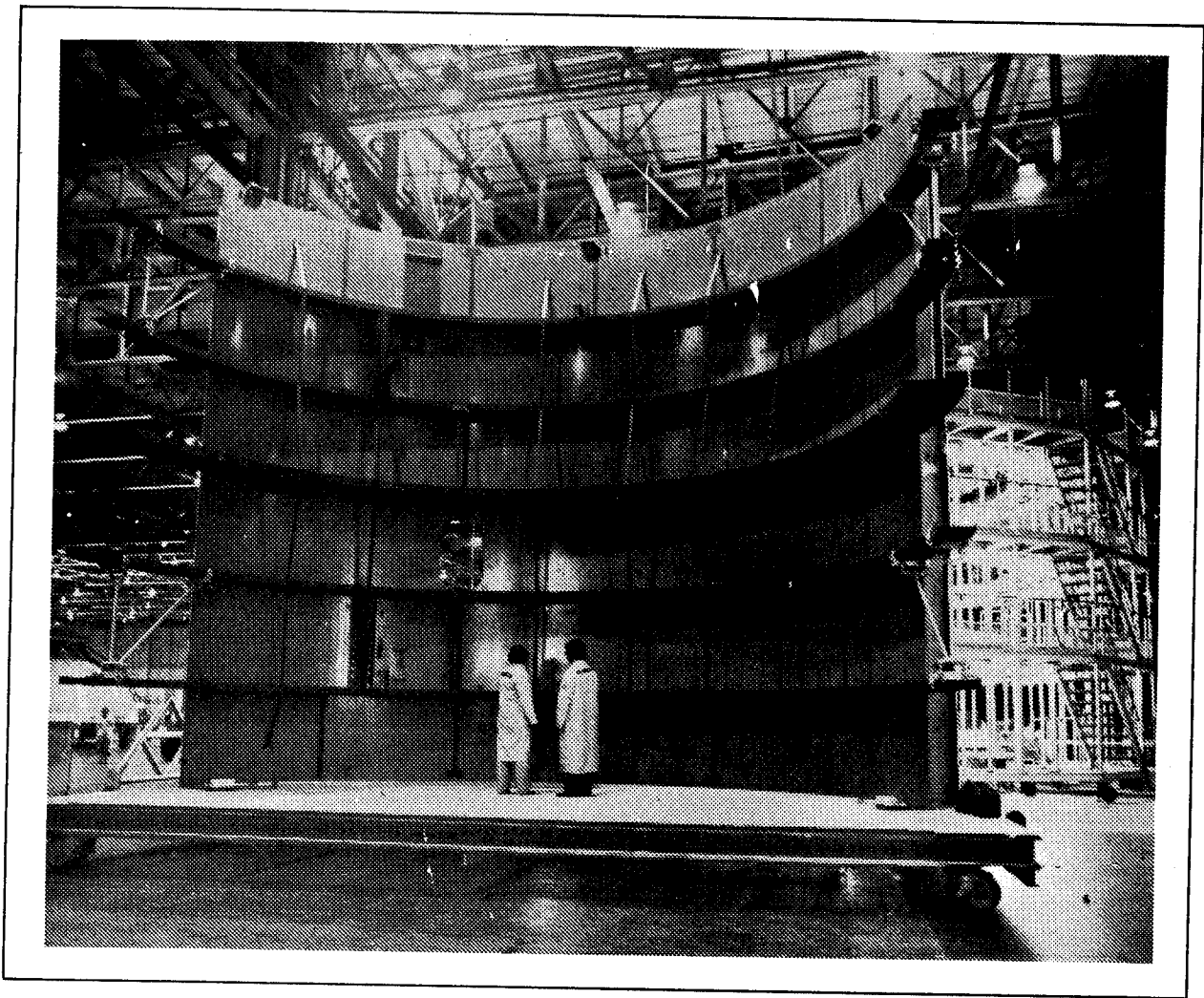
Figure 4.
Intertank Half Section On Transportation Dolly.

These two tooling positions as well as the foundation foot-print for the Automatic Riveting System are shown in Figure 5.

The second position in the family will be the Automatic Riveting System which will install the fasteners to secure the skin panels to the frames and complete the butt splices. The majority of the fasteners used in this operation are 1/4 inch A286 Hi-Sets.

SYSTEM DESCRIPTION

The Automatic Riveting System utilizes a new and unique system of driving the drill/rivet heads under computer numerical control on vertical inner and outer columns with the work piece rigidly supported on a 360 degree rotary positioner. This Vertical Drivmatic is capable of installing any one piece fastener, including slugs, up to 3/8 inch diameter without displacing the workpiece. The inner

81
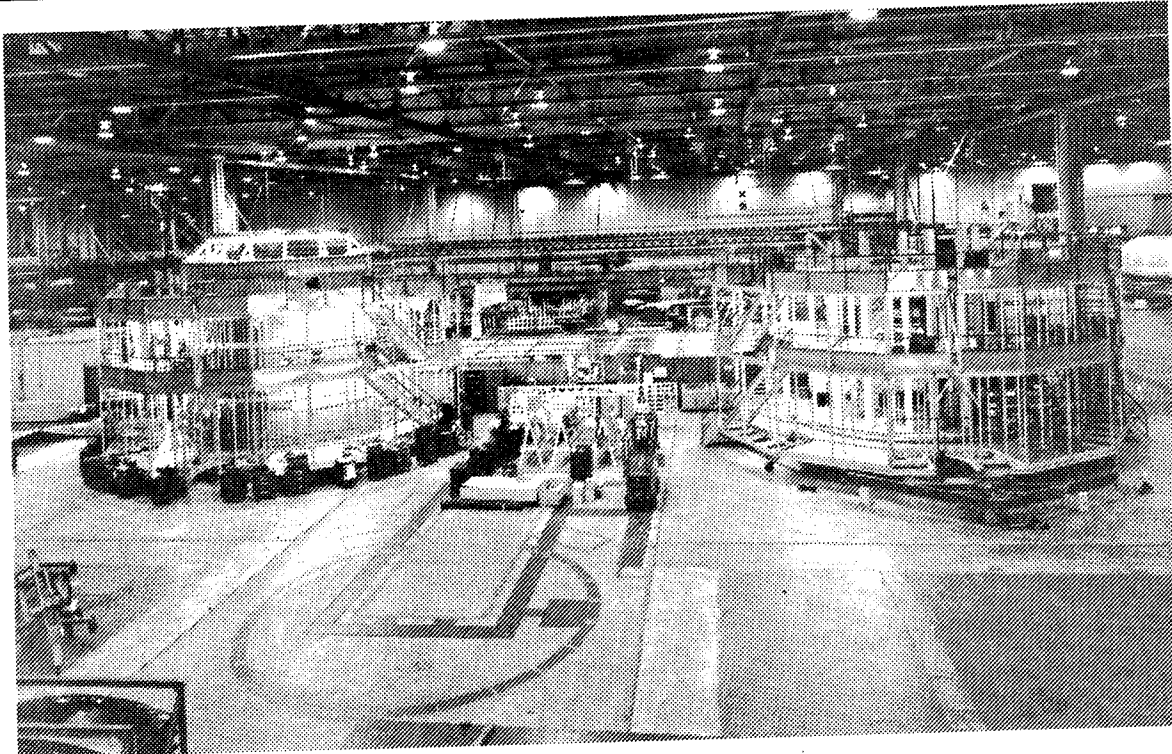
Figure 5.
Footprint For Intertank Automatic Riveting System
Shown Between First and Third Tooling Positions.

to outer head load bias to the workpiece is limited to a maximum of 50 pounds under the heaviest riveting·conditions.

The system is capable of riveting structures with both internal and external stiffening. The rivet installation rate exceeds twelve fasteners per minute in the Dual head mode and seven per minute in the single head mode. The key features of the system are described in the following paragraphs.

Vertical Drill/Rivet Columns - Rotary Positioner

The columns are 33 feet high and measure eight feet by ten feet at the base. Two sets of opposing carriages, Z axis, are positioned by electro servomotor rack and pinion drives with dual hydraulic motor counterbalances. This arrangement

permits 28.5 feet of vertical travel or 20.7 feet of working range with either set of carriages parked. Each pair of carriages are controlled by separate CNC systems. The inner column carriages (slaves) provide synchronous movement to the outer carriages and are positioned accordingly. See Figure 6.

The outer Z-axis carriage houses the Y-axis carriage which, in turn, houses the transfer head. The transfer head carries the drill spindle, hole inspection system, and bucking ram and is actuated by the transfer cylinder. The outer Z-axis carriage also mounts the automatic tool changer, automatic injector changer, vision system and TV camera. Six inches of in and out head travel, Y axis, is provided for clearing external stiffeners and accommodating work plane variations.

The inner column carriage contains the upset ram which has 24 inches of programmable retraction and programmable rotation of 350 degrees about the rivet centerline.

Plus or minus one-half inch X - axis translation is provided in each carriage to permit independent edge margin control.

The CNC rotary positioner, C axis, is a 28 foot diameter ring shaped rotary table which positions the part holding fixture and work piece for the drill rivet operations.
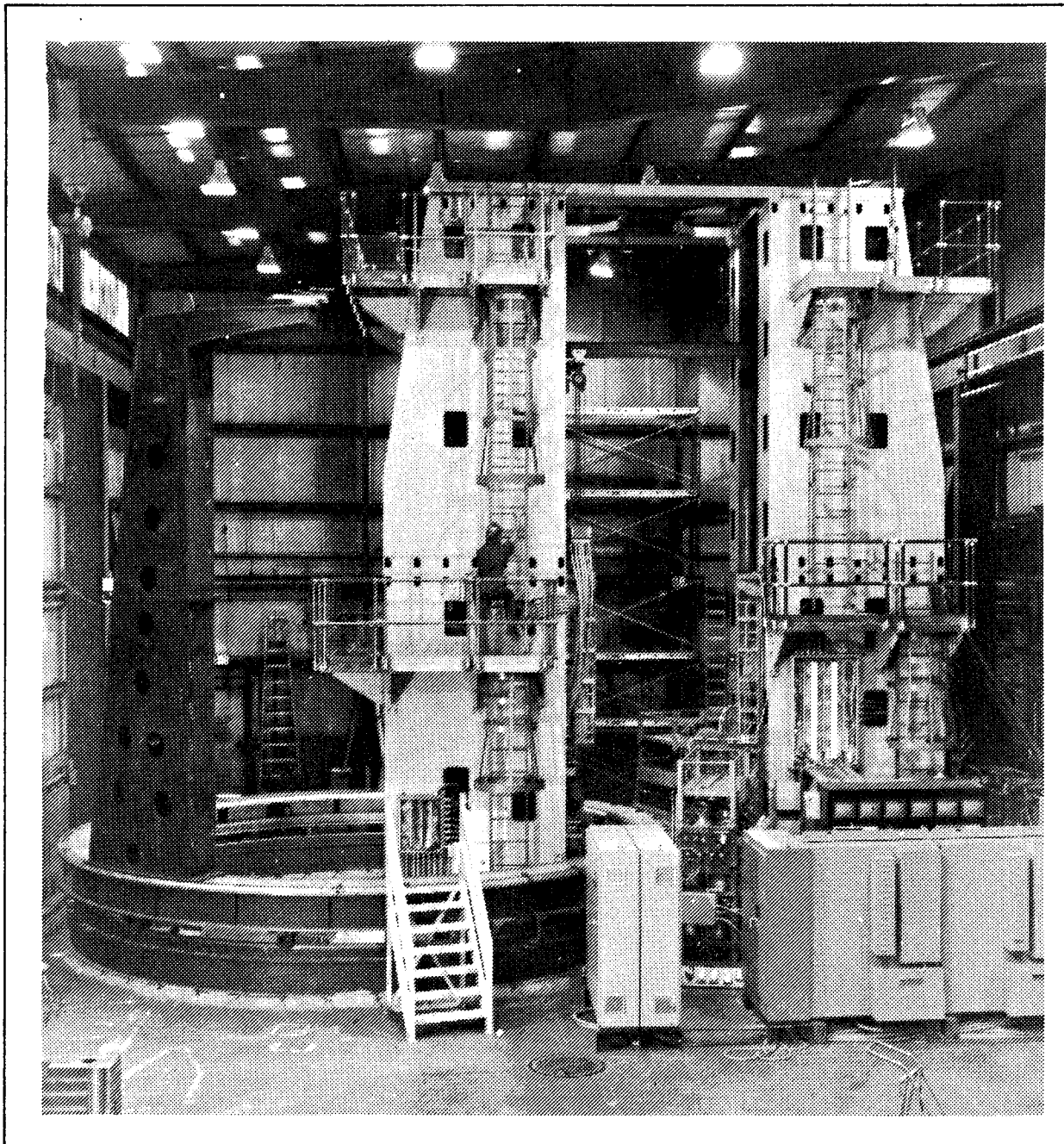
Figure 6.
GEMCOR Automatic Riveting System During Preliminary Checkout.

Control System

The Control system includes the operator's console; two Allen-Bradley 7320 Computerized Numerical Controls (CNC); three Allen-Bradley Programmable Logic Controllers (PLC 2/30); and the General Electric Vision System. The controls are interfaced to permit independent and simultaneous operation of both sets of heads. The control system block diagram is shown in Figure 7.

Primary control of the Vertical Drivmatic is accomplished through utilization of two CNC controllers. One controls the Upper Head, while the other controls Lower Head movement. With the dual CNC system one will be considered the master, which controls the 'C' Axis programming and is responsible for locking out any head motion that could cause workpiece damage. Either CNC can have the capability of controlling the C Axis, but only one at a time will do so.

Head functions will be controlled by two PLC's in communication with the CNC. In addition a third PLC will be used to control both ARS Systems. The Tack Resynchronization Visual System provided for each head will interact with its associated CNC.

The Operator's console houses all operator controls in a single main control panel. The two
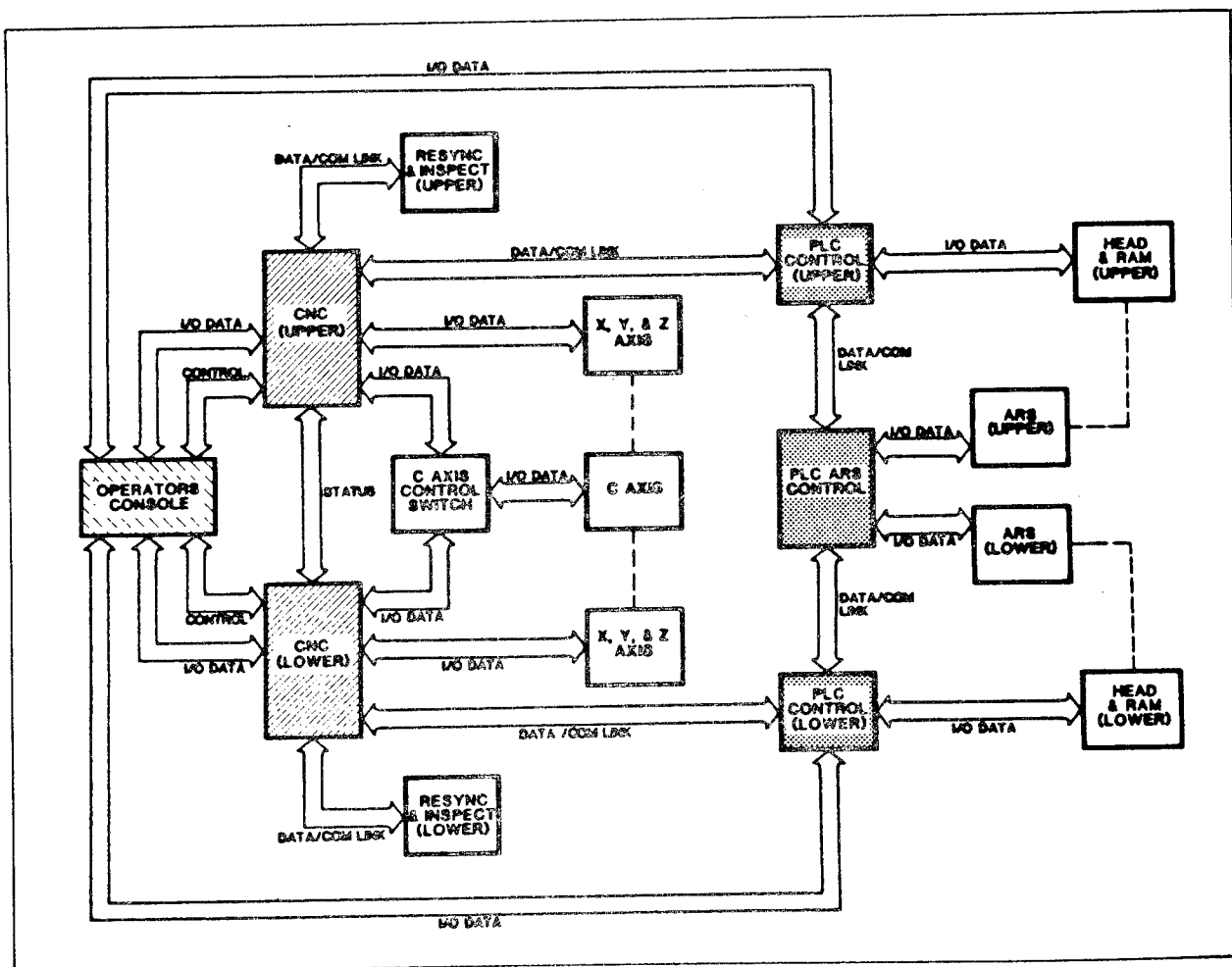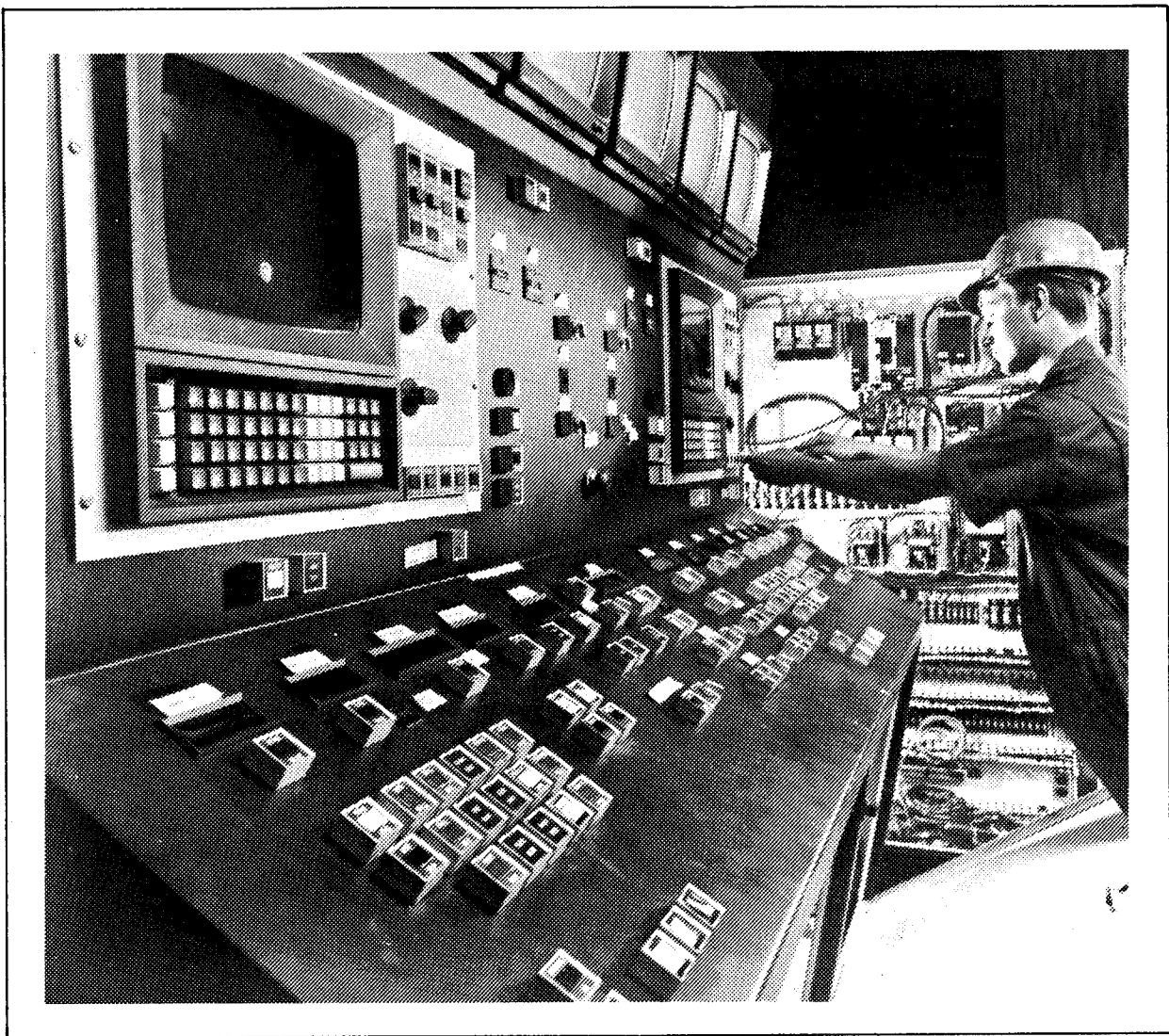

Figure 7.
Control Systems Block Diagram.

Figure 8.
Operator's Console Provides Independent Control of Dual Drill/Riveting Systems.

Allen-Bradley CNC main control panels with the CRT display and alpha-numeric keyboard are located in the operator's console along with all controls and indicators necessary for the operation of the system and riveting process. The Operator's Console, shown in Figure 8, also houses the color TV monitors and vision system displays for each set of heads.

The system is capable of controlling the riveting process by either servo upset force or head height control. The mode of operation as well as the

upset force or head height can be selected from the console or the parts program.

Rigid Workpiece Location And Clamp

The Automatic Riveting System locates the work plane of the rigidly mounted Intertank half section and completes the riveting process without displacing the work piece. The following explains the GEMCOR developed method of applying rivet upset forces while putting less than fifty pounds of bias force

85

on the workpiece. The Y-Axis carriage moves in under system pressure. When the pressure foot, which is at low pressure, touches the work surface and collapes, the pressure foot encoder senses movement and stops the Y-Axis carriage. The Y-Axis then retracts until the encoder indicates home position. The pressure foot is now fully extended and can be pressurized with system pressure.

The inner ram now advances until the clamp makes contact with the work surface. The clamp then switches from low to high pressure and the work piece is fully clamped. The Drivmatic Drill and riveting process is then initiated.

Edge Margin And Tooling Hole Resynchronization Vision System

The vision system has the capability to detect the edge of a part and shift rivet location for a single hole or group of holes using X-axis translation so that a predetermined minimum margin is maintained. This mode of operation will be used to locate the edge of hat sections when riveting Intertank panels to frames. In the hole resynchronization mode, the vision system has the capability of resynching the parts program to a tooling hole. The resynchronization is accomplished by means of X-axis translation and/or Z-axis move. The system also has the capability of resynching on a second tooling hole, computing the offsets for intermediate fasteners, and shifting the fastener locations accordingly.

Automatic Tool Changer

An Automatic Tool Changer on each outer carriage changes the drill and bucking anvil by means of the CNC parts program or operator console input. The tool changer has the capability of accomplishing the tool change without moving the workpiece. The GEMCOR developed Automatic Tool Changer has 18 tool positions comprising six bucking anvil positions and 12 drill positions. An Automatic Injector Changer accommodates up to five injectors.

The Automatic Tool Changer can complete a drill change in less than 30 seconds and a bucking anvil and injector change in 30 seconds. The Automatic Tool Changer is shown in Figure 9.

Automatic Rivet Selection System

An independent Automatic Rivet Selection System (ARS) is provided for each set of riveting heads. Each ARS has a floor mounted feed station containing 16 vibratory bowl feeders for unscrambling and aligning the rivets. The rivet selection is controlled by the CNC using a miscellaneous (M) function, an automatic stock thickness measurement system, or through the operator console. Selected rivets are automatically dispensed one at a time, blown through the injector tube to the injector and fed into the drilled holes as part of the automatic riveting cycle. A backup or reserve feed capability is included to permit manual feed from three individual drop tubes for each riveting head. The ARS, which can be expanded to include additional feeders, is shown in Figure 10.

Automatic Inspection

A programmable probe type hole inspection system is incorporated in the outer head which performs a plug gage type inspection. A precision conical probe is inserted into the drilled hole and its displacement measured with a Linear Variable Displacement Transducer (LVDT).
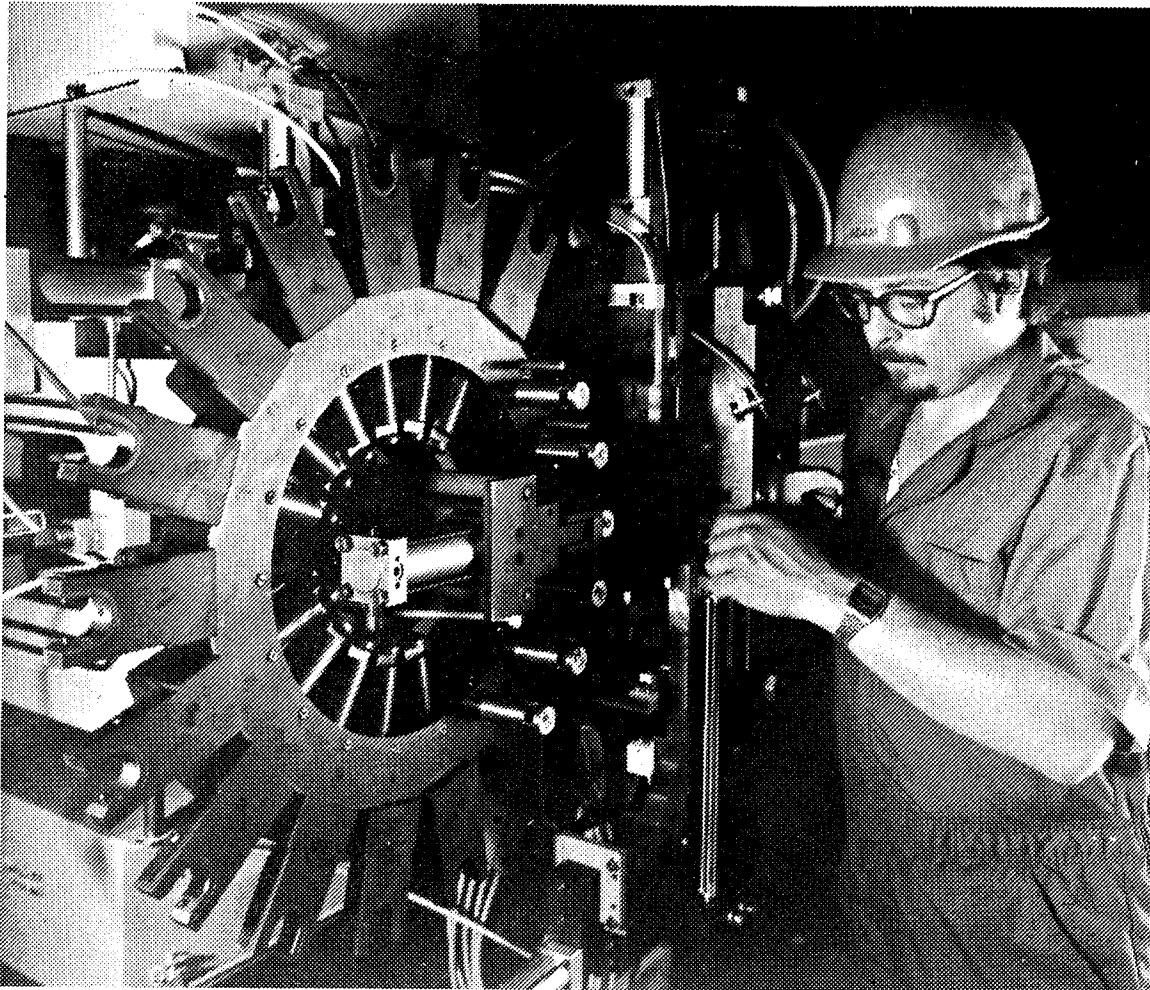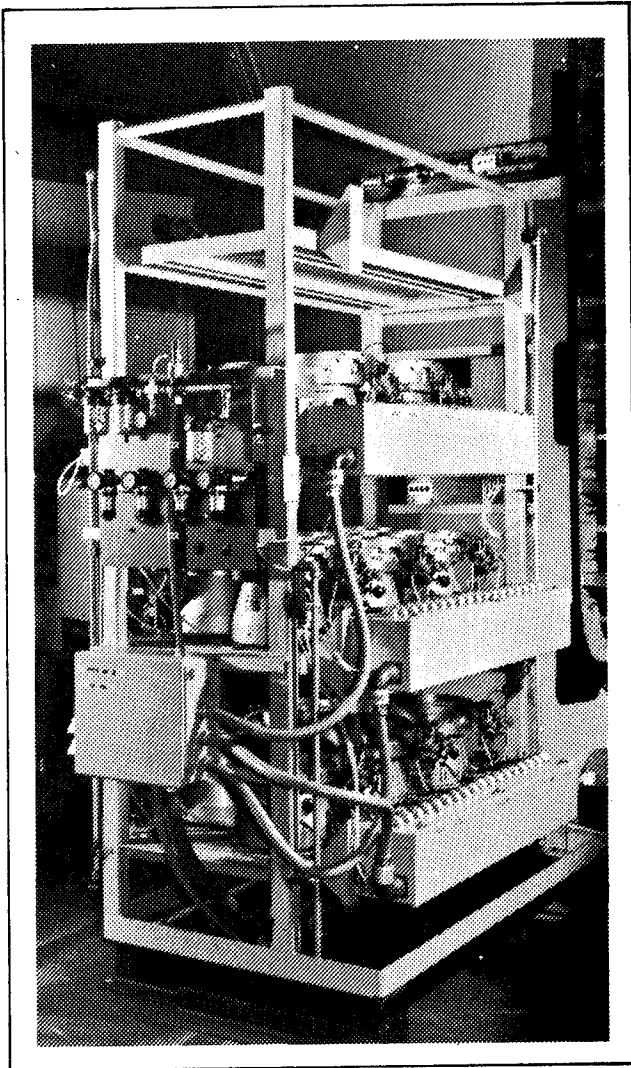
Figure 9.
Automatic Tool Changer Holds 12 Drills and 6 Bucking Anvils.

From the linear displacement data, the hole diameter is computed and compared to the established tolerances prior to rivet insertion. The system is interfaced with the CNC system to provide the capability of interrupting the drill/rivet cycle and displaying an operator message on the CRT when a drill change becomes necessary to maintain hole tolerance.

A rivet process data system provides real time hard copy printout of sequence number, upset force, hole size, and rivet head height. The frequency of printout is programmable to provide data as desired from every rivet cycle down to an exception only (out of tolerance) basis.

The system is capable of programming the hole size, upset force, and head height tolerances and the frequency of hole size inspection. The basic programming of the frequency of hole inspection is not accessible from the operator's console; however, the operator has the capability to selectively add inspection of any holes without changing the basic program.

87

Figure 10.
Automatic Riveting Selection System
Selects & Feeds Fasteners From 16
Vibratory Bowl Feeders.

SUMMARY

This Automatic Riveting System, being procured from GEMCOR by Martin Marietta Aerospace for NASA, will incorporate a new and unique automatic riveting system approach. It will bring to the Michoud Assembly Facility and External Tank Program the latest automatic riveting technology permitting further ET cost reductions and capability for low cost production of large structures for future space programs.

STRESS CORROSION RESISTANT FASTENERS

Thomas A. Roach

SPS Technologies
Jenkintown, PA

This paper describes a family of high performance aerospace fasteners made
from corrosion resistant alloys for use in applications where corrosion
and stress-corrosion cracking are of major concern. The materials discussed
are mainly A-286, Inconel 718, MP35N* AND MP159. Most of the fasteners
utilize cold worked and aged materials to achieve the desired properties.
The fasteners are unique in that they provide a combination of high strength
and immunity to stress corrosion cracking not previously attainable. A dis-
cussion of fastener stress corrosion failures is presented including a re-
view of the history and a description of the mechanism. Case histories are
presented to illustrate the problems which can arise when material selection
is made without proper regard for the environmental conditions. Mechanical
properties and chemical compositions are included for the fasteners discussed.
Several aspects of the application of high performance corrosion resistant
fasteners are discussed including galvanic compatibility and torque-tension
relationships.

*MP35N is a registered trademark of SPS Technologies.

89

HIGH PERFORMANCE BOLTING-CIRCA 1960

ALLOY STEEL-
TO 180 KSI-CYANIDE CADMIUM

H-11 -
220 KSI-FLUOBORATE CADMIUM
260 KSI-VACUUM DEPOSITED
CADMIUM OR DIFFUSED
NICKEL CADMIUM

INTRODUCTION

Fasteners made from alloy steel and modified tool steels have
been used in critical aerospace applications for decades with
a great deal of success. Tensile strengths as high as 260
KSI and even 300 KSI have been achieved and used in applica-
tions which required a high degree of integrity and on which
the integrity of the structure depended. Field failures
occurred as a result of stress corrosion cracking although
the failures were uncommon and not well understood until re-
cently. As the need for lightweight structures increased,
fastener sizes decreased, preloads increased, and design
redundancies were reduced to provide the maximum mission
capability at the lowest cost. One result was an increase
in the incidence of stress corrosion cracking failures. The
susceptibility of the noncorrosion resistant materials, the
general higher stresses, and the presence of corrosive en-
vironments were the main contributors to the increase.
Coatings were found to extend the fastener life somewhat,
but were not capable of totally preventing stress corrosion
cracking. Attempts were made to protect the area of the
fasteners from corrosion with various sealants, but these
were only partially successful. In recent years, the most
critical applications for high performance fasteners have
been filled by those fasteners made from corrosion resistant
materials.

STRESS CORROSION CRACKING REQUIRES THREE SIMULTANEOUS CONDITIONS

STRESS

SUSCEPTIBILITY

S.C.C.

SPECIFIC CORRODENT
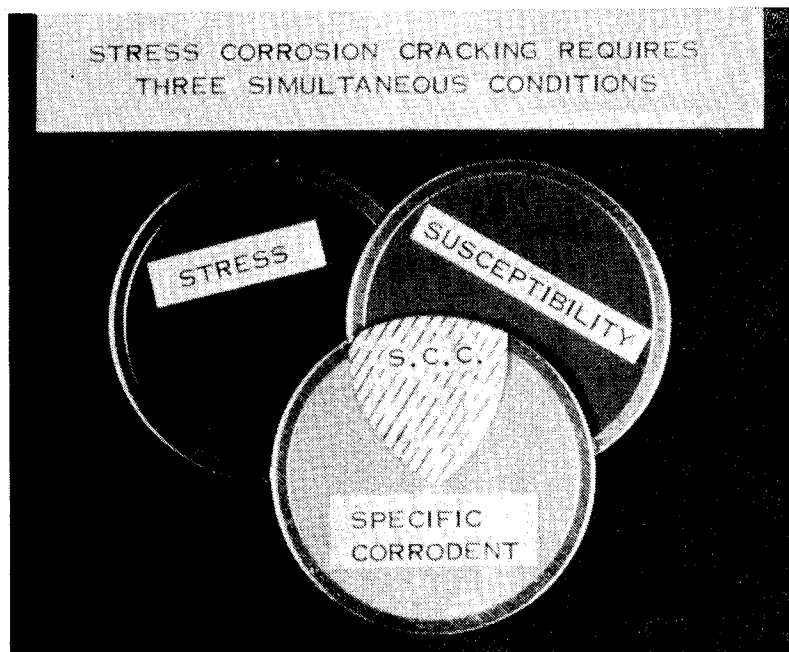
HISTORY OF STRESS CORROSION FAILURES IN SERVICE

A review of the history of stress corrosion failure of fasteners reveals that the majority of failures have occurred in bolts with 220 KSI and 260 KSI psi minimum tensile strengths. These parts are almost universally made of AMS 6487, an alloy developed from the basic H-11 steel composition. For airframe applications, these bolts are usually coated with fluoborate cadmium per NAS 672 (220 KSI fasteners) or vacuum-deposited cadmium per MIL-C-8837 (260 KSI fasteners).

CRACKING USUALLY OCCURS AT CREVICE LOCATION,

RESULTING IN FRACTURE FACE LIKE THIS
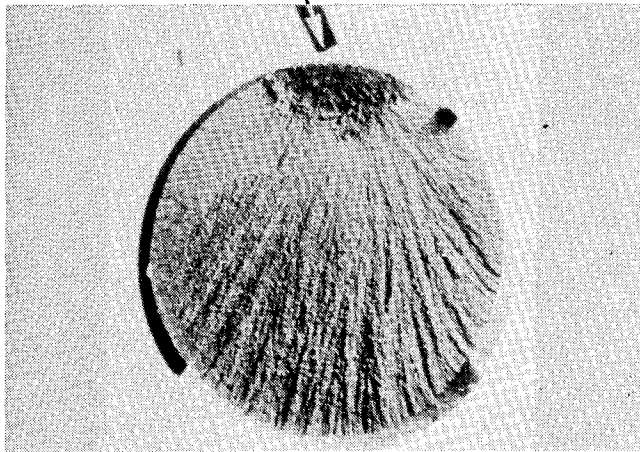
Stress corrosion failures exhibit a classic fracture with the crack initiation occurring at a surface corrosion pit generally associated with a crevice condition in the joint. The corrosion aided crack propagates to an extent dependent on the stress on the part and the fracture toughness of the material. When the crack grows to the extent that the uncracked section can no longer sustain the stress in the presence of the sharp crack, the part fails. A typical stress corrosion failure is shown in this photograph.
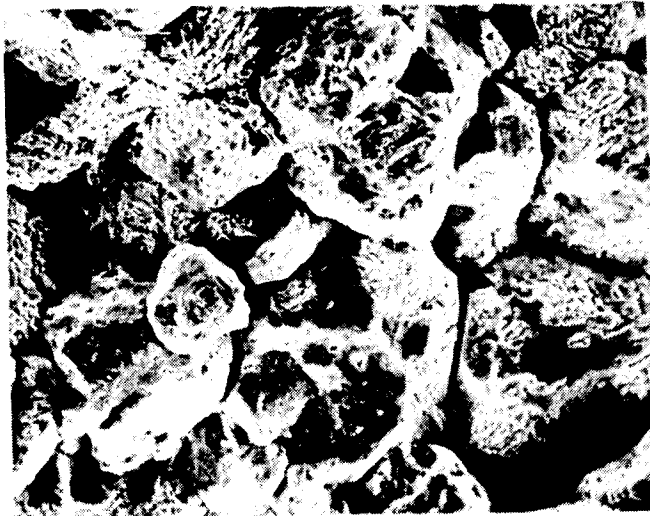
SEM FRACTOGRAPH   AMS 6487 SHCS   X700
INTERGRANULAR FRACTURE WITH CORROSION
          PRODUCTS.

A typical stress corrosion failure fractograph exhibits a
"rock candy" like fracture face. Secondary cracking is
extensive and corrosion product covers the exposed facets
of the individual grains.

MIL-STD-1312 TEST 9

STRESS- 75% OF MIN. UTS

SOLUTION- 3.5% SODIUM CHLORIDE

CYCLE- IN SOLUTION-10 MINUTES

AIR DRY-50 MINUTES

REPEAT TO FAILURE

LABORATORY STRESS CORROSION TESTS

Concern over stress corrosion cracking failure led to the development of a standard test which was ultimately adopted as a military standard (MIL-STD-1312 test no. 9). This test requires preloading the nut and bolt to be tested into a cylinder of similar material by a reproducible method such as measured bolt extension. The preloaded assembly is placed in an apparatus which immerses it in 3.5% NaCl solution for 10 minutes and then places it into moving air for 50 minutes. This cycle is repeated until failure occurs. The time to failure is recorded.
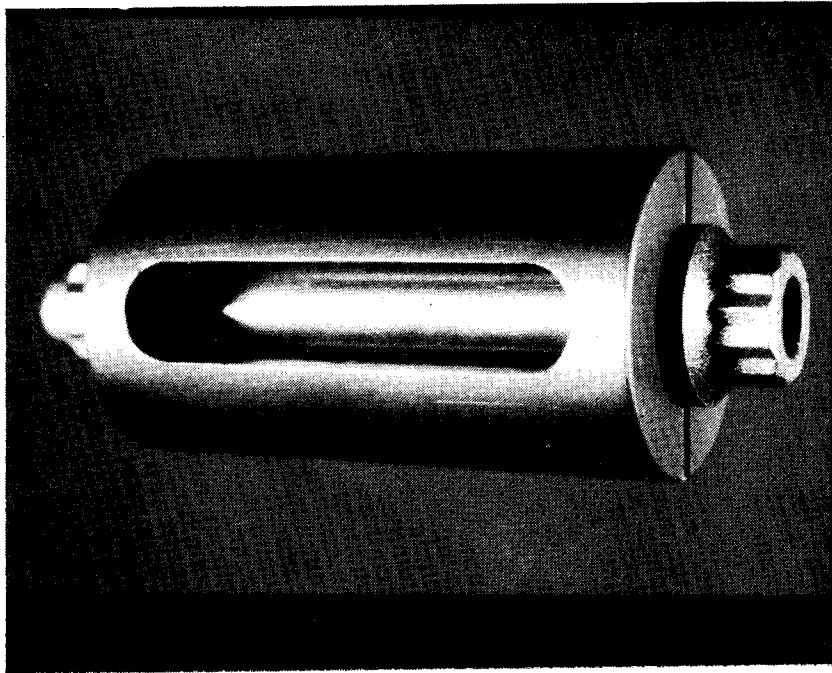
The test assembly consists of a bolt and nut tightened into
a cylinder of the appropriate material as shown. Preload is
generally developed by developing a predetermined amount of
bolt extension while tightening the bolt nut combination.
The extension is determined by running a load-extension
curve to failure and selecting the elongation at the appro-
priate preload, usually 75% of ultimate tensile strength.

The test facility consists of plastic containers of 3½% NaCl
solution and a device which immerses the test assemblies
in the solution for 10 minutes and removes them for 50
minutes into moving air. The cycle is repated to failure
or to a predetermined number of cycles.

EFFECT OF COATING ON STRESS CORROSION CRACKING RESISTANCE OF H-11 BOLTS
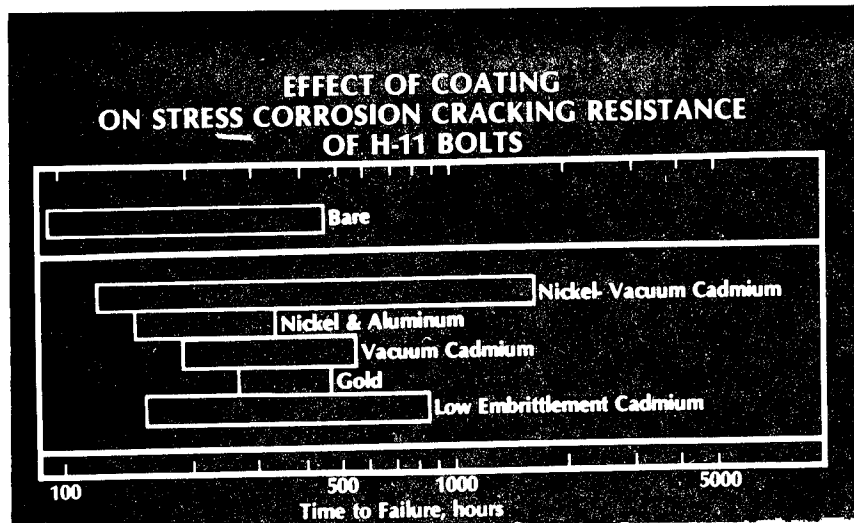
Laboratory testing produces, in a relatively short time, failures with fracture topography identical to that of field failures, providing a laboratory means to assess the relative stress corrosion cracking susceptibility of various materials, strength levels, and coatings at various stress levels. Such tests indicate that coatings can provide some protection to 260 KSI fasteners, but that failures can occur at times not significantly longer than those experienced with bare fasteners.

A new fastener material designated as Multiphase Alloy MP35N offers a combination of characteristics never before equalled in fastener history: high strength, toughness, outstanding corrosion and stress corrosion cracking resistance, and excellent cryogenic properties. Multiphase is a quaternary alloy system with a nominal composition of 35Ni-35Co-20Cr-10Mo. Through a combination of cold working, transformation, and aging, Multiphase can be strengthened to 260,000 psi tensile strength, resulting in the most corrosion resistant high-strength fastener ever manufactured.

ALTERNATE IMMERSION TEST
(S.C.C. SUSCEPTIBILITY)

75 %
UTS

No Failure AFTER 5000 HRS.
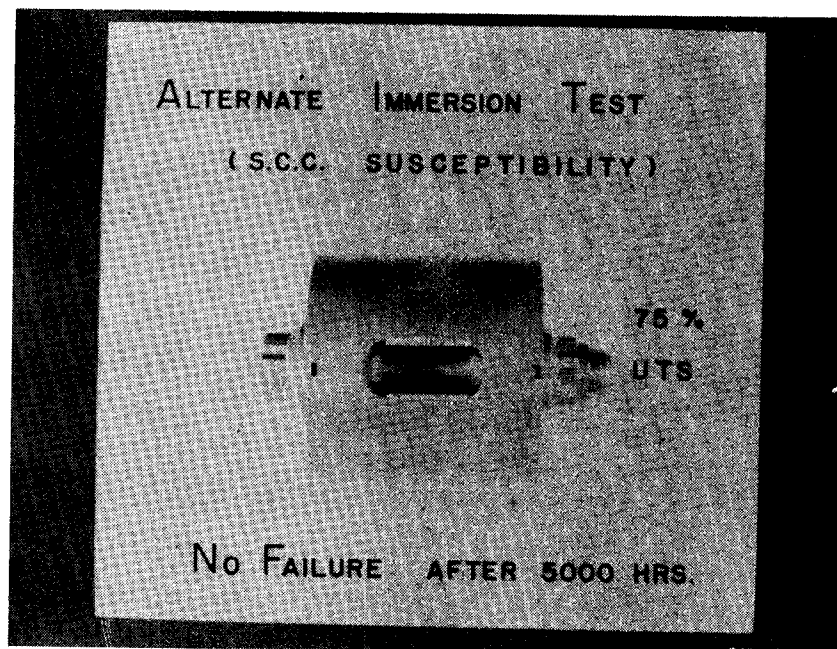
MP35N fasteners subjected to the MIL-STD-1312 test experienced
no failures in 5000 hours and no stress corrosion failures have
occurred in the field despite exposure to high stresses and
highly aggressive environments.
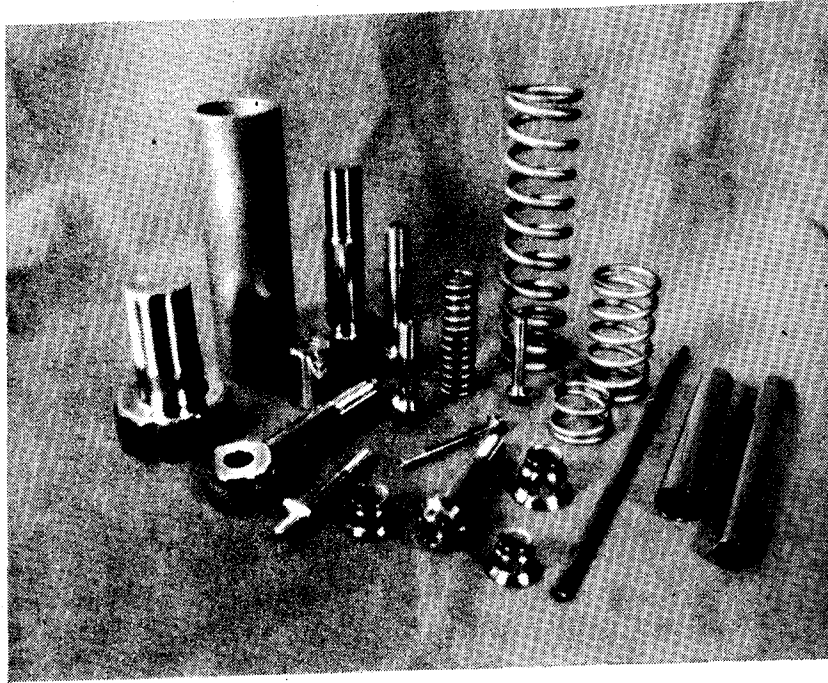
MP35N has been applied to a wide variety of products including
bolts, nuts, tubing, springs, shear pins and prosthetic devices.

The application of high strength corrosion resistant fasteners to aerospace structure has taken place in both original design and rework as a result of field failures with noncorrosion resistant fasteners. The largest single application involves the use of MP35N alloy and Inconel 718 fasteners in the space shuttle. The original design of the orbiters, solid rocket boosters, and expendable fuel tanks made extensive use of these fasteners to provide reliable fastening in the presence of extremely high loads and aggressive, seacost environments. Inherent corrosion resistance was further mandated because the vacuum conditions of space prohibit the use of cadmium plating or other protective coatings. An MP35N alloy application on Harpoon missile canisters resulted from a series of tests comparing PH13-8Mo to MP35N in resistance to corrosion and stress corrosion cracking. The MP35N alloy was chosen and has been used exclusively for the fasteners which join the individual canisters together and attach the canister assemblies to the launch support structure.
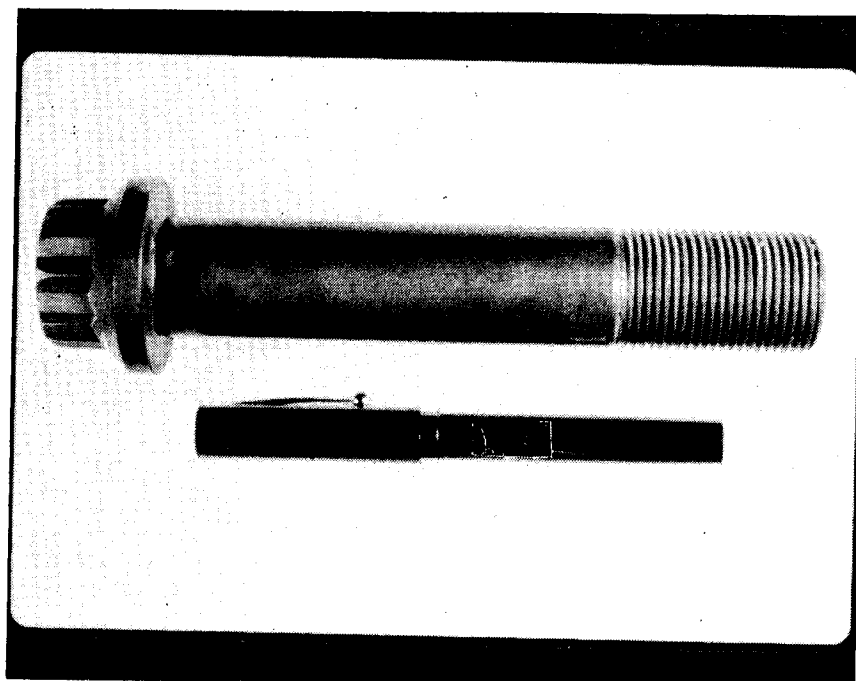
MULTIPHASE ALLOY COMPOSITION

	Co	Ni	Cr	Mo
MP 35N	35	35	20	10
MP 159	35	26	19	7

	Fe	Ti	Cb	Al
MP 159	8	3	.6	.2

A derivative of the MP35N alloy, MP159 was developed to provide improved high temperature properties and hot forgeability. The MP159 alloy has found many applications in the gas turbine industry, where it provides properties superior to those of Inconel 718.

INCONEL 718

Inconel 718 was developed for applications up to 1200°F. In
its most commonly used condition, solution treated and aged,
it has a minimum tensile strength of 180 KSI. This strength
level has permitted its use in applications which would
normally use alloy steel fasteners such as MS21250s but in
which concern over corrosion and stress corrosion cracking
dictates the use of inherently corrosion resistant materials.
For applications which require 220 KSI fasteners for which
AMS 6487 or alloy steel would have been used, the ideal ma-
terial for corrosion critical applications is Inconel 718.
This is produced by the cold work and age method and the
resulting fasteners are mechanically equivalent to their
noncorrosion resistant counterparts.

103

S.C.C. CRITICAL APPLICATIONS

130 KSI-200 KSI UTS — A-286

180 KSI-220 KSI UTS — INCONEL 718

260 KSI UTS ——————— MP35N-MP159

CONCLUSIONS

Recent developments in materials and fasteners have created
new design options for the designer of critical structures.
Where stress corrosion cracking is of some concern, a family
of fasteners has been developed to provide virtual immunity
to failures resulting from interaction with aggressive en-
vironments. While the purchase price of those fasteners
exceeds that of conventional fasteners, the total life cycle
cost is attractive when the cost of periodic inspection, re-
placement, and product liability is considered.

The use of corrosion resistant fasteners will continue to
increase as the demand for higher integrity structures grows.

DERIVATION AND TEST OF ELEVATED TEMPERATURE THERMAL-STRESS-FREE FASTENER CONCEPT

James Wayne Sawyer, Max L. Blosser and Robert R. McWithey
NASA Langley Research Center
Hampton, Virginia

ABSTRACT

Future aerospace vehicles must withstand high temperatures and be able to function over a wide temperature range. New composite materials are being developed for use in designing high-temperature lightweight structures. Due to the difference between coefficients of thermal expansion for the new composite materials and conventional high-temperature metallic fasteners, innovative joining techniques are needed to produce tight joints at all temperatures without excessive thermal stresses. A thermal-stress-free fastening technique is presented that can be used to provide structurally tight joints at all temperatures even when the fastener and joined materials have different coefficients of thermal expansion. The derivation of thermal-stress-free fasteners and joint shapes is presented for a wide variety of fastener materials and materials being joined together. Approximations to the thermal-stress-free shapes that result in joints with low-thermal-stresses and that simplify the fastener/joint shape are discussed. The low-thermal-stress fastener concept is verified by thermal and shear tests in joints using oxide-dispersion-strengthened alloy fasteners in carbon-carbon material. The test results show no evidence of thermal stress damage for temperatures up to 2000°F and the resulting joints carried shear loads at room temperature typical of those for conventional joints.

INTRODUCTION

Future aerospace vehicles must withstand high temperatures and be able to function over a wide temperature range. New composite materials are being developed for use in designing high-temperature lightweight structures. Many of the high temperature structural composite materials have coefficients of thermal expansion (CTE) that are considerably different from those of high-temperature metallic fasteners. Thus, conventional high-temperature metal fasteners and fastening techniques do not provide structurally tight joints for the complete use temperature range without introducing severe thermal stresses that can result in premature failure. The difficulties in designing a tight structural joint for all temperatures are illustrated by the accompanying sketch and table. If the fastener material has a higher CTE than the material joined together, a standard cylindrical fastener which is snug at room temperature will produce high thermal stresses at elevated temperatures. If sufficient radial clearance is provided at room temperature to reduce the thermal stress at elevated temperature, the fastener will be loose in the radial direction at room temperature and loose in the axial direction at elevated temperatures. An axially snug joint at elevated temperature can be achieved by providing high clamping pre-stresses in the joint at room temperature but the high pre-stresses may be detrimental to the joint. Thus, new joining techniques are needed for the high-temperature composite materials.

A thermal-stress-free fastener concept has been developed at the Langley Research Center that can be used to provide structurally tight joints at all temperatures even when the fastener and joined materials have different coefficients of thermal expansion. The derivation of thermal-stress-free fasteners and joint shapes is presented herein for many combinations of fastener material and joined material. Approximations to the thermal-stress-free shapes that result in joints with low-thermal-stresses and that simplify the fastener/joint shape are discussed. Results of thermal and shear tests are also presented from an ongoing experimental program to verify a low-thermal-stress joint concept which consists of oxygen-dispersion-strengthened (ODS) alloy fasteners in carbon-carbon material.

106

PROBLEM AREAS FOR CONVENTIONAL JOINTS IN HIGH-TEMPERATURE APPLICATIONS

Fastener coefficients-of-thermal expansion greater than that for joined materials
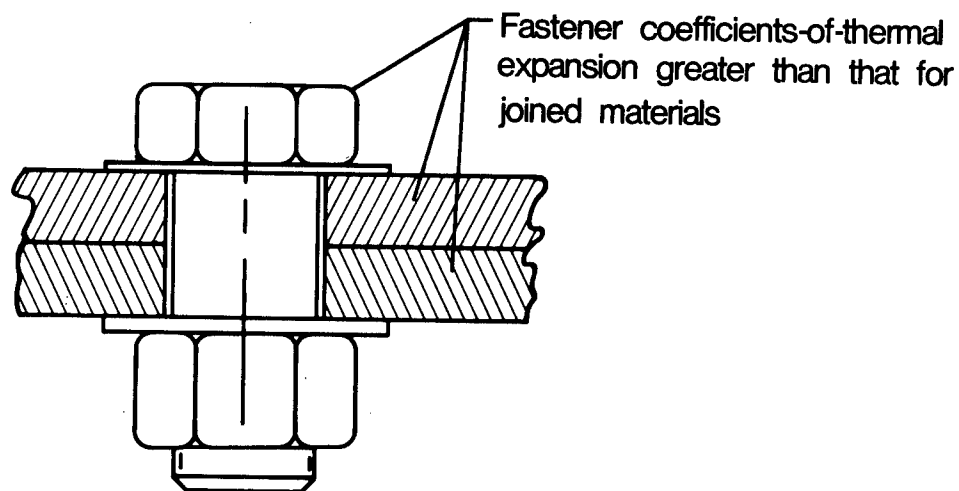
	Joint condition	
	Room temperature	Elevated temperature
Radial direction	Snug Loose	High thermal stresses Snug
Axial direction	Snug Pre-stressed	Loose Snug

THERMAL-STRESS-FREE METAL FASTENER
## CONCEPT FOR HIGH-TEMPERATURE JOINTS

The thermal-stress-free fastener concept (Ref. 1) is illustrated by the sketch. A typical high-temperature joint with a metal fastener joining material with a different CTE is shown. The metallic components of the joint consist of a conical fastener, washer, and nut. The remaining components of the joint consist of two plates and a washer made of the material being joined together. The thickness of the washer made from the same material as the plates is determined so that the origin (apex) of the conical fastener is located at the outer plane of the washer as shown. The inner diameter of the washer must have a clearance fit with the shank of the fastener if the CTE of the fastener is greater than the CTE of the material being joined. The clearance is determined by the difference between the coefficients of thermal expansion between the two materials and the temperature extremes for which the joint is designed. Because the metal fastener and the composite material have a different CTE, heating or cooling the joint results in different amounts of expansion for the two materials. However, if the fastener material and the material being joined both have an isotropic CTE, relative expansion or contraction between the fastener and the material takes place on radial lines projecting from the origin of the conical fastener. Thus, the expansion or contraction does not result in tightening or loosening of the joint and does not introduce thermal stresses into the material.

High-temperature metal fastener

Material to be joined with coefficient-of-thermal expansion different from fastener

Metal washer

Hex nut
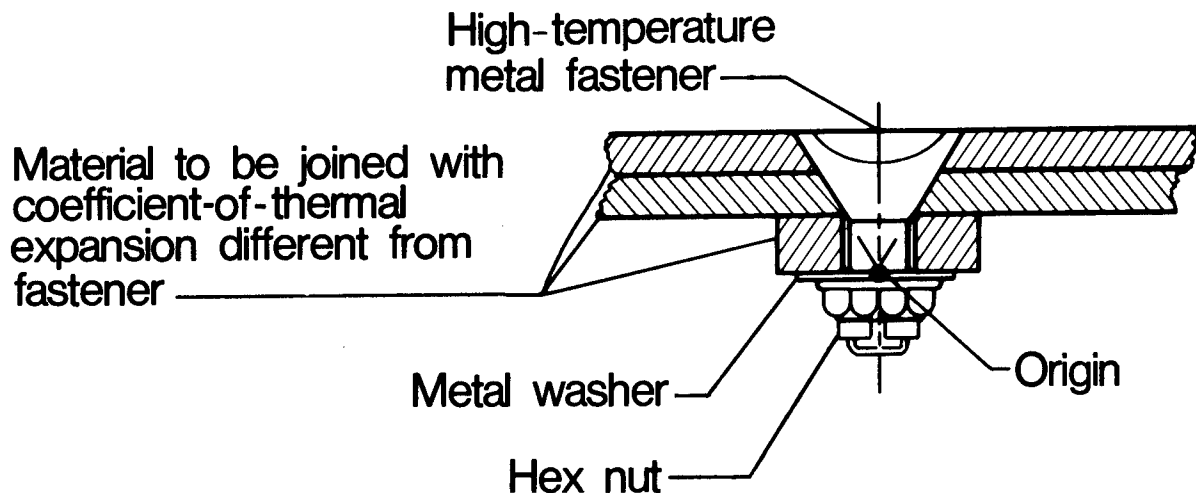
Origin

● **Joint is thermal-stress-free if fastener and material being joined have isotropic coefficients-of-thermal expansion**

THERMAL EXPANSION OF THERMAL-STRESS-FREE CONCEPT

Thermal expansion relative to the origin for the thermal-stress-free concept is illustrated in the two sketches. The dashed lines show an exaggerated view of the expanded shapes assuming that the fastener has a higher CTE than the joined material. The larger expansion of the fastener is evident. For the joint with isotropic CTE (sketch on left), the thermal expansion does not result in any interference or clearance between the fastener and the joined material and does not have thermal stresses or become loose at the high temperatures. However, for the joint with the joined material having a non-isotropic CTE (sketch on right), there is an interference zone due to a reduction in the cone angle for the joined material. The change in cone angle is due to the inplane CTE being smaller than the CTE through-the-thickness for the joined material. (An inplane CTE larger than the CTE through-the-thickness would result in an increase in cone angle and therefore a loose fit at high temperatures.) Thus, for materials that do not have an isotropic CTE, the conical fastener configuration reduces but does not eliminate the thermal stresses. Since many of the high-temperature composite materials do not have isotropic CTE, a thermal-stress-free fastener configuration is needed that is applicable to materials that have different CTE in the inplane and through the thickness directions (specially orthotropic materials).

Isotropic CTE   **Non-Isotropic CTE**
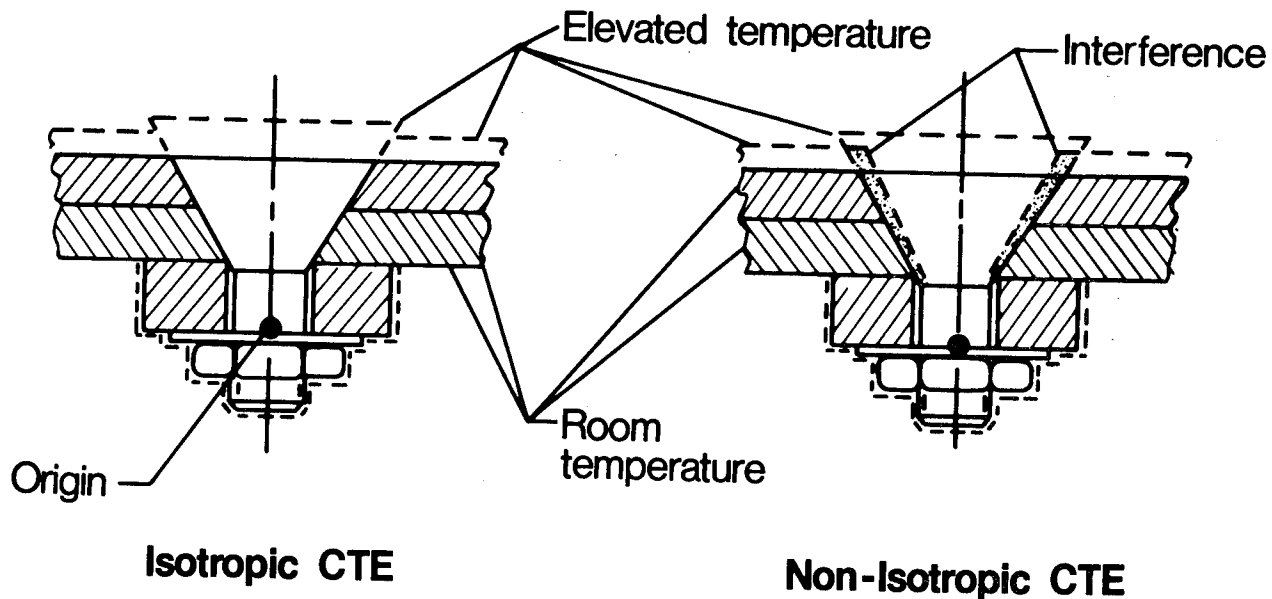
DERIVATION OF THERMAL-STRESS-FREE BOUNDARY

A general description of the shape of the thermal-stress-free boundary between the fastener material and the joined material is desired in which both materials have these specially orthotropic characteristics. Derivation of the desired thermal-stress-free boundary between the two materials requires an interface along which the two materials will remain in contact without interference or separation as temperature changes. The boundary between the two materials is illustrated in the sketch and is given by y=f(x) at the initial temperature. The desired boundary is shaped so that, as the temperature is increased or decreased, points located on the boundary at the initial temperature may move relative to each other but must remain on a common boundary for all temperatures. The boundary may change shape with a change in temperature, as shown, but all points of both materials initially on the boundary will remain on the boundary. Such a boundary can be found if the following assumptions are made: the CTE is constant with temperature and location for both materials; the temperature is uniform in both materials; and there is no friction along the boundary. Derivation of the thermal-stress-free boundary is discussed in reference 2.
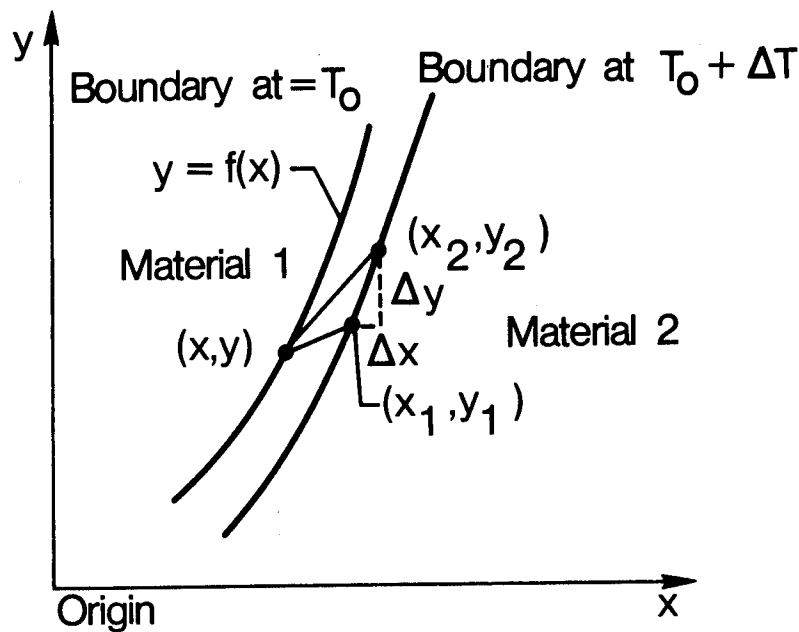
Assumptions

- CTE constant with temperature and location
- Uniform temperature
- No friction along boundary

110

THERMAL-STRESS-FREE BOUNDARIES

A family of thermal-stress-free boundaries exists and is given by the equation shown, where c is an arbitrary constant and p is the ratio of the differences between the CTE for the two materials in the through-the-thickness and the inplane direction. The value of c, although arbitrary for defining a family of thermal-stress-free boundaries, is determined by the fastener diameter and washer thickness when deriving a specific fastener shape. The family of thermal-stress-free boundaries is shown in the figure. The curvature of the different boundaries is determined by the relationship between the CTE of the two materials as defined by p. Each of the thermal-stress-free boundaries shown is derived in two dimensions but if the inplane CTE of each material is independent of direction, then the boundary can be rotated about an axis to produce axisymmetric thermal-stress-free fasteners. Note that for p=1, which would result for joints involving different isotropic materials, the thermal-stress-free boundary is a straight line which results in a conical fastener. Thus, the initial conical fastener concept discussed previously is a subset of the thermal-stress-free boundaries given above.

$$y = cx^p \quad ; \quad \text{where } p = \frac{\alpha_{y1} - \alpha_{y2}}{\alpha_{x1} - \alpha_{x2}}$$
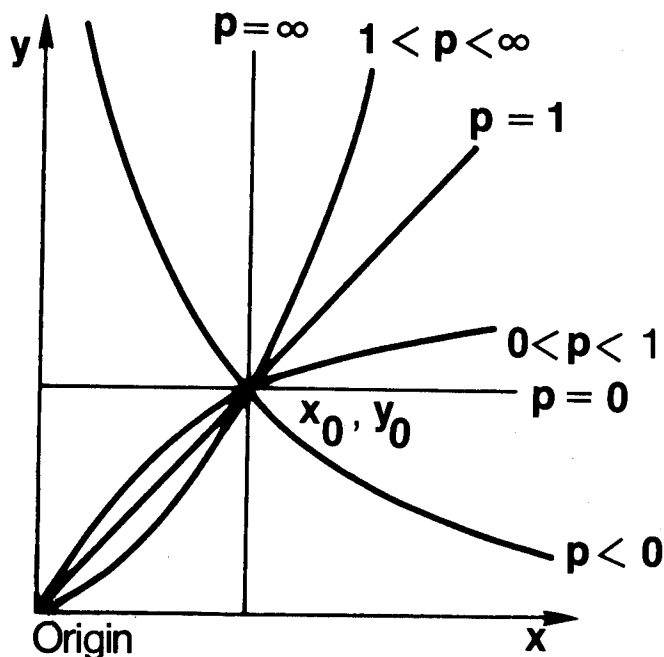
TYPICAL THERMAL-STRESS-FREE FASTENER CONFIGURATIONS

Typical thermal-stress-free fastener configurations which utilize the derived thermal-stress-free boundaries are shown in the figure. The fastener configurations shown for p greater than zero appear practical to use for making conventional joints. For p between 0 and 1, the fastener has a concave shape; whereas, for p greater than 1 it has a convex shape. As pointed out previously, a value of p equal to 1 results in a conically shaped fastener. Note that if the diameter of the cylindrical portion of the fastener is maintained fixed as shown, the washer thickness varies widely depending on the value of p. A clearance between the washer and the shank of the fastener must be maintained at all temperatures to avoid thermal stresses. For values of p less than zero, the thermal-stress-free boundaries do not result in a conventional joint configuration. The sketch shows one possible thermal-stress-free configuration for the case where p is less than zero. The configuration shown is rather inefficient as the joint shear load would have to be carried in bending of the fastener. However, the joint is thermal-stress-free and may be the only joint configuration possible for certain combinations of materials. An example of high-temperature materials that would require such a fastener is graphite/polyimide (Gr/PI) materials being joined together by a high-temperature metal fastener. The negative value of p is due to the difference in in-plane and through-the-thickness CTE for Gr/PI being large and the CTE for the fastener being between the two values for Gr/PI. Most other high-temperature composite materials and metal fastener combinations have positive values of p which result in more practical thermal-stress-free configurations.

112
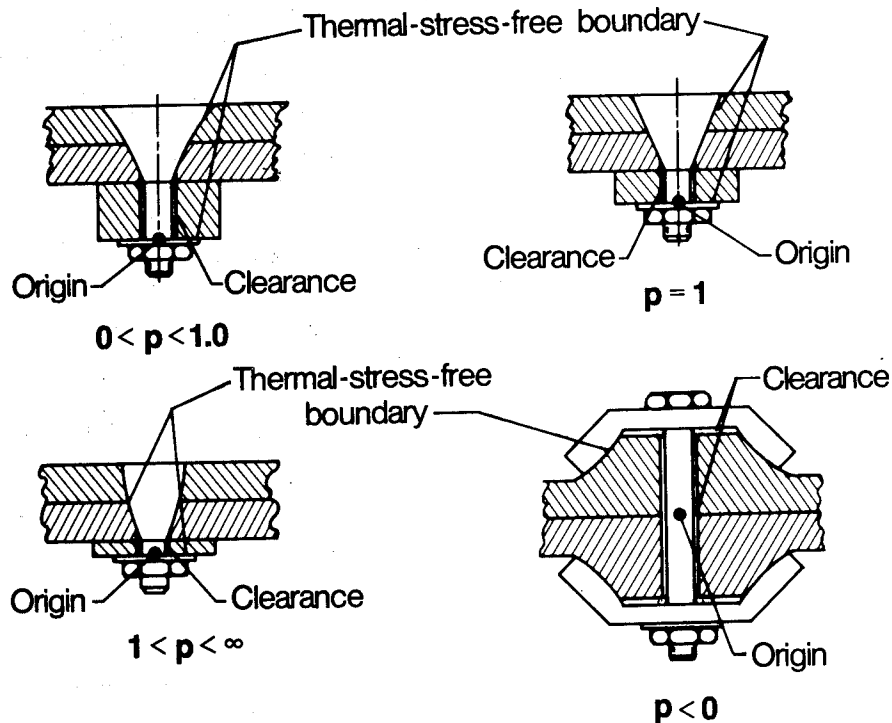
# EFFECT OF DESIGN PARAMETERS W AND R ON FASTENER PROPORTIONS

The thermal-stress-free boundary for a particular fastener configuration is determined by the constant c and by the relative values of the CTE for the fastener and the materials joined together. The constant c is determined from two design parameters --the washer thickness W and the radius r of the cylindrical portion of the fastener by the relationship $c = W/R^p$. The effect of changes in these two parameters on the fastener and joint configuration is shown in the figure for a typical combination of materials (p=constant). The baseline fastener configuration is shown in the sketch in the center of the figure. Increasing the radius of the fastener while keeping the washer thickness constant (decreasing c) results in a fastener with a much larger head as shown in the sketch in the upper left-hand corner of the figure. Increasing the washer thickness and keeping the radius constant (increasing c) results in a fastener with a much smaller head as shown in the sketch in the lower right-hand corner of the figure. Changing both the radius and the washer thickness results in a wide variation of possible fastener configurations and gives the designer a wide range of choices in determining the desired fastener joint configuration.
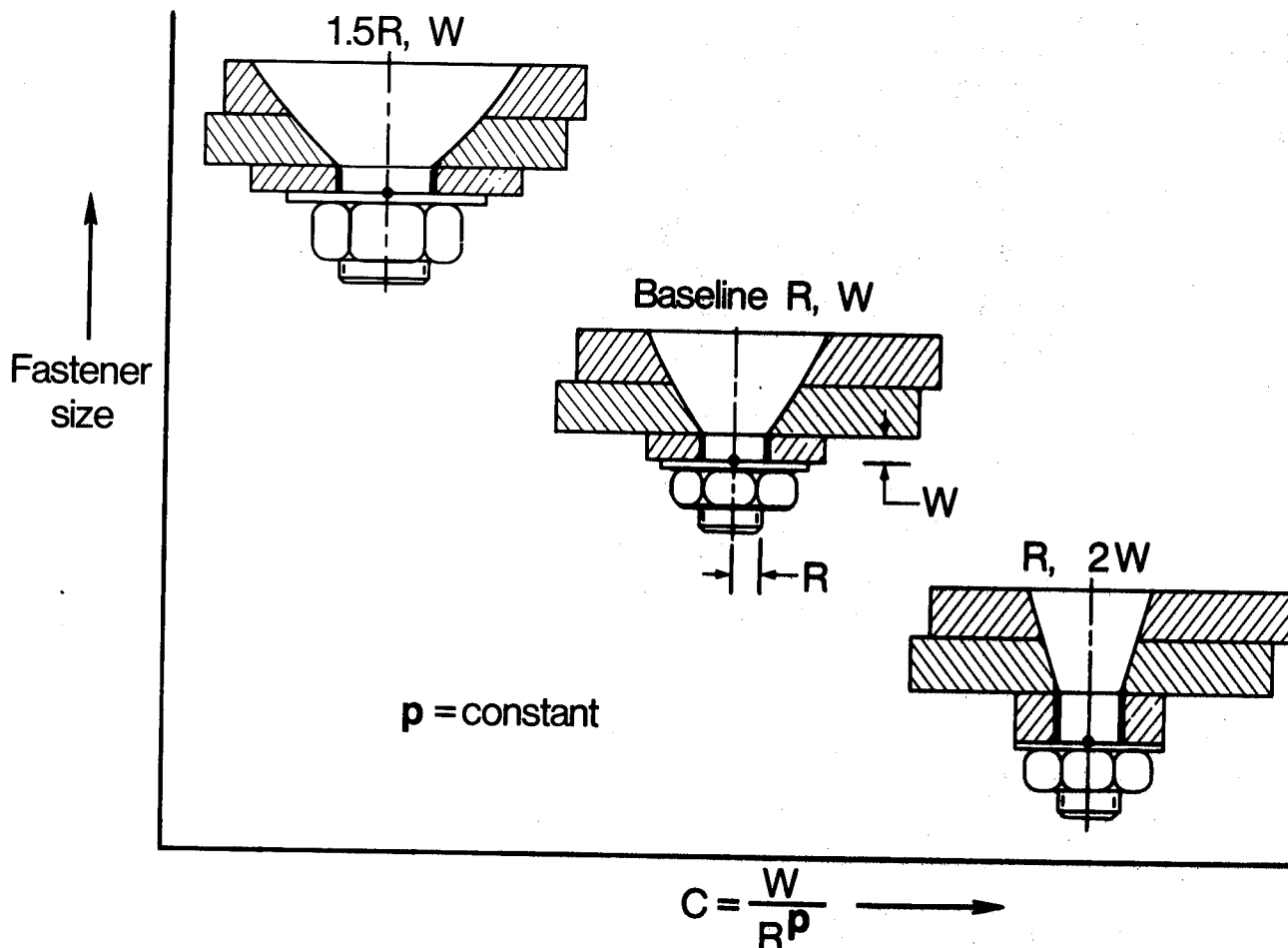
THERMAL-STRESS-FREE FASTENER FOR CARBON-CARBON MATERIAL

A thermal-stress-free fastener design for an ODS alloy fastener joining two pieces of carbon-carbon material together is shown in the sketch. Each plate of carbon-carbon material is 0.15-inch thick and the diameter of the shank of the fastener is 0.25 inch. The thermal-stress-free boundary is the curved solid line indicated on the sketch. A relatively thick carbon-carbon washer is required to properly position the origin of the thermal-stress-free boundary.

Due to the difficulty of machining a fastener with the curved thermal-stress-free shape, it is desirable to simplify the shape as much as possible without destroying the low-thermal-stress properties of the joint. The curved shape can be approximated by a straight line as shown which results in a conically shaped fastener and hole. For the fastener configuration shown, the straight line approximation results in a maximum deviation of 0.005 inch from the curved thermal-stress-free boundary and thus should still result in a low-thermal-stress joint. Note that to approximate the thermal-stress-free fastener configuration with a conical fastener, the washer thickness is determined by the origin of the thermal-stress-free boundary and not that of the origin of the cone. The location of the origin of the conical fastener is offset inside the free surface of the washer as shown. Thus, by simply offsetting the origin, conical fasteners, which are considerably less expensive to machine and much easier to apply than curved thermal-stress-free fasteners, can probably be used for many other combinations of materials and still give joints that have low-thermal-stresses when heated or cooled. A thermal stress analysis is needed to investigate the stresses introduced by making the conical approximation for various combinations of materials.
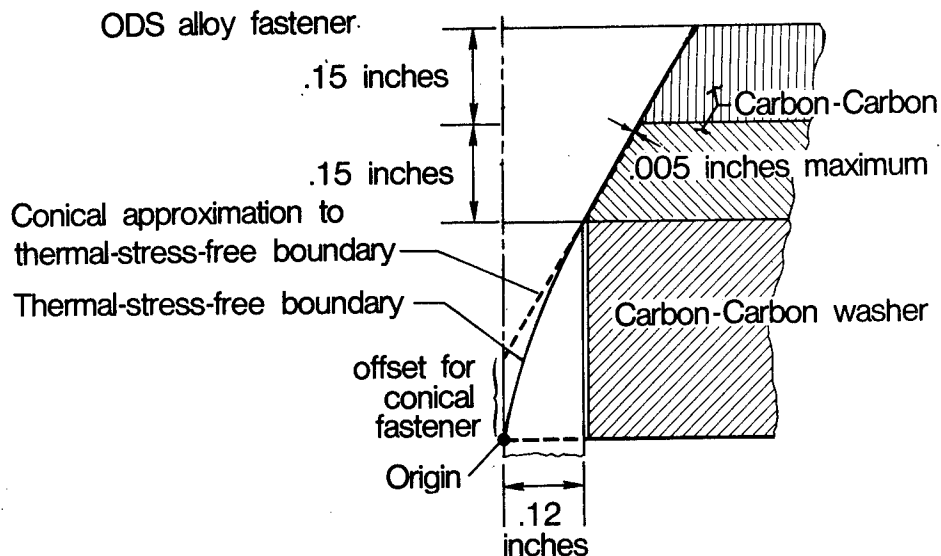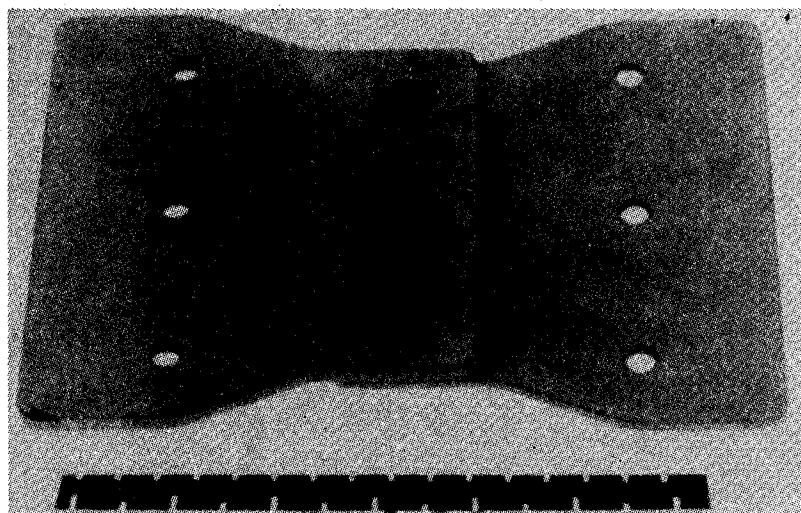
CARBON-CARBON LOW-THERMAL-STRESS JOINT TEST SPECIMEN

A test program was initiated to verify the low-thermal-stress concept using ODS alloy conically shaped fasteners in carbon-carbon material (see Ref. 3). Twelve specimens were tested, one of which is shown in the photograph. The specimens consist of two carbon-carbon plates connected by a single line of three low-thermal-stress fasteners. Three specimens each of four design configurations were tested. The configurations were chosen to represent typical structural joints and included various plate thicknesses and load transfer levels. The plates for the four joint designs contained the following number of plies of fabric: 7/8, 10/11, 11/18, and 18/21. The joint configuration at each fastener location consisted of an ODS-alloy metal fastener which passed through the two carbon-carbon plates , the carbon-carbon washer, and the ODS alloy metal washer and nut. The fastener had a 60 degree included-angle conical head and a number 10 machine screw threaded shaft. As previously mentioned, in approximating the thermal-stress-free configuration, the origin of each conical fastener was offset slightly inside the outer surface of the carbon-carbon washer.

The specimens were manufactured by Vought Corporation using their standard process for ACC-4 (four densifications) cross-ply (alternate layers of 0 and 90 degree fabric) material. The specimens were machined and then given a silicon carbide coating, followed by a Tetraethyl Orthosilicate high-temperature sealer and an LB (Vought Corporation designated for proprietary sealer) low-temperature sealer. After the coating and sealers were applied, the conical fastener holes were lightly reamed to provide good fit for the fasteners.

CARBON-CARBON LOW-THERMAL-STRESS CONICAL FASTENER TEST PROGRAM

The test program consisted of thermal-cycle tests and shear load tests. One specimen was subjected to a thermal cycle with no mechanical loading, ten specimens were tested to failure in shear at room temperature, and the other specimen was subjected to both a thermal-cycle test and a shear-to-failure test at room temperature. The specimens were assembled with the fasteners torqued to 5 in-lbs for each test.

The thermal tests consisted of drying the specimen at 250°F and 0.005 mm of mercury pressure for 12 hours and then heating to 2000°F and holding at that temperature for one hour in an oxidizing atmosphere. The atmospheric pressure for the specimen was gradually increased from 0.005 mm to 27 mm of mercury during heatup of the specimen and was maintained at that pressure for the remainder of the test. The specimen was then cooled and inspected for cracks or visual surface damage. Neither of the thermally cycled specimens showed any evidence of damage or cracking as a result of thermal stresses. Although the joints were not checked to determine if they maintained contact at the high temperatures, the behavior of the fasteners appears to be as expected.

● THERMAL CYCLE

    ● 2000° F FOR ONE HOUR

    ● .04 ATMOSPHERE PRESSURE

● SHEAR LOAD TESTS

SHEAR TEST SETUP FOR CARBON-CARBON LOW-THERMAL-STRESS JOINTS

For the shear tests, attachment brackets were bolted to each carbon-carbon sheet as shown in the sketch. The test specimen assembly was mounted in a hydraulic universal test machine and loaded in tension to failure at a constant displacement rate of 0.05 in./minute. The tension load applied a linear shear load through the center of the row of fasteners and failed the specimens in shear. The tests were conducted at ambient temperature and pressure. Load was recorded as a function of crosshead displacement using an X-Y recorder.

THERMAL-STRESS-
FREE FASTENER

TEST SPECIMEN

LOAD ATTACHMENT BRACKET
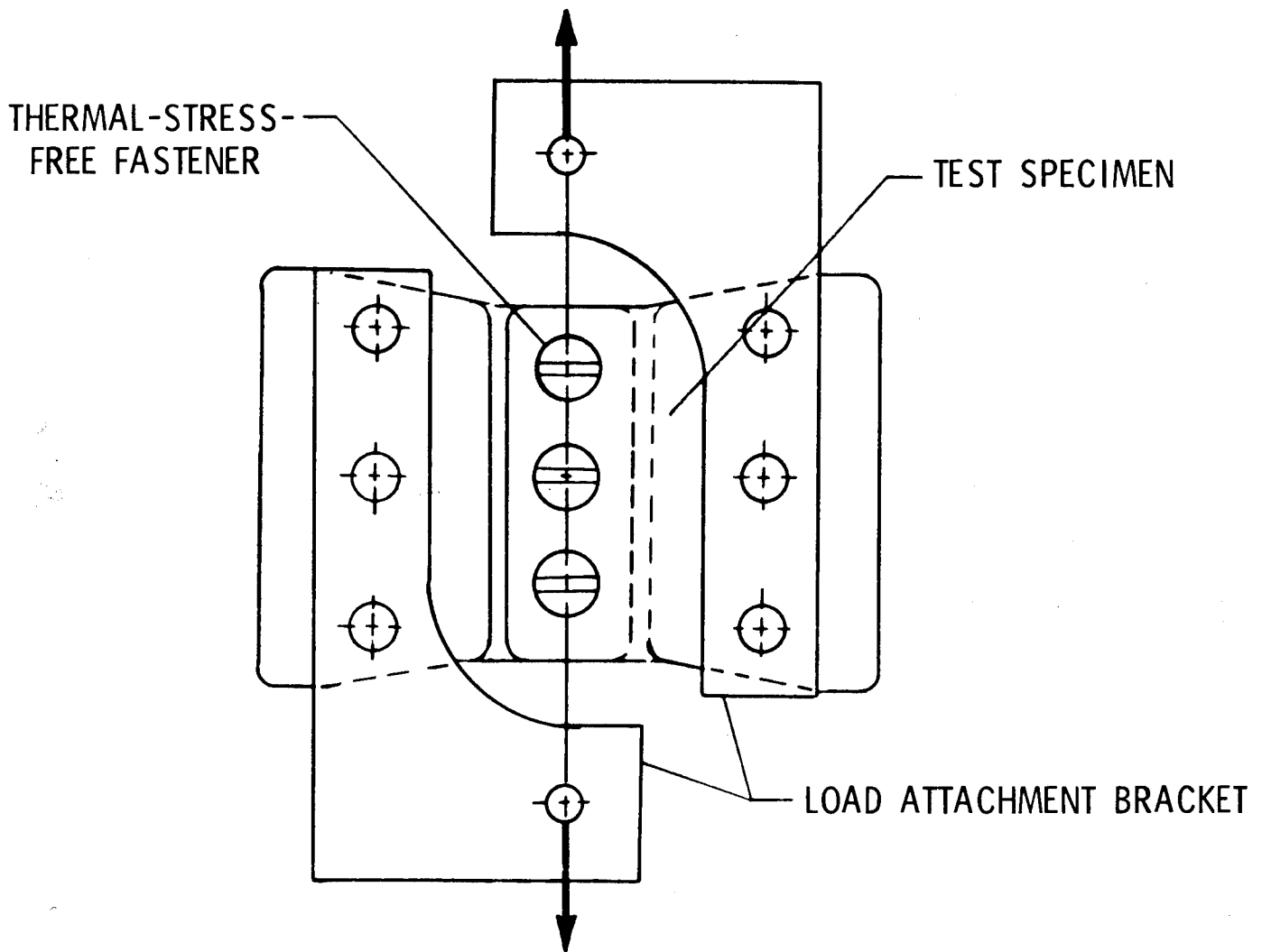
TYPICAL SHEAR FAILURE MODE FOR CARBON-CARBON
LOW-THERMAL-STRESS JOINT

A typical shear failure mode for the specimens is shown in the figure. Joint failure results in bulging of the carbon-carbon material near the conical bolt head and under the carbon-carbon washer, rotation of the fasteners, and cracking of the carbon-carbon washer.
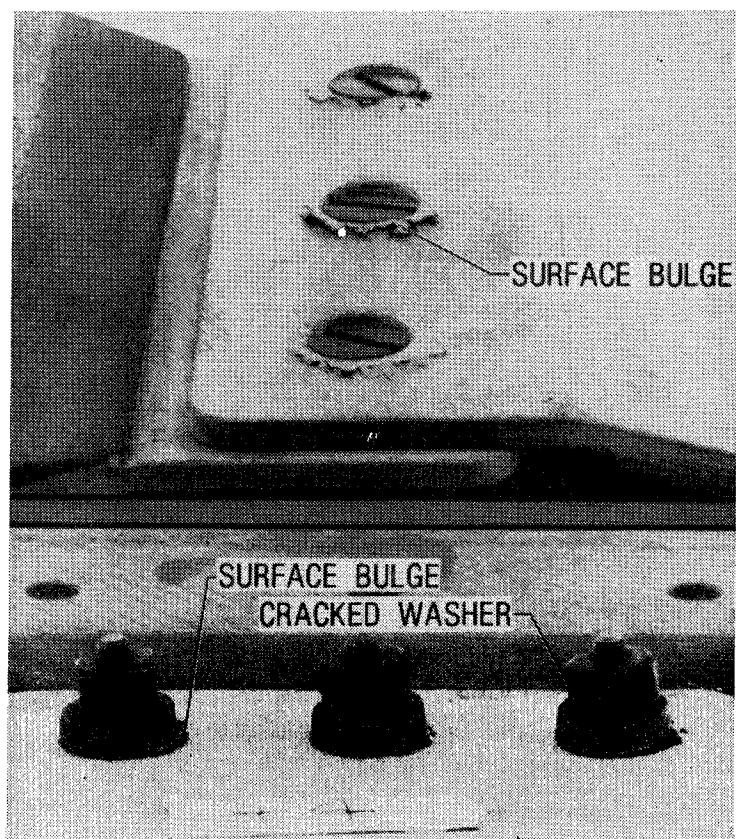
CROSS SECTION OF FAILED CARBON-CARBON LOW-THERMAL-STRESS JOINTS

The shear specimens all failed in the same manner. A cross-section view of a typical failed joint is shown in the photographs. Joint failure is thought to occur as follows: bearing failure occurs at the locations indicated by the arrow thus allowing fastener rotation and localized shear crippling failure to occur at the bearing failure points. Additional loading causes the failed zone to propagate circumferentially around the fastener and along a line from the bearing failure point to the free edge of the plate. Observation of the test indicates that the maximum strength of the joint is obtained approximately when the shear failure reaches the surface as indicated by a bulging of the carbon-carbon material near the head of the fastener and under the carbon-carbon washer. The displacement of the material under the washer applies a moment to the carbon-carbon washer until it cracks.
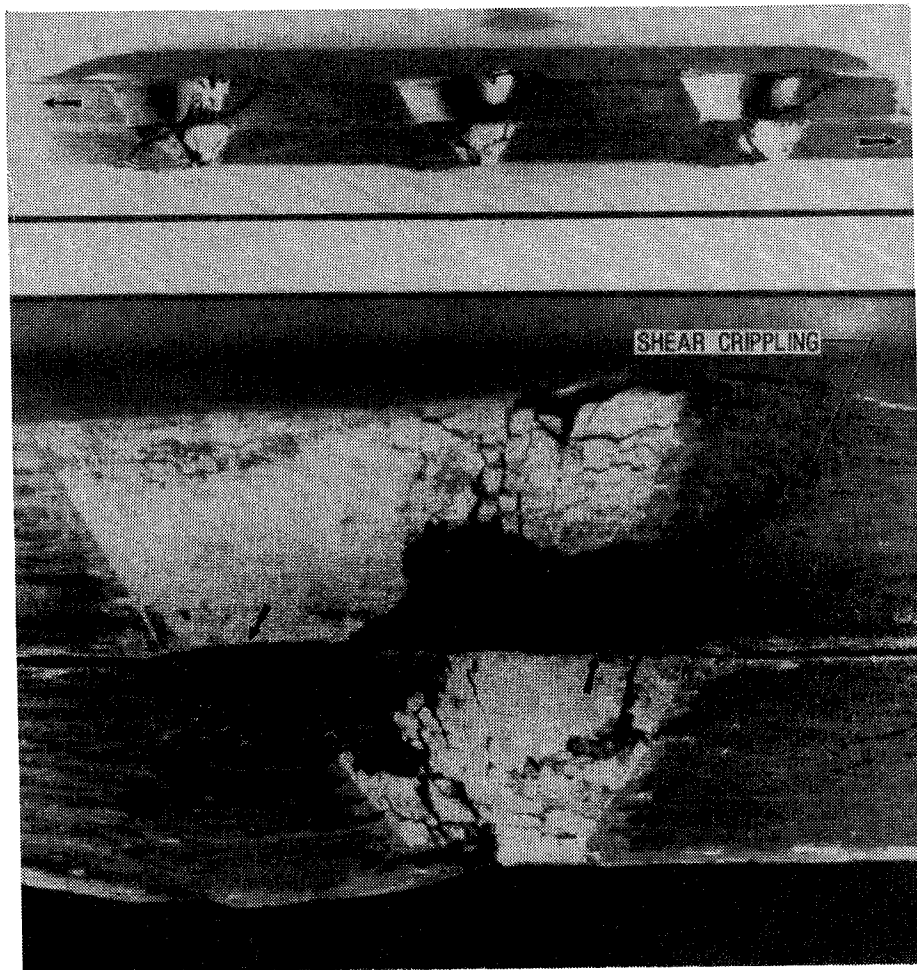
SHEAR STRENGTH OF CARBON-CARBON LOW-THERMAL-STRESS JOINTS

Relative shear strengths for the specimens are shown in the figure as a function of the number of plies in the plate subject to the highest bearing stress (thinner plate in each case). The solid line is a predicted bearing failure strength based on bearing ultimate strength obtained from cylindrical bolt bearing tests. The bearing failure criteria are reasonably accurate to predict the failure loads. For the thicker joints, the bearing failure criteria predict failure loads slightly higher than those obtained experimentally. Cross-section cuts through the center of the joint did not show any significant difference in failure modes for the different thickness specimens. The good agreement with the bearing failure criteria and the observed failure modes indicates that the low-thermal-stress joints have failure modes and strengths similar to conventional joints. One of the specimens that was thermally cycled was also tested to failure in shear at room temperature and is shown on the figure by the triangle symbol. Thermal cycling the joint did not have a significant effect on the joint strength nor on the failure mode.
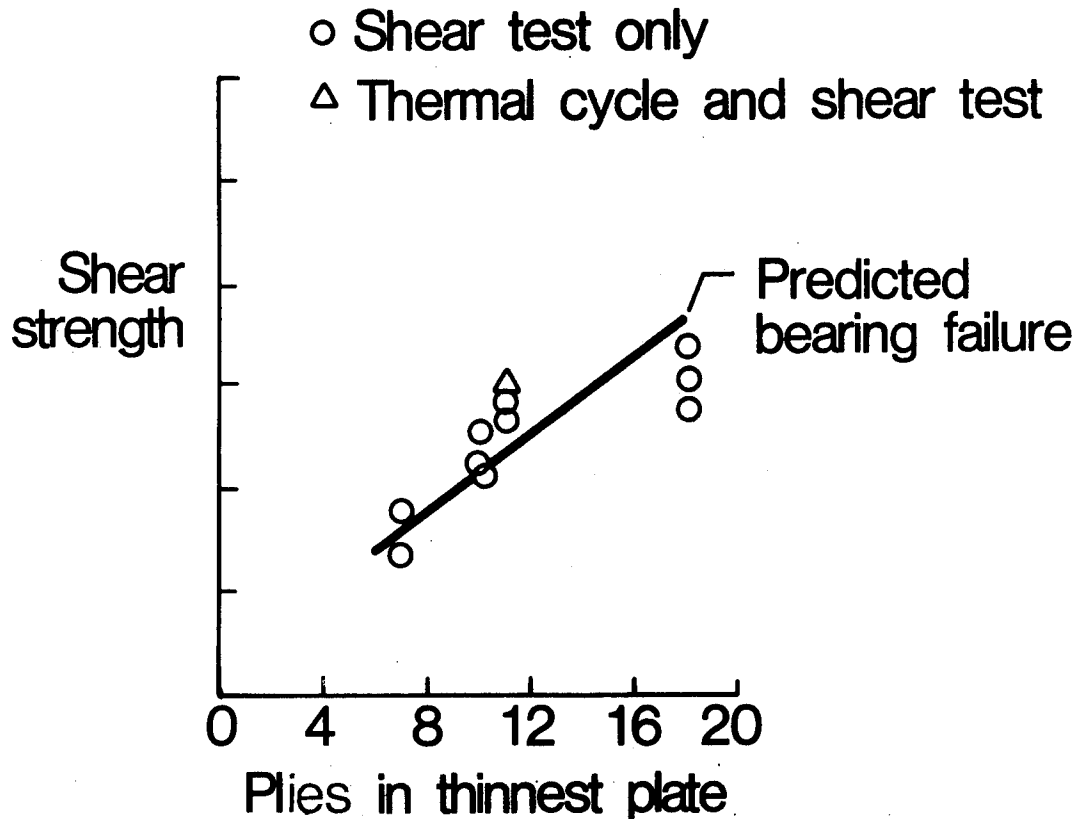
SUMMARY

Future aerospace vehicles must withstand high temperatures and be able to function over a wide temperature range. New materials are being developed for use in designing high-temperature lightweight structures. Due to the differences in coefficients of thermal expansion for the new materials and conventional high temperature metallic fasteners, innovative joining techniques are needed to produce tight joints at all temperatures without excessive thermal stresses. The thermal-stress-free fastening technique presented here can be used to provide structurally tight joints at all temperatures even when the fastener and joined materials have different coefficients of thermal expansion. The derivation of thermal-stress-free fasteners and joint shapes is presented for many combinations of fastener material and material being joined together. Approximations to the thermal-stress-free shapes that simplify the fastener/joint shape and that should result in joints with low-thermal-stresses are discussed. The low-thermal-stress fastener concept is verified by thermal and shear tests in joints using ODS alloy fasteners in carbon-carbon material. The test results show no evidence of thermal stress damage for temperatures up to 2000°F and the resulting joints carried shear loads at room temperature typical of those for conventional joints. Static failure strengths for the low-thermal-stress joints are predictable using bearing failure strengths and the failure modes are typical of those for conventional fasteners.

SUMMARY

- Thermal - stress -free fastener concept presented

- Fastener configuration determined by analysis

- Conical approximation to thermal - stress - free fastener shape
  with offset origin may be adequate for many materials

- Conical concept verified by thermal and shear tests

- Static failure strength of joints using conical fastener predictable
  using bearing failure strength

REFERENCES

1. Jackson, L. R.; Davis, Randall C.; Taylor, Allan H.; McWithey, Robert R.; Blosser, Max L.: DAZE Fastener, Inserts, Bushings. NASA Tech Brief LAR-13009, August 1983.

2. Blosser, Max L.; McWithey, Robert R.: Theoretical Basis for Design of Thermal-Stress-Free Fasteners, NASA TP-2226, November 1983.

3. Sawyer, James Wayne: Experimental Evaluation of Thermal-Stress-Free Fastening Technique for Two-Dimensional Carbon-Carbon Structures. Presented at Fifth JANNAF Rocket Nozzle Technology Meeting, Colorado Springs, Colorado, Dec. 6-8, 1983.

EXPLOSIVE WELDING IN THE 1990'S

Narain S. Lalwaney and Vonne D. Linse

Battelle's Columbus Laboratories
505 King Avenue
Columbus, Ohio 43201

INTRODUCTION

Explosive bonding is a unique joining process with the serious potential to produce composite materials capable of fulfilling many of the high-performance materials needs of the 1990's. The process has the technological versatility to provide a true high-quality metallurgical bond between both metallurgically compatible and incompatible systems. Metals routinely explosively bonded include a wide variety of combinations of reactive and refractory metals, low and high density metals and their alloys, corrosion resistant and high strength alloys, and common steels. The major advantage of the process is its ability to custom design and engineer composites with physical and/or mechanical properties that meet a specific or unusual performance requirement. Explosive bonding offers the designer unique opportunities in materials selection with unique combinations of properties and high integrity bonds that cannot be achieved by any other metal joining process.

Twenty years have passed since the explosive bonding process was first commercialized. While its true potential has already been demonstrated in many instances as much as 15 years ago, it has not been extensively utilized. The explosive bonding process has simply not lived up to its expectations or technological potential. Instead of being the $200 million/yr full-fledged high-tech, high growth industry of the 1980's as predicted, it has become a marginal industry at best with annual domestic sales stagnated at less than $10 million and no projected breakthroughs in sight. In addition to the chemical process industry where it has found its greatest use, explosively bonded products were projected to find extensive use in the high performance aerospace and defense related materials needs of the 1970's and 1980's. These projections have not materialized. In modern times, no other industry has developed so much technological content with so little commercial success.

The failure of the explosively bonded product to live up to its expectation may be attributed to a number of reasons. It is the intent of this paper to discuss in some detail the reasons for the limited acceptance of the process and the steps that will be required for it to gain wider acceptability in the 1990's commensurate with technological capability. Initially, the process mechanism will be very briefly

reviewed and its applications to date outlined to provide an understanding of the nature of the process and its potential.

Explosive Bonding Process

In literature as well as this paper, the terms "explosive bonding", "explosive welding", and "explosive cladding" are used synonymously. The fundamentals of the process are well understood. The process is basically simple and only the rudiments are presented here. Excellent review articles[1-4] are available for those interested in more details .

A typical setup for explosive bonding is shown schematically in Figure 1a. The explosive is placed in a layer usually in direct contact with the upper or exposed surface of the prime or cladding component. The opposite or bonding surface of the cladding component is then placed at a specified distance above the surface of the base component to which is is to be bonded. This separation is usually known as the "standoff gap". For most explosive bonding operations, particularly large plate cladding, this gap is usually constant over the entire area being bonded.

The mechanisms that occur during the actual bonding event are shown schematically in Figure 1b. As the detonation front in the explosive passes over the surface of the cladding component, the pressure and expanding gases combine to bend and accelerate the cladding component across the standoff gap toward the base component at a high velocity. The high velocity cladding component then impacts the base component at an angle generating extreme localized pressures at the collision point which are several orders of magnitude above the yield strength of both metals being welded. Under the influence of this high pressure, angular collision, the surrounding metal surfaces act as viscous fluids around an obstacle and a few microns of the component surfaces are jetted into the standoff gap ahead of the progressing collision point. The jet consists of a combination of surface contaminants, a few microns of the metal surface layers, and compressed air. As the detonation progresses, the jet travels ahead of the collision point sweeping the contaminants from the surfaces. This enables the the two cleaned metallurgical surfaces to come into intimate contact under extreme pressure at and behind the collision point and become bonded due to interatomic forces. The collison is characterized by the collision velocity (V_c) and the collision angle (0). There is a critical collision velocity below which no bonding occurs and similarly a minimum collision angle below which no jetting will occur regardless of the collision velocity.

There is no heat associated with the process other than that generated by the plastic working near the interface and the adiabatic compression temporarily imposed on the metals. Since the process is almost instantaneous, no diffusion takes place. Therefore, explosive bonding can directly join dissimilar, metallurgically incompatible and reactive metals without the significant formation of intermetallic compounds that are harmful to the properties of the bond and the ultimate performance of the composite.

Most explosively bonded composites have a wavy bond zone that can be explained on the basis of hydrodynamics. A flat bond zone is indicative of a bond being made at the lower limits of collision energy and has the potential to display marginal and/or nonuniform properties. When properly made, the bond strength is normally equal to or slightly greater than the weaker of the two components being bonded. Figure 2 shows a typical explosively bonded interface between commercially pure titanium and steel in which the small amount of brittle iron-titanium intermetallic that exists is isolated in small areas that are surrounded by ductile direct bond. Closer examination of the bond interface usually reveals that the weld is a combination of direct weld on the crests and in the valleys of the waves, and intermittent pockets of trapped jet material on the front and back slopes (Figure 3). Figure 4 similarly shows a wavy interface in aluminum/magnesium alloy with pockets of entrapped jet material near the crests. Depending on the energy input into the bond, the trapped jet pockets will range from a mechanical mixture of the two materials being bonded to a totally melted and solidified structure. Excessive energy inputs during bonding with resultant excessively large jet pockets typically produce bonds with less than optimum properties.

Present Applications

Since its initial commercialization in the mid 1960's, the flat-plate cladding applications grew rapidly until the early 1970's and then leveled off. From 1970 onward, most new applications were in the area of specialty products other than flat plate configurations.

Flat-Plate Clads

The largest and most extensive commercialization to date of explosively bonded products has been in the form of flat-plate clads which are subsequently fabricated into a structure. The most important application has been in chemical process pressure vessels. Commercial applications can be broadly divided into the following three categories:

1. Pressure Vessels

     Products: Ti/steel, Zr/steel, Ta/steel, Inconel/steel, Hastelloy/steel (Figures 5 and 6)

     Industry: Chemical process industry

2. Tube Sheets for Heat Exchangers

     Products: Ti/steel, Inconel/steel, stainless steel /steel, bronze/steel (Figure 7)

     Industry: Chemical process industry

3. Transition Joints

Products: Al/Al/steel (Figure 8)

Industry: Shipbuilding-structural transition joints for
both new construction and repair work

Products: Cu/Al

Industry: Electrorefining industry

In the chemical process related industries, the major
applications have been for corrosion resistant clads in pressure
vessels and tube sheets for heat exchangers. The corrosion resistant
clad is almost always bonded onto a steel backer which becomes the
pressure carrying component of the vessel or tube sheet for these
applications. This process has made it possible to economically use
expensive, high-density metals such as tantalum for a tantalum/copper
clad steel pressure vessel in the recovery of chlorine from HCl at
higher temperature and pressure.

In the shipbuilding industry, aluminum alloy/aluminum/steel
structural transition joints replace bolted or riveted aluminum/steel
joints thus avoiding crevice corrosion. The aluminum part of the joint
is then conventionally welded to the aluminum superstructure and the
steel part is welded to the steel decking/coaming. Similarly
copper/aluminum and aluminum/steel transition joints are used in the
electrorefiniong industry to replace bolted/riveted joints in high
current density systems.

Other applications of explosively bonded flat plate product
have been for stainless steel clad steel boiler plates in the nuclear
industry and helium leakproof tubular transition joints of
aluminum/stainless steel with either titanium or silver interlayers
for cryogenic applications.

Cylindrical Products

Up to now the use of explosively clad cylindrical products has
been customized and not widespread. Several industries have used both
small and large diameter explosively clad titanium/steel, stainless
steel/steel, and Inconel/steel concentric cylinders. In other cylin-
drical configuration applications, direct explosively bonded alumi-
num/steel tubular transition joints in various diameters such as shown
in Figure 9 are made by overlap cylindrical bonding techniques and
being used in significant numbers in the nuclear industry. The joining
of large sections of oil and gas pipelines, 36, 42, and 48 inches in
diameter, by explosive welding has been successfully developed and
placed into commercial application.[5]

126

Specialty Products

Multilayer laminates of three or more layers of metals explosively bonded together have been used for various applications such as coinage stock, condensers, electrodes, etc. Figure 10 shows one such configuration of thirteen explosively bonded 1/8-inch-thick layers of Alclad aluminum. With the explosive bonding process, laminate structures can be designed with specific combinations of metals and layer thicknesses to modify or control heat/electrical conduction properties or to improve fracture toughness or fatigue crack arresting capabilities.

The repair and buildup of worn flat and cylindrical components is another specialty area of explosive bonding that has not been utilized to its full potential. Figure 11 shows an explosively welded repair buildup sleeve over the remachined worn area of a high speed turbine shaft.(6)

In Europe, explosive bonding is used to simultaneously bond tubes into tubesheets in the fabrication and retubing of heat exchangers, in lieu of conventional welding where seal welds are required. This application has not yet gained wide acceptance in the United States where the use of explosives to expand but not weld tubes into tubesheets has been used successfully for quite some time. Explosive bonding is used for plugging leaky tubes during heat exchanger repairs in both the United States and Europe.

Present Status

The entire explosive metalworking or fabrication area (bonding, forming, powder compaction, etc) has experienced relatively little commercialization of its products with respect to its overall potential. The reasons for this lack of use vary depending on the process. The most serious lack of use with respect to its overall potential in the technological and manufacturing community to date however is explosive bonding. The basic understanding of process fundamentals and manufacturing procedures for making high quality explosively clad product has been thoroughly established and is available. Well over 300 similar and dissimilar combinations of metal and their alloys have been explosively bonded and many more are capable of being bonded if the need arises. Yet, explosive bonded materials are seemingly used only as a last resort, with those systems that have been commercialized being ones that cannot be produced by any other joining technique.

The major reason for the lack of use of explosively bonded products is graphically illustrated in Figure 12. Large engineering/informational gaps exist between the three major components that are involved with the explosively bonded product throughout its life. As a result the growth potential of the product has not been realized.

The user typically specifies the material in terms of type, properties, sizes, etc that he desires for his end product based on his need and the available information and design data for the material. The greatest area of deficiency is the almost total lack of good

design support data and information on explosively bonded product that are universally available for the end user to input to his design and materials selection. As a result, only a few large repetitive end users are cognizant of the product and its capability and have consistently utilized the product.

The large chemical companies in the U.S. and abroad have treated explosive bonding and its product as an extension of their explosive product lines rather than treating it as an entity of its own. They have incorporated these products into their own designs only after expending large engineering efforts to evaluate clad materials, establish their own user criteria, and work out fabrication and repair proceedures for use by the fabricators. The information created thus becomes proprietary and not available for general use by industry.

Fabricators in the past have had little or no information made available to them from either the end user or the material manufacturer on how to fabricate explosively bonded product into an end product such as a pressure vessel. The responsibility for developing these fabrication procedures has thus fallen to a few custom fabricators who do little process designing. Once again the fabrication proceedures developed become very specialized and propietary and not always technically and economically the most effective.

The materials/clad manufacturers provide guidance/information only as to the bond integrity and strength of the product which they manufacture. None possess the facilities for intermediary processing of the clad product such as hot/cold conversion rolling, extrusion, etc., to enhance its technical quality and/or its economical attractiveness. The intermediary processing requires a much higher level of technology than the simple forming of plates during standard fabrication. The availability of this technology is very restricted and supplied mostly through the clad manufacturer. It is therefore either very expensive or oftentimes unavailable because the technology does not exist. Again much of the property data and secondary processing information on explosively bonded products has become propietary to the materials manufacturer and is not available on a general basis.

Until recently, there has been no attempt to bridge these engineering/informational gaps between the three major components so the potential end user can select and utilize explosively bonded products to their fullest potential.

Future Opportunities

Mechanistically and parametrically, the explosive bonding process is well understood; therefore, the basic, fundamental research and development on the process is primarily behind us. Likewise the previous restrictions to market entry into the field imposed by basic patent protection or any other barriers have now disappeared. Urgently needed is market development via new thrusts into application areas where the need for composite materials having unique properties or performance capabilities is present. The development of process technology and material data and information that will be readily

128

available to all who need it for these new markets will be the overriding factor is the future implementation of explosive bonding.

There are several areas of opportunity for explosively bonded products that hold considerable promise and need to be addressed:

- Very lightweight/high strength composites for application in both aircraft frame and engine components and land vehicles.

    Examples: aluminum/titanium, beryllium/titanium, aluminum/magnesium

- Thin composite foils for the electronic and areospace industries.

    Examples: multilayer composites of a number of metals having the combined desired properties explosively bonded and susequently conversion rolled to the desired foil thickness.

- Multilayer composites that provide the proper combination of densities and strengths, with the added benefit of significantly improved fatigue and fracture toughness properties.

- Advanced composite materials for neutron capture/impermeability in managing nuclear wastes.

- Remote joining of metals in hostile, hazardous, or inaccessible areas such as nuclear reactor repairs, underwater welding, or assembly of structures in earth orbit or space. Such an application with seam welding has been demonstrated. [7]

- Repair and renovation of worn or damaged parts or components especially in situ will become more popular as materials and new replacement parts become more expensive. The costs of critical materials, although stable at present, are subject to significant increases in the future depending on the world political situation. An example is such as those in Africa where the major supplies of the raw materials for many of our critical metals are located.

Needs of the 1990's

A number of critical aspects of the explosive bonding area must be addressed in the remaining years of the 1980's in order that the process and its products will be ready to meet the high tech materials requirements of the 1990's. These aspects include:

- Create reliable design data that is readily available and easy to disseminate to those who need it. The data base should include representative mechanical and physical properties for each material system along with typical applications, fabrication methods, repair procedures, etc. This will help the designing engineer to consider and employ new materials. The data base should be continuously expanded to include new materials which can be produced but are not presently being commercialized.

- Develop more meaningful product specifications and testing methods (user friendly) so that potential users can easily establish their own criteria to better meet their needs. Present specifications like shear tests, etc., as standards for acceptance in many cases are not realistic from the user's viewpoint.

- Provide innovation into high tech, high performance materials through innovations in the explosive bonding process. One potential area is in the welding of very high strength, low impact materials which are susceptible to fracture during bonding at room temperature. The basic feasibility of using elevated temperature bonding has already been demonstrated as one solution to this problem.

- Reduce the costs to the end user. Not only is the explosive bonding process presently expensive but the cost of susequently fabricating the product is also expensive. From the explosive bonding viewpoint, the cost of the bonded product is proportional to the area clad. The cost of bonding can be considerably reduced in many instances by cladding thicker components and subsequently rolling flat-plate clads or extruding clad cylinders to increase the bond area and thus reduce its unit cost.

  In fabrication, the cost can be considerably reduced by developing better and more economical techniques for joining or welding clad components. For example, the cost for joining titanium/steel clads in the fabrication of pressure vessels can run as much as $150/linear foot while that for joining tantalum/copper clad steel may run to $300/foot. Reducing the amount of welding by simply increasing the initial overall size of the bonded plate would bring significant fabrication savings. Oftentimes the thickness of the composite bonded plate, both clad and base, is significantly greater than necessary. Reduction of the thickness along with improved fusion welding techniques to handle it would also help to further reduce the overall costs of the process. In many instances such as titaniun/steel composite, the clad may be as much as three to five times as thick as necessary for corrosion protection

only because the technology for fusion welding it in thinner layers does not exist.

NEW DEVELOPMENTS

There are several recent developments that suggest the industry may be undergoing some change in the near future.
For example:

1. Several large metallurgical companies, both domestic and foreign, are looking seriously at the potential U.S. explosive metalworking market with several captive inhouse and export applications in mind now that there are no market barriers.

2. Serious and increasing Soviet effort in the high energy rate fabrication field is under way in several institutions. Some of these are solely devoted to explosive metalworking with potential military applications. Our own defense needs will have to keep these developments under scrutiny.

3. Battelle recently announced the opening of an explosive metalworking application center at Columbus, Ohio to bridge the information/engineering gaps discussed above.

4. The Center for Explosive Technology recently opened at the New Mexico Institute of Mining and Technology.

These activities suggest a new era of activity in the explosive fabrication field. If successful, these developments could lead to new commercial applications that will once again produce growth within the industry.

ACKNOWLEDGEMENTS

REFERENCES

1. "Explosive Welding", Metals Handbook, Ninth Edition, Vol 6; Welding, Brazing, and Soldering, American Society of Metals, pp 705-718.

2. G. R. Cowan, O. R. Bergman, A. H. Holtzman, "Mechanism of Bond Zone Wave Formation in Explosion-Clad Metals", Metallurgical Transactions, Vol. 2, November, 1971.

3. V. D. Linse and N.S. Lalwaney, "Explosive Welding", Journal of Metals, Vol 36, No. 5, May, 1984, pp 62-65.

4. B. Crossland, "Review of the Present State-of-the-Art in Explosive Welding", Metals Technology, January, 1976.

5. Method of Welding Pipe Sections with Explosives", U.S. Patent #4,231,506, November 4, 1980.

6. "Explosion Welding", Welding Handbook, Seventh Edition, Vol. 3, American Welding Society, pp 263-278.

7. L. J. Bement, "Practical Small-Scale Explosive Seam Welding", Mechanical Engineering, September, 1983.
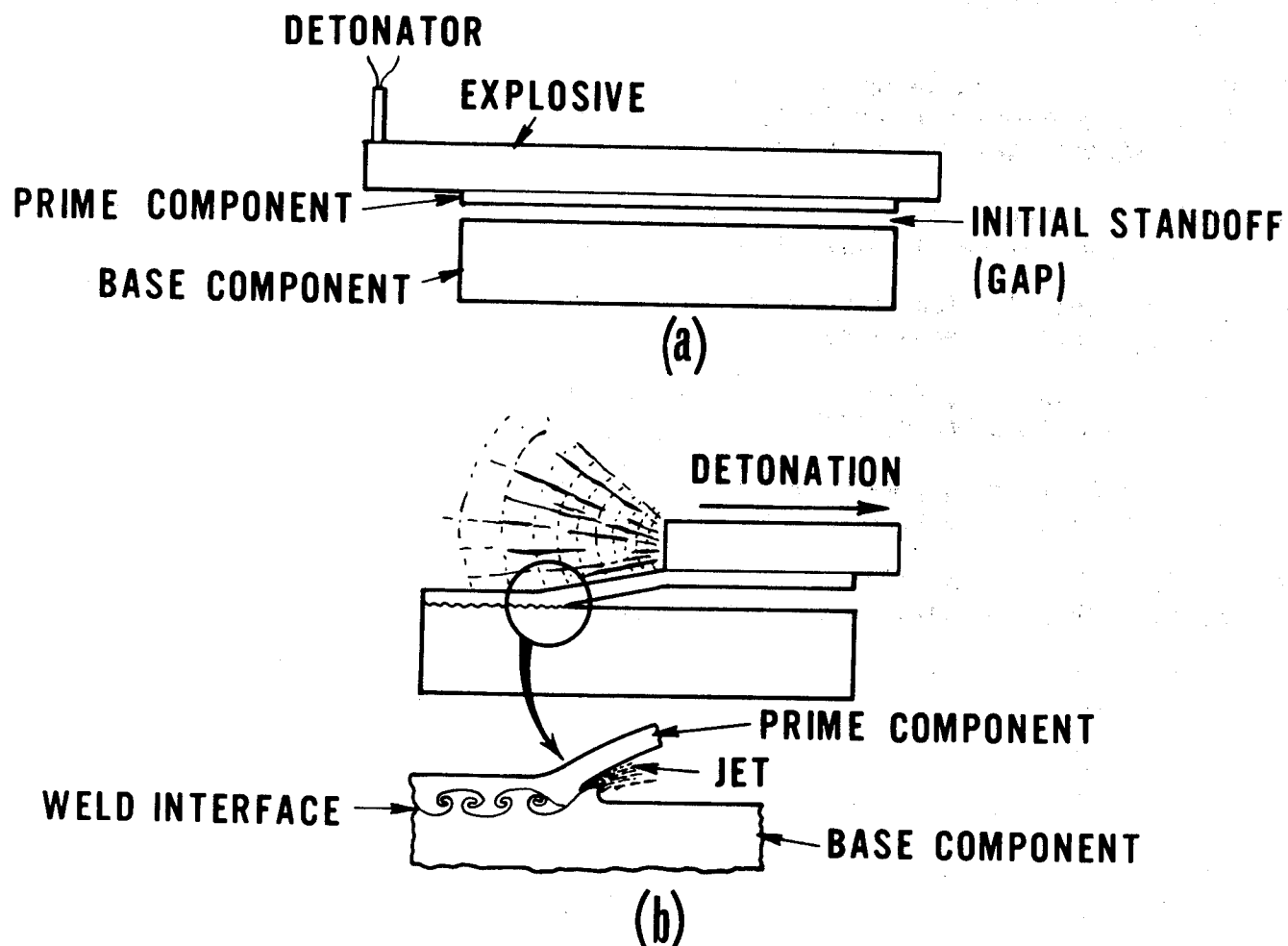
FIGURE 1. SCHEMATIC OF EXPLOSIVE BONDING PROCESS
(a) SETUP (b) PROCESS MECHANISM
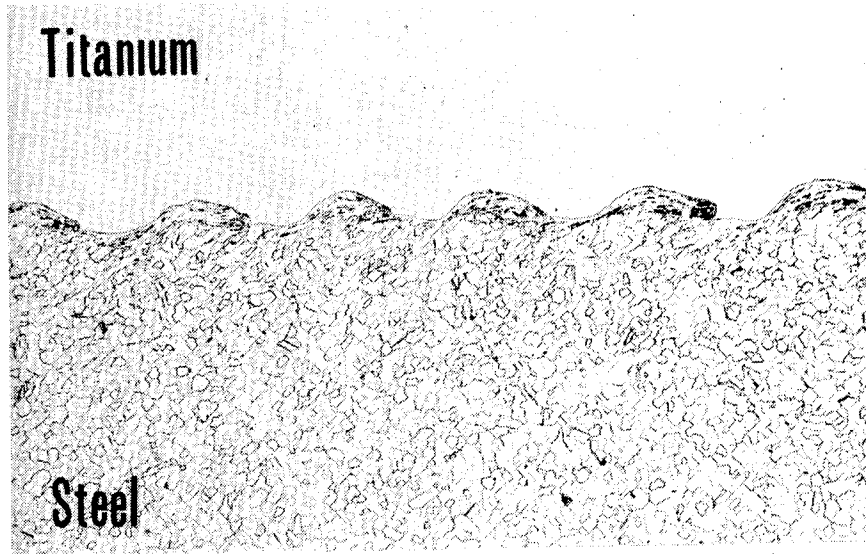
FIGURE 2.   PHOTOMICROGRAPH OF A SKEWED WAVE PATTERN
IN MISMATCHED SYSTEM OF TITANIUM (TOP)
TO LOW CARBON STEEL (BOTTOM).   100 x.
(LOW DENSITY/HIGH DENSITY) SYSTEM
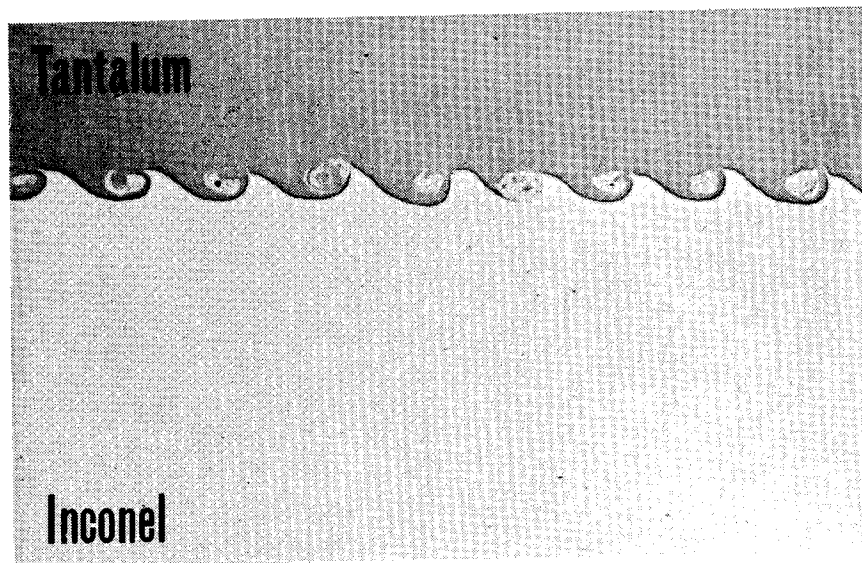
FIGURE 3.   EXPLOSIVE WELD BETWEEN TANTALUM AND
INCONEL SHOWING POCKETS OF ENTRAPPED
JET MATERIAL (50 x)
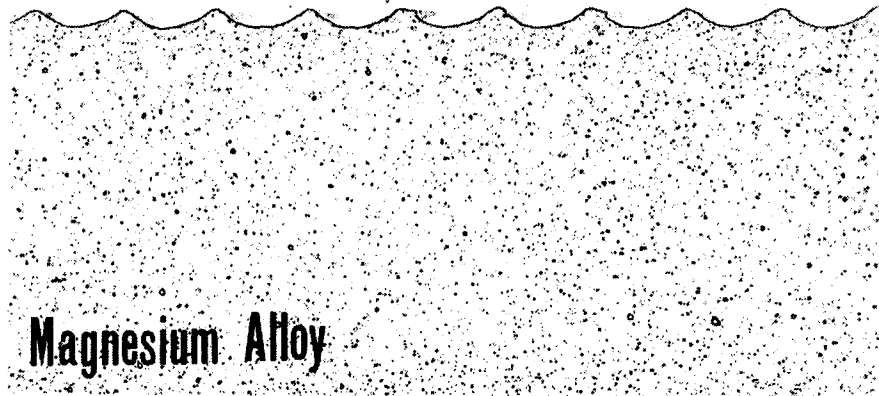
FIGURE 4. EXPLOSIVE WELD BETWEEN ALUMINUM 1100 (TOP) AND MAGNESIUM ALLOY SHOWING POCKETS OF ENTRAPPED JET MATERIAL. (VERY LOW/VERY LOW DENSITY) (20 x)
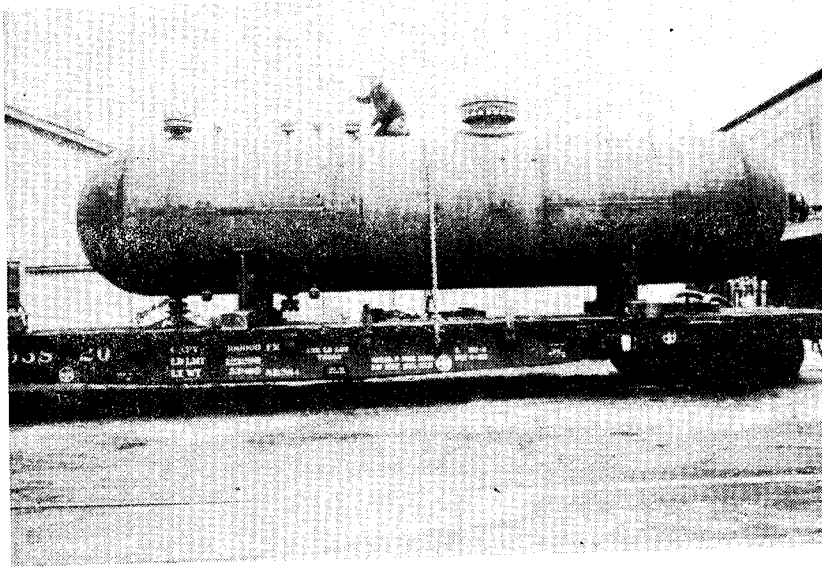
FIGURE 5. TITANIUM/STEEL PRESSURE VESSEL MADE
FROM EXPLOSIVELY BONDED CLAD PLATE
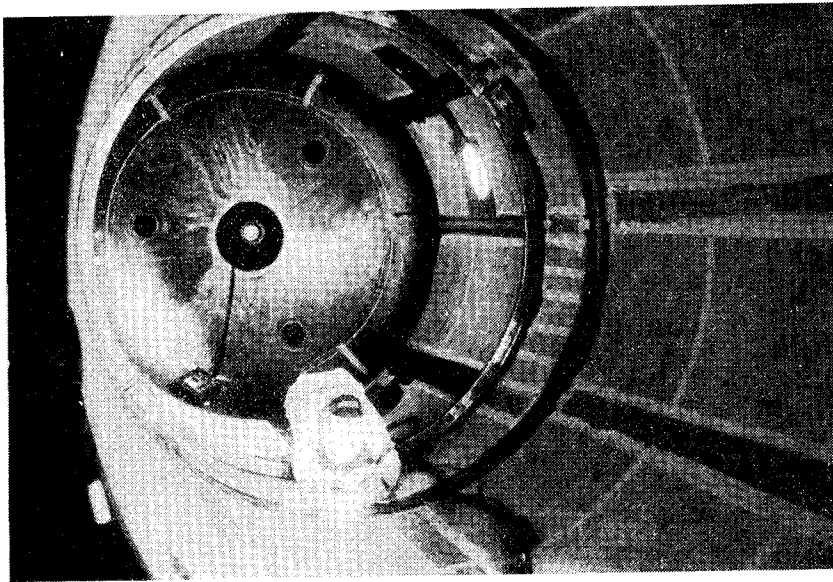
FIGURE 6. INTERIOR OF 8 BY 60 FT. DIAMETER VESSEL
FABRICATED FROM EXPLOSION-CLAD TANTALUM
TO COPPER TO CARBON STEEL
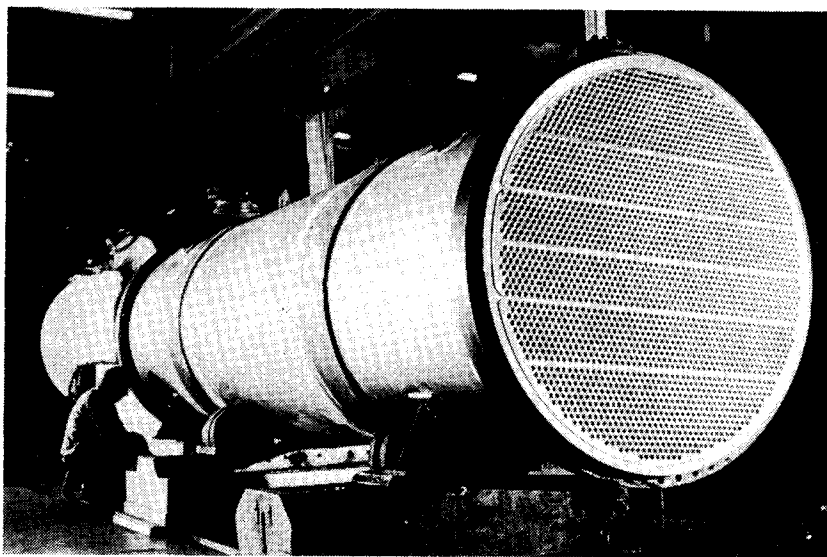
FIGURE 7.   TITANIUM TUBE SHEET EXPLOSIVELY BONDED
            TO MONEL 400
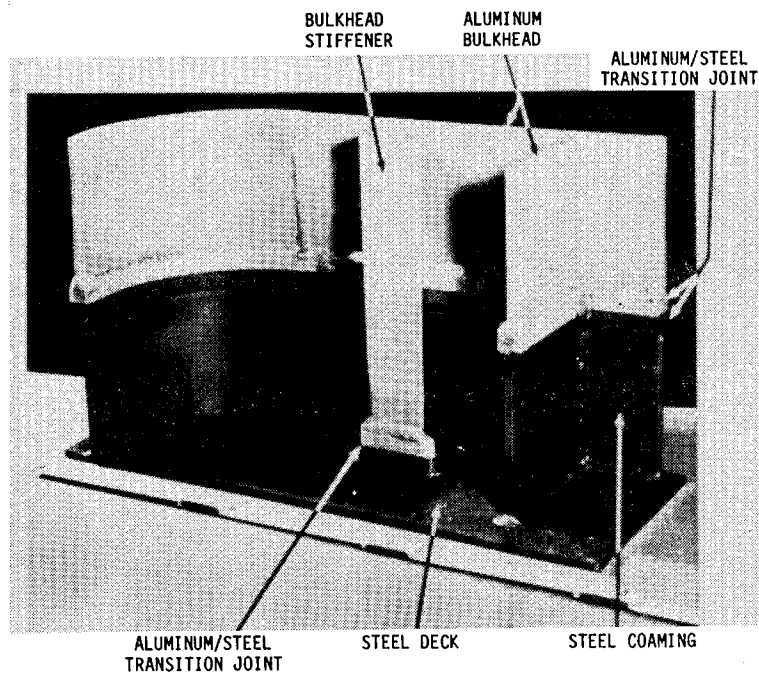
FIGURE 8. ALUMINUM SUPERSTRUCTURE AND STEEL
DECK CONNECTION USING A1/A1 STEEL
TRANSITION JOINT
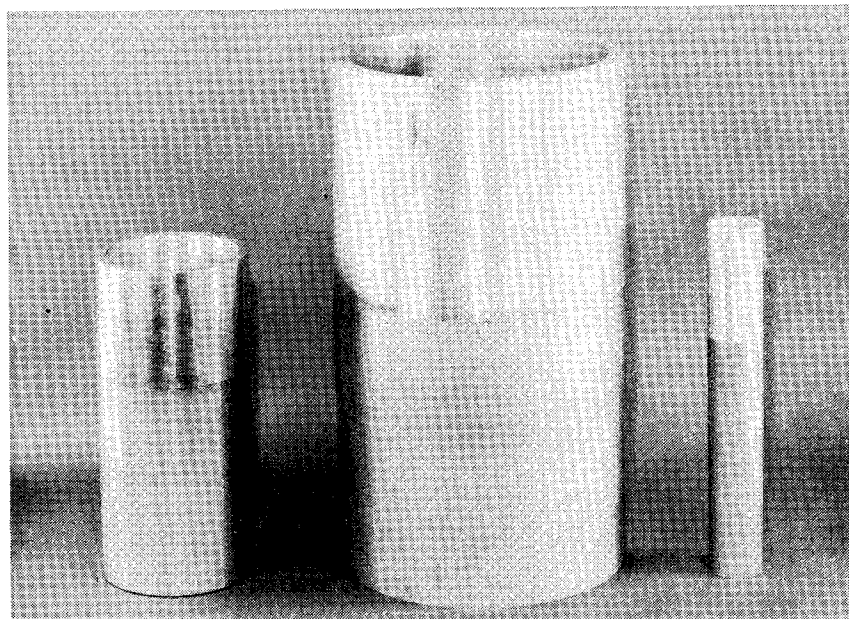
FIGURE 9. EXPLOSIVELY WELDED ALUMINUM-STEEL
TUBULAR TRANSITION JOINTS
(NOMINAL DIAMETERS LEFT TO RIGHT,
6, 12, AND 2 IN.)

138
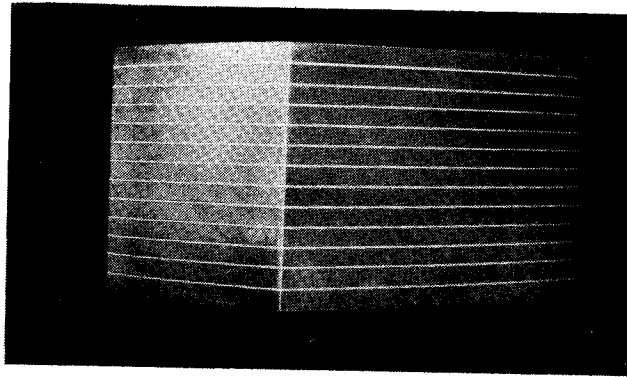
FIGURE 10. MULTILAYER LAMINATE OF
EXPLOSIVELY WELDED
ALCLAD 6061-T6 ALUMINUM
LAYERS (TOTAL THICKNESS
4.1 cm)
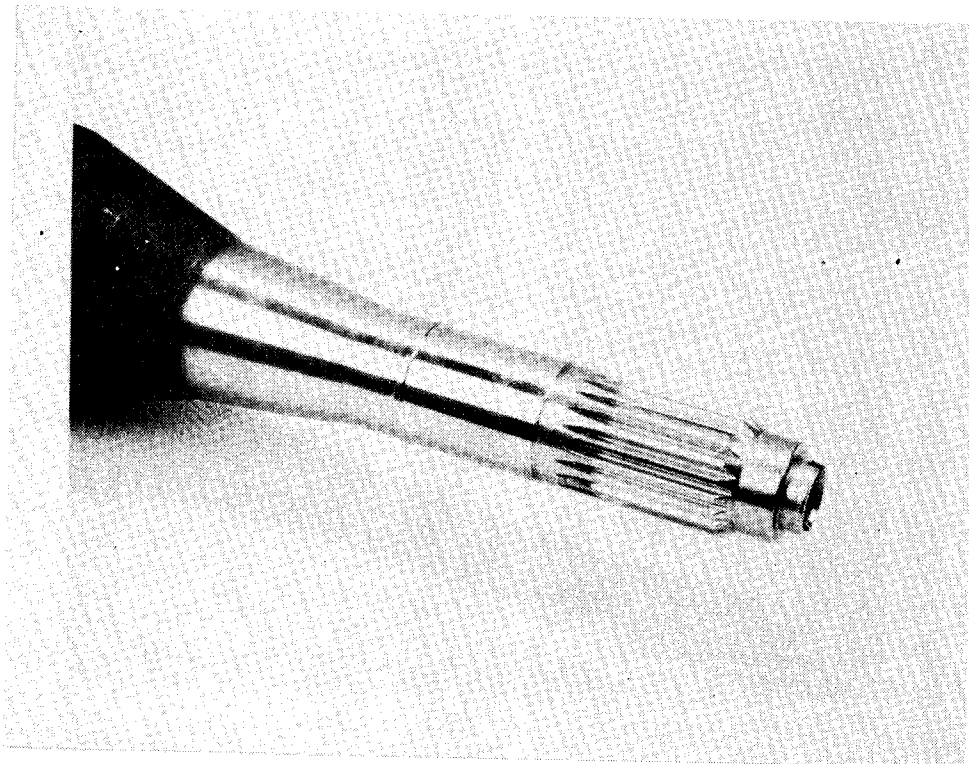
FIGURE 11. EXPLOSIVE WELD REPAIRED BEARING JOURNAL
ON HIGH-SPEED TURBINE SHAFT
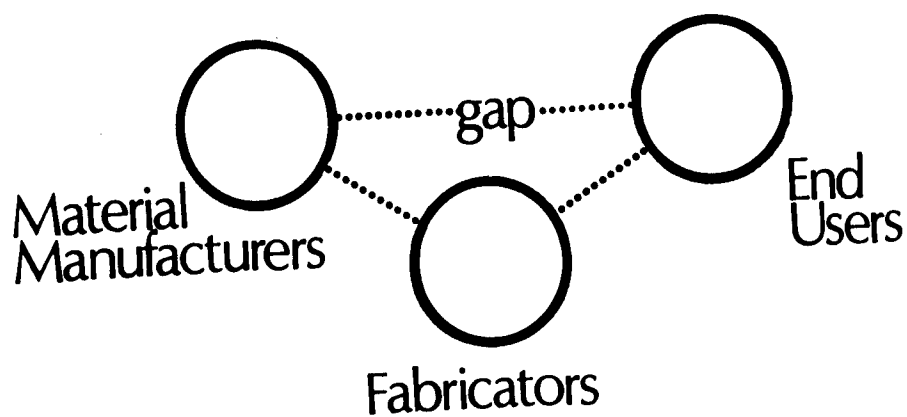
FIGURE 12. ENGINEERING/INFORMATIONAL GAPS BETWEEN ALL
COMPONENTS OF EXPLOSIVE METALWORKING
INDUSTRY

EXPLOSIVE WELDING OF TUBULAR CONFIGURED JOINTS
FOR CRITICAL APPLICATIONS

Roy Hardwick
Explosive Fabricators, Inc.
Louisville, Colorado 80027

ABSTRACT

Explosive welding can provide the answer to problems of permanently joining metals typically used in the aerospace industry.

The explosive bonding process is a solid state bonding process enabling material incompatibility problems associated with fusion welding to be overcome. In addition, heat affected zones are eliminated thus enhancing joint strength, properties and performance.

The process requires the parts being joined to be impelled, by means of explosives, to collide with each other. Certain critical collision parameters must be met and controlled and these parameters are defined. Various component geometries which satisfy the collision parameters are described.

Examples of transition joints used in the aerospace industry are described and illustrated.

INTRODUCTION

Metallic components used in the aerospace industry are often required to be permanently joined together. The materials of construction, however, are quite varied and are often incompatible for fusion welding. In demanding environmental situations of thermal or fatigue cycling, it may also be desirable to avoid the use of fusion welded joints because of their inherent strength limitations. These limitations are associated with the cast structure and heat affected zones of the fusion weld.

Explosive welding can provide an answer when fusion welding should or must be avoided.

Explosive welding has been used primarily for the construction of flat plate clads and much of the technology is derived from this source. A second common application of the technology is the explosive welding of heat exchanger tube/tubeplate joints. Such joints are tubular in section. The combination of these two technologies permits methods of producing tubular transition or coupling joints to be devised. Such tubular configured joints represent a large number of metal joining requirements in the aerospace industry.

The unique welding mechanism and weld properties make the explosive welding process extremely useful for aerospace applications.

a) Unlike fusion welded joints, the weld area can be several times the tubular wall thickness.

b) The joint is stronger than the parent metal.

c) Being a solid state bonding process, dissimilar metals of widely differing melting points can be welded.

d) Metal combinations which cannot be fusion welded due to the formation of brittle intermetallics can be welded by explosive welding techniques.

e) There is no cast structure within the joint, nor are there any heat affected zones.

f) There is no dilution of the alloys at the interface.

Cladder Metal

Metal Jet

Pressure Isobars

Unburnt Explosive

Surface layer which becomes entrained in the jet.

Backer Metal

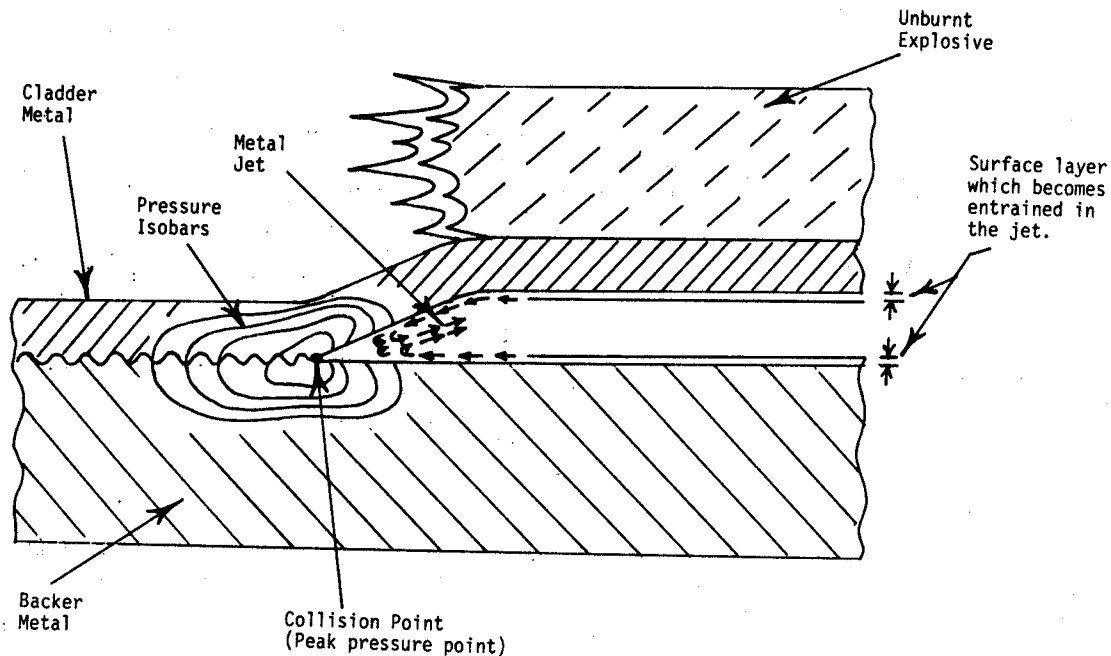Collision Point (Peak pressure point)

FIGURE 1

g)   No filler metals are required.

h)   Once the correct welding parameters are established, the process is highly reproducible given reasonable levels of quality control.

Because of these numerous advantages, an increased level of interest is being shown by the aerospace industry in producing explosively welded joints.

FUNDAMENTAL REQUIREMENTS FOR EXPLOSIVE WELDING

Explosive welding requires certain geometrical dispositions of the component parts to be joined. This is because the parts must be thrust together by the explosion, during welding, to cause collision of the parts in a very precise and controlled manner. These collision parameters, though critical, are highly reproducible and are as follows:

a) The two surfaces to be joined must be brought together progressively over their surface area.   This will produce a collision front which traverses the two surfaces (Figure 1).

b) The collision front must travel at a velocity below the sonic velocity of the materials being joined. This will allow the associated pressure front to precede the collision front. As a result, the two approaching metal surfaces are subjected to an increasing pressure, culminating at a peak pressure on impact at the collision front.

c) The peak pressure at the collision front must significantly exceed the yield strength of the materials being joined. Plastic deformation of the component surfaces will then occur.

Provided the above requirements are met, the plastically deformed surfaces are projected forward into the lower pressure area of the interfacial gap ahead of the collision front. A jet is thus formed from the component surfaces which includes the surface oxides and other surface contaminants originally present. This jet precedes the collision front to be finally ejected from the interfacial gap. By this mechanism the surface contaminants are removed ahead of the collision front allowing the cleaned surfaces to be brought together in the solid state and under pressure. A bond is then formed due to inter-atomic attraction, or electron sharing, at the interface.

The depth of surface removed into the jet is a function of collision pressure; the greater the pressure, the greater the layer depth removed. The collision pressure is itself a function of cladder momentum and, as such, the controlling variable is the explosive load. It is desirable to minimize the explosive load for several reasons and consequently the level of contamination upon the surfaces prior to welding must be minimized to ensure it is fully removed into the jet. Similarly the surface topography must be closely controlled to ensure surface inperfections and machining marks are minimized to a degree where they also are within the layer depth removed by the jet. In practice, the surfaces to be bonded are machined or ground to specified standards of surface finish which are closely monitored. Degreasing of the surfaces is also a standardized procedure prior to assembly of the parts.

ALTERNATIVE METHODS OF EXPLOSIVE WELDING

The fundamental requirements of explosive welding described above are usually achieved by two alternative methods. There are others, but their limitations result in their less frequent use. The two principal set-ups are:

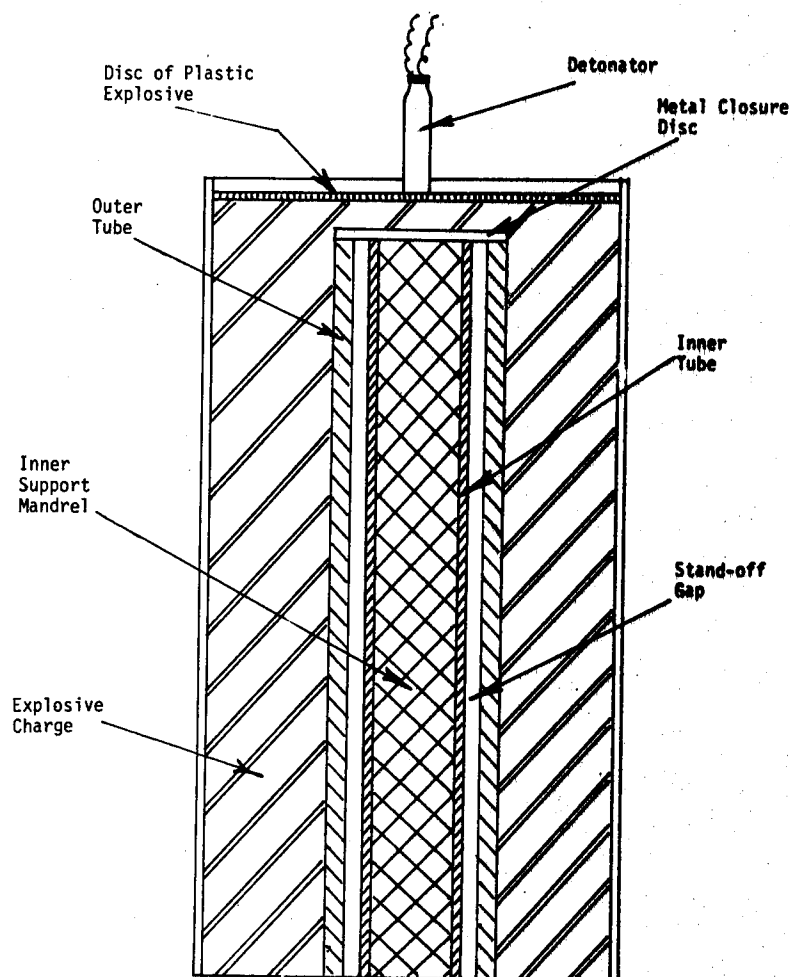The parallel geometry, and
The angular geometry.

144

FIGURE 2

Parallel Geometry

This set-up is so called because the two surfaces to be welded are set a small distance apart and parallel to each other. The distance apart is called the stand-off gap. In a tubular configuration, the stand-off gap is annular in form. An explosive charge is used to propel the inner and outer tubular components together and this can be done in two ways:

    a)   Implosion Method

    The basic set-up of this method is shown in Figure 2. A loose composite assembly of inner and outer tubes is set up with an annular stand-off gap between the components. Spacers are used at the tube extremities to achieve concentricity between the components and ensure uniformity of the annular gap. This loose composite is concentrically placed within a cardboard or plastic tube to form a second annular gap into which an explosive charge is poured. The dimension of this second annular gap is controlled to contain the requisite amount of explosive necessary to weld the tubes together.
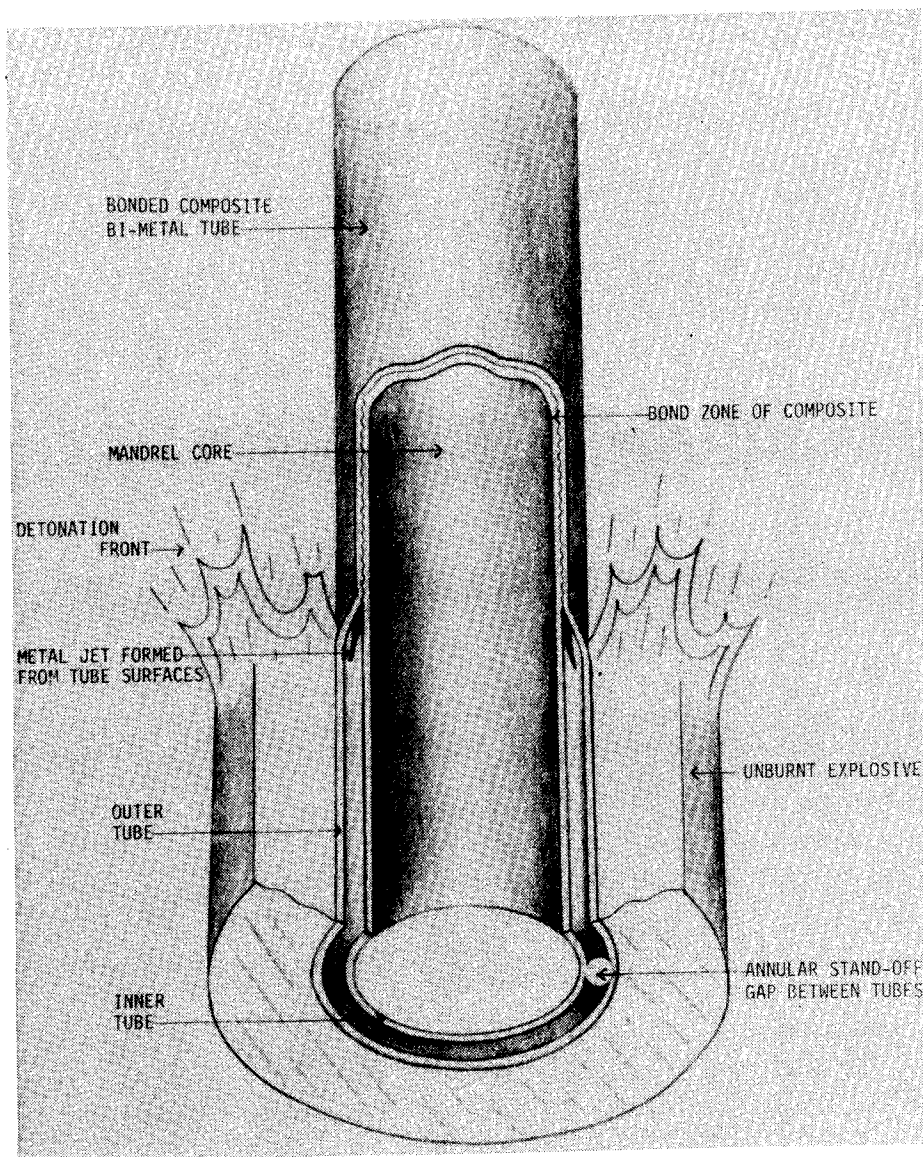
FIGURE 3

The explosive charge is initiated at one end by a disc of cap sensitive plastic explosive causing a detonation front to pass down the explosive charge. Immediately alongside the detonation front, the outer tube is propelled inwards over the stand-off gap to collide with the outer surface of the inner tube.

Because the outer surface of the inner tube and the inner surface of the outer tube are initially parallel to each other, the stand-off gap is uniform over its length. The distance that the collapsing tube must travel before colliding with the inner tube is, therefore, constant. Consequently, the collision front which has been generated will travel at a velocity identical to that of the explosive

detonation velocity. If the collision velocity is to travel
at a velocity less than the material sonic velocity then so
also must the detonation velocity be "subsonic".

Alternatively, the inner component may be a solid cylinder
but if it is tubular in form, it may require internal
support to prevent its collapse.

A schematic illustration of the implosion welding process in the
dynamic situation is shown in Figure 3. The jet formed at the
collision front can be seen and this jet, containing the surface
contaminants originally present, is finally ejected from the
interface.
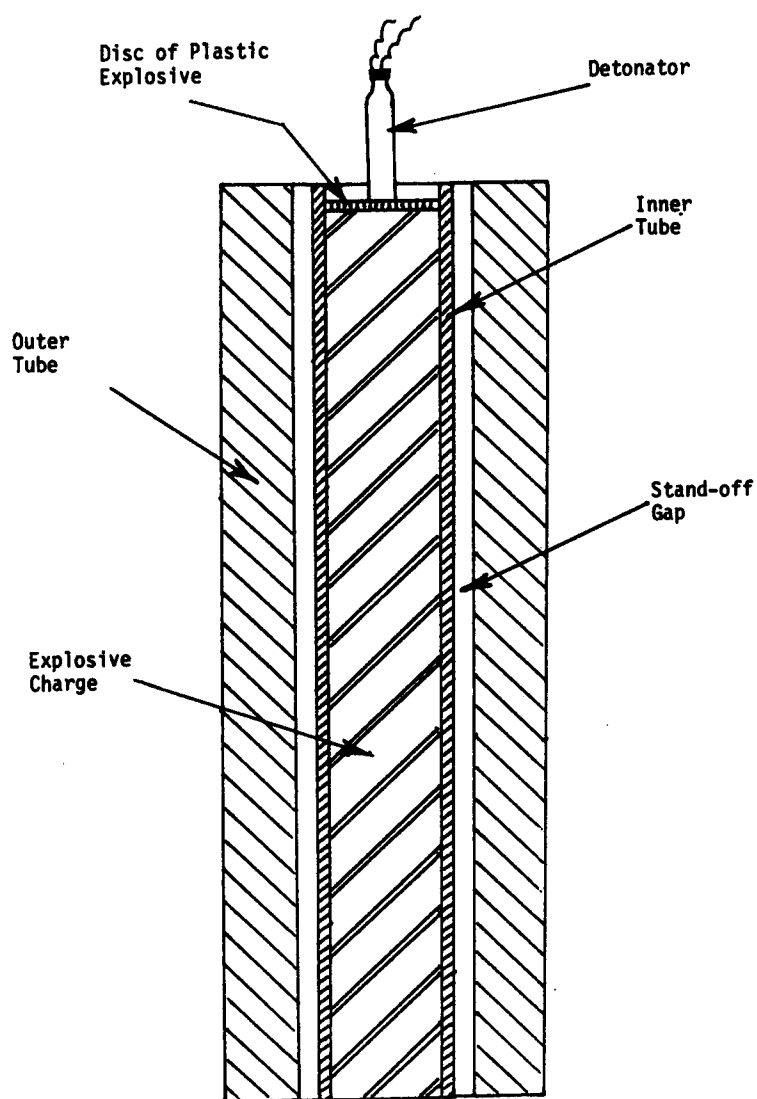
FIGURE 4

b) Expansion Method.

Figure 4 illustrates the set-up for welding by the
expansion method. Once again a loose composite of the inner
and outer tube components is set up with a concentric
annular gap. The explosive charge usually fills up the bore
of the inner tube and it is again initiated at one end by a
disc of cap sensitive plastic explosive. The detonation
front passes down the explosive and the inner tube is
expanded radially at the detonation front to collide with
the bore of the outer tube. A collision front is formed
which travels down the annular stand-off gap. As the gap is
again uniform over its length, the collision front and
detonation velocities will be identical and a "subsonic"
detonation velocity explosive must be used.

The outer tube component will ideally be of a substantial
thickness which will withstand the impact of the expanding
inner tube without distortion. If the thickness of the
outer component is not adequate, an external die must be
used.

Angular Geometry

As the name suggests, this set-up differs from the parallel
geometry in that the two surfaces to be bonded lie initially at
a pre-set angle to each other. In the case of tubular
components, the stand-off gap is again annular in form but of a
progressively increasing distance. Usually the inner tube is
expanded outwards over the stand-off gap with the angular gap
being contrived by either:

A divergent angle on the bore of the outer component or,

A convergent angle on the outer surface of the inner
component.

a) Expansion Method

The most convenient method of expanding is shown
schematically in Figure 5(a). An angular stand-off gap is
achieved by countersinking the bore of the outer component
which, in the illustration shown, is a tubular fitting.

The explosive charge is initiated at the innermost end
coincident with the smallest stand-off gap and this produces
a detonation front which travels outward toward the tube
extremity. The inner tube is expanded radially at the
detonation front to collide with the angular bore of the
fitting. Because the distance that the tube must travel is
progressively increasing, the collision front velocity is
reduced substantially below that of the explosive detonation

Polyethylene Transmitting Insert

Explosive contained within detonator

Angle machined in bore of fitting.

Fitting

Tube

(a)

Fitting

Angle machined on tube outer surface

Explosive charge shaped to maintain E/M ratio.

Tube

(b)

Fitting

Angle swaged on tube
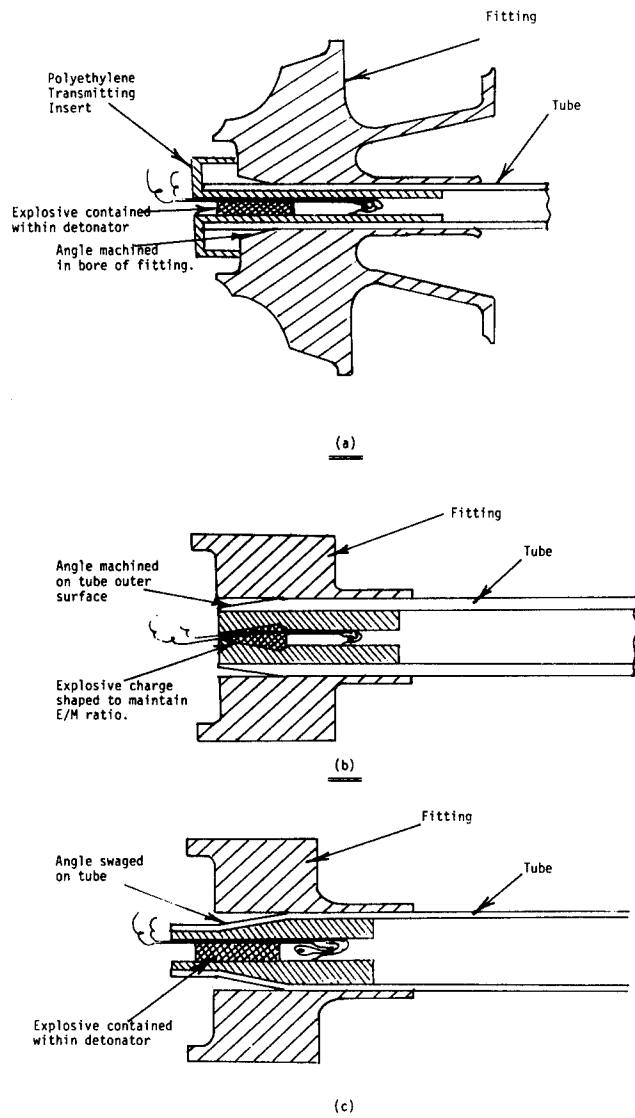
Tube

Explosive contained within detonator

(c)

FIGURE 5

velocity. This feature creates the principal advantage of this geometry: A high "supersonic" detonation velocity explosive can be used while still maintaining a "subsonic" collision front velocity. Such explosives are of higher density and strength than "subsonic" explosives. As the tube bore size must ultimately determine the maximum volume of explosive that it will accommodate, the use of the more powerful "supersonic" explosive will allow smaller tubes to be welded.

The smallest tube welded to date by this method is a 0.260" O.D. x 0.204" I.D. 316L stainless steel tube which was welded into an Inconel 625 fitting similar that shown in Figure 5(a). The bond length achieved was one of 0.28" and a minimum length of 0.25" could not be separated by a chisel.

Figures 5(b) and 5(c) show alternative expansion methods in which the angular stand-off gap is achieved by either machining an angle on the tube 5(b) or swaging the tube 5(c).

Method 5(b) has the advantage of simplicity. Its disadvantage is a changing wall section which, if a constant explosive/metal mass ratio over the length is to be maintained, requires the use of a correspondingly shaped inwardly tapered charge. The positioning of this shaped charge is critical and must be accurately maintained. The wall thickness of the tube also limits the choice of angle in that, to achieve an adequate bond length, the angle must be shallow when the wall thickness is small.

Angle machined within bore of fitting.

Tube

Detonator

External explosive charge shaped to maintain E/M ratio.

Mandrel

(a)

Angle flared in bore of fitting

Tube

Detonator

External explosive charge

Mandrel

(b)

Angle machined on outer surface of tube.

Tube

Detonator

External explosive charge

Mandrel

(c)
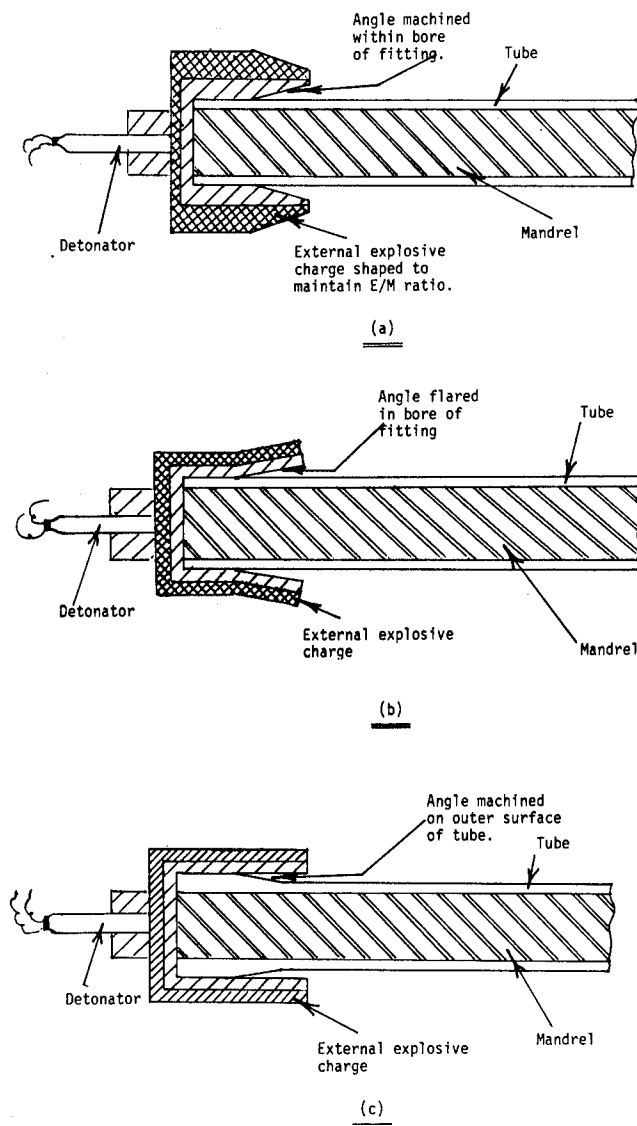
FIGURE 6

Method 5(c) requires the tube to be mechanically swaged but is otherwise less complex. The constant wall thickness gives much greater freedom in the choice of angle and does not require charge shaping.

Alternatively the outer tube can be imploded onto the inner component.

b) Implosion Method

A schematic representation of three alternative methods of imploding using angular geometries is shown in Figure 6. (a, b, and c).

Figure 6(a) shows an external fitting countersunk to create an angular stand-off gap. The high detonation velocity explosive surrounds the circumference of the fitting and it is initiated at the outer end to progressively collapse the fitting onto the inner tube or bar. Ideally the charge should be shaped to maintain the explosive/metal mass ratio over the bond length.

Figure 6(b) shows an alternative arrangement with the external fitting mechanically flared to create the angular gap. The constant wall thickness of the fitting avoids the necessity of shaping the charge.

Figure 6(c) illustrates a set up in which the angular gap is contrived by machining the angle on the outer surface of the inner component.

CHARACTERISTICS OF THE WELD

Metallographic examination of an explosive weld will usually show a characteristic wave form at the interface (Figure 7). A wave form is not necessary for bond strength, and flat interfaces are in some instances even desirable.

Associated with the peaks and troughs of the waves are discrete islands of "melt". This melt is material, originally molten, which has been rapidly chilled. If this material is an intermetallic formed from the component materials, it will be brittle. If bond strength is to be adequate, therefore, the collision parameters must be controlled to minimise the volume of these intermetallics. This can be achieved by avoiding excessive collision pressures and controlling the dynamic angle. If the collision parameters can be further controlled to form a straight interface, the intermetallics are entirely excluded. This degree of control is difficult to achieve in practice, however, and provided the "melt" is kept to acceptable proportions, the bond strength is very high and more than adequate.

151
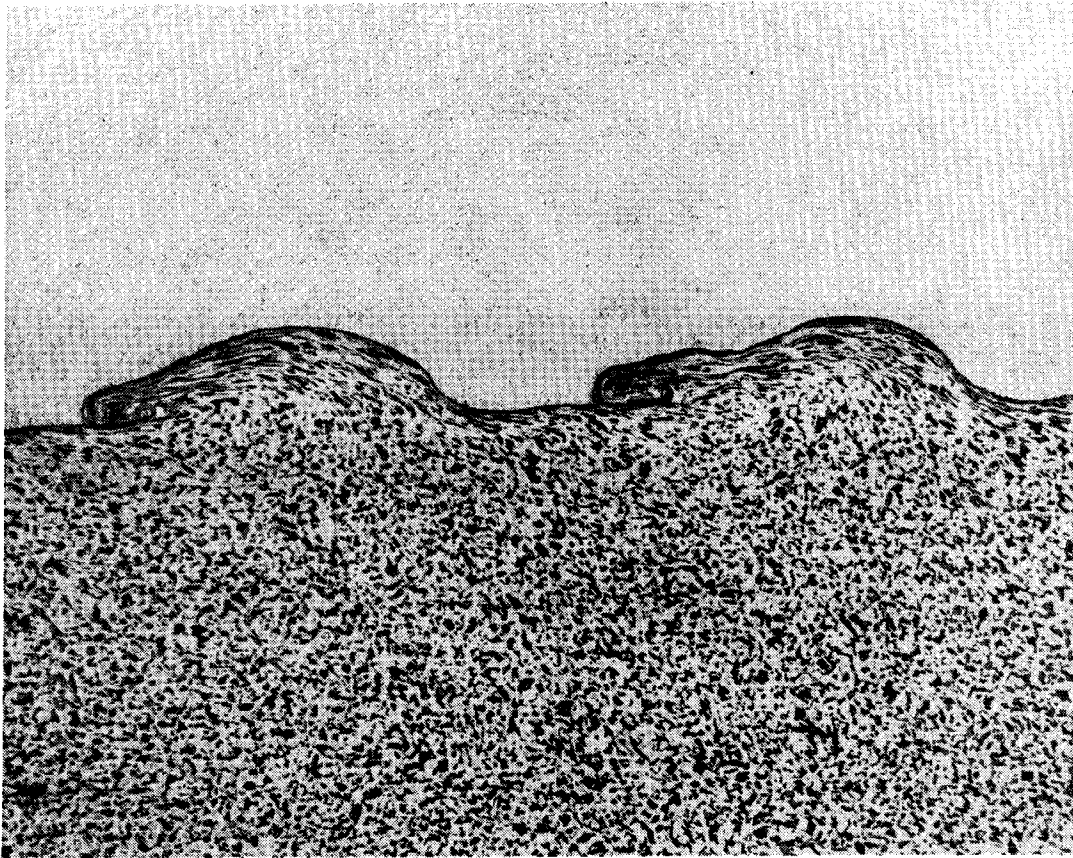
FIGURE 7

Destructive tests will usually result in failure of the weaker of the parent materials. Metal combinations which are a mix of hexagonal and cubic structured metals are more prone to fail at the bond. The strength of the bond may be more than adequate and the bond area can be increased to a point which will result in prior failure of the component parts.

Once the welding parameters are correctly established the welds are highly reproducible. An example of this reproducibility is demonstrated by the process of tube to tubesheet joining. In this instance, tube/tubesheet joints are fabricated by the angular technique with the tube being expanded into a countersunk tubeplate hole. Some 400,000 such joints have been made over a period of 15 years, and there is no recorded instance of joint failure.

Repairs of conventional tube/tubesheet joints have a similar unblemished record. In the repair situation a hollow plug is machined from solid bar and the open end is swaged in a similar manner to Figure 5(c).

TESTING OF JOINTS

Ultrasonic examination is the most commonly used non-destructive test method used for the inspection of explosively welded products. In the pulse-echo mode, the transducer is placed against the metal surface to transmit an ultrasonic pulse into the metal. If the metals are unbonded, the ultrasonic pulse is reflected by the interface. Alternatively, if the metals are bonded, the ultrasonic pulse passes through the interface and is reflected from the reverse side of the composite. In both cases, the reflected signal is received by the transducer and is displayed upon an oscilloscope screen as a deflection of the illuminated base line. The difference in pulse time travel between composites in the bonded and unbonded state is identified by the position of the deflection on the screen and is readily apparent.

The transducer used for the inspection of clad plates is usually about 1" in diameter. Small diameter transducers have been used to inspect many thousands of explosively welded tube to tube plate joints over a period of 20 years and the process has proved highly reliable. The same test apparatus and procedures can be used to inspect explosively welded tube to fitting joints. Ultrasonic testing, when combined with careful process controls and periodic destructive testing, can provide excellent assurance of product integrity.

Other forms of non-destructive tests which are commonly used are helium, hydraulic and pneumatic leak tests. All these tests provide additional assurance of bond quality.

Tensile, shear and compression tests are useful destructive tests which can be applied when determining bonding parameters. All give measures of the joint strength. Hydraulic testing to destruction gives a concomitant evaluation of joint strength and leak tightness should this be required. This is usually the case in tubular joint configurations.

SOME TYPICAL APPLICATIONS

Aluminum/Stainless steel is a metal combination often used in the aerospace industry. Obviously these two materials cannot be fusion welded together and transition joints are required if permanent connections are to be made. Figure 8 shows a typical transition joint in which a 1/8" O.D. x 1/16" bore, Type 321 stainless steel tube is bonded within a Type 6061-T6 aluminum boss. The 6061 aluminum has been bonded directly to the stainless steel and also with a type 1100 aluminum interlayer. In the particular joint configuration illustrated, the 6061 was imploded directly onto the stainless steel tube.
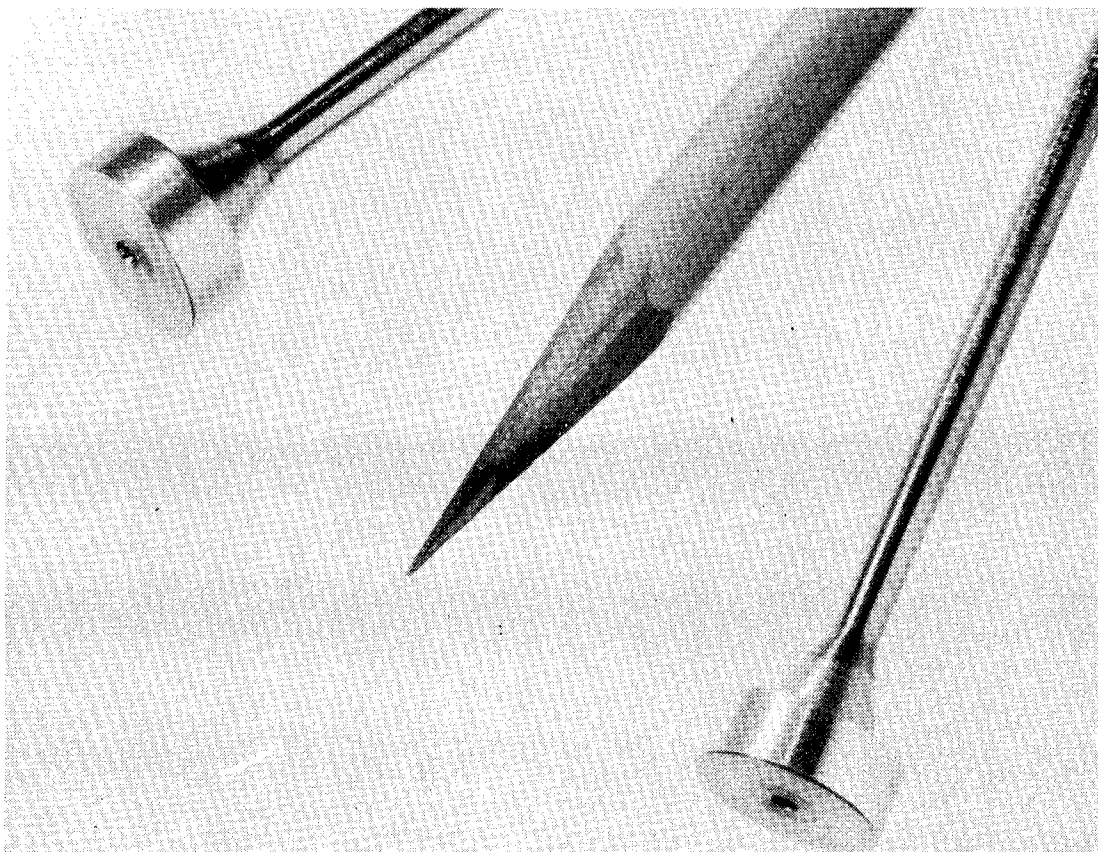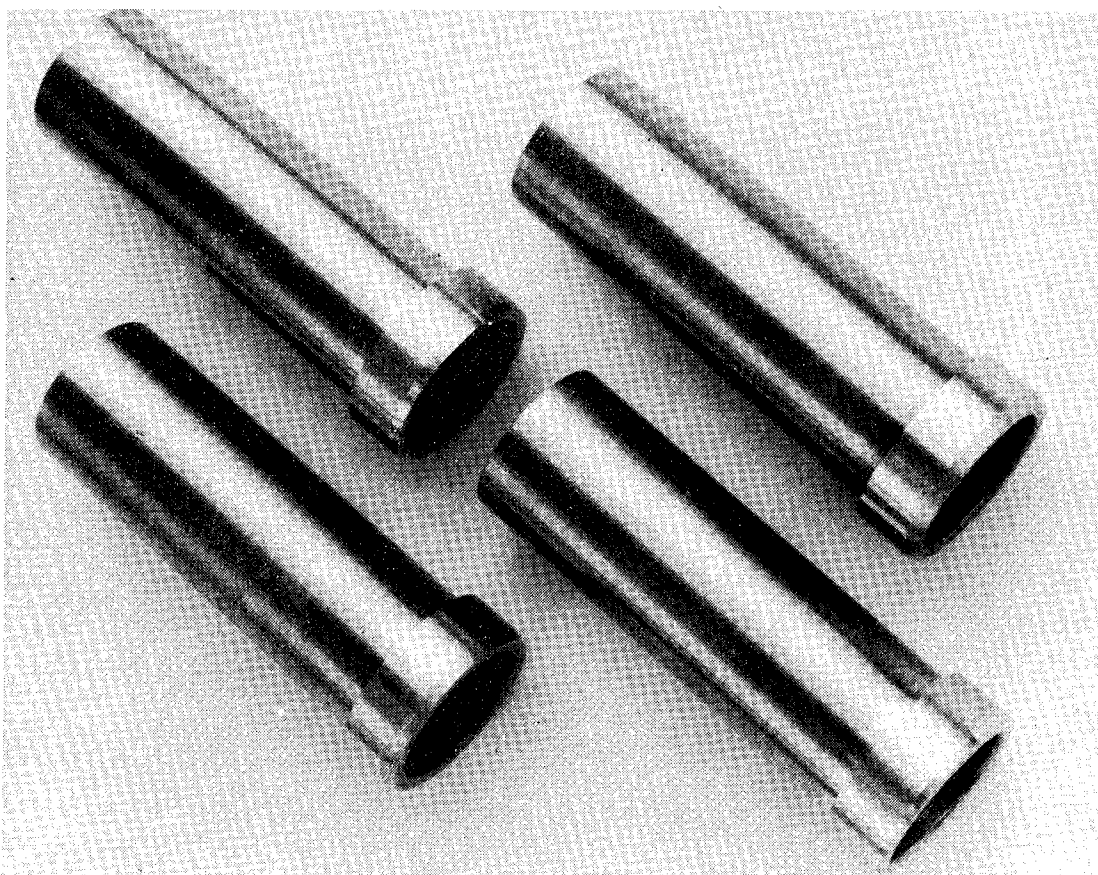
FIGURE 8

FIGURE 9

Figure 9 shows a second transition joint between a Type 304L stainless steel collar and a 3AL-2.5V titanium alloy tube. The very high yield strength of the titanium alloy tube has, in the past, made this particular metal combination impossible to explosively weld. The parameters for bonding are now established and welding can be just as readily and reproducibly achieved as with more familiar and frequently used metal combinations. The joint illustrated was again fabricated by implosion of the stainless steel collar onto the titanium alloy tube.

The particular shapes of transition joints are many and varied. It is necessary to approach each required configuration individually to decide the most appropriate geometry for its manufacture. The most appropriate method will be that which has the greatest commercial and technical viability.

EXPLOSIVE TUBE-TO-FITTING JOINING OF SMALL-DIAMETER TUBES

Laurence J. Bement
NASA Langley Research Center
Hampton, VA

An effort is currently under way by NASA Marshall Space Flight Center to upgrade the Space Shuttle main engine through the use of improved materials and processes. Under consideration is the use of the Langley Research Center explosive seam welding process, as stated in the objective.

OBJECTIVE - DEMONSTRATE THE FEASIBILITY OF JOINING SPACE SHUTTLE MAIN ENGINE TUBE-TO-FITTING COMPONENTS IN AN OXYGEN HEAT EXCHANGER, USING THE NASA LaRC EXPLOSIVE SEAM WELDING PROCESS

The Space Shuttle Main Engine liquid oxygen tank pressurization heat exchanger assembly is shown in this figure. Located at the output of the oxygen turbopumps, just prior to the engine's main combustion chamber, this assembly's function is to convert a liquid oxygen supply to gaseous oxygen to pressure the oxygen vessel of the external tank. Liquid oxygen enters a 0.260-inch O.D. stainless-steel tube (inboard-directed arrow, lower left). The tube is wrapped around the inside of the heat exchanger, expands to a 0.5-inch O.D. in a split internal fitting, and penetrates the wall of the assembly at the outboard-directed arrow, lower left. The explosive joining effort described in this presentation was directed at joining the 0.260 and 0.500-inch diameter tubes to their respective fittings.

**LOX TANK PRESS
HEAT EXCHANGER ASSY**

INCOLOY 903
718L
HAYNES 188
INCONEL 625
INCONEL 718
HOT GAS
HOT OXYGEN
COLD OXYGEN
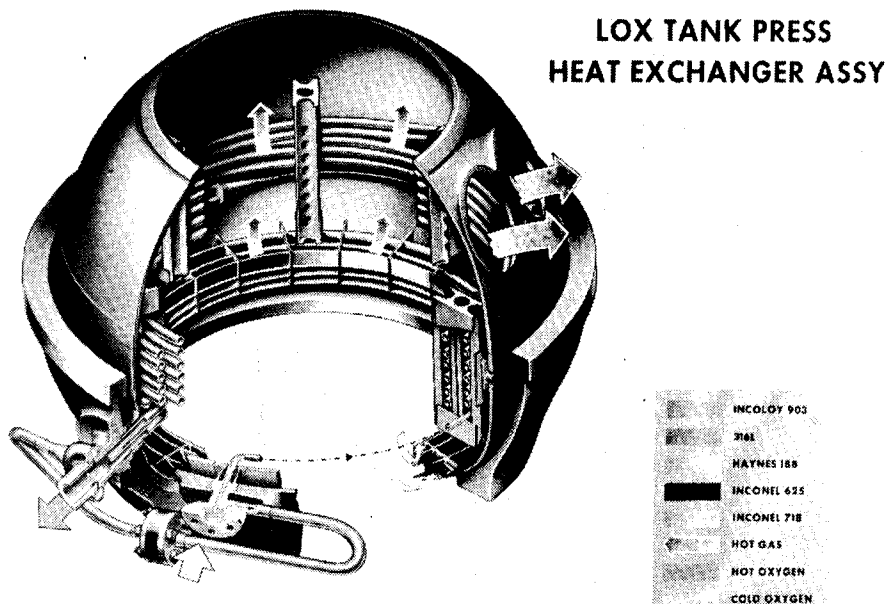
This figure details the materials, sizes, and temperature extremes at the input and output of the heat exchanger. All materials are refractory; each material has individual advantages and disadvantages in terms of strength, fracture toughness and the ability to be fusion welded.

Should the tube fail, the high-pressure oxygen pumped through the turbine would overpressurize the external tank with catastrophic results.

SHUTTLE HEAT EXCHANGER CONDITIONS/HARDWARE

- 316 L CORROSION-RESISTANT STEEL SEAMLESS TUBING

- AT INLET:
    -260°F
    .260 O.D., .026-INCH WALL

- HEATED BY +800°F TURBINE GASES

- AT OUTLET:
    +390°F
    .500 O.D., .035-INCH WALL

- THREE CANDIDATE MATERIALS FOR SHROUD FITTINGS:
    HAYNES 188, INCONEL 625, INCOLOY 903

- MOST CATASTROPHIC FAILURE MODE IN ENGINE IS FAILURE OF TUBING

The explosive joining goals of this program are listed here.

1. Make the tube-to-fitting joint only through the mouth of the tube inserted in each fitting. No other external tooling or access would be required.

2. All other joining processes would be complete prior to the explosive joining of the tubes to the fittings.

3. Simplicity in tooling and process with easily inspectable assembly of all components of the tool and explosive materials would be required.

4. The output of the explosive, yielding the explosive joint, would have to be highly predictable and controllable.

5. The explosive joining process, which generates very high pressure, short-duration impulses, must not damage surrounding structure or fusion welds.

6. The bond between the tube and the fitting must have at least twice the strength of the tube.

7. The joint must be completely inspectable once made.

8. The joint shall exhibit absolute sealing capability with no indication of helium leaks at any required differential pressure across the joint.

9. No loss in strength or sealing capability will be allowed due to exposure to system temperature extremes in any cycle.

10. Reliability is paramount in all aspects of material preparation, tool assembly, the joining process, and the final joint.

SHUTTLE ENGINE TUBE-TO-FITTING EXPLOSIVE JOINING JOINING GOALS

1. EXTERNAL ACCESS (MOUTH OF TUBE)
2. LAST STEP IN ASSEMBLY
3. SIMPLE
4. HIGHLY PREDICTABLE/CONTROLLABLE
5. NO DAMAGE TO SURROUNDING STRUCTURE/WELDS
6. JOINT HAVE LARGE STRUCTURAL MARGINS
7. INSPECTABLE
8. ABSOLUTE SEALS
9. UNAFFECTED BY THERMAL EXTREMES
10. RELIABLE

This figure describes the explosive joining process, which produces metallurgical bonds that are impossible to achieve by any other joining process. A several million psi explosive pressure wave accelerates the flyer plate into a high-velocity, angular collision with the base plate. On impact, the kinetic energy is converted to skin-deep melts, which are stripped from the surface and squeezed out (ejected) by the closing angle. The pure surface allows interatomic linkup through electron sharing. Bulk powder explosive is spread over the flyer plate and detonated along the line entering the plane of the paper to sweep from left to right (See "Practical Small-Scale Explosive Seam Welding" by L. J. Bement, NASA TM 84649, April 1983).
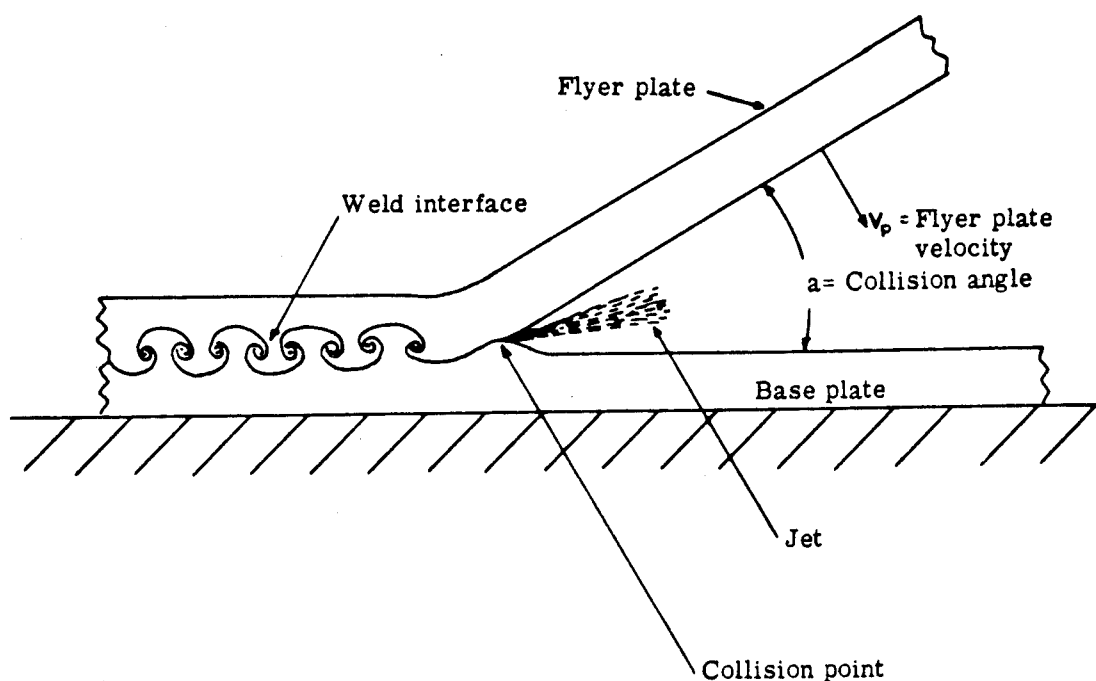
High-velocity angular collision of metal plates in an explosive welding operation.

161

This figure describes the Langley explosive joining process. A "ribbon" explosive is placed on separated plates and detonated at one end. The explosive pressure wave drives the plate downward, contacting in the center, producing two high-velocity, angular impacts outward at 60° angles from the centerline of the indentation. This process is ten times more efficient in terms of bond area produced by equivalent explosive quantities. Very small quantities of explosive are used.
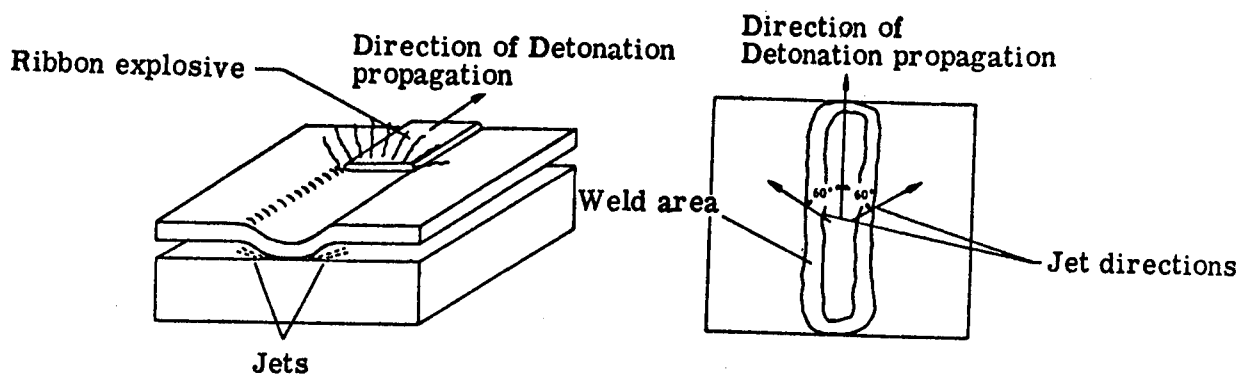
Mechanisms involved in small-scale explosive seam welding process.

The "ribbon" explosive, a lead-sheathed, flattened tube filled with RDX (cyclotrimethylene trinitramine) explosive, is shown here for six different loads. A grain unit is small: there are 7,000 grains in a pound, 15.4 grains in a gram.

Cross-sectional Dimensions of Linear Ribbon RDX Explosive

Explosive Load, grains/foot	Thickness, inch	Width, inch
7	0.020	0.220
10	0.020	0.300
15	0.025	0.315
20	0.030	0.365
25	0.035	0.370
30	0.035	0.510

163
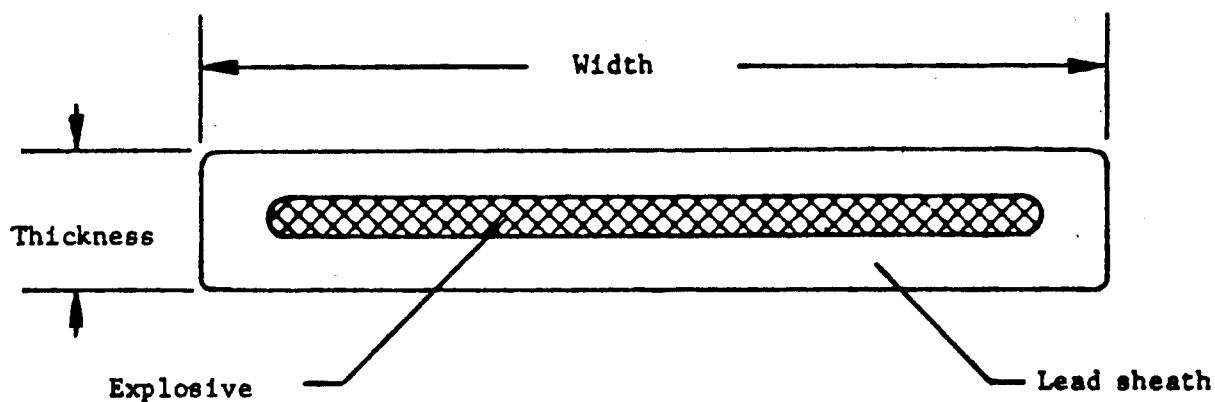
This table lists the metals and range of thicknesses in which 100% strength joints can be obtained. The plates to be joined were placed in parallel (except as noted), separated by 0.015 inch. The ribbon explosive was placed on the outer sides of the plates, directly opposing and simultaneously initiated.

Like Metals Joinable by Explosive Seam Welding
(100% Strength Joints)

Metal	Range of Thickness (inch)
a. Iron/steel Low-carbon to 300 and 400 stainless	0.001 to 0.050
b. Aluminum - any fully annealed alloy and all age and work-hardened alloys except 2024 and 7075	0.010 to 0.188
c. Copper/brass	0.010 to 0.150
*d. Titanium (Ti-6Aℓ-4V)	0.005 to 0.050

*Each plate prebent 5° ⎯⎯⎯⎯⎯⎯⎯

This process can metallurgically join a wide variety of metal combinations, as well as different tempers and conditions.

Metal Combinations Joinable by Explosive Seam Welding

a. Low-carbon to series 300 and 400 stainless steel are joinable in any combination

b. All aluminum alloys and conditions are joinable to any other alloy and condition, except a combination of 2024-T3, T4, etc. and 7075-T3, T6, etc.

c. Any combination of copper, aluminum, and brass can be joined

The explosive joining compatibility of the 316L stainless steel was first evaluated using flat stock. A 0.035-inch sheet of 316L stainless steel (top of figure) was joined to the three alloys of interest: Inconel 625, Incoloy 903, and Haynes 188. The base plates were machined with a V notch to allow the flyer plate (316L) to be in full contact and maximize the explosive joining efficiency. The lower plates show the machined notch, which is dimensionally described on the next figure. The upper figure shows the indent in the 316L, which was driven into the notch by the ribbon explosive. The vertical indents are where the 316L was driven into the small spaces between the base plates. The top joints were cross sectioned, pull-tested, and examined microscopically. The bond area for all three plates was several times that needed to support the full strength of the 316L.
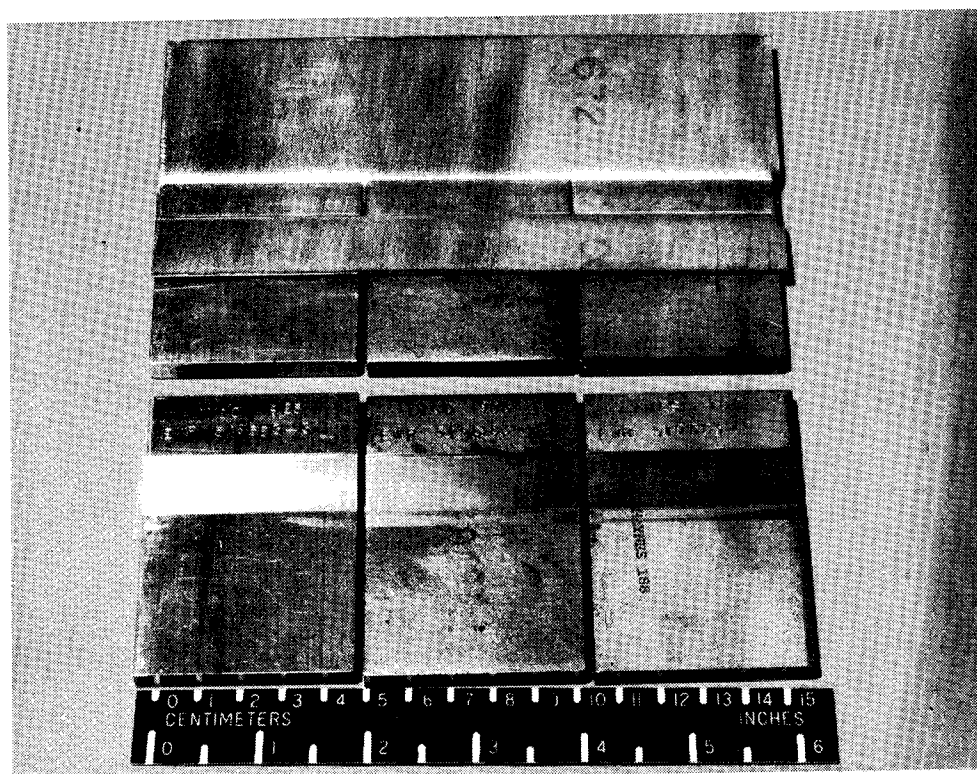
This figure shows the dimensions of the "V"-notch, which was cut into the flat plates and the internal circumference of the fittings for the tube joining operation. The "V" immediately establishes the necessary collision angle for explosive joining. The tube outside diameter matched the fitting inside diameter to less than 0.002-inch tolerance. Past tests with 8-inch diameter tubes indicated this match was not critical. A joint was successfully made with a 0.060-inch diameter undersized tube. See "Explosive Seam Welding Application to Reactor Repair" by A. E. Aikens and L. J. Bement, presented at the 3rd Annual Conference of the Canadian Nuclear Society, Toronto, Canada, June 9, 1982.

SHUTTLE ENGINE TUBE-TO-FITTING EXPLOSIVE JOINING
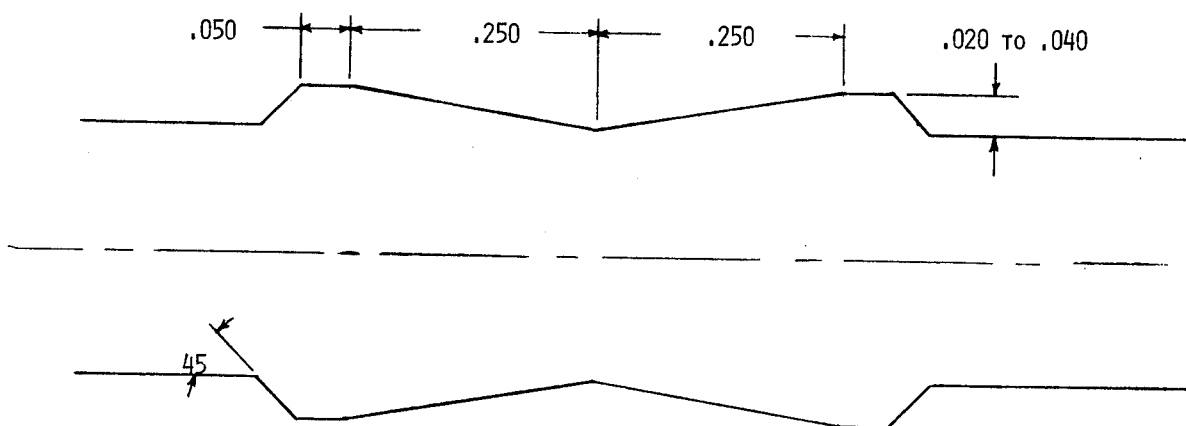
CROSS SECTION OF EXPLOSIVE WELDING INTERFACE WITHIN FITTINGS

167

This photograph depicts the explosive materials and the explosive joining tool in various stages of assembly. The explosive joining principle is to insert the loaded tool inside the tube, and on initiation of the explosive, the tube is driven into the V notch in the fitting. The top object is the initiator, which consists of a 0.090-inch diameter, 0.005-inch wall, 1-inch long 304 stainless-steel tube containing a 0.40-inch length of packed RDX. Bonded into this tube is an 8 grains/foot RDX, lead sheathed mild detonating fuse (MDF). The white object is a nylon rod machined to accommodate the ribbon explosive and ultimately match the inside diameter of the tube to be joined. The 30 grains/foot ribbon explosive (third object) is wrapped around the tool (held in place with sticky-back tape) and trimmed to the dimensions of the initiator. The initiator is then inserted into an axial hole in the tool. This photograph shows a teflon tape overwrap to match the inside diameter of the tube to be joined. A different approach was more effective, using modeling clay around the explosive, fully contained by heat-shrinkable plastic tubing.
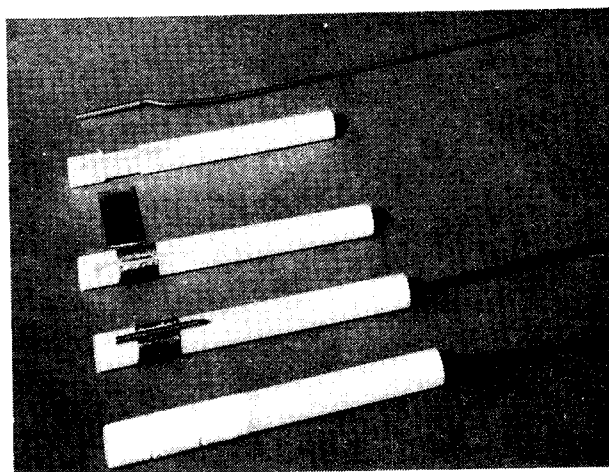
This photograph shows the loaded tool, a 0.5-inch tube and an experimental fitting in which has been machined the V notch. The fitting on the right contains an explosively joined tube.
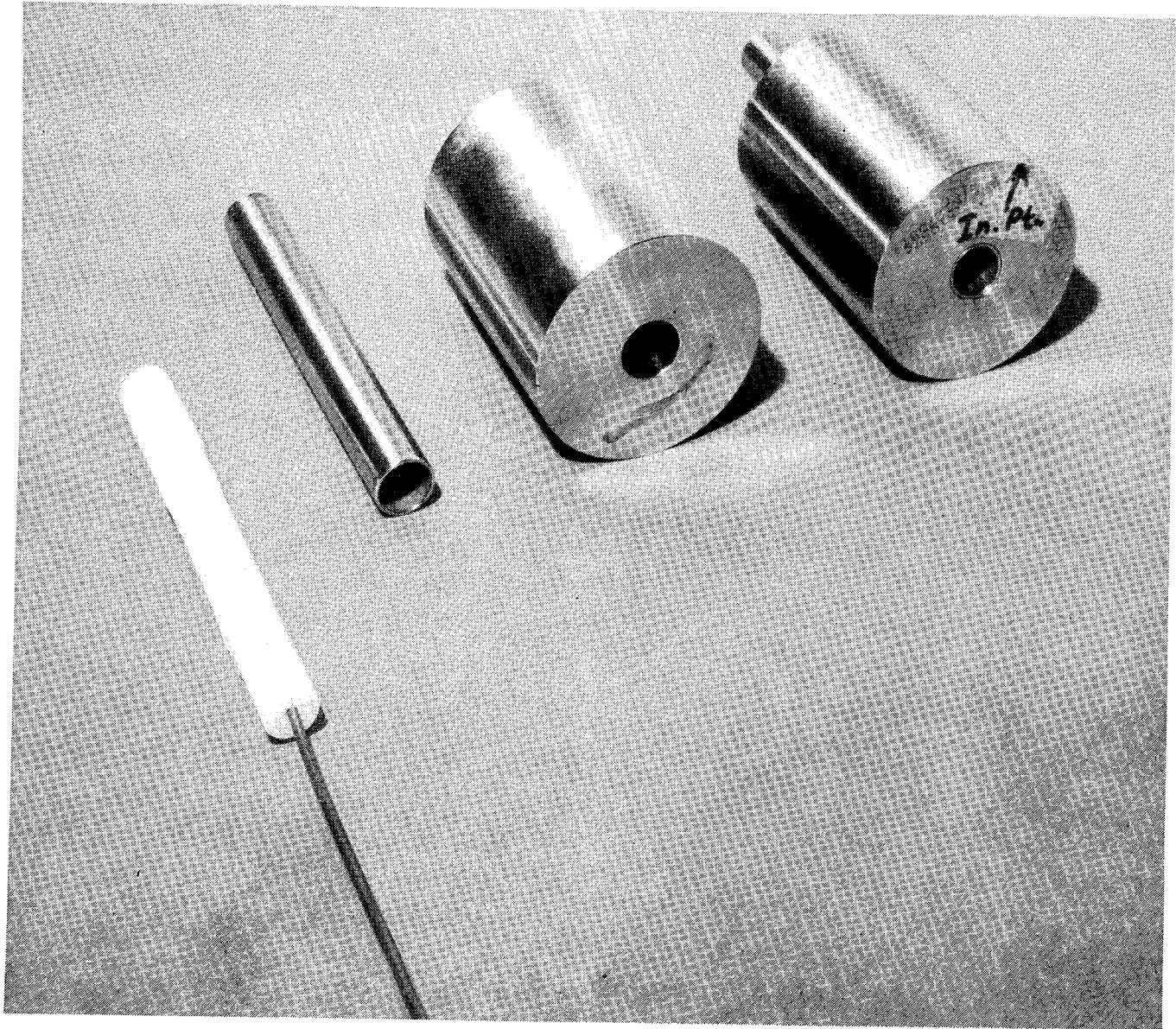
This photograph shows the fitting in the previous photograph, cross sectioned on its axis. The 0.5-inch tube was driven into the notch at the indented area. However, ultrasonic inspections and peel tests showed only partial bonds. Furthermore, lead from the ribbon explosive had been imbedded into the interior surface of the tube. The teflon tape had not exactly matched the tube's interior, leaving air gaps. Since the air is compressible, the explosively driven lead penetrated the teflon and impinged into the tube. The modeling clay with shrink tube described on the previous figure completely filled the internal volume, preventing lead transfer to the tube wall.
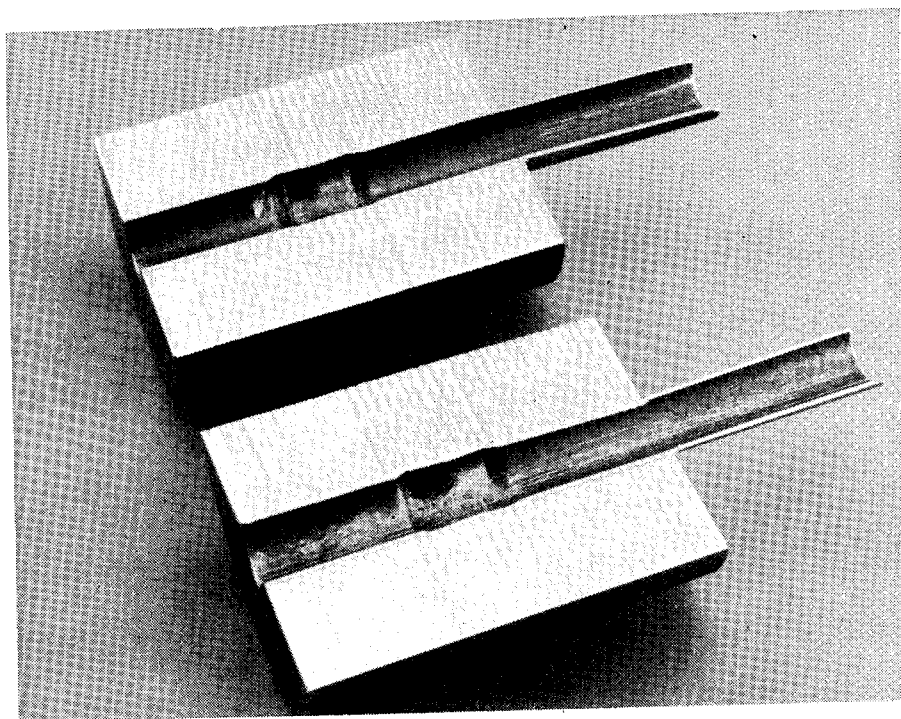
The 0.260 diameter, 0.026-inch wall fitting proved to be much more effective in terms of bond. A 15 grains/foot ribbon explosive was used in this test. The upper section was used for a peel test, shown in the next photograph.
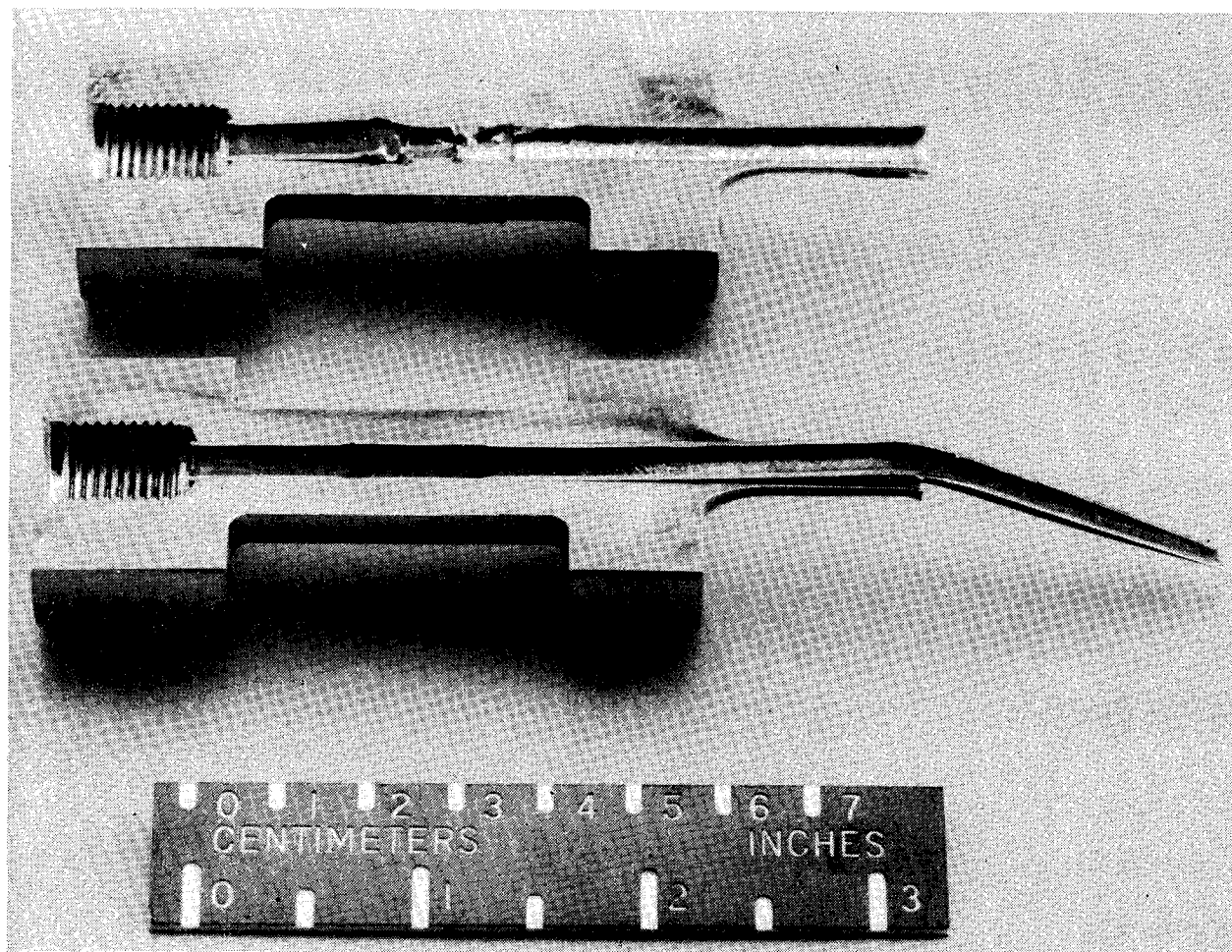
A cold chisel was driven into the bond interface as far as possible. In this case, approximately 0.25 inch of the tube length was bonded, nine times the 0.026-inch wall thickness. Only a bond length of 0.052 inch would fully support loads that would fail the tube.
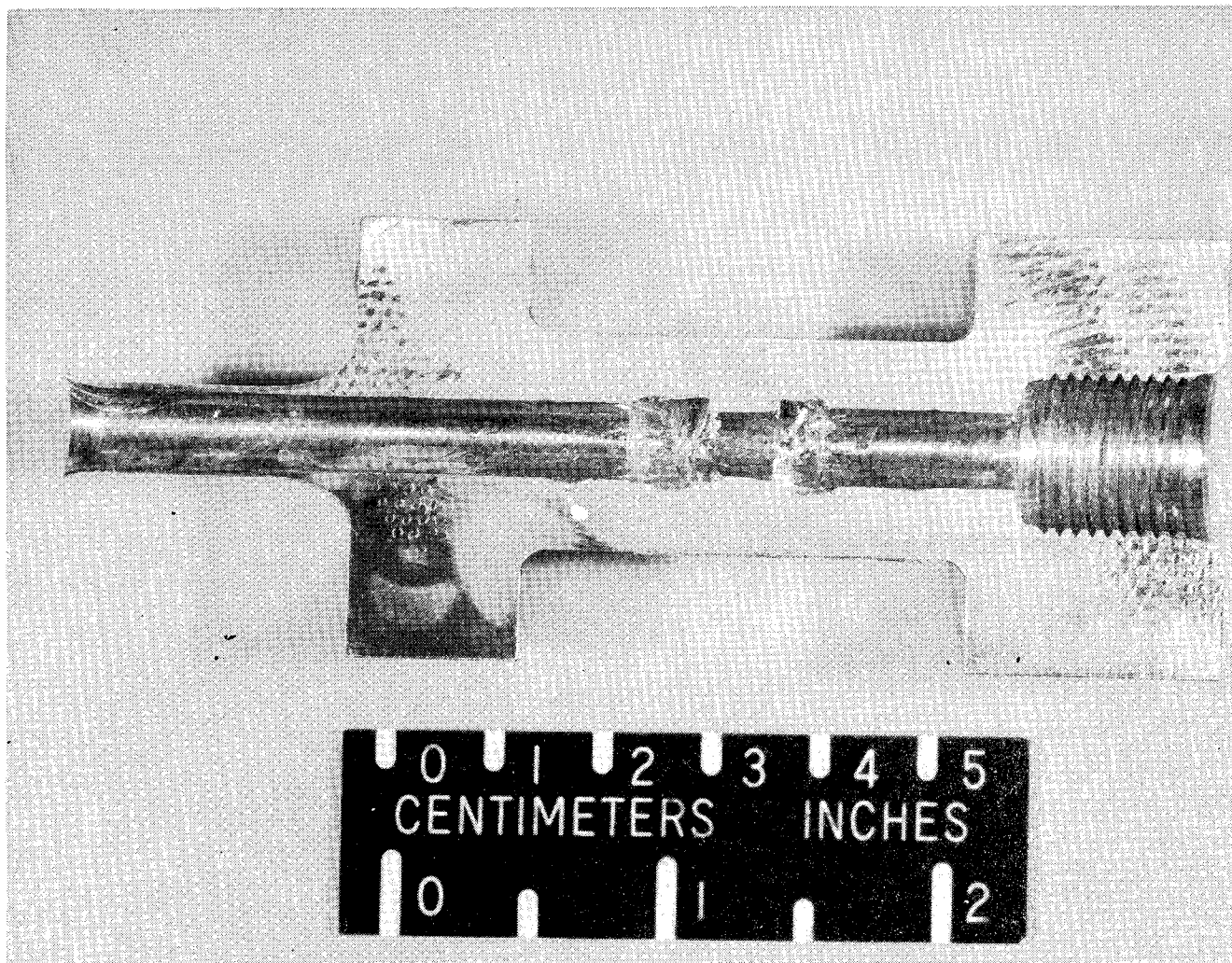
This photograph shows a portion of the bond in the 0.260 diameter tube, which has the typical "wave" pattern of explosive joining. The largest "wave" pattern to the right has peak-to-peak dimensions of less than 0.001 inch.

To evaluate the effect of reduced explosive loads, a second test was conducted with a 10 grain/foot ribbon explosive. The bond length was reduced to approximately 0.150 inch.
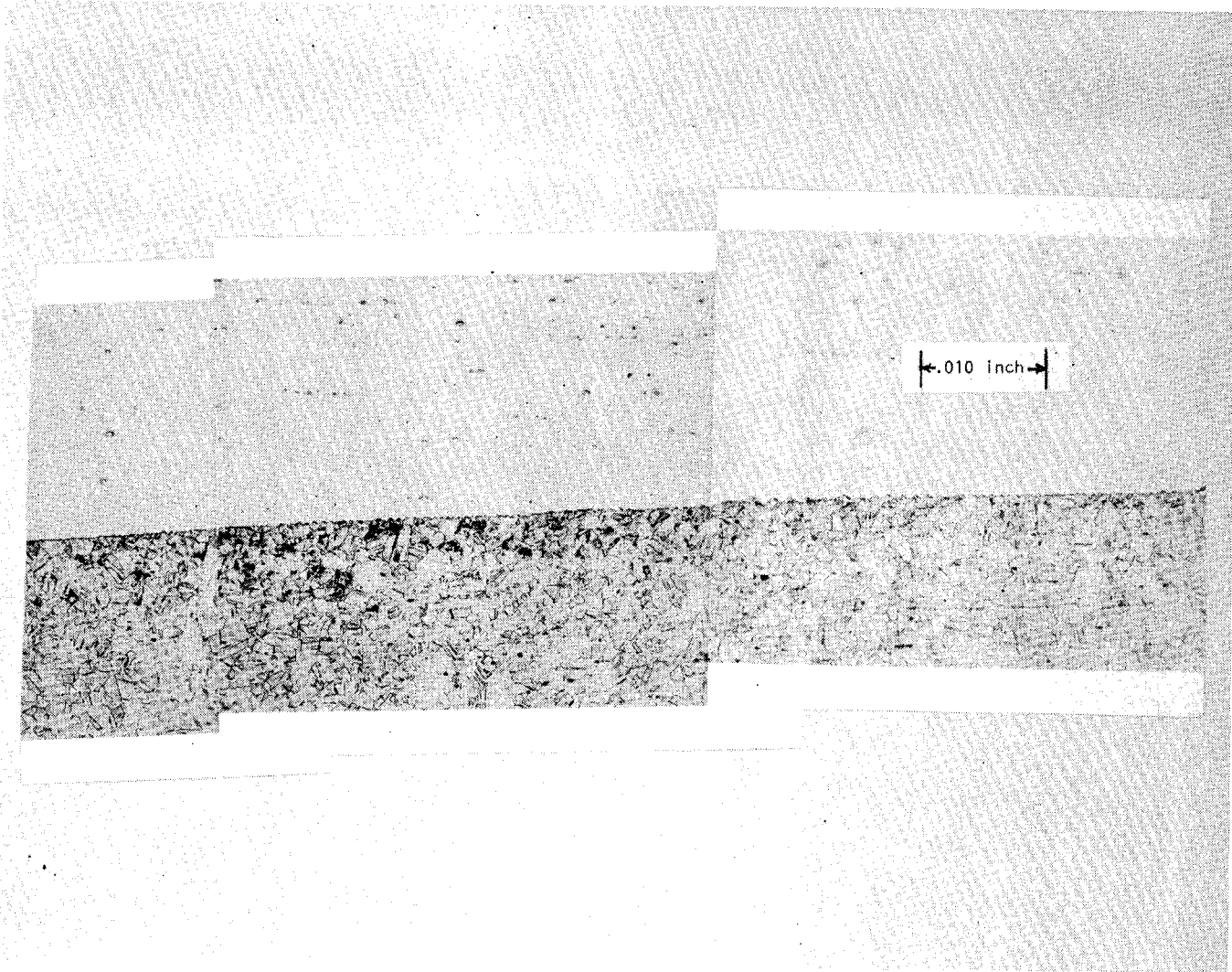
The current results of the tube-to-fitting explosive joining evaluation are shown here.

1. The 316L is completely compatible with the three candidate refractory materials for explosive joining.
2. The 0.260 diameter tube has successfully met all joining requirements with excellent margins.
3. Planned are thermal shock tests in which the joints will be transferred from liquid nitrogen (-320°F) to a $+400^\circ$F stabilized oven.
4. The 0.500-inch diameter tube is not bonded due to air entrapment in the V notch. The 30 grains/foot ribbon explosive's 0.510-inch width creates a pressure wave that forces the tube into the fitting wall and prevents the air in the V notch from escaping as the tube collapses into the notch. Narrower ribbon explosives have been attempted, but the more promising improvement would be to widen the notch and vent the air out of the fitting.
5. Helium leak checks are not a good indication of a good joint. Perfect seals were achieved without explosive bonding. The tube had only been swaged into the V notch.
6. Ultrasonic inspection utilizing pulses of sound, which reflect from opposite surfaces, provides an excellent evaluation method for explosive joining. An ultrasonic probe placed on the outside of the fitting provides a highly accurate measurement of the interior V-notch surface. Once "mapped," the process is repeated for the explosive joint. A bonded joint will appear as simply a greater thickness. Areas with no bond display a complex reflected signal from two surfaces instead of one.

SHUTTLE ENGINE TUBE-TO-FITTING EXPLOSIVE JOINING

CURRENT RESULTS
- 316 L COMPATIBLE WITH ALL THREE FITTING MATERIALS
- THE .260 O.D. TUBE JOINT MET ALL TESTS TO DATE WITH EXCELLENT MARGINS
- NOT YET CONDUCTED THERMAL SHOCK TESTS
- THE .500 O.D. TUBE JOINT NOT BONDING
    - AIR ENTRAPMENT DURING JOINING OPERATION
    - USE NARROWER RIBBON EXPLOSIVE OR WIDER NOTCH
- HELIUM LEAK CHECKS NOT INDICATION OF GOOD JOINT; EXPLOSIVE SWAGE PRODUCED ABSOLUTE SEAL
- ULTRASONIC INSPECTION IS EXCELLENT
    - EXTERNAL TO FITTING APPROACH
    - MAP INTERNAL SURFACE OF FITTING
    - COMPARE MAP WITH PROFILE OBTAINED WITH TUBE INSTALLED

The current conclusions are:

1. The Langley explosive joining process is indeed viable for this tube-to-fitting application.
2. No incompatibility of materials has been detected.
3. Ultrasonic inspection provides the best evaluation of the joint and will provide the needed confidence of the joint in the final application.
4. The 0.500-inch diameter tube has not yet been adequately joined. Success is anticipated with a wider V-notch that allows the trapped air to vent during explosive joining.
5. Thermal shock testing (-320 to +400°F) will be conducted. Past experience with explosively bonded joints in steel has indicated no problems.

SHUTTLE ENGINE TUBE-TO-FITTING EXPLOSIVE JOINING

CURRENT CONCLUSIONS

- LaRC EXPLOSIVE JOINING IS VIABLE FOR THIS APPLICATION

- NO INCOMPATABILITY OF MATERIALS HAS BEEN DETECTED

- ULTRASONIC INSPECTION IS THE BEST NON-DESTRUCTIVE TESTING

- THE .500 DIA JOINT EXPERIENCES INTERFACE PROBLEMS

- THERMAL TESTING HAS YET TO BE ACCOMPLISHED

175

THE USE OF EXPLOSIVE FORMING FOR

FASTENING AND JOINING STRUCTURAL AND PRESSURE COMPONENTS

J. Wayne Schroeder
Foster Wheeler Development Corporation
Livingston, N.J. 07039

ABSTRACT

Explosive expansion of tubes into tubesheets has been used for over 20 years in the fabrication and repair of shell and tube heat exchangers.

The use of explosives to perform these expansions has offered several distinct advantages over other methods. First, the process is fast and economical and can be performed with minimal training of personnel. Secondly, explosive forming does not cause the deleterious metallurgical effects which often result from other forming operations. In addition, the process can be performed remotely without the need for sophisticated handling equipment.

The expansion of tubes into tubesheets is only one of many possible fastening and joining applications for which explosive forming can be used to achieve highly successful results.

This paper describes the explosive forming process and where it has been used. In addition, some possible adaptations to other joining applications are identified and discussed.

INTRODUCTION

The expansion of tubes into tubesheets of heat exchangers is performed for several reasons. First, the expansions may provide the pressure seal between the primary and secondary sides of the heat exchanger to prevent mixing of the two mediums which are being heated or giving off heat. Secondly, the expansion provides the axial strength of the joint. This strength requirement may be quite large, depending upon the design of the exchanger. Lastly, the expansions close the annular gap between the drilled hole and the tube outside diameter, preventing the accumulation of possible corrodents which may attack the tube or tubesheet materials.

TYPICAL TUBE-TUBESHEET JOINT DESIGNS

Tube-to-tubesheet joints which require expansion are generally one of the three following types, see Figure 1.

The first type uses a weld at the front face of the tubesheet that provides the pressure tight seal. The expansion is done to close the annular gap to exclude space for the accumulation of corrodents and to provide joint strength so the weld is not subjected to vibration or axial loads. This design is used for high pressure applications.

For the second type the tube is expanded for the full depth of the tube hole. The expansion provides both the seal and axial strength to the joint. This design is normally used where the pressure differential across the joint is low.

The third design incorporates circumferential grooves within the tubesheet hole. The grooves provide additional axial joint strength and also disrupt axial drill marks, thus increasing the sealing ability of the joint. This design is used for both high and low pressure applications.

THE EXPLOSIVE EXPANSION PROCESS

The explosive tube expansion process is achieved by placing a uniform carefully sized explosive charge into an energy transmitting medium which is sized to fit the inside of the tube, see Figure 2. The length of the charge/medium package, called an insert, is the same as the desired expansion. A flange at one end of the insert facilitates proper placement with the tube bore. The continuing explosive at the front end of the insert provides the means of detonation.

The explosive generally used because of its availability, consistency and safety is detonating cord. The detonating cord, which is commercially available to many charge sizes, uses PETN (pentaerythritoltetranitrate) as the explosive core load.

The body of the insert that positions and transfers the energy from the detonating explosive is usually made from low density polyethylene. Polyethylene has been selected because of its low cost and availability. In addition the absence of halogens, sulfur and heavy metals in its constituency make it safe to use when expanding materials which may be sensitive to stress corrosion cracking.

Selecting the proper charge size to perform the expansion is achieved by conducting a series of expansions using prototypical tubes and test tubesheets. Once the optimum charge size is determined for a particular material and size combination this data is retained and used for all subsequent expansions having these parameters.

The number of tubes that can be expanded simultaneously is limited only by the noise and shock wave constraints at the expansion site. As few as one and as many as 5000 tubes have been successfully expanded in one detonation.

ADVANTAGES OF EXPLOSIVE EXPANSION

The explosive expansion of tubes into tubesheets offers several distinct advantages over the once common practice of Mechanical rolling.

Mechanical rolling is accomplished by rotating tapered rollers, held within a metal cage, about the inside of the tube. These tapered rollers are rotated and forced toward the tube wall by a mandrel, which is also tapered, that is placed between the rollers. As the mandrel is rotated and driven inward the rollers gradually force the tube into contact with the tube hole. Additional force is applied until the tube is cold worked sufficiently to become tight within the hole. This method which can produce strong tight joints also causes severe local surface distortion to the tube inside surface. This cold work often leaves the tube very susceptible to stress corrosion caused failures in service.

Metallurgical examinations have shown that explosive expansion results in an almost undisturbed material structure as shown in Figure 3.

Mechanical expansion is also dependent upon the skill of the operator to achieve correct and uniform results. Explosive expansion, because of the consistency of the explosives used, produces the same degree of expansion each time.

The explosive expansions can be performed easily in remote or relatively inaccessible areas. Other methods require more space and access because of the size of the necessary tooling.

Finally, especially when the tubesheets are thick and the quantity of tubes large, there is an appreciable savings in the time required to perform the expansions.

OTHER APPLICATIONS OF EXPLOSIVE EXPANSION

The expansion of tubes into tubesheets is only one of many possible applications of explosive expansion of tubular components. The process can readily be adapted to joining tubular members into an almost endless variety of structural shapes. Identified below are only a few of the possible variations.

Tubular prefabricated sections, Figure 4, could easily be assembled and the connections explosively expanded at any location to form a ladder or other structure. Properly sized explosive charges placed into the ends of the smaller tubes would, when detonated, cause expansion of this tube at both sides and the interior of the larger tube. These expansions will firmly lock these members together.

Figure 5 shows a method of reinforcing a structure by adding a truss. These trusses would also be explosively expanded in place. Strategic locations would provide an extremely rigid structure.

Figure 6 indicates how the process can be adapted to square as well as round tubing. Finally Figure 7 shows how rotation of the expanded tubular connections can easily be prevented by premachining a key or notch into the drilled hole.

The examples shown are only a few of the many possible configurations for fastening structural components using explosive forming methods. What these examples do show is that structures could be erected and securely fastened anywhere without the need for special tools or personnel skills.

For application in remote or difficult environments the explosive charges can be pre-assembled and secured into the structural members prior to delivery to the erection site. Thus the amount of handling required during actual construction is reduced to a minimum.

CLOSURE

It has been shown that explosive forming can be used to join and fasten tubular members to form structures. The applications are endless and with the knowledge of the process in hand engineers have another tool to use when designing structures for use in the remote areas of the earth or in space.
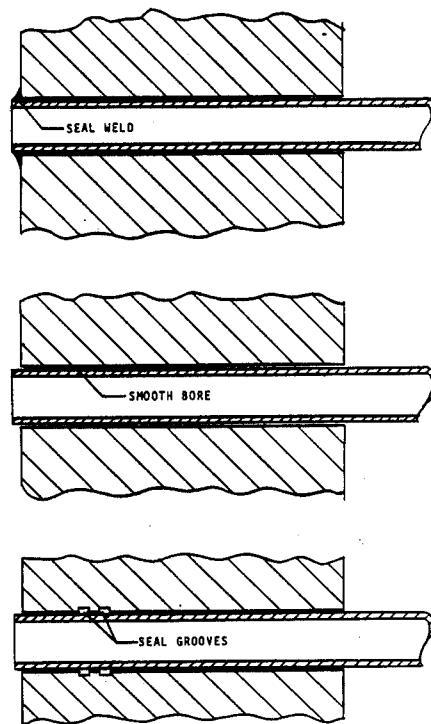
Figure 1. Typical heat exchanger tube to tubesheet joints.
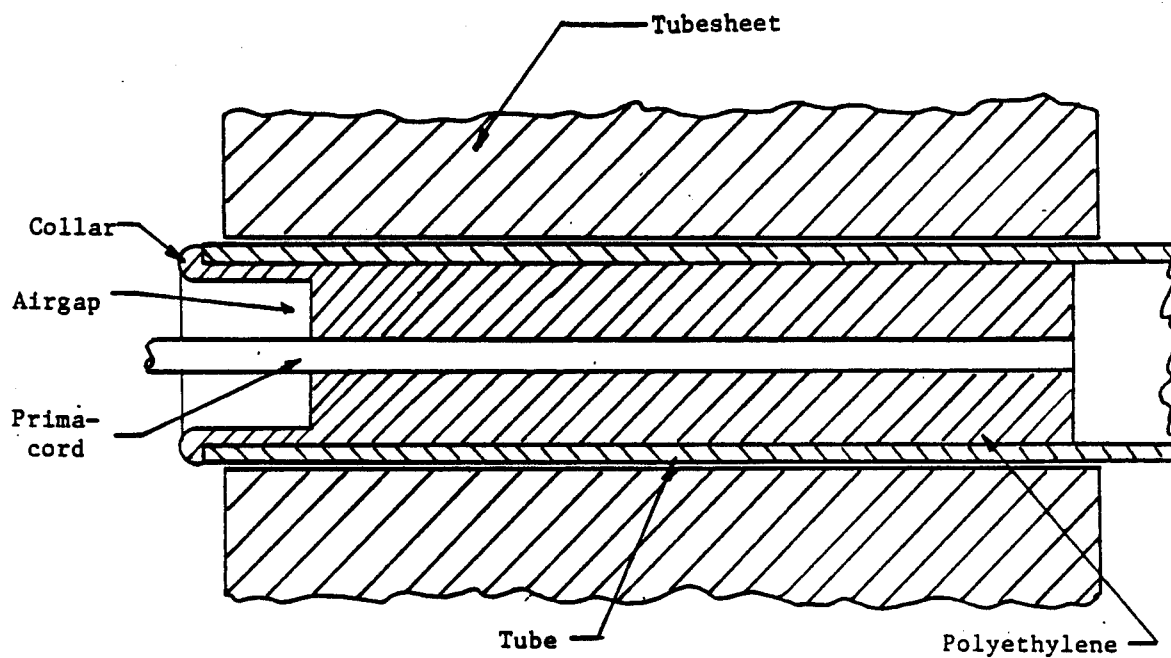
Figure 2. Explosive insert positioned in a tube and tubesheet assembly.
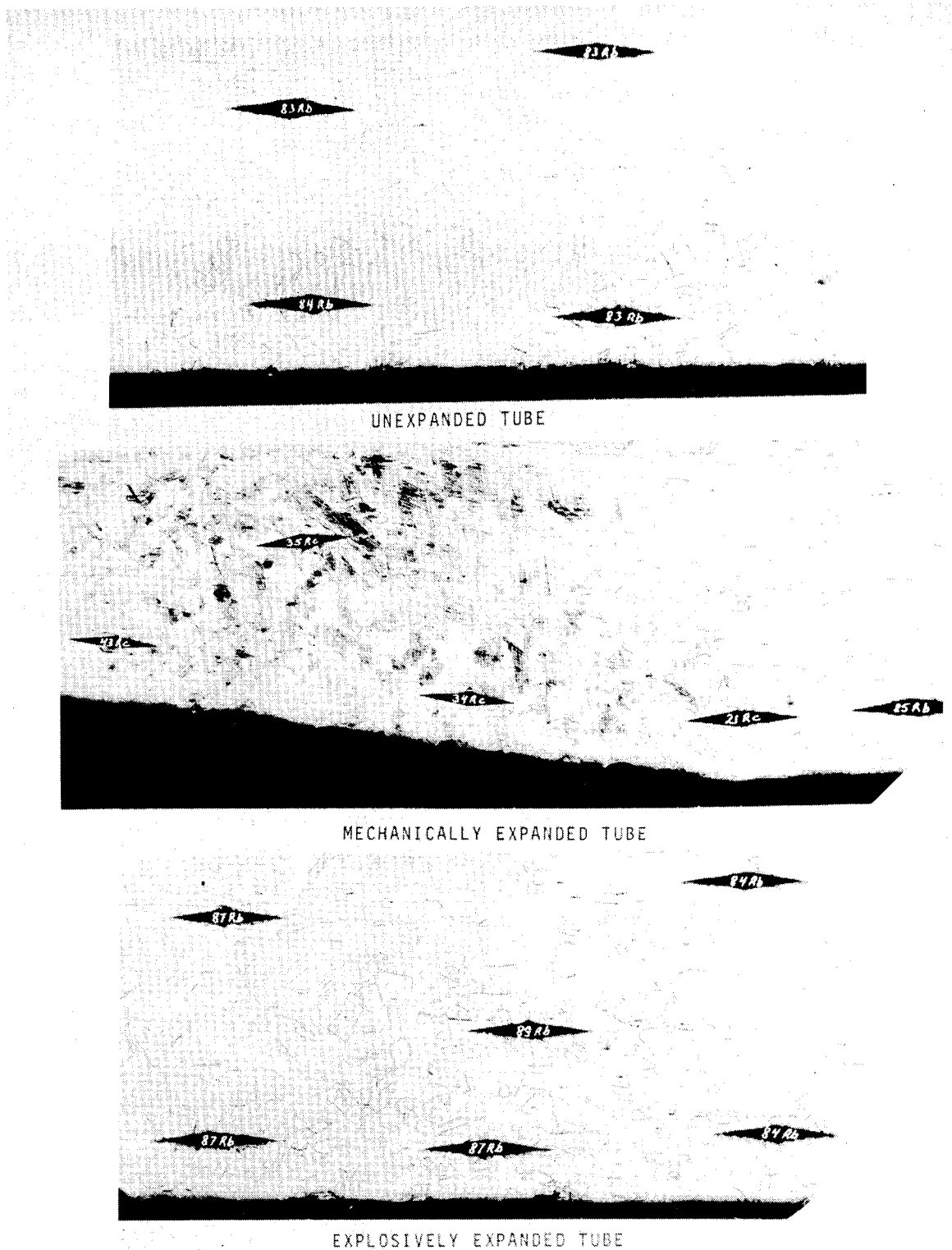
Figure 3. 100X photomicrographs showing grain structure and micro-hardness values of unexpanded, mechanically expanded and explosively expanded type 304 stainless-steel tubes.
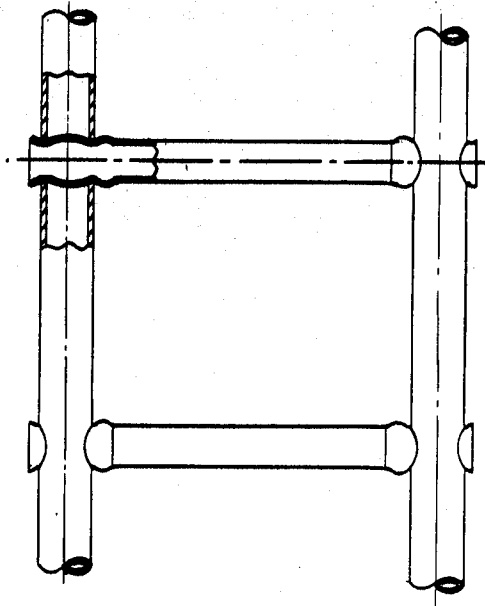
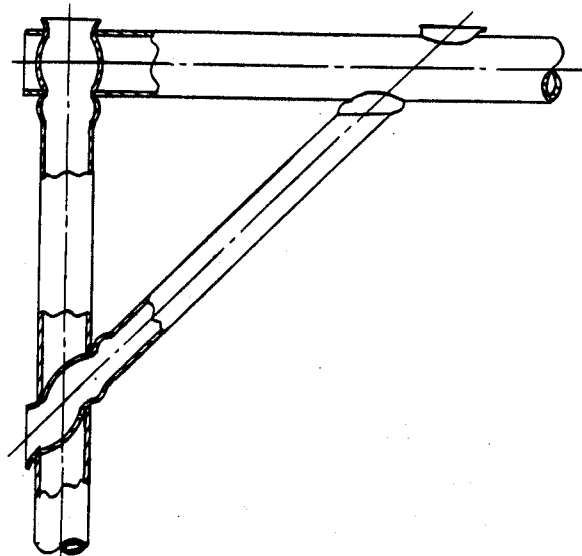Figure 4.   Assembly of tubular components to form a rigid structure.

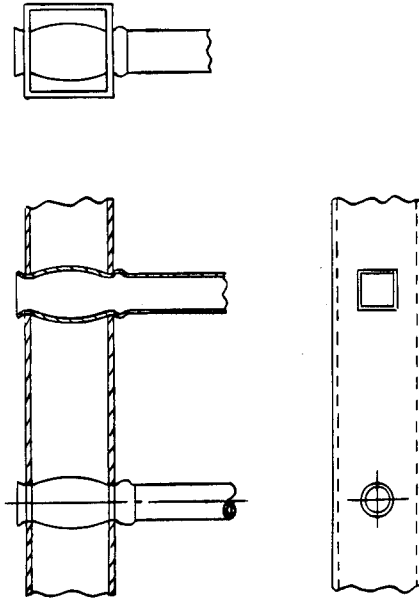Figure 5.   Reinforcement of structure by addition of a truss.

Figure 6. Application using square or rectangular tubing.
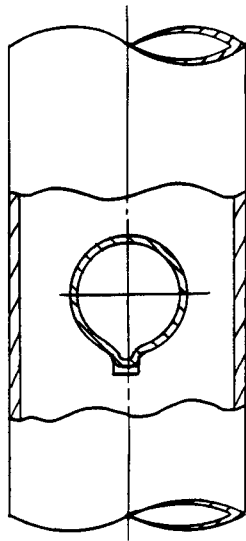
Figure 7. Method of keying to prevent rotation of round structural connections.

EXPLOSIVE WELDING OF ALUMINUM, TITANIUM AND ZIRCONIUM TO COPPER SHEET METAL

Abdel-Aziz Hegazy*
Helwan University
Helwan, Cairo, Egypt

Jim D. Mote
Chemical and Materials Sciences
Denver Research Institute
University of Denver
Denver, CO

ABSTRACT

The main material properties affecting the explosive weldability of a certain metal combination are the yield strength, the ductility, the density and the sonic velocity of the two metals. Successful welding of the metal combination depends mainly on the correct choice of the explosive welding parameters; i.e. the stand-off distance, the weight of the explosive charge relative to the weight of the flyer plate and the detonation velocity of the explosive.

Based on the measured and the handbook values of the properties of interest, the explosive welding parameters were calculated and the arrangements for the explosive welding of the Al-alloy 6061-T6, titanium and zirconium to OFHC-copper were determined. The relatively small sheet metal thickness (1/8") and the fact that the thickness of the explosive layer must exceed a certain minimum value were considered during the determination of the explosive welding conditions. The results of the metallographic investigations and the measurements of the shear strength at the interface demonstrate the usefulness of these calculations to minimize the number of experimental trials.

INTRODUCTION AND OBJECTIVES

Cladding of dissimilar sheet metals can be achieved by explosive welding (1-4). The parallel configuration shown in Figure 1 is used when the sheet metals are of relatively large planar dimensions. The main explosive welding parameters are the detonation velocity of the explosive, the weight of the explosive charge relative to that of the flyer plate (c/m ratio) and the stand-off distance between the flyer and the base plate. The determination of the explosive welding parameters, which produce good metallurgical bond at the interface, is governed by the density, the sonic velocity, and the plastic properties of the flyer and base plate materials besides the thickness of the flyer plate.

The objectives of this program were to clad OFHC-copper plates to plates of the aluminum alloy 6061-T6, titanium (ASME SB265GR2) and zirconium (ASTM B551-79). The explosive welding parameters were calculated and the quality of the resulting bond was evaluated.

MATERIAL PROPERTIES

The yield strength ($\sigma_{0.5}$), the ultimate tensile strength σ_u and the percent elongation δ of the materials used in this program were measured, while the density, the sonic velocity C and the melting temperature T_m are the handbook values (5), Table 1.

Table 1: Material Properties

Property	Material			
	Al6061-T6	OFHC Copper	Titanium ASME SB 265 GR2	Zirconium ASTM B 551-79
$\sigma_{0.5}$ (N/mm^2)	276	277	353	416
σ_u (N/mm^2)	334	243	492	534
δ (%)	10	40	24	20
ρ (g/cm^3)	2.7	8.96	4.54	6.44
ρC (m/s)	5105	3580	5100	3600
ρC (g.m/cm^3.s) (Impedance)	13784	32077	23154	23184
T_m (^{o}C)	660	1083	1725	1850
Thickness (mm)		3.18	(1/8")	

SELECTION OF THE WELDING PARAMETERS

The explosive welding parameters were selected using the approach summarized by Ezra (2) and experimentally verified by Hegazy and Badawi(6).

The stand-off distance, i.e. the initial gap between the two plates, was taken equal to the thickness of the flyer plate = 3.175 mm. The detonation velocity of the explosive should be between 1/2 and 2/3 of the sonic velocity of the slower of the two metals. Since copper is the common material and it has the lowest sonic velocity of 3580 m/s, Table 1, the detonation velocity of the explosive in the three metal combinations Cu/Al, Cu/Ti and Cu/Zr should be higher than 1790 m/s and lower than 2386 m/s. Amatol with 80% ammonium nitrate and 20% TNT was used in the powder form as an explosive. The detonation velocity of Amatol was found to change with the thickness of the explosive layer as indicated in Figure 2. Explosive layers with a thickness less than 25 mm may produce unreliable detonation. The choice of the thickness of the explosive layer is governed by the density and the thickness of the flyer plate. This is evident from the following relation

$$\frac{c}{m} = \frac{\rho_{ex} \cdot t_{ex}}{\rho_f \cdot t_f} \qquad (1)$$

Where c = weight per unit area of the explosive
      m = weight per unit area of the flyer plate
      t = density and thickness
         The subscripts ex and f refer to the explosive and the flyer plate respectively.

Copper is chosen as a flyer plate for the following reasons:

   i.   Copper has the highest ductility, Table 1, and hence it can withstand the higher plastic deformations due to double plastic bending.

   ii.   Copper has the highest density, Table 1, and hence the c/m ratio, Eq (1), can be kept as low as c/m = 0.9 taking into consideration that the thickness of the explosive layer may not be less than 25 mm and the density of the explosive ρ_{ex} 1 g/cm^3. Higher values of c/m will reduce the bonding strength (6).

Referring again to Figure 2, the detonation velocity corresponding to an explosive layer of 25 mm is about 3500 m/s. This value is higher than the maximum allowable detonation velocity of 2386 m/s. Addition of salt to Amatol reduces the detonation velocity as shown in Figure 3. Using an Amatol-salt mixture of 18% salt gives in the average a detonation velocity of V_d = 2300 m/s.

The estimated values of the explosive welding parameters are therefore as follows:

```
stand-off distance = 3.175 mm
c/m ratio = 0.9
(copper as flyer plate)
detonation velocity $V_d$ = 2300 m/s
```

These values will be used to check the resulting plate impact velocity Vp and the resulting impact pressure P at the interface. The approximate relation (2)

$$P = \frac{\rho_1 C_1 \cdot \rho_2 C_2}{\rho_1 C_1 + \rho_2 C_2} V_p \qquad (2)$$

can be used to obtain the impact pressure, where $_1$, c_1, and $_2C_2$ are the acoustic impedances of the colliding plates and Vp is the impact velocity. Figure 4 shows a graphical representation of Eq (2) for the required material combinations Cu/Al, Cu/Ti and Cu/Zr using the values of the impedence given in Table 1.

The plate impact velocity may be related to the detonation velocity and the c/m ratio through the empirical equation of Deribas et al. given in Reference (2)

$$V_p = 1.2 \ V_d \ \frac{x-1}{x+1} \qquad (3)$$

$$\text{where } x = (1+1.185 \ \frac{c}{m})^{\frac{1}{2}}$$

Substituting the values of c/m = 0.9 and V = 2300 m/s gives V = 496 m/s. From Figure 4 the plate impact pressure will be 4850 N/mm for Cu/Al and 6600 N/mm^2 for Cu/Ti and Cu/Zr. Comparing those values with the static yield strength of the metals ($\sigma_{0.5}$), Table 1, the impact pressure is about 18 times the yield strength of the stronger Al-alloy (Cu/Al) and about 19 times the yield strength of the stronger titanium (Cu/Ti) and about 16 times the yield strength of the stronger zirconium (Cu/Zr). These figures are higher than the values reported by Ezra(2) of 10-12 times the yield strength of the stronger of the two metals. However, an analysis carried out by Hegazy and Badawi(6) of the experimental results of Zhengkui et al.(7) showed that good welding is achieved at impact pressures which are up to 25 times the yield strength of the stronger of the two metals.

EXPLOSIVE WELDING EXPERIMENTS

The calculated explosive welding parameters were checked experimentally using plates of 150 x 300 mm planar dimensions. A No. 8 detonator and 10g Detasheet booster are used to initiate the explosive reaction along the plate length. A 19-mm thick hard board is used as an energy sink. Before assembling the mating surfaces of the metal plates were cleaned and degreased.

QUALITY OF WELDMENTS

The quality of the weldments was evaluated through metallographic investigations and shear strength measurements at the interface. Figures 5, 6 and 7 show the shape of the interface along sections parallel and normal to the direction of detonation for the metal combinations Cu/Al, Cu/Ti and Cu/Zr respectively. A straight interface resulted between copper and aluminum, a uniform wavy interface resulted between copper and titanium and nonuniform wavy interface was achieved between copper and zirconium. Satisfactory welds can be obtained with all three types of interfaces (8) provided no excessive melting takes place at the interface. Theoretical and experimental analysis of wave formation during explosive welding has been the subject of many publications, e.g. (9,10)

The shear strength at the interface was also measured parallel and normal to the direction of detonation in the way shown schematically in Figure 8. The cross-sectional area of the tested interface ranges between 3 and 20 mm^2. The results of the shear tests are summarized in Table 2 together with the shear strength ($\approx \frac{1}{2} \sigma_u$) of the metals before cladding.

Table 2: Results of the shear tests at the weld
interface for the three metals combinations

Metal combination	Initial shear strength N/mm^2	Shear strength at the interface N/mm^2	
		parallel	normal
Cu/Al	121/167	148	140
		143	162
Cu/Ti	121/246	174	134
		193	132
Cu/Zr	121/267	191	204
		201	203

It can be seen from Table 2 that the shear strength at the interface of all material combinations is higher than the initial shear strength of the weaker metal.

CONCLUSIONS
1. The calculated explosive welding parameters for the used material combinations produced high-quality weldments after the first shot.
2. The impact pressure at the interface can be as high as 19 times the yield strength of the stronger of the two metals without causing excessive melting.

REFERENCES
1. Rinehart J. and Pearson, T., "Explosive Working of Metals". Pergamon Press, New York, 1963.

2. Ezra, A.A., "Principles and Practice of Explosive Metal Working", Industrial Newspapers Limited, London, 1973.

3. Crossland, B., "Explosive Welding of Metals and its Applications", Clarendon Press, Oxford, 1982.

4. Blazynski, T.Z., ed., "Explosive Welding, Forming and Compaction", Applied Science Publishers, London, 1983.

5. Miner, D., and Seastone, J., "Handbook of Engineering Materials", John Wiley and Sons, New York, 1955.

6. Hegazy, A.A., and Badawi, G., "Estimation of the Charge Weight for an Explosive Welding Process". Second PEDAC Conf. of the Alexandria University, Alexandria, Egypt, 27-29 Dec. 1983.

7. Zhengkui, Z., and Shaoyao, W., "The Determination of the Weldability Window and the Reasonable Charge for Explosive Welding Copper to Steel by the Use of the Semi-Cylinder Method". 7th Int. HERF Conference, Leeds, England, 14-18 September 1981.

8. Szecket, A. et al., "Explosive Welding of Aluminium to Steel; A Wavy Versus a Straight Interface". 8th Int. HERF Conference, San Antonio, Tx, USA, 17-20 June 1984.

9. El-Sobky, H. and Blazynski, T.F. "Experimental Investigation of the Mechanics of Explosive Welding by Means of a Liquid Analogue", 5th Int. HERF Conference, Denver, CO, USA, 24-26 June 1975.

10. Hampel, H. and Richter, U., "Formation of Interface Waves and the Explosive Cladding Parameters". 7th Int. HERF Conference, Leeds, England, 14-18 September 1981.
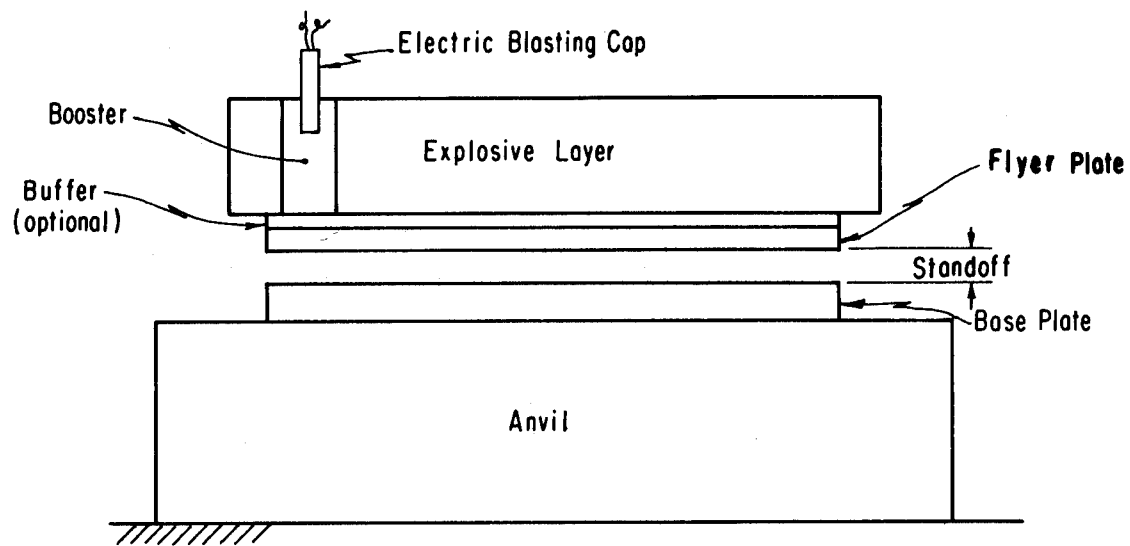
Figure 1: Parallel configuration for the explosive welding of two plates
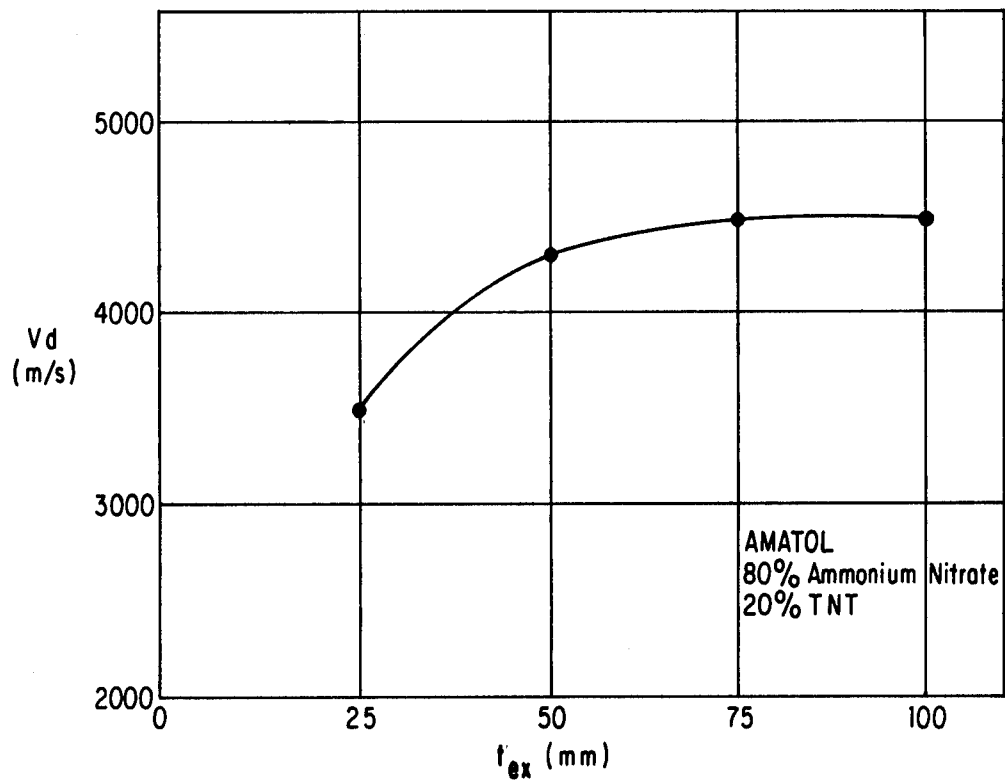
Figure 2: Effect of the thickness of the explosive layer t_{ex} on the detonation velocity Vd
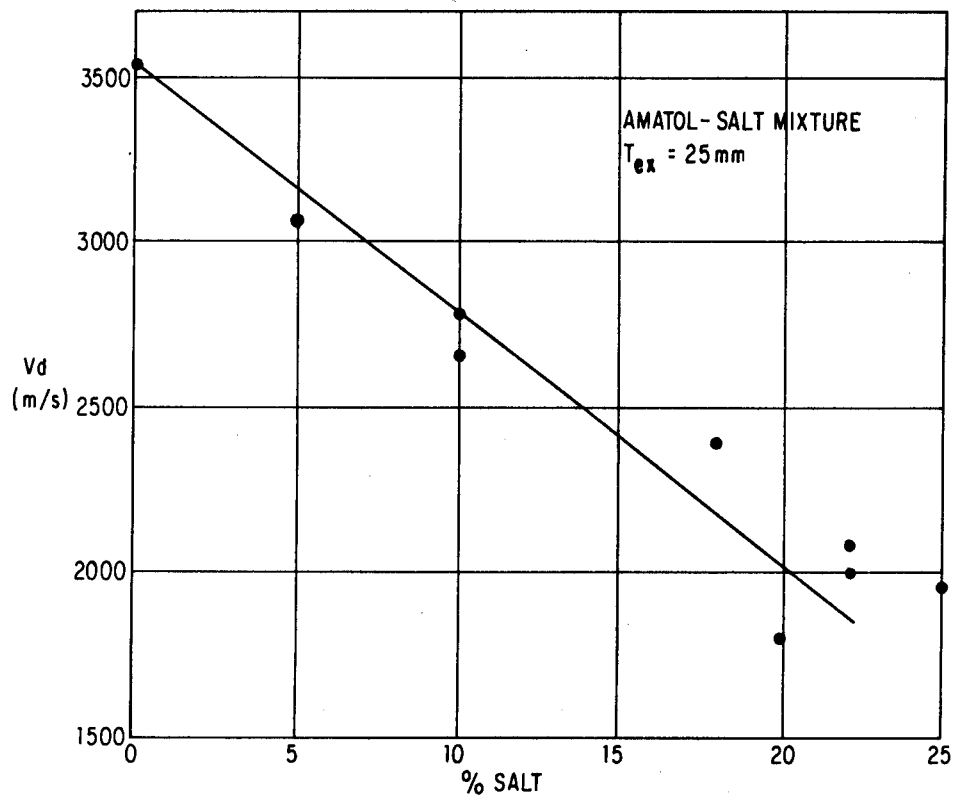
Figure 3: Effect of the percent salt on the detonation velocity Vd for an explosive layer of a thickness of 25 mm
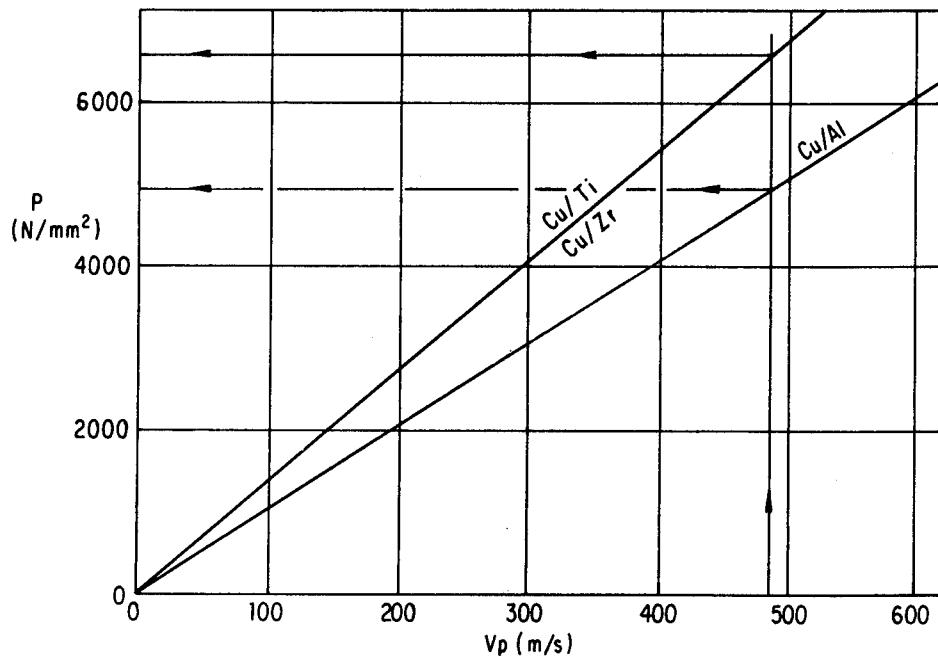
Figure 4: Relations between the impact velocity Vp on the impact pressure P at the interface for the material combinations Cu/Al, Cu/Ti and Cu/Zr
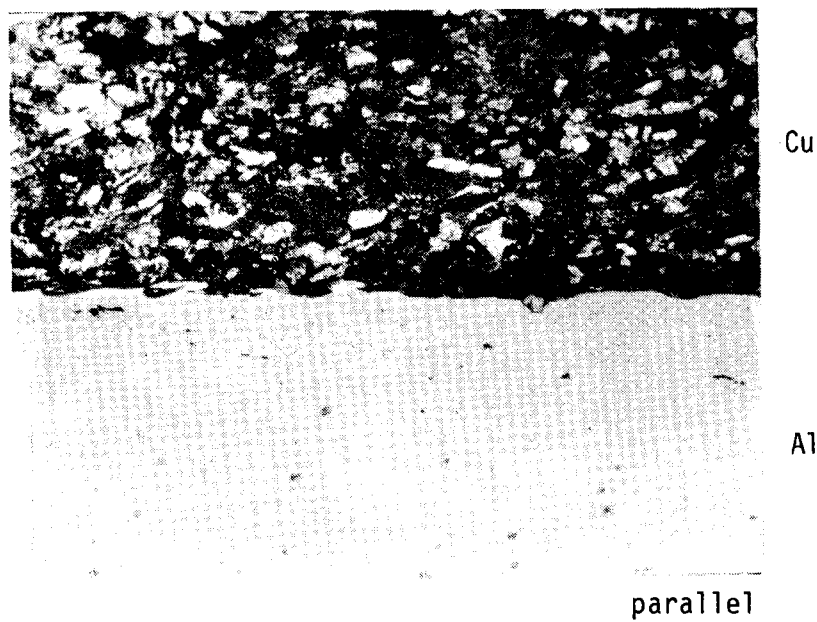
Cu

Al

parallel

Cu

Al
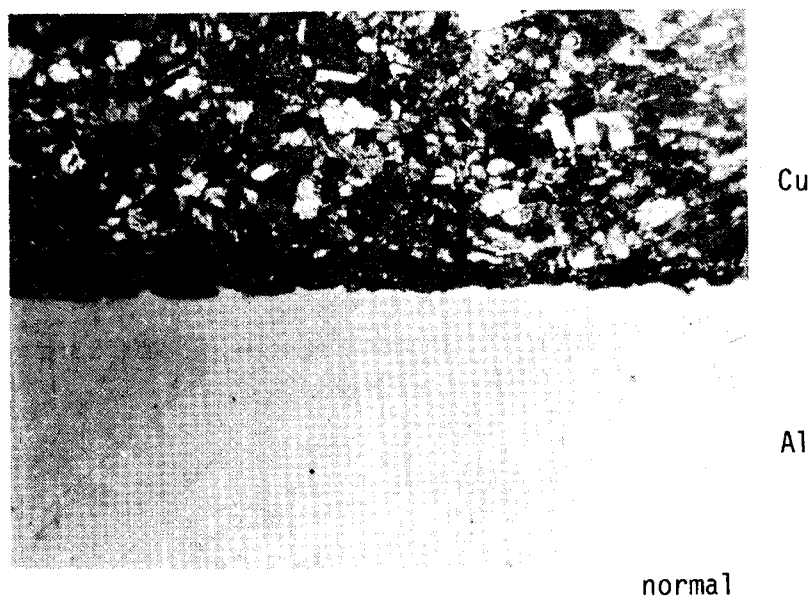
normal

Figure 5: Cu/Al-interface parallel and normal to the direction of denotation. Copper is etched for contrast, 150X

Cu

Ti

parallel

Cu

Ti
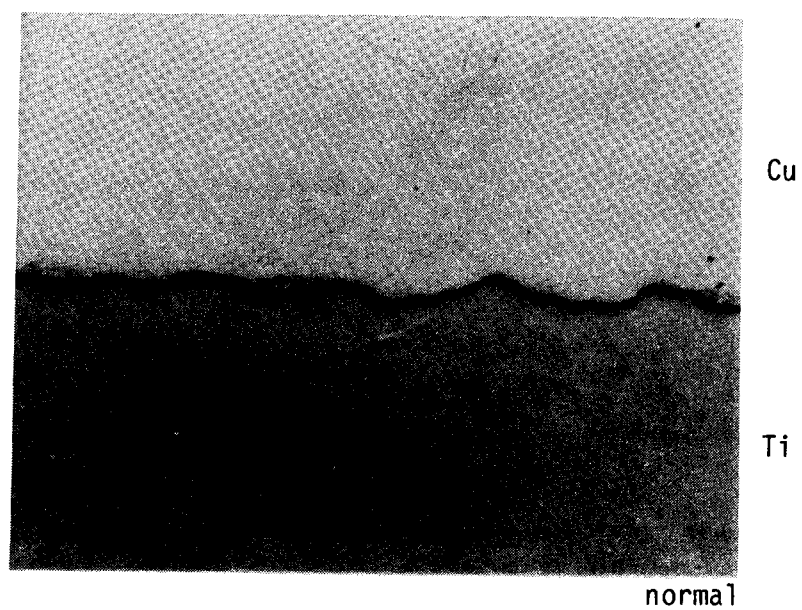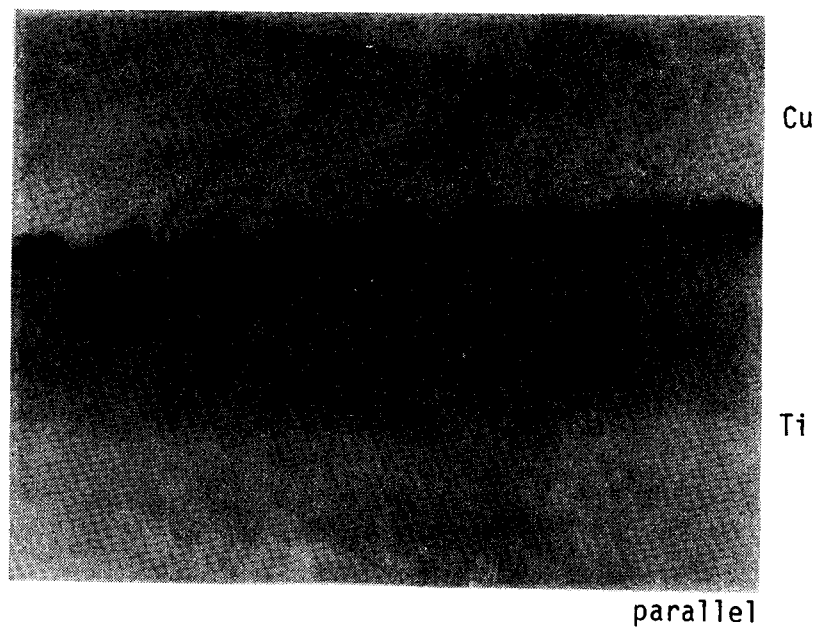
normal

Figure 6:   Cu/Ti-interface parallel and normal to the direction of
detonation, 77X

Cu

Zr

parallel

Cu

Zr
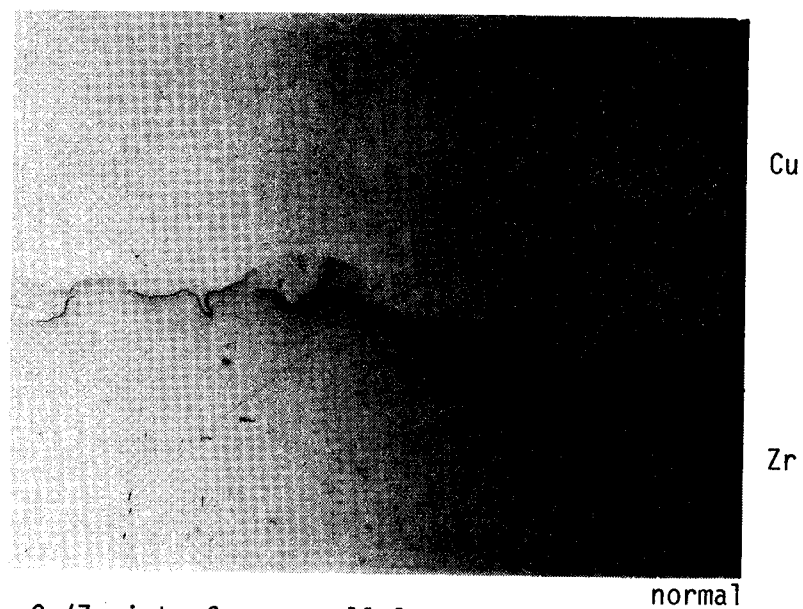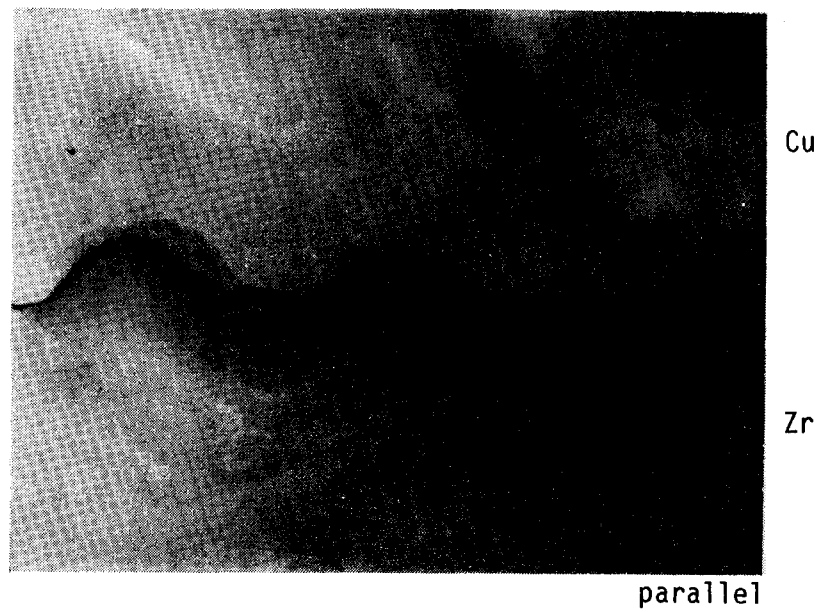
normal

Figure 7: Cu/Zr-interface parallel and normal to the direction of detonation, 150X
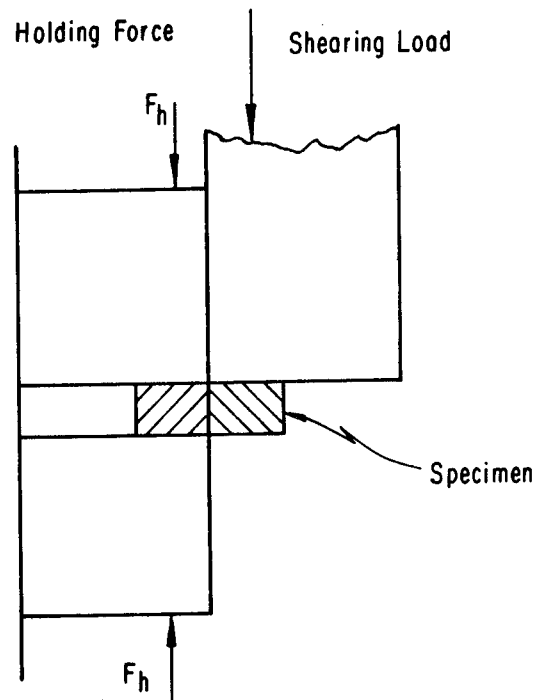
Figure 8: Schematic representation of the shear strength measurement at the interface

NONDESTRUCTIVE ULTRASONIC MEASUREMENT OF BOLT PRELOAD USING THE PULSED-PHASE LOCKED-LOOP INTERFEROMETER

S. G. Allison and J. S. Heyman
NASA Langley Research Center
Hampton, Virginia 23665

ABSTRACT

Achieving accurate preload in threaded fasteners is an important and often critical problem which is encountered in nearly all sectors of government and industry. Conventional tensioning methods which rely on torque carry with them the disadvantage of requiring constant friction in the fastener in order to accurately correlate torque to preload. Since most of the applied torque typically overcomes friction rather than tensioning the fastener, small variations in friction can cause large variations in preload. An instrument called a pulsed-phase locked-loop interferometer, which was recently developed at NASA Langley, has found widespread use for measurement of stress as well as material properties. When used to measure bolt preload, this system detects changes in the fastener length and sound velocity which are independent of friction. The system is therefore capable of accurately establishing the correct change in bolt tension. This high-resolution instrument has been used for precision measurement of preload in critical fasteners for numerous applications such as the Space Shuttle landing gear and helicopter main rotors.

INTRODUCTION

Several years ago, NASA Langley Research Center began developing a technique for accurately measuring preload in threaded fasteners. As a result of this effort, today we have just such an instrument called a pulsed-phase locked-loop interferometer. This new measurement system offers vast improvement over torque for meeting the objective of threaded fasteners, i.e., obtaining the desired amount of clamping force or preload holding an assembly together. The problem with the conventional torque approach for obtaining preload is that since most of the applied torque goes toward overcoming friction, large errors are caused by variations in friction. Conventional use of torque achieves preload accuracy of 20 percent at best, and it is not at all unusual to expect an accuracy of only 50 percent or even worse using torque to measure bolt preload. The solution is to measure stress, not torque. The pulsed-phase locked-loop system ultrasonically measures bolt "stretch" without measuring friction. With this new system, bolt preload can be measured with accuracies ranging from better than 1 percent for good geometry bolts to approximately 3 percent for fasteners having poor geometry and with measurement resolution of 1 psi.

This report describes some basic problems associated with the conventional use of torque for bolt preload measurements and shows data illustrating the improvements obtainable with some ultrasonic techniques. The report gives background information about previous instruments which led to development of the current pulsed-phase locked-loop system and discusses some of the earlier limitations which have been eliminated by the current state-of-the-art system. The present pulsed-phase locked-loop system is described giving examples of bolt preload measurement applications as well as describing other capabilities of this versatile measurement instrument.
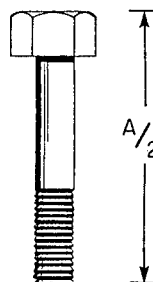
ULTRASONIC BOLT MEASUREMENTS

$$F_j = \frac{jV}{A}$$
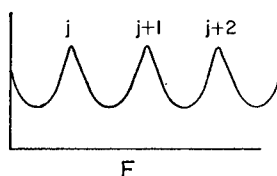
$$\Delta F_j = \frac{jV}{A}\left(\frac{1}{V}\frac{dV}{dA} - \frac{1}{A}\right)\Delta A$$

$$\Delta F_j = F_j \left[\frac{1}{V}\frac{dV}{dS} - \frac{1}{E}\right]\Delta S$$

$$\frac{dV}{dS} = \frac{-1}{6\rho(\lambda+2\mu/3)V}\left[2\ell + \lambda + \frac{\lambda+\mu}{\mu}(4m+4\lambda+10\mu)\right]$$

EXAMPLE FOR MILD STEEL

$$\Delta F = 0.632 \ \Delta S \ (POUNDS/IN.^2) \ AT \ 5MHz$$

In order to illustrate how bolt preload can be measured ultrasonically, an analogy can be made to the pipe organ. A pipe organ uses pipes of different lengths so that each pipe has a different resonance frequency in accordance with its length. If one of these pipes was to be made slightly longer or shorter, and if the sound velocity of the gas in the pipe was changed, the resonance frequency would shift in proportion to the change in length and gas sound speed. In a similar manner, continuous wave (CW) type bolt monitors use the bolt as an ultrasonic resonator (like the organ pipe). An ultrasonic transducer is placed on the end of the bolt producing sound waves within the bolt. The insonified bolt typically has several resonance frequencies (see Fig. above), i.e., the fundamental plus a number of harmonics which are integral multiples of the fundamental. When the bolt is tightened, the length and sound velocity changes cause a proportional change in resonance frequency. By tracking the resonance frequency changes, the bolt monitor is also tracking stress (preload) changes since the change in resonance frequency is equal to a constant times the change in stress.

INTRODUCTION TO THE MEASUREMENT SYSTEMS

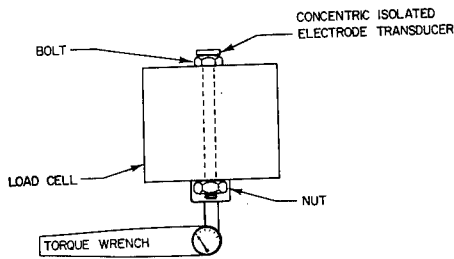## EVOLUTION OF NASA BOLT MONITOR

TOUS

ROUS — Won IR-100 award in 1976

PCW

SQ

P^2L^2 — Named NASA Invention of the Year in 1982
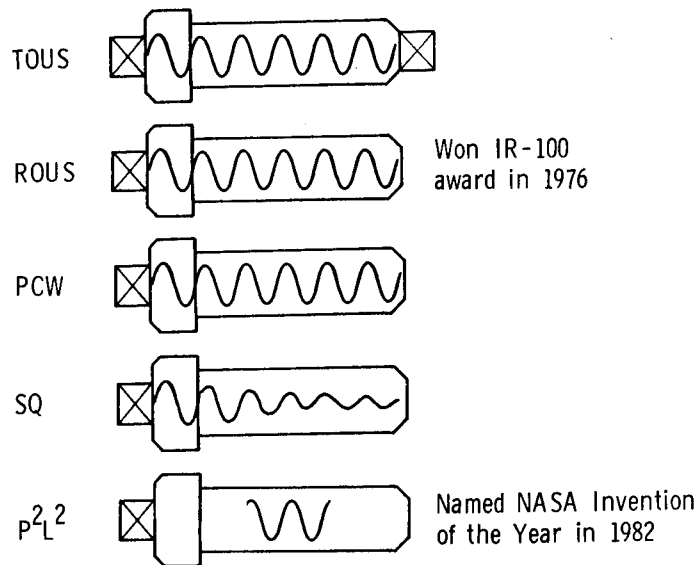
The pulsed-phase locked-loop (P^2L^2) system evolved from several predecessors including the transmission oscillator ultrasonic spectrometer (TOUS), the reflection oscillator ultrasonic spectrometer (ROUS), the pseudo-continuous wave (PCW) system and the spoiled Q (SQ) system. Each predecessor to the P^2L^2 offered great improvement over the conventional torque method but also had some special requirements. For example, the CW TOUS (Ref. 1) could measure bolt preload with great precision but required the use of a transducer at each end of the bolt and also required bolt preparation, i.e., machining of the bolt ends to be smooth, flat and parallel. The CW ROUS system (Ref. 2), which won an IR-100 Award in 1976, also measured preload with great precision and offered the additional advantage of requiring the use of only one transducer so that access to only one end of the bolt was required. The ROUS, however, still required bolt end preparation and also required use of a special complex transducer that could continuously transmit and receive signals simultaneously. The PCW system (Ref. 3) eliminated the need for a complex transducer but still required bolt preparation. In addition, the PCW began to move away from a pure CW system. The SQ system moved further away from a pure CW concept and eliminated the requirement for bolt preparation, but, in doing so, it sacrificed the ability to make bolt preload measurements with the degree of precision achieved by previous bolt monitors. Finally, the P^2L^2 system (Ref. 4) eliminated all of the special requirements, i.e., it provided a means of measuring bolt preload with great precision (parts in 10^7) using one simple transducer and without requiring any bolt preparation. The P^2L^2 was named NASA Invention of the Year in 1982 and has been used to verify bolt preload in a number of critical applications. It is neither CW or broadband pulsed. Instead, it is between a frequency domain instrument and a time domain instrument.

MEASUREMENT SYSTEM DETAILS

R O U S BOLT MONITOR
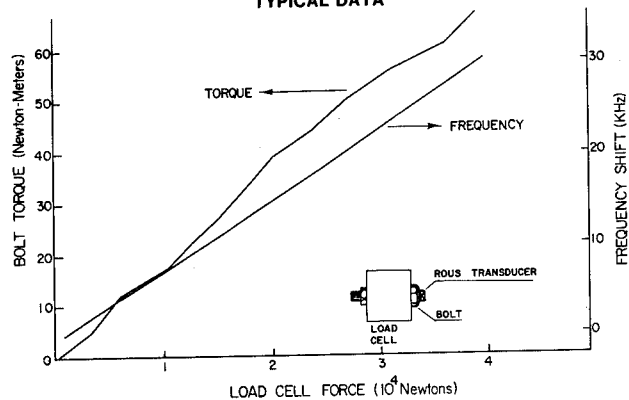

ACOUSTIC SPECTRA VERSUS LOAD
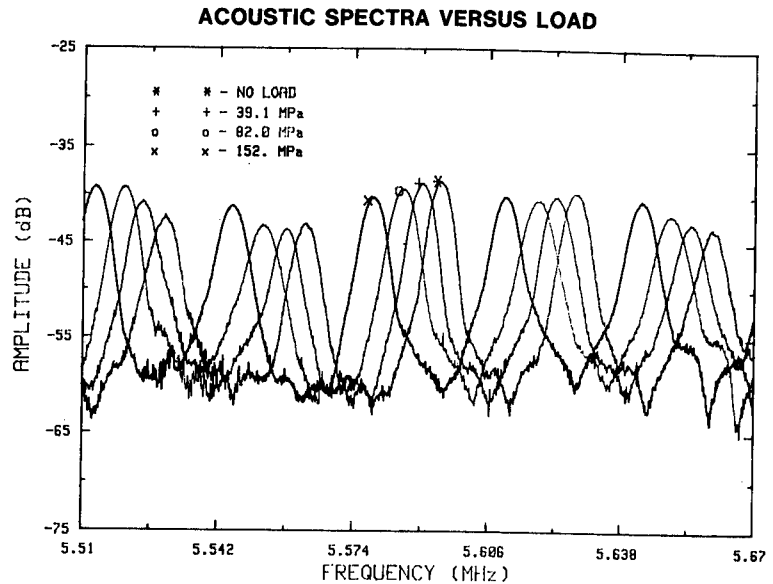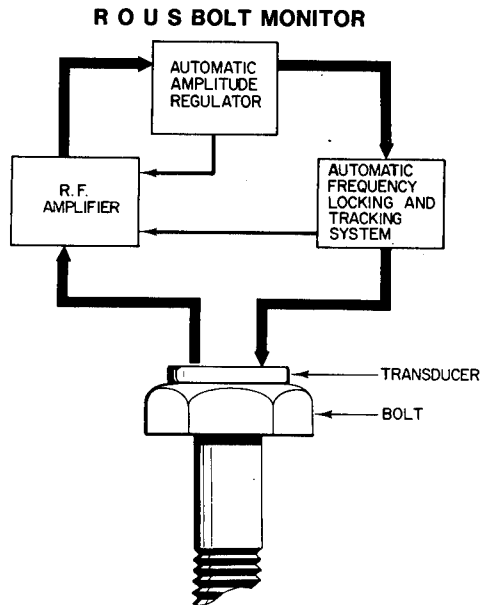
The ROUS system, as previously mentioned, uses a complex transducer acoustically coupled to the bolt to transmit and receive ultrasonic waves. The electronics system incorporates a special marginal oscillator which uses resonance feedback from the bolt to track stress-induced resonance frequency changes. By examining the above typical acoustic spectral response of a bolt at different preload levels, one can see that tightening of the bolt causes the resonance frequency to shift. The ROUS bolt monitor measures these stress-induced changes in bolt resonance frequency with a high degree of accuracy.
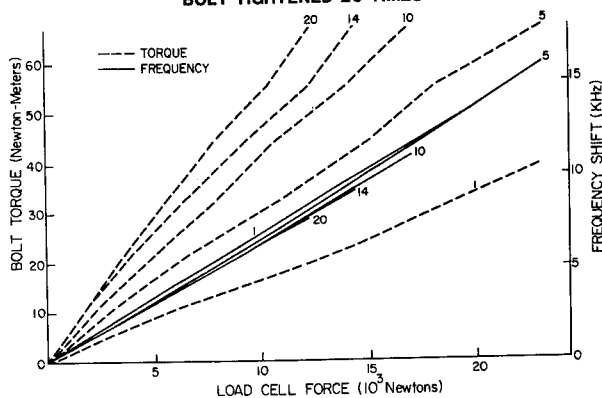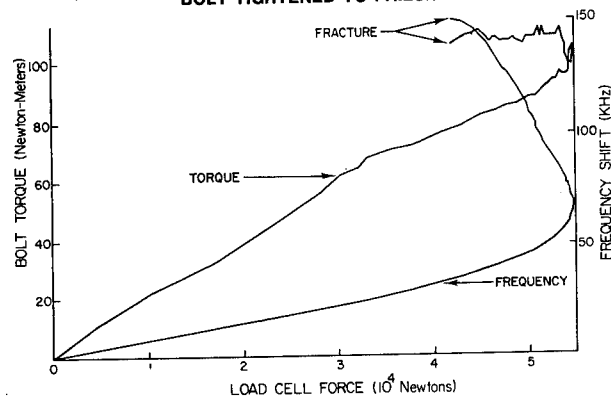
TEST ARRANGEMENT

CONCENTRIC ISOLATED
ELECTRODE TRANSDUCER

BOLT

LOAD CELL

NUT

TORQUE WRENCH

TYPICAL DATA

BOLT TORQUE (Newton-Meters)

FREQUENCY SHIFT (KHz)

TORQUE

FREQUENCY

ROUS TRANSDUCER

BOLT

LOAD CELL

LOAD CELL FORCE (10^4 Newtons)

BOLT TIGHTENED 20 TIMES

---- TORQUE
—— FREQUENCY

BOLT TORQUE (Newton-Meters)

FREQUENCY SHIFT (KHz)

LOAD CELL FORCE (10^3 Newtons)

BOLT TIGHTENED TO FAILURE

FRACTURE

TORQUE

FREQUENCY

BOLT TORQUE (Newton-Meters)

FREQUENCY SHIFT (KHz)

LOAD CELL FORCE (10^4 Newtons)

In order to show the relationship between actual bolt preload, applied tightening torque, and acoustic resonance frequency, the test arrangement shown in the top left figure above is used. In this arrangement, a bolt is placed through a load cell and a torque wrench is used to tighten the bolt to a known load level. A ROUS system measures stress-induced resonance frequency shifts in the bolt. Typical torque and frequency shift data are shown in the top right figure as a function of load cell force. This illustrates that frequency is much more directly related to bolt preload than is torque.

In the lower left figure, data for a bolt tightened 20 times illustrate that use of torque can result in large variations in bolt preload. In this case, retightening of a bolt 20 times results in a 70% change in bolt preload. Note that the ultrasonic data consistently track bolt preload regardless of changes in friction. The slight change in slope of the ultrasonic data is due to a small change in load length resulting from yielding of the fastener threads. In the lower right figure a bolt is tightened to failure showing that the ultrasonic frequency data track bolt stress all the way to fracture. One can see from this that the ultrasonic system can even be used to detect yielding of the fastener since the ultrasonic frequency will continue to increase after the applied torque stops increasing.

P^{2}L^2 MEASUREMENT SYSTEM

BLOCK DIAGRAM
PULSED-PHASE LOCKED-LOOP INTERFEROMETER
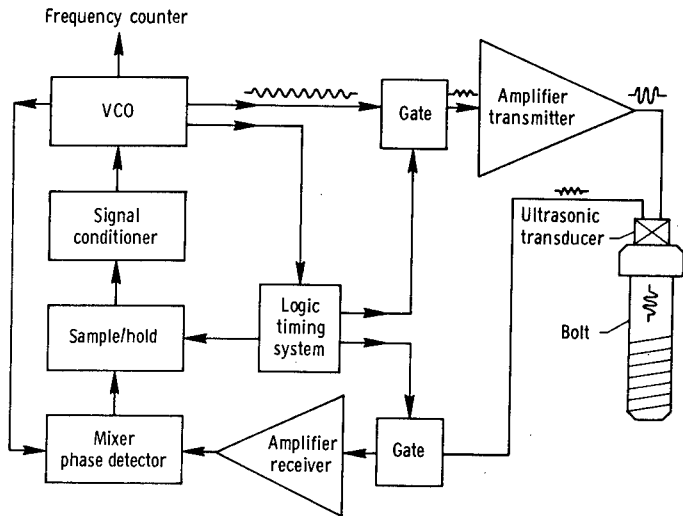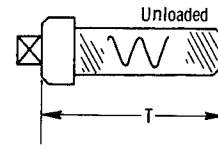
THEORY OF OPERATION

TIME DOMAIN

$$T = \frac{L}{V} \qquad (T = 2 \text{ way propagation time})$$

$$\frac{dT}{d\sigma} = \frac{1}{V}\frac{\partial L}{\partial \sigma} - \frac{L}{V^2}\frac{\partial V}{\partial \sigma}$$

$$\frac{dT}{d\sigma} = T\left[\frac{1}{L}\frac{\partial L}{\partial \sigma} - \frac{1}{V}\frac{\partial V}{\partial \sigma}\right]$$

$$\frac{dT}{T} = \left[\frac{1}{L}\frac{\partial L}{\partial \sigma} - \frac{1}{V}\frac{\partial V}{\partial \sigma}\right] d\sigma$$

$$\frac{\Delta T}{T} = \left(\frac{\Delta L}{L} - \frac{\Delta V}{V}\right)$$
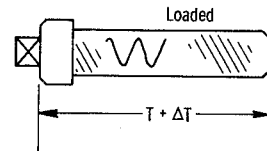
FREQUENCY DOMAIN

$$\Phi = 2\pi F T$$

$$\frac{d\Phi}{d\sigma} = 2\pi\left[F\frac{\partial T}{\partial \sigma} + T\frac{\partial F}{\partial \sigma}\right] \equiv 0$$

$$F\frac{\partial T}{\partial \sigma} = -T\frac{\partial F}{\partial \sigma}$$

$$\frac{\Delta F}{F} = \frac{-\Delta T}{T}$$

$$\frac{\Delta F}{F} = \left(\frac{\Delta V}{V} - \frac{\Delta L}{L}\right)$$

Unloaded

Loaded

The P^{2}L^2 system is the state-of-the-art instrument offering high resolution without the limitations of previous bolt monitors. The P^{2}L^2 shown in the above block diagram uses a voltage-controlled oscillator (VCO) and gate to send out an electronic pulse consisting of a few cycles of RF energy to drive an ultrasonic transducer. This produces an acoustic tone burst or sound wave pulse that travels down the length of the bolt and bounces off of the far end. The returning echo produces an electronic signal that is received back into the P^{2}L^2, is amplified and goes to a phase detector. The phase detector compares the phase of the received signal to that of the signal that went out, generates a voltage proportional to the difference in phase, and (when the instrument is locked) changes the frequency of the VCO such that the phase of the signal out is held constant with respect to the phase of the signal in. With this arrangement, a change in acoustic phase in the bolt causes a corresponding change in output frequency of the P^{2}L^2 system. Therefore, when we preload the bolt we change the acoustic pathlength as well as the velocity of sound and cause a change in the output frequency of the P^{2}L^2.

The P^2L^2 system is actually measuring small changes in acoustic propagation time in the bolt. The right-hand figure on the preceding page shows a bolt in the unloaded and loaded configurations. Before loading, the pulse propagation time (or time of flight) is T whereas after preloading the propagation time becomes T + ΔT. This small change in propagation time, ΔT, can be measured in the time domain or in the frequency domain. In the time domain, the time of flight is the acoustic pathlength, L, divided by the velocity of sound, V. If we take the derivative of T with respect to stress, we obtain an expression containing stress-induced length and velocity changes. This expression simplifies to show that a change in propagation time is proportional to a material strain and an ultrasonic velocity change. Time domain measurements involve thresholds, noise, amplitude variations and complex propagation laws. Of course, the P^2L^2 instrument is more of a phase velocity device which is not subjected to the group velocity constraints of a time domain device. Because of inaccuracies inherently associated with measuring in the time domain, the P^2L^2 system was developed to measure in the frequency domain in which stress-induced acoustic phase shifts can be measured with great precision. Since the acoustic phase, ϕ, is a function of acoustic frequency, F, and propagation time, T, the derivative of the phase with respect to stress is a function of the stress-induced changes of propagation time and frequency as shown on the preceding page. Since our P^2L^2 system maintains constant phase, the stress derivative of the acoustic phase is forced to equal zero. The above expression then simplifies to show that the stress-induced frequency shift measured by the P^2L^2 is directly related to the small stress-induced change in ultrasonic pulse propagation time. This can be rewritten to show that the stress-induced frequency shift is proportional to a stress-induced strain and a stress-induced velocity change.
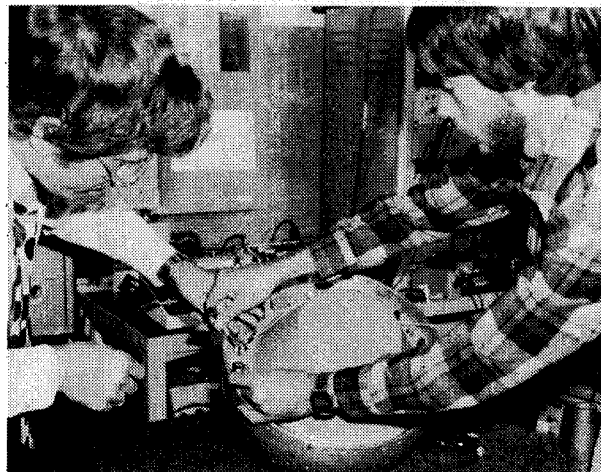
TYPICAL CRITICAL FASTENERS
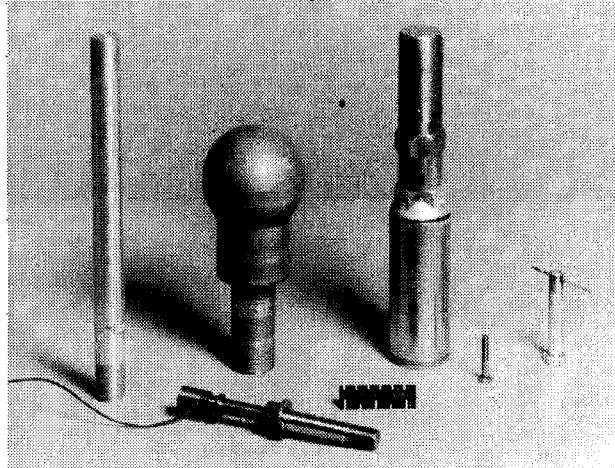
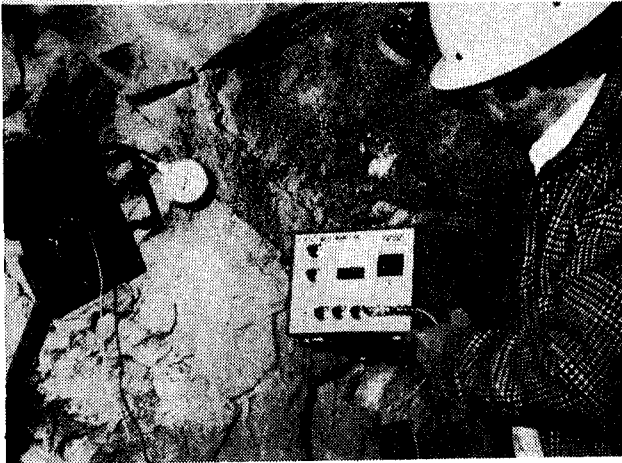

NTF TURBINE ROTOR BLADE BOLTS
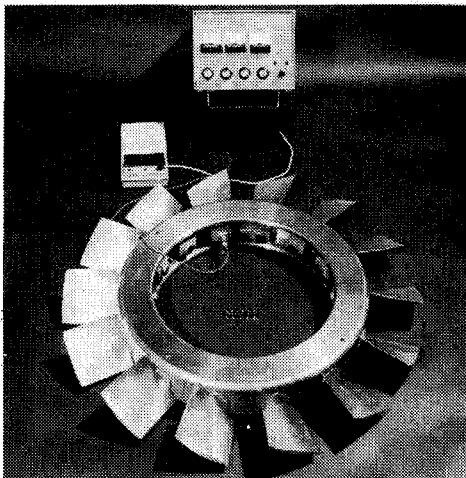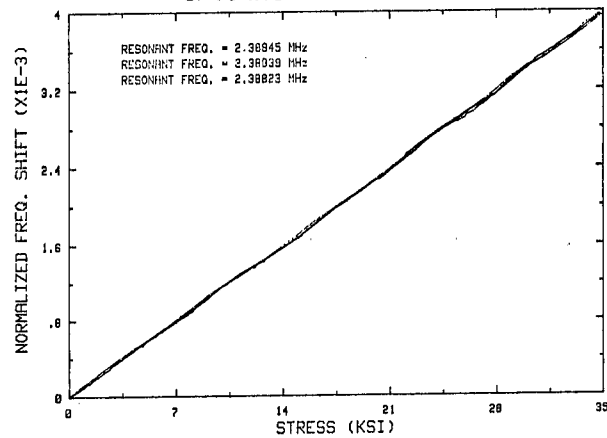

SILTS SAFETY DOME BOLTS

Some typical critical fasteners for which preload was verified using the P^2L^2 are shown in the upper figure. The bolt shaped like a trailer hitch ball holds an external solid-rocket booster onto the Delta Launch Vehicle. The large fastener to the right holds the front of the Space Shuttle orbiter to the external fuel tank. Other bolts shown include a Space Shuttle landing gear wheel bolt, a Shuttle Infrared Leeside Temperature Sensor (SILTS) bolt and a typical aircraft bolt. Also shown is a typical test sample rod used for experimental work.

The bottom left figure shows preload verification for critical fasteners holding blades on a scaled turbine rotor for the National Transonic Cryogenic Wind Tunnel Facility (NTF) at NASA Langley. The lower right figure shows preload measurements being made for the SILTS safety dome bolts. These fasteners are critical to the safety of the Space Shuttle since the safety dome prevents combustible hydrazine from coming into contact with possible ignition sources within the SILTS electronics.
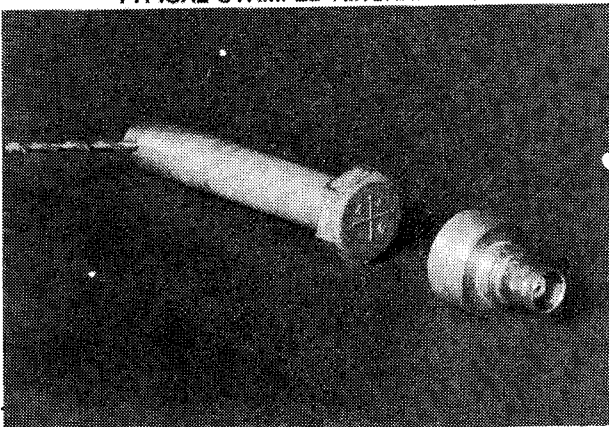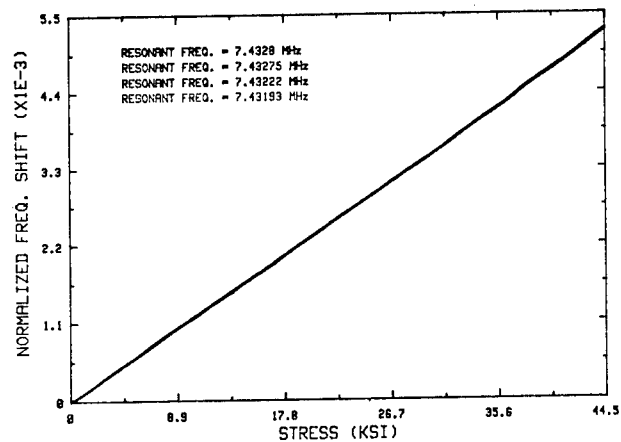
MINE SAFETY ROOF BOLTS

9/16 INCH MINE BOLT

RESONANT FREQ. = 2.38945 MHz
RESONANT FREQ. = 2.38039 MHz
RESONANT FREQ. = 2.38823 MHz

NORMALIZED FREQ. SHIFT (X1E-3)

STRESS (KSI)

TYPICAL STAMPED AIRCRAFT BOLT

1/2 INCH STAMPED BOLT

RESONANT FREQ. = 7.4328 MHz
RESONANT FREQ. = 7.43275 MHz
RESONANT FREQ. = 7.43222 MHz
RESONANT FREQ. = 7.43193 MHz

NORMALIZED FREQ. SHIFT (X1E-3)

STRESS (KSI)

Preload measurements were made for mine safety roof bolts which perform the critical function of keeping the roof rock material under compressive stress to prevent cave-ins. Typical frequency versus stress data for three tightening cycles of a 6-foot-long roof bolt shows that the data are very linear and repeatable. As previously mentioned, the P^2L^2 system can even measure preload accurately for poor geometry fasteners. Even though the typical stamped aircraft bolt shown above has raised markings on the head and a safety wire hole at the end, stress versus frequency data obtained during four tightening cycles is seen to be very linear and repeatable.
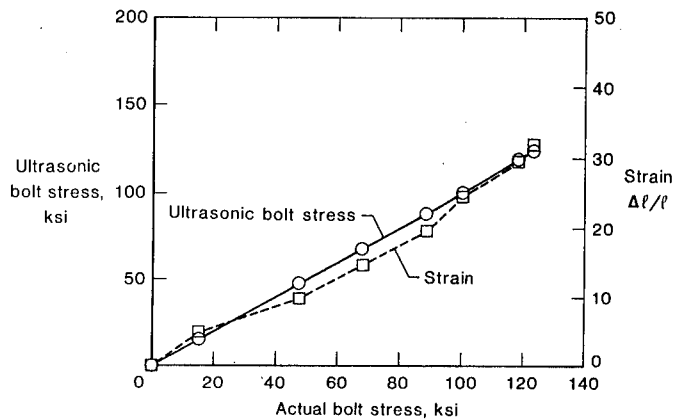
206

P²L² IN PORTABLE CARRYING CASE
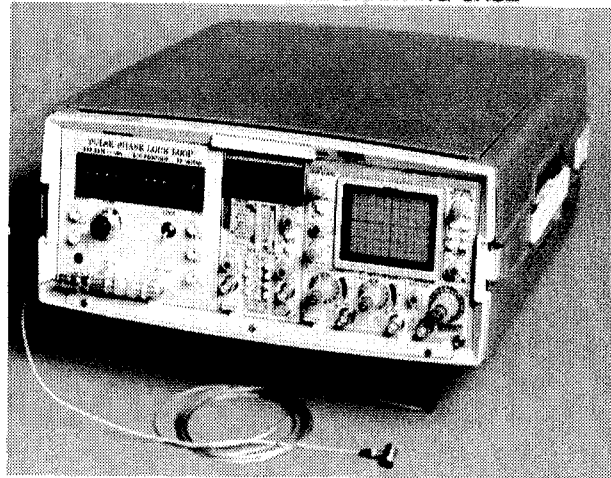
**ARMY HELICOPTER CRITICAL MAIN ROTOR BOLTS**


AH-64 HELICOPTER 27% ROTOR

The latest state-of-the-art P^2L^2 system is packaged in a carrying case the size of a small suitcase. This system can be carried into the field for performing preload measurements such as those made for the Army AH-64 helicopter main rotor bolts. Actual bolt stress versus strain and ultrasonic P^2L^2 frequency data shows that the P^2L^2 gives an even better indication of bolt stress than does strain measured with a micrometer.
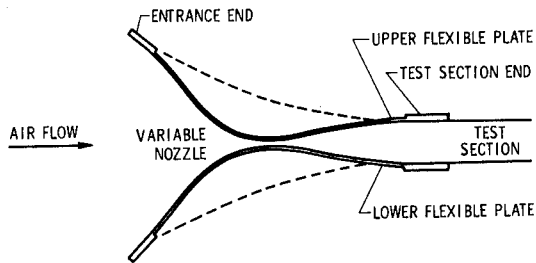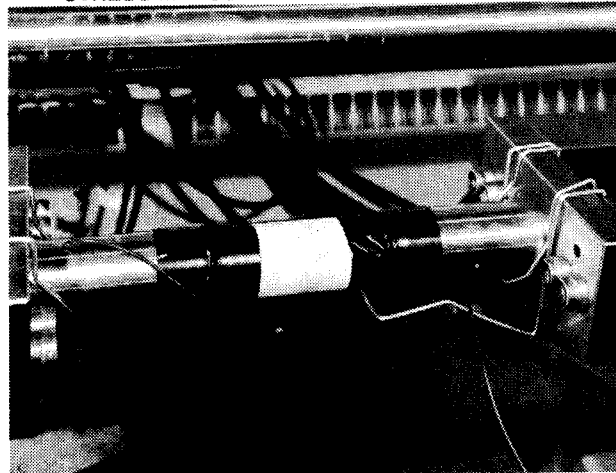
STRESS MEASUREMENTS FOR TUNNEL NOZZLE PLATES

WIND TUNNEL NOZZLE PLATES
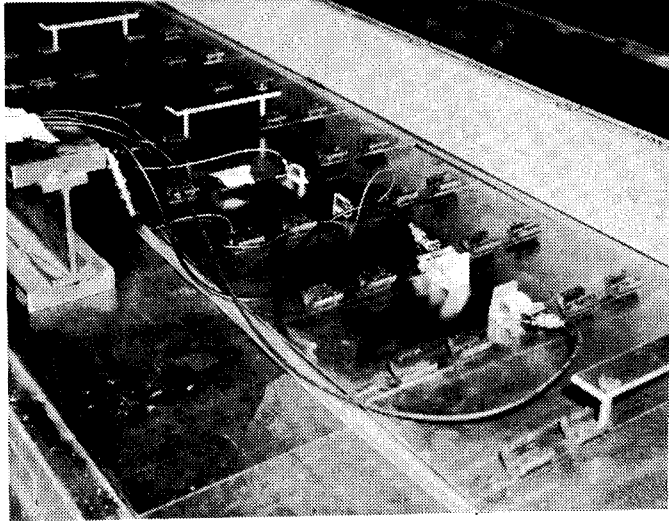
STRESS MEASUREMENTS FOR ROCK SAMPLE

As previously pointed out, the P^2L^2 system has found widespread use for measurements other than bolt preload. For example, this system was used to measure stress in two flexible steel plates (Ref. 5) which comprise the variable nozzle of a critical NASA wind tunnel. The P^2L^2 measured plate stress changes using transducers (top right Fig.) to send and receive sound waves across the plate surface. The P^2L^2 system has even been used to measure stress changes in rock as can be seen in the bottom figure in which a rock sample is compressively stressed with a hydraulic loading machine with transducers (hidden from view) sending sound waves through the rock sample. The P^2L^2 also measures material properties and has been used for a number of material studies (Refs. 6, 7, and 8).

208

CONCLUDING REMARKS

In conclusion, ultrasonic techniques provide an excellent means to measure changes in bolt preload and to reverify bolt preload. Conventional techniques which rely on torque are very inaccurate because they measure friction which can vary to a great extent. The pulsed-phase locked-loop system measures bolt preload with accuracies ranging from better than 1% for prepared (good geometry) bolts to about 3% for poor geometry bolts. Use of the P^2L^2 system eliminates the need for costly alternatives such as strain gauge bolts and is suitable for a small portable instrument. Reliability of this system to make accurate bolt preload measurements has been demonstrated through a number of critical aerospace and other field applications within both the government and private sector. In addition to measurement of bolt preload, the pulsed-phase locked-loop system has been successfully used to measure stresses in a variety of other components including wind tunnel nozzle plates. This technique has also expanded materials characterization to include measurement of higher order (nonlinear) elastic material properties.

REFERENCES

1. M. S. Conradi, J. G. Miller, and J. S. Heyman: "A Transmission Oscillator Ultrasonic Spectrometer," Rev. Sci. Instrum., Vol. 45, No. 3, (March 1974).

2. J. S. Heyman: "A CW Ultrasonic Bolt Strain Monitor," Exp. Mech., Vol. 17, pp. 183-187 (1977).

3. J. S. Heyman: "Pseudo Continuous Wave Instrument," United States Patent #4,117,731 (1978).

4. J. S. Heyman: "Pulsed Phase Locked Loop Strain Monitor," NASA Patent Disclosure LAR-12772-1 (1980).

5. S. G. Allison, J. S. Heyman, and K. Salama, "Ultrasonic Measurement of Residual Deformation Stress in Thin Metal Plates Using Surface Acoustic Waves," Proceedings, 1983 IEEE Ultrasonic Symposium, Atlanta, GA.

6. J. S. Heyman and E. J. Chern: "Characterization of Heat Treatment in Aluminum Based on Ultrasonic Determination of the Second and Third Order Elastic Constants," Proceedings, 1981 IEEE Ultrasonic Symposium, Chicago, IL.

7. J. S. Heyman, S. G. Allison, and K. Salama: "Influence of Carbon Content on Higher-Order Ultrasonic Properties in Steels," Proceedings, 1983 IEEE Ultrasonic Symposium, Atlanta, GA.

8. S. G. Allison, J. S. Heyman, K. Smith, and K. Salama: "Effect of Prestrain Upon Acoustoelastic Properties of Carbon Steel," Proceedings, 1984 IEEE Ultrasonic Symposium, Dallas, TX.

LANGLEY RESEARCH CENTER STANDARD
FOR THE EVALUATION OF SOCKET WELDS

Robert F. Berry, Jr.
NASA Langley Research Center
Hampton, Virginia

I. SCOPE

This specification shall be utilized for the nondestructive evaluation of socket type pipe joints at Langley Research Center (LaRC). The scope of hardware shall include, but is not limited to, all common pipe fittings – tees, elbows, couplings, caps, and so forth – socket type flanges, unions, and valves. In addition, the exterior weld of slip-on flanges shall be inspected using this specification.

II. INSPECTION TECHNIQUES

At the discretion of the design engineer, standard practice engineer, Fracture Mechanics Engineering Section, Pressure Systems Committee, or other authority, four nondestructive evaluation techniques may be utilized exclusively, or in combination, to inspect socket type welds. These techniques are visual, radiographic, magnetic particle, and dye penetrant. Under special circumstances, other techniques (such as eddy current or ultrasonics) may be required and their application shall be guided by the appropriate sections of the American Society of Mechanical Engineers (ASME) Boiler and Pressure Vessel Code (B&PVC).

III. VISUAL INSPECTIONS

At the discretion of cognizant authority, socket type weld joints shall be inspected for surface defects using visual techniques.

Visual inspections within the scope of this specification shall be restricted to the weld contour and adjacent pipe and fitting surfaces. Inspections shall be conducted in accordance with the most current editions of the American National Standard Institute (ANSI) Power Piping Code B31.3, Chapter VI, Paragraph 336.4.2 and the ASME B&PVC, Section V, Article 9, with the following modifications:

A. Inspection Personnel

1. Inspection personnel shall demonstrate the ability to implement inspection techniques, interpret visual data and make quality assessments with respect to the acceptance criteria contained within this document.

2. Inspectors shall have successfully passed an eye examination to demonstrate near-distance acuity such as the J-11 letters on a standard Jaeger Test Chart, in accordance to the following schedule:

   - Under age 35, every 12 months
   - Over age 35, every 6 months

B. **Inspection Condition**

Unless otherwise specified, all welds shall be contour ground and free of rust, scale, slag or other conditions that would obscure the surface condition.

C. **Acceptance Criteria**

1. Fillet size - weld fillets shall comply with the requirements of ANSI B31.3 - 1976, Figures 327.4.2, A-C. In lieu of a specified pressure design thickness "t," the nominal pipe wall thickness "Tw" shall be substituted. (See Figures 1 and 2.)

2. Weld Surface

   a. The weld surface and adjacent base metal shall be free of cracks, incomplete fusion (IF), arc strikes, weld spatter, gouges, mishandling marks, and other sharp surface irregularities. (See Figures 3 and 4.)

   b. The weld fillet shall blend uniformly into the pipe wall and socket rim. The undercut shall not exceed the lesser of 1/32 inch or Tw/4 (Tw = nominal pipe wall thickness). (See Figure 5.)

   c. Surface porosity and/or slag is not permitted. (See Figure 6.)

3. Misalignment - unless otherwise specified, axial misalignment, between the pipe and fitting, shall not exceed 5°.

D. **Inspection Report**

Upon completion of visual inspections, a report shall be furnished containing, as a minimum, the following information:

1. System identification

2. Drawing number

3. Location

4. Sketch or description of each component/weld

5. Material type

6. Surface condition

7. Discrepancies noted

8. Inspector's name

9. Inspection data

IV. RADIOGRAPHIC INSPECTIONS

At the discretion of cognizant authority, socket type weld joints shall be inspected for defects using radiographic techniques.

These radiographic inspections shall be conducted in accordance with the most current edition of the ASME B&PVC, Section V, Articles 2 and 22, as modified by the following paragraphs. Any item not specifically herein addressed will revert to the provisions of Section V.

A. Personnel Qualifications

All inspection personnel shall be qualified in accordance with the American Society for Nondestructive Testing (ASNT) SNT-TC-1A "Recommended Practice for Nondestructive Testing Personnel Qualification and Certification." Personnel qualified to Level I shall be utilized only under the field supervision of Level II or III inspectors. In addition to the above requirement, radiographic interpreters shall have demonstrated acuity as specified under Section III A 1 and 2 and shall be familiar with weld fabrication techniques.

B. Safety

All radiographic inspection operations conducted at LaRC shall be in accordance with applicable Nuclear Regulatory Commission (NRC) regulations ("Notice, Instructions, and Reports to Workers; Inspections," NRC Part 19, April 1975; "Standards for Protection Against Radiation," NRC Part 20, April 1975) and shall, in addition, be in compliance with the NASA Langley Safety Manual, LHB 1710.5, "Ionizing Radiation."

C. Surface Preparation

Unless otherwise specified, all welds shall be contour ground and free of surface irregularities which could mask or be confused with discontinuities.

D. Direction of Radiation

Each socket weld exposure setup shall be aligned so as to pass the radiation central ray parallel to and in line with the socket rim. (See Figure 7.)

➤ NOTE: This requirement may, at the discretion of the NASA Technical Monitor, be relaxed to allow the simultaneous exposure of closely spaced weld joints. Three views of each weld joint taken at 60° to each other are the minimum acceptable coverage for pipe having a nominal size greater than 1 inch. For pipe having a nominal size of 1 inch or less, two views of each weld joint taken at 90° to each other are the minimum acceptable coverage. (See Figure 7.)

E. Shim Block Thickness, Size, and Material

1. The shim block thickness shall be established for each joint by utilizing the formula:

213

$$2\ Tw + R$$

where

Tw = the nominal pipe single wall thickness
R = the component of weld reinforcement measured perpendicular to the pipe axis at the socket rim. (See Figure 2.)

2. The shim block shall be of sufficient size to allow placement of a penetrameter and identification markers. Shim material shall be radiographically similar to the subject weld/pipe material.

F. Penetrameter Selection and Essential Holes

The penetrameter selection shall be based on the calculated shim thickness as follows:

SHIM THICKNESS (2 Tw + R)	PENETRAMETER	ESSENTIAL HOLE
0 thru 0.375	10	4T
Over 0.375 thru 0.625	12	4T
Over 0.625 thru 0.875	15	4T
Over 0.875 thru 1.00	17	4T
Over 1.00 thru 1.50	25	2T
Over 1.50 thru 2.00	30	2T
Over 2.00 thru 2.50	35	2T

G. Identification Markers

In lieu of detailed system schematics, weld numbers shall be permanently marked on each inspected joint utilizing low stress stamping. If the radiographic view depicts more than one weld joint, ID numbers shall be included in the image to positively identify each weld. Film printer identification techniques are prohibited. Each radiograph shall, as a minimum, have the following information permanently included in its image:

1. Weld number

2. View number

3. NASA quality assurance (QA) or contract number

4. Radiographic contractor identification

5. Date of exposure

H. Shim Block/Penetrameter Placement

The shim block with identification numbers and penetrameter shall be aligned parallel to the subject pipe axis with the penetrameter center adjacent to the socket rim. (See Figure 7.)

I. Radiographic Density

The calculated shim thickness from Section IV E 1 shall be utilized to determine exposure values. Film image density shall be measured through the shim block/penetrameter combination and shall equal 3.0 ± 0.5. (See Figure 7.)

J. Source Strength

Unless otherwise specified, the radiation source energy shall be equal to or greater than 35 curies for IR 192 and 150 KEV for x-ray machines.

K. Scattered Radiation

To prevent backscatter radiation, all film cassettes shall be backed up with a minimum of 1/16-inch-thick lead sheeting. This sheeting shall be at sufficient size to completely cover the cassette and shall be covered with tape to prevent lead smearing. (See Figure 7.)

L. Quality of Radiographs

All radiographs shall be free of mechanical, chemical, or other blemishes to the extent that they cannot mask, or be confused with, the image of any discontinuity within the area of interest. Such blemishes include, but are not limited to:

1. Fogging

2. Processing defects such as streaks, water marks, or chemical stains

3. Scratches, finger marks, crimps, dirt, static marks, smudges, or tears

4. Loss of detail due to poor screen-to-film contact

5. False indications due to defective screens or cassette faults

M. Geometric Unsharpness/Source-to-Film Distance

Geometric unsharpness of the radiographic image shall not exceed 0.020 inches and the radiation source-to-film distance, unless otherwise specified by the NASA Technical Monitor, shall be not less than 14 inches.

N. Acceptance Criteria

1. Cracks

   No cracks of any nature or extent are acceptable. (See Figure 8.)

2. Incomplete Penetration (IP)

   IP is defined as the failure of weld material to extend completely into and become integral with the intersection of the socket rim

inner diameter and cylindrical pipe wall. Incomplete penetration is not acceptable. (See Figure 9.)

3. Incomplete Fusion (IF)

   IF is defined as an isolated, discontinuous or continuous area of no weld material fusion at the weld-socket, weld-pipe interface, or between consecutive weld passes. Incomplete fusion is not acceptable. (See Figure 10.)

4. Pipe-to-Socket Bottom Gap

   A gap of 1/16 inch ± 1/32 inch shall be maintained between the pipe end and socket bottom after welding. (See Figures 2 and 11.)

5. Porosity and Rounded Indications

   An individual pocket of porosity shall not exceed the lesser of $T_w/3$ or 1/8 inch in its greater dimensions. Adjacent indications shall be separated by a minimum $T_w/2$ of sound weld. The summation of diameters for aligned rounded indications shall not exceed T_w in length for any 6 T_w of weld. (See Figure 12.)

6. Slag and Elongated Defects

   The developed length of any single slag inclusion or elongated defect shall not exceed $T_w/3$. Adjacent slag inclusions shall be separated by a minimum $T_w/2$ sound weld. The total cumulative developed length of slag inclusions and/or elongated defects shall not exceed T_w in any 6 T_w of weld. The width of a slag inclusion shall not exceed the lesser of 3/32 inch or $T_w/3$. Slag inclusions or elongated defects that infringe upon the root area are not acceptable to any extent. (See Figure 13.)

7. Melt Through

   Melt through is defined as a localized area of pipe metal melting and resolidification, usually on the pipe inner diameter. Melt through shall be reviewed on an individual case basis and shall not:

   a. Reduce the nominal pipe wall thickness greater than 12-1/2%

   b. Present severe internal flow restrictions

   c. Include icicle type areas which could become dislodged (See Figure 14.)

8. Burn Through

   Burn through shall not reduce the nominal pipe wall thickness greater than 12-1/2%.

216

O. **Radiographic Technical Log and Interpretation Report**

The inspector shall furnish, in addition to the radiographic film, a technical log and interpretation report relative to each inspected weld. The log/report shall contain, as a minimum, the following data:

1. System identification

2. Drawing number

3. Location

4. Sketch or description of each component/weld

5. Material type

6. Pipe nominal wall thickness $\underline{Tw}$

7. Weld thickness $\underline{R}$

8. Shim block thickness – $\underline{2\ Tw + R}$

9. Penetrameter size/essential hole

10. Isotope or x-ray machine, size/type/energy

11. Film type/manufacturer

12. Screen type, thickness, placement

13. Source-to-film distance

14. Exposure time/milliamp-minutes (MAM)

15. Radiographer's name

16. Inspection date

17. Discrepancies noted

18. Interpreter's name

19. Interpretation date

V. **MAGNETIC PARTICLE/DYE PENETRANT INSPECTIONS**

At the discretion of cognizant authority, socket type weld joints shall be inspected for surface defects utilizing magnetic particle and/or dye penetrant techniques. When so specified, this work shall be conducted in accordance with the ASME B&PVC, Section V, Articles 7 and 25, for magnetic particles and Articles 6 and 24 for dye penetrants, with the following modifications.

A. **Surface Conditions**

   Weld joint surfaces and adjacent areas (within a minimum of 1 inch)
   shall be free of any irregularities which could mask indications due
   to discontinuities. Prior to inspection, these areas shall be dry
   and free of all paint, dirt, grease, lint, scale, welding flux, and
   splatter, oil or other extraneous matter that could interfere with
   the examination.

B. **Personnel Qualifications**

   Inspection personnel shall be qualified in accordance with
   ASNT-SNT-TC-1A. Personnel qualified to Level I shall be utilized
   only under the field supervision of Level II or III inspectors.

C. **Magnetic Particle Technique**

   1. Magnetization Method

      The inspector has the option of utilizing a coil encirclement or
      yoke magnetization technique.

   2. Field Adequacy

      Magnetizing field adequacy shall be verified through the utili-
      zation of a magnetic particle field indicator as illustrated in
      ASME B&PVC, Section V, Article 25, Section SA-275, Figure 8.
      This verification shall be conducted at the beginning of each
      period of work or shift change and as a minimum every 4 hours
      during the work period.

   3. Coverage

      All surface areas of the weld joint and adjacent pipe and socket
      material (for a minimum of 1 inch) shall be 100% inspected.

D. **Dye Penetrant Technique**

   1. Dwell Time

      Unless otherwise specified, dwell time shall be not less than
      10 minutes.

   2. Temperature

      When the surface temperature of the area to be inspected is out-
      side of the 60° F to 125° F range, the testing procedure shall
      be qualified as per the requirements of ASME B&PVC, Article 6,
      Paragraph T-660, "Qualification of Techniques for Nonstandard
      Temperatures."

E. **Acceptance Criteria**

   The following defects shall constitute rejectable conditions:

   1. Cracks

218

2. Incomplete fusion (IF)

3. Surface open slag or porosity

F. **Inspection Report**

Upon completion of magnetic particle and/or dye penetrant inspections, the inspector shall furnish a report containing, as a minimum, the following information:

1. System identification

2. Drawing number

3. Location

4. Description or sketch of inspected item

5. Technique

    a. If there is a dye penetrant, then include:

        (1) Penetrant type/manufacturer

        (2) Part temperature

        (3) Dwell time

        (4) Cleaning method

        (5) Development method

    b. If there is a magnetic particle, then include:

        (1) Magnetization method

        (2) Equipment manufacturer

        (3) AC/DC

        (4) Current settings

        (5) Power type/manufacturer

6. Discrepancies noted

7. Inspector's name

8. Date of inspection

WELD SIZE LESS
THAN Tw x 1.25
OR 1/8 IN.

WELD SIZE LESS
THAN Tw x 1.25
OR 1/8 IN.
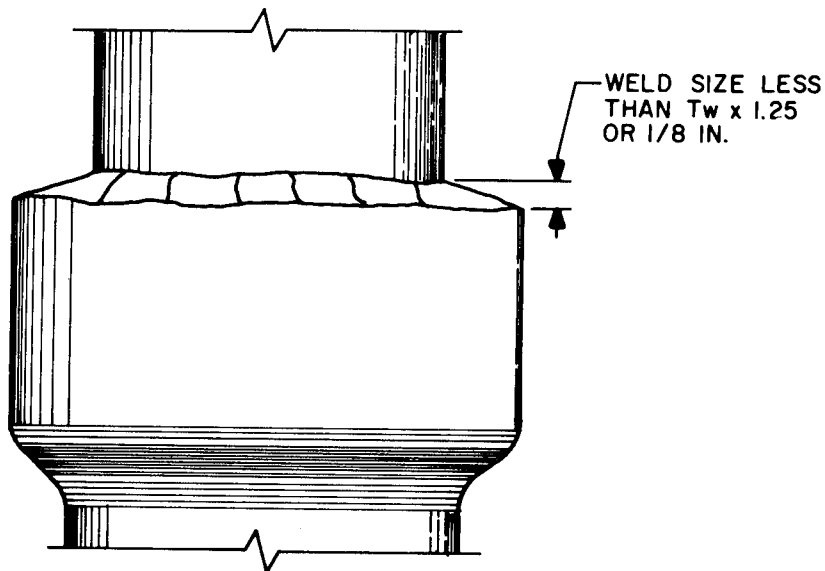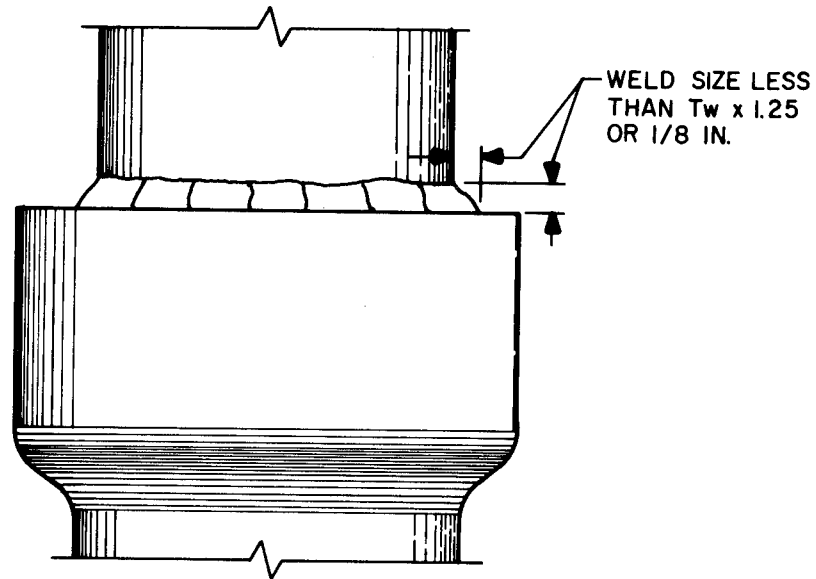
Figure 1.   Unacceptable socket weld fillet sizes for components other than flanges.
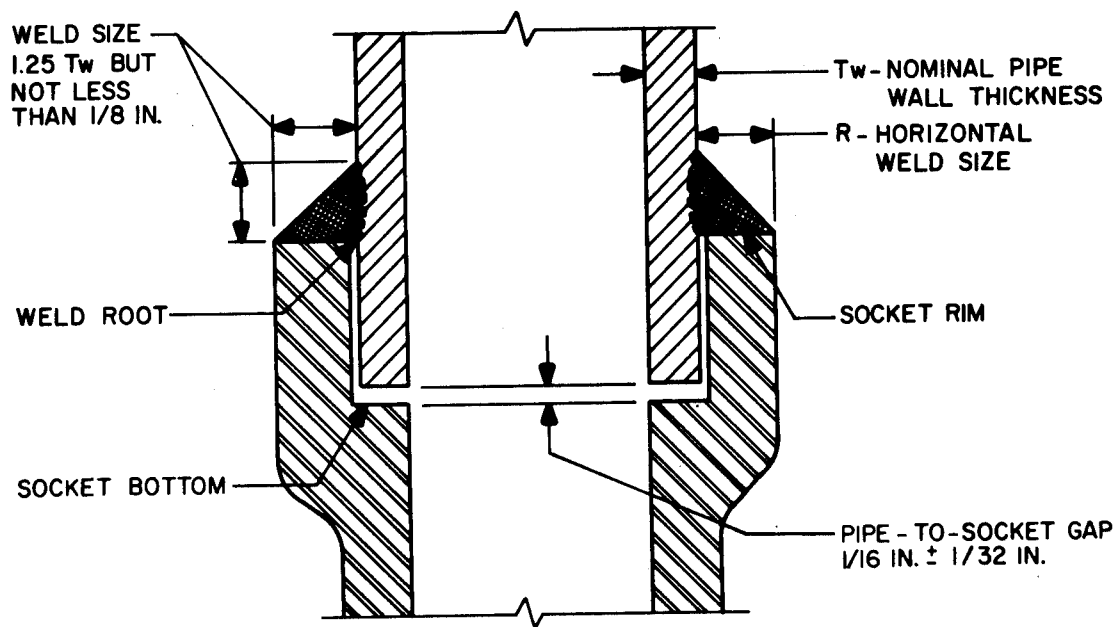
Figure 2. Weld nomenclature and minimum dimensions for socket weld components other than flanges.
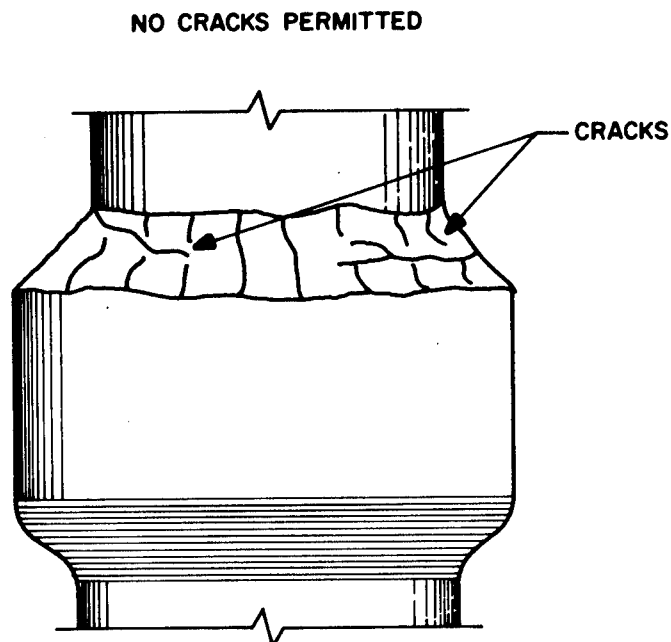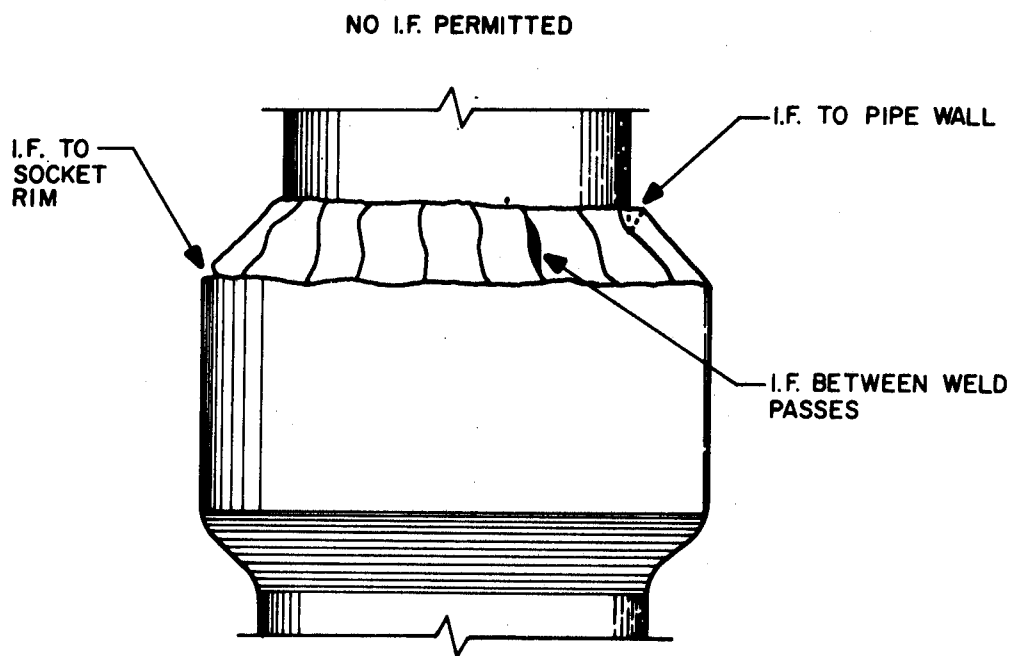
NO CRACKS PERMITTED

Figure 3. Cracks.

I.F. TO SOCKET RIM

I.F. TO PIPE WALL

I.F. BETWEEN WELD PASSES

Figure 4.   Incomplete fusion (I.F.).

UNDERCUT NOT TO EXCEED 1/32 IN. OR Tw/4 WHICHEVER IS LESS
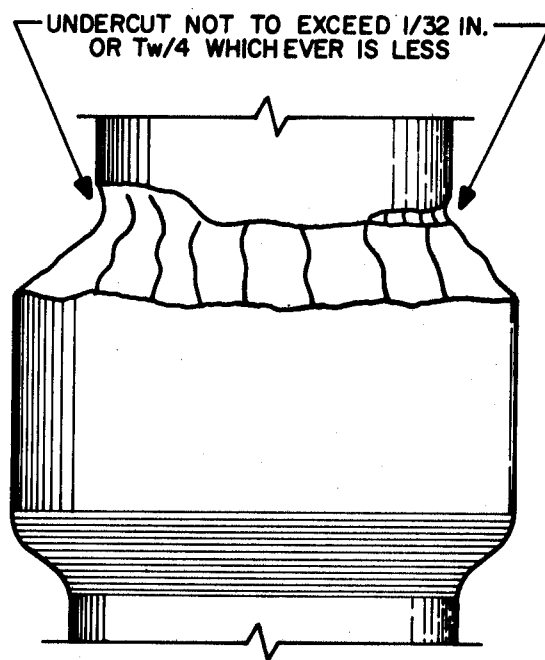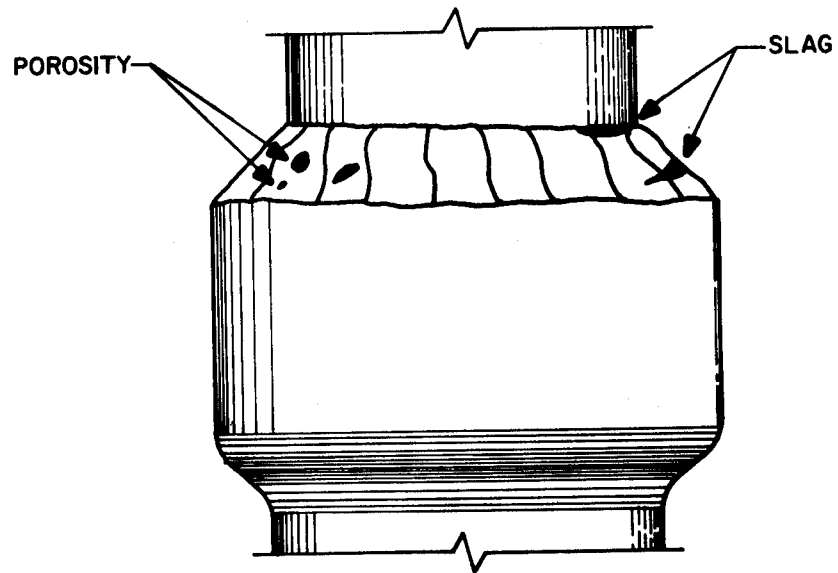
Figure 5.   Undercut.

NO SURFACE SLAG OR POROSITY PERMITTED

Figure 6. Surface slag porosity.
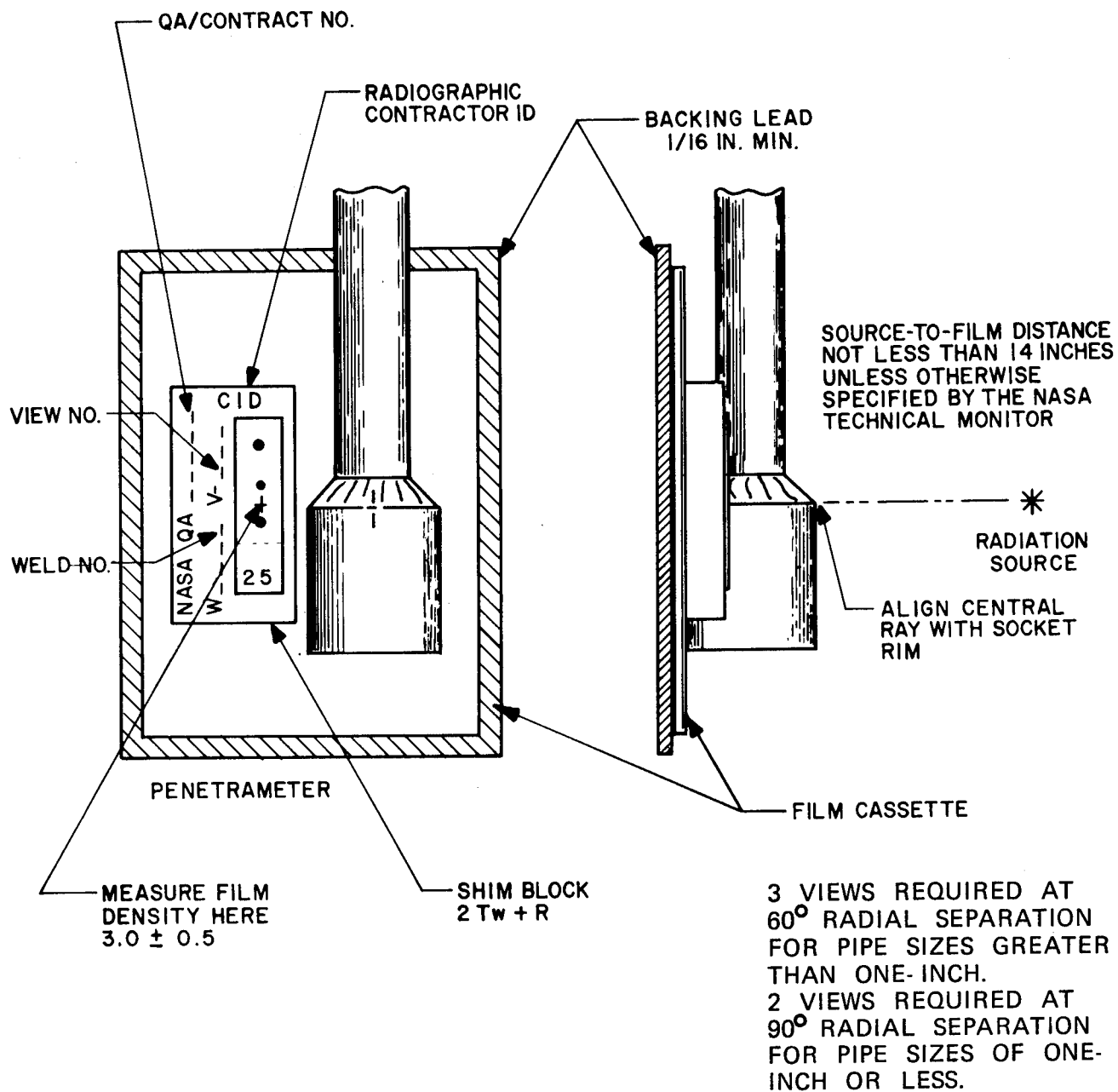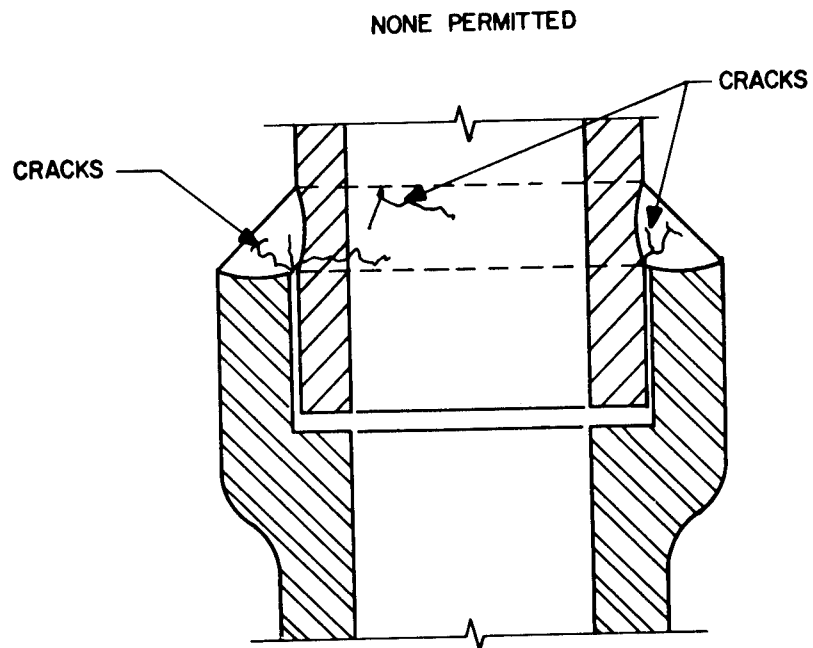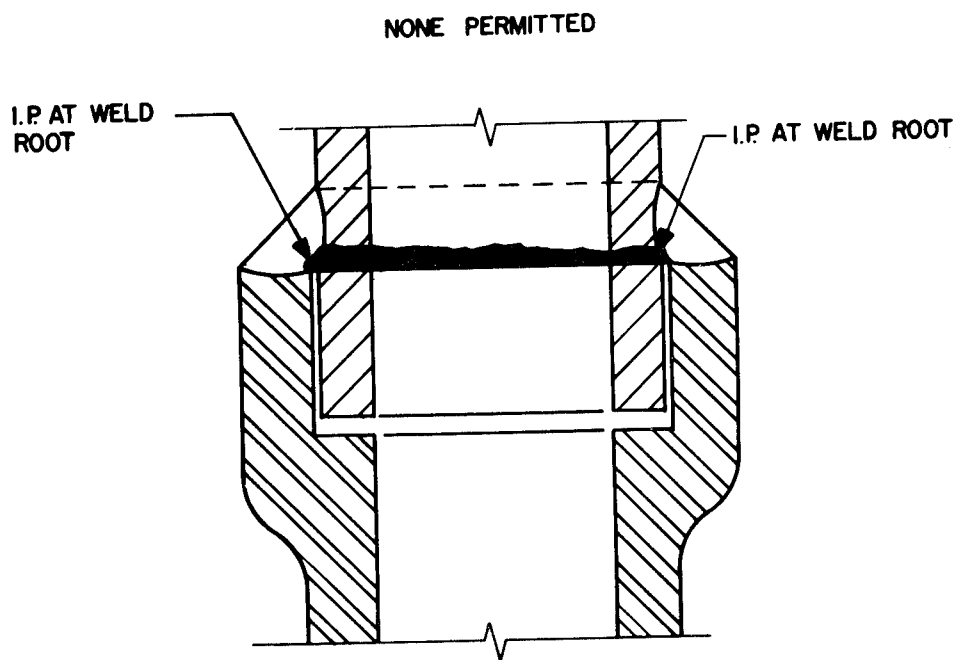
Figure 7. Radiographic exposure technique.

NONE PERMITTED

CRACKS

CRACKS

Figure 8. Cracks.

NONE PERMITTED

I.P. AT WELD ROOT

I.P. AT WELD ROOT

Figure 9. Incomplete penetration (I.P.).

225
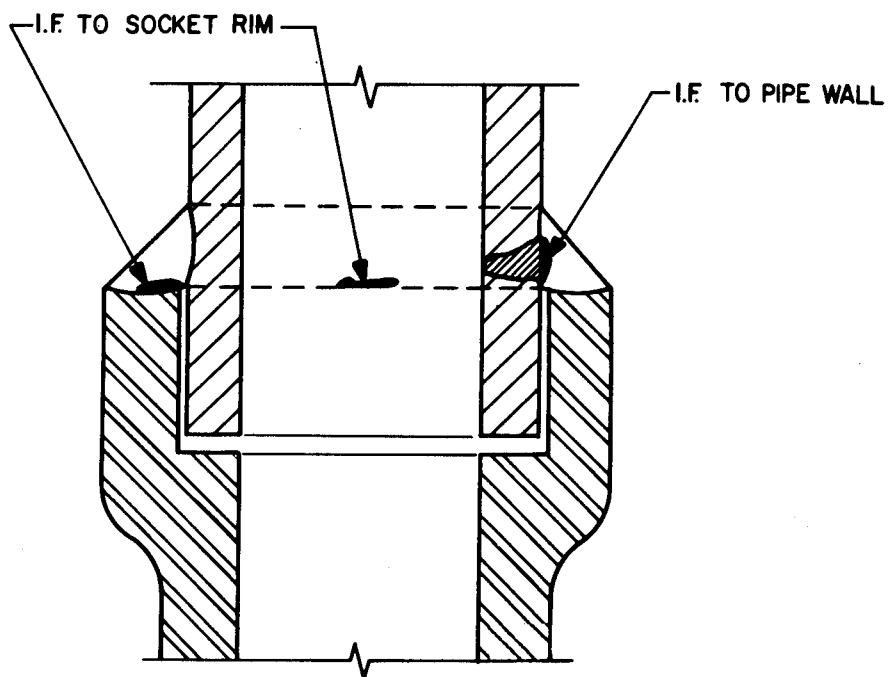
Figure 10. Incomplete fusion (I.F.).
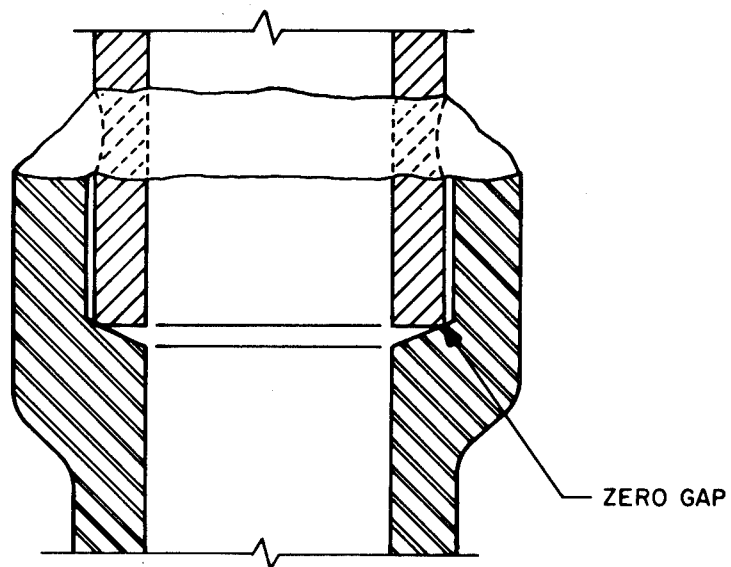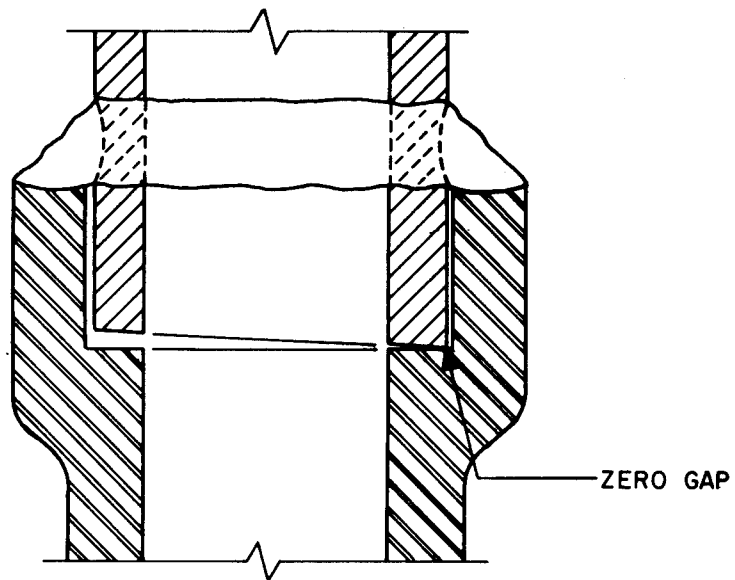
ZERO GAP

ZERO GAP

Figure 11.   Unacceptable pipe-to-socket gap.
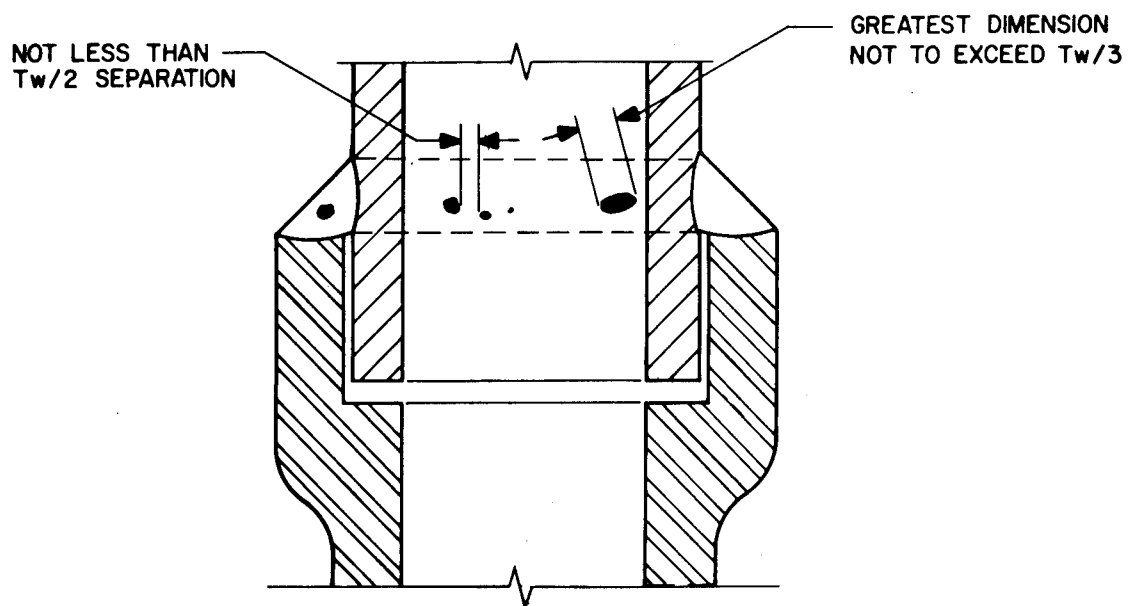
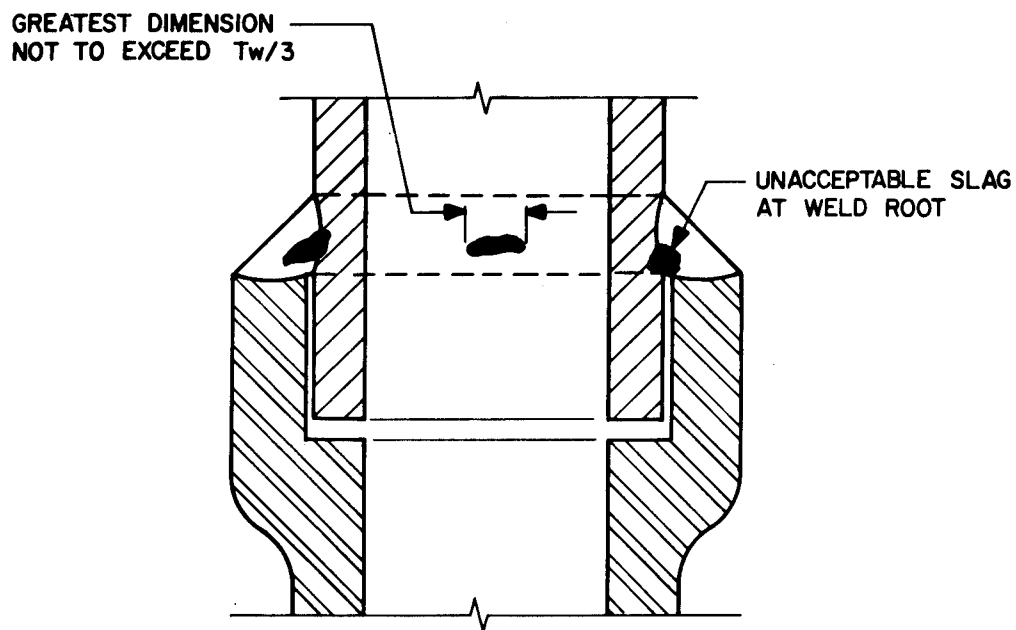Figure 12. Porosity and rounded indications.
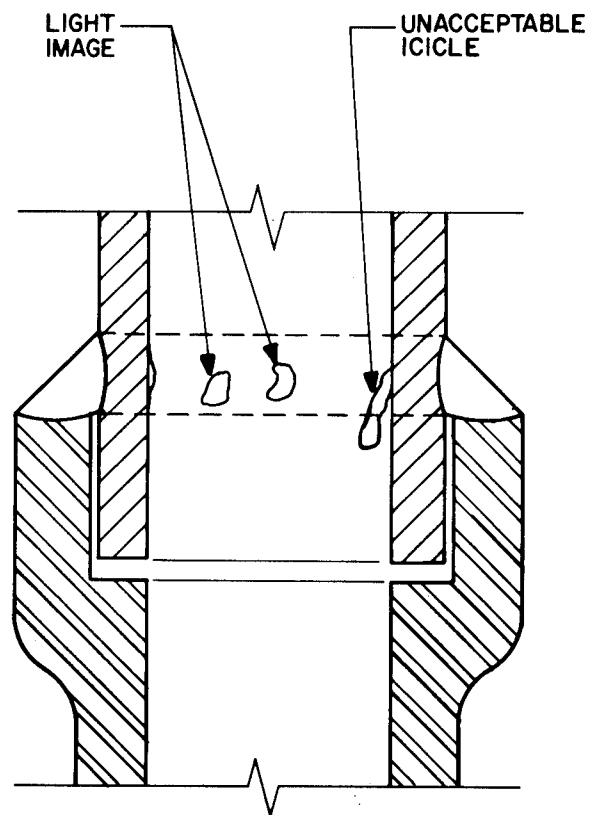

Figure 13. Slag inclusions.

Figure 14.   Melt through.

SOLID-STATE BONDING OF SUPERPLASTIC ALUMINUM ALLOY 7475 SHEET

Thomas D. S. Byun and Ramsevak B. Vastava
Northrop Corporation
Aircraft Division
Hawthrone, California

ABSTRACT

Experimental works were carried out to study the feasibility of solid-state bonding of superplastic aluminum 7475 sheet. Amount of deformation, bonding time, surface cleaning method and intermediate layer were the process parameters investigated. Other parameters, held constant by the superplastic forming condition which is required to obtain a concurrent solid-state bonding, are bonding temperature, bonding pressure and atmosphere. Bond integrity was evaluated through metallographic examination, x-ray line scan analysis, SEM fractographic analysis and lap shear tests. The early results of the development program indicated that sound solid-state bonding was accomplished for this high strength 7475 alloy with significant amounts of deformation. A thin intermediate layer of the soft 5052 aluminum alloy aided in achieving a solid-state bonding by reducing the required amount of plastic deformation at the interface. Bond strength was substantially increased by a post bond heat treatment.

INTRODUCTION

Superplastic forming of titanium combined with solid-state bonding (frequently called SPF/DB) has demonstrated substantial cost and weight savings in fabricating aircraft structures. Superplastic forming aluminum is a new technology emerging in aerospace industries to form complex net formed parts of high strength aluminum. While the aluminum superplastic forming technology is ready for implementation into production, to date only limited success has been realized in solid-state bonding of aluminum especially high strength aluminum alloy. The major difficulty in the solid-state bonding of aluminum comes from its tenacious surface oxide film which cannot be avoided under normal manufacturing conditions. As a result, methods should be developed to achieve intimate metallic contact between faying surfaces in the presence of this film.

A company-funded program was started to study the feasibility of solid-state bonding as a concurrent process with superplastic forming of aluminum. The early phase of this program concentrated on obtaining solid-state bonding of alloy 7475 sheet at superplastic forming temperature. Bonding experiments were conducted using methods to disrupt the surface oxide film to expose a clean metal surface prior to bonding. Some of the bonding parameters including an intermediate layer as a bonding aid were evaluated for use in the later phase of this program. Since there are no standard test procedures which apply to solid-state bonding, reliable tools had to be selected to measure bond quality.

FEATURES OF SOLID-STATE BONDING
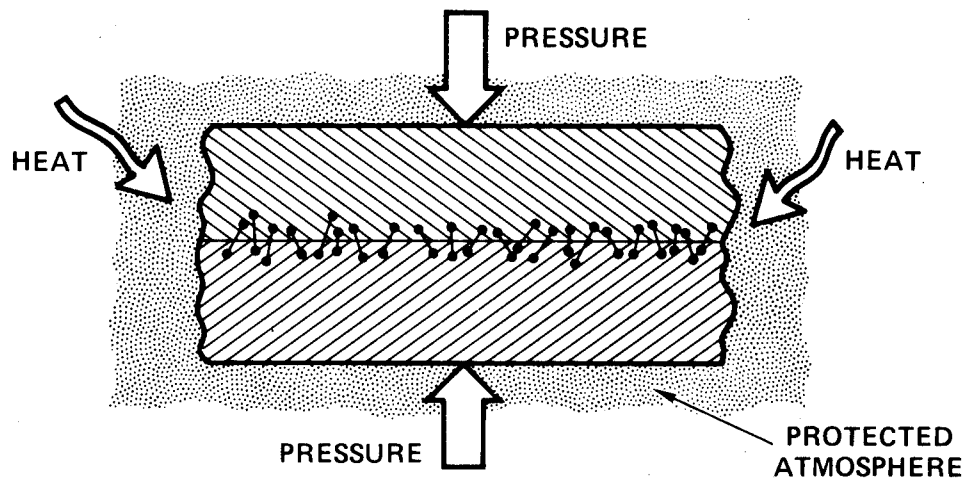
- JOINT PROPERTIES ARE SAME OR VERY SIMILAR TO THOSE OF BASE ALLOY

- IT IS APPLICABLE TO UNWELDABLE ALLOYS

In solid-state bonding two cleaned pieces of metals are put together with pressure applied normal to the bond interface at elevated temperature. Bond interface has to be protected from oxidation in either vacuum or inert gas. It is generally believed that solid-state bonding is completed through two stages. At the first stage plastic flow disrupts oxide film to expose the clean metallic surface and produces intimate contact. Bonding is established by atomic inter-diffusion and recrystallization and/or grain growth across bond interface at the second stage.

PROCESS PARAMETERS FOR SOLID-STATE BONDING

- SURFACE CLEANING

- AMOUNT OF DEFORMATION

- INTERMEDIATE LAYER

- BONDING TIME

- POSTBOND HEAT-TREATMENT

- BONDING TEMPERATURE

- BONDING PRESSURE

- ATMOSPHERE

The process parameters investigated are surface cleaning, amount of deformation, intermediate layer and bonding time. Besides these parameters there are three more important variables in the solid-state bonding process: bonding temperature, bonding pressure and atmosphere; these were kept constant by superplastic forming conditions in our bond experiments.

SURFACE CLEANING PROCEDURE

```
        ┌─────────────────────┐
        │   VAPOR DEGREASE    │
        └─────────────────────┘
                  │
                  ▼
        ┌─────────────────────┐
        │   ALKALINE CLEAN    │
        └─────────────────────┘
                  │
                  ▼
          ┌──────────────┐
          │    RINSE     │
          └──────────────┘
                  │
                  ▼
        ┌─────────────────┐
        │    DEOXIDIZE    │  ─   SELECTION OF DEOXIDIZER
        └─────────────────┘
                  │
                  ▼
          ┌──────────────┐
          │    RINSE     │
          └──────────────┘
                  │
                  ▼
        ┌─────────────────┐
        │    AIR DRY      │
        └─────────────────┘
```

MECHANICAL CLEAN

BONDING TEST

BONDING TEST
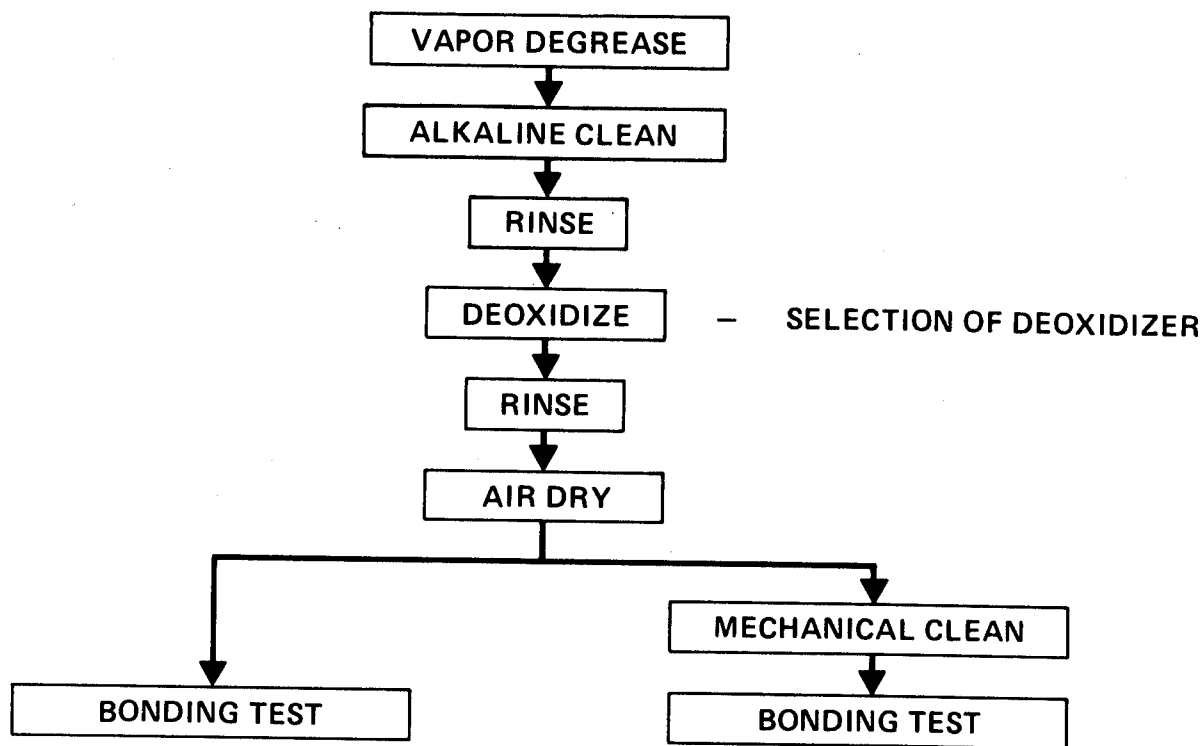
Surface cleaning of the as-received aluminum alloy 7475 sheets was started with vapor degreasing followed by alkaline cleaning to remove oil and other dirts. Surface oxide film was removed through a deoxidizing process. Mechanical cleaning subsequent to chemical cleaning was beneficial to solid-state bonding of alloy 7475.

LAP SHEAR SPECIMEN

FLAT BOTTOM NOTCHES (1/16 INCH WIDE)

0.5 INCH

3.0-3.5 INCHES

BOND LINE
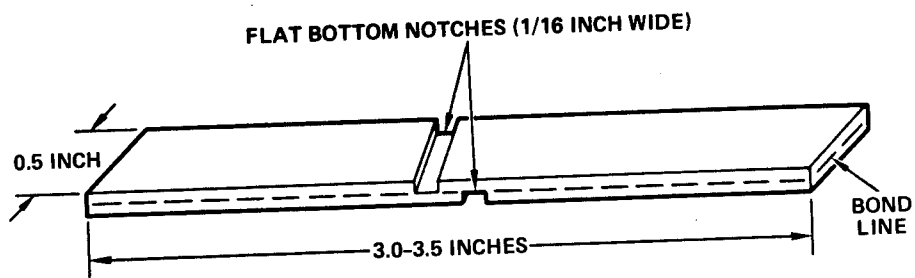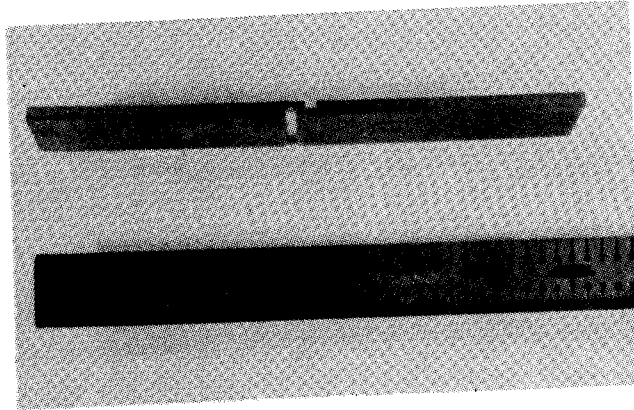
A single shear test was chosen to measure bond equality. The test specimen was designed to break at lap joint between two flat bottom notches when it was pulled lengthwise.

# EFFECTS OF INTERMEDIATE LAYERS AND AMOUNT OF DEFORMATION ON BOND STRENGTH
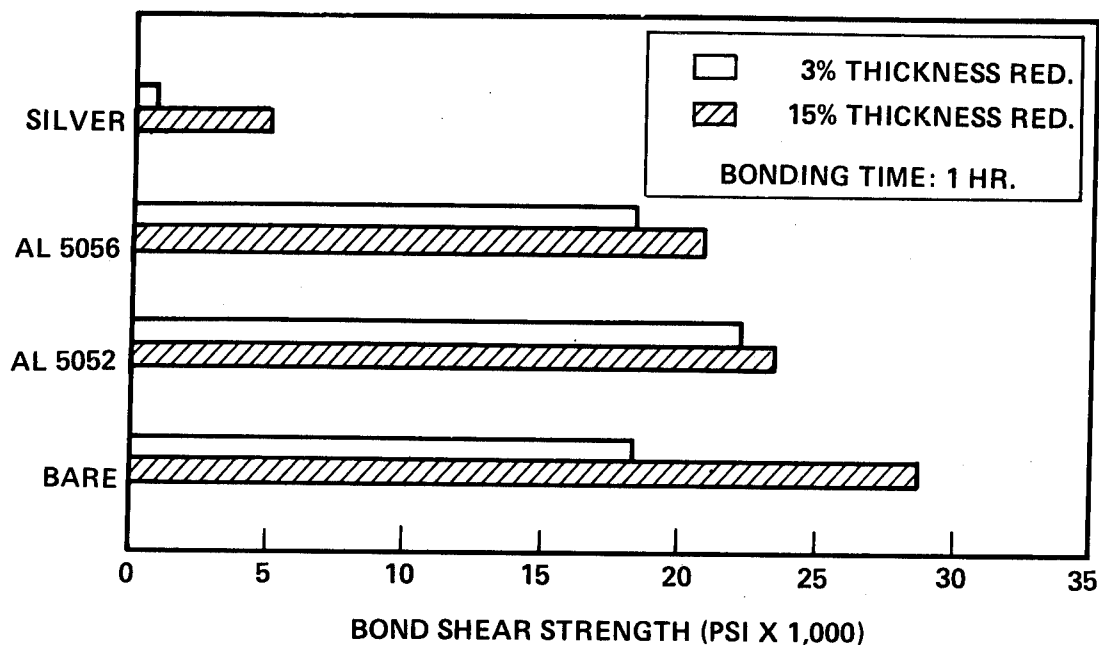
Three different types of intermediate layers were investigated as bonding aids, and the bond strength results were compared with self-bonding of alloy 7475. With low bond deformation a thin layer of alloy 5052 produced the highest bond strength. Electroplated silver did not aid solid-state bonding of alloy 7475. Bond quality with alloy 5056 foil as an interlayer was slightly lower than that with alloy 5052 intermediate layer.

Bond lap shear strength was significantly increased with increasing bond deformation from 3% to 15% in terms of total thickness reduction. This deformation effect on bond strength was most pronounced in self-bonding without using any intermediate layer. Since bonding with high deformation was considered to limit the application, solid-state bonding of alloy 7475 with alloy 5052 intermediate layer which reduced the amount of required bond deformation was selected for further investigation.

237

COMPLETION OF SOLID-STATE BONDING

AS-POLISHED   100X   KELLER'S   100X

BOND LINE
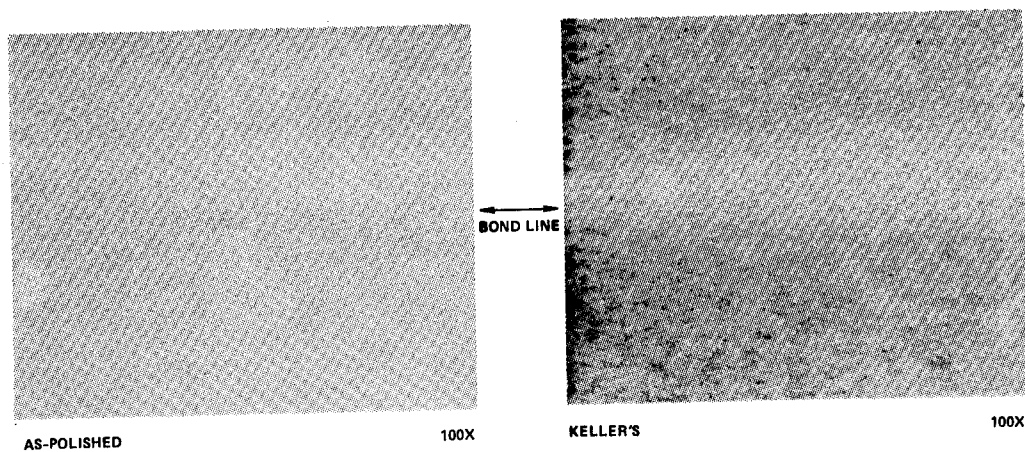
The photomicrographs show a solid-state bond of alloy 7475 with the intermediate layer of alloy 5052 foil as a bonding aid. Microstructure is continuous over bond interface without showing any significant interface voids or detectable original bond line.

238

CHEMICAL COMPOSITION OF BASE
AND FILLER ALLOYS

| ELEMENTS	ALLOY 7475 (WT. %)	ALLOY 5052 (WT. %)
SILICON	0.04	0.12
COPPER	1.45	0.04
MANGANESE	0.01	0.04
MAGNESIUM	2.50	2.35
CHROMIUM	0.20	0.20
ZINC	5.70	0.06
TITANIUM	0.02	0.01
ALUMINUM	REMAINDER	REMAINDER

When the chemical composition of filler alloy 5052 is compared with that of
base alloy 7475, the major differences between two alloys are the contents of
copper and zinc. Therefore, concentrations of these two elements were ana-
lyzed at the joint area.

ELEMENT DIFFUSION PROFILE
ACROSS BOND INTERFACE
(INTERMEDIATE LAYER: Al 5052)

COPPER   ZINC
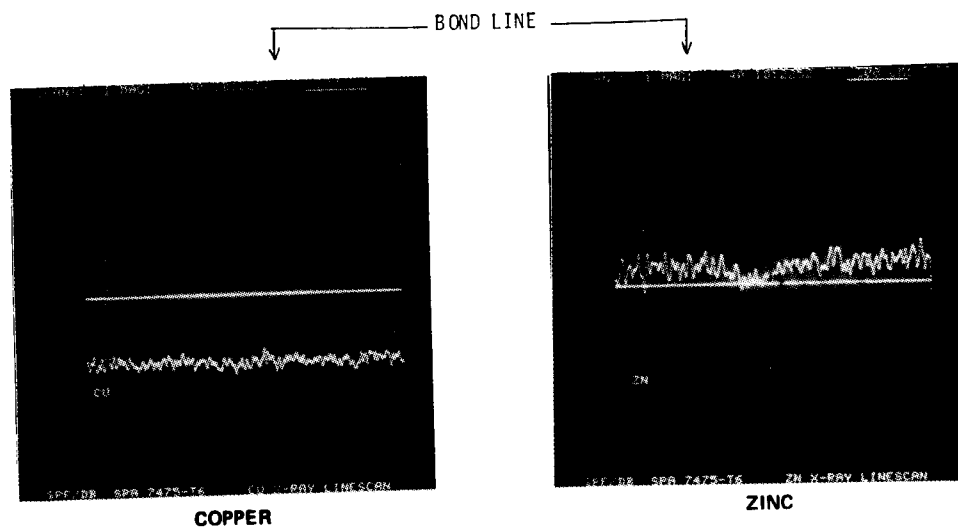
X-ray line scan analyses were made for the elements copper and zinc to obtain qualitative diffusion profiles. A bonded specimen was placed on a scanning electron microscope. Using an x-ray line scan system, diffusion profiles for copper and zinc were determined across the bond interface. The solid white lines in the photos show the electron beam path for each analysis. The line profile for the element zinc shows a concentration decrease at the bond area where alloy 5052 was interlayed while the line profile for the element copper does not indicate any change across the bond line.

QUANTITATIVE ANALYSIS OF ZINC
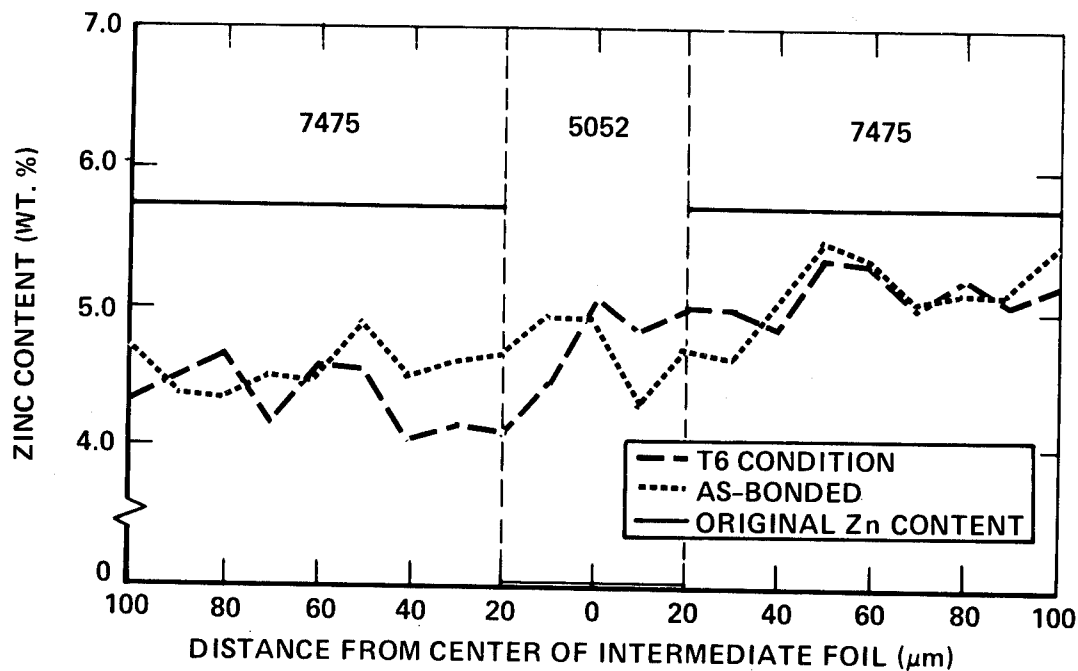
With concern over the concentration drop of zinc as seen, quantitative analyses were performed. Energy dispersive x-ray analyses were conducted at 10 μm steps, then the data obtained were reduced by a computer to give quantitative weight percent. Zinc contents ranged from 4.5 wt % to 5.5 wt % while the original zinc content was 5.7 wt % in alloy 7475 and 0.06 wt. % in alloy 5052. The diffusion profiles clearly indicate elements inter-diffused across interfaces during the solid-state bonding. Post bond T6 heat treatment did not significantly change the diffusion profile of zinc at the joint.

MICROSTRUCTURE AND MICROHARDNESS
OF SOLID-STATE BONDED SPA 7475

KELLER'S

KNOOP HARDNESS NUMBER 120   112   113 114   110   108

200X
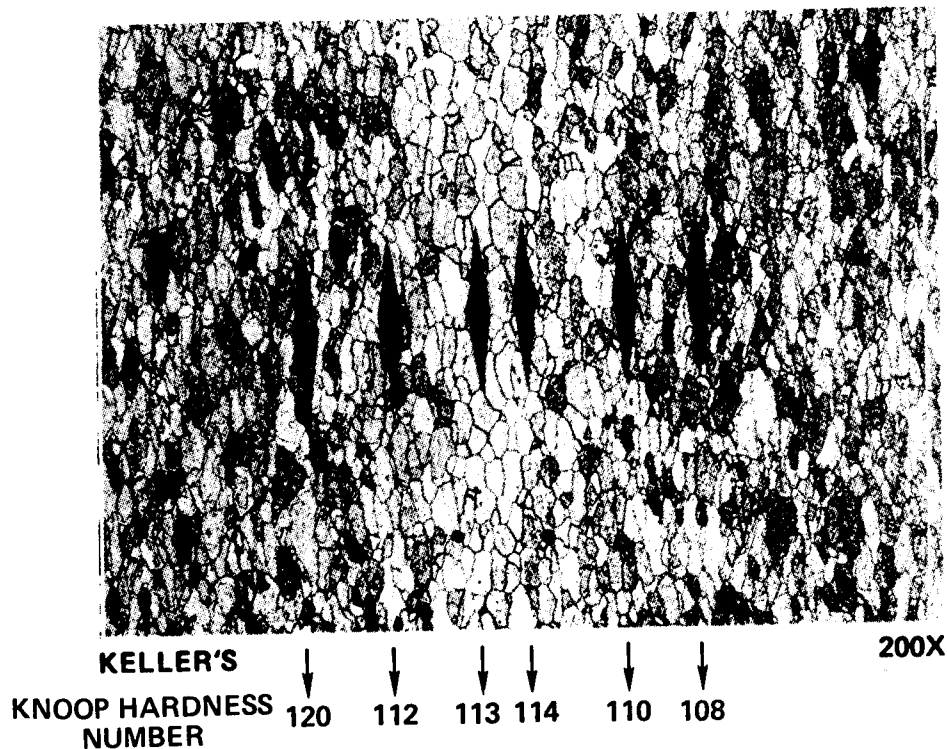
Knoop hardness numbers at the joint ranged from 108 to 120, which are somewhat lower than the hardness number that one can expect from the base alloy 7475. The microhardness numbers were closely related to the content of zinc. The photo shows the details of microstructure for perfectly bonded alloy 7475 as well as dark indentations from microhardness testings.

BONDING TIME VS. BOND STRENGTH
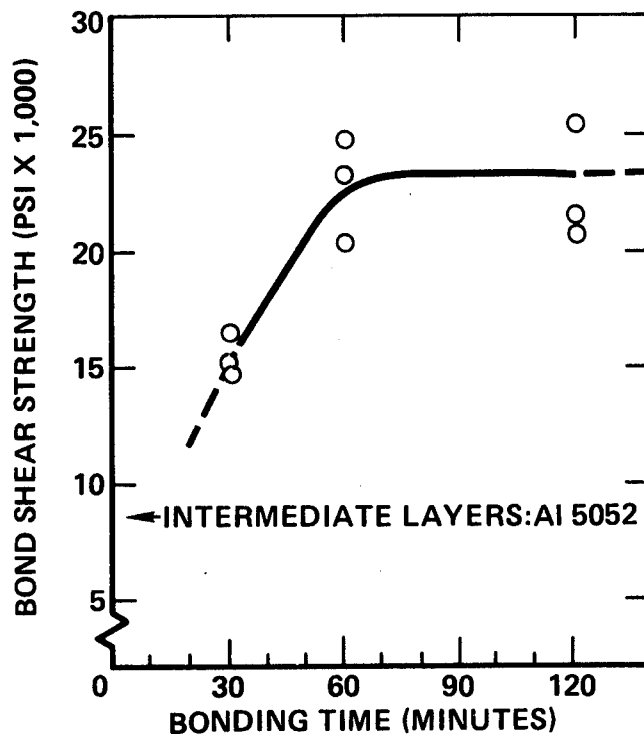
The bond experiment started with 60 minutes bonding time. Bond shear strength
sharply decreased with reducing the bonding time from 60 minutes to 30 minutes.
When the bonding time was increased from 60 minutes to 120 minutes, no change
of bond strength was observed. Although the data are not enough to determine
the optimum bonding time, 60 to 90 minutes is considered to be enough bonding
time to produce sound bonding of alloy 7475.

# EFFECT OF POSTBOND HEAT-TREATMENT
ON BOND STRENGTH
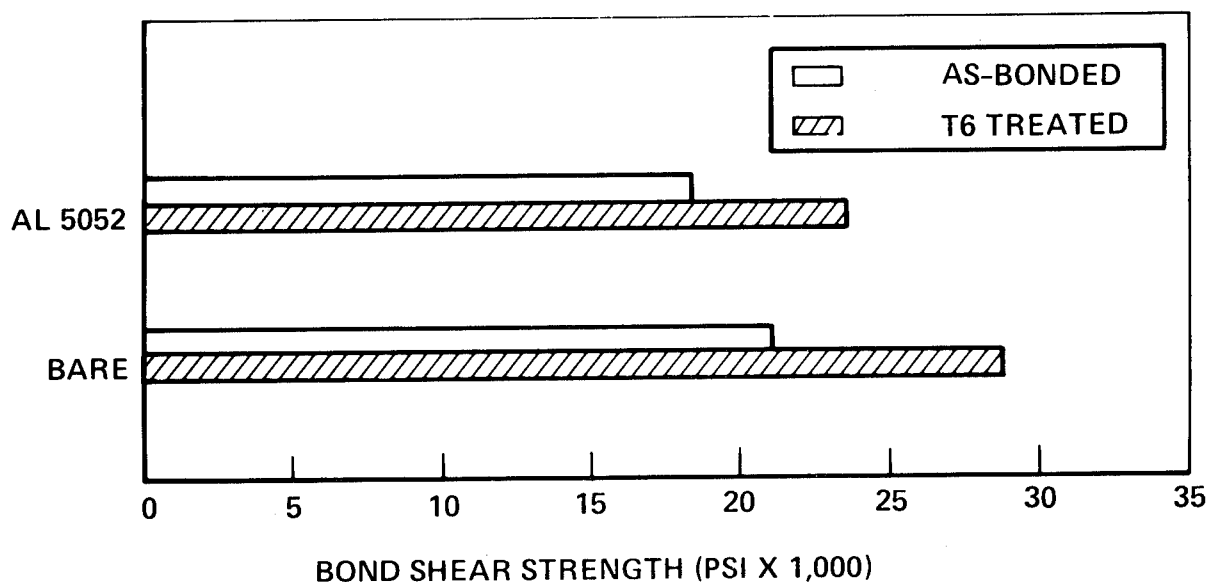
Solid-state bonded structure responded well to postbond T6 heat-treatment with substantial increase of bond strength. The heat-treatment response was more distinct in self-bonding than in the bonding with the intermediate layer. This can be explained by the zinc concentration decrease at the joint when alloy 5052 was used as bonding aid.

SEM FRACTOGRAPHS OF BONDING INTERFACE
(BOND SHEAR STRENGTH:15,000 PSI)
SHOWING INSUFFICIENT BONDING
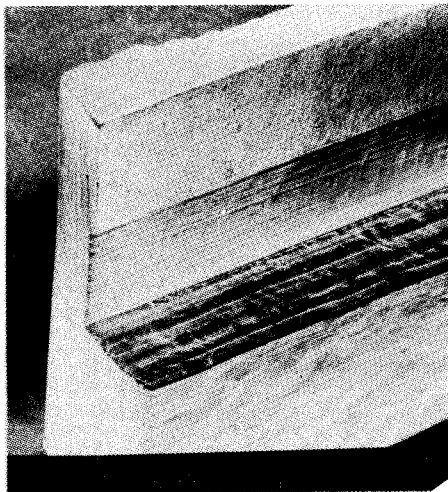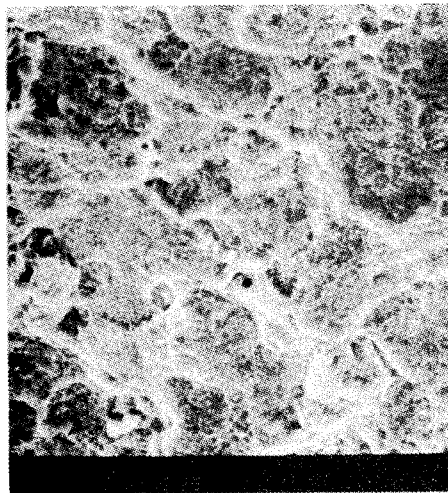
20X   1000X

Fractographic analysis of the failed bond interface characterizes integrity of
the solid-state bond. Lap-sheared bond specimens were examined on a scanning
electron microscope for this purpose. In the above fractographs fracture
occurred along the bond interface, and significant areas of the fractured
surface are essentially featureless. These fractographic features indicate
that the bonding was not sufficient. The bond strength of the shear specimen
used here was 15,000 psi.

SEM FRACTOGRAPHS OF BONDING INTERFACE
SHOWING SOUND BONDING
(BOND SHEAR STRENGTH: 30,000 PSI)
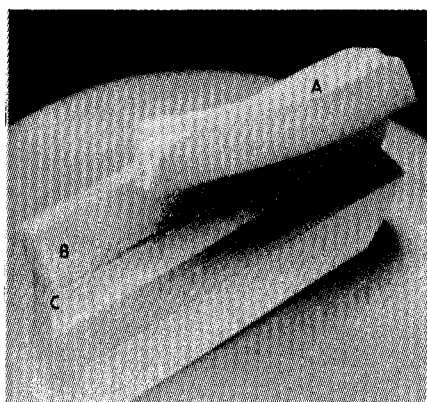
10X

BONDING PLANE = B
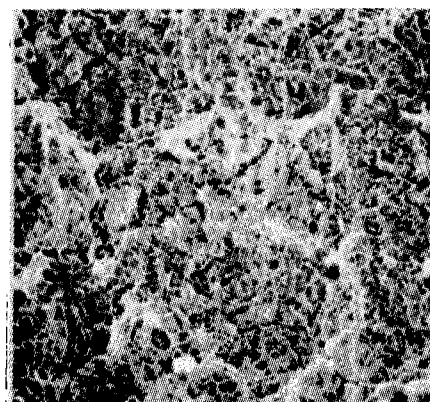
1000X

PLANE B

Another lap sheared specimen which represents 30,000 psi bond strength was chosen for SEM fractographic analysis. Here fracture occurred both at bond interface (Plane B) and at parent alloy (Plane A). A secondary crack, which is indicated as C, was also observed at the corner of a machined notch. Examination of Plane B with higher magnification revealed a typical failure mode of overload dimpled rupture by microvoid coalescence. This failure mode of ductile rupture is a good indicator for a completed bonding with good integrity.

246

APPLICATIONS FOR SOLID-STATE BONDING

- **ELECTRONIC COMPONENTS**

- **NUCLEAR REACTORS**

- **MISSILES**

- **AIRCRAFT STRUCTURES**

    - **AS A JOINING METHOD FOR UNWELDABLE ALLOYS**

    - **AS A CONCURRENT PROCESS WITH SUPERPLASTIC FORMING**

The applications of solid-state bonding are found in the industries where stringent joint requirement is necessary and high joint efficiency is required. Solid-state bonding or diffusion bonding of titanium has been utilized for aircraft structural parts. The ultimate goal of this program is to develop solid-state bonding technology as a concurrent process with superplastic forming of high strength alloy 7475 for aircraft structural application.

GRAIN STRUCTURE OF
SUPERPLASTIC ALUMINUM 7475

MAG 250X
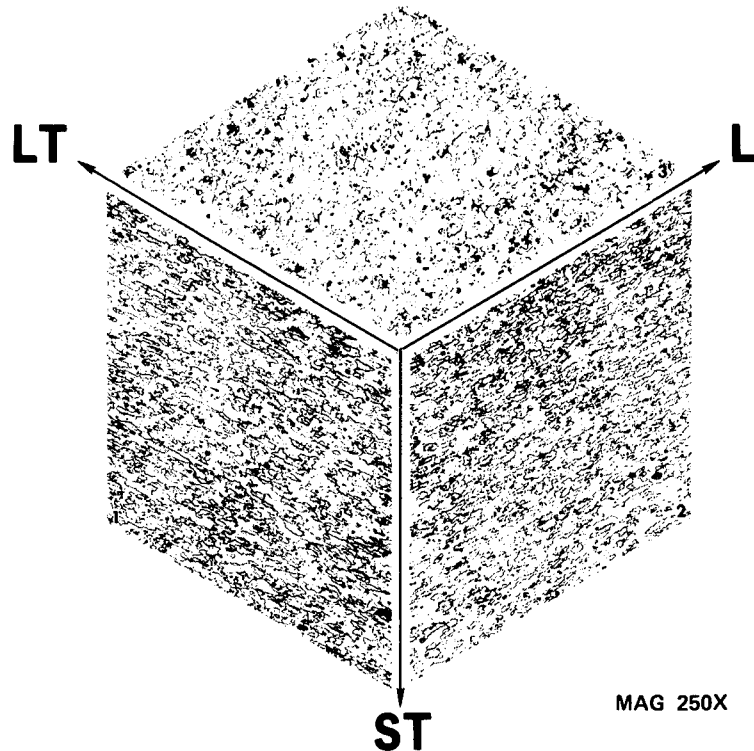
The photomicrograph shows a three-dimensional grain aluminum 7475 alloy sheet, which was used in the bonding experiments. Conventional aluminum alloy sheets are not superplastic because of coarse grains. Thermo-mechanical process can effectively reduce the grain size of the 7475 alloy to a sufficiently small size and stable state to permit the development of superplastic deformation. The grain size of the alloy shown in the photo is approximately 10 μm.

DEFORMATION CHARACTERISTICS OF SUPERPLASTIC ALUMINUM 7475
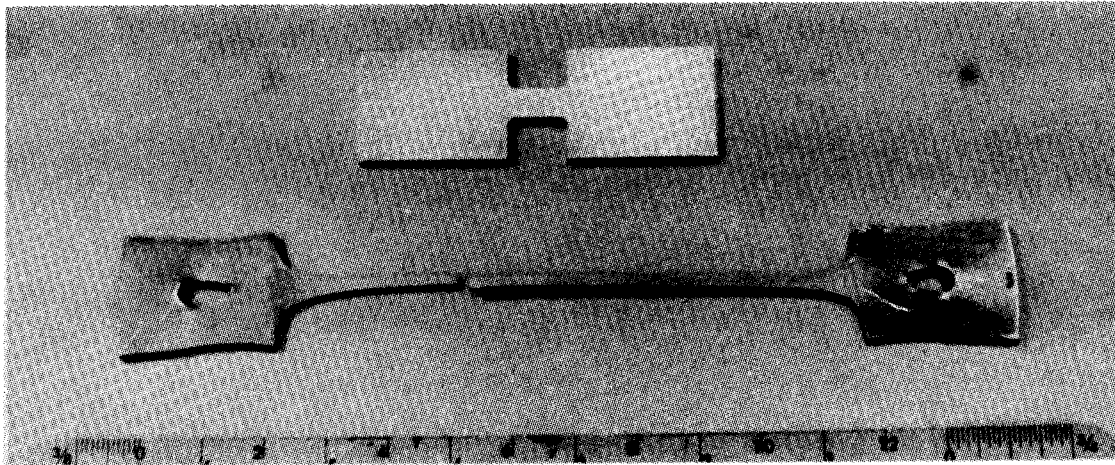
Superplastic behavior is characterized by extremely high elongation before necking occurs. When a tensile specimen of fine-grained 7475 alloy was tested at 960° F at a controlled strain rate, the total elongation was approximately 950% at fracture.

INTEGRALLY STIFFENED STRUCTURES
FOR POTENTIAL SPF/SSB APPLICATION
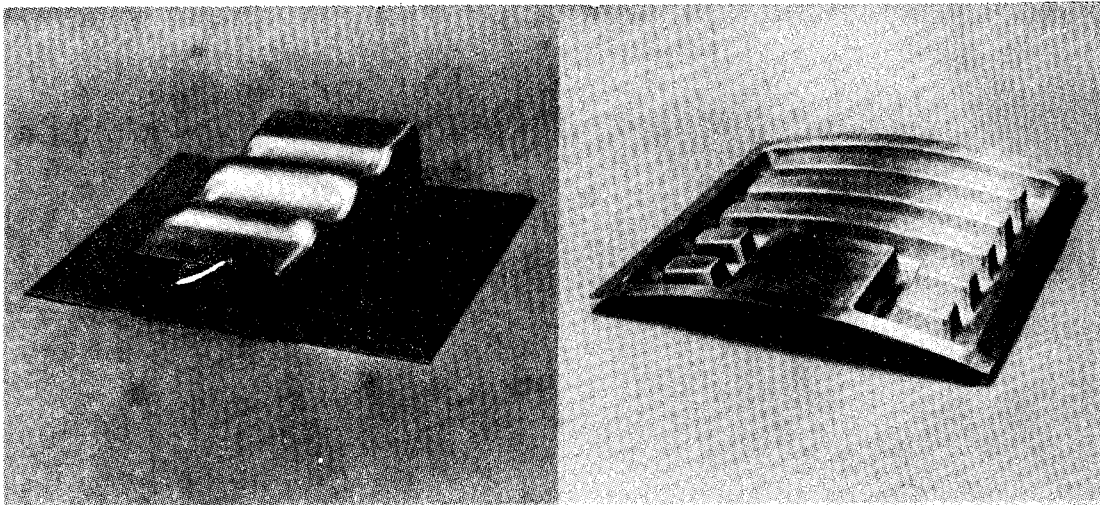
Superplastic forming of aluminum will result in reduction of number of details and fasteners, which consequently leads to cost and weight savings. When the solid-state bonding is combined with the superplastic forming process, further gains will be realized. Two integrally stiffened structures of high strength aluminum which were superplastically formed are the examples of potential superplastic forming solid-state bonding because these formed parts have to be eventually joined to skin sheet.

CONCLUSIONS

1. Feasibility of solid-state bonding was demonstrated for superplastic aluminum 7475 sheet.

2. Plastic deformation was required to obtain solid-state bonding, and bond strength increased with an increase in the amount of deformation.

3. A thin intermediate layer of alloy 5052 aided the solid-state bonding in reducing the required bond deformation.

EVALUATION OF SUPERPLASTIC FORMING AND WELD-BRAZING FOR FABRICATION OF TITANIUM COMPRESSION PANELS

Dick M. Royster, Thomas T. Bales, and Randall C. Davis
NASA Langley Research Center
Hampton, Virginia 23665

ABSTRACT

Studies have been conducted at NASA Langley Research Center to demonstrate the processing advantages of superplastic forming and weld-brazing for the fabrication of full-size titanium skin stiffened structural components. The studies were conducted in three phases. The initial phase included fabrication and testing of 10-inch-long single stiffener compression panels of varying configurations, including advanced designs to explore improved structural efficiency. The second phase consisted of scaling up the process to fabricate and test multiple stiffener panels approximately two ft by three ft in area. The panel configurations selected for evaluation included a conventional hat stiffened design and the beaded web hat stiffened design which exhibited highest structural efficiency in the initial phase results. The multiple stiffeners for each panel were superplastically formed in a single operation from a single sheet of titanium and then joined to a titanium skin by weld-brazing.

In the third phase of the study, an alternative approach (designated the half-hat process) was developed for superplastically forming and weld-brazing the titanium compression panels. This process involved superplastically forming individual half-hat stiffener segments which minimized thinning of the titanium compared to results obtained in the earlier phases. The half-hat segments were then incorporated into full-size compression panels by weld-brazing the segments to titanium caps.

Results from these studies verify that the superplastic forming process can be designed and controlled to provide close tolerances, and that weld-brazing is a highly effective joining technique for fabrication of full-scale, full-size compression panels.

SUPERPLASTIC FORMING/WELD-BRAZING (SPF/WB) PROCESS

INTRODUCTION

o INITIAL DEVELOPMENT
o SCALE-UP
o REFINEMENT

In the past few years the aerospace industry has been involved in the research and development of the advanced forming and joining method for titanium alloys known as superplastic forming and diffusion bonding. The research at the Langley Research Center (LaRC) of NASA has taken a different approach where superplastic forming was combined with weld-brazing to fabricate structural hardware. This is a summary paper on this long-standing in-house research program.

This paper discusses the research program beginning with the initial process development phase that demonstrated that single stiffener structural panels of advanced design could be fabricated by the superplastic forming/weld-brazing process and that these panels could be used to explore structural efficiency. The second phase of the program was to scale-up the process to fabricate full-size panels having multiple stiffeners. In the recent phase of the program the superplastic forming/weld-brazing process was refined in an attempt to reduce metal thinning during superplastic forming.

SUPERPLASTIC FORMING OF TITANIUM

AS-MACHINED

SUPERPLASTICALLY FORMED

1.0 INCH
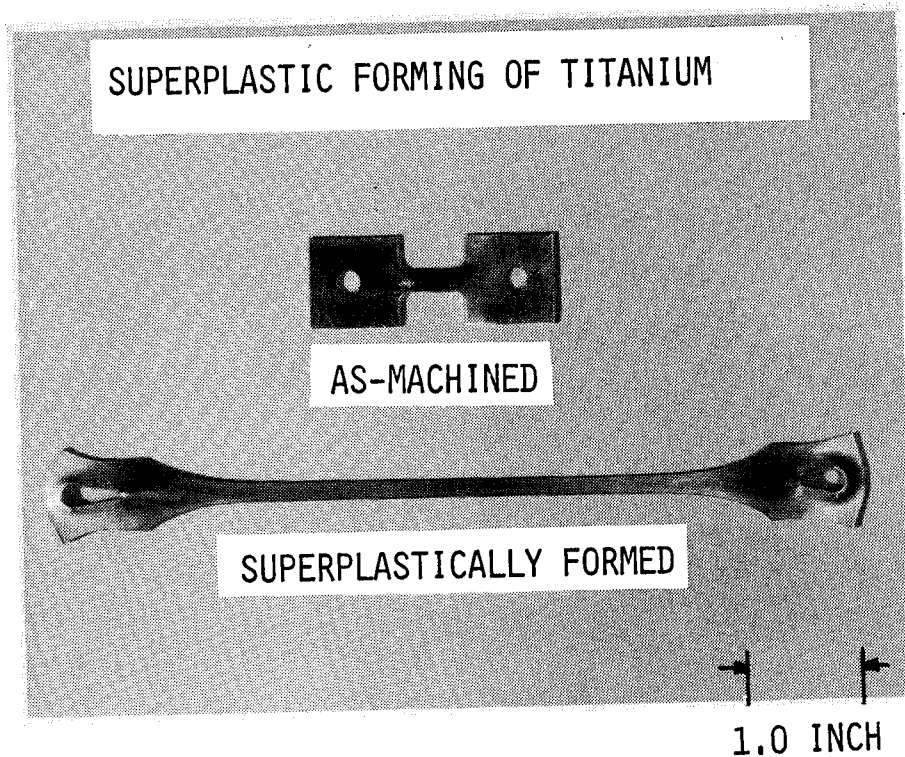
The NASA LaRC program combined two established titanium alloy forming and joining processes, superplastic forming and weld-brazing. The superplastic forming of titanium alloys has been researched by the aerospace industry for several years. To demonstrate and develop the superplastic forming process, the initial work was usually done on tensile specimens. The figure shows a Ti-6Al-4V titanium alloy tensile specimen in the "as-machined" condition and after being "superplastically formed." In the as-machined condition the test section is one-half inch long. The superplastically formed specimen has been elongated approximately 1100 percent by heating the specimen to 1700°F and loading at a strain rate of 0.0002 per second. Low flow stresses of one to two ksi were developed. The specimen was superplastically formed with a uniform elongation and no localized necking.

TOOLING FOR SUPERPLASTIC FORMING OF STIFFENERS
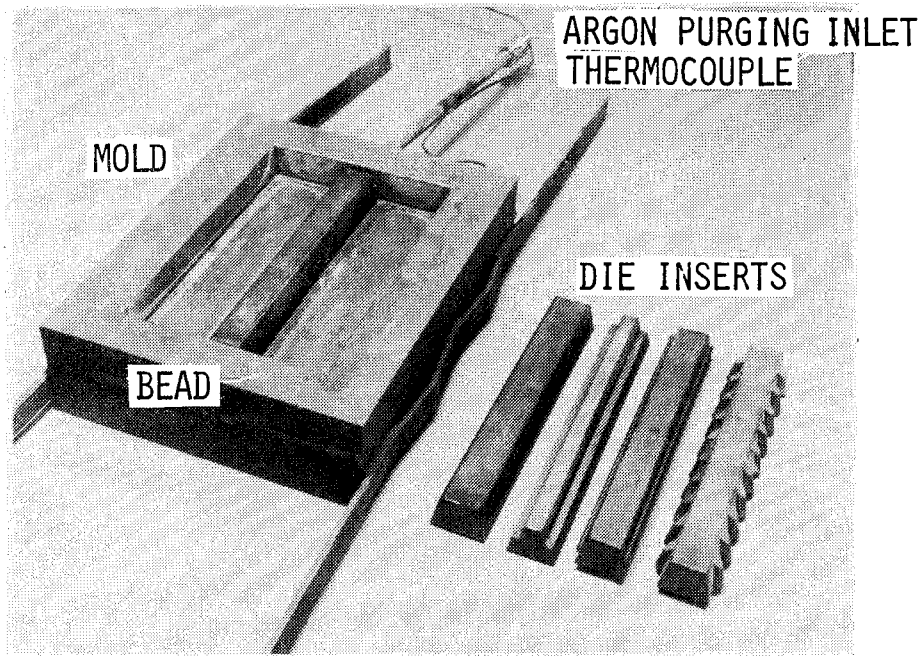
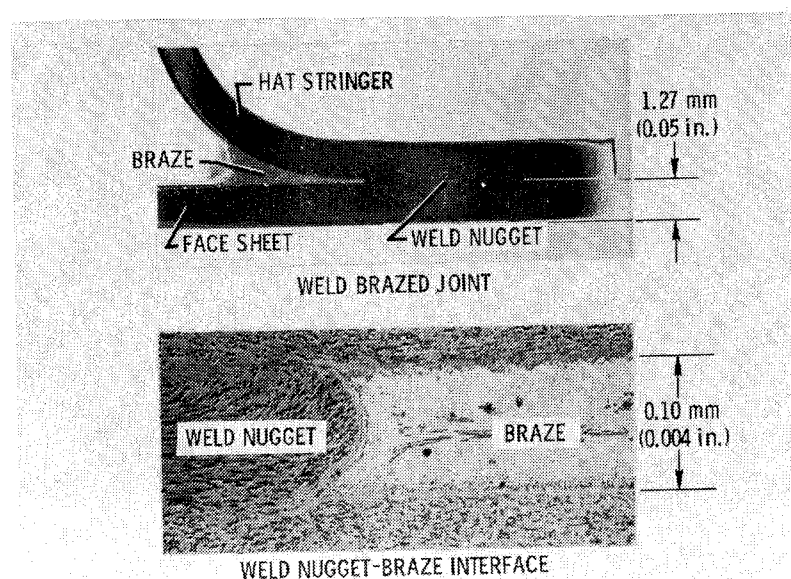As a result of the low flow stresses required for superplastic forming, titanium sheet material can be readily blown into molds using argon gas pressure. This was the procedure utilized to fabricate stiffeners for this program (reference 1). A mold with several die inserts for the stiffener configurations evaluated is shown in the figure. The mold, machined from 2249 steel, was designed such that the titanium in the crown of the formed stiffener would equal the approximate thickness of the titanium sheet prior to forming. The resulting webs and flanges of the stiffeners had variable thicknesses due to thinning associated with superplastic forming.

The die inserts were machined from 2249 steel and positioned in the mold. One of the inserts was used to form conventional shaped hat stiffeners. The remaining die inserts were used to form stiffeners with a stepped shaped web, a ribbed shaped web, and a beaded shaped web. These complex shaped stiffeners were either difficult to form or could not be formed by conventional titanium forming methods. Stiffener shapes were selected on the basis of structural efficiency, taking advantage of the superplastic forming characteristics of the titanium alloy.

Ti-6Al-4V stiffeners were superplastically formed to the shape of the dies by placing a sheet of titanium over the lower mold. The cover plate, which has an inlet for pressurizing with argon gas, was placed over the titanium sheet. The assembled tooling was placed between heated ceramic platens mounted in a press. After the tool was heated to 1700°F, argon gas was induced through the cover plate which forces the titanium sheet into the shape of the die and lower mold cavity. Argon gas pressure was applied up to a pressure of 125 psi for a period of 90 minutes. Power to the ceramic platens was turned off and the formed titanium stiffener was cooled in the mold using argon gas.

VACUUM WELD-BRAZED JOINT

HAT STRINGER

BRAZE

FACE SHEET — WELD NUGGET

1.27 mm
(0.05 in.)

WELD BRAZED JOINT

WELD NUGGET — BRAZE — 0.10 mm
(0.004 in.)

WELD NUGGET-BRAZE INTERFACE

Weld-brazing was a joining process developed at NASA LaRC in the early 1970's which combined resistance spot-welding with brazing (reference 2). The process was used successfully to join titanium structural members using an aluminum braze alloy. The first step in the process was to establish spot-welding parameters which resulted in expansion of the weld nugget to provide a predetermined uniform gap between the faying surfaces in order to optimize the thickness of the subsequent brazed joint. Following resistance welding, braze alloy foil in appropriate quantities was placed along the exposed edge of the joint. The assembly was then brazed in a vacuum furnace to produce the specimen joint shown in the figure. During brazing, the braze alloy melted and was drawn into the existing gap by capillary action. The braze is shown to have drawn through the gap to form a fillet between the face sheet and the inner radius of the hat stiffener. The lower photomicrograph of the weld-brazed joint shows good integrity of the joint in the vicinity of the weld-nugget.

SINGLE-OVERLAP TENSILE-SHEAR DATA
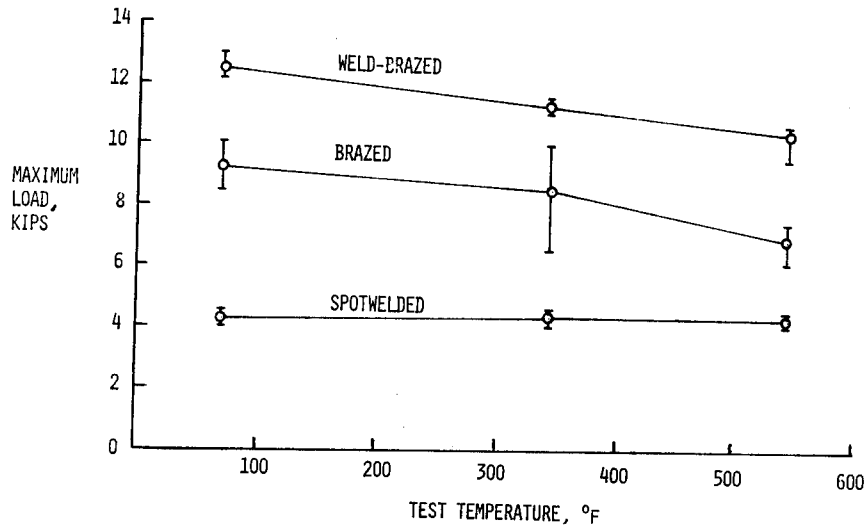
The tensile-shear results obtained at ambient temperature, 350°F, and 550°F for titanium specimens fabricated by spot-welding, brazing, and weld-brazing are shown in the figure where the maximum load is plotted against test temperature. The data points are the average of a minimum of three tests with the data spread indicated. The tensile-shear properties of the weld-brazed specimens are shown to be greater than those of the brazed or spot-welded specimens and are approximately equal to the sum of the values shown for the spot-welded and brazed specimens. The strength of the weld-brazed specimens apparently decreases linearly with increasing temperature.

258

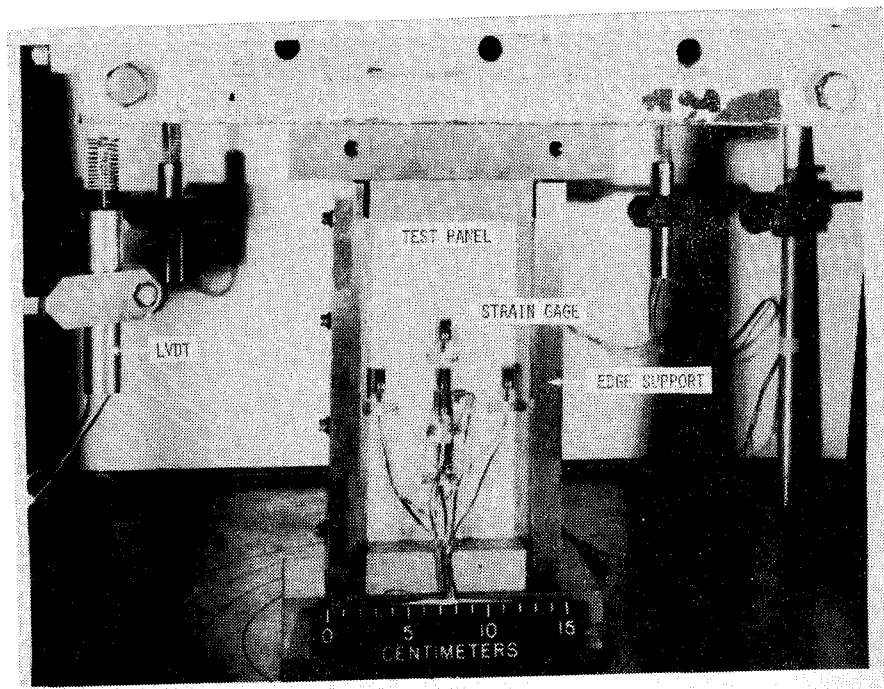# SUPERPLASTICALLY FORMED/WELD-BRAZED TITANIUM COMPRESSION PANEL
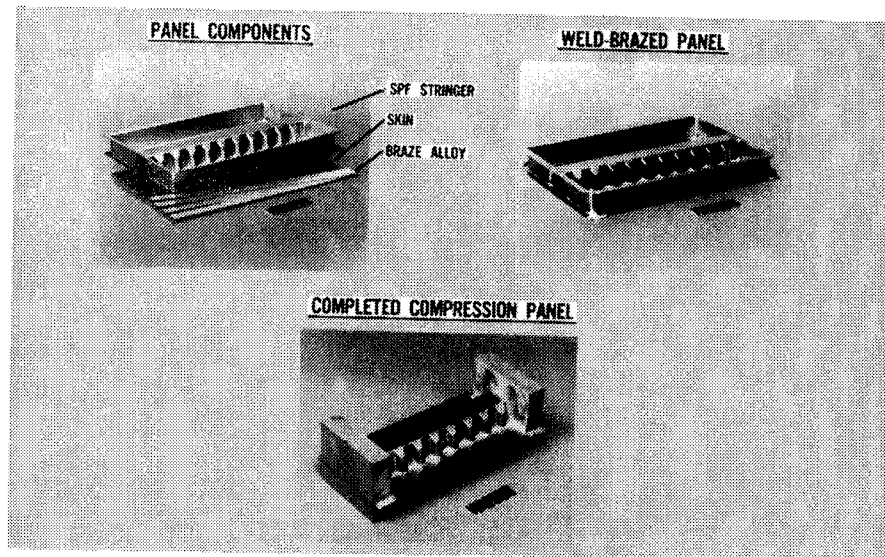
The steps involved to combine superplastic forming and weld-brazing to fabricate a compression panel are shown on the figure. The components of a panel include the superplastically formed stiffener, the panel skin and the 3003 aluminum braze alloy. Both the stiffener and skin material are 0.050-inch thick Ti-6AL-4V titanium alloy. Weld-brazing of a panel consisted of spot-welding the stiffener to the skin and then brazing. Following chemical cleaning, two rows of four spot-welds each were used to attach each flange of the stiffener to the skin. Welding parameters were developed so that weld nugget expansion established a faying surface gap 0.002 to 0.003 inches between the flanges of the stiffener and the skin. Braze alloy strips were placed adjacent to the joints to be brazed and the panel placed in the brazing furnace. Fixturing provided by the spot welds was sufficient to maintain alignment and no tooling was required for brazing of the panel.

Brazing of the panel was accomplished in a vacuum furnace at a temperature of 1250°F. Upon melting, the 3003 aluminum braze alloy was drawn into the faying surface gap by capillary action. The panel was allowed to cool from the brazing temperature to room temperature before being removed from the furnace. Visual and radiography inspection verified good wetting between the stiffener and skin and establishment of a good integral joint.

Following brazing the superplastically formed/weld-brazed panel was trimmed on the edges and ends. After trimming, the panel was potted on both ends using an epoxy potting compound. Potting compound was used to facilitate grinding the ends of the panel flat, parallel to each other, and perpendicular to the skin. The potting also served to prevent local failure of the ends during compression testing.

259

TEST SETUP FOR SKIN-STIFFENED PANELS

The superplastically formed/weld-brazed structural panels were tested in end compression using a 300 kip hydraulic testing machine. The edges of the panels were supported with knife edges. Relative motion between the upper and lower heads of the testing machine was measured using linear variable differential transformers. Foil strain gages were attached to the stiffener and skin and were used to measure local strains. Strain reversal was used to define onset of elastic buckling.

UNIQUE SPF STIFFENER CONFIGURATIONS
INCREASE STRUCTURAL EFFICIENCY

RELATIVE
BUCKLING
STRENGTH
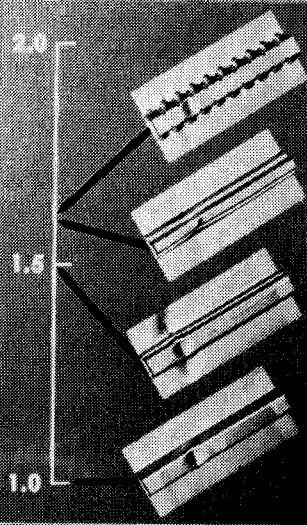
Three panels were fabricated and tested from each of the four stiffener config-
urations (conventional shaped hat, stepped shaped web, ribbed shaped web, and
beaded shaped web) at room temperature. The buckling strengths of the complex
shaped stiffener configurations were compared with those of the conventional
shaped hat stiffener. The data in the figure show that the panels with the
complex shaped stiffener configurations were 50 to 60 percent more efficient
than the panels with the conventional shaped hat stiffener. This increase in
structural efficiency was obtained with no increase in panel weight or cross-
sectional area. The improvement in structural efficiency was attributed to
the advanced structural shapes that were formed by the superplastic forming
process.

SUPERPLASTIC FORMING FACILITY

ARGON GAS REGULATORY SYSTEM

HEATED CERAMIC PLATENS

TEMPERATURE PROGRAMMER

300 KIP JACK

GAS PRESSURE PROGRAMMER
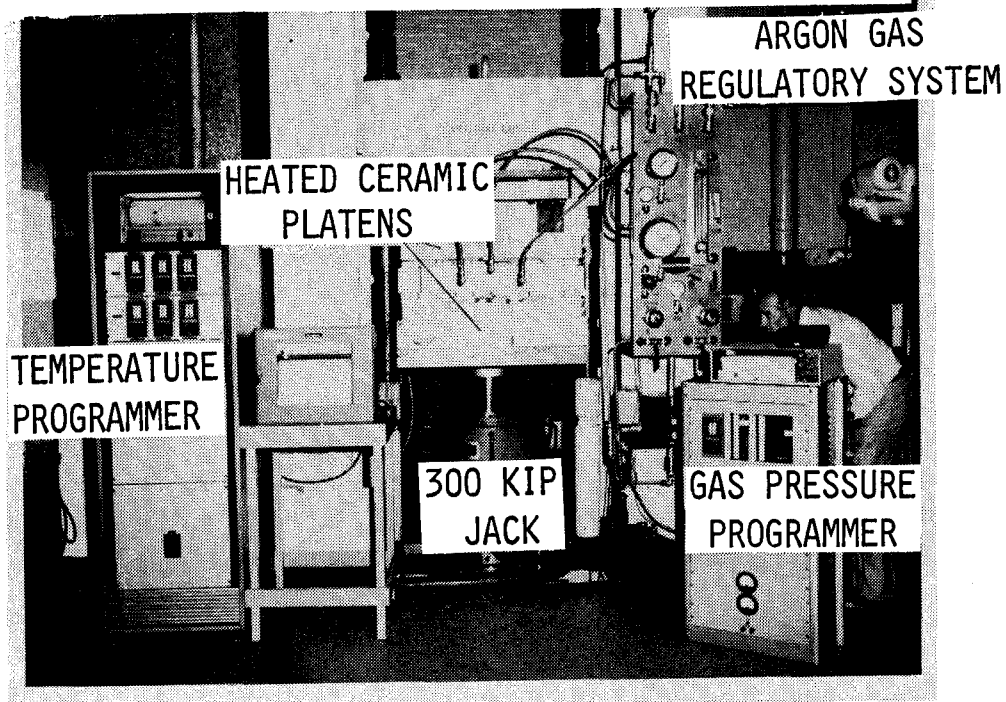
The second phase of the superplastic forming/weld-brazing program was to scale-up the process to fabricate full-size panels. The figure shows the superplastic forming facility located at LaRC. Using this facility, three-ft by two-ft multi-stiffener panels were formed with either conventional shaped hat stiffeners or beaded web shaped stiffeners. The superplastic forming temperatures and pressures were similar to those utilized in the superplastic forming of the single element panels. The ceramic platens heated the tooling to 1700°F and the 300 kip jack reacted to the gas forming pressure. Both the temperature and argon gas forming pressure were automatically programmed.

MULTIPLE STIFFENER COMPRESSION PANELS

CONVENTIONAL SHAPED HAT

BEADED SHAPED WEB
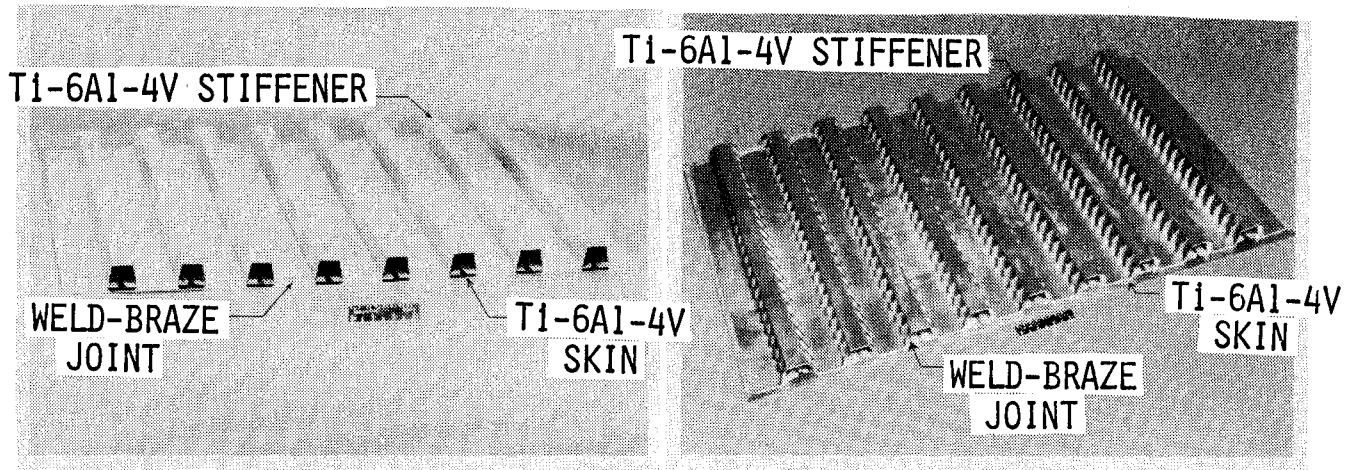
Multi-stiffener panels were superplastically formed from one sheet of titanium in a single forming operation. The three-ft by two-ft panels with either conventional shaped hat stiffeners or beaded web shaped stiffeners are shown in the figure following weld-brazing to titanium skins. To accomplish the brazing, sufficient braze alloy was placed adjacent to each joint at both ends of the panels. Following inspection the panels were trimmed, the ends were potted, and the panels were machined to the proper length. The panels were instrumented with strain gages and tested at room temperature to failure in end compression in a hydraulic test machine.

263

AVERAGE BUCKLING LOADS FOR SPF/WB
FULL-SIZE PANELS
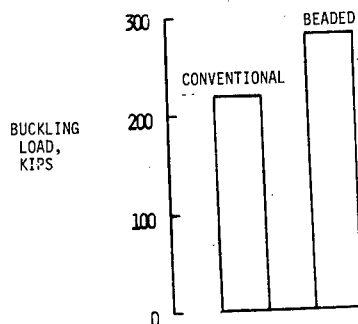
The buckling loads for the two full-size panel configurations are shown in the figure. The data are the average of two tests for the panel with the conventional shaped hat stiffener design and a single test for the panel with the beaded web shaped stiffener design. The panels with the conventional shaped hat stiffener buckled at an average load of 219 kips, which was in excellent agreement with analysis. An analysis of the buckling mode showed that the web of the hat was the critical element in that its local buckling strength was lower than the local buckling strength of any other element. The next lowest buckling element was the skin segment under the hat stiffener. The local buckling strength of the skin segment was calculated to be 29 percent higher than that of the webs.

By beading the webs they become nonload-carrying structural members which made the critical element for local buckling the skin element under the beaded hat stiffener. Taking into account the reduced extensional stiffness caused by the loss of load-carrying capacity in the beaded webs, analysis predicted that the panel with the beaded web shaped stiffeners should carry 28 percent more load than the panels with the conventional shaped hat stiffeners. This was in excellent agreement with the test results that showed that the panel with the beaded web shaped stiffeners buckled at a load of 280.5 kips or 29 percent higher than the panels with the conventional shaped hat stiffeners.

264

ANALYSIS OF CURVED-CAP CORRUGATION INDICATES SIGNIFICANT IMPROVEMENT IN STRUCTURAL EFFICIENCY IS POSSIBLE
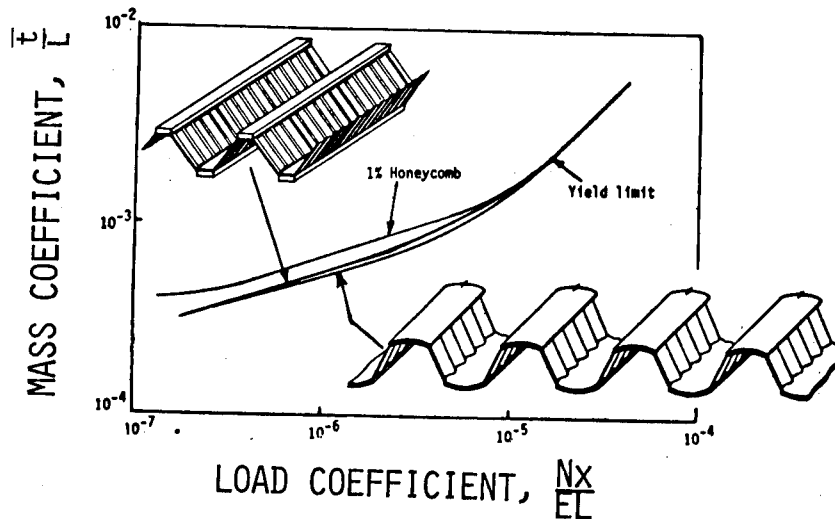
The recent phase of the program was begun by conducting an analytical study on structural efficiency of advanced panel design concepts. The results of analysis on these configurations are shown in the figure. In the mass coefficient, $\bar{t}/L$, $\bar{t}$ is the mass-equivalent thickness for the corrugated cross section and L is the panel length. In the load coefficient, Nx/EL, Nx is the compressive load-per-unit width, E is the elastic modulus and L is the panel length. The mass-strength data are dimensionless and are, therefore, independent of the materials used to make the panels. The mass-strength data for a one-percent honeycomb sandwich are a standard of comparison for low mass structures. This standard represents the desired goal in mass efficiency and is considered just beyond the current state of art in manufacturing technology. As the figure shows, some advanced configurations show mass-strength efficiencies better than one-percent honeycomb. These configurations can be fabricated with current state-of-art superplastic forming techniques. Panels fabricated using lightweight sine wave webs with minimized thinning in the flanges are an important design goal. This goal has lead to the development of new tooling for superplastic forming and a new fabrication procedure to explore the possibility of fabricating panels similar to those shown on the figure.

TOOLING CONCEPTS FOR SUPERPLASTIC FORMING
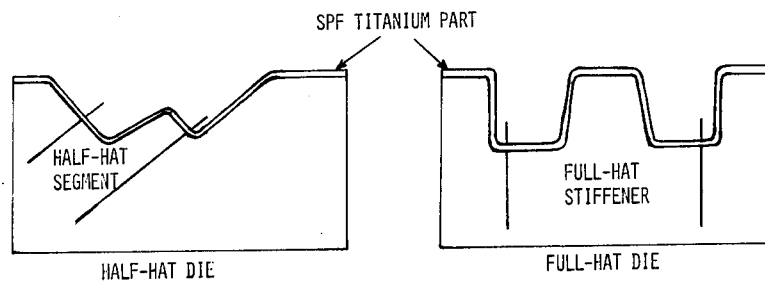
Two tooling concepts for superplastic forming stiffeners are shown in the figure. The full-hat male-die concept was utilized to form the stiffeners discussed previously in this report. After forming a stiffener, the thickness of the titanium in the crown of the stiffener was equal to the approximate thickness of the titanium sheet prior to forming. The resulting webs and flanges of a stiffener had variable thicknesses. The half-hat die concept was developed to reduce metal thinning across the web and to develop equal thicknesses in the flanges. In the half-hat die concept only half of a hat segment was superplastically formed in one operation. Two half-hat segments were weld-brazed to a cap segment to fabricate a full hat stiffener. Thinning was reduced by rotating the half-hat segment in the mold requiring lower strain levels to achieve given design dimensions than the deeper full-hat mold. The required strains or deformations were less and the effects of thinning were, therefore, minimized.

SPF TITANIUM HALF-HAT SEGMENTS
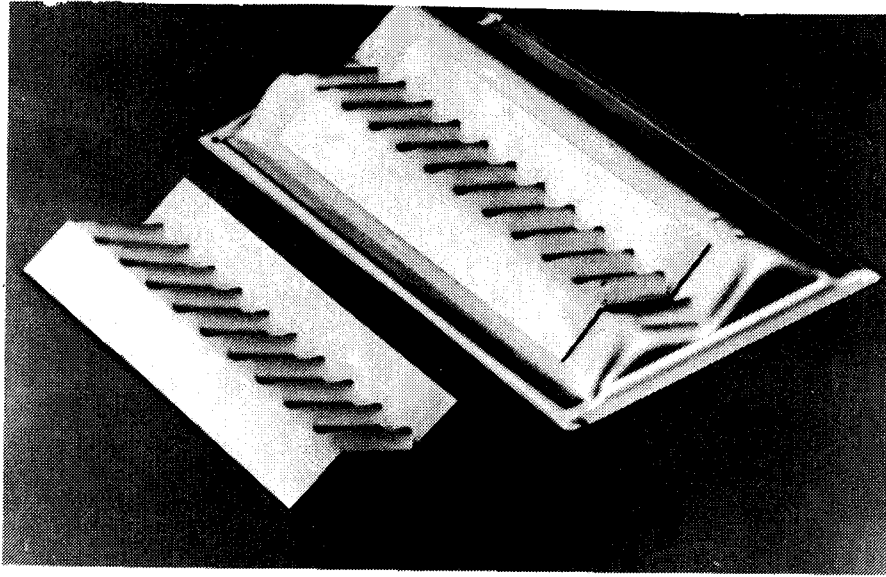
This figure shows a superplastically formed part and two half-hat segments. One half-hat segment shows the location on the part from which the half-hat segment was machined. The second half-hat segment is shown after trimming and ready for weld-brazing. A constant thickness was maintained in both flanges in the half-hat segment by using this die concept.

SPF/WB BEADED WEB COMPRESSION PANELS

SINGLE-STIFFENER
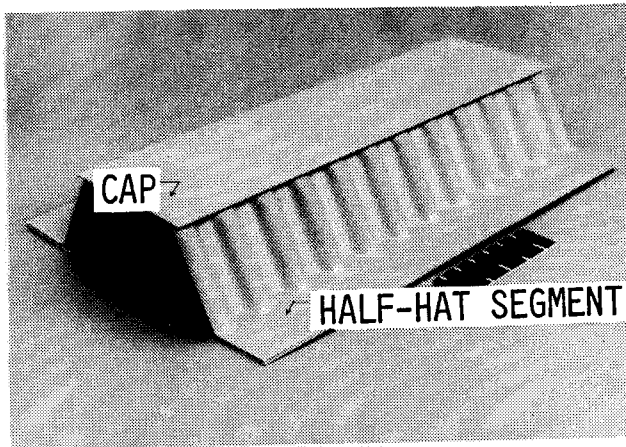
MULTIPLE-STIFFENER
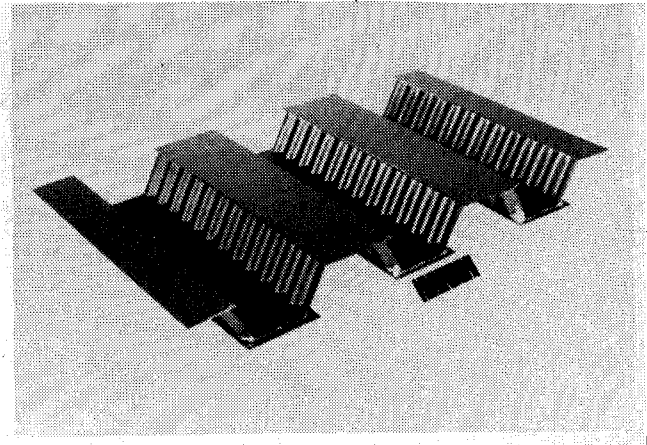
The half-hat process was utilized to fabricate both single-stiffener panels and multi-stiffener panels as shown in the figure. The half-hat segments were joined to caps by the weld-braze process. The process offers the opportunity to fabricate full-size multi-stiffener panels limited only by the size of the brazing furnace. During superplastic forming of the half-hat segments, the thickness of the titanium material was reduced 16 percent from the original thickness in the highest strained regions.

AVERAGE BUCKLING LOADS OF SPF/WB PANELS
USING HALF-HAT PROCESS
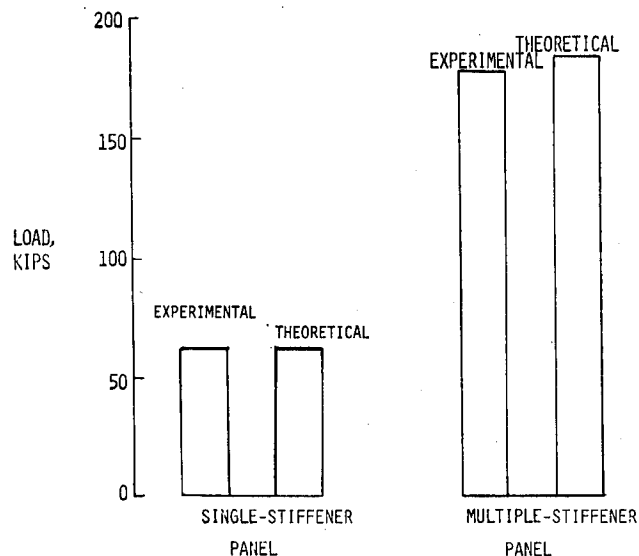
Following fabrication, three panels of each configuration were tested to failure in compression at room temperature. The figure shows the average buckling load and the calculated theoretical buckling load for both panel configurations. The experimental buckling load was within three percent of the calculated theoretical load for both panel configurations, verifying that the superplastic forming process can be used to achieve controlled tolerances and that the weld-brazing process was a highly effective technique for joining panel elements.

CONCLUDING REMARKS

o SUPERPLASTIC FORMING
  - COMPLEX SHAPES
  - SIMPLE TOOLING
  - INSPECTABILITY

o WELD-BRAZING
  - NO TOOLING
  - DUCTILE JOINTS

o SPF/WB PANELS
  - INCREASED STRUCTURAL EFFICIENCY
  - SCALE-UP DEMONSTRATED

The two titanium processing procedures, superplastic forming and weld-brazing, were successfully combined to fabricate titanium skin-stiffened structural panels. Stiffeners with complex shapes were superplastically formed using simple tooling. These stiffeners were formed to the desired configuration and required no additional sizing or shaping following removal from the mold. The weld-brazing process by which the stiffeners were attached to the skins utilized spot-welds to maintain alignment and no additional tooling was required for brazing. The superplastic formed/weld-brazed panels having complex shaped stiffeners developed up to 60 percent higher buckling strengths than panels with conventional shaped hat stiffeners.

The superplastic forming/weld-brazing process was successfully scaled up to fabricate full-size panels having multiple stiffeners. The superplastic forming/weld-brazing process was also successfully refined to show its potential for fabricating multiple-stiffener compression panels employing unique stiffener configurations for improved structural efficiency.

REFERENCES

1. Royster, Dick M.; Bales, Thomas T.; and Wiant, H. Ross: Superplastic Forming/Weld-Brazing of Titanium Skin-Stiffened Compression Panels. Materials Overview for 1982, Volume 27 of National SAMPE Symposium and Exhibition, Society for the Advancement of Material and Process Engineering, 1982. pp. 569-582.

2. Bales, Thomas T.; Royster, Dick M.; and Arnold, Winfrey E., Jr.: Development of the Weld-Braze Joining Process. NASA TN D-7281, 1973.

FEASIBILITY OF REMOTELY MANIPULATED WELDING IN SPACE -
A STEP IN THE DEVELOPMENT OF NOVEL JOINING TECHNOLOGIES

Koichi Masubuchi
John E. Agapakis
Andrew DeBiccari
and Christopher von Alt

Massachusetts Institute of Technology
Cambridge, Massachusetts 02139

ABSTRACT

A six-month research program entitled "Feasibility of Remotely Manipulated Welding in Space - A Step in the Development of Novel Joining Technologies" was performed at the Massachusetts Institute of Technology for the Office of Space Science and Applications, NASA, under Contract No. NASW-3740. The work was performed as a part of the Innovative Utilization of the Space Station Program. The final report from M.I.T. was issued in September 1983 (ref. 1). This paper presents a summary of the work performed under this contract.

The objective of this research program was to initiate research for the development of packaged, remotely controlled welding systems for space construction and repair. The research effort included the following tasks:

Task 1: Identification of probable joining tasks in space
Task 2: Identification of required levels of automation in space welding tasks
Task 3: Development of novel space welding concepts
Task 4: Development of recommended future studies
Task 5: Preparation of the final report.

Probable joining tasks have been classified, depending upon the complexities and scales of the tasks, into the following three categories:

Category 1: Construction and repair of simple, small tools, equipment, components, and structural members
Category 2: Maintenance and repair of major members of space stations
Category 3: New construction of large, complex structures.

The following six research programs have been recommended for further developing technologies for space welding:

Program #1: Development of space stud welding which can be remotely manipulated
Program #2: Development of "instamatic®" GTAW systems for space applications which can be operated by an astronaut with no welding training
Program #3: Development of flexible space welding systems
Program #4: Research on space welding using GMAW, EBW, and LBW processes
Program #5: Research on spatial joining techniques suited for space applications
Program #6: Development of integrated fabrication systems for certain complex structures.

INTRODUCTION

The objective of this six-month research program was to initiate research for the development of packaged, remotely controlled welding systems for space construction and repair. The research effort included the following tasks

Task 1: Identification of probable joining tasks in space
Task 2: Identification of required levels of automation in space welding tasks
Task 3: Development of novel space welding concepts
Task 4: Development of future studies
Task 5: Preparation of the final report.

In order to establish permanent human presence in space we must develop technologies of constructing and repairing space stations and other space structures. In early states of the Space Station Program, most construction jobs will be performed on earth and the fabricated modules will then be delivered to space by the Space Shuttle. Only limited final assembly jobs, which may be primarily mechanical fastening, will be performed on site in space. Such fabrication plans, however, limit the designs of these structures, because each module must fit inside the transport vehicle and it must withstand launching stresses that could be considerable. It is evident that large-scale utilization of space will necessitate more extensive construction work on site. Furthermore, continuous operations of space stations and other structures will require maintenance and repairs of these space structures. It is therefore very important to develop metal joining technology, and especially high-quality welding, in space.

It should be mentioned that close relationships exist between welding technologies and structural designs. Many space structures designed so far appear to be based on an assumption that welding fabrication in space is not possible. Much more versatile structural design can be achieved once the space welding technology is well developed.

Welding is a relatively complicated joining process which requires certain scientific knowledge and human skills. Proper processes, equipment, and consumables, as well as joint design and welding conditions (welding current, arc voltage, torch travel speed, etc.) must be used to successfully weld certain materials in given thicknesses. Welding operations, including manipulation of the welding torch, must be performed in a proper manner in order to produce a weld free from defects such as cracks, lack of fusion, porosity, and slag inclusion. Welding engineers have spent considerable effort to minimize the adverse effects caused by oxygen, nitrogen, and hydrogen.

Welding in space certainly creates great challenges and opportunities for welding engineers. The lack of an atmosphere in space will be helpful in obtaining uncontaminated welds and also will readily permit the use of high power-density welding processes such as electron beam welding. However, a number of problems will be posed by the particular nature of the space environment and the great distance from the earth. In order to successfully perform welding construction and repair in space, we must first study problems associated with welding in space and then develop welding technologies suitable for space applications.

ADVANTAGES OF WELDING OVER MECHANICAL JOINING AND ADHESIVE BONDING

HIGHER STRENGTH OVER A WIDE RANGE OF TEMPERATURES

MORE RIGIDITY

AIR AND WATER TIGHTNESS

COMPLEX CHARACTERISTICS OF WELDING FABRICATION

1. MANY DIFFERENT PROCESSES, MATERIALS, AND STRUCTURES

2. ADDITIONAL PROBLEMS WITH WELDING FABRICATION OF COMPLEX STRUCTURES

3. SKILLS REQUIRED

4. WELDING IS ONLY A PART OF TOTAL FABRICATION SYSTEM INCLUDING:

   A. PLATE CUTTING, FORMING (IF NECESSARY), AND EDGE PREPARATION

   B. ASSEMBLY OF PARTS TO BE WELDED AND TACK WELDING

   C. WELDING

   D. INSPECTION

Before discussing welding in detail, let us discuss briefly the advantages of welding over mechanical joining such as riveting and adhesive bonding. First of all, welded joints normally have higher strengths over a wide range of temperatures than mechanical and adhesive-bonded joints. Welded joints have higher rigidity than mechanical and adhesive-bonded joints. It is easier to obtain air and water-tight welded joints than mechanical and adhesive-bonded joints.

Although welding is widely used because of its advantages over other joining methods, there are some problems with welding fabrication, one of which is that it is rather complicated and requires some knowledge and skill.

First, there are many different processes which are commercially available today. Many of these processes may be used for space applications. In space applications, on the other hand, we must consider many different materials and different structures.

Even though the welding of simple joints in a certain material is successfully made, it does not necessarily mean that welding fabrication of a complex structure would be successfully achieved. There are certain problems associated with welding fabrication of complex structures composed with a number of members. One of the problems is related to residual stresses and distortion.

Manual arc welding, which is still widely used, is performed by people who are specially trained and qualified. Even in the case of automatic welding, most machines need to be operated by people who have received special training.

Welding is only a part of total fabrication system that includes (a) plate cutting, forming (if necessary), and edge preparation, (b) assembly of parts to be welded and tack welding, (c) welding, and (d) inspection. In considering welding in space, we must also consider how to perform total fabrication in space.

NUMBER OF EXISTING PUBLICATIONS ON SPACE WELDING
AND RELATED SUBJECTS

(a) Classification by Countries

	WELDING AND BRAZING	OTHER	TOTAL
U.S.A.	15	52	67
U.S.S.R.	22	11	33
GERMANY	12	5	17
U.K.	3	0	3
FRANCE	1	0	1
TOTAL	53	68	121

(b) Classification of Publications on Welding and Brazing

ELECTRON BEAM WELDING	10
BRAZING	6
SOLAR ENERGY WELDING	4
COLD WELDING AND DIFFUSION BONDING	3
EXPLOSIVE WELDING	2
GENERAL	28
TOTAL	53

As the first step for identifying probable joining tasks in space, a survey was made on examining publications on space welding and related subjects. The result of the literature survey is presented in APPENDIX A of reference 1. The emphasis of the discussion is placed on identifying (a) those who are studying, (b) which processes are being considered, (c) which materials are being used, and (d) which kinds of applications are being examined.

Serious technical publications on space welding started to appear around 1966, when Lawrence and Schollhammer prepared a report entitled "Hand Held Electron Beam and External Power Supply" (ref. 2). APPENDIX A of reference 1 contains 121 citations on space welding and related subjects, of which 53 publications cover welding and brazing as major topics (see table above). Most of the information on space welding and fabrication has been generated by two countries, U.S.A. and U.S.S.R. In preparing the table, efforts have been made as much as possible to identify the country where the work was performed. For example, when a Soviet author presented a paper in a technical journal published in U.S.A., the paper was regarded as a publication from U.S.S.R. On the other hand, when an author in U.K. wrote a paper referring to work done in U.S.S.R., the paper was regarded as a publication from U.K. Papers published in the Federal Republic of Germany and the German Democratic Republic are combined and listed as papers from Germany.

Among the 53 publications on welding and brazing, electron beam welding has been discussed in the largest number of articles, as shown in the table above. Other processes that have been discussed for space applications include solar energy welding, cold welding and diffusion bonding, and explosive welding.

PAST WELDING EXPERIMENTS ON SPACESHIPS

I. U.S.S.R., SOYUZ-6, 1969

PROCESSES: ELECTRON BEAM
PLASMA ARC
GMA

MATERIALS: STAINLESS STEEL
ALUMINUM ALLOY
TITANIUM ALLOY

2. U.S.A., SKYLABS, 1973

A. METALS MELTING EXPERIMENT, M551
B. BRAZING EXPERIMENT, M552
C. SPHERE FORMING EXPERIMENT, M553

M551: ELECTRON BEAM
ALUMINUM ALLOY, STAINLESS STEEL, NICKEL
M552: EXOTHERMIC BRAZING OF STAINLESS STEEL TUBES
M553: ELECTRON BEAM
TUNGSTEN

So far, there have been only two sets of welding experiments performed aboard a spaceship whose results have been published. They are those performed in 1969 by the U.S.S.R. during the Soyuz-6 mission and those performed in 1973 by the U.S.A. on board the Skylab. APPENDIX A of reference 1 presents a summary of the results obtained in these experiments. Both experiments, however, were aimed at demonstrating experimentally that welding of metals could be achieved in space.

(1) Soyuz-6 Experiments. Descriptions presented here come primarily from a paper by Paton (ref. 3). Welding experiments were performed in an enclosed unit, called the "Vulkan" welder, especially designed for the experiments. As an autonomous unit, it was connected to the vehicle system only with telemetry cables. It had two sections, one of which contained the welding burners and an electron beam gun, and a rotating table with samples. The second module consisted of power sources, control devices for measuring and converting units, and automatic communication systems. The machine was activated by pilot-cosmonauts. The experiments were performed using the three processes and the three materials shown above.

(2) Skylab Experiments. On board the Skylab, 54 experiments were performed. Among them, 18 were related to materials science and manufacturing processes. Experiments related to welding were performed in M551, M552, and M553.

In the M551 experiment, the electron beam was used to conduct typical welding tests. Experiments were performed on three materials including (a) an aluminum alloy (22019), (b) a stainless steel (321), and (c) a thoria dispersed nickel.

The M552 experiments were performed with the primary objective of demonstrating feasibility of brazing as a method of space repair and maintenance. A single assembly comprising four brazing packages was mounted in the same vacuum chamber as M551.

The M553 experiment was not exactly on welding, but it was closely related to welding. The main objective of the M553 experiment was to study the mechanisms of sphere melting under zero gravity. The experiment was performed using the same equipment used for the M551 experiment.

UNIQUE REQUIREMENTS FOR SPACE WELDING FABRICATION

(1) DIFFERENCES IN ENVIRONMENTS

	Space			Earth
	Case 1 Outside Space Station	**Case 2** In a Chamber Inside Space Station	**Case 3** Inside Space Station	
Gravity	Zero	Zero	Zero	One
Atmosphere	Vacuum	Vacuum	Air	Air
Temperature	Extreme	Room Temperature	Room Temperature	Room Temperature
Space Suit	Yes	No	No	No

(2) REMOTENESS FROM THE EARTH

    (A) TELEPRESENCE OF EXPERTS
    (B) REMOTE MANIPULATION
    (c) PACKAGING OF OPERATIONS INVOLVED IN WELDING FABRICATION
        -"INSTAMATIC"® WELDING SYSTEMS -

Welding construction and repair in space have rather unique requirements, different from ordinary welding jobs on earth. Major differences between space welding and ordinary welding on earth come from (1) differences in environment and (2) remoteness of space welding from the earth.

1. Differences in Environment. The table shown above compares differences in environments between space welding and ordinary welding on earth. The space welding environments may be divided into the following three cases:

Case 1: Outside a space station. Gravity is zero. The atmosphere is a vacuum, and the temperatures are extreme. Welding may be done manually, but a worker is in a space suit which greatly restricts his/her movements.

Case 2: In a vacuum chamber inside a space station. Gravity is zero. The atmosphere is a vacuum, but the temperature is at room temperature. A worker does not wear a space suit, but welding must be done remotely or through gloves attached to the chamber. The M551, M552, and M553 experiments performed in the Skylab were done under Case 2.

Case 3. Inside a space station. Gravity is zero. The atmosphere is air, and the temperature is at room temperature. Workers wear no special space suits.

2. Remoteness from the earth. Space welding must be performed in locations extremely far from the earth, where there are no large numbers of people with vast knowledge and experience and no abundant amounts of material and energy resources. In a space station, only a small view is available.

CLASSIFICATION OF PROBABLE JOINING TASKS IN SPACE

- **Category 1:** CONSTRUCTION AND REPAIR OF SIMPLE, SMALL TOOLS, EQUIPMENT COMPONENTS, AND STRUCTURAL MEMBERS

- **Category 2:** MAINTENANCE AND REPAIR OF MAJOR MEMBERS OF SPACE STATIONS

- **Category 3:** NEW CONSTRUCTION OF LARGE, COMPLEX SPACE STRUCTURES

Probable joining tasks in space may be classified, depending upon the complexities and scales of the tasks, into the three categories shown above. We believe that it is a good idea to start working on simple cases (Category 1) and gradually expand the effort to cover more and more complex cases (Categories 2 and 3) as the technology develops.

Category 1. It would be extremely useful if techniques could be developed in the welding of various joints of tools, equipment components and structural sections in space. Some welding jobs will be done inside a space station, while other jobs will need to be done outside the space station. One could probably say that most of necessary welding jobs inside a space station could be done almost immediately, if experienced welding engineers and qualified welders were sent to a space station. However, this would be difficult to do, since a space station will be manned by a limited number of crew members who must do many things besides welding. Therefore, the major problem here is how to accomplish simple welding tasks without having welding engineers and welders present.

Category 2. There will also be the need for developing capabilities of performing limited maintenance and repair jobs on some major structural members, such as platforms, bulkheads, shell structures, etc., of space stations. However, since these jobs tend to require complex and delicate operations, only limited jobs will be performed in the near future.

Unlike structures such as ships, pressure vessels, and even automobiles which are mainly fabricated with metal plates and sheets, space structures are mainly fabricated with composite panels. These panels may be made with thin metals in honeycomb structures, they may be made with metals and non-metals, or they may even be made with non-metals such as fiber reinforced plastics. Welding repairs of these composite panels are very difficult, and in some cases impossible. Nevertheless, there still will be some maintenance and repair jobs which can be done by welding. A few such examples are presented later.

Category 3. The use of welding to assemble large complex structures has many advantages. Due to Space Shuttle payload considerations, it will be more economical to launch only structural components, saving the final joining of these sub-structures until they are in orbit.

APPLICABILITIES OF EXISTING WELDING PROCESSES TO SPACE

(I) PROCESSES WHICH APPEAR TO HAVE BROAD, GENERAL APPLICATIONS

GAS TUNGSTEN ARC WELDING (GTAW)
GAS METAL ARC WELDING (GMAW)
PLASMA ARC WELDING AND CUTTING (PAW AND PAC)
ELECTRON BEAM WELDING AND CUTTING (EBW AND EBC)
LASER BEAM WELDING AND CUTTING (LBW AND LBC)

(2) PROCESSES WHICH APPEAR TO HAVE LIMITED BUT UNIQUE APPLICATIONS

STUD WELDING
EXOTHERMIC BRAZING
SOME RESISTANCE WELDING PROCESSES

One could perhaps say that almost all welding processes which are currently in use on earth can be used in space. This is because the only environmental difference between ordinary welding on earth and space welding inside a space station (Case 3) is the lack of gravity. It does not mean, however, that almost all welding processes will be or should be used in space. On the contrary, only a limited number of processes will actually be used in space in the near future.

An important factor is that many space structures will be made of light and high-performance materials such as aluminum alloys, titanium alloys, stainless steels, etc., since it is extremely costly to transport anything from the earth to a space station. To achieve light weight, most structures will be made with thin plates and composite materials. Very few structures will be made with plates over 12 mm (1/2 inch) thick. Therefore, the welding processes which may be used in space will be those which are suitable for joining light and high-performance metals. It is important that these processes do not require heavy equipment using a large amount of electrical power.

Efforts have been made to identify welding (and cutting) processes which appear to be suitable for space applications. The results are given in two different categories: (1) processes which appear to have broad, general applications and (2) processes which appear to have limited but unique applications.

Those welding and cutting processes which appear to have broad, general applications in space include gas tungsten arc welding (GTAW), gas metal arc welding (GMAW), plasma arc welding and cutting (PAW and PAC), electron beam welding and cutting (EBW and EBC), and laser beam welding and cutting (LBW and LBC). Detailed discussions regarding possible uses of these processes are presented in reference 1.

A number of welding processes may be used for limited but unique applications in space. However, it is rather difficult to identify these processes and their possible applications without knowing specific structures and tools to be welded. Once specific joint tasks, including materials and plate thicknesses, are identified, one could select the process most suitable for the specific applications. The uses of stud welding, exothermic brazing, and some resistance welding processes have been discussed

PROBABLE JOINING TASKS IN SPACE

Category I: CONSTRUCTION AND REPAIR OF SIMPLE, SMALL TOOLS, EQUIPMENT COMPONENTS, AND STRUCTURAL MEMBERS

The information generated thus far, including that obtained during welding experiments performed in space ships, indicates that welding of metals in space can be achieved using processes similar to those which have been used for fabricating similar structures on earth. Vacuum and microgravity do not seem to cause significant problems with welding metals. In fact, when joining some metals using certain processes, it is easier to weld them in space than on earth.

The major problem associated with space welding comes from the fact that the work must be performed by a limited number of crew members with no or little knowledge, experience, and skills in welding, using limited supplies of materials (welding machines, filler metals, shielding gas, etc.) and energy resources (electricity, etc.).

There are obviously many joining tasks to be performed in space using various processes to join different materials in different shapes and thicknesses used for a variety of structures. However, it is rather difficult to determine details of joining tasks such as joint designs, processes to be used, and welding conditions employed, unless some details of structural designs are defined.

Nevertheless, certain discussions still can be made if we focus on certain types of generic welding technologies which can be used for construction and repair of various structures in space. For example, once the technology of welding fabrication of aluminum structures for airplanes is established the same basic technology can be used for fabricating aluminum structures for space applications, or even ships and storage tanks. Since the major objective of this research program is to develop novel welding technologies that could be used for fabricating and repairing various tools, machine components, and structures in space rather than to develop details of welding procedures for certain specific applications, discussions here are focused on the development of generic technologies of space welding fabrication.

Probable joining tasks in space have been classified into Categories 1, 2, and 3 as discussed earlier. Presented in the following are some examples of Category 1 joining tasks, which are to construct and repair simple, small tools, equipment components, and structural members.
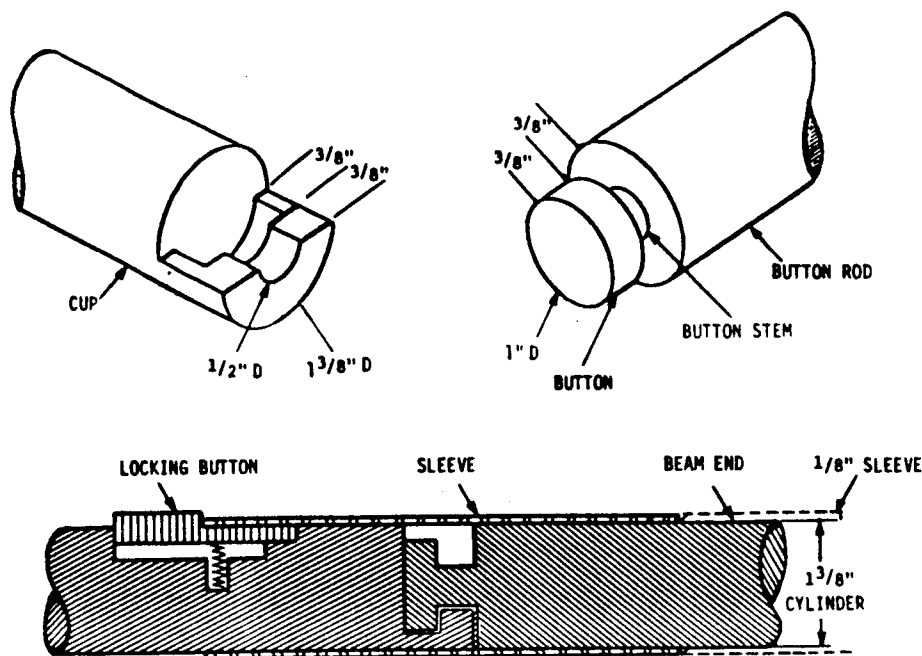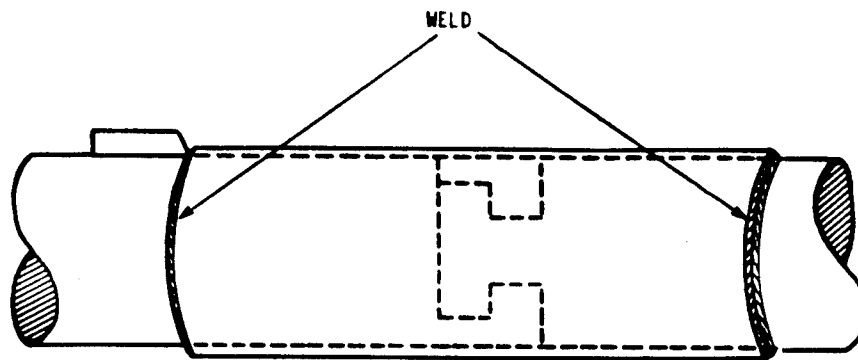
M.I.T. CONNECTOR DESIGN

An example of the use of welding machines to perform simple construction tasks is the seal welding of mechanical joints. Although mechanical fastening is simple, it has some inherent problems as follows:

(a) Mechanical joints do not have high rigidity. Therefore, it is rather difficult to maintain their exact shapes, especially when a number of modules are joined.

(b) Mechanical joints may become loose during service.

(c) It is difficult to obtain air tightness during service.

Many structures that are currently being considered for construction in space utilize the joining of pipes to form truss elements. These structures are designed to be assembled by hand by the astronauts in an extra-vehicular (EVA) mode. This will require joints that can be easily fit-up and assembled.

A prototype of this joint has been designed by the Space Systems Laboratory of the Massachusetts Institute of Technology, and is shown above. The joint uses two cylinder machines in such a manner that they interlock. A sleeve is attached to one of the interlocking cylinders, and this sleeve is pushed into place over the connected joint to keep the pieces in place. The sleeve is held in place by a spring lock. This prototype has been used to construct a number of truss elements in the Marshall Neutral Buoyancy Facility.
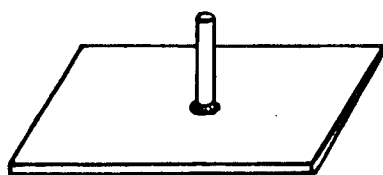
WELD

Possible permanent fastening of the M. I. T. connector

Mechanical joints are designed to have some play in them in order to aid the astronaut/builder in fitting up the pieces to be assembled and also to allow the connector to perform properly even if some dirt or other contaminant should somehow get in the way. Also, some clearance is necessary to prevent the sleeve from cold welding itself to a cylinder before the connection is completed.

However, once the joint connection has been completed, it would be beneficial if all potential motions in the joint could be eliminated (remove the play in the joint). This could be accomplished by welding the connecting sleeve in place after the mechanical fastening is done. Two welds, one at each end of the sleeve, as shown above, would fix the joint in place permanently. This would allow for the ease in assembling structures and still obtaining high rigidity of the structure.

For the welding of the sleeve, a device similar to that used to automatically weld pipes on earth could be developed. This space pipe welder would only need to be placed into position by the astronaut. Once in place, the welding machine would automatically make the circumferential weld needed. This totally automatic welding machine would eliminate the need for a welding engineer in space for this task, and an astronaut could be trained to use it in a minimum amount of time. Some examples of totally automatic welding systems which are capable of performing certain simple, prescribed tasks are discussed in the following page.
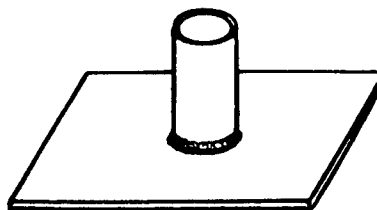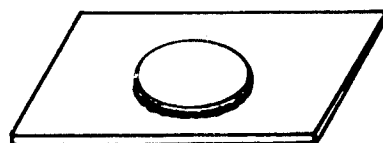
a. Stud Welding a Bar to a Flat Plate
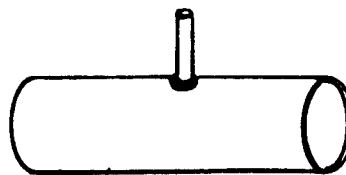
b. Stud Welding a Bar to a Pipe
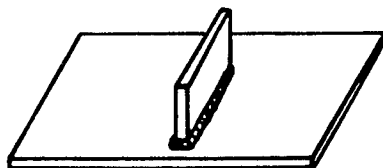
c. Joining a Plate to a Plate by Fillet Welding

d. Joining a Pipe to a Plate by Fillet Welding

e. Lap Welding a Cover Plate to a Flat Plate

f. Replacing a Section of a Pipe

"Instamatic®" systems

It is technically possible to develop totally automatic welding systems capable of enabling an astronaut with little or no training for welding to perform certain simple, prescribed tasks in space. In fact, researchers at M.I.T. under the direction of Professor K. Masubuchi have been working during the last several years to develop a group of fully automated and integrated welding systems which package many operations involved in welding, including feeding the electrode and manipulating the torch. These machines have been nicknamed "instamatic welding systems", since they are similar to easy-to-operate "instamatic®" cameras with which a person with little knowledge of photography can take good pictures. The idea of developing "packaged dedicated welding systems" was originally conceived while M.I.T. researchers were studying means of performing underwater welding in deep sea.

In past research programs at M.I.T. the six types of joints shown above were studied:

Type 1: Stud welding of a bar to a flat plate
Type 2: Stud welding of a bar to a pipe
Type 3: Joining of a flat plate to a flat plate by fillet welding
Type 4: Joining of a pipe to a flat plate
Type 5: Lap welding of a cover plate to a flat plate
Type 6: Replacing a section of a pipe

Actual hardware for Types 1, 3, and 5 joints has been built and tested. Further details of these designs are presented in APPENDIX B of reference 1. We believe that similar systems could be developed for space applications.

282

Category 2: MAINTENANCE AND REPAIR OF MAJOR MEMBERS OF SPACE STATIONS

- **1.** ON-SITE WELDING OF STUDS FOR MECHANICAL FASTENING OF STRUCTURAL MODULES OF SPACE STATIONS

- **2.** PLACING STUDS FOR VARIOUS PURPOSES

- **3.** WELDING PATCHES ON SOME STRUCTURAL MEMBERS

Now we would like to discuss welding jobs under Category 2. There will be some maintenance and repair jobs which can be done by welding, of which a few examples are:

(1) On-site welding of studs for mechanical fastening of structural modules of space stations,
(2) Placing studs for various purposes, and
(3) Welding patches on some structural members.

On-Site Welding of Studs. As stated earlier, most construction jobs in the early stages of the Space Station Program will be performed on earth, and fabricated modules will be joined, probably by mechanical fastening methods such as bolts and nuts. Although most bolts will be placed on earth, we may find it necessary to place some bolts on site in space. Or we may find that some joints are mismatched, requiring some bolts to be cut and new bolts placed in different locations. The stud welding process can be extremely useful for welding studs on site.

Placing Studs for Various Purposes. Stud welding may be useful for placing studs on some major structural components for various purposes. For example, there will be many occasions in which insulation materials will need to be placed over some structural members. By using stud welding it is possible to place studs without piercing holes through the structural members; then these studs can be used to secure the insulation materials.

Welding Patches. Some structural members may be damaged during service. For example, a hole may be pierced in a wall of a space station when it is hit by a meteorite or other space debris. It is possible to develop techniques for repairing some of the damages on site, for example by placing a patch over the damaged areas - a "bandage" over the damaged area of the space station. Three typical methods of placing a patch over a damaged structural member of a space station are shown on the next page.
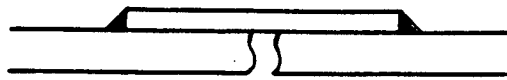
a. Attach a patch by lap welding
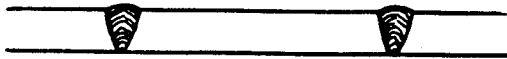
b. Butt weld an insert plate
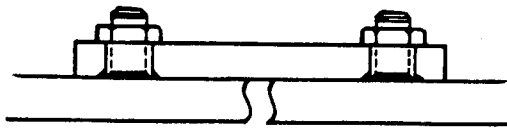
c. Stud weld bolts on the structure and
then securely fasten the cover plate
work holes by nuts

Three typical methods of placing a patch plate over a damaged structural member of a space station

A patch may be lap welded to the structure as shown in Figure a. In the case shown in Figure b, the damaged areas are removed, and an insert plate is butt welded to the structural member. In the case shown in Figure c, bolts are stud welded to the structure, and a patch plate with holes is placed over the structure to cover the damaged areas; then the patch plate is securely fastened to the structure by tightening nuts on the bolts.

Each of the above three methods has advantages and disadvantages over the other methods. In repairing the structural members of a space station which is composed of light structures in thin metals, the third method of placing bolts by stud welding may be a good method because stud welding can be made with very little heat effect to the structure.

Category 3: New Construction of Large, Complex Space Structures. There will be a need for welding fabrication of new, large and complex structures in space. For example, by performing the final construction in space, the structure does not have to be designed to withstand the high stresses which could occur during launch. The M.I.T. final report discusses a few examples including:
- (a) Attachment of a multiple docking adapter/airlock module to an external fuel tank used for an orbital platform, and
- (b) The beam builder

However, details of these discussions are not given here, since welding jobs under Category 3 will not be performed until welding jobs under Categories 1 and 2 are successfully accomplished.

284

TASK 2: IDENTIFICATION OF REQUIRED LEVEL OF AUTOMATION IN SPACE WELDING TASKS

1. WELDING TASK ANALYSIS

    A. GENERAL TASK CONSIDERATION
    B. TOOL MANIPULATION
    C. SELECTION OF PROCESS TYPE AND PARAMETERS
    D. PROCESS CONTROL
    E. INSPECTION AND QUALITY CONTROL

2. OPERATIONAL MODES FOR SPACE WELDING FABRICATION

    A. MANUAL WELDING BY AN OPERATOR AT THE REMOTE SITE
    B. REMOTELY MANIPULATED WELDING
    C. TOTALLY AUTONOMOUS SYSTEMS

3. EXPERIMENTAL STUDY

Under Task 2 efforts were made to identify the required level of automation in space welding tasks. In order to rationally decide on the degree of required or attainable automation and autonomy in space welding applications, one should consider the requirements of the task on hand, the availability of human operators on site, and the current or projected state of the art in the field. The following studies were made:

(1) Welding task analysis
(2) Operational modes for space welding fabrication, and
(3) Experimental study.

Welding Task Analysis. Due to the limitations of the existing technology, most of the currently planned space structures are not designed for welded construction. Therefore, only a limited number of possible welding tasks can be fully identified at this point. Efforts were made to identify some "generic" welding tasks. The analysis covered the following subjects:

(a) General task consideration
(b) Tool manipulation
(c) Selection of process type and parameters
(d) Process control, and
(e) Inspection and quality control.
Details are presented in reference 1.

Operational Modes. Some discussions are presented on the next page.

Experimental Study. An experimental study was initiated at M.I.T. in order to rationally establish the fundamental components of the generic remote joining tasks that can or should be automated. Since the current state of the art limits the extent of such automation, there will be necessarily some higher level tasks that need to be performed by the human operator. The tasks that are most difficult (or even impossible) to effectively perform remotely, and that disproportionately increase the total completion time, are more likely to be passed on to a local computer. In the confines of this initial investigation, only the positioning and path tracking manual control tasks were examined. For simulation of remote manipulation, the facilities in the Machine Systems Laboratory of the Mechanical Engineering Department at M.I.T. were used. The results obtained to date indicate that welding performance can be significantly impaired during remote manipulation, especially when time delay is present. The results are presented in APPENDIX D of reference 1.

OPERATIONAL MODES FOR SPACE WELDING

A. MANUAL WELDING BY OPERATOR ON-SITE

A.1 WELDING IN ENCLOSED LIFE-SUSTAINING HABITAT
A.2 WELDING OUTSIDE AN ENCLOSED HABITAT
    A.2.1 UNAIDED EXTRA-VEHICULAR ACTIVITY (EVA)
    A.2.2. AIDED E.V.A.
        MANNED MANEUVERING UNIT (MMU)
        OPEN CHERRY PICKER (OCP)

B. REMOTELY MANIPULATED WELDING

B.1 REMOTELY MANIPULATED WELDING
    B.1.1. MANIPULATION USING REMOTE MANIPULATOR SYSTEM (RMS)
        OF THE SHUTTLE
    B.1.2. MANIPULATION FROM A MANNED REMOTE WORK STATION (MRWS)
B.2 REMOTE MANIPULATION FROM EARTH (TELEPRESENCE)

C. FULLY AUTONOMOUS UNMANNED WELDING SYSTEMS

A number of different operational modes for space welding are possible. These modes range from fully manned to fully autonomous and can be classified as shown above, depending upon the level to which a human operator is used, his/her proximity to the task site, and the means used for translation and effecting the work task.

Manual Welding. If welding is performed inside an enclosed life-sustaining habitat, then it is no different, operationally, than that performed on earth. However, if welding is performed outside the space station by an operator in a space suit, then we can further discriminate between the following modes:
    (1) Unaided extra-vehicular activity (EVA), and
    (2) Aided E.V.A. in which other means are used to transport and position the operator in the remote site. This case is further classified into:
    2.1. Manned maneuvering unit, and
    2.2. Open cherry picker
A manned maneuvering unit is a self contained system which can provide the operator with a pressurized means for translation to and from the welding site. An open cherry picker is a special platform mounted on the end of a manipulator system which can provide means for transporting and positioning an EVA operator.

Remotely Manipulated Welding. Remote teleoperation is essentially an interim case between fully manual and fully autonomous operations. Remotely manipulated welding can be further classified into:
    (1) Remotely manipulated welding
    1.1. Manipulation using a remote manipulation system of the shuttle
    1.2. Manipulation from a manned remote work station
    (2) Remote manipulation from earth (telepresence of welding experts).

Fully Autonomous Welding. In both the previously mentioned cases, a human operator is available and performs certain tasks. In a completely autonomous system, on the other hand, the role of the operator will be diminished and the computer will handle all the decision making. However, it is not feasible to develop such a welding system in the near future.

TASK 3: DEVELOPMENT OF NOVEL SPACE WELDING CONCEPTS

1. DEVELOPMENT OF SPACE WELDING TECHNOLOGIES WHICH DO NOT REQUIRE THE ON-SITE PRESENCE OF WELDING ENGINEERS AND WELDERS

1.A. COMPLETELY REMOTE WELDING TECHNOLOGY

1.B. INTEGRATED AND AUTOMATED WELDING SYSTEMS WHICH CAN BE OPERATED BY PERSONS WITH NO WELDING SKILL

1.C. WELDING TECHNOLOGIES THROUGH TELEPRESENCE

2. DEVELOPMENT OF NEW WELDING PROCESSES AND PROCEDURES UNIQUELY SUITED FOR SPACE APPLICATIONS

In order to successfully accomplish construction, maintenance, and repair of space stations, we need to develop novel welding concepts. The necessary research and development efforts may be classified into:
  (1) Efforts to develop space welding technologies which do not require the on-site presence of welding engineers, and
  (2) Efforts to develop new welding processes and procedures uniquely suited for space applications.

Space Welding Technologies Which Do Not Require On-Site Presence. The efforts necessary to develop space welding technologies which do not require the on-site presence of welding engineers and welders will include the following:
  (1) Efforts to develop welding systems which can perform certain welding jobs through completely remote manipulation,
  (2) Efforts to develop welding systems by which operators with no welding knowledge and skill can perform certain welding jobs, and
  (3) Efforts to develop technologies for performing certain welding jobs through proper guidance and assistance from the earth station (telepresence of welding experts).

Welding Technologies for Special Applications. There is also a need to develop new welding technologies uniquely suited for space applications, which are radically different from the welding technologies used on the earth. A few examples are as follows:

(1) Electron Beam Welding. One can develop a new system of electron beam welding uniquely suited for space applications. Electron beam welding guns small enough to be portable may also be developed. Some efforts along this line have already been made.

(2) Exothermic Brazing. Some basic work was already done during the M552 experiment on the feasibility of accomplishing the joining of tubes by exothermic brazing. It is worth exploring the feasibilities of developing designs for devices which can perform certain joining tasks in space.

(3) Solar Welding. Another very likely method of welding in space is to utilize solar heat by use of properly designed optical lens systems. Again, some efforts along this line have already been made.

TASK 4: RECOMMENDED FUTURE STUDIES

GROUP A: RESEARCH PROGRAMS RECOMMENDED TO BE PERFORMED IMMEDIATELY

PROGRAM #1: SPACE STUD WELDING SYSTEMS WHICH CAN BE REMOTELY MANIPULATED

PROGRAM #2: "INSTAMATIC"® GTAW SYSTEMS FOR SPACE APPLICATIONS WHICH CAN BE OPERATED BY AN ASTRONAUT WITH NO WELDING TRAINING

PROGRAM #3: FLEXIBLE SPACE WELDING SYSTEMS

GROUP B: RESEARCH PROGRAMS RECOMMENDED TO BE PERFORMED AFTER SOME RESULTS OF GROUP A RESEARCH HAVE BEEN OBTAINED

PROGRAM #4: SPACE WELDING USING GMAW, EBW, AND LBW PROCESSES

PROGRAM #5: SPECIAL JOINING TECHNIQUES SUITED FOR SPACE APPLICATIONS

PROGRAM #6: INTEGRATED FABRICATION SYSTEMS FOR CERTAIN COMPLEX SPACE STRUCTURES

Under Task 4 efforts were made to develop recommended research programs on space welding. Six research programs as shown above have been recommended. Discussions on the first group including Research Programs #1, #2, and #3 are rather specific and in detail, since we already have concrete ideas about (a) what should be done and (b) what is perhaps achievable. On the other hand, discussions on the second group including Research Programs #4, #5, and #6 are rather general and brief, since plans for these programs may be significantly affected by the outcome of Programs #1, #2, and #3.

In developing space welding technologies, we must recognize that not a single actual weld has ever been made in space. Welding experiments were performed in 1969 by the U.S.S.R. during the Soyuz-6 mission and in 1973 by the U.S.A. during the Skylab mission. However, these were scientific experiments to demonstrate that welding can be achieved successfully under microgravity conditions.

If we compare the state of the space welding technology to that of a human, we could probably say the present state of the space welding technology is similar to that of an unborn fetus. What we are proposing under the Research Programs #1, #2, and #3 is equivalent to an effort to make an infant successfully crawl and totter a few steps. This would lead to a healthy, walking child who will soon run and jump. Just like parents of a child who would like to see their child grow as soon as possible, we are very anxious to see space welding technologies develop as fast as possible and as far as possible. But we must have enough patience to develop the technologies step by step, first developing methods of performing simple welding tasks using processes which we know will work, and then gradually expanding our capability to perform increasingly more complex tasks using more sophisticated techniques.

Program I: STUD WELDING SYSTEMS WHICH CAN BE
REMOTELY MANIPULATED

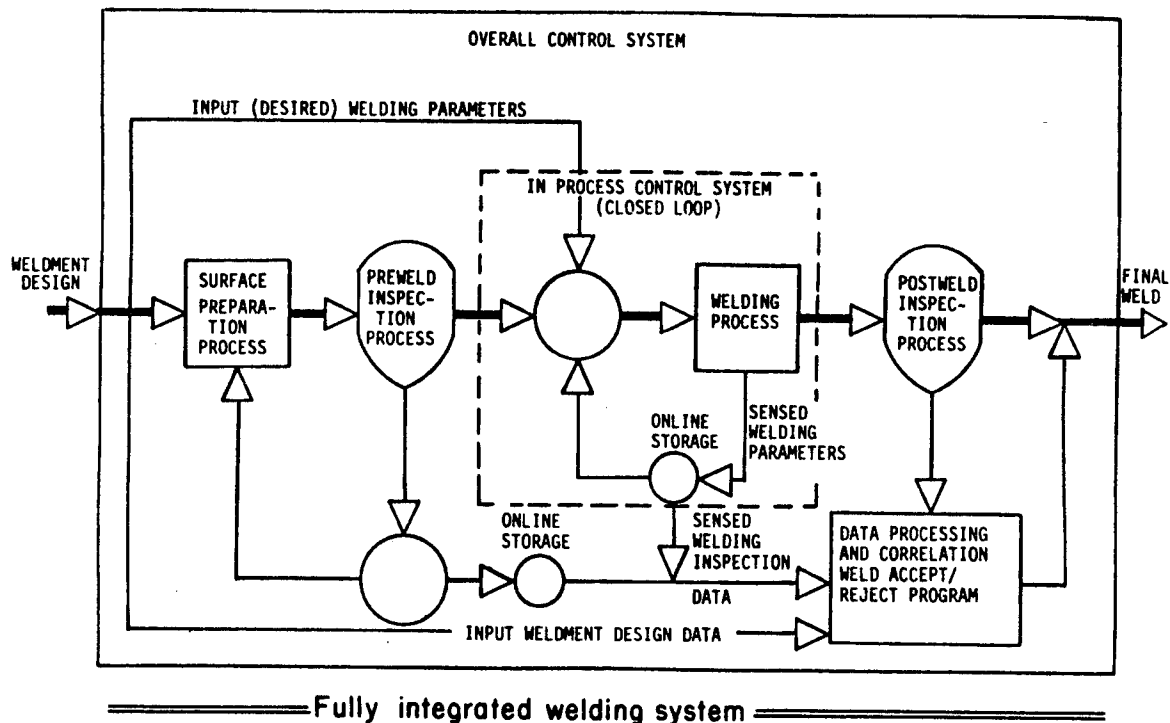| RESEARCH PHASES	YEARS AFTER THE INITIATION OF THE RESEARCH PROGRAM									
	1	2	3	4	5	6	7	8	9	10
PHASE 1: BASIC STUDY	██									
PHASE 2: LABORATORY TESTING OF THE FIRST GENERATION STUD WELDING SYSTEM			██							
PHASE 3: SIMULATED ZERO GRAVITY TESTING OF SYSTEMS DEVELOPED IN PHASE 2			██							
PHASE 4: DEVELOPMENT AND LABORATORY TESTING OF INTEGRATED STUD WELDING SYSTEMS				██						
PHASE 5: SIMULATED ZERO GRAVITY TESTING OF SYSTEMS DEVELOPED IN PHASE 4					██					
PHASE 6: TESTING IN SPACE OF THE INTEGRATED STUD WELDING SYSTEMS						██				

It is recommended that a research program be carried out with the objective of developing space stud welding systems which can be remotely manipulated. The only thing that an operator aboard a space station must do is to place the welding system at the right location, either manually or using a simple manipulator. Then all other necessary operations, including selection of appropriate welding parameters and activation of the welding, are to be performed in the command station. APPENDIX C of reference 1 identifies some technical problems which need to be solved in order to achieve the objective, and discusses possible ways for solving the problems.

It is recommended that the research be carried out in six phases with different specific objectives and time frames as shown above. We should be ready for testing in space of the integrated space stud welding systems (Phase 6) in six years after completing Phases 1 through 5. Reference 1 discusses details of these phases. Given below is a brief discussion of Phase 1, the objective of which is to conduct a basic study on space stud welding.

Phase 1, which will be completed in two years, will consist of the following steps:
>   Step 1-1:   Stud welding experiments in a vacuum
>   Step 1-2:   Development of stud welding materials and optimum welding conditions for selected 2000 series aluminum alloys
>   Step 1-3:   Development of initial designs of the first generation space and stud welding systems.

In Step 1-1, a study will be made to determine whether it is possible to perform stud welding in a vacuum. The experiments will be performed using the pressure chamber presently installed at M.I.T. Efforts will include determining whether the existence of certain gases or mixture of gases would facilitate the initiation and maintenance of an arc in a vacuum. In selecting the materials and stud sizes to be investigated, close contacts will be made with representatives from NASA. Our choices at present are 2219 (primary) and 2014 (secondary) as materials, and stud size of 1/4 inch (6.4 mm) in diameter as the primary candidate. Step 1-3 is to develop initial designs of the first generation space stud welding system, the hardware of which will be constructed in Phase 2.

OVERALL CONTROL SYSTEM

INPUT (DESIRED) WELDING PARAMETERS

IN PROCESS CONTROL SYSTEM
(CLOSED LOOP)

WELDMENT
DESIGN

SURFACE PREPARA-TION PROCESS

PREWELD INSPEC-TION PROCESS

WELDING PROCESS

POSTWELD INSPEC-TION PROCESS

FINAL WELD

ONLINE STORAGE

SENSED WELDING PARAMETERS

ONLINE STORAGE

SENSED WELDING INSPECTION DATA

DATA PROCESSING AND CORRELATION WELD ACCEPT/ REJECT PROGRAM

INPUT WELDMENT DESIGN DATA

========Fully integrated welding system========

In order to develop a reliable welding fabrication system, it is essential to develop an integrated system which covers all important operations involved in welding fabrication. Development of an integrated system is especially important for welding fabrication in space, where no experienced welding engineers and skilled welders are present. Although development of such an integrated system for various welding processes can become very complicated, we strongly believe that stud welding is simple enough that an integrated system can be developed within the time and cost anticipated in the proposed research.

The above figure shows schematically what subsystems should be included in an integrated stud welding system (in time sequence of from left to right):
(1) A subsystem to prepare surface conditions suitable for stud welding,
(2) Make sure that the surface conditions are adequate, before commencing welding. If the surface conditions are not adequate, recondition the surface.
(3) Select appropriate welding conditions, including welding current, arc voltage, and welding time, for particular applications (materials, plate thickness, etc.),
(4) Inspect the weld after it is completed. The inspection may be performed by use of a non-destructive testing method such as the ultrasonic technique and the acoustic emission technique, or it may be done by applying some external load to the stud.

We do not expect to develop a completely integrated stud welding system shown above in Phase 2; however, we should be able to develop in Step 1-3 an initial design of a system which will incorporate at least some portions of the system shown above.

290

Program 2: DEVELOPMENT OF "INSTAMATIC"® GTAW WELDING SYSTEMS FOR SPACE APPLICATIONS WHICH CAN BE OPERATED BY AN ASTRONAUT WITH NO WELDING TRAINING

RESEARCH PHASES		YEARS AFTER THE INITIATION OF THE RESEARCH PROGRAM									
		1	2	3	4	5	6	7	8	9	10
PHASE 1:	IDENTIFICATION OF SEVERAL TYPES OF "INSTAMATIC"® WELDING SYSTEMS	▬									
PHASE 2:	CONSTRUCTION AND LABORATORY TESTING OF SOME PROTOTYPE MODELS		▬	▬							
PHASE 3:	CONSTRUCTION AND LABORATORY TESTING OF THE FIRST GENERATION INTEGRATED "INSTAMATIC"® WELDING SYSTEMS				▬	▬					
PHASE 4:	SIMULATED ZERO GRAVITY TESTING OF SYSTEMS DEVELOPED IN PHASE 3					▬					
PHASE 5:	CONSTRUCTION AND LABORATORY TESTING OF INTEGRATED "INSTAMATIC"® WELDING						▬	▬			
PHASE 6:	FURTHER IN-FLIGHT TESTING OF HARDWARE SYSTEMS DEVELOPED IN PHASE 5							▬			
PHASE 7:	TESTING IN SPACE OF INTEGRATED "INSTAMATIC"® WELDING SYSTEMS								▬	▬	

It is recommended that a research program be carried out with the objective of developing "instamatic®" gas tungsten arc welding (GTAW) systems, or enclosed welding boxes which can perform certain prescribed welding jobs by an operator with no welding training. The research should be started immediately to cover the first two phases (Phases 1 and 2) shown above. If the results of the initial two phases are positive, the research program should be continued to cover Phases 3 through 7. Presented below is a short discussion of Phase 1. Reference 1 contains further details of Research Program #2.

The objective of Phase 1 of Research Program #2 are (1) to identify several types of joints for which "instamatic®" welding systems can be developed for space application and (2) to develop initial designs for these systems. Phase 1 is extremely important for the success of Research Program #2, because we must select examples which are simple enough so that "instamatic®" welding systems can be developed within the time and research budget available, yet these examples must be important for activities using the Space Station. Close coordination among M.I.T. researchers, representatives from NASA, and people in the space industry is important in identifying the examples to be investigated. Attempts also will be made to identify some joints which are useful for some other research projects included in the Innovative Utilization of the Space Station Program.

Reference 1 presents some discussions on four types of joints which are likely to be selected. They include (a) joining a flat plate to a flat plate by fillet welding, (b) lap welding a circular cover plate over a flat plate, (c) seal welding along a girth joint between two cylinders mechanically fastened, and (d) replacing a section of a pipe. These joining tasks are already explained in earlier portions of this report.

291

PHASES WHICH WILL BE INCLUDED IN THE RESEARCH PROGRAM #3: DEVELOPMENT OF
MAN-MACHINE GTAW SYSTEMS FOR PERFORMING CERTAIN WELDING JOBS THROUGH
PROPER GUIDANCE AND ASSISTANCE FROM THE COMMAND STATION CN EARTH

RESEARCH PHASES	YEAR AFTER THE INITIATION OF THE RESEARCH PROGRAM									
	1	2	3	4	5	6	7	8	9	10
Phase 1: Identification of several welding tasks and development of strategies for developing man-machine GTAW systems	▬									
Phase 2: Development of initial designs for man-machine GTAW systems for certain applications and plans for later phases		▬								
LATER PHASES	DETAILED PLANS WILL BE DEVELOPED IN Phase 2									

The objective of Research Program #3 is to develop flexible systems capable of performing various types of space welding jobs with the necessary guidance and assistance from a command station on earth. It is recommended that Phases 1 and 2 be initiated immediately as shown above. Presented below is a brief discussion on Phase 1.

The objective of Phase 1 is to (a) identify several welding tasks and (b) develop strategies for developing man-machine gas tungsten arc welding (GTAW) systems. Phase 1 is extremely important for the success of Research Program #3, because we must select welding tasks which are (1) simple enough so that the proposed systems can be developed within the time and budget available, and (2) important for activities using the Space Station. Close coordination among M.I.T. researchers, representatives from NASA, and people in the space industry is very important in identifying the examples to be investigated. Attempts also will be made to identify some welding tasks which will be useful for other research projects included in the Innovative Utilization of the Space Station Program.

Discussions on the six types of welding tasks being considered are presented below (see figures shown on the next page). They represent different types of welds with different levels of complexity in welding fabrication.

Welding Task No. 1: Joining Two Flat Plates by Butt Welding. Joining of two flat plates by butt welding, as shown in Figure (a) on the next page, is perhaps the most fundamental welding task. Therefore, any flexible system able to perform useful welding tasks ought to be able to perform this task, at least. The task will be simple if joints to be welded are always the same. That is, if they are of the same material, same thickness, and same joint preparation. If they are different, however, we must find some way to select the right filler metal and right welding conditions (welding current, arc voltage, arc travel speed) for each joint condition.
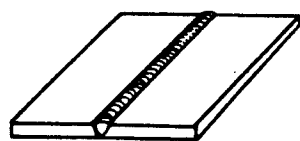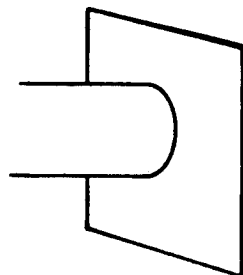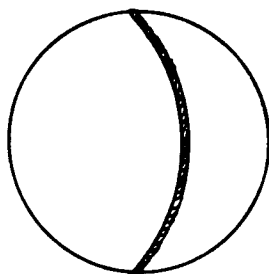
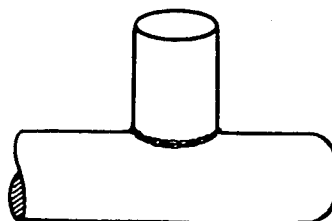(a) BUTT WELDING FLAT PLATES
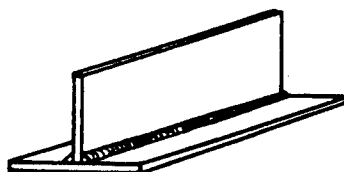
(b) FABRICATING A T-BEAM

(c) JOINING OF PIPES

(d) JOINING OF A PIPE TO A FLAT PLATE

(e) JOINING OF TWO SEMI-SPHERICAL SHELLS

(f) JOINING OF TWO INTERSECTING PIPES

═══════ Welding tasks in Program #3 ═══════

Welding Task No. 2: Fabricating a T-Beam. T-beams and I-beams are commonly used as elementary members of many structures. Instead of fabricating these beams on earth and transporting them to space, it will be more economical to simply transport the metal pieces and join them in space.

Welding Task No. 3: Joining of Pipes. Joining of pipes in a fixed position, especially in a small diameter, can be performed by using an "instamatic" welding system. However, joining of larger-diameter pipes will probably require a more flexible welding system.

Welding Task No. 4: Joining of a Pipe to a Flat Plate. The joining of a pipe to a flat plate is another basic welding task.

Welding Task No. 5: Joining Two Semispherical Shells. The joining of two semispherical shells to form a spherical hull is an important but difficult fundamental joining problem. We may have difficulties in finding ways to securely hold the pieces to be welded during welding, due to distortion. If one could successfully perform this task, this would demonstrate that many other complex structures could be fabricated in space.

Welding Task No. 6: Joining of Two Intersecting Pipes. This task is again cited to test the limit of the technical capabilities of flexible welding systems.

PROGRAMS # 4, # 5, and # 6

RESEARCH PROGRAMS	YEAR AFTER THE INITIATION OF THE RESEARCH PROGRAM									
	1	2	3	4	5	6	7	8	9	10
RESEARCH PROGRAM #4: SPACE WELDING USING GMAW, EBW, AND LBW PROCESSES PHASE 1: INITIAL STUDY LATER PHASES		▆	DETAILED PLANS WILL BE DEVELOPED IN Phase 1							
RESEARCH PROGRAM #5: SPACE JOINING TECHNIQUES SUITED FOR SPACE APPLICATIONS PHASE 1: INITIAL STUDY LATER PHASES				▆	DETAILED PLANS WILL BE DEVELOPED IN Phase 1					
RESEARCH PROGRAM #6: INTEGRATED FABRICATION SYSTEMS FOR CERTAIN COMPLEX SPACE STRUCTURES PHASE 1: INITIAL STUDY LATER PHASES			▆	DETAILED PLANS WILL BE DEVELOPED IN Phase 1						

Research Program #4. The reason for recommending Research Programs #1, #2, and #3 is that we think that NASA would be interested in having some welding systems which can do certain welding jobs in space as soon as possible. When we think about the distant future, however, we must consider uses of such processes as gas metal arc welding (GMAW), electron beam welding (EBW), and laser beam welding (LBW). EBW and LBW may well be prime joining processes in space in the future. It is recommended that an initial Phase 1 study be conducted perhaps during the second year of the Space Welding Fabrication Research, as shown above.

Research Program #5. There will be a number of joining processes which are uniquely suited for some applications under space environments. They include solar welding, exothermic brazing, diffusion bonding, explosive welding, ultrasonic welding, etc. It is recommended that an initial Phase 1 study be conducted perhaps during the fourth year, as shown above.

Research Program #6. There are basically two approaches in developing technologies of fabricating structures. One is to think about welding processes first and then develop the technologies of using these processes. This approach has been taken in planning Research Programs #1 through #5. The other approach is to think in the reversed direction, that is to think about structures first and develop fabrication techniques most suitable for the structures being considered. This second approach can be useful in fabricating some structures. It is recommended that a research program be carried out to look at welding problems from the view point of the structures being fabricated. We recommend an initial Phase 1 research with the following objectives:

    (1) To identify space structures being planned, to which introductions of new concepts in welding may make significant effects, and

    (2) To develop future plans of further R & D work.

CLOSING REMARKS

A study was made on feasibilities of remotely manipulated welding in space. Major results obtained in this study may be summarized as follows:

(1) Literature Survey. As the first step for identifying probable joining tasks in space, a survey was made of existing publications on space welding and related subjects. The result of the survey is presented in APPENDIX A of reference 1, which contains 121 citations.

(2) Unique Requirements for Space Welding Fabrication. Welding construction and repair in space has rather unique requirements, different from ordinary welding jobs on earth. Major differences between space welding and ordinary welding on earth come from (a) differences in environment and (b) remoteness of space welding from earth.

(3) Probable Joining Tasks in Space. Probable joining tasks in space may be classified, depending upon the complexities and scale of the tasks, into the following three categories:

Category 1: Construction and repair of simple, small tools, equipment components, and structural members,
Category 2: Maintenance and repair of major members of space stations,
and Category 3: New construction of large, complex space structures. We believe that it is a good idea to start working on simple cases and gradually expand the effort to cover more and more complex cases.

(4) Required Levels of Automation in Space Welding. Under Task 2, studies were performed on (a) analysis of welding tasks in space, (b) operational modes for space welding fabrication, and (c) simple experiments on supervisory control of torch positioning and seam tracking.

(5) Development of Novel Space Welding Concepts. In order to successfully accomplish construction, maintenance, and repair of space stations, we need to develop novel welding concepts. Discussions have been held on (a) efforts to develop space welding technologies which do not require the on-site presence of welding engineers and (b) efforts to develop new welding processes and procedures uniquely suited for space applications.

(6) Recommended Future Studies. Six research programs have been recommended. Discussions on the first group including Research Programs #1, #2, and #3 are rather specific, since we already have concrete ideas about (a) what should be done and (b) what is perhaps achievable. Discussions on the second group including Research Programs #4, #5, and #6 are rather general and brief, since plans for these programs may be significantly affected by the outcome of Programs #1, #2, and #3.

REFERENCES

1. Masubuchi, K.; Agapakis, J. E.; DeBiccari, A.; and von Alt, C.: Feasibility of Remotely Manipulated Welding in Space - A Step in the Development of Novel Joining Technologies. NASA CR-175437, 1983.

2. Lawrence, G. S.; and Schollhammer, F. R.: Design, Fabrication, and Evaluation of Hand Held Electron Beam Gun and External Power Supply for Electron Beam Welding in Space. NASA CR-62059, 1966.

3. Paton: Welding Engineering, Jan. 1972.

ADVANCES IN JOINING TECHNIQUES USED IN
DEVELOPMENT OF SPF/DB TITANIUM
SANDWICH REINFORCED WITH METAL MATRICES*

J. E. Fischler
Douglas Aircraft Company
McDonnell Douglas Corporation
Long Beach , CA

ABSTRACT

Three- and four-sheet expanded titanium sandwich sheets have been developed at Douglas Aircraft Company, a division of McDonnell Douglas Corporation, under contract to NASA Langley Research Center. In these contracts, spot welding and roll seam welding were used to join the core sheets. These core sheets were expanded to the face sheets and diffusion bonded to form various type cells.

The advantages of various cell shapes and the design parameters for optimizing the wing and fuselage concepts are discussed versus the complexity of the spot weld pattern.

In addition, metal matrix composites of fibers in an aluminum matrix encapsulated in a titanium sheath were aluminum brazed successfully to the titanium sandwich face sheets. The strength and crack growth rate of the SPF/DB titanium sandwich with and without the metal matrix composites are described.
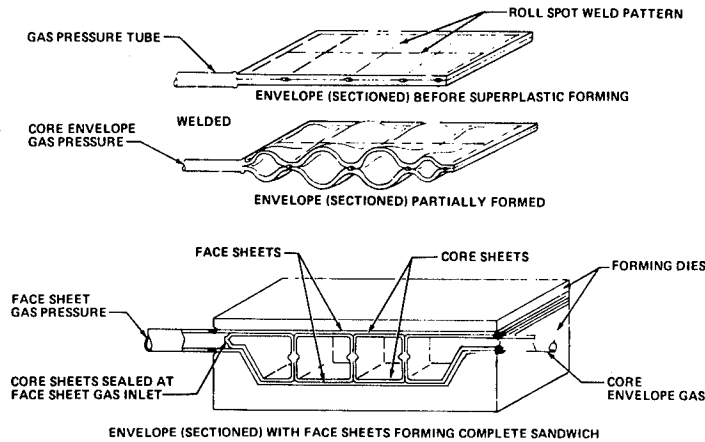
INTRODUCTION

A superplastic-formed/diffusion-bonded (SPF/DB) titanium sandwich, utilizing a unique method of spot welding core sheets that was developed at Douglas Aircraft Company, creates sandwich structure that can be tailored to the design loads. In this process, after spot welding the core sheets to the most optimum pattern for the loadings, the core is expanded and diffusion bonded to the doubler and face sheets to form a finished sandwich. The result is a very efficient sandwich construction with all the parts bonded by a very strong metal-to-metal diffusion bond. If built in production quantities, the process could provide significant weight and cost savings with proper designs.

The panels utilized were: a 3- by 5-foot four-sheet SPF/DB titanium sandwich wing panel; a 3- by 3-foot, three-sheet SPF/DB titanium sandwich forward wing panel; an SPF/DB titanium sandwich primary structure wing panel with a DC-10 size access door; and a truss type, hat-stiffened, 3- by 5-foot primary structure fuselage panel, made by using the unique Douglas-developed, three-sheet roll seam welded sandwich concept, as well as smaller panels fabricated by aluminum brazing metal matrix composites to an SPF/DB titanium sandwich.

Static compression tests reveal that the SPF/DB titanium sandwich and the metal matrix composites brazed to the sandwich are structurally very efficient. Also, the SPF/DB titanium sandwich has a lower rate of crack growth starting from surface damage on one side.

Some of the problems of designing ultra-lightweight SPF/DB titanium sandwich are described briefly and some solutions presented in the following text.

SPF/DB PHASES OF FABRICATION
FOUR-SHEET SANDWICH

ROLL SPOT WELD PATTERN

GAS PRESSURE TUBE

ENVELOPE (SECTIONED) BEFORE SUPERPLASTIC FORMING

CORE ENVELOPE GAS PRESSURE

WELDED

ENVELOPE (SECTIONED) PARTIALLY FORMED

FACE SHEETS — CORE SHEETS — FORMING DIES

FACE SHEET GAS PRESSURE

CORE SHEETS SEALED AT FACE SHEET GAS INLET

CORE ENVELOPE GAS

ENVELOPE (SECTIONED) WITH FACE SHEETS FORMING COMPLETE SANDWICH

The SPF/DB titanium sandwich developed at Douglas Aircraft Company is shown above. The top sketch illustrates the spot weld pattern made by the designer to meet the load requirements. These two core sheets, when partially formed from core envelope gas pressure, are shown in the middle sketch. Additional core pressure forces the pillow shape into vertical walls, and the core top and bottom surfaces are diffusion bonded to the outer face sheets. A very efficient titanium sandwich is formed in one operation.

CORE PATTERNS

RECTANGULAR   **TRIANGULAR AND HEXAGONAL**
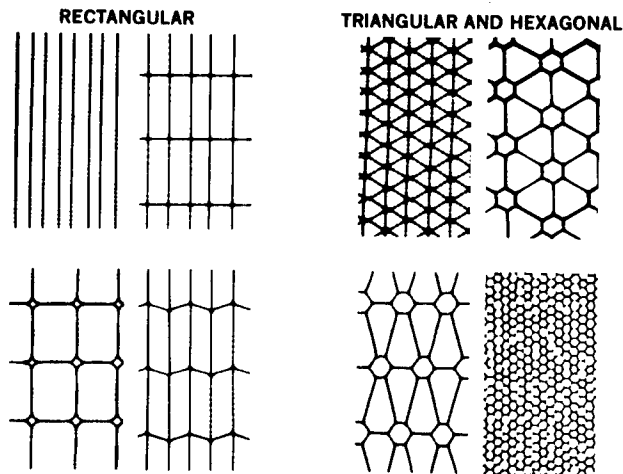
Various core patterns have been fabricated. The upper left sketch shows roll spot welds that form vertical walls with continuous longitudinal webs. This pattern can be used for high axial loading efficiency when hardly any transverse loading or shear loading is present. The upper left-right pattern is used for typical aircraft structure when some transverse loading and/or shear loading is present. The upper right-left pattern is desirable when thin sheet shear buckling and axial loading are present. The upper right-right pattern is when higher axial loading, pressure loading (bending), and shear loading are present. The vertexes of the triangles are spot welded to form hexagonal shapes. These walls prevent thinning at the vertexes. The bottom left-left pattern has a diamond wall at the vertexes of the rectangular pattern for higher strength (by reducing thinning). The bottom left-right staggered transverse pattern was used to reduce the fatigue stress concentration factor. The bottom right-left pattern was developed to sustain high axial loads with high shear loadings. The bottom right-right pattern is an SPF/DB substitute for honeycomb sandwich.

299

FABRICATION COMPLEXITY

CORE TYPE	WELDING	PRESSURE CYCLE
STRAIGHT WEBS	1	1
RECTANGLES	2	2
TRIANGLES	3	8
INTERRUPTED RECTANGLES	8	6
ISOGRID	10	6
COLUMNS 1.27-CM (1/2-INCH) SPACING AND GREATER	4	1
1.90-CM (3/4-INCH) HEXAGONS	8	4
0.79-CM (5/16-INCH) HEXAGONS	10	5
SINE WAVE WEBS	10	2
STRAIGHT WEBS AND COLUMNS	2	3

- COMPLEXITY RATED ON 1-TO-10 SCALE

The complexity of fabricating various core patterns (which influences the cost) is based on the core type. The welding complexity is based on automated spot weld equipment that can easily go in straight lines but cannot be programmed for triangles, isogrid, and sine wave webs. These shapes must be scribed by hand. Future capital equipment could be programmed to automate the shapes. However, this would not be done unless a production quantity is desired.

CANDIDATE WING CONCEPTS
SPF/DB SANDWICH

RECTANGLE CORE

SINGLE-TRUSS CORE

ISOGRID CORE

COMBINED CORE
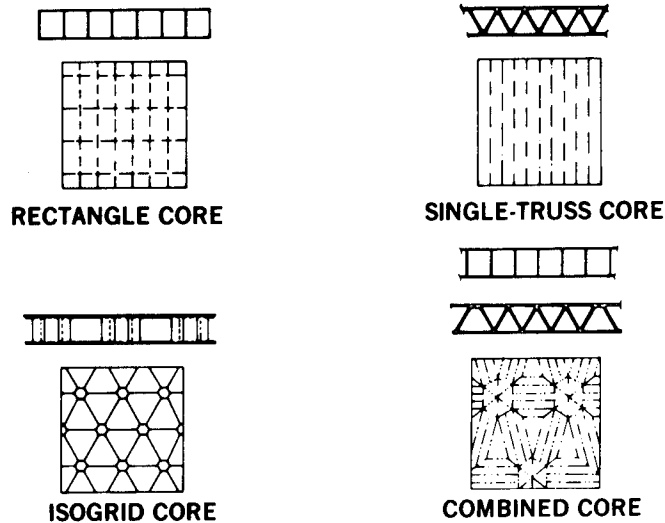
The candidate core patterns for the primary wing of a supersonic transport are shown. Only one pattern can be selected. Analysis indicates that the upper left rectangular core will be the best compromise for weight and cost.

FATIGUE PANEL RECTANGULAR CORE SANDWICH

The wing fatigue panel design is shown. Sheets of titanium, chamfered to avoid stress risers, are placed over the two rectangular spot welded core sheets and formed in one "blow" to the panel final shape.

3- BY 5-FOOT WING TEST PANEL
LAY-UP DETAIL

The lay-up details of the wing panel are shown. The edge bars are compressed and provide the side restraint to prevent the core sheets from pulling out when the core sheet forming pressure is applied.
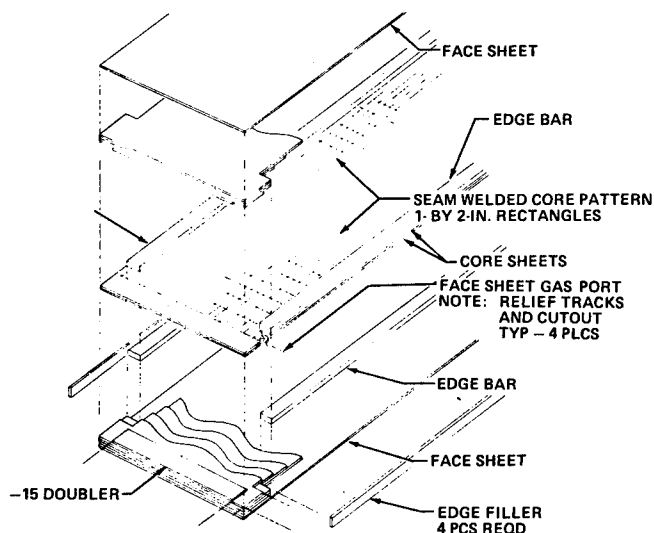
301

3- BY 5-FOOT WING PANEL PRIOR TO TESTING
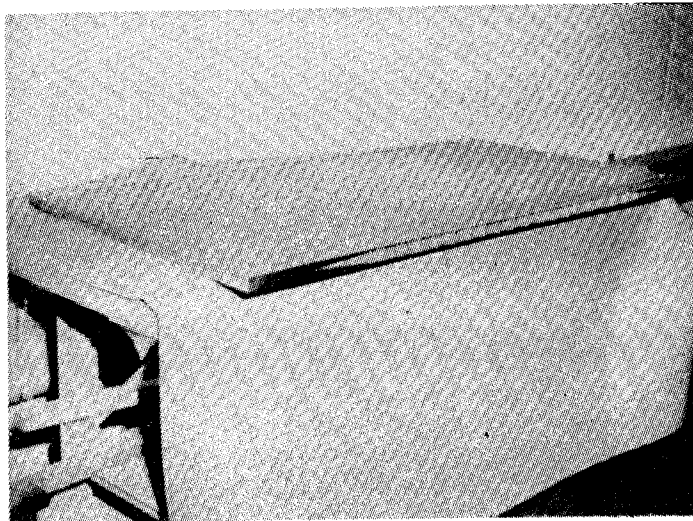
The wing fatigue panel is machine finished and prepared for testing.

HAT-STIFFENED GEOMETRY

DIMENSIONS = cm (IN.)

CONCEPT A — COMPUTER-OPTIMIZED HAT-STIFFENED GEOMETRY

CONCEPT B — FABRICATION FEASIBLE GEOMETRY

CONCEPT C — FABRICATION FEASIBLE GEOMETRY
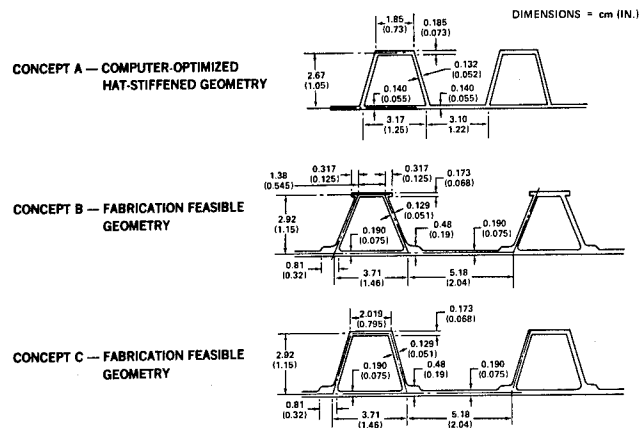
The hat-stiffened geometry desired for the fuselage was obtained by a computer-optimized program. The results are shown in Concept A. Using a three-sheet process developed at Douglas Aircraft Company, Concept B can be fabricated by roll seam welding two sheets together (at the 0.19-inch dimension), then blowing one sheet to form the web and upper skin and caps. The sheet between the caps is cut off, leaving a stringer with a high moment of inertia. Concept C was also considered if the cutouts of Concept B could not be fabricated. Available forming pressure and restraint fixture strength influenced the fabrication of feasible geometry.

3- BY 5-FOOT FUSELAGE PANEL
ASSEMBLY SCHEMATIC
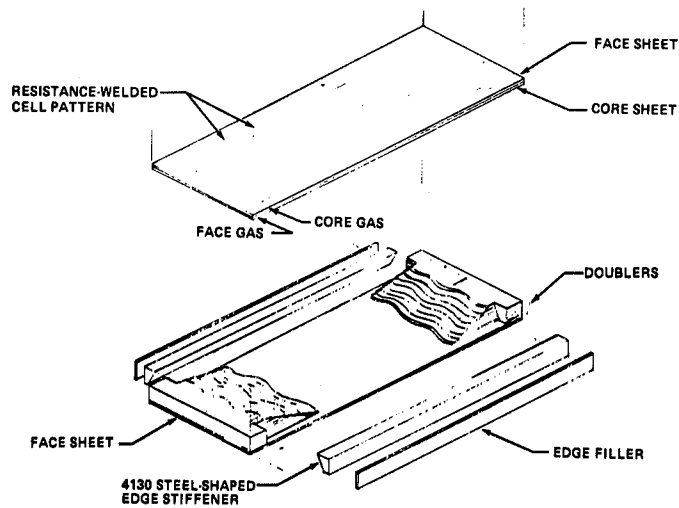
The assembly schematic for the fuselage panel is shown. The core sheet is blown down to the doublers to form the hat-stiffened pattern. The difference in pressure between the alternate small and large cells results in the required truss angle.

EDGEWISE COMPRESSION (1.4) SPECIMEN
NY DIRECTION
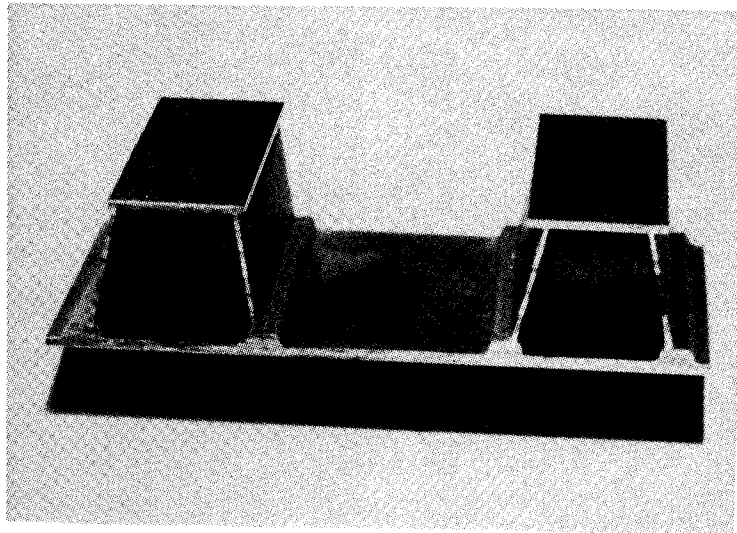
A small section of the completed panel for the "three-sheet" fuselage is shown. The high structural efficiency in compression of this specimen has been verified in test.

SPF/DB EXPANDED SANDWICH WITH
BRAZED METAL MATRIX COMPOSITE
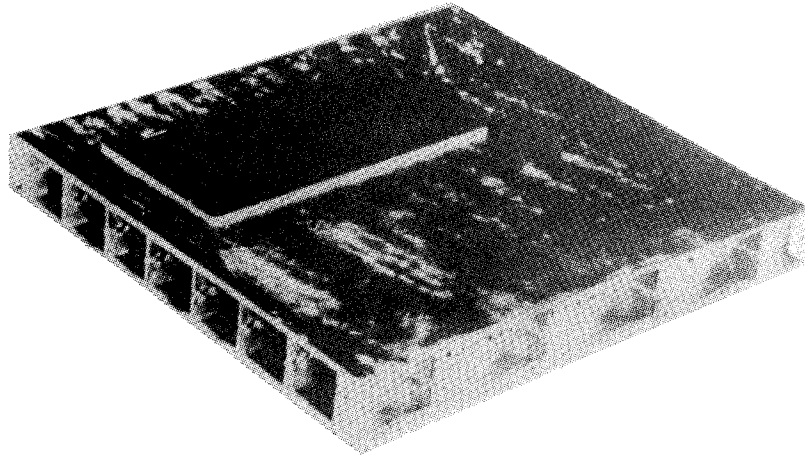
A titanium SPF/DB sandwich is shown as the base sandwich with an aluminum metal matrix brazed to it. The brazed panel was excised with a similar sized small compression panel shown in the next figure.

EDGEWISE COMPRESSION TEST SPECIMENS
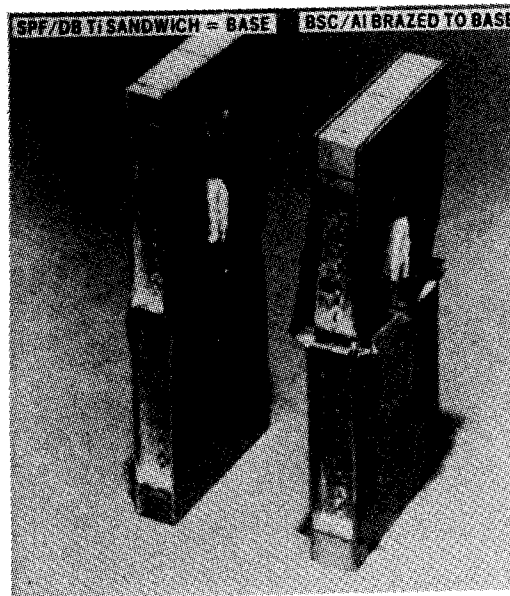
The base SPF/DB titanium sandwich is shown on the left. The similar sized panel with the metal matrix composite brazed to it is shown on the right. The local buckling mode of failure is shown on the left. The metal matrix panel has approximately the same shape. However, the failure occurs at a higher load. The failure could be from bending of fibers or web shear, or failure of the braze, or any combination of these.

SPF/DB TITANIUM SANDWICH AND MMC TEST RESULTS

Specific Strength $= \dfrac{Fc}{\rho}$ $\left(\dfrac{PSI \cdot IN.^3}{LB} \times 10^{-6}\right)$ bar chart:
- ALUMINUM — REFERENCE: 0.507
- Ti SANDWICH — TEST VALUE: 0.59
- Ti SANDWICH — TEST VALUE: 0.683
- $(B_4 C/B\text{-}Al)$Ti — B_4C/AL ON Ti SANDWICH: 1.22 *
- (BSC-Al)Ti — BSC/AL ON Ti SANDWICH: 1.36 x *
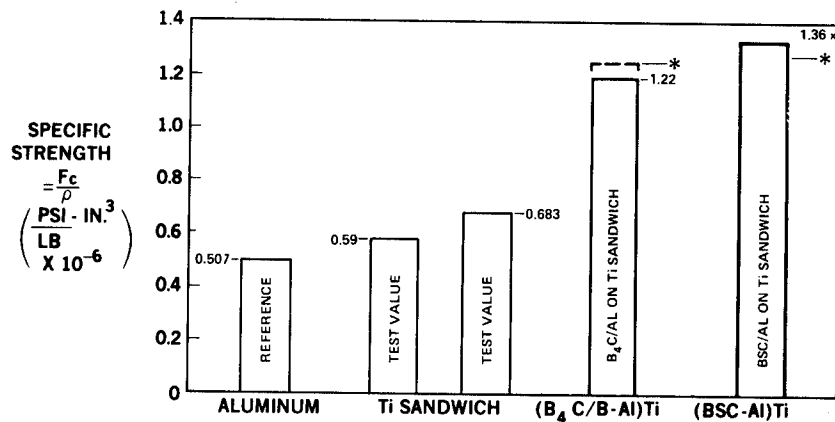
*ASSUMING NO BRAZE FAILURE AT ROOM TEMPERATURE (ROM)

A comparison of the critical short column compression stress divided by density is shown for sandwich structures at room temperature. Adding the metal matrix continuous fibers in an aluminum matrix significantly increases the specific strength.

SUPERPLASTIC FORMING PROGRESS; CALCULATED CURVE VERSUS CONSTANT PRESSURE
(U.S. UNITS)

CURVE	PARAMETERS
STRESS	1300 PSI
STRAIN RATE	0.0004 IN./IN./SEC
THICKNESS (START)	0.016 INCH
1/2 PITCH	0.325 INCH
HEIGHT (H)	0.50 INCH
CORE DESIGN	
3/4-INCH BY 2-1/4-INCH RECTANGLES	
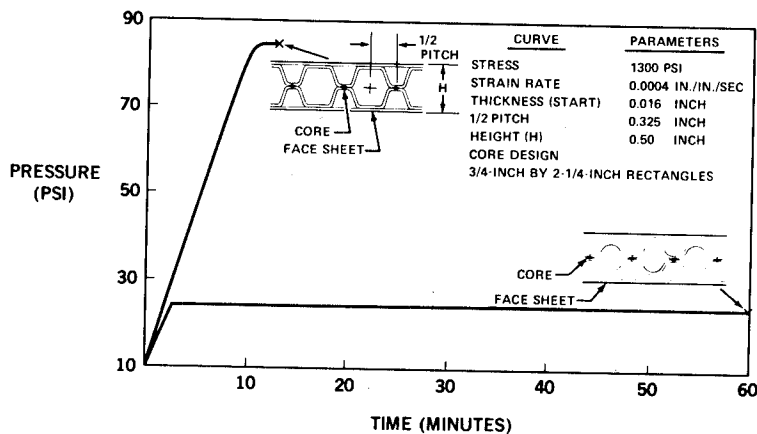
With the spot weld spacing and geometry as shown, a desirable constant strain rate can be achieved with the pressure as shown and the calculated result produces cells that have reached the face sheets after a short time. Then, the pressure can be increased to form the rectangular corners. The lower curve shows that the reduced pressure will not form the rectangular cells, even after a long time.

305

REDUCED CYCLE TIME INNOVATIONS

CORE DESIGN: 1.90 CM (3/4)-INCH HEXAGONS
CORE THICKNESS: 0.05 CM (0.020) INCH

BASIC DIMENSIONS – CM
(   ) DIMENSIONS – IN.

TEMPERATURE (1300°F) 704.4°C (1720°F) 937.78°C
815.5°C
(1500°F)
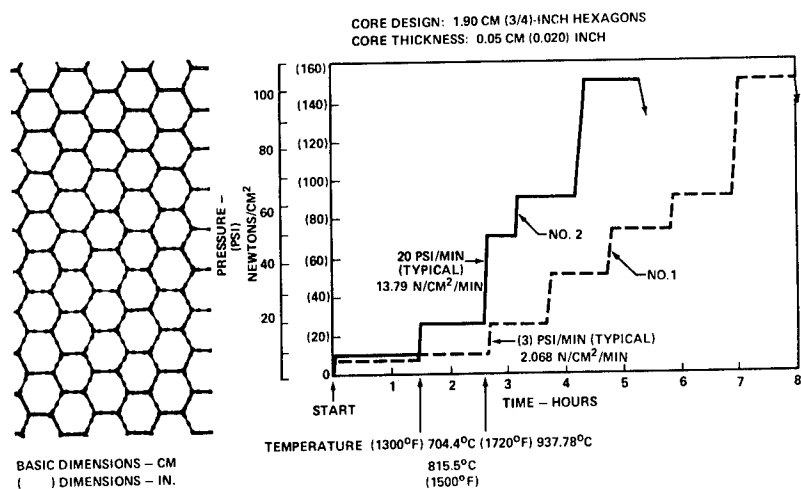
Hexagonal cells have been created for the SPF/DB sandwich using the pattern on the left. Early forming at 1,300°F with higher pressure is one way to reduce the cycle time. Too much pressure at low temperatures could cause thinning and failure. Computer programs were created to prevent this.

WELDED CORE ASSEMBLY FOR
3- BY 5-FOOT WING PANEL
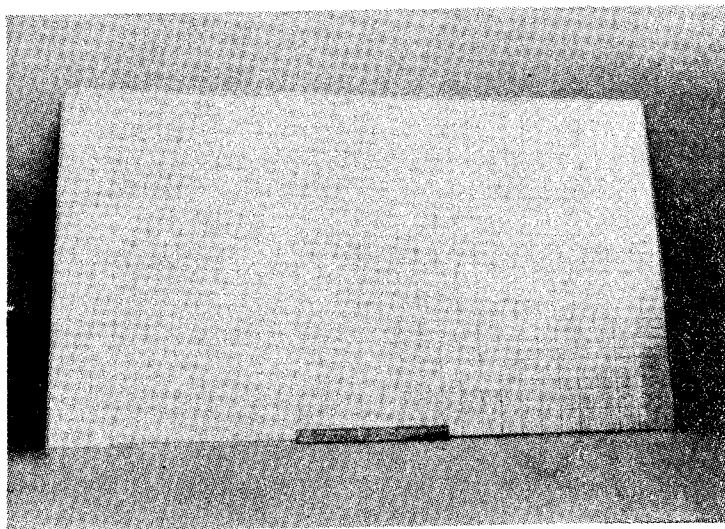
The spot weld pattern for the core sheets for 1- by 2-inch cells is shown for a 3- by 5-foot wing panel.

306

FACE SHEET AND DOUBLER ARRANGEMENT — WING
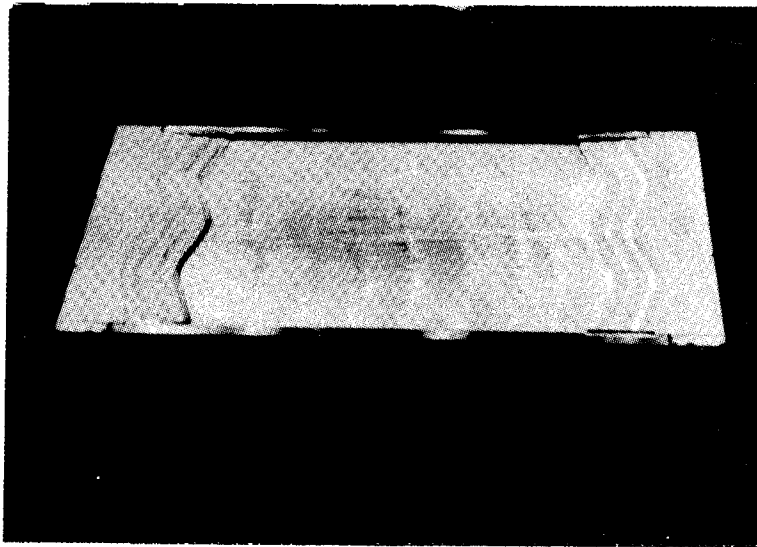
The internal end machined doublers (for one side) are shown.

3- BY 5-FOOT WING PANEL AFTER MACHINING
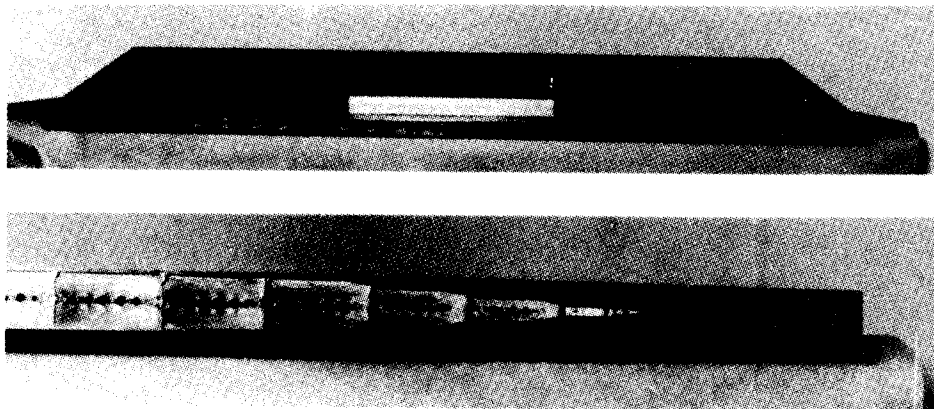
The edge view of the SPF/DB panel shows the final machined doublers, all from initial flat sheets, which have been formed in one blow. This is how the SPF/DB process holds the fabrication costs down.

-1 BOX ASSEMBLY — Al BRAZED Ti HONEYCOMB
## WING BASE CONFIGURATION
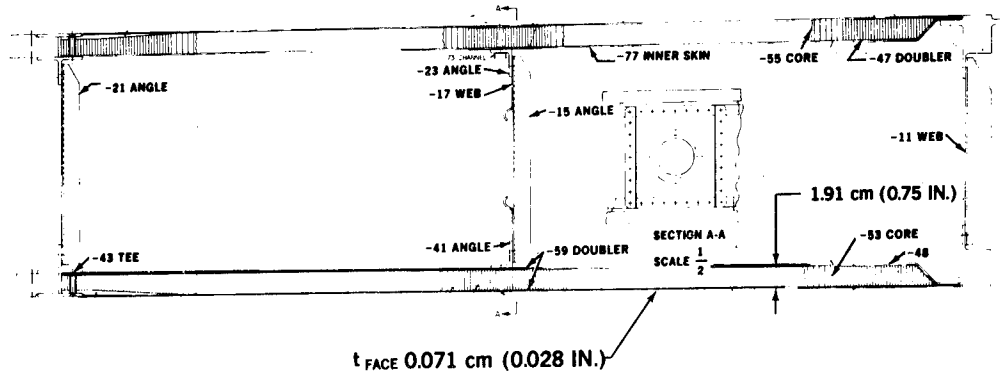
An aluminum brazed titanium honeycomb wing panel box is shown as the "base" conventional structure. It should be noted that fabrication must include the machining of the end doublers, the machined end densified core, the many fasteners, and the brazing of the sandwich panel.

-501 BOX ASSEMBLY — SPF/DB
SANDWICH Ti CONCEPTS
RECTANGULAR CELL WITH FUEL CELL ACCOMMODATIONS
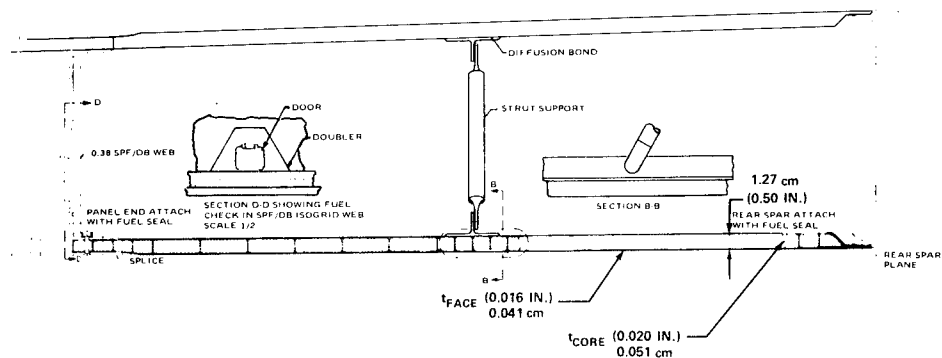
The SPF/DB sandwich box is shown. End doublers are incorporated in the wing panels. A tee spar cap is diffusion bonded to the wing panels and strut tubes are used for the intermediate spar. The major spars are of isogrid SPF/DB sandwich construction, as shown in Section D-D.

WING SPAR — TUBE STRUTS ATTACHED
# TO TEE SPAR CAP AND SPF/DB COVER PANELS
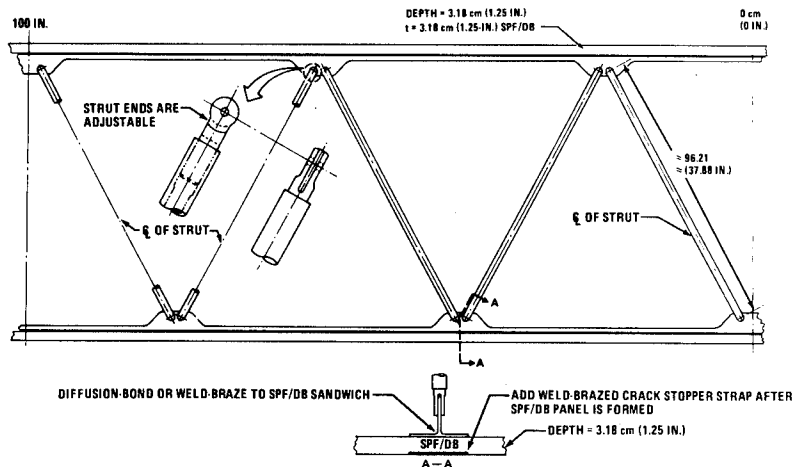
The intermediate spar details are shown. The strut end fittings are adjustable for quick installation of the struts at the holes in the spar cap tees.

# SPF/DB SANDWICH PANEL WITH INTEGRAL
DOUBLERS AND ATTACHED TEE
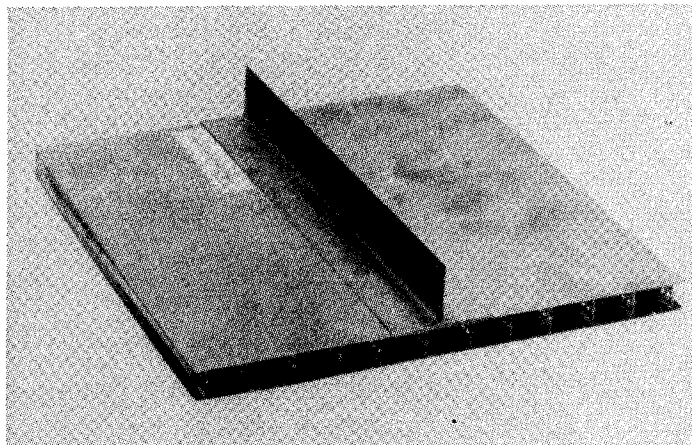
This panel with the tee spar cap was fabricated in one "blow." The tee was set in the die on the face sheet and when all parts were heated, the core sheets were blown to the face sheets and pressure was applied at SPF temperatures to diffusion bond all the parts.

FORWARD WING STRUCTURE
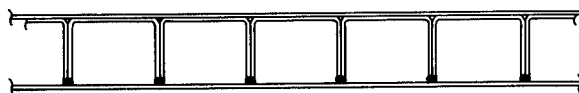
AREA REPRESENTED BY
TEST STRUCTURE ASSEMBLY
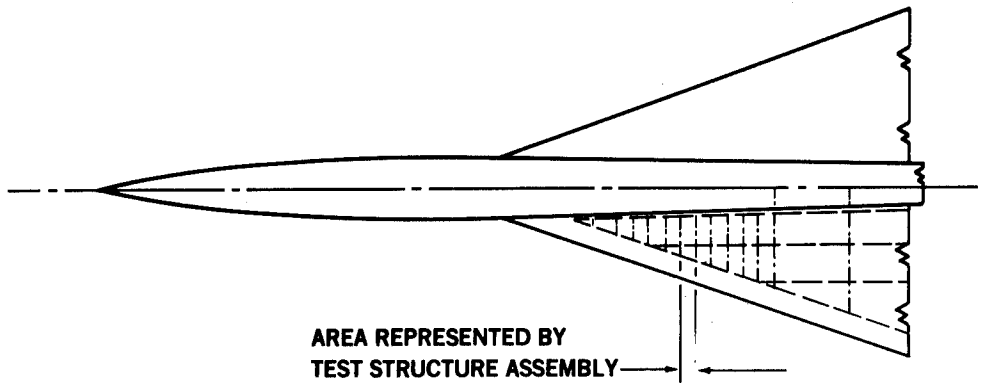
The forward wing structure of a supersonic transport wing has lightly loaded structure. Minimum-weight panels can be formed in this area using the SPF/DB titanium sandwich process.

WING PANEL DETAIL
OPTIMUM GAUGES FOR MINIMUM WEIGHT
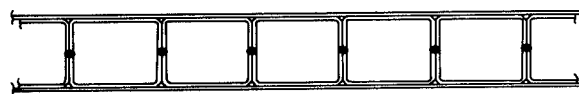
**4-SHEET CONSTRUCTION**

2 FACE SHEETS OF 0.016
2 CORE SHEETS OF 0.008

3-SHEET CONSTRUCTION

1 TOP FACE SHEET OF 0.013
1 BOTTOM FACE SHEET OF 0.016
1 CORE SHEET OF 0.008

To obtain minimum wing panel weight, a four-sheet construction and a three-sheet construction were considered. The three-sheet construction was chosen since it is lighter in weight when the available minimum core gage is the critical parameter.
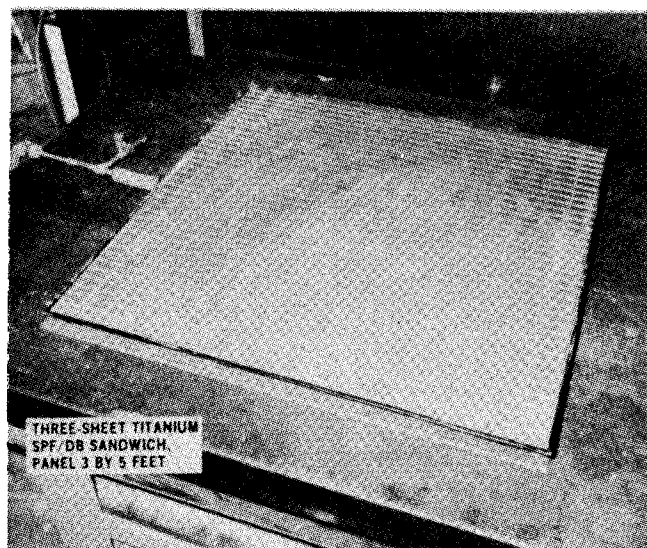
## OUTER SKIN SIDE, FORWARD WING
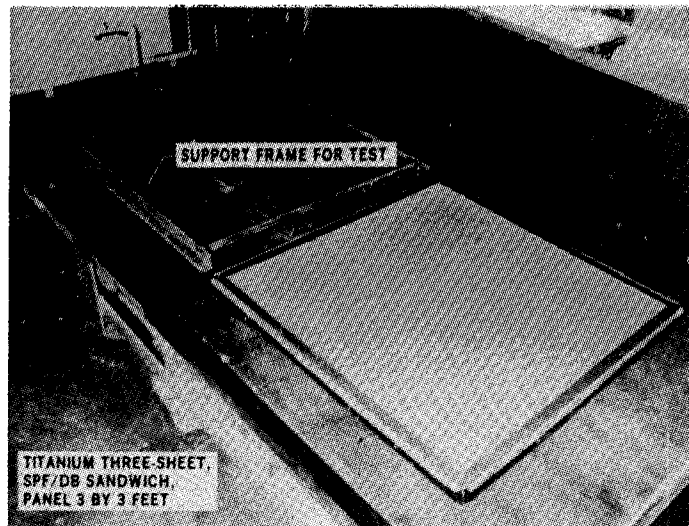
A three-sheet SPF/DB titanium sandwich was fabricated for the forward wing. The smooth side that faces the outer skin is shown on the bottom right. The upper left is a frame for testing the panel.

INNER SKIN SIDE, FORWARD WING

The inner skin side shows the spot welds of the single core sheet to the inner face sheet. Sufficient compression buckling of these panels is available so the slight amount of "eyebrowing" is not objectionable.

311

SECTION OF SPF/DB Ti SANDWICH
WING ACCESS PANEL
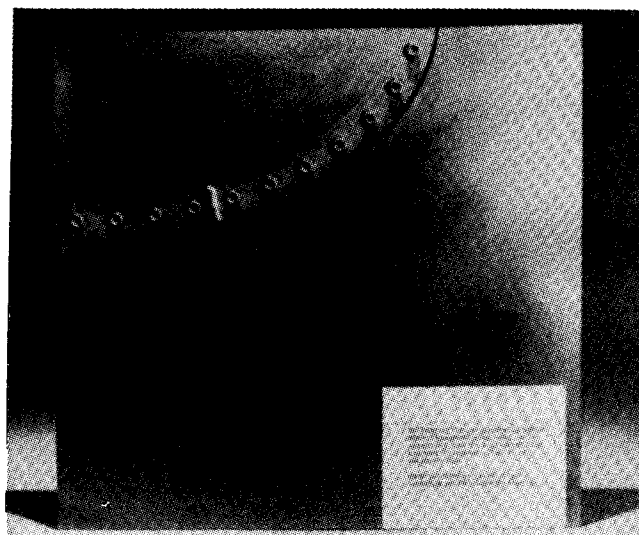
One-fourth of a 3- by 3-foot panel with a DC-10 size access door is shown after being compression tested to the design ultimate axial loading of 204,000 pounds. This panel is a typical supersonic primary wing structure.
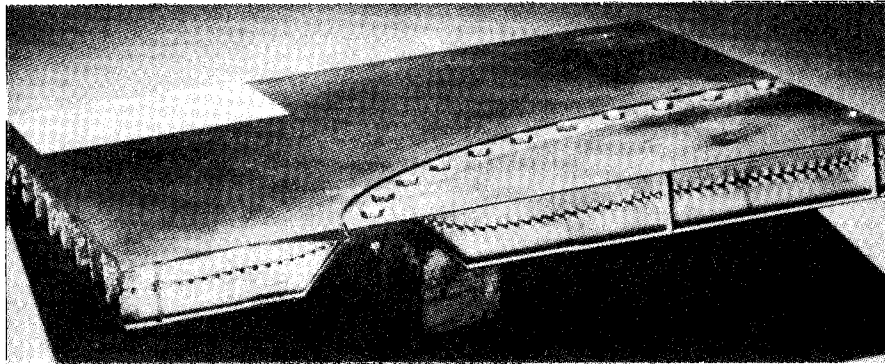
SECTION OF WING TEST PANEL WITH ACCESS DOOR
SPF/DB TITANIUM SANDWICH AFTER ULTIMATE LOADING
VIEW SHOWING AXIAL LOADED CELLS
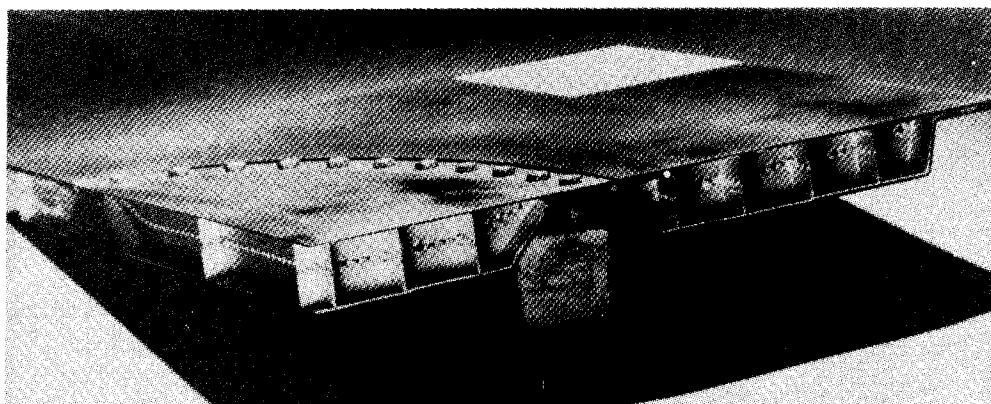
The view in this picture shows the more closely spaced axial loaded cells after testing to ultimate load.

SECTION OF WING TEST PANEL
WITH ACCESS DOOR
SPF/DB TITANIUM SANDWICH AFTER ULTIMATE LOAD
VIEW SHOWING TRANSVERSE LOADED CELLS

This view shows the more lightly loaded transverse cells in the wing test panel with the access door. The panel was tested only in the axial direction to ultimate loading. To reduce the cost, no countersunk holes or countersunk bolts were used. However, multilayer sheets were diffusion bonded to provide sufficient thickness for a countersink.

SECTION OF WING TEST PANEL WITH ACCESS DOOR
SPF/DB TITANIUM SANDWICH AFTER ULTIMATE LOADING
## LOAD CARRY-THROUGH DETAILS
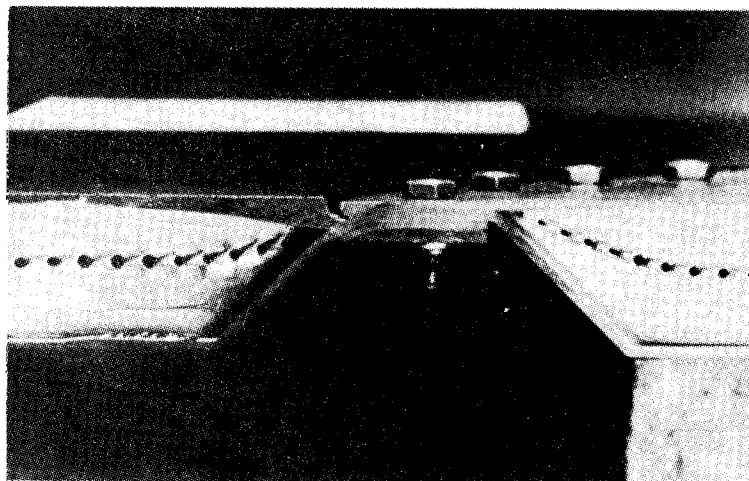
A close-up is shown of the joint between the wing panel and access door. The two core sheets are "blown" to the many layers of doublers necessary for load carry-through.

313

ULTRALIGHT SANDWICH

| PROBLEM	SOLUTION
NONUNIFORM MATERIAL THICKNESS	SELECTED CORE STOCK WITH MATCHING GAGE AND UNIFORM THICKNESS
TEMPERATURE NONUNIFORMITY	REVISED HEATER DESIGN TO MINIMIZE EDGE EFFECT OF TEMPERATURE
CORE DEPTH AND CELL CONFIGURATION	DEVELOPED TIME, TEMPERATURE, AND PRESSURE CYCLES TO ACCOMMODATE CONFIGURATION
LEAKS • EXCESSIVE STRAIN/STRAIN RATE BRITTLENESS	EXPERIMENTED WITH CYCLE AND MINIMUM GAGE
POOR FLOW-THROUGH CLEAVAGE	ELIMINATED LEAKS
SURFACE CONTAMINATION	SELECTED CONTAMINATION-FREE STOCK
POOR AVAILABILITY OF PROPER MATERIAL SIZE — WIDTH AND GAGE	MILL PROBLEM — WILL IMPROVE WITH INCREASED USAGE

The problems associated with designing and fabricating ultralight sandwich SPF/DB titanium structures are listed. Also, on the right, some possible solutions are suggested.

SURFACE CONDITION OF 8-MIL FOIL

AS RECEIVED 500X   AS RECEIVED 5,000X

AS RECEIVED (BENT) 1,000X   AS RECEIVED (BENT) 1,000X
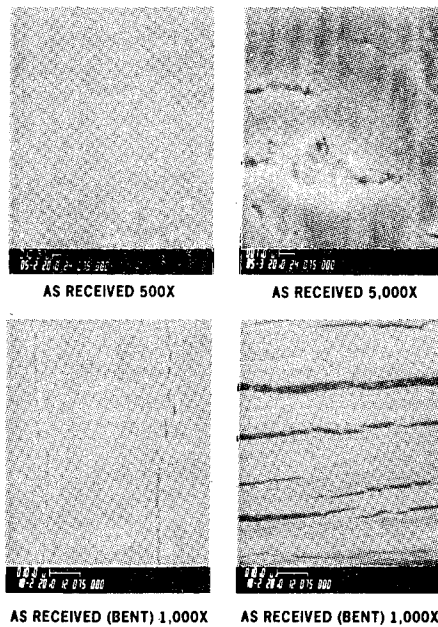
The poor nonuniform condition of 8-mil foil that was considered for ultra-lightweight SPF/DB sandwich panels is shown above. Notice that at 1,000X and 5,000X magnification, the material is not very uniform. Eight-mil foil is made by rolling heavier thicknesses down. The cost and material condition could be carefully controlled if large amounts are needed.

314
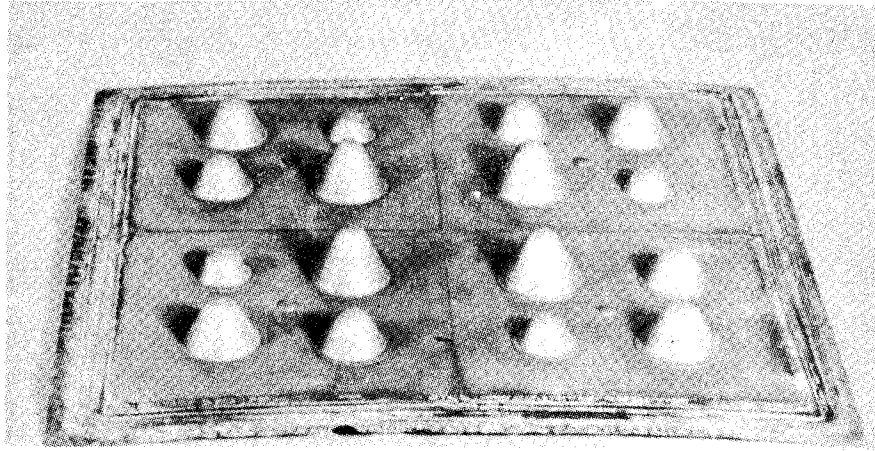
8-MIL CONE TESTS

Cone tests on 8-mil foil show how severely the thickness and material properties vary when superplastically formed. Core thicknesses were increased to prevent failure due to excessive thinning.

DIFFUSION BOND AT EDGE OF CLEAVAGE
CORE TO CORE

NEG LW-240   MAGNIFIED 300X
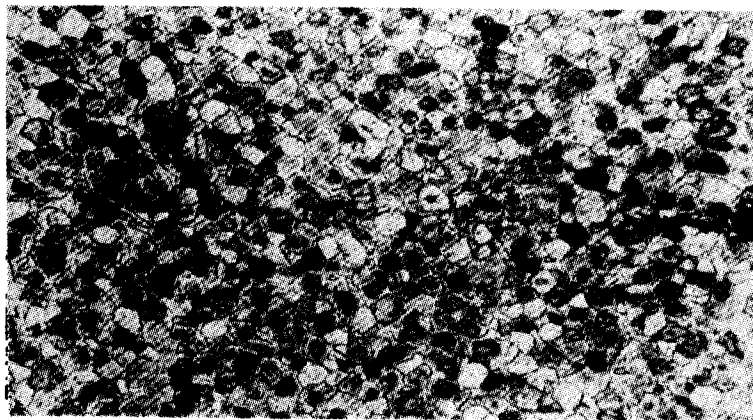
The core-to-core diffusion bonding looks excellent. At the right center is the edge of the cleavage. It is difficult to distinguish the original boundary of the thicknesses to the left of the cleavage.

315

DIFFUSION BOND AT EDGE OF CLEAVAGE
CORE-TO-FACE SHEET
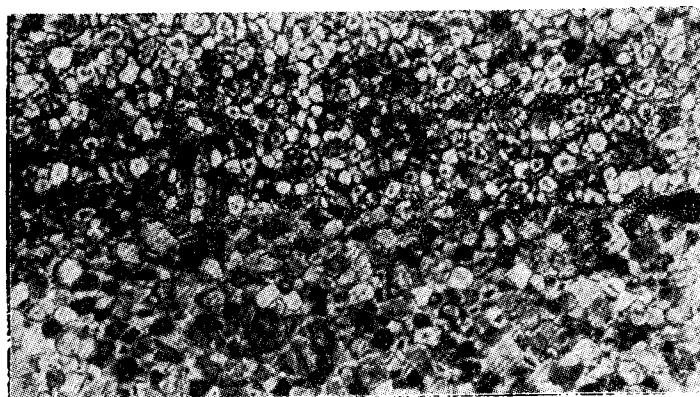

NEG LW-239   MAGNIFIED 300X

The core-to-face sheet diffusion bonding is good, but not as good as the core-to-core bonding. The difference shown in grain size is due primarily to the larger elongation of the core compared to the face sheet and some temperature differences. However, to the left of the cleavage, the grains seem to intermingle and it is difficult to distinguish the boundary of the original thicknesses.

CORE FAILURE DUE TO EXCESSIVE STRAIN RATE
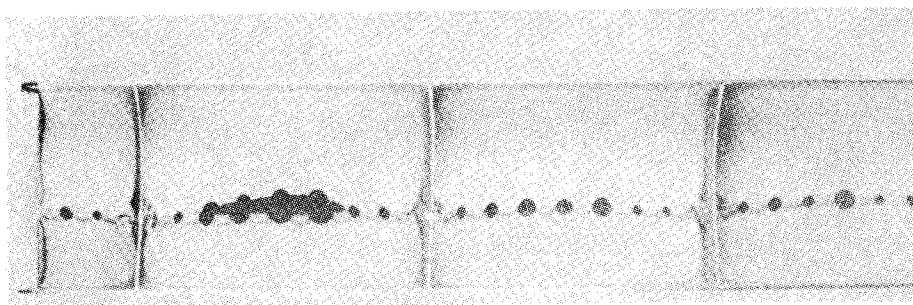
Excessive strain/strain rate brittleness can occur to cause the core failure shown. The best pressure-temperature-time cycle, with the poor surface conditions and nonuniform material thicknesses for minimum gage material, may still result in core failure.

316

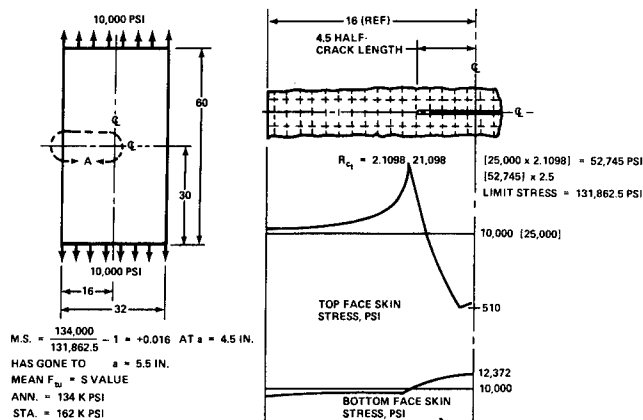## SPF/DB RECTANGULAR CORE SANDWICH PANEL
THEORETICAL AND ACTUAL

HALF CRACK LENGTH, a (IN.), ALONG TOP SKIN

0.80

0.60

0.40

0.20

0

UNSTIFFENED SHEET THEORETICAL

ACTUAL BY TEST (SANDWICH)

THEORETICAL (SANDWICH)

WEB CRACKED

RECTANGULAR SANDWICH WEB LOCATION

REQUIRED FLIGHTS

0   10   20   30

FLIGHTS (1000)
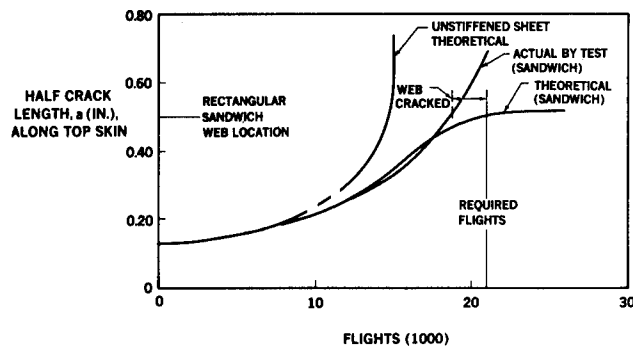
The unstiffened sheet panels and SPF/DB rectangular core sandwich panels were analyzed starting from an 0.125-inch half-crack length elox slot.* The theoretical SPF/DB sandwich, starting from an elox slot on one side, can sustain one lifetime of 21,100 flights. The unstiffened sheet panel cannot sustain one lifetime starting from an initial elox slot. Verification has been attained by test. It should be noted that a web crack occurred in the SPF/DB titanium sandwich before one lifetime of testing. This was found using a fiber optic probe on a 3-1/2-inch-wide allowables crack propagation specimen. The probe was inserted through the gas holes from the side of the specimens.

*Elox is an electronic discharge that creates a slot.

THEORETICAL MARGIN OF SAFETY USING FINITE-ELEMENT ANALYSIS AND R_{c_t} FOR SPF/DB TITANIUM SANDWICH

10,000 PSI

60

30

10,000 PSI

16

32

16 (REF)

4.5 HALF-CRACK LENGTH

R_{c_t} = 2.1098, 21,098

[25,000 x 2.1098] = 52,745 PSI
[52,745] x 2.5
LIMIT STRESS = 131,862.5 PSI

10,000 [25,000]

TOP FACE SKIN STRESS, PSI

510

12,372
10,000

BOTTOM FACE SKIN STRESS, PSI

M.S. = $\frac{134,000}{131,862.5}$ − 1 = +0.016 AT a = 4.5 IN.
HAS GONE TO   a = 5.5 IN.
MEAN F_{tu} = S VALUE
ANN. = 134 K PSI
STA. = 162 K PSI

A finite-element model of a 32-inch-wide SPF/DB titanium sandwich panel was analyzed to determine the theoretical R_{c_t} value to expect with a half-crack length of 4.5 inches (on one side). The analysis showed a value of 2.1098. Applying this, using the mean value of the ultimate strength in MIL-HDBK-5, a margin of safety of 1.6 percent is available at limit stress (assuming the 6Al-4V annealed properties). The actual panel went to a half-crack length of a = 5.5 inches and sustained limit stress.

R_{c_t} DERIVED FROM TEST

$$R_{c_t} = \frac{\text{CRACK TIP STRESS IN UNSTIFFENED PANEL}}{\text{CRACK TIP STRESS IN STIFFENED PANEL}}$$

MEASURED a_c = 5.5 INCHES AFTER LIMIT LOAD WAS APPLIED

MEASURED DATA, K_c = 130,000 PSI $\sqrt{\text{IN.}}$

σ_R = GROSS LIMIT STRESS APPLIED
= 62,500 PSI (2.5 x 25,000 PSI)
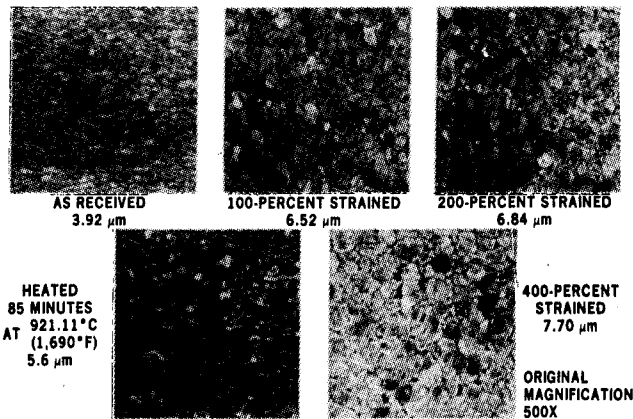
THEREFORE, FROM EQUATIONS ON PREVIOUS SLIDE:

$$R_{c_t} = \frac{\sigma_R \sqrt{\pi a_c}}{K_c}$$

$$R_{c_t} = \frac{62,500 \sqrt{\pi \times 5.5}}{130,000}$$

$$R_{c_t} = 1.998 \approx 2.0$$

The R_{c_t} derived from the test of the SPF/DB titanium wing panel with a half-crack length of 5.5 inches at limit gross stress of 62,500 psi (using a 1g stress of 25,000 psi), indicated that the R_{c_t} value is 1.998 ≈ 2.0. Therefore, from theory (previous figure) or from test, the SPF/DB sandwich reduces the crack tip stress of an unstiffened panel by a factor of approximately 2.0.

EFFECT OF THERMAL PROCESSING ON GRAIN SIZE OF Ti-6Al-4V 0.127 cm (0.050 IN.)

AS RECEIVED
3.92 μm

100-PERCENT STRAINED
6.52 μm

200-PERCENT STRAINED
6.84 μm

HEATED
85 MINUTES
AT 921.11°C
(1,690°F)
5.6 μm

400-PERCENT
STRAINED
7.70 μm

ORIGINAL
MAGNIFICATION
500X

The grain sizes increase with higher percent elongation during the SPF pressure-temperature-time cycle. At 400 percent strained, the grain size has almost doubled. The effect of the heating and time (no elongation) accounts for approximately 43 percent of the increase in grain size (compared to the 400-percent strained specimen). The increase in grain size, which occurs in superplastic forming, does deteriorate the strength. However, if the designer minimizes the elongations, and diffusion bonds to create a sandwich, the damage tolerance and rate of crack growth are superior for the sandwich SPF/DB panel (compared to an unstiffened sheet or a sheet-stringer).
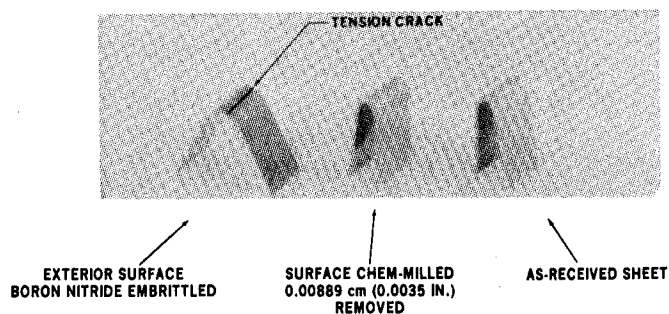
318

SPF/DB TITANIUM SANDWICH WITH MMC CRACK STOPPERS AND EXTERNAL DOUBLERS Al BRAZED
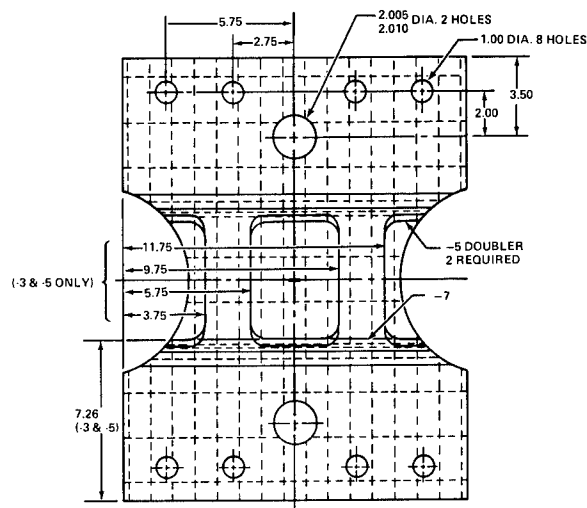
The above sketch is a crack propagation panel that has a metal matrix composite crack stopper doubler brazed to an SPF/DB titanium sandwich. An elox slot starts a crack that propagates across the 9.5-inch throat. A supersonic transport fatigue spectrum is imposed through the bolts and doublers. The number of lifetimes with and without the metal matrix composite doublers is compared.

BEND TESTS: SURFACE CONDITION AFTER SUPERPLASTIC FORMING
MAGNIFICATION: 0.5X

EXTERIOR SURFACE
BORON NITRIDE EMBRITTLED

SURFACE CHEM-MILLED
0.00889 cm (0.0035 IN.)
REMOVED

AS-RECEIVED SHEET

The bend test puts tension on the outer fibers. After using boron nitride as a stop-off* and then subjecting the sheet to a typical SPF/DB cycle, the part is then bent as shown. It should be noted that a crack forms from the tension stress. If the surface is chem-milled and the "white layer" removed, the part can be bent 180 degrees without cracking (middle picture). Also, as-received sheet can be bent without cracking. Therefore, only the combination of pressure, temperature, and time of the superplastic process causes the embrittlement. Accordingly, Douglas would not consider using stop-off on the inner core to face sheet. At Douglas, it is used only on an exterior surface where the "white layer" can be removed.

*A stop-off is a chemical compound that inhibits diffusion bonding of the parts.

SECTION THROUGH A THREE-ELEMENT PANEL
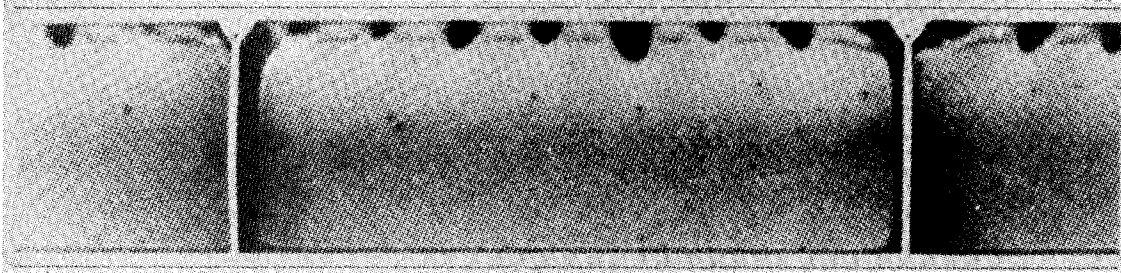
The three-sheet sandwich structure is a unique Douglas design. The top face sheet and core sheet are spot welded into rectangular cells and the core sheet is then blown to the bottom face sheet where it is diffusion bonded. Ultra-lightweight strong sandwich structures can easily be formed by this process.
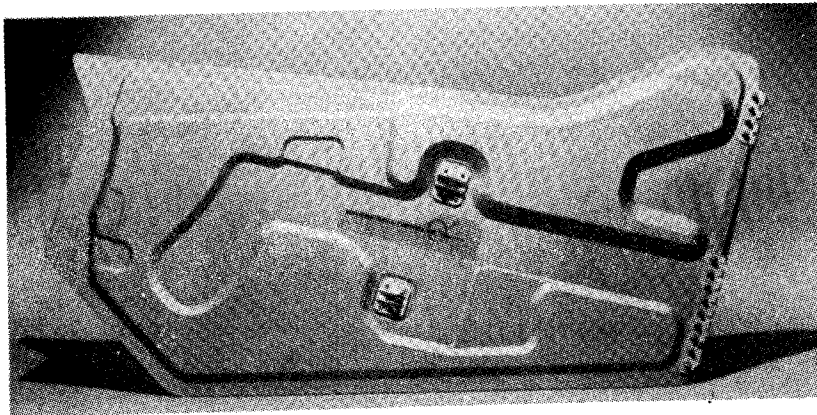
WING TRAILING-EDGE SECTION
SPF/DB SANDWICH (RECTANGULAR PATTERN)
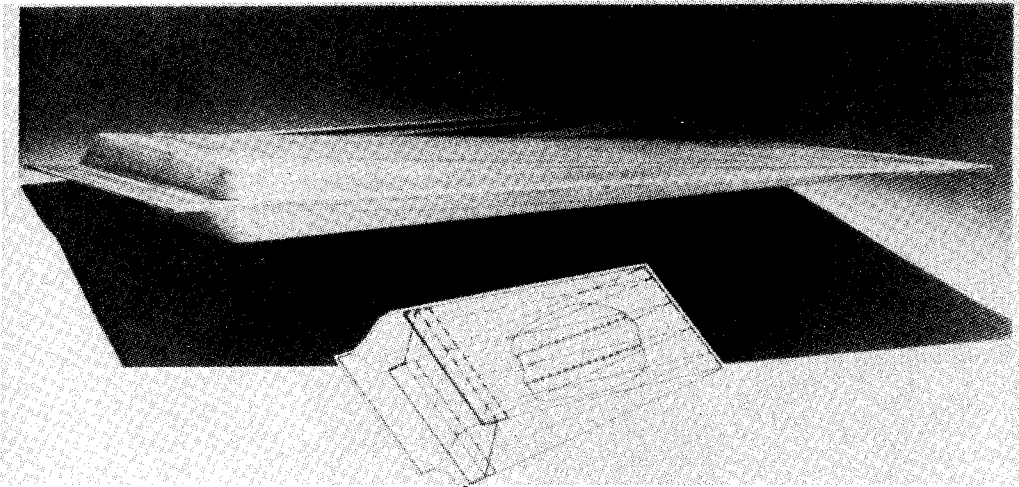
A typical trailing-edge four-sheet process has been successfully developed at MDC for application to a trailing-edge structure of a fighter aircraft.

T-38 MAIN LANDING GEAR DOOR

SPF/DB SANDWICH (RECTANGULAR PATTERN)
RELATIVE STIFFNESS + 10 PERCENT
RELATIVE WEIGHT — 8 PERCENT

The four-sheet SPF/DB titanium sandwich has been successfully developed as a substitute for the main landing gear door panels in the T-38 which are currently made from aluminum honeycomb sandwich. The SPF/DB titanium sandwich is 10-percent stiffer for 8-percent less weight.

3- BY 5-FOOT TITANIUM
SPF/DB SANDWICH
WING FATIGUE PANEL — INSTRUMENTED FOR TEST
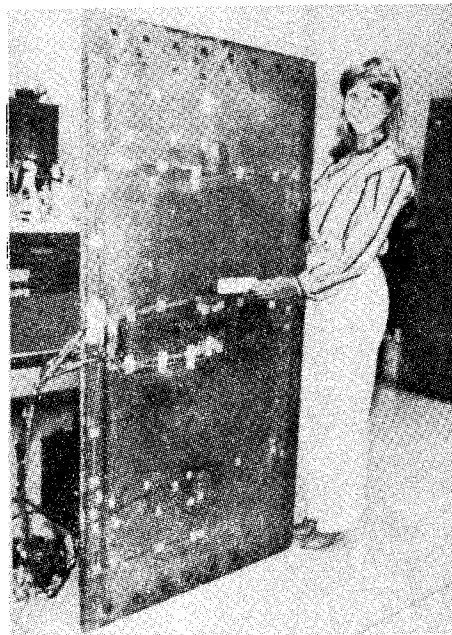
The above wing fatigue test panel has undergone one complete fatigue lifetime, and then was checked for limit load, elox slotted, and instrumented for crack propagation tests. Since then, it has achieved another one full lifetime after the initial crack. It has been checked again for limit load and is still stable (crack size will still hold).

321

CONCLUDING REMARKS

In conclusion, three methods of joining have been described that are applicable to SPF/DB titanium sandwich and its reinforcement with metal matrix composites. The core materials are joined by spot welding and/or roll seam welding and then, by applying enough heat and pressure to make the titanium superplastic, the core sheet cells are "blown" and diffused to the face sheets and doublers. Diffusion bonding is very effective — repeated tests and nondestructive evaluation confirm that a very efficient sandwich structural assembly is obtained. Many examples have been illustrated, with the largest a 3- by 5-foot wing panel. In addition, by aluminum brazing metal matrix composites to lightweight SPF/DB titanium sandwich, the structural efficiency has been enhanced significantly.

Scale-up of the SPF/DB titanium sandwich concepts to larger wing and fuselage sections should be attempted as soon as possible and should result in additional weight and cost savings. The larger the panel, the smaller the effects of the edge doublers and splice attachment parts, therefore reducing the number of parts and resulting in lower cost per square foot. Scale-up of large SPF/DB titanium sandwich panels that are double contoured can easily be achieved at superplastic temperatures. The dies for this are initially expensive, but worth investigating if a quantity production run is expected.

Brazing of reinforcement sheets to ultra-lightweight titanium sandwich can be done in a braze oven or a heated autoclave. In the past, Douglas has successfully fabricated large titanium panels by spot welding and then aluminum brazing. Similarly, brazing metal matrix composite reinforcement strips or sheet to titanium ultra-lightweight panels should be considered for scale-up for future aircraft.

SPF/DB titanium sandwich is very good for resisting stress corrosion. Also, the three-sheet sandwich, which has been developed successfully by Douglas and has been described previously, can be made into ultra-lightweight panels. These panels can compete in structural efficiency with aluminum honeycomb panels and aluminum conventional panels for new aircraft, and are especially efficient in their damage tolerance and life-cycle costs.

COMPARISON OF BOND IN ROLL-BONDED
AND ADHESIVELY BONDED ALUMINUMS

R. J. Schwensfeir, Jr., G. Trenkler,
R. G. Delagi and J. A. Forster
Texas Instruments Incorporated
Attleboro, MA 02703

ABSTRACT

Lap-shear and peel test measurements of bond strength have been carried out as part of an investigation of roll bonding of 2024 and 7075 aluminum alloys. Shear strengths of the bonded material in the 'F' temper are in the range of 14-16 ksi. Corresponding peel strengths are 120-130 lb/inch. These values, which are three to five times those reported in the literature for adhesively bonded 2024 and 7075, are a result of the true matallurgical bond achieved. The effects of heat-treating the bonded material are described and the improvements in bond strength discussed relative to the shear strength of the parent material. The significance of the findings for aerospace applications is discussed.

INTRODUCTION

Roll bonding is one of a number of methods used for joining metals by the production of a solid-phase weld at their interface. Bonding is carried out continuously by sqeezing constituent metal sheets together between a set of work rolls. The pressure from the rolls causes the metals to deform so that the interfacial contact is intimate enough to produce atomic bonding between virgin metal surfaces - i.e., to produce a solid-phase weld. An exhaustive treatment of solid-phase welding - including history, theory, methods, research and results - has been given by Tylecote.[1] A shorter review is contained in a book by Schwartz[2] while current work has been summarized by Melhorn.[3]

The first definitive experimental research on roll bonding was done by Vaidyanath et al.[4] The analytical mechanics of roll bonding have been presented in detail by Parkins[5] and summarized by Backofen.[6]

Roll bonding has been in use at Texas Instruments (TI) - Attleboro for a number of years in the production of metallurgically bonded metals and alloys, commonly called clad metals.[7] From its origin as a method for bonding decorative gold or silver surfaces onto base metals, the cladding process has been developed to the point where it is today sophisticated technology used in hundreds of applications.[8,9] These range from electronic connectors and automobile trim to composite coins with the density and appearance of those made from silver.

Developmental work at TI has recently been concerned with roll bonding of the high-strength, precipitation-hardening aluminum alloys 2024 and 7075.

This paper summarizes the results of the studies to date as they pertain to the strength of the metallurgical bond which is achieved in these materials.

BONDING

The roll bonding was done in the Metallurgical Laboratory on a two-high mill with 6-inch roll diameters. Following standard preparation, the sheets of material to be bonded were assembled into a layered "pack" which was introduced between the rolls manually. All roll bonding was performed at room temperature.

Initial experiments with 7075 produced a rather weak and brittle metallurgical bond. This problem was eliminated by using a sheet of softer aluminum between the 7075 sheets. The same situation was found with the 2024 alloy. The use of a soft interliner has been noted briefly in generic terms by Tylecote.[1]

Excellent results have been obtained using 6061 as the interliner. This was chosen for two reasons. First, its chemical composition is similar to that of the 2024 or 7075 alloy. Consequently the interdiffusion that occurs in subsequent thermal treatment of the bonded material does not cause significant strength reduction due to alloy dilution. Second, if a heat-treatable interliner is used, then some strengthening in the interliner can be anticipated when the composite is heat-treated to attain maximum strength - i.e., the effect of property dilution due to the presence of the interliner is reduced.

POST-BONDING TREATEMENT

Consistent with the findings of Tylecote and Wynne,[10] the morphology and consequently the strength of the bond are enhanced significantly by a post-bonding thermal treatment. The standard schedule selected was one hour at 260°C, with heating and cooling rates uncontrolled. This treatment produces about a five-fold increase in bond strength. The metallurigical mechanisms of bonding during rolling, and the formation of the solid phase weld, have been discussed by a number of authors.[4,10,11] Fig. 1 is a typical photomicrograph of the interface between the 6061 and 2024 of a bonded and heat treated 2024-T6 sample. The elemental diffusion and consequent grain growth that has occurred across the interface demonstrate clearly the formation of a metallurgical bond.

MEASUREMENT OF BOND STRENGTH

Bond strength was measured by both peel and lap-shear tests as described below:

Peel Testing

Peel specimens in the form of strips one inch wide and 15 inches long were cut from bonded packs. To permit separation of the bonded layers for testing, a stop-off medium was introduced at the interface at one end of the

pack prior to bonding. Specimen edges were smoothed before testing to eliminate stress concentrators.

Peel strength was measured using a fixture developed by Aero Research, Ltd. during the 1950's to evaluate adhesive materials and is described in detail by Benson.[12] As shown in Fig. 2, the specimen is clamped around a rotating drum sector with one of the separated layers free for peeling. Fig. 3 is a photograph of the fixture installed in the Instron testing machine, where the force required to peel the bond is measured. Note that the application of the peel force is always perpendicular and that as the material is peeled the drum rotates to maintain this geometry. In this way a quasi-steady state peel process is obtained. A typical autographic record of the peel force as a function of displacement is shown in Fig. 4. The force increases to a maximum as peeling is initiated, then falls off to an essentially steady-state value. Peel strength in pounds per unit width is determined by dividing the steady-state peel force by specimen width. The peel rate in all experiments was 0.05 inches/min (0.02 mm/sec).

To establish the repeatability of the method, a series of peel tests was run over a three-day period on two specimens with significantly different bond strengths. The results for both specimens were normally distributed, with standard deviations in the range of 6 to 8 percent of the mean as seen from Table 1.

Lap-Shear Testing

Lap-shear specimens one inch wide and nominally 7 1/2 inches long were cut from bonded packs. A groove was machined on opposite sides to approximately half the specimen thickness to produce the desired overlap area as shown in Fig. 5. The edges of the specimen were smoothed as for peel specimens. The specimen was placed in the Instron tester and pulled in tension at 0.01 inches/min (0.004 mm/sec). The force required to pull the specimen apart at the lap joint was recorded and the ultimate shear strength determined from:

$$\text{Ultimate Shear Strength} = \frac{\text{Maximum Load}}{\text{Overlap Length} \times \text{Sample Width}} \tag{1}$$

Peel and lap-shear testing as described above was carried out on 2024 and 7075 laminates after post-bonding thermal treatment and after further heat-treatment to a T6 temper. The thermal histories of the samples are given in Table 2.

RESULTS

The results of peel and lap-shear tests on the 2024 and 7075 are presented in Tables 3 and 4 for 'F' and 'T6' temper materials, respectively. Typical values for the bond strength of adhesives reported in the literature[13-16] are also given for comparison. The superior bond strength of the metallurgically roll bonded material is evident.

It should be noted that in determining the bond strength adhesives a piece of 2024-T3 0.032 inches thick (0.8 mm) is used for the face material.

In this way some uniformity is brought to the test and the adhesive quality of the "glue" is tested.

This is remarkably different for roll bonded materials, where the shear strength of the bonded materials is tested. Consequently any improvement in the strength of the bonded materials, whether by further cold rolling or thermal treatments, can produce an improvement in the bond strength. This is clearly seen in Table 4, where the lap shear strength of the materials, heat treated to a T6 temper, is 30% higher than that presented in Table 3 for the 'F' temper material.

Peel test results for the T6 temper materials are not presented since meaningful peel tests could not be performed. In any peel test, the value for the peel strength is affected by the size of the radius of the bend in the peeled member at the advancing disbond. This is, in turn, related to the flexural strength of the member and can, as discussed elsewhere,[17] significantly affect the results due to the introduction of a sizable bending load.

DISCUSSION

The results given in Tables 3 and 4 show that the strength of the bond produced in roll-bonded 2024 and 7075 aluminum is in the range of three to five times that reported in the literature for adhesive bonding. This is a direct consequence of the true metallurgical bond achieved during roll bonding and its ready enhancement by subsequent thermal processing.

The bond strength of roll-bonded metals can be determined theoretically if the shear strength of the material is known. Vaidyanath et al.[4] have discussed the use of a constraint factor developed by Orowan et al.[18] and have shown that for aluminum alloys that have been work hardened, the shear strength of the bond (σ_b), relative to the shear strength of the parent material (σ_p), is given by

$$\frac{\sigma_b}{\sigma_p} = R(2-R),\tag{2}$$

Where R is the fractional thickness reduction during bonding.

In the present work, R = 0.6 and Eq. (2) predicts that the theoretical ratio is

$$\frac{\sigma_b}{\sigma_p} = 0.6\ (1.4) = 0.84.\tag{3}$$

Since the mechanical properties of aluminum alloys are a function of the theromechanical history, values of the shear strength of the parent

326

material, σ_p, for the 2024 and 7075 were determined by measuring the shear strength of monolithic material subjected to the same process schedule.

The value of the ratio of the bond/parent shear strength can thus be experimentally determined and is presented in Table 5 for the 'F' temper samples. Recall that Equation (2) is only valid for materials which have been significantly strain hardened and cannot be applied to the case of thermally treated (i.e., T6) samples. The shear strength of the bond for both materials is 16-17 ksi shich is 90% of the parent material yield strength. This bond strength is significantly better than the shear strengths of adhesives which are typically in the range of 1-5 ksi.[15,16] The similarity of the bond shear strength for the 2024 and 7075 presented in tables 3 and 4 may be coincidental; however we believe it is because the failure is through the 6061 interliner. This subject is being investigated further.

The correlation between experimental and theoretical predictions for the bond strength ratio is excellent. Work is continuing on a theoretical understanding of the bond strength and the influence of subsequent thermomechanical processing schedules in roll bonded materials.

The physical attributes of roll-bonded high-strength aluminum alloys 2024 and 7075 suggest a number of advantages. However, because roll bonding cannot be done in situ, the applications would be restricted to parts having dimensions compatible with the width limit imposed by the bonding process.

The superior bond strength relative to adhesives with no penalty in weight could permit weight reductions, since for equivalent overall strength, joint area might be made smaller. Another advantage could be the replacement of fasteners such as rivets with a roll-bonded joint. This would not only eliminate problems with pronounced stress concentrations, but could also reduce fabrication costs incurred in the labor-intensive process of installing fasteners.

The metallurgical bond is hermetic. Thus, its resistance to environmental degradation by temperature of moisture would be superior to that of adhesives.

Finally, the fatigue response is expected to be better than that of an adhesive bond and probably better than that of a riveted joint. Fatigue studies on roll-bonded 2024 and 7075 are just getting under way at TI. There are some preliminary indications that the fatigue crack growth may be arrested at the bond interface.

AEROSPACE APPLICATIONS

The interest at TI in the bond strength of roll bonded aluminum alloys is prompted by development efforts to produce finished parts without using rivets or adhesives. This technology[9] holds the promise of reduced weight and cost due to the elimination of heavy sections for riveting and the associated assembly costs. Figure 6 shows a demonstration part, typical of a number of access panels, which was fabricated using this cladding process. There are no rivets or adhesives used in this part, which results in a 30% weight reduction and a potential cost reduction of 30%. Other applications of this technology

are being developed and the bond strength of the clad metal is of paramount importance. From the work reported here, and ongoing in our laboratory, it is clear that the strength of roll-bonded materials is significantly higher than that usually thought of in the aerospace industry. The shear strength of the bond is typicaly 3 to 10 times greater than that for adhesives and approaches the strength of the parent or face material.

CONCLUSIONS

The strength of the solid-phase weld produced in roll-bonded 2024 and 7075 aluminum has been examined. Bond strength was measured by the peel-test and lap-shear methods for material given an isothermal post-bonding treatment and for material subsequently heat-treated to a T6 temper. Bond strengths were found to be in the range of three to five times those reported in the literature for adhesively bonded 2024 and 7075. Lap-shear strength of bonded material after a thermal treatment was in excellent agreement with theoretical predictions. Potential aerospace applications of roll-bonded 2024 and 7074 aluminum were discussed.

REFERENCES

1. R. F. Tylecote: The Solid Phase Welding of Metals, St. Martin's Press, New York, NY, 1968.

2. M. M. Schwartz: Modern Metal Joining Techniques, Wiley Interscience, New York, NY 1969, Chap. 9.

3. H. Melhorn: Schweisstechnik, 1983, vol. 33, p. 24.

4. L. R. Vaidyanath, M. G. Nicholas, and D. R. Milner: Brit. Welding J., 1959, vol. 6, p. 13.

5. R. N. Parkins: Mechanical Treatment of Metals, George Allen and Unwin, Ltd., London, 1968, pp. 106-135.

6. W. A. Backofen: Deformation Processing, Addison-Wesley Publishing Company, Reading, MA, 1972, pp. 176-190.

7. G. Durst: J. Met., 1956, vol. 8, p. 328.

8. R. G. Delagi: Machine Design, vol, 52, no. 27, Nov. 20, 1980, p. 79: no. 28, Dec. 11, 1980, p. 148.

9. Texas Instruments: Clad Metals, brochure no MMAB001, 1983.

10. R. F. Tylecote and E. J. Wynne: Brit. Welding J., 1963, vol. 10, p. 385.

11. J. A. Cave and J. D. Williams: J. Inst. Metals, 1973, vol. 101, p. 203.

12. N. K. Benson: in Adhesion and Adhesives, R. Houwink and G. Salomon, eds., Elsevier Publishing Company, Amsterdam, 1967, vol 2, p. 517.

13. E. A. Podaba, S. P. Kodali, R. C. Curley, D. McNamara, and J. D. Venables: Appl. Surface Sci, 1981, vol. 9, p. 359.

14. P. K. Nelson: Am. Machinist, vol, 126, no. 12, Dec. 1982, p. 87.

15. T. Renshaw, D. Wongwiwat, and A. Sarrantonio: J. Aircraft, 1983, vol. 20, p. 552

16. T. Smith: J. Adhesion, 1982, vol. 14, p. 145.

17. N. A. deBruyne: in Adhesion and Adhesives, N. A. deBruyne and R. Houwink, eds., Elsevier Publishing Company, Amsterdam, 1951, p. 480.

18. E. Orowan, J. F. Nye, an W. J. Cairns: Ministry of Supply, England, Armament Research Department, Theoretical Research Report No. 16/45, 1945.

19. U. S. Patent NO. 4434930.

TABLE 1

RESULTS OF PEEL-TEST REPEATABILITY STUDY

SPECIMEN ID NUMBER	MEAN PEEL STRENGTH lb/in (N/mm)	STANDARD DEVIATION OF THE MEAN lb/in (N/mm)
A-1	113 (19.8)	9.1 (1.6)
A-2	96 (16.8)	5.9 (1.0)

TABLE 2

THERMAL HISTORIES OF THE BONDED SAMPLES

THERMAL PROCESS	2024 TEMP °F(°C)	TIME	7075 TEMP °F(°C)	TIME
POST-BONDING THERMAL TREATMENT	500(260)	1 HR	500(260)	1 HR
HEAT-TREATMENT TO T6				
SOLUTIONIZATION	920(493)	35 MIN	900(482)	35 MIN
ARTIFICIAL AGING	375(191)	9 HRS	250(121)	24 HRS

TABLE 3

BOND STRENGTH AFTER POST-BONDING THERMAL TREATMENT. THE ERROR QUOTED IS ONE STANDARD DEVIATION.

MATERIAL	PEEL STRENGTH lb/in (N/mm)		SHEAR STRENGTH ksi (MPa)	
	TI	ADHESIVE	TI	ADHESIVE
2024	131 ± 12 (22.9 ± 2.1)	22-60[a]	15.7 ± 0.7 (108 ± 5)	1-5[b]
7075	136 ± 15 (23.8 ± 2.6)	"	17.0 ± 0.6 (117 ± 4)	"

(a) REFERENCES 13 AND 14

(b) REFERENCES 15 AND 16

TABLE 4

BOND STRENGTH IN MATERIAL HEAT-TREATED TO T6 TEMPER. THE ERROR QUOTED IS ONE STANDARD DEVIATION.

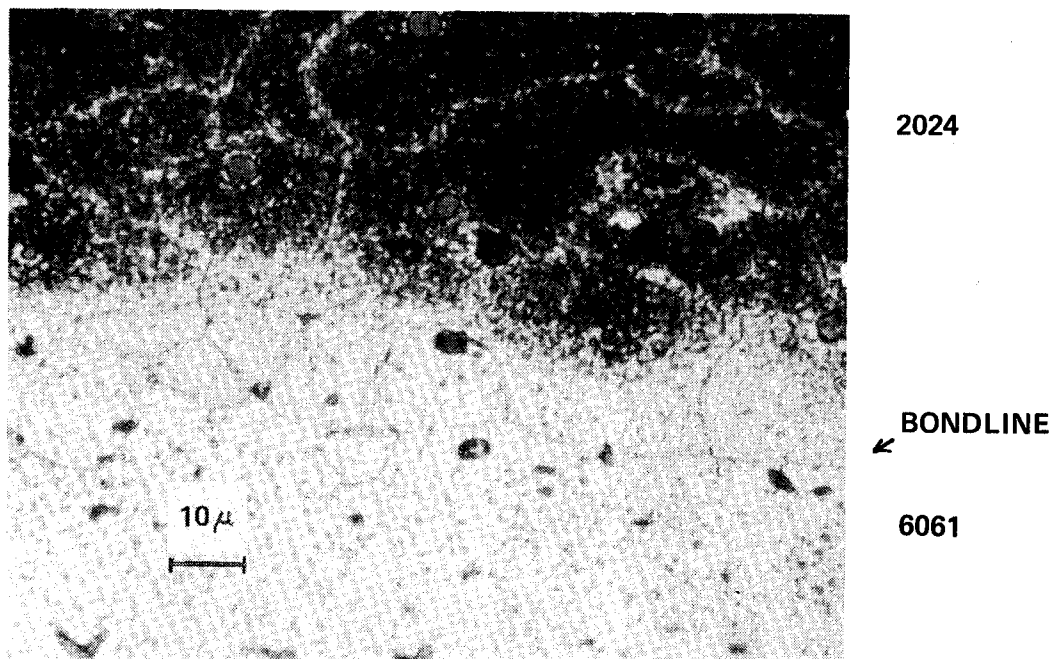| MATERIAL	SHEAR STRENGTH KSI (MPa)	
	TI	ADHESIVE
2024-T62	21.3 ± 1.3 (147 ± 9)	1-5[a]
7075-T6	20.6 ± 1.3 (142 ± 9)	"

(a) REFERENCES 15 AND 16.

TABLE 5

COMPARISON OF SHEAR STRENGTH OF THE BOND WITH SHEAR STRENGTH OF THE PARENT MATERIAL. THE QUOTED ERROR IS ONE STANDARD DEVIATION.

MATERIAL	σ_b (ksi)	σ_p (ksi)	σ_b/σ_p
2024	15.7 ± 0.7	17.1 ± 1.5	0.92 ± 0.09
7075	17.0 ± 0.6	18.6 ± 1.0	0.91 ± 0.06

Labels in figure (a): 2024, BONDLINE, 6061, BONDLINE, 2024, 10μ

Labels in figure (b): 2024, BONDLINE, 6061, 10μ
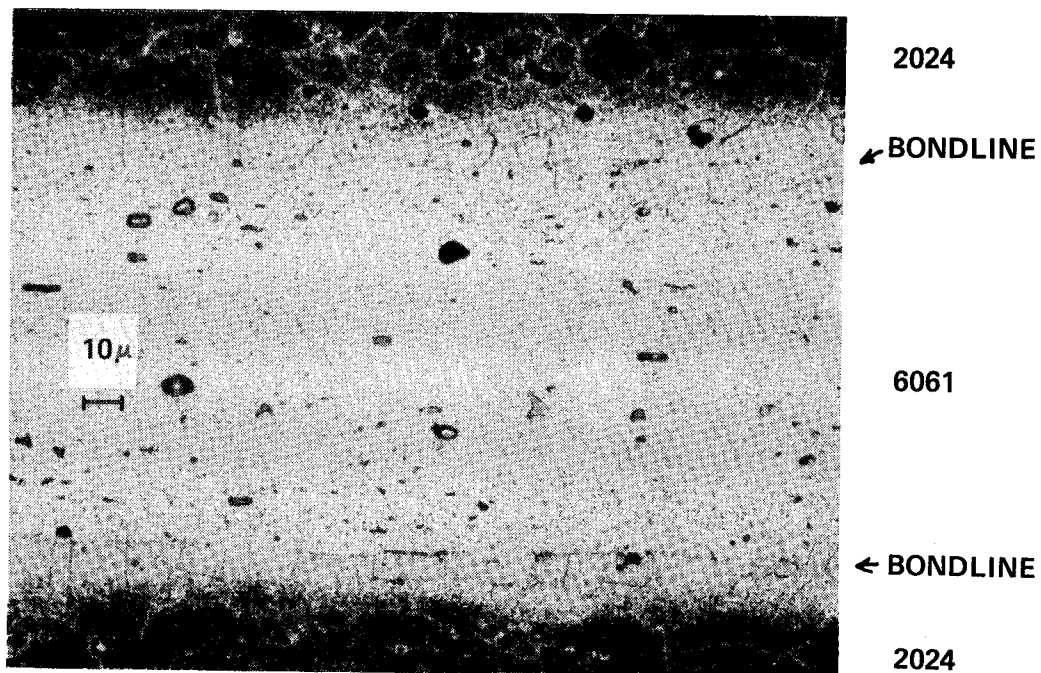
(a)

(b)

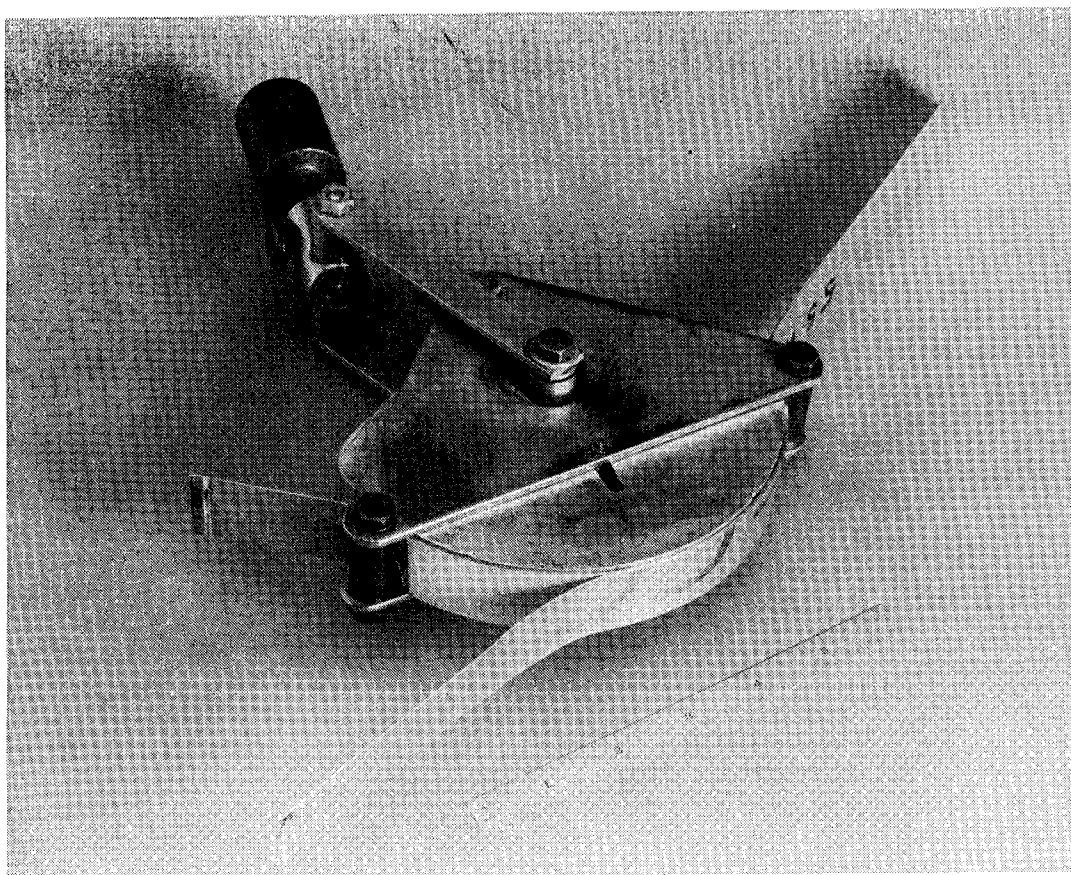FIG. 1. BOND INTERFACE IN 2024-T6 MATERIAL. (a) 500X. (b) 1000X. KELLER'S ETCH.
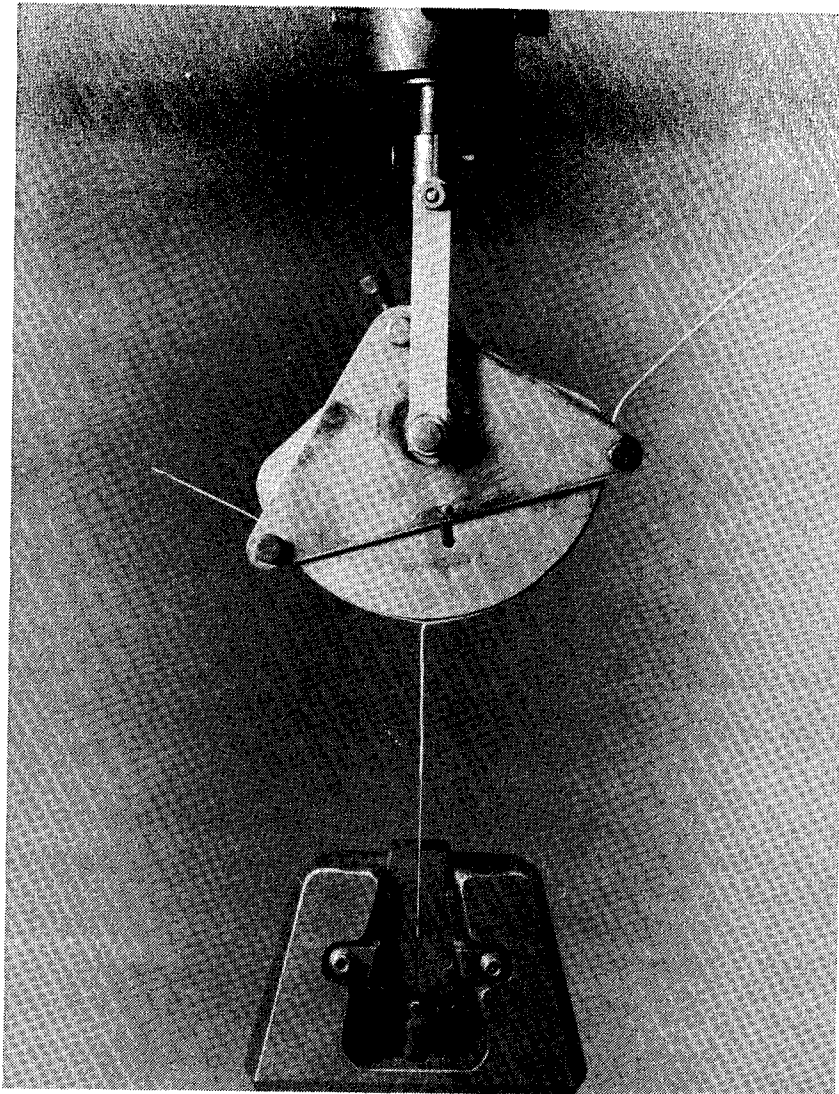
FIG. 2. PEEL-TEST FIXTURE.

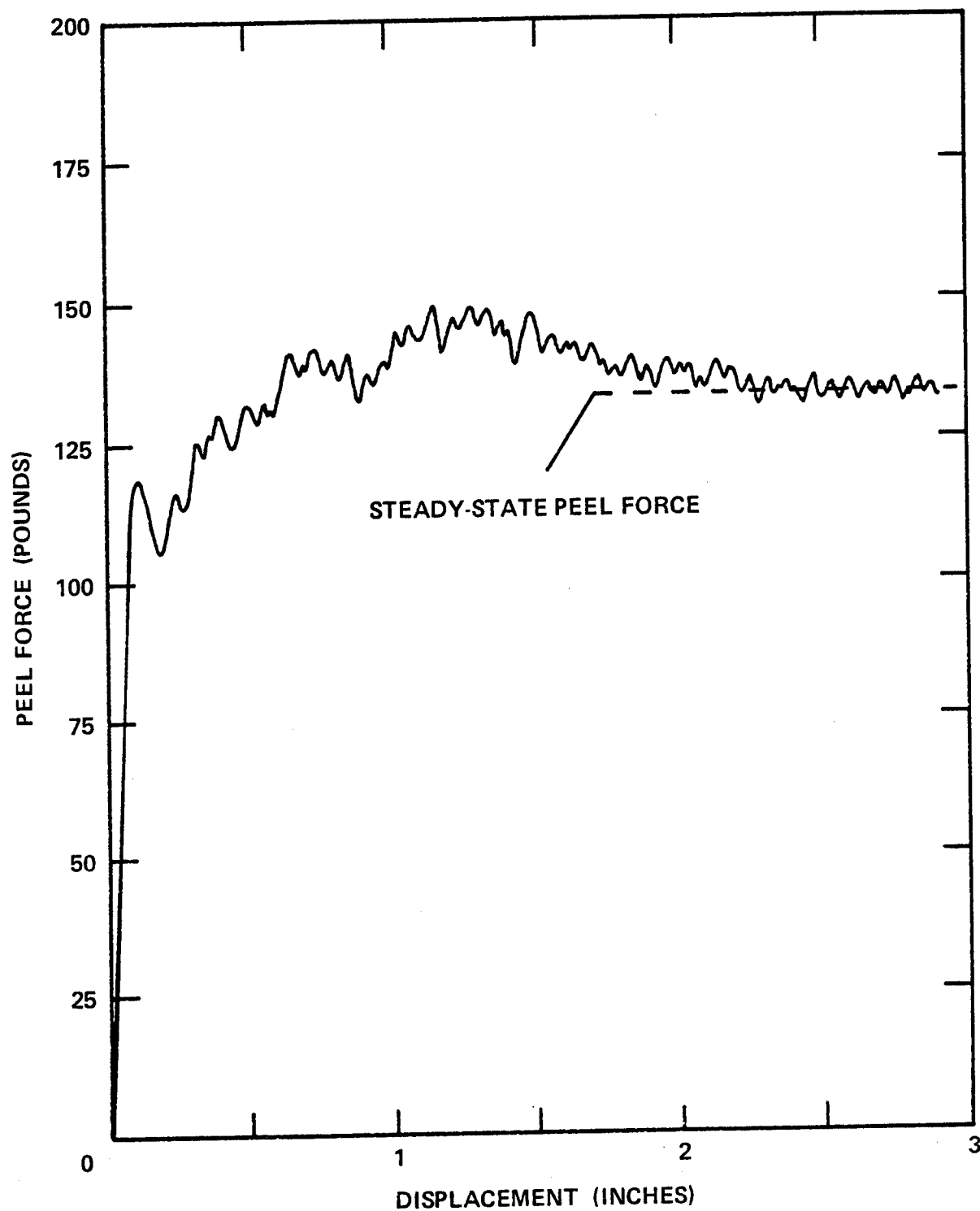FIG. 3. PEEL-TEST FIXTURE IN INSTRON TESTER.

FIG. 4. TYPICAL AUTOGRAPHIC RECORDING OF PEEL FORCE (SCHEMATIC).

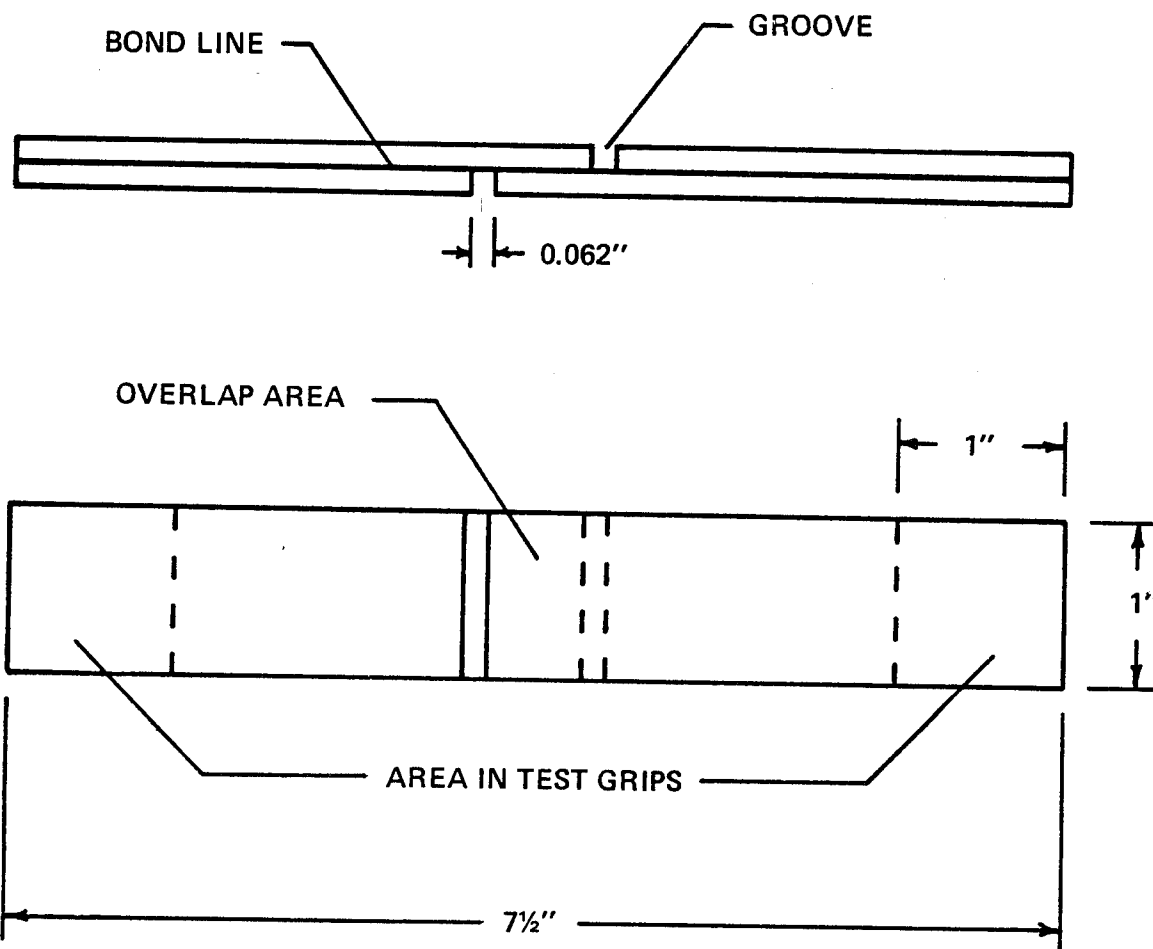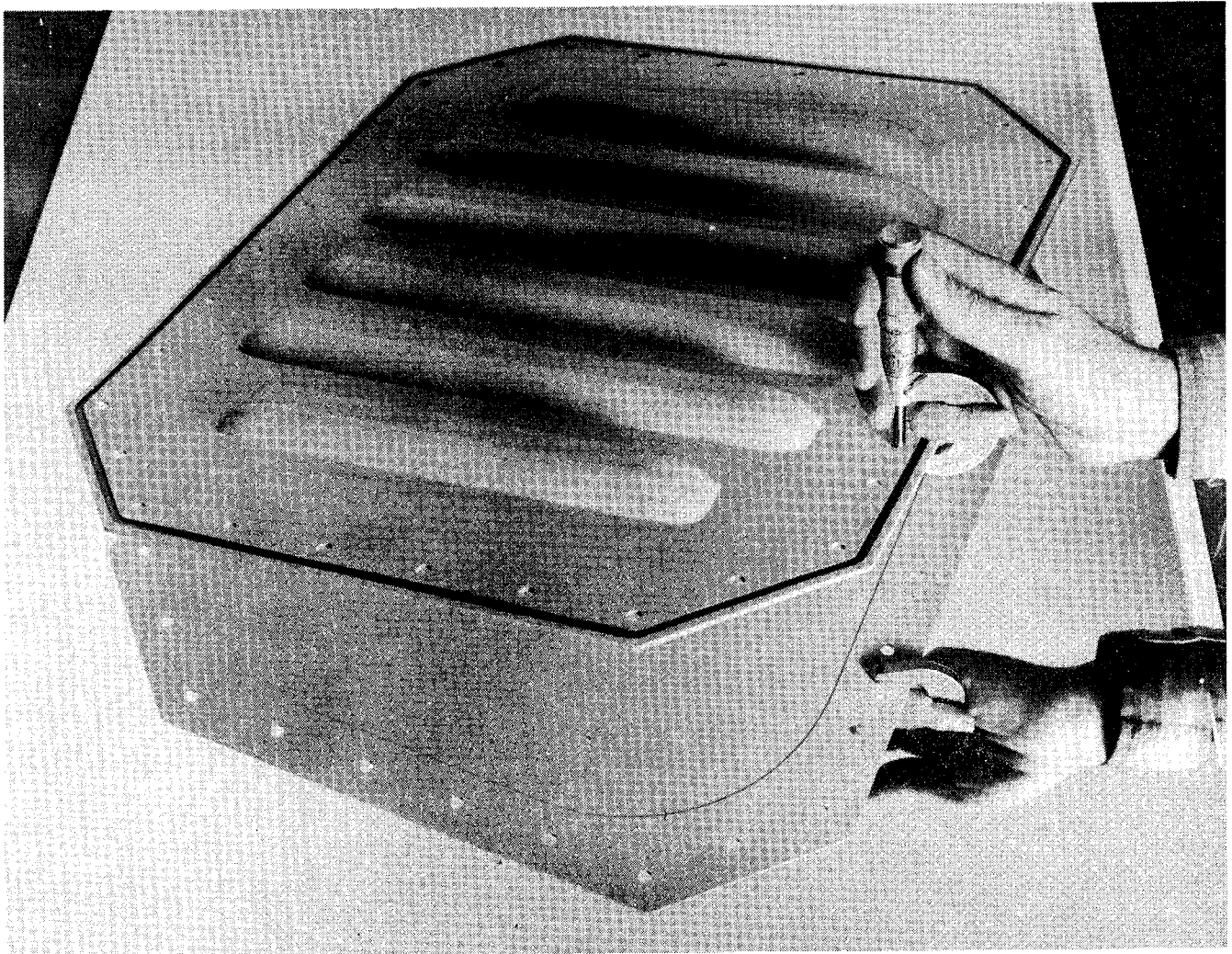FIG. 5. LAP-SHEAR TEST SPECIMEN.

FIG. 6. ROLL-BONDED ACCESS PANEL.

ADHESIVES FOR AEROSPACE

L. E. Meade
Staff Engineer - Advanced Structures
Program Manager - Honeycomb Repair Center
Lockheed-Georgia Company
Marietta, Georgia 30063

INTRODUCTION

The industry is hereby challenged to integrate adhesive technology with the total structure requirements in light of today's drive into automation/ mechanization. The state of the art of adhesive technology is fairly well meeting the "needs" of the structural designers, the processing engineer, and the inspector, each on an individual basis. But the total integration of these needs into the "factory of the future" is the next collective hurdle to be achieved. Improved processing parameters to fit the needs of automation/mechanization will necessitate some changes in the adhesive forms, formulations, and chemistries.

ELEMENTS OF BONDING

In addressing the needs of adhesives for the aerospace industry, the entire structure to be bonded must be considered. A bonded joint is only as good as the weakest element of the total. Figure 1 shows the elements of a typical bonded joint in an aircraft bonded structure. The adherend, surface treatment, primer, adhesive, and core (if sandwich) plus the processes used all must be considered. Figure 2 presents the state of the art for each of these adhesive bonding elements over the past two and one-half decades.

The Lockheed-Georgia Company has applied bonded structure on aircraft, starting 32 years ago on the C-130 (Figure 3)[1]. As seen in this figure, the applications were for fairings, secondary structure and some control surfaces. The JetStar (C-140) aircraft seen in Figure 4, designed in 1959, utilized a limited amount of bonded structure similar to the C-130. The C-141 (Figure 5) followed the C-130 by ten years, in 1962, and used approximately 10,000 square feet of bonded honeycomb structures, considerably more than the C-130. These included several primary structures plus fairings, leading edges, control surfaces, wing tips, landing gear doors, aft cargo doors and other secondary structure. The C-5A aircraft (Figure 6) used approximately three times as much bonded structure as did the C-141,
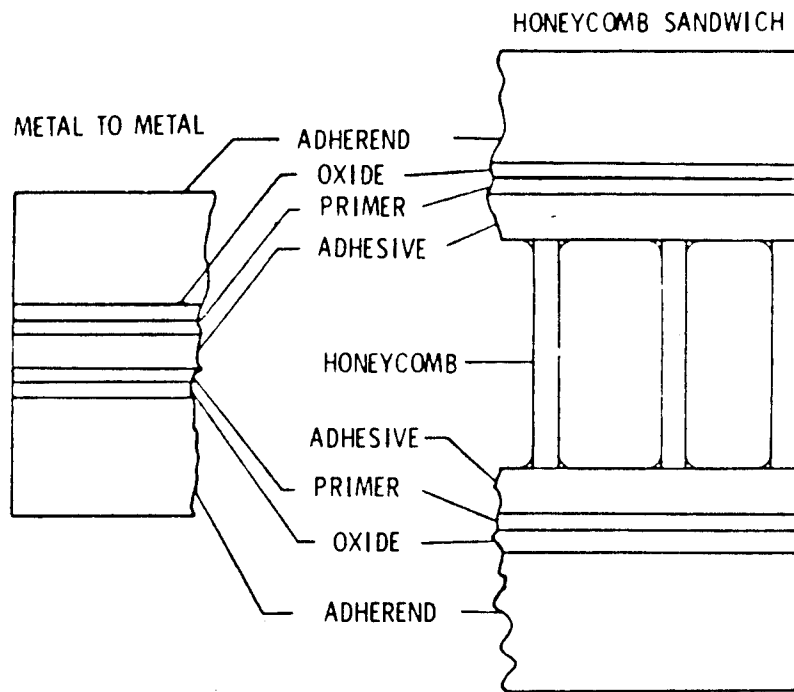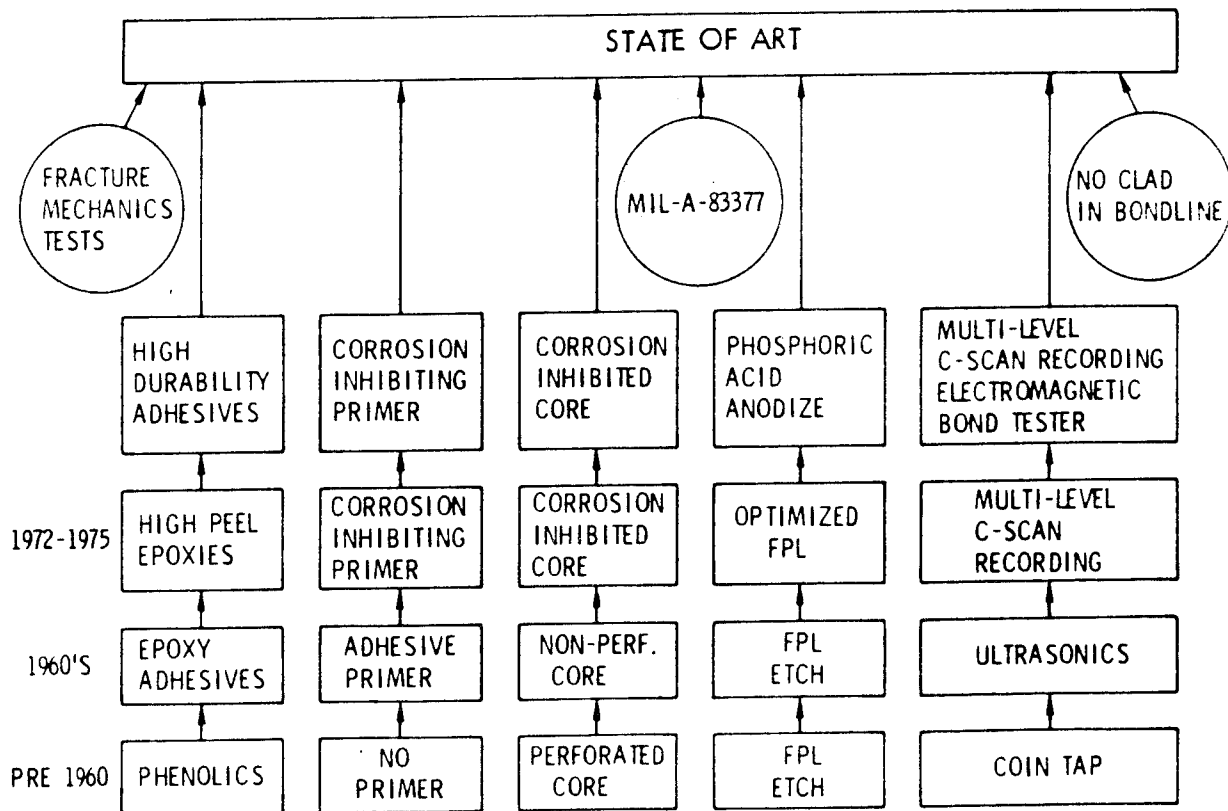
Figure 1. Elements of Bonding

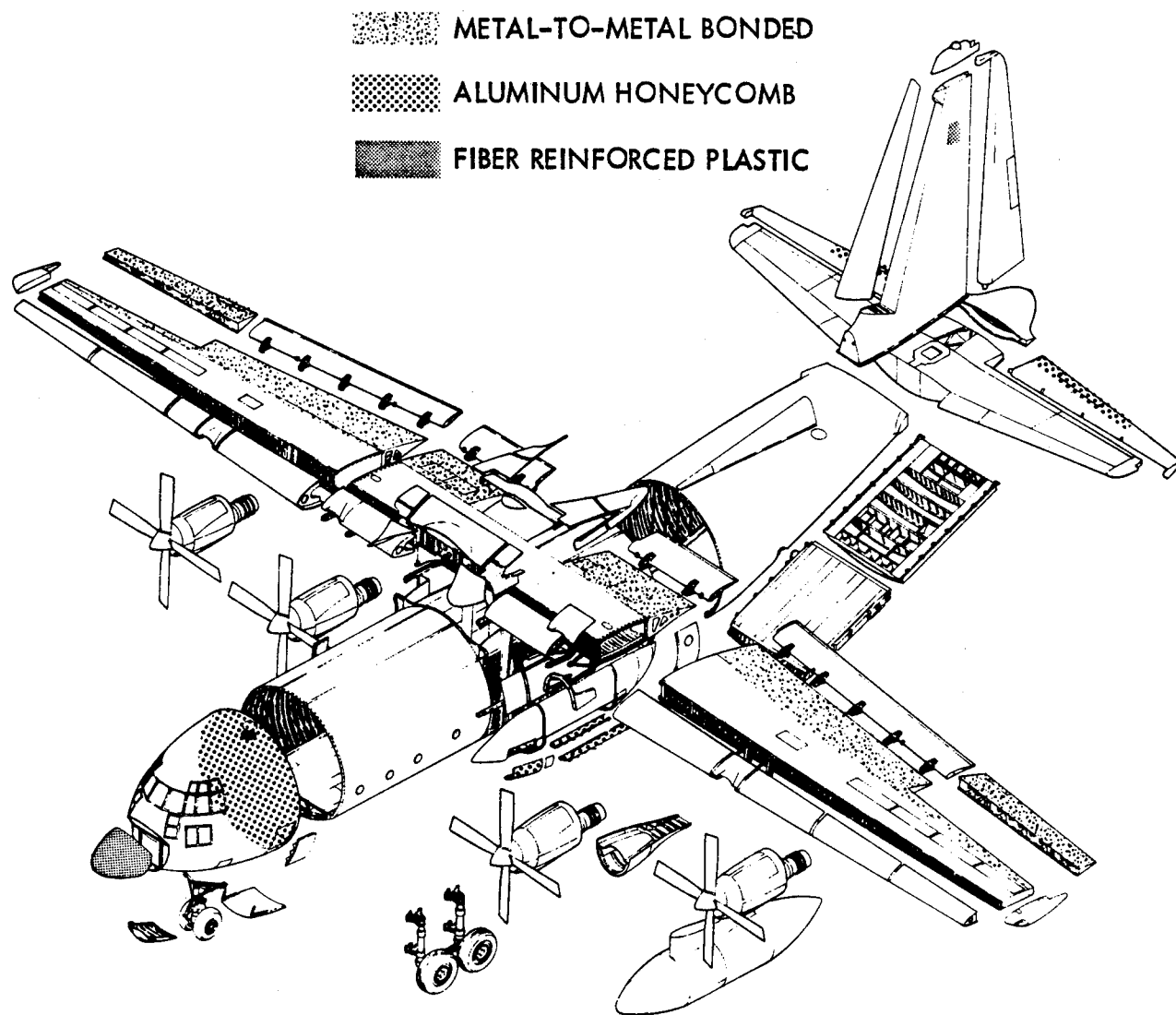Figure 2. State of Art Bonding Technology

METAL-TO-METAL BONDED

ALUMINUM HONEYCOMB

FIBER REINFORCED PLASTIC

Figure 3.   C-130 Bonded Structure

METAL-TO-METAL BONDED

ALUMINUM HONEYCOMB

FIBER REINFORCED PLASTIC
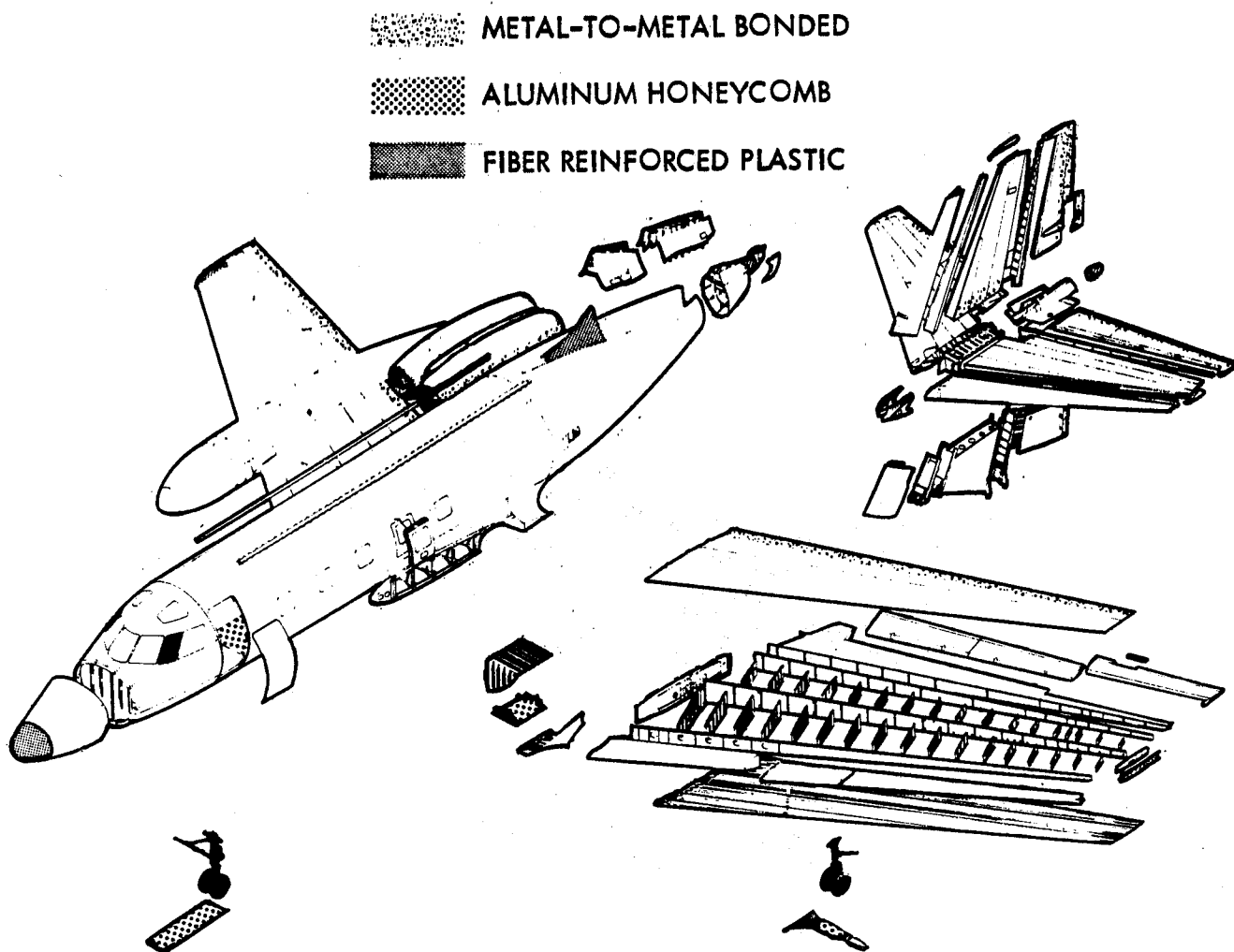
Figure 4.   JetStar Bonded Structure

METAL-TO-METAL BONDED

ALUMINUM HONEYCOMB

FIBER REINFORCED PLASTIC

Figure 5.   C-141 Bonded Structure

METAL-TO-METAL BONDED

ALUMINUM HONEYCOMB

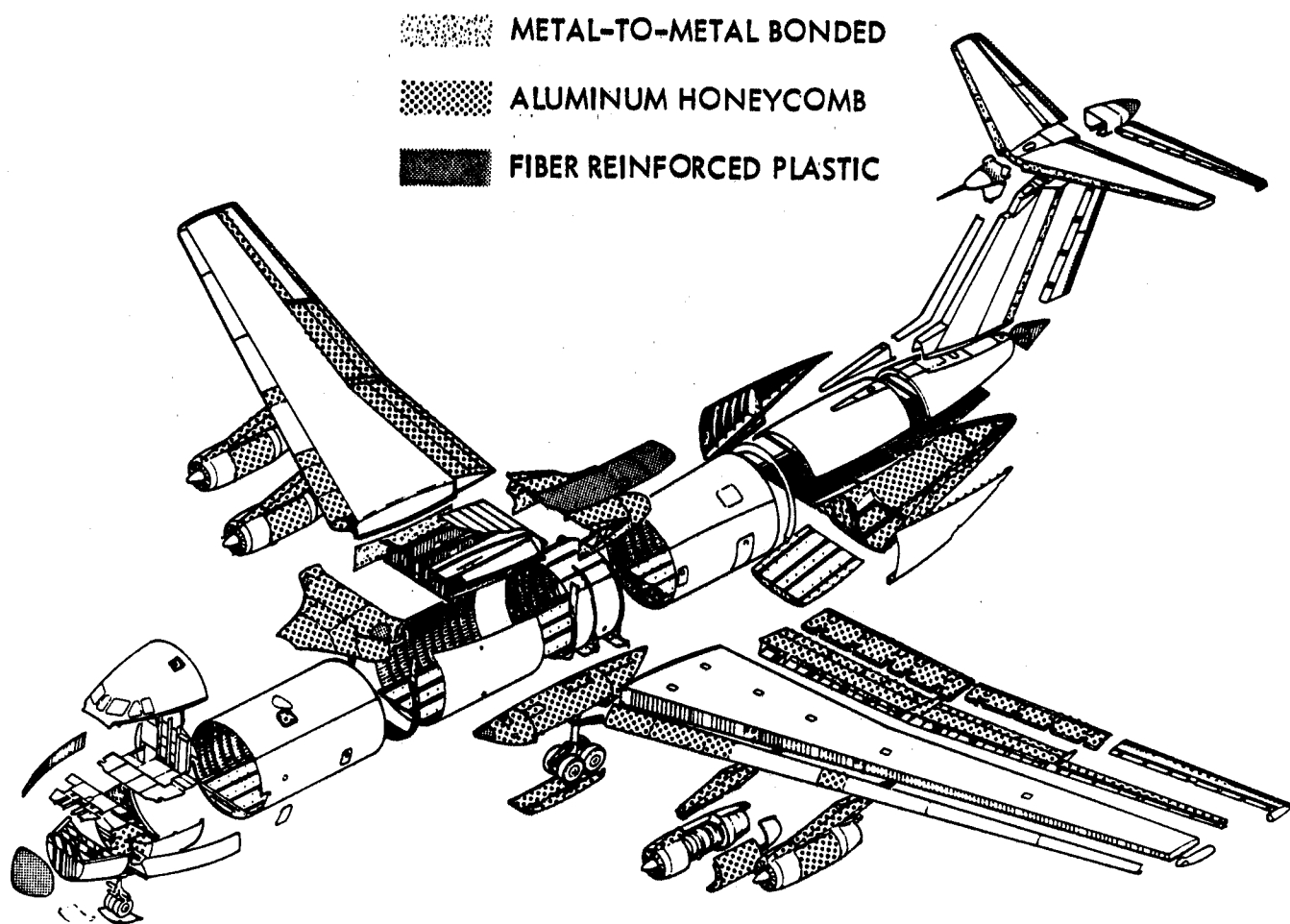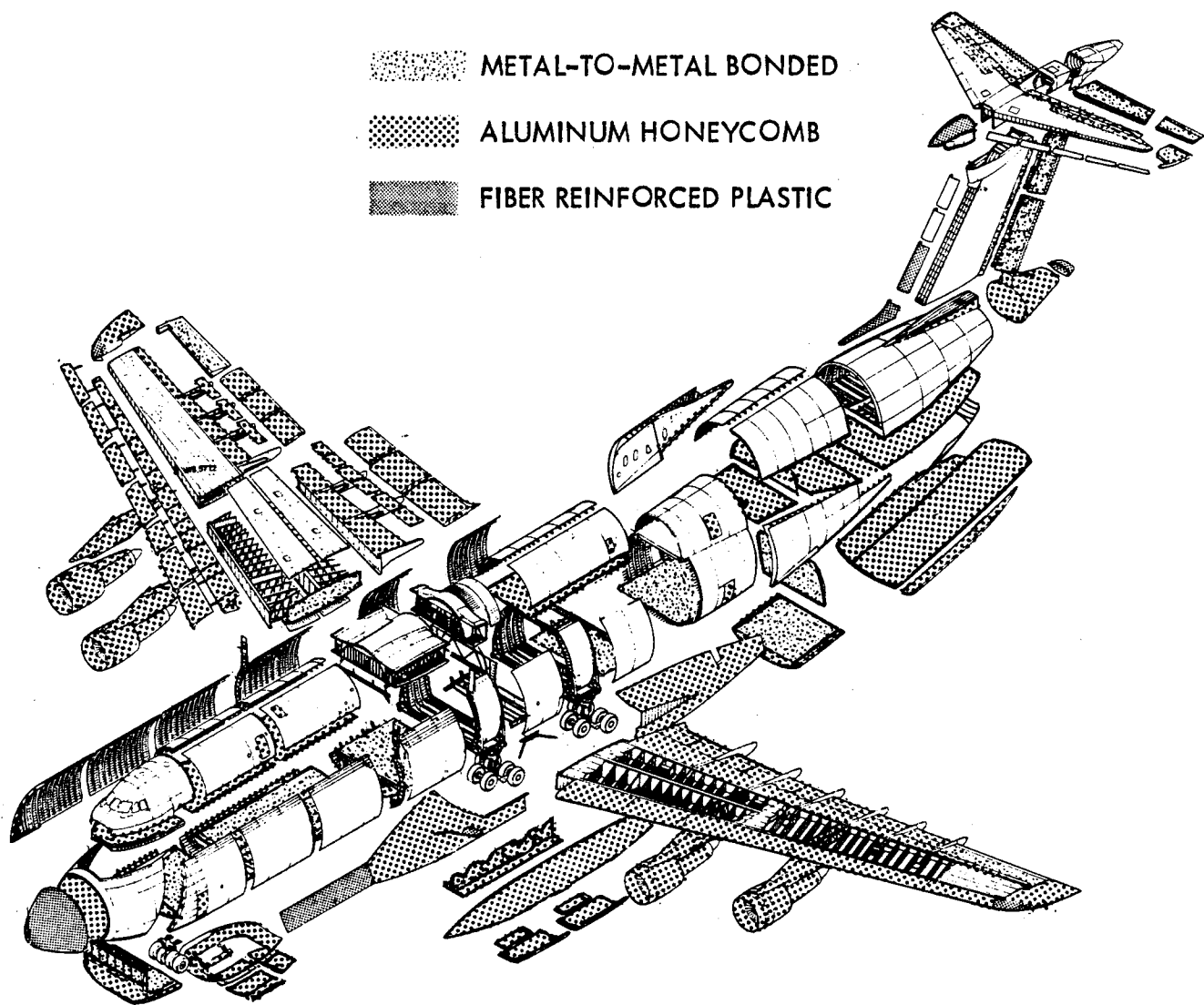FIBER REINFORCED PLASTIC

Figure 6.   C-5 Bonded Structure

and went into production in 1966. Primary structure that was bonded
extended to underfloor bulkheads, cargo floor, troop compartment floor,
and pressure bulkheads. A comparison of the honeycomb and metal-to-metal
bonded structure on the four different aircraft is shown in Figure 7.
These four aircraft, covering over three decades, progressed with
adhesive and surface preparation developments up to the presently used
PABST (Primary Adhesive Bonded Structure Technology) type adhesives and
phosphoric acid anodize on C-130 spares at the current time [1,2].

For most of aerospace's bonding needs, aluminum and composites make up the
majority of substrates to be bonded. The surface treatments most widely
used for aluminum are Optimized Forest Products Laboratory (OFPL) etch,
unsealed chromic acid anodize, and phosphoric acid anodize. The surface
morphology of these treatments (the oxide produced) is improved by the
use of corrosion inhibitors in adhesive based primers [3]. Much work has
been accomplished on new systems currently being used. Most of the current
primers are solvent carried, but environmental pollution regulations are
increasingly requiring no solvent emission and as such are driving our needs
toward aqueous based primers for either spray or electro-deposited
processes [4]. Several companies are working on electro-deposited primers
to meet these needs [5].

Composite substrates (the resin matrix composites) need fresh resin surfaces
exposed for wetting by the adhesive or adhesive primers. Either peel ply or
grit blast process are used to provide surfaces that are receptive to
adhesive materials. Primers will enjoy increased use on composites for
(a) surface protections against contamination during shop handling and
storage and (b) promotion of improved wetting of the cured composite surface
by the adhesive.

The adhesive films available to all of us today are vastly improved from a
decade ago [2], but there is an ever-increasing need for better toughness
along with hot-wet strength property improvements. At the same time, we
need to improve the economics of processing by lower cure temperature,
longer out time, and less sensitivity to storage conditions and cure
pressures (private conversations with S. Westerback, Grumman Aerospace
Corporation; E. House, Boeing Company; M. Williams, GD/Ft. Worth; J. Morrow,
Rohr/Ind; M. Lindsey, Lockheed-Georgia Company; B. Silverman, PRC, Inc.).
The corrosiveness of by-products from the cure process needs further
attention to ensure that the adhesive materials are neutral from a corrosion
standpoint.

The overall adhesive bonding processes and the manufacturing technologies
used to produce the finished assembly need consideration at the time of
structure design. Advanced bonding techniques have not yet been fully
integrated into bonding facilities, as suggested by Figure 8. The adhesive
bonding and composite fabrication factories of the future will encompass
much automation. These techniques will encompass many mechanized systems
taking the human guesswork and variables out of the process. Increased
emphasis will be placed upon material consistency, narrower tolerances,
and instrumental analysis means of verification of both the material
chemistry and its optimum processing [6]. Adhesives suppliers will need to
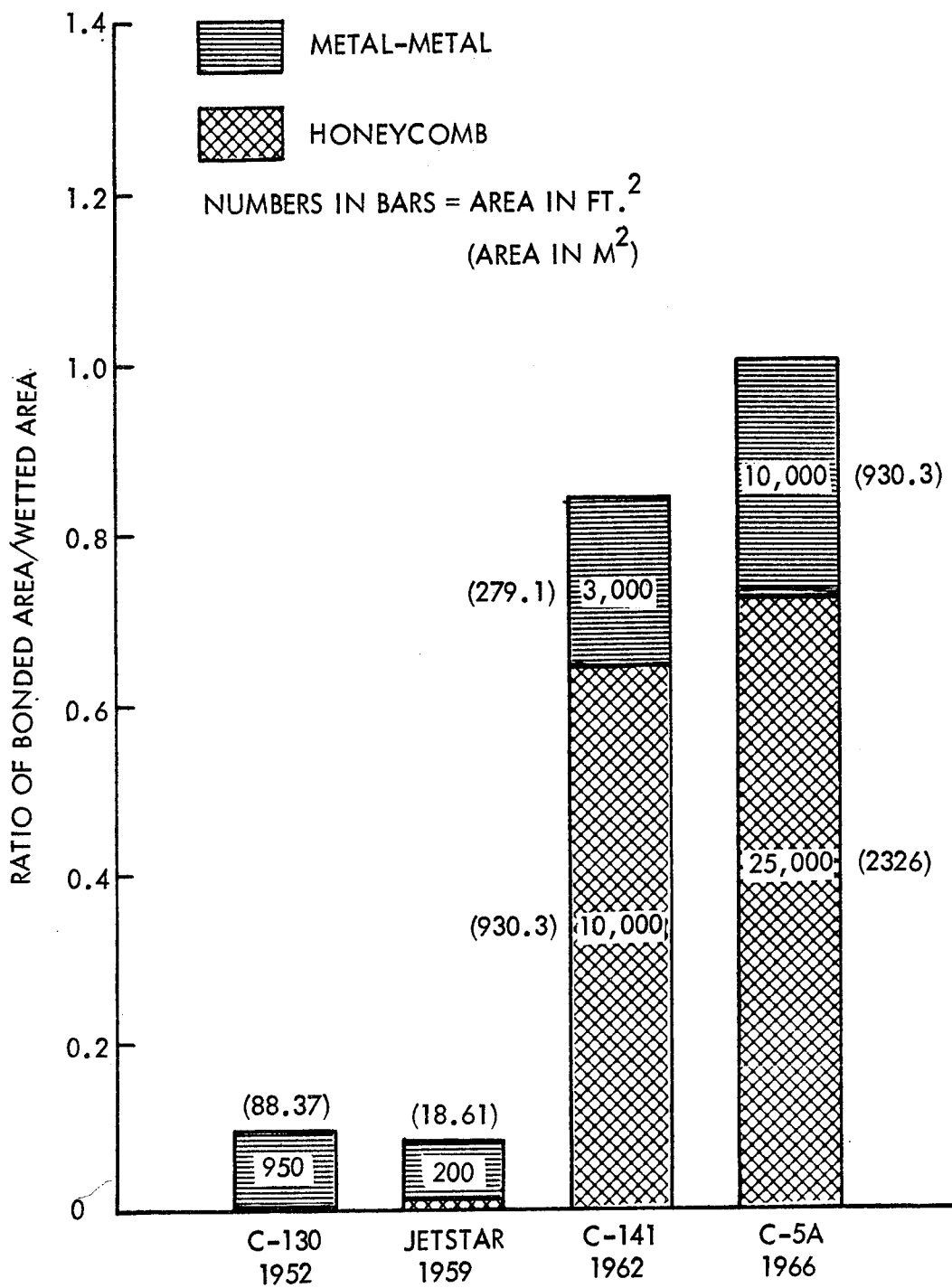
Figure 7.   Ratio of Bonded Area to Aircraft Wetted Area
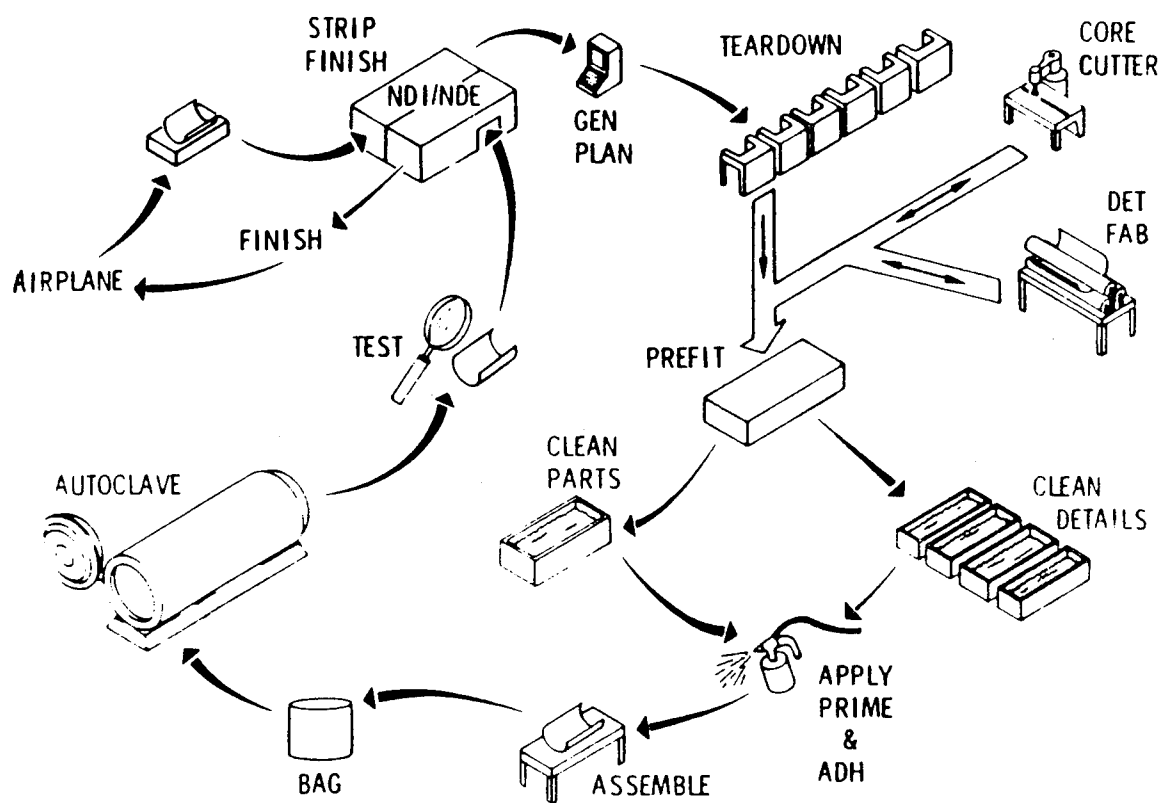
Figure 8.   Preliminary "To Be" Concept - Honeycomb Bonding Center

work ever more closely with structure designers, factory layout engineers, process engineers and quality assurance personnel in the formulation and manufacture of new materials.

The use of structural adhesive bonding as the primary means of sealing fuel cell structures has been well demonstrated by the F102, F100, 880 and 990 aircraft. Advanced made in adhesives and surface treatments make this approach even more desirable today. Much work is being concentrated on integrating all of the required elements to achieve the highest degree of producibility with the latest technology in adhesively sealed, bonded/fastenered fuel cell structure both in fighters (as is being accomplished on the F16), and in future transport applications.

CONCLUSIONS

(1) Adhesives have, for the most part, kept up with the "needs" of the aerospace industry, normally leading the rest of the industry in developments.

(2) The "wants" of the aerospace industry still present a challenge to encompass all elements, achieving a totally integrated joined and sealed structural system.

(3) Better toughness with "hot-wet" strength improvements is desired.

(4) Lower cure temperatures, longer out times, and improved corrosion inhibition are desired.

348

REFERENCES

(1) "Bonding and Durability", Fehrle and McDougal, Lockheed-Georgia Company, SAE Technical Paper #790561, April 1979.

(2) "Primary Adhesive Bonded Structure Technology", Air Force Contract #F33615-75-C-3016, Douglas Aircraft Company, Long Beach, California, 1975.

(3) "Exploratory Development of Corrosion Inhibiting Primers", Air Force Contract #F33615-76-C-5301, Northrop Corporation, 1976.

(4) "Development of Improved Electro-Deposited Corrosion Inhibiting Primer", Air Force Contract #F33615-78-C-5050, Northrop Corporation, 1978.

(5) "Interfacial Bond Integrity (350°F Service)", Air Force Contract #F33615-80-C-5069, Northrop Corporation, 1980.

(6) "Manufacturing Technology for Integration of Advanced Repair Bonding Techniques", Air Force Contract #F33615-82-C-5054, Lockheed-Georgia Company, 1982.

HIGH-TEMPERATURE ADHESIVE
DEVELOPMENT AND EVALUATION

Carl L. Hendricks and Jeremy N. Hale
Boeing Aerospace Company
Seattle, Washington

ABSTRACT

High-temperature adhesive systems were evaluated for short- and long-term stability at temperatures ranging from 232°C to 427°C. The resins selected for characterization included: NASA Langley developed polyphenylquinoxaline (PPQ), and commercially available polyimides (PI). The primary method of bond testing was single lap shear. The PPQ candidates were evaluated on 6Al-4V titanium adherends with chromic acid anodize and phosphate fluoride etch surface preparations. The remaining adhesives were evaluated on 15-5 PH stainless steel with a sulfuric acid anodize surface preparation. Preliminary data indicate that the PPQ adhesives tested have stability to 3000 hours at 450°F with chromic acid anodize surface preparation. Additional studies are continuing to attempt to improve the PPQ's high-temperature performance by formulating adhesive films with a boron filler and utilizing the phosphate fluoride surface preparation on titanium. Evaluation of the polyimide candidates on stainless-steel adherends indicates that the FM-35 (American Cyanamid), PMR-15 (U.S. Polymeric/ Ferro), TRW partially fluorinated polyimide and NR 150B2S6X (DuPont) adhesives show sufficient promise to justify additional testing.

Objective

To evaluate and test various polymers as adhesives for potential high temperature (450 °F – 800 °F) aerospace vehicle applications

INTRODUCTION

Increasing demands for improved structural performance and efficiency of advanced aerospace vehicle systems have severely stressed existing material designs. For additional improvement in this area, new materials and processes must be developed to meet these stringent requirements. High-temperature adhesives could be utilized to improve the reliability and durability of advanced composite, metallic, and ceramic designs.

The purpose of this effort is to evaluate and test various available polymers as adhesives for potential high-temperature applications. The two candidate polymers are polyphenylquinoxaline and polyimide. The three PPQ polymers, designated X-PQ, PPQ-2501 and PPQ-HC, are currently under evaluation as adhesives for long-term 232°C applications under contract NAS1-15605. The six PI candidates, designated FM-35, PMR-15, TRW-PFPI, NR150B2S6X, LARC-TPI, and IP-600, are also candidates for short-term applications (15 minutes) at temperatures ranging from 316°C to 427°C.

The following presentation details some of the work accomplished by the Materials and Processes Group of the Boeing Aerospace Company.

352

Polymers Selected for Study

1. Polyphenylquinoxalines (NAS1-15605)
    A.   X-PQ   (NASA Langley)
    B.   PPQ-2501 (King Mar Laboratories)
    C.   PPQ-HC   (Hunt Chemical)

2. Polyimides (IR&D)
    A.   PMR-15   (U.S. Polymeric)
    B.   FM-35   (American Cyanamid)
    C.   TRW-PFPI (TRW)
    D.   NR150   (DuPont)
    E.   LARC-TPI (Mitsui Toatsu)
    F.   IP-600   (National Starch and Chemical)

Selected Polymers

The polymers selected for study as high-temperature adhesives include polyphenylquin-oxaline (PPQ) and polyimide (PI).

The PPQ adhesive candidates are currently under evaluation as $232^{\circ}C$ structural adhesives on NASA Contract NAS1-15605. In this study, titanium lap shear, crack extension and climbing drum peel specimens were fabricated and then subjected to various environmental conditions before testing. These conditions included temperature ranges from $-54^{\circ}C$ to $232^{\circ}C$, humidity exposure ($49^{\circ}C$/95% R.H.) and aircraft fluid immersion (Skydrol). Exposure times in these environments ranged from 0-3000 hours.

In addition, boron-filled PPQ adhesives are being evaluated on a Boeing Independent Research and Development (IR&D) Program to improve their high-temperature ($427^{\circ}C$) performance. This is being done in conjunction with a phosphate fluoride titanium surface preparation.

All PI candidates are being evaluated on a Boeing (IR&D) Program. These adhesives are being assessed for short-term stability at high temperatures (above $316^{\circ}C$) on stainless-steel adherends. The surface preparation is sulfuric acid anodize. A majority of this testing was completed on single lap shear specimens at test temperatures from $-54^{\circ}C$ to $427^{\circ}C$.

TRW-PFPI (4BDAF/PMDA)
## Partially Fluorinated Polyimide
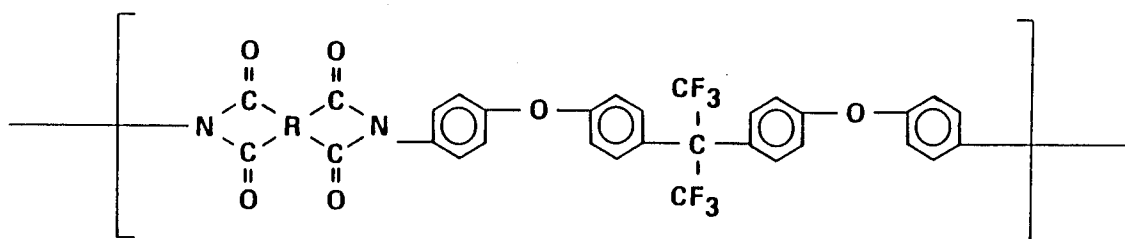
Where R = aromatic ring structure

This figure shows the general molecular structure of the partially fluorinated polyimide, a linear aromatic condensation polyimide that can be utilized as a thermo-oxidative/corrosive protective coating. The glass transition temperature for this polymer is approximately $390^{\circ}C$ ($734^{\circ}F$).

354

DuPont NR150 B2S6X
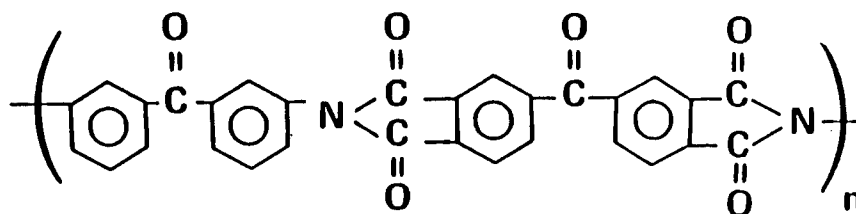
Thermoplastic Polyimide
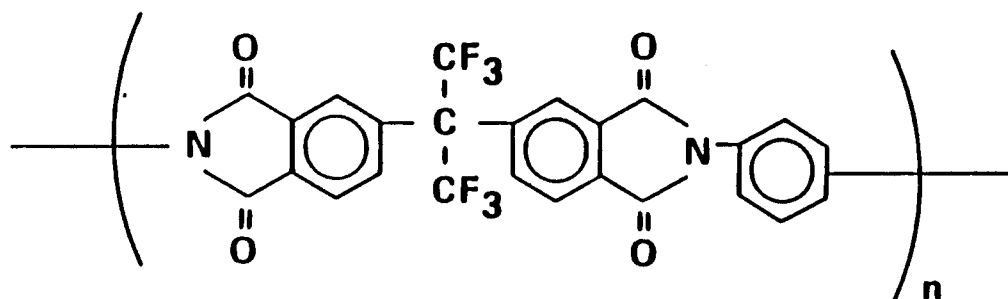
This figure shows a NR 150 condensation polyimide from DuPont supplied as a precursor solution in diglyme solvent; it is a polymer that exhibits excellent thermal and oxidative stability with a glass transition temperature of approximately $375^{\circ}C$ ($707^{\circ}F$).

Mitsui Toatsu LARC-TPI
Thermoplastic Polyimide

This figure shows the molecular structure of a NASA Langley-developed linear thermoplastic polyimide produced by Mitsui Toatsu Chemicals, Inc., Japan. In its fully imidized form, LARC-TPI exhibits excellent toughness and thermo-oxidative stability. This condensation polyimide has a glass transition temperature of 259°C (498°F).

PPQ Processing Parameters

- **Adhesive tape preparation:** Polymer solution was applied to 112 E-glass scrim. Individual coats of polymer were dried at 65 °C/1 hour; tape thickness was built up to .010″. Final film was cured at 185 °C/1 hour. Flow and volatile tests were conducted to check processing techniques.

- **Adherend:** Adherend was 6Al-4V titanium.

- **Adherend surface preparation:** It was 10V chromic acid anodize, primed immediately with a dilute solution consisting of 3 parts solvent (1:1 mixture of m-cresol/xylene) and 1 part polymer solution.

- **Bonding conditions:** All specimens were autoclave cured under 22 in. Hg vacuum and 200 psi for 90 minutes at 329 °C.

The processing conditions for the PPQ polymer system were characterized in earlier work (Ref. 1). Processes optimized included adhesive film preparation techniques, surface preparation methods and cure cycles.

The PPQ polymers were supplied in solutions of M-cresol and xylene solvent with a solid content of approximately 20% by weight. Adhesive film construction involved applying layers of the polymer solution to a 112 E-glass scrim. Typically the fiberglass was stretched in an aluminum frame and the polymer solution was spread onto the surface by either brush or squeegee application. Each layer of polymer solution was subsequently oven dried to remove the majority of the residual solvent. After the desired film thickness (.010″) has been acheived, the film is then oven cured at 185°C for 1 hour to further reduce the volatile content. Flow and volatile tests were then conducted to check the processing methods. After processing the PPQ films usually exhibited very little melt flow at 600°F/200 psi and a volatile content of from 0.5% to 3.0% by weight.

Surface preparation of the titanium adherends included the following process steps:

1. Trichloroethylene degrease
2. Alkaline clean
3. Nitric-hydrofluoric acid etch
4. Chromic acid anodize

After surface preparation, the adherends are immediately primed with a dilute polymer solution, and then oven dried at 163°C for one hour.

Fabrication of the test specimens (lap shear, crack extension and climbing drum peel) required the assembly of appropriately sized adhesive films and the primed titanium adherends. All specimens were subsequently vacuum bagged and autoclave cured at 329°C for ninety minutes.

Data Summary for X-PQ Adhesive

Test Condition	Lap Shear MPa (psi)	Crack Extension mm (inches)	Climbing drum peel, N-M (in/lb)
Ambient (68° F) Initial	26.6 (3850)	22.1 (.87) 24.1 (.95) 1/	1.3 (11.7)
219 K (-67° F) Initial	29.9 (4340)	–	–
450 K (350° F) Initial	25.5 (3700)	23.9 (.94)	–
505 K (450° F) Initial	16.1 (2330)	24.6 (.97)	5.6 (49.7)
Ambient after exposure to 322 K (120° F)/95% R. H. 1000 hrs	16.6 (2400)	34.8 (1.37)	0.4 (3.5)
450 K (350° F) after exposure to 322 K (120° F)/95% R. H. 1000 hrs	17.6 (2550)	64.9 (2.55)	–
Ambient after exposure to Skydrol at ambient stressed to 25% of ultimate	28.2 (4090)	–	–
450 K (350° F) after exposure to to Skydrol at ambient stressed to 25% of ultimate 1000 hrs		–	–
450 K (350° F) after exposure to 450 K (350° F) in air 1000 hours 3000 hours	24.6 (3570) 20.6 (2980)	25.7 (1.01) 25.9 (1.02)	– –
505 K (450° F) after exposure to 505 K (450° F) in air 1000 hours 3000 hours	13.4 (1950) 4.7 (680) 2/	28.1 (1.11) 44.2 (1.74)	– –
450 K (350° F) stressed to determine creep resistance	N		
505 K (450° F) stressed to determine creep resistance	F		

1/ Crack length measured after 1000 hours exposure.
2/ 2 specimens failed prematurely.

F — Failed at 2832 hours.
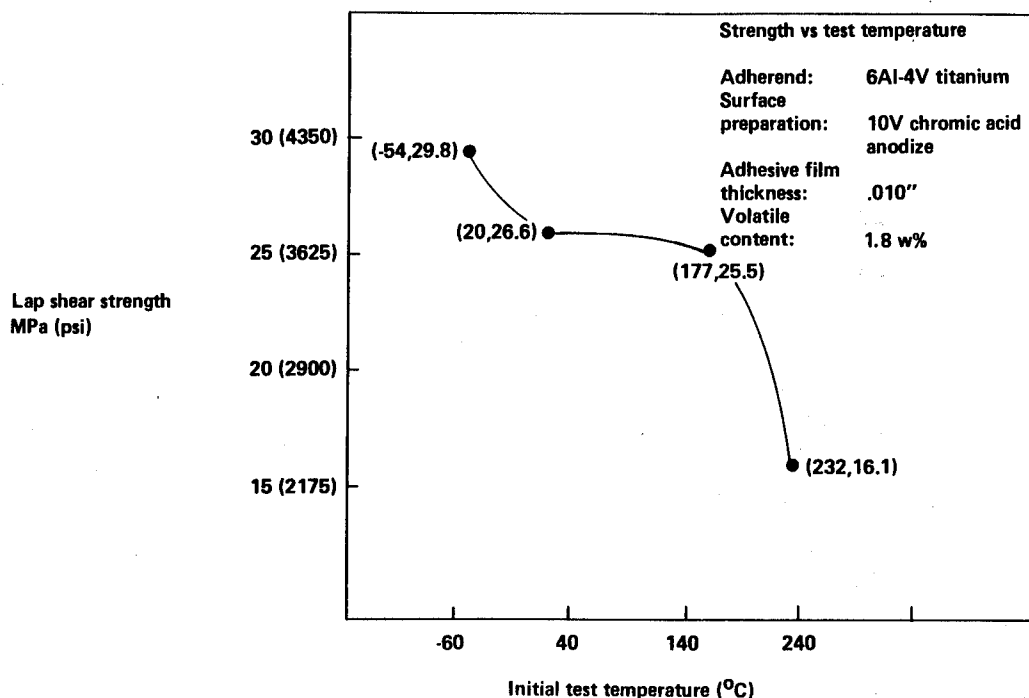N — No creep recorded at 3000 hours.

Data Summary (X-PQ)

Examination of the data generated for the X-PQ adhesive supplied by NASA Langley reveals the following trends:

. Shear-strength and toughness decrease with increasing temperature.
. After 1000 hours humidity exposure, shear strength, peel strength, and toughness all decrease.
. . X-PQ adhesive lap shear strength is very stable in Skydrol.
. X-PQ has excellent retention of shear strength and toughness after long-term exposure (3000 hours) at 177°C in both stressed and unstressed conditions.
. X-PQ has substantial degradation of shear strength and toughness after long-term exposure (3000 hours) at 232°C, especially the specimens stressed at 25% of ultimate strength.

X-PQ Adhesive

Strength vs test temperature

Adherend:	6Al-4V titanium
Surface preparation:	10V chromic acid anodize
Adhesive film thickness:	.010"
Volatile content:	1.8 w%

Lap shear strength MPa (psi)

Data points: (-54,29.8), (20,26.6), (177,25.5), (232,16.1)

Y-axis: 30 (4350), 25 (3625), 20 (2900), 15 (2175)

X-axis: Initial test temperature (°C): -60, 40, 140, 240

Lap Shear Strength Versus Temperature (X-PQ)

As expected, the lap shear strength of the X-PQ adhesive decreases with increasing temperature. At 177°C, the test specimens retained 96% of the room temperature properties. However, at 232°C, the room temperature retention was only 60%. Improvements in the lap shear strength at temperature could probably be achieved by reducing the volatile content and post-curing the test specimens.

X-PQ Adhesive Strength at 177 °C
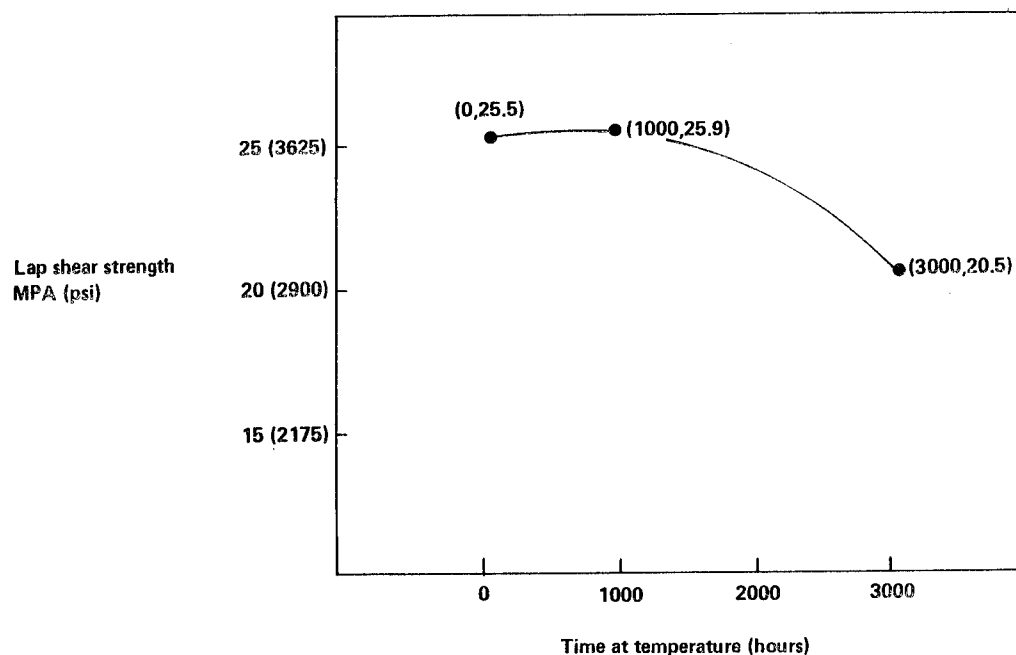
Lap Shear Strength Versus Exposure Time at 177°C (X-PQ)

The excellent thermo-oxidative stability of X-PQ at 177°C is apparent from this figure. Exposure for a period of 3000 hours resulted in only a 20% decrease in lap shear strength.

Data Summary for PPQ-2501 Adhesive

Test Condition	Lap Shear MPa (psi)	Crack Extension mm (inches)	Climbing drum peel, N-M (in/lb)
Ambient (68° F) Initial	21.1 (3060)	22.8 (0.90) 28.1 (1.11) 1/	0.6 (5.1)
219 K (-67° F) Initial	25.2 (3650)	—	—
450 K (350° F) Initial	20.0 (2900)	25.4 (1.00)	0.2 (2.0)
505 K (450° F) Initial	8.1 (1180)	29.0 (1.14)	—
Ambient after exposure to 322 K (120° F)/95% R. H. 1000 hrs	16.9 (2450)	36.6 (1.44)	0.4 (3.2)
450 K (350° F) after exposure to 322 K (120° F)/95% R. H. 1000 hrs	15.3 (2220)	40.9 (1.66)	—
Ambient after exposure to Skydrol at ambient stressed to 25% of ultimate	F	—	—
450 K (350° F) after exposure to to Skydrol at ambient stressed to 25% of ultimate 1000 hrs	F	—	—
450 K (350° F) after exposure to 450 K (350° F) in air 1000 hours 3000 hours	 21.2 (3080) 24.1 (3490)	 30.5 (1.20) 30.5 (1.20)	 — —
505 K (450° F) after exposure to 505 K (450° F) in air 1000 hours 3000 hours	 15.6 (2260) 13.4 (1950)	 39.1 (1.54) 39.1 (1.54)	 — —
450 K (350° F) stressed to determine creep resistance	N		
505 K (450° F) stressed to determine creep resistance	F		

1/ Crack length measured after 1000 hours exposure
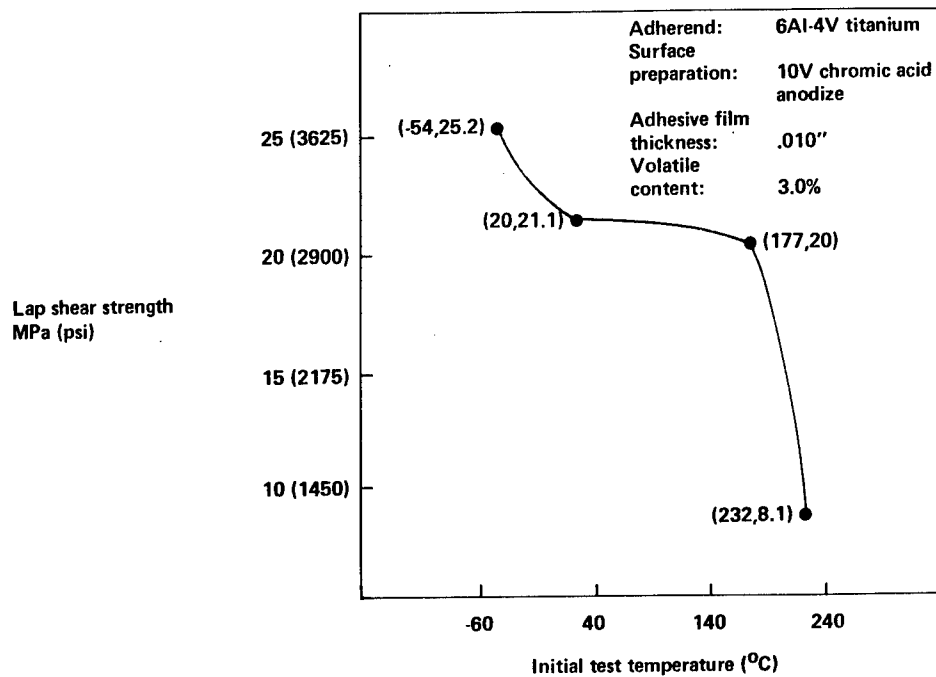
F — Specimens failed after 120 hour exposure
N — No creep recorded at 3000 hours

Data Summary (PPQ-2501)

The following observations can be made from the data generated from King Mar Laboratories PPQ-2501:

- A decrease in shear strength and toughness generally with increasing temperature
- A noticeable decrease in shear strength and toughness after humidity exposure
- Premature lap shear specimen failure in stressed Skydrol condition, suggesting a sensitivity to this fluid
- Increased shear strength after 1000 hour exposure at both 177°C and 232°C exposure temperatures, possibly indicating the need for additional post-cure

PPQ-2501 Adhesive Strength vs Test Temperature

Adherend: 6Al-4V titanium
Surface preparation: 10V chromic acid anodize
Adhesive film thickness: .010"
Volatile content: 3.0%

Lap shear strength MPa (psi)

25 (3625) — (-54,25.2)
20 (2900) — (20,21.1) · (177,20)
15 (2175)
10 (1450) — (232,8.1)

-60   40   140   240

Initial test temperature (°C)

Lap Shear Strength Versus Temperature (PPQ-2501)

As expected the lap shear strength of the PPQ-2501 adhesive decreases with increasing temperature. At 177°C, the test specimens retained 95% of their room temperature properties. And at 232°C, retention was 38%. Additional data indicate that these properties could be improved by post-curing the test specimens.

Data Summary for PPQ-HC Adhesive

Test Condition	Lap Shear MPa (psi)	Crack Extension mm (inches)	Climbing drum peel, N-M (in/lb)
Ambient (68° F) Initial	22.8 (3300)	21.8 (.86) 26.1 (1.03) 1/	1.4 (12.5)
219 K (-67° F) Initial	25.1 (3640)	—	—
450 K (350° F) Initial	19.4 (2820)	23.1 (.91)	1.9 (17.0)
505 K (450° F) Initial	12.3 (1790)	22.1 (.87)	—
Ambient after exposure to 322 K (120° F)/95% R. H. 1000 hrs	21.9 (3170)	31.8 (1.25)	1.9 (16.6)
450 K (350° F) after exposure to 322 K (120° F)/95% R. H. 1000 hrs	8.8 (1280)	36.8 (1.45)	—
Ambient after exposure to Skydrol at ambient stressed to 25% of ultimate	12.8 (1860)	—	—
450 K (350° F) after exposure to to Skydrol at ambient stressed to 25% of ultimate 1000 hrs	1.4 (210) 2/	—	—
450 K (350° F) after exposure to 450 K (350° F) in air 1000 hours 3000 hours	29.7 (4300) 25.3 (3670)	27.4 (1.08) 31.5 (1.24)	— —
505 K (450° F) after exposure to 505 K (450° F) in air 1000 hours 3000 hours	13.9 (2020) 14.6 (2110)	32.5 (1.28) 32.6 (1.29)	— —
450 K (350° F) stressed to determine creep resistance	N		
505 K (450° F) stressed to determine creep resistance	F		

1/ Crack length measured after 1000 hours exposure.
2/ Premature failure of 2 specimens.

F — Specimens failed after 120 hour exposure.
N — No creep recorded at 3000 hours.

Data Summary (PPQ-HC)

Examination of the data generated for PPQ-HC supplied by Hunt Chemical indicates the following trends:

- The shear strength decreases with increasing temperature; however, the crack extension values (toughness) remain stable over the same temperature range
- After a 1000-hour humidity exposure, shear strength and toughness both decrease
- Stressed exposure in Skydrol results in a substantial decrease in shear strength
- An increased shear strength after 1000 hour exposure at 177°C and 232°C conditions is seen, possibly indicating the need for additional post-cure
- The premature failure of all test specimens at the stressed 232°C condition indicates some potential thermal stability problems
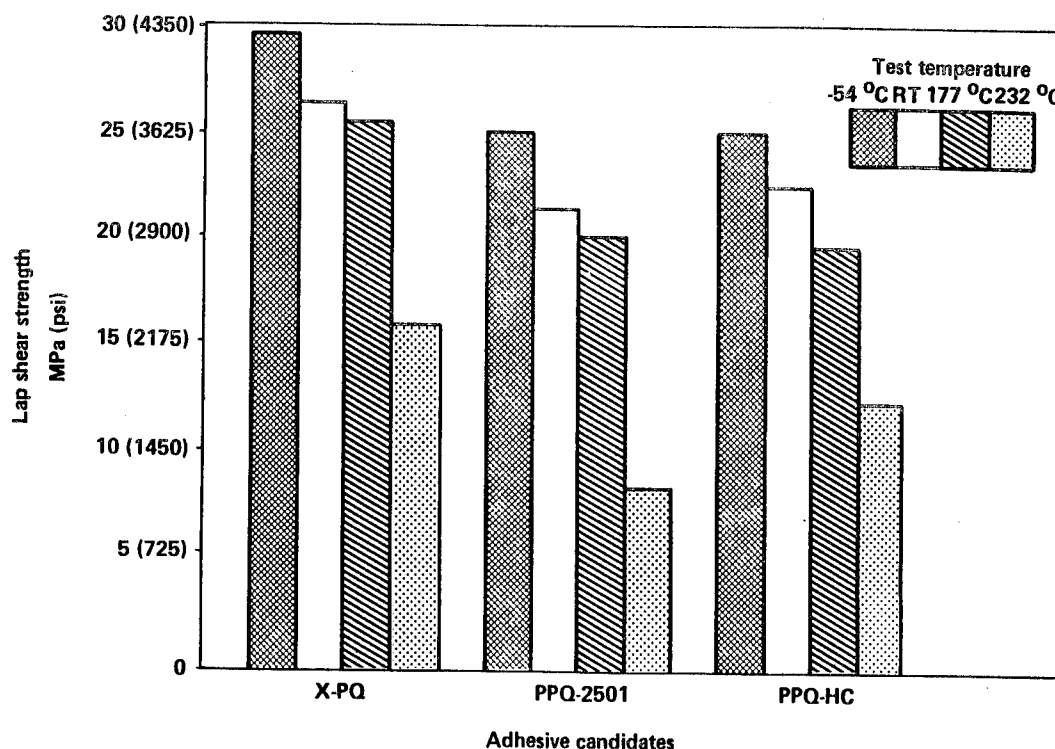
PPQ-HC Adhesive Strength vs Test Temperature
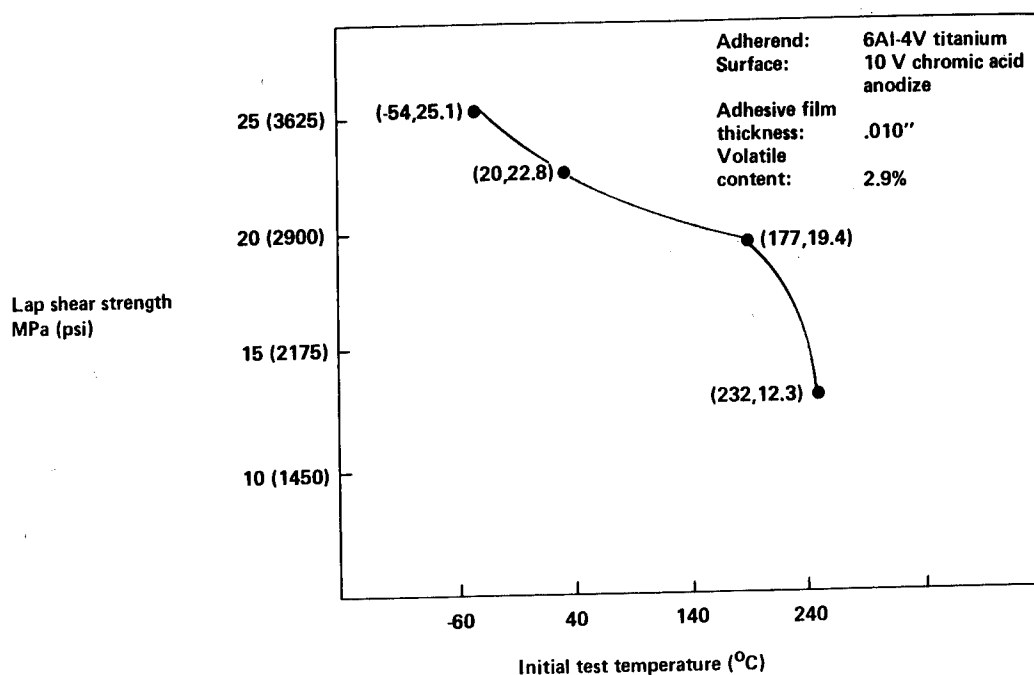
Lap Shear Strength Versus Temperature (PPQ-HC)

As found with the other PPQ candidates, a general decrease in shear strength is observed with increasing test temperature. Retention of room temperature properties at 177°C and 232°C was 85% and 54% respectively.
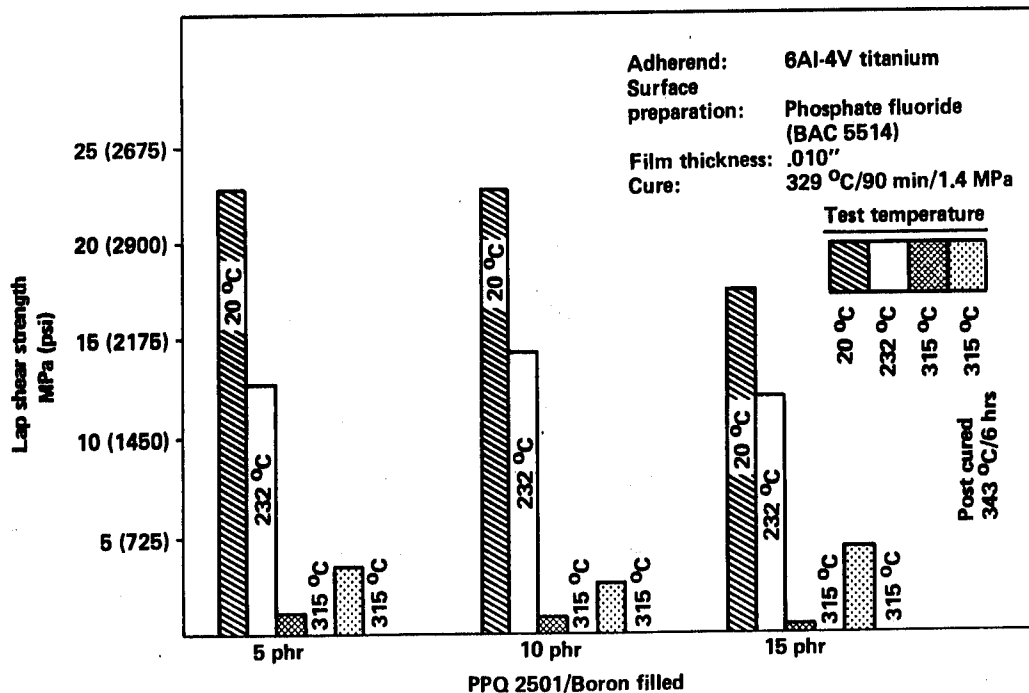
Comparison of Initial Lap Shear Data

Comparison of Initial Lap Shear Data

The best overall lap shear strength properties are clearly exhibited by X-PQ. However, conclusions should not be drawn based solely on lap shear data. To select an adhesive for high-temperature/high-performance applications, careful consideration must be given to all available data.

PPQ-2501/Boron Filled System

Adherend: 6Al-4V titanium
Surface preparation: Phosphate fluoride (BAC 5514)
Film thickness: .010"
Cure: 329 °C/90 min/1.4 MPa

Lap shear strength MPa (psi)

25 (2675)
20 (2900)
15 (2175)
10 (1450)
5 (725)

5 phr   10 phr   15 phr

PPQ 2501/Boron filled

Boron-Filled PPQ-2501 System

To improve the high-temperature performance (above 232°C) of the PPQ adhesive systems, additional studies were conducted by formulating adhesive films with an amorphous boron filler and utilizing a phosphate fluoride surface preparation for titanium. Previous work (Ref. 2) conducted by Boeing Aerospace has shown that the chromic acid anodize surface preparation can produce adhesive failure when exposed to temperatures above 700°F.

The boron filler improves bond strengths probably through improvement of the differential coefficient of thermal expansion between the titanium and the adhesive layers, and an improvement in the thermo-oxidative stability of the adhesive.

Analysis of the room temperature and 232°C data shows a general improvement in shear strength at all filler loading levels, except 15 phr (room temperature). Additional testing done at 315°C indicates only a 10% to 20% retention of room temperature properties.

Polyimide Processing Parameters

Adherend: 15-5 PH stainless steel

Surface preparation: Sulfuric acid anodize

Adhesive cure schedule:

FM-35/PMR-15 — 329 °C/1.4 MPa/2 hours/full vacuum

TRW-PFPI — 454 °C/.7MPa/15 minutes/full vacuum
Post-cure 371 °C/6 hours

NR150-B2S6X — 371 °C/1.4 MPa/30 minutes/full vacuum

X-PQ — 329 °C/1.4 MPa/1.5 hours/full vacuum

IP-600 — 260 °C/.7 MPa/2 hours/full vacuum

Polyimide Processing Parameters

For the preliminary analysis of the PI candidates, manufacturers recommendations for processing were followed except for FM-35/PMR-15. Previous processing optimization for these two candidates has been completed on an Independent Research and Development Program. The polyimide polymers were supplied as follows:

- FM-35 – Aluminum-filled supported film, primer
- PMR-15 – resin, supported film
- TRW-PFPI – resin, unsupported film
- NR150-B2S6X – resin
- LARC-TPI – resin
- IP-600 – powder

Adhesive film construction was as previously described.

Surface preparation of the stainless-steel adherends included the following process steps:

1. Trichloroethylene Degrease
2. Alkaline Clean
3. Sulfuric Acid Anodize

After surface preparation, the adherends are immediately primed with a dilute polymer solution and then oven dried.

Fabrication of the lap shear test specimens required the assembly of the primed adherends and the adhesive film. All specimens were then vacuum bagged and autoclave cured according to schedule.
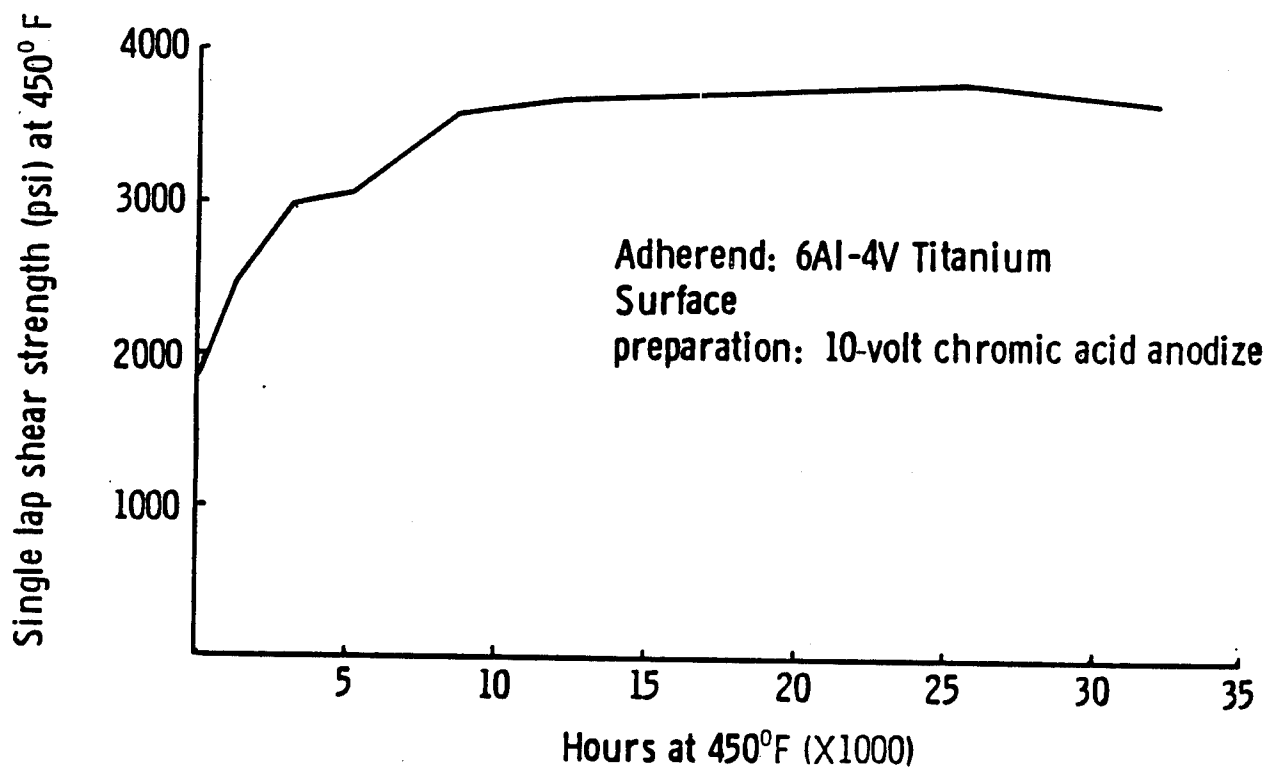
Comparison of Polyimide candidates:
Lap Shear Strength vs Test Temperature
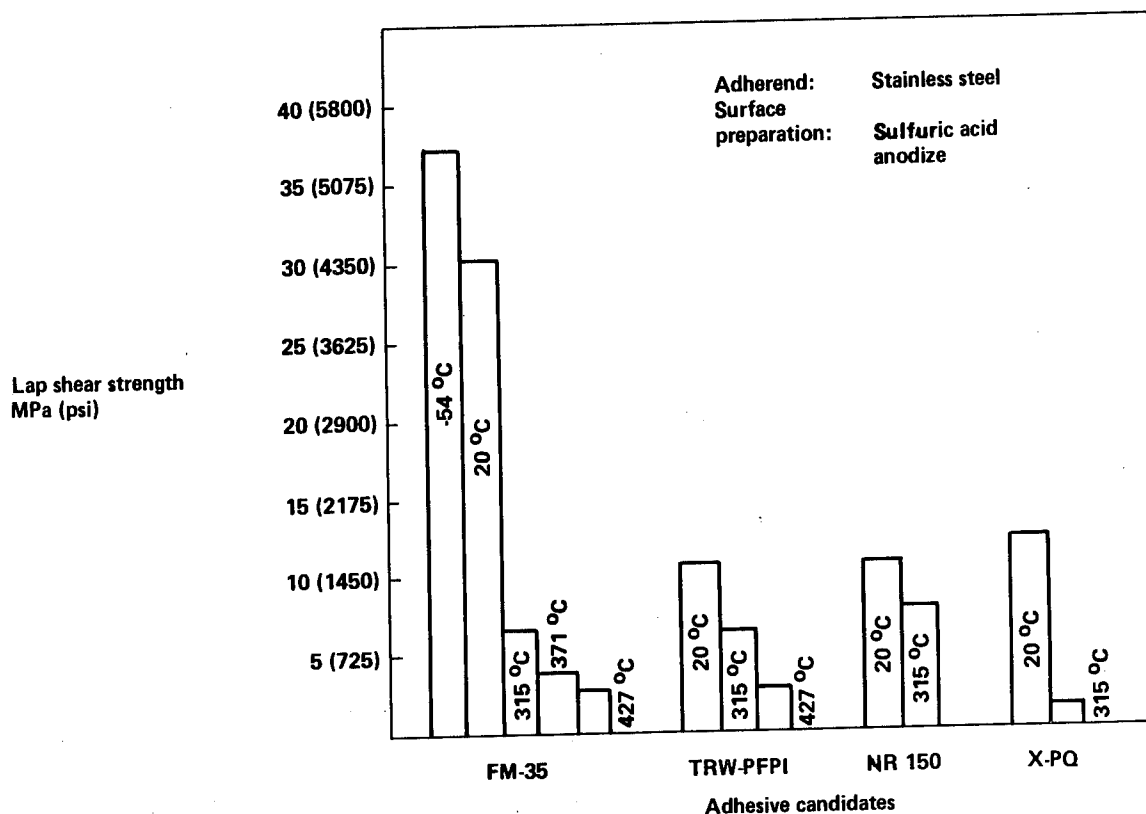
Comparison of Polyimide Candidates

Of the candidates tested, FM-35 exhibits the best overall lap shear strength at room temperature. However, at 315°C the three polyimide candidates (FM-35, TRW-PFPI, NR150) show similar strengths.

LARC-2 Aging Studies

Thermal aging of LARC-2 (TPI) adhesively bonded titanium with a chromic acid anodize surface preparation is shown in this figure. The excellent thermal stability of the LARC-TPI adhesive over 32,000 hours is clearly exhibited.

CONCLUSIONS/RECOMMENDATIONS

Various polymers have been evaluated and tested for potential high-temperature (232°C to 427°C) aerospace vehicle applications.

Three PPQ polymers (X-PQ, PPQ-2501, PPQ-HC) have been evaluated as high-temperature structural adhesives on NASA Contract NAS1-15605. X-PQ exhibits the best overall adhesive properties of the three polymers tested. Although some problems are noted with the bond stability of X-PQ at 232°C (stressed/unstressed exposure), this could be resolved by further optimization of the film processing, surface preparation and post-curing methods.

Significant problems were also noted with the commercially produced PPQ-2501 and PPQ-HC, specifically, with thermo-oxidative stability, solvent and humidity exposure sensitivity. The PPQ polymers appear to be excellent candidates for metal-to-metal adhesive bonding; however, further work is necessary to optimize this adhesive system

Several PI polymers were also evaluated on Boeing Aerospace IR&D Programs. Preliminary testing of these candidates reveals several promising commercially available polymers. These include FM-35, PMR-15, NR150, TRW-PFPI and LARC-TPI. Further evaluation is continuing in the area of large area bonds, dissimilar material bonding and filler loading.

REFERENCES

1. S. G. Hill, P. D. Peters, and C. L. Hendricks, "Evaluation of High-Temperature Structural Adhesives for Extended Service," NASA Contractor Report 165944, July 1982.

2. Boeing Company 1985 IR&D Technical Plan, Document Number D1-8299-3.

USE OF HYDRATION INHIBITORS TO IMPROVE

BOND DURABILITY OF ALUMINUM ADHESIVE

JOINTS*

G.D. Davis, J.S. Ahearn, L.J. Matienzo, J.D. Venables
Martin Marietta Laboratories
Baltimore, Maryland   21227

ABSTRACT

The adsorption of selected organic hydration inhibitors onto Forest Products Laboratory (FPL)-etched aluminum surfaces and the subsequent hydration of the treated surfaces have been studied using X-ray photoelectron spectroscopy (XPS) and surface behavior diagrams (SBD's) supplemented by Fourier Transform Infrared Spectroscopy (FTIR). Wedge tests were used to evaluate performance of these inhibitors in improving bond durability and the locus of failure was identified by XPS and high resolution scanning electron microscopy (X-SEM). The results indicate that nitrilotris methylene phosphonic acid (NTMP) and related compounds adsorb to the alumina surface via the POH bonds of the phosphonic acid groups, resulting in a displacement of water normally adsorbed onto the surface. A model of adsorption was developed which suggests that after treatment with very low concentrations of inhibitor ($\sim$ 1 ppm), only one leg of the NTMP molecule adsorbs onto the surface although at higher concentrations ($\sim$ 100 ppm) all three legs adsorb. Hydration is a three-step process: 1) reversible physisorption of water, 2) slow dissolution of the inhibitor followed by rapid hydration of the freshly exposed Al_2O_3 to boehmite (AlOOH), and 3) further hydration of the AlOOH to bayerite [$Al(OH)_3$]. Analysis of the adsorption, hydration, and wedge test results using different inhibitors suggests the following five inhibitor characteristics that promote good bond performance: 1) displacement of water and occupation of all active sites on the Al_2O_3 surface, 2) formation of strong inhibitor surface bonds, 3) insolubility of the resulting inhibitor-aluminum complex in aqueous solutions, 4) compatibility with the adhesive or primer, and 5) coupling of the inhibitor to the adhesive.

1. Introduction

The performance of adhesively bonded aluminum structures is judged primarily by the initial bond strength and the long-term durability of the bond. The high initial bond strength provided by commercial aerospace bonding processes[1,2] is a consequence of the microscopically rough aluminum oxide formed during the etching or anodization treatment. When polymeric adhesive is added, it penetrates the oxide pores and surrounds the oxide whiskers, resulting in a physical interlocking that ensures a much stronger bond than that possible with a smooth oxide surface.[3,4]

The oxide morphology also partially governs long-term bond durability in moist environments in that the mechanical interlocking of an adhesive and a rough aluminum oxide can maintain high bond strength even if their chemical interaction between the oxide and polymer is diminished. In this case, a crack propagates only if interlocking is destroyed or failure occurs cohesively in that adhesive. In previous work crack propagation occured as the aluminum oxide hydrated to the oxyhydroxide, boehmite, allowing failure either at the boehmite-metal or boehmite-adhesive interface prior to a cohesive failure in the adhesive, the ultimate performance limit of an adhesive bond.[5-7]

These findings have prompted investigations of methods to inhibit the oxide-to-hydroxide conversion process and thereby to improve the long-term durability of adhesively bonded aluminum structures. One such procedure is to treat a Forest Products Laboratory (FPL) sodium dichromate/sulfuric-acid-etched adherend with certain organic acids (amino phosphonates).[8] With a saturation inhibitor coverage of approximately one monolayer, these surfaces exhibit a much higher resistance to hydration (up to two orders of magnitude) than untreated FPL surfaces and have a corresponding increase in long-term bond durability.[9]

In previous studies,[6,7,9,10] we have examined the mechanical properties of adhesive bonds formed with FPL and phosphoric-acid-anodized (PAA) adherends treated with hydration inhibitors, particularly nitrilotris methylene phosphonic acid (NTMP, $N[CH_2P(O)(OH)_2]_3$). We showed that: 1) NTMP-treated FPL bonds and PAA bonds exhibited similar long-term durability 2) the durability of NTMP-treated PAA bonds was better than that of untreated PAA bonds and 3) an inhibitor's effectiveness depended both on its ability to inhibit the oxide-to-hydroxide conversion and on its compatibility with the adhesive.

In this paper, we address the following issues: Why do inhibited aluminum oxide surfaces eventually hydrate? What causes failure of bonds made from inhibited adherends? What properties of an inhibitor are important in achieving good bond durability? To answer these questions we used X-ray photoelectron spectroscopy (XPS), supplemented with Fourier-Transform Infrared Spectroscopy (FTIR), to examine both the adsorption of NTMP and similar inhibitors onto FPL-prepared adherends and the hydration behavior of the inhibited surfaces. Using the model for hydration thus developed, we modified the inhibitor molecule and performed wedge tests using

adherends treated with these modified inhibitors. Based on the relative performances of the wedge-tested bonds and on a failure analysis of the aluminum panels, we have identified five important characteristics determining the effectiveness of inhibitors in improving bond durability.

2. Experimental Procedure

2.1. Surface Preparation

Test coupons and panels of bare 2024 Al were degreased by a 15-min immersion in an agitated solution of Turco 4215* (44 g/1) at 65°C and then rinsed in distilled, deionized water. Degreasing was followed by a standard FPL treatment,[1] consisting of a 15-min immersion in an agitated aqueous solution of sodium dichromate dihydrate (60 g/1) and sulfuric acid (17% v/v) held at 65°C, after which samples were rinsed in distilled, deionized water and air dried. Some FPL-treated panels were then treated using the PAA process.[2] These panels were anodized in a 10%(w/w) phosphoric acid solution at a potential of 10 V for 20 min, rinsed in distilled, deionized water, and air dried.

The coupons were immersed for 30 min in a dilute aqueous solution of the inhibitor held at room temperature. Solution concentrations ranged from 0.1 to 500 ppm for the adsorption experiments and from 100 to 300 ppm for the hydration studies and wedge tests. In a separate experiment, the time of immersion of FPL surfaces in a 300 ppm NTMP solution was varied from 5 s to 30 min. The samples were then thoroughly rinsed in distilled deionized water, forced-air dried, and stored in a dessicator until analysis.

Samples used in the hydration experiments were suspended vertically in a humidity chamber and exposed to air saturated with water vapor at 50°C. The samples were removed at different intervals, dried with forced air, and also stored in a dessicator.

Panels for wedge tests (6 x 6 x 0.125-in.) were bonded together using American Cyanamid FM 123-2 epoxy adhesive cured at 120°C and 40 psi for 1 h. The bonded panels were cut into 1 x 6-in. test strips and a wedge (0.125-in. thick) was inserted between the two adherends to provide a stress at the bondline. After 1-h equilibration at ambient conditions, the wedge-test samples were placed in a humidity chamber held at 60°C and 98% relative humidity. In order to determine the extent of crack propagation, the test pieces were periodically removed from the humidity chamber and examined under an optical microscope to mark the position of the crack front. When the test was complete, usually after 150 to 160 h, calipers were used to measure the positions of these marks, which determine crack length as a function of time.

---

*An alkaline cleaning agent manufactured by Turco Products.

2.2 Inhibitor Selection and Preparation

Each of the seven compounds shown in Fig. 1 was selected to investigate various aspects of the inhibitor process. NTMP serves as our standard. Ethylene diamine tetramethylene phosphonic acid {EDTMP, $[-CH_2N[CH_2P(O)(OH)_2]_2]^2$} increases the potential bonding sites to the aluminum oxide surface (POH groups) from six to eight. The inhibitor (n-Butyl) nitrilobis methylene phosphonic acid { (n Bu)NBMP: $CH_3(CH_2)_3N[CH_2P(O)(OH)_2]_2$} decreases the potential bonding sites to four, but exposes an extended hydrophobic end for possible micro-mechanical interlocking with the adhesive. The inhibitor (t Butyl) nitrilobis methylene phosphonic acid { (t Bu)NBMP,$(CH_3)_3C-N[CH_2P(O)(OH)_2]_2$} also decreases the potential adsorbate-surface bonds to four, but is expected to expose a bulky hydrophobic end to the adhesive or aqueous environment. The remaining inhibitors -- amino methylene phosphonic acid [AMP, $H_2NCH_2P(O)(OH)_2$,] , methylene phosphonic acid {MP, $CH_3P(O)(OH)_2$} and phosphoric acid [PA, $P(O)(OH)_3$] -- represent smaller sections of the NTMP molecule or, in the case of PA, an analogy to the phosphoric acid anodized (PAA) surface without its more complex morphology.[3]

Four of the inhibitors investigated -- NTMP, AMP, PA, and MP -- are commercially available; the others were synthesized according to the methods of Plaza.[11] Melting point measurements for these compounds were within the ranges previously reported.[11] Elemental analyses were close to the calculated values; in some cases intermediate products with fewer phosphonic acid groups may also have been present in small amounts.
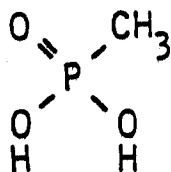
2.3 Surface Analysis

The surface composition of treated coupons was determined by XPS. Measurements were made on a Physical Electronics Model 548 spectrometer, which consists of a double-pass cylindrical mirror analyzer (CMA) with pre-retarding grids and a coaxial electron gun, a Mg anode X-ray source, a rastering 5-keV sputter ion gun, a sample introduction device, and a gas-handling system used to backfill the chamber to 5×10^{-5} Torr Ar. Operating pressure was in the low 10^{-9} Torr range. The XPS measurements were sometimes supplemented by Auger electron spectroscopy (AES) and ion sputtering to obtain an elemental distribution with depth.

Atomic concentrations were determined from high-resolution (50-eV pass energy) XPS spectra of the O1s, Al2p, and P2p peaks.[12] The results were interpreted with the use of surface behavior diagrams (SBD's),[12,13,14] a recently developed method for analyzing quantitative surface-sensitive results. These diagrams resemble ternary or quaternary phase diagrams in that they represent the surface composition as the sum of the compositions of three or four basis compounds. They differ, however, in that they display compositional data rather than structural
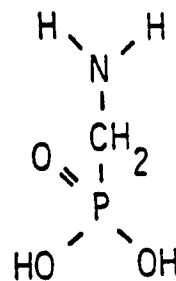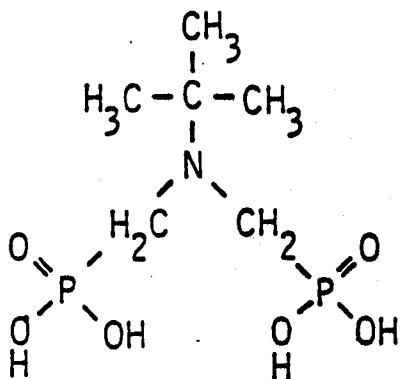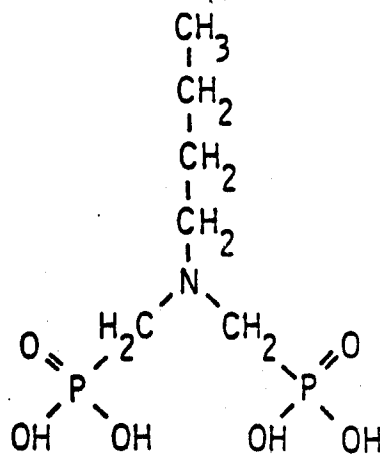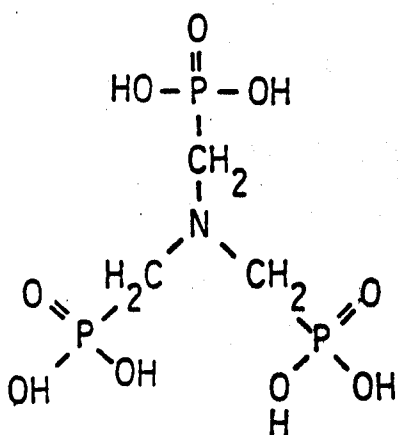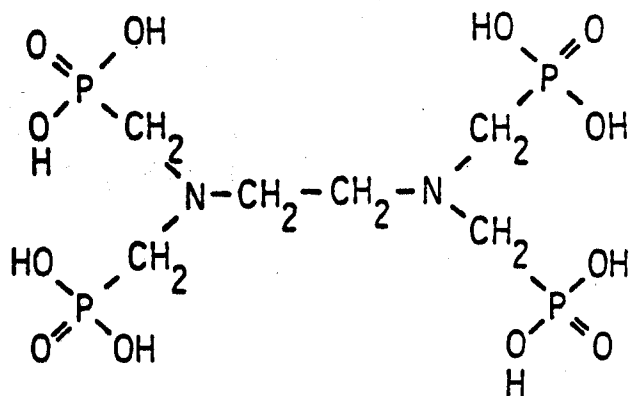
Figure 1. Inhibitors tested: a) denotes compounds commercially available and b) denotes compounds synthesized.

data. In addition, the equilibrium condition is relaxed for SBD's, so that the surface can be described during non-equilibrium processes such as hydration. To this end, the SBD's graphically display the changes in the surface composition as a function of reaction time, solution concentration, anodization voltage, depth in the sample, or other parameters of interest. The measured changes can then be compared to those predicted by various models during analysis of the results.

In this study, the atomic concentrations of O, Al, and P were usually converted to molar concentrations of Al_2O_3, inhibitor, and H_2O using the following assumptions. All the P was assigned to the inhibitor, the Al was assigned to Al_2O_3, and enough O was used to satisfy the inhibitor and Al_2O_3 stoichiometric requirements. Any excess O was assumed to be bonded to H as H_2O. For example, AlOOH has a composition equivalent to $Al_2O_3 + H_2O$ even though it is not a two-phase mixture of these compounds. The molar concentrations were then plotted on the appropriate SBD. In certain cases, the atomic concentrations were also directly plotted onto an Al-P-O SBD.

Additional measurements were obtained from FTIR with a Nicolet 7199 spectrometer using the diffuse reflectance (DRIFT) technique. The samples were mixtures of the material of interest and KBr powder.

In some cases, wedge-test specimens were pulled apart following exposure to high humidity, and the near-crack-tip regions were examined by XPS or ultrahigh resolution scanning electron microscopy (X-SEM) using a JEOL 100CX STEM to determine the locus of failure during the humidity exposure. Prior to examination by X-SEM, the samples were coated with an extremely thin vacuum-evaporated Pt-Pd coating to reduce charging, but without obscuring the fine structure present on FPL surfaces.[3]

3. Results

3.1. Adsorption

The adsorption of NTMP on FPL surfaces was studied as a function of solution concentration and immersion time. The dependence of the surface coverage and composition on solution concentration is shown in the adsorption isotherm (Fig. 2) and in the Al_2O_3-NTMP-H_2O surface behavior diagram (Fig. 3). In the SBD, the solution concentration increases from left to right. The approximately horizontal position of the curve corresponds to the saturation coverage of P/Al $\approx$ 0.15 observed in Fig. 2. The adsorption process can be described as the displacement by NTMP of water or hydroxyl groups initially bound to the aluminum oxide surface. If the water were not removed during adsorption, the surface composition would evolve along a path directly toward the inhibitor.
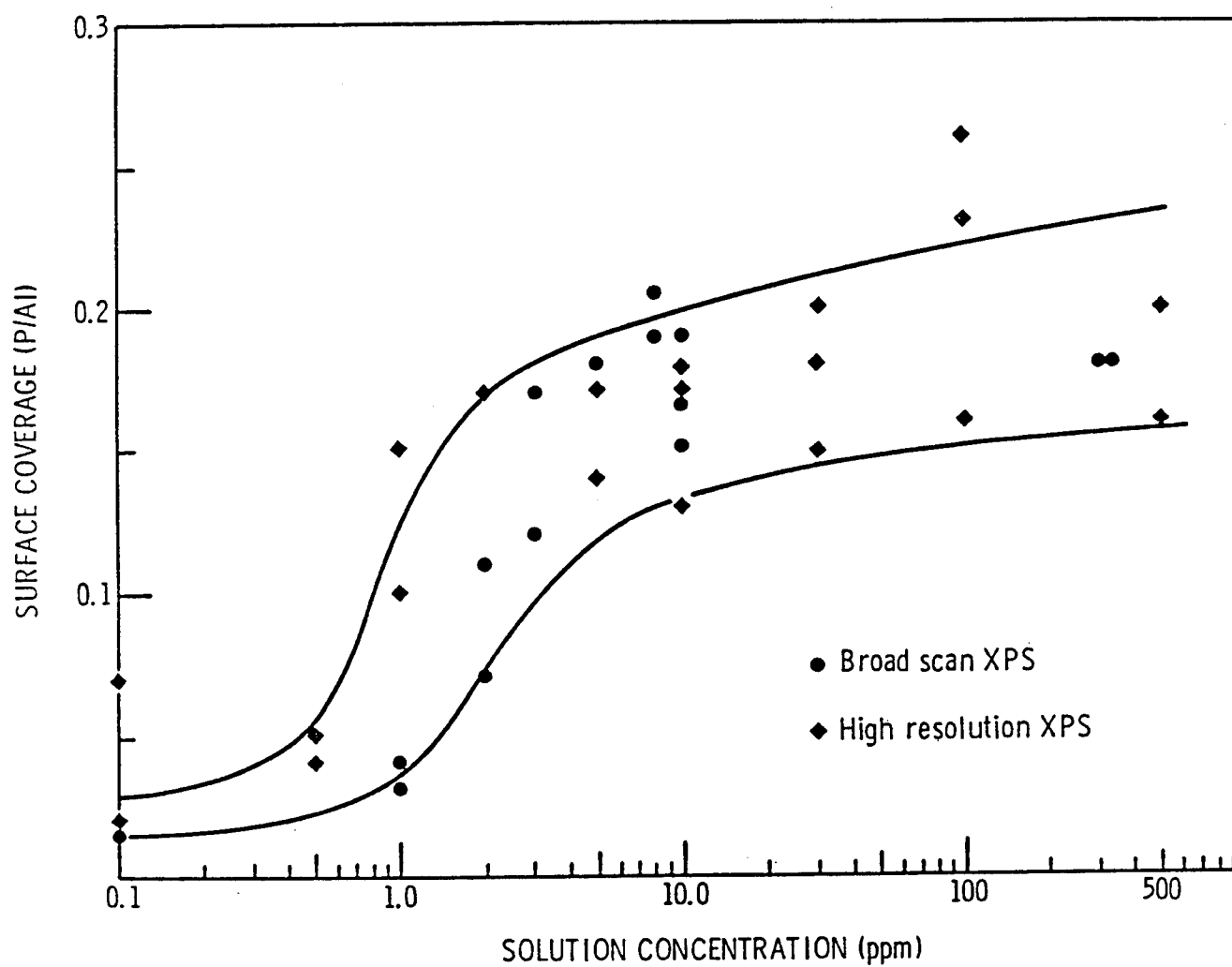
Figure 2. NTMP coverage (P/Al) of FPL-etched surfaces as a function of solution concentration.
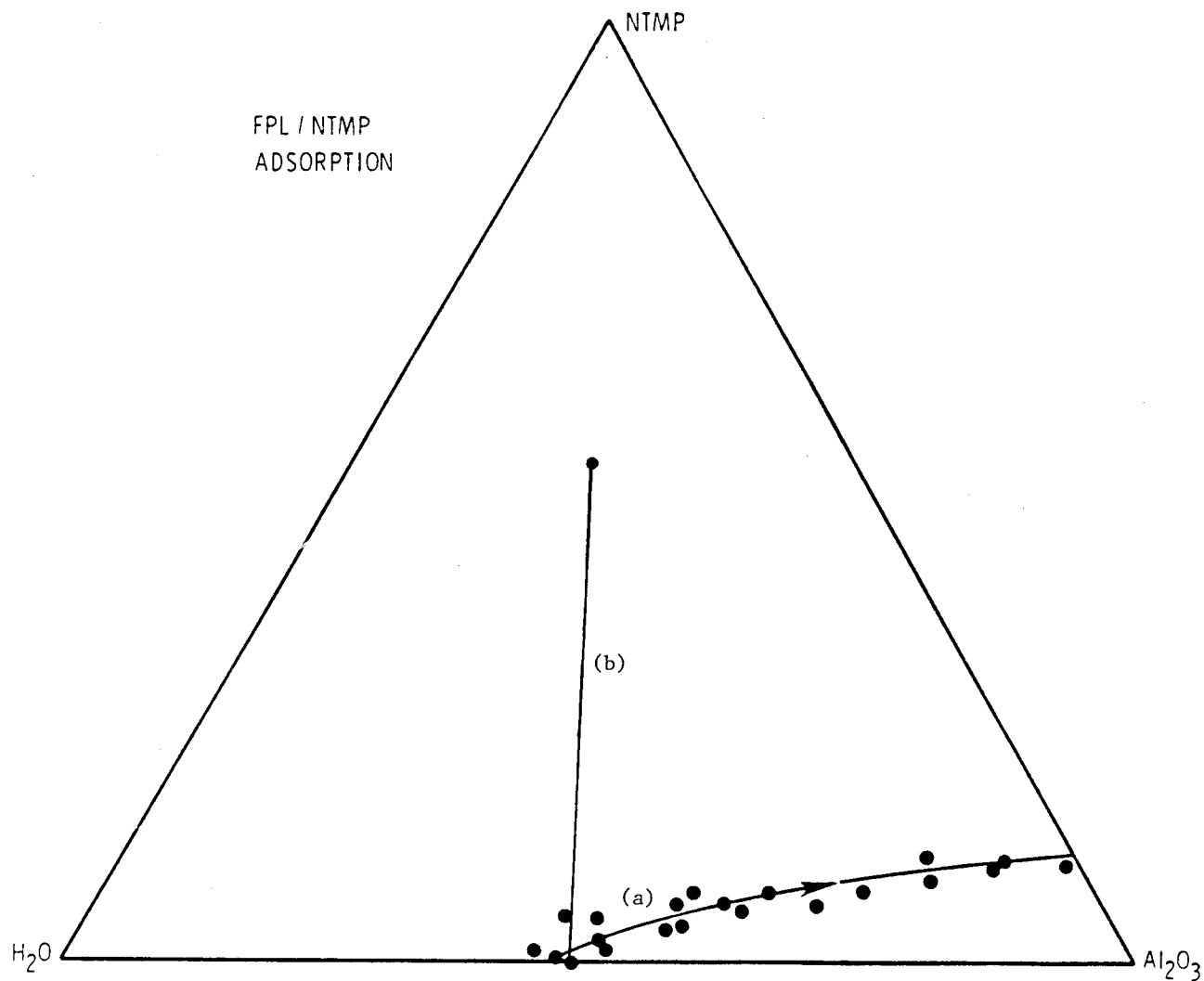
Figure 3. Al_2O_3-NTMP-H_2O SBD showing a) surface composition of FPL-etched surfaces after 30-min immersion in aqueous solutions of NTMP at concentrations ranging from 0.1 to 500 ppm, solution concentration increases from left to right; and b) path representing no displacement of water.

NTMP saturation coverage on FPL surfaces is rapidly achieved on immersion. Figure 4 indicates that the NTMP layer grows to monolayer thickness in less than 5 s and remains at this level even after a 30-min (1800 s) immersion.

Similar adsorption studies on the effect of solution concentration were done for AMP and (n Bu)NBMP on FPL. The adsorption of the two inhibitors (Figs. 5 and 6) are qualitatively similar to that of NTMP on FPL, i.e., a displacement reaction of the inhibitor in exchange for adsorbed water. Subtle differences between the NTMP and AMP adsorption behavior, which are reflected in the different evolutionary paths in the Al-P-O elemental SBD shown in Fig. 7, will be discussed later.

The FTIR spectrum of solid NTMP is shown in Fig. 8a, and the assignments of the various peak absorbances are given in Table 1. Because of

Table 1

FTIR Band Assignments

	Wave numbers (cm^{-1})	
Assignment	NTMP	Al-NTMP
OH	3500–2800	3500–2800
NH^+	3020	3026
OH	1653	1646
CH_2	1435	1434
P=O	1188–970	1160
Al-O		956
PO_3^{2-}	808–723	
P-O-Al		751

the high degree of symmetry in the molecule, the infrared spectrum is very weak and is comprised of broad bands. Analysis of the FTIR results and determination of the bonding between NTMP and the aluminum surface were facilitated by studying the DRIFT spectrum of an Al-NTMP complex formed by reacting $Al(NO_3)_3$ with NTMP in a 2:1 molar ratio[15] (Fig. 8b and Table 1). Significant changes in the P=O and P-O bonds (1200–700 cm^{-1}) are evident. The formation of an Al-O-P bond is indicated by the band at 956 cm^{-1} as well as by the shift to lower wave numbers of the PO_3^{2-} group. Additional evidence is seen in that the P=O bond for Al-NTMP is much sharper than that for NTMP, indicating a decrease of symmetry on the PO_3^{2-} group. By analogy, we can conclude that the NTMP molecule adsorbs to the aluminum oxide surface via the initially present P-OH groups of the phosphonic acid.
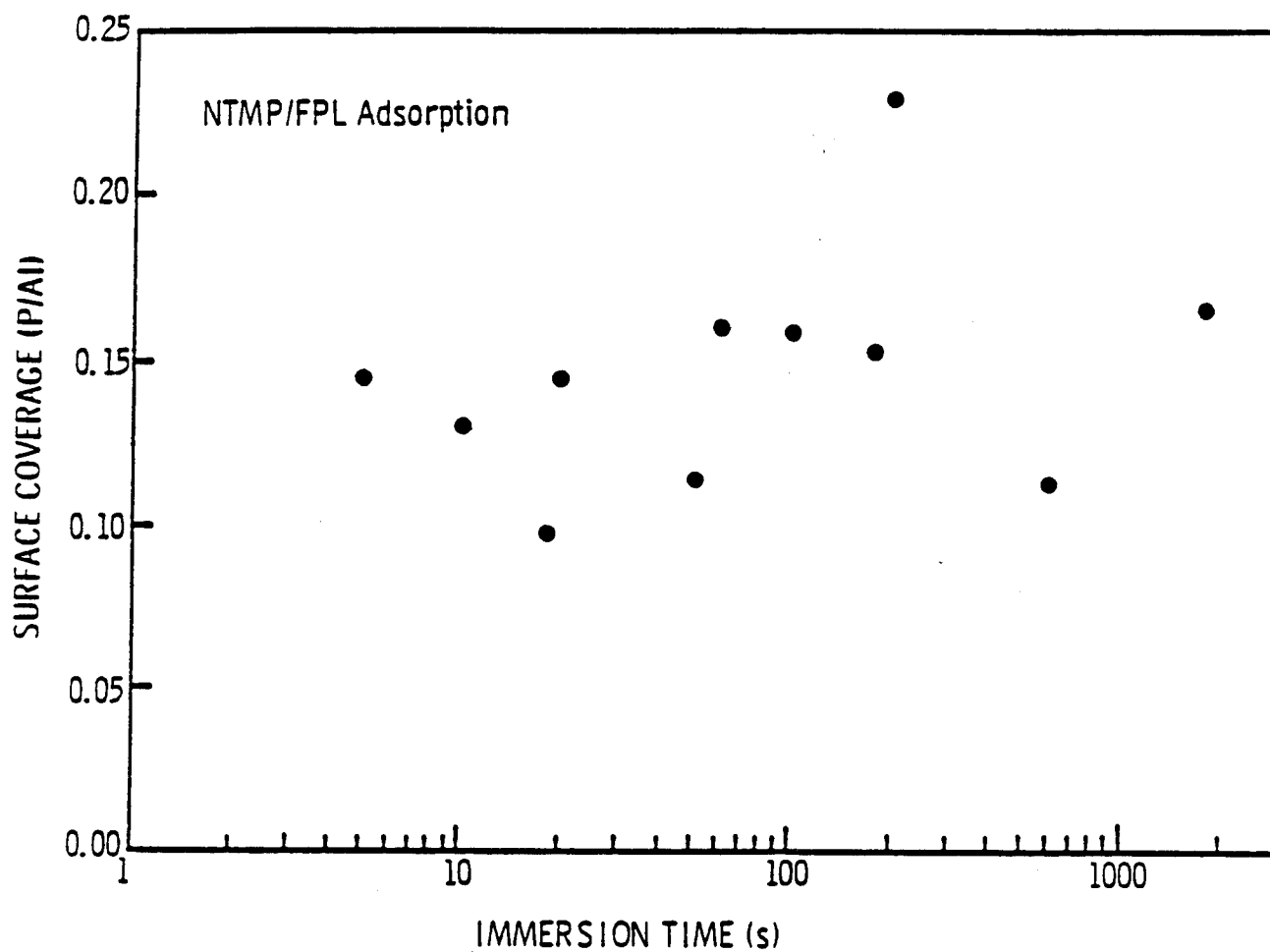
Figure 4. NTMP coverage (P/Al) of FPL-etched surfaces as a function of immersion time in a 300-ppm NTMP solution.
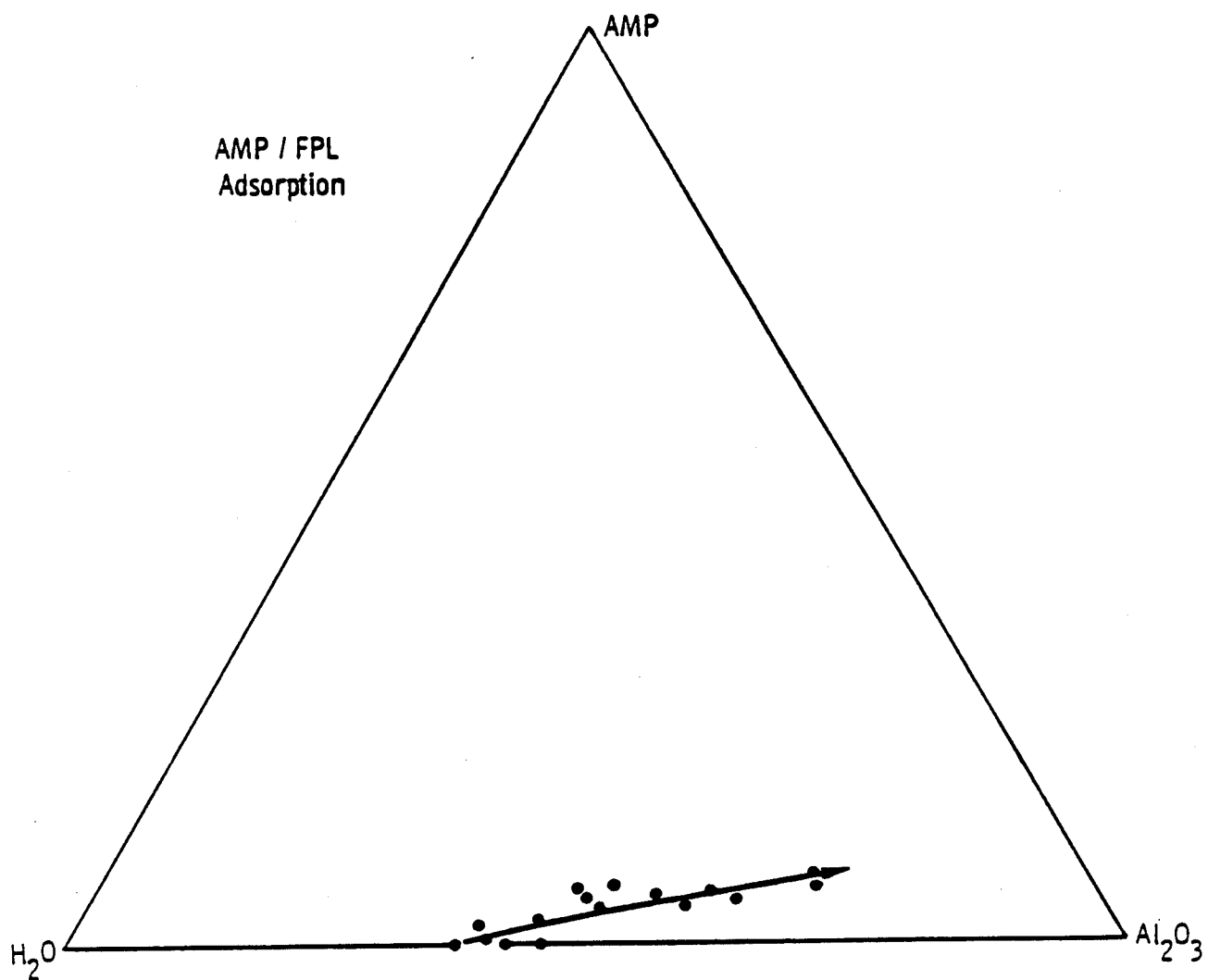
Figure 5. Al$_2$O$_3$-AMP-H$_2$O SBD showing the surface composition of FPL-etched surfaces after immersion in solutions of AMP at concentrations of 1 to 300 ppm.
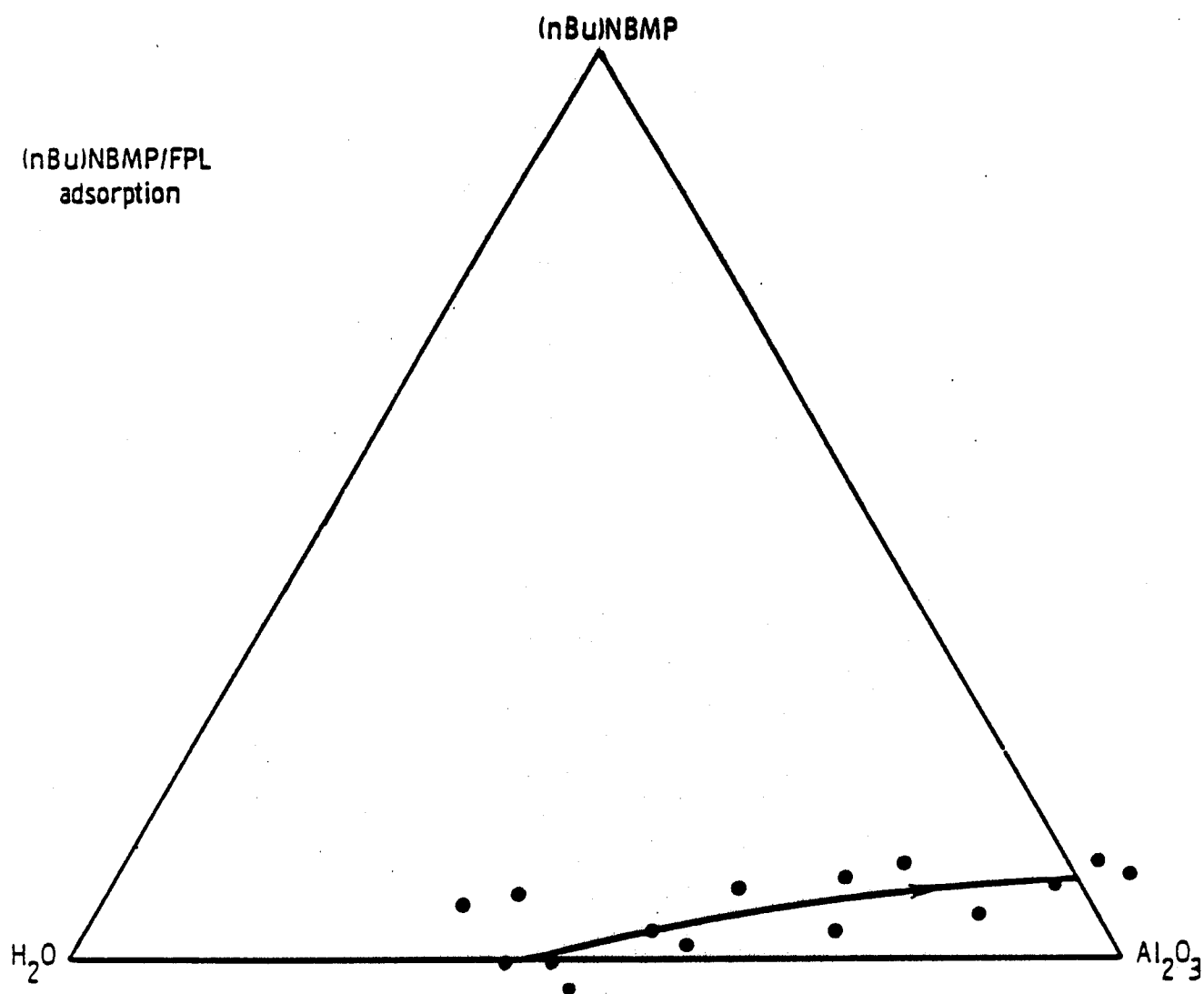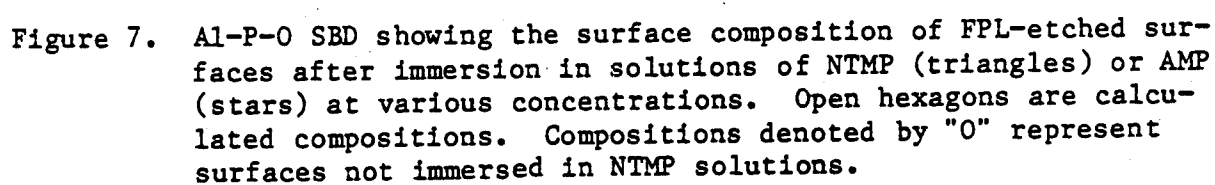
Figure 6. Al_2O_3-(n Bu)NBMP-H_2O SBD showing the surface composition of FPL-etched surfaces after immersion in solution of (n Bu)NBMP at concentrations of 1 to 300 ppm.

Figure 7. Al-P-O SBD showing the surface composition of FPL-etched surfaces after immersion in solutions of NTMP (triangles) or AMP (stars) at various concentrations. Open hexagons are calculated compositions. Compositions denoted by "0" represent surfaces not immersed in NTMP solutions.
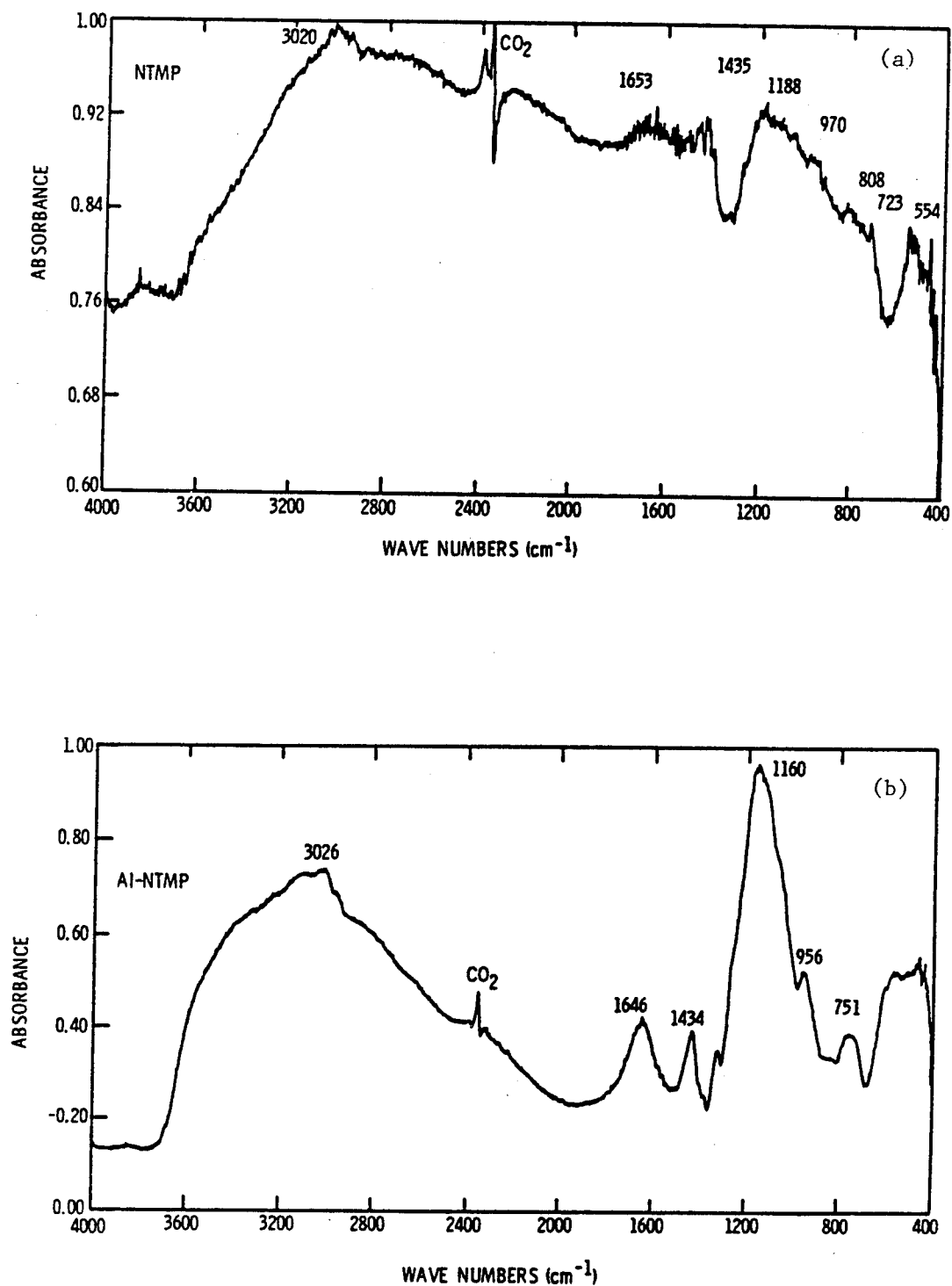
Figure 8. FTIR DRIFT spectrum of: a) dried NTMP and
b) AL-NTMP complex.

3.2. Hydration

The hydration of NTMP-treated FPL surfaces in 100% relative humidity at 50°C has also been investigated using XPS and SBD's. As shown in Fig. 9, the hydration path proceeds from an NTMP-covered Al_2O_3 surface to a boehmite [AlOOH] surface (line "a") and then to one of bayerite [$Al(OH)_3$]. Variation in this data is caused by physisorbed water,[12,14] represented by line "b", which was calculated by the addition of approximately one monolayer of water to surface compositions along line a. Surfaces with compositions along line b lost this physisorbed water after several days exposure to ultrahigh vacuum (UHV), so that their final composition was near line a. Finally, Auger depth profiles of several samples revealed no subsurface concentration of phosphorus for coupons without surface phosphorus.

Similar hydration behavior is also observed for FPL surfaces treated with (n Bu)NBMP. The surface again evolves directly from Al_2O_3 with a monolayer of inhibitor to AlOOH, and then to $Al(OH)_3$.

3.3 Wedge Tests

Wedge tests were performed with FPL adherends treated with NTMP and several variants shown in Fig. 1.

From the results shown in Figs. 10-12, we can classify the inhibitors into three groups: (I) MP and PA, which provide either worse performance or no improvement over the untreated FPL specimens; (II) AMP and (t Bu)NBMP, which provide some improvement over the control; and (III) NTMP, (n Bu)NBMP, and EDTMP, which provide the best performances. In each case, however, the performance is not as good as that limited by the adhesive[7] (Fig. 10).

To determine the locus of failure of the wedge-test specimens, X-SEM micrographs and/or XPS measurements of the near-crack-tip region were obtained for selected samples in each of the three groups. The XPS results are summarized in Table 2. The failure of MP-, PA-, NTMP-, and

Table 2

Surface Composition of Failed Surfaces (at. %)

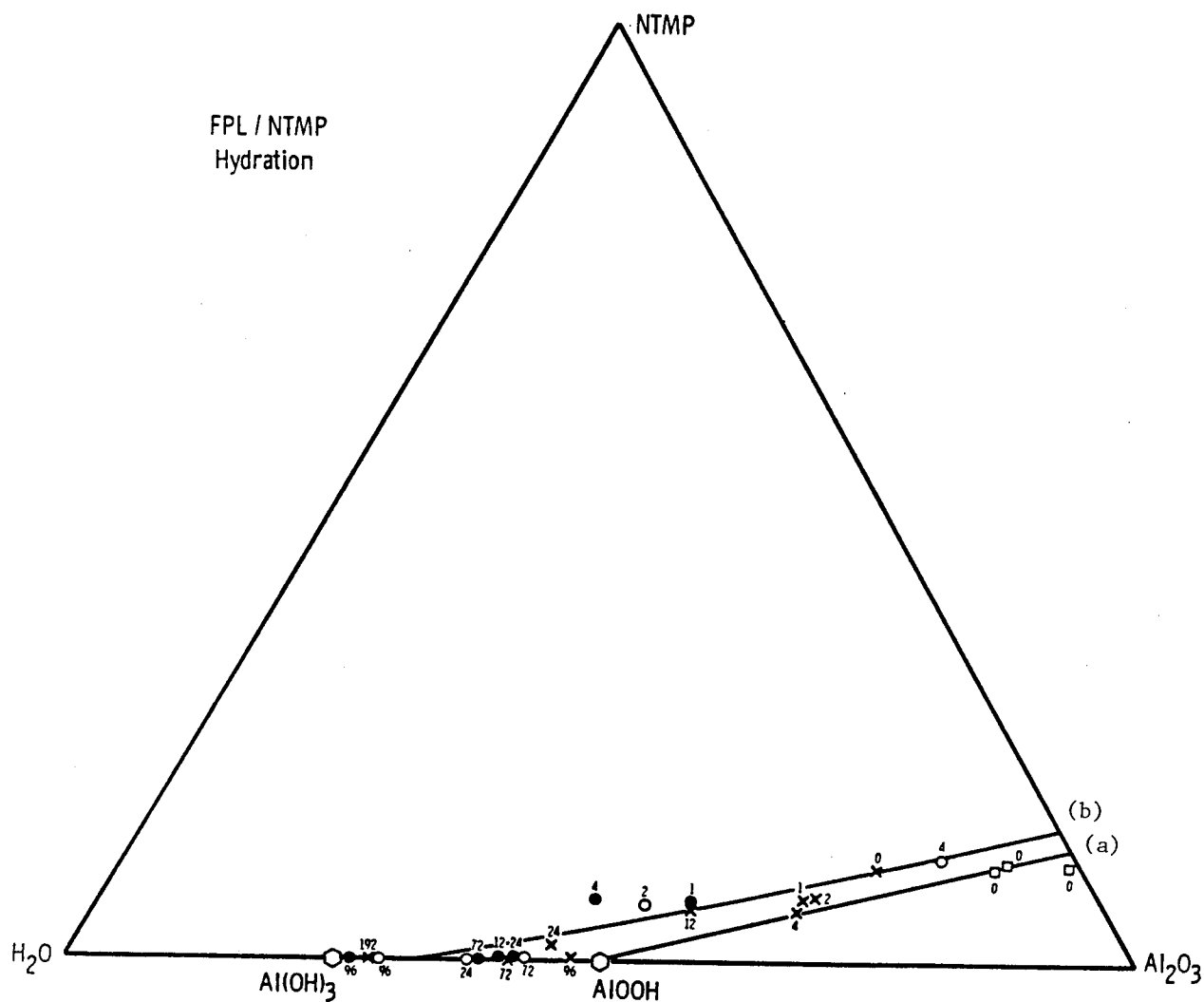| Group	Inhibitor	Al M^a	Al A^b	O M	O A	C M	C A
	Adhesive	—	0	—	8	—	92
	Control	22	24	44	47	34	30
I	MP	20	0	50	21	29	78
I	PA (66 ppm)	25	2	49	25	25	73
II	(t Bu)NBMP	30	29	59	58	10	12
III	NTMP	30	14	56	38	13	47
III	EDTMP	29	19	59	45	12	36
III	(n Bu)NBMP	31	30	56	58	13	11

a metal side
b adhesive side

385

Figure 9. Al_2O_3-NTMP-H_2O SBD showing the evolution of the surface composition of FPL-etched surfaces treated with saturation coverages of NTMP as a function of exposure time in 100% relative humidity at 50°C. The different symbols represent different experimental runs; the numbers are the exposure time (h).
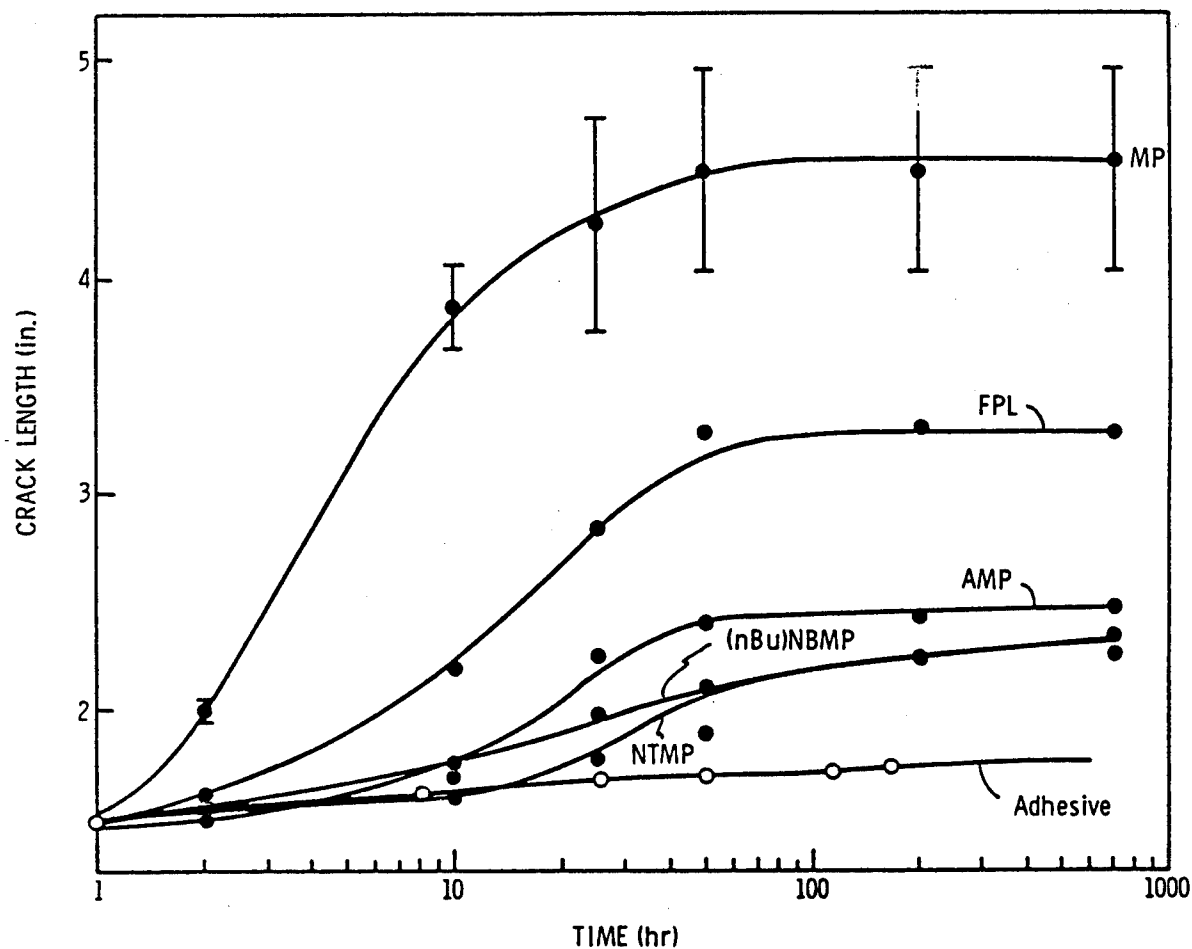
Figure 10. Wedge-test results (crack length as a function of time) for FPL adherends treated in solutions of MP, AMP, (n Bu)NBMP, and NTMP and for untreated FPL adherends. Also shown is the limiting performance of bonds made with FM 123-2.
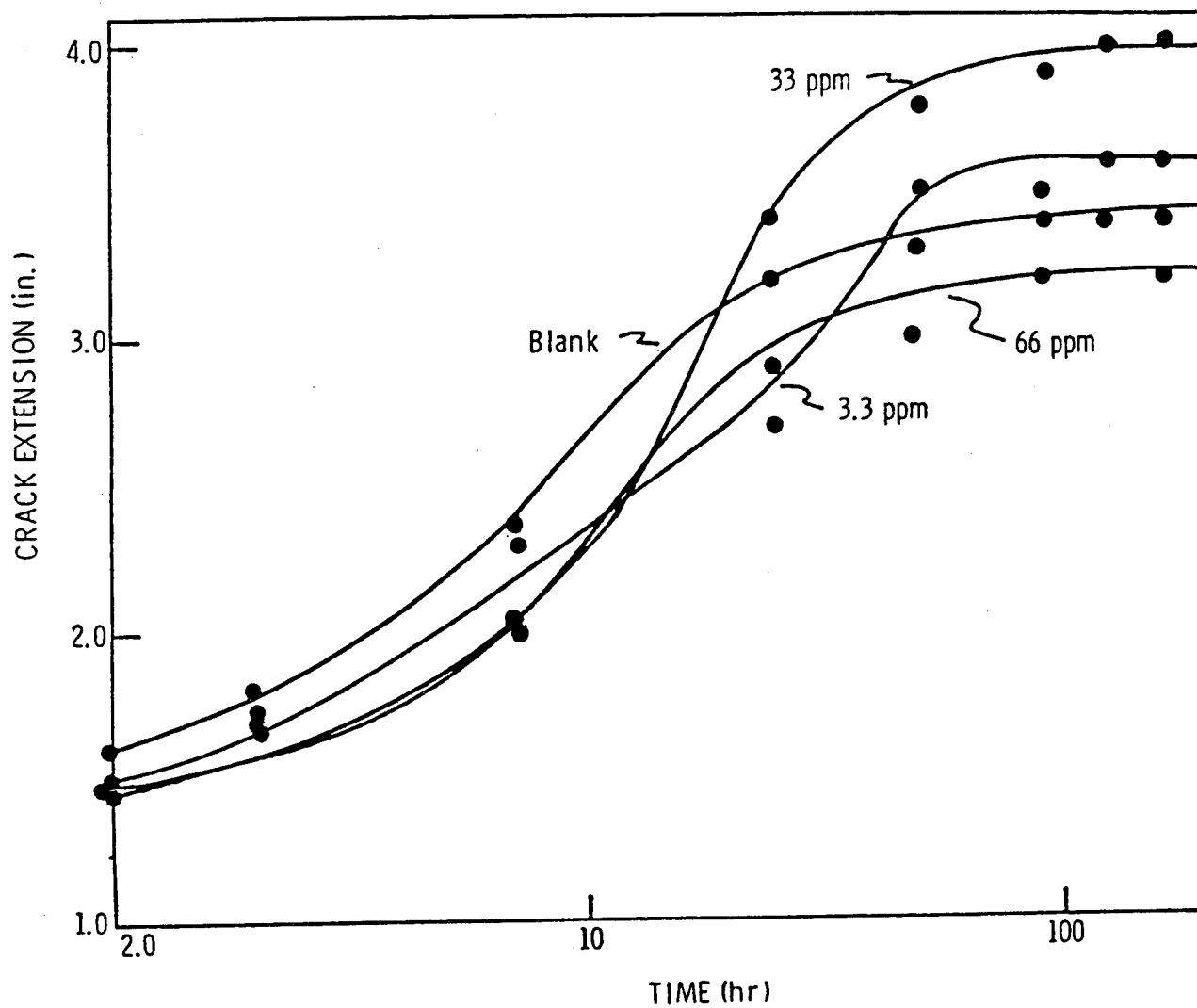
Figure 11. Wedge-test results (crack length as a function of time) for FPL adherends treated in solutions of PA and for untreated FPL adherends.
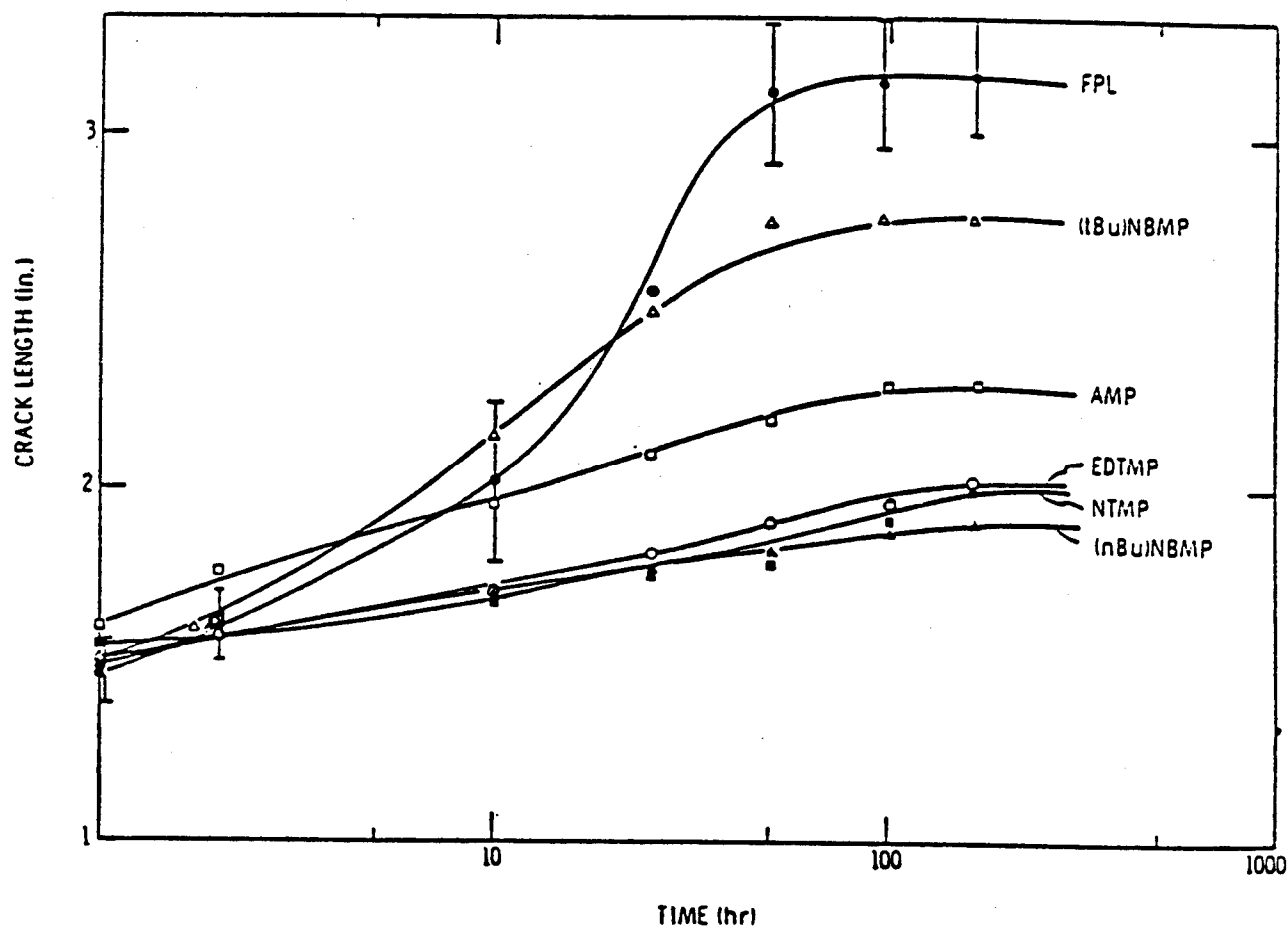
Figure 12. Wedge-test results (crack length as a function of time) for FPL adherends treated in solutions of AMP, (n Bu)NBMP, (t Bu)NBMP, NTMP, and EDTMP and for untreated FPL adherends.

EDTMP-treated specimens occurs near or at the adhesive adherend interface because substantial differences are seen between the metal and adhesive sides of the failure with high Al (and O) denoting aluminum oxide or hydroxide and high C denoting the adhesive. (Al and some O on the adhesive side of NTMP and EDTMP-treated bonds result from aluminum hydroxides solution-deposited from the condensed water vapor. Similarly the C on the metal side results from adventitious hydrocarbon contamination.) In contrast, the two surfaces of the FPL control and specimens treated with (t Bu)NBMP and (n Bu)NBMP exhibit high Al and O and low C indicating that the locus of failure is in the oxide/hydroxide or at the interface between the oxide/hydroxide and the metal with subsequent hydration or corrosion of the metal surface. For all cases, because the failures are not cohesive in the adhesive, further improvement in the bond performance may be possible using other inhibitors.

The micrographs of the near-crack-tip region of NTMP-treated panels reveal a "shiny" aluminum area right at the crack tip and a "dull" region further along the crack (Fig. 13). Closer examination shows the shiny area to exhibit an FPL morphology while the dull area exhibits the corn-flake morphology of a hydrated surface.[3] In this case, the crack has apparently propagated in advance of the hydration of the aluminum oxide; only after additional exposure to the moist environment does hydration occur.

In other specimens that show improvement over the control, bond failure apparently occurred as a result of hydration. This hydration is demonstrated in Fig. 14, which shows the crack-tip region of panels treated with AMP and (n Bu)NBMP. Here cornflake morphology is present up to the crack tip. In some areas, more extensive hydration is also seen with bayerite crystallites on top of the boehmite.

4. Discussion

4.1. Adsorption

The adsorption of each of the three amino phosphonates studied proceeds by the displacement of the physisorbed water on the FPL surface. (This water can also be removed by storing the coupon in UHV for several days; the surface, however, regains the water upon exposure to the normal humid atmosphere.) For NTMP and (n Bu)NBMP this reaction continues at room temperature until most, if not all, physisorbed water is replaced by approximately one monolayer of chemisorbed inhibitor. However, it appears that AMP is less efficient at displacing physisorbed water, so that some water remains even at the highest AMP coverages achieved at room temperature. This presence of residual water is consistent with the lower phosphorus content on the surface at saturation.[9] Our model of adsorption suggests one phosphorus atom for every two water molecules removed from the surface (assuming that all the inhibitor's POH groups bond to the Al_2O_3). Since the AMP-treated surface has a significantly lower P/Al ratio, less water would have been displaced from the surface.
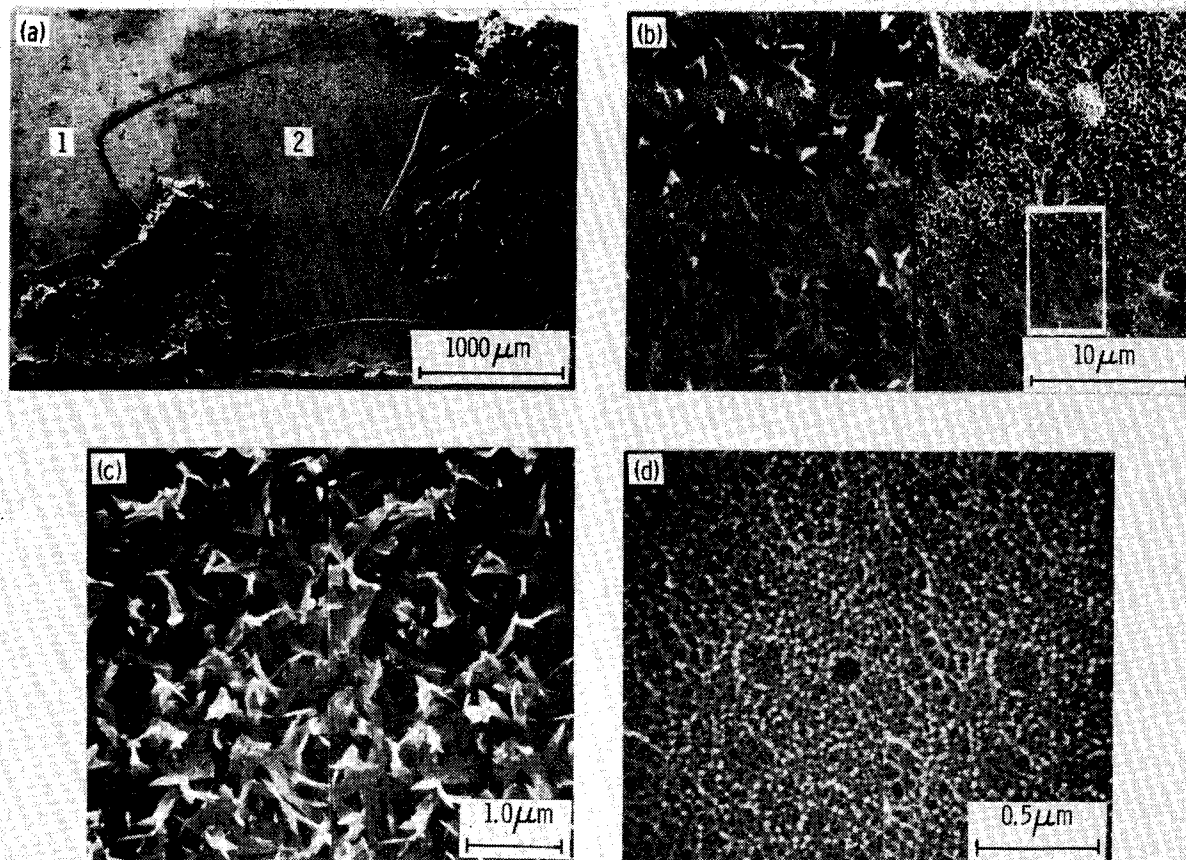
Figure 13. Scanning electron micrographs of the near-crack-tip region of the
aluminum side of an NTMP-treated FPL-etched wedge test specimen:
a) low magnification view showing 1) the dull aluminum area and
2) the shiny aluminum area, and the cohesive failure in the adhesive
after the wedge test was completed (at right); b) the beginning of
hydration in the boundary region between dull and shiny areas,
enlargement of the blocked-in area in inset is at left; c) higher
magnification stereo view of the dull area showing the cornflake
boehmite structure; and d) high-magnification stereo view of the
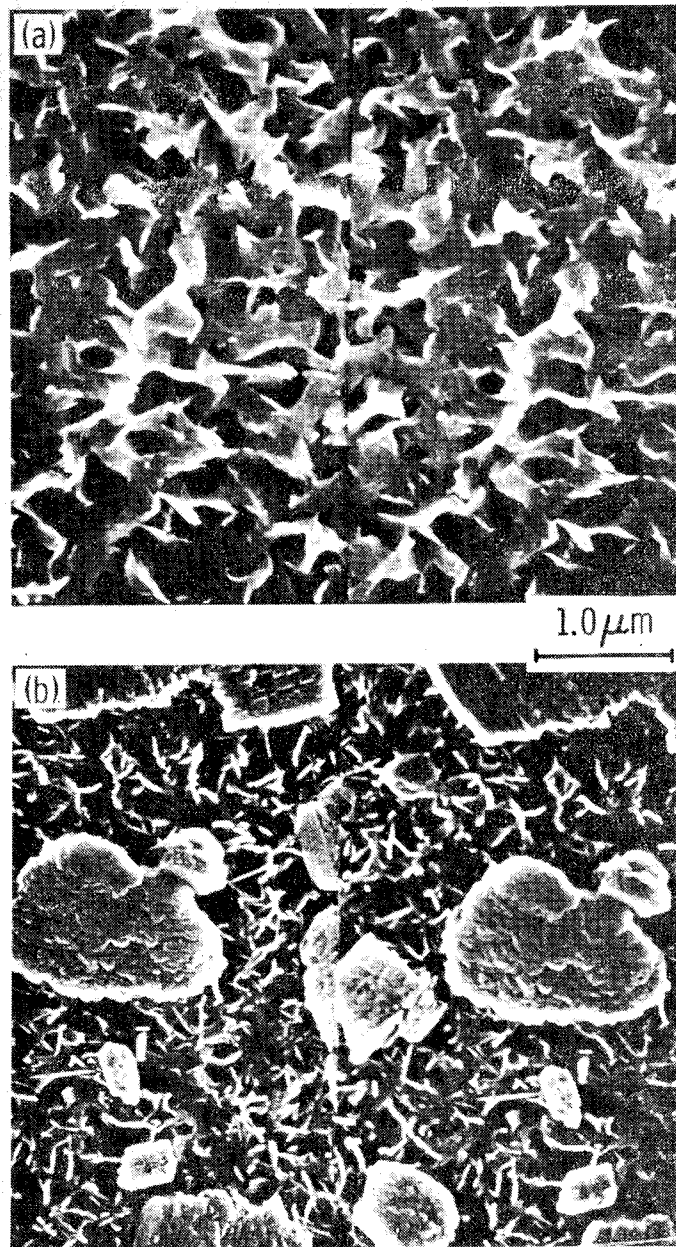shiny area showing the original FPL morphology.

Figure 14. Scanning electron micrographs of the near-crack-tip region of the aluminum side of two inhibitor-treated FPL-etched wedge test specimen: a) AMP-treated surface exhibiting cornflake (boehmite) morphology and b) (nBu)NBMP-treated surface exhibiting bayerite crystallites on top of boehmite.

The adsorption data of NTMP on FPL (Fig. 3) show the adsorption isotherm to be concave downward. This is indicative of a two-step adsorption process more clearly illustrated in Fig. 7, which shows the isotherm proceeding at first in the general direction of NTMP, but then heading away from the H_2O vertex. These results suggest that at very low solution concentrations, NTMP adsorbs with only one $PO_3^=$ group bonded to the surface. Consequently the inhibitor coverage, as determined by the amount of P on the surface, increases faster than the water concentration on the surface decreases. At higher concentrations, however, the NTMP competes more successfully with water for adsorption sites, and the other $PO_3^=$ groups of the molecule become bonded to the surface, displacing additional water without increasing the inhibitor coverage.

A similar two-step process is expected for (n Bu)NBMP adsorption on FPL, although a single-step process is expected for AMP, since it has only one phosphonic acid group per molecule. The SBD's shown in Figs. 5, 6, and 7 support these ideas. Figure 7 clearly shows only a slight curvature in the surface composition evolutionary path for AMP on FPL, in contrast to the distinct two-step adsorption process for NTMP on FPL.

4.2. Hydration

The behavior of the surface composition during the hydration of NTMP-treated FPL surfaces (Fig. 8) is very similar to that observed during the hydration of PAA surfaces.[12] First, a reversible physisorption of water occurs. Then the surface hydrates to boehmite. Finally, bayerite crystallites grow on top of the boehmite. In fact, the linear evolutionary path of the surface composition from the monolayer of NTMP on Al_2O_3 to boehmite, together with the absence of any subsurface phosphorus in the hydration product, indicates that hydration only occurs as the NTMP-aluminum complex dissolves from the surface. Apparently, the limiting step in the hydration is the dissolution of this complex.

These findings, which have been generalized to include the corrosion of NTMP-treated steel samples[14] as well as the hydration of PAA surfaces,[12] suggest that at an ideal inhibitor should: 1) displace water and occupy all the active sites on the surface, 2) bond strongly to the surface, and 3) form an insoluble complex with aluminum.

4.3. Wedge Tests

Wedge test results allow us to identify two additional properties of an ideal inhibitor. Treatment with MP accelerates bond failure compared to FPL adherends while treatment with PA provides no change in performance even though it does confer hydration-resistance to the unbonded surface (J. S. Ahearn and A. I. Desai, unpublished results). For both bonds, the crack propagated along the adhesive-oxide interface. The inhibitors apparently weakened this interface, making it susceptible to attack by moisture either by interfering with the curing of the epoxy adhesive at the surface or by passivating the adherend surface and preventing the formation of adhesive-oxide or adhesive-inhibitor chemical bonds. In either case, compatibility of the inhibitor with the adhesive is necessary to prevent rapid bond failure.

A final criterion for a good inhibitor – coupling to the adhesive – can be deduced from the micrographs of the crack-tip region and from the relative performance of adherends treated with the two (Bu)NBMP compounds. Samples treated with (t Bu)NBMP and AMP exhibit only moderate bond durability. Failure occurs as the oxide hydrates, leading to crack propagation within the hydroxide, or along the weak hydroxide-metal interface with subsequent hydration of the exposed metal surface.

Even treatment with (n Bu)NBMP, although it gives good bond durability, leads to failure by hydration. We attribute the improved performance of these samples over those treated with (t Bu)NBMP to a molecular mechanical interlocking or good dispersion of the n-butyl tail in the polymeric adhesive. This mechanical coupling would make the inhibitor less vulnerable to aqueous attack and improve bond durability. It is not sufficient, however, to fully compensate for the reduced number of inhibitor-oxide bonds. As a result, treatment with (n Bu)NBMP fails to provide superior performance to that of NTMP-treated adherends. A similar effect may occur with AMP-treated bonds. The addition of the amino group to MP makes a dramatic difference in the performance of the respective bonds. This amino group is capable of reacting with the epoxy adhesive, thus strengthening the inhibitor-adhesive interface. At the same time, by making a less soluble complex, the inhibitor probably increases the hydration resistance of the oxide, even though the water that remains on the surface can act as initiation sites for hydration. These initiation sites prevent the hydration resistance from becoming as high as that of NTMP-treated oxides.

The failure of the NTMP-treated specimens, on the other hand, occurs not upon hydration, but prior to hydration. In these cases, the hydration rate is slowed sufficiently so that it is no longer the limiting factor in bond durability. Instead, failure occurs along the inhibitor-adhesive interface, and only after subsequent exposure does the oxide surface hydrate. These results, then, suggest that further improvement in bond durability can be achieved by strengthening the inhibitor-adhesive interface by either chemical or mechanical coupling while maintaining strong inhibitor-oxide bonding.

5. Summary

We have investigated the mechanisms by which nitrilotris methylene phosphonic acid (NTMP) and related compounds adsorb onto oxidized aluminum surfaces, inhibit the hydration of this oxide, and increase the durability of adhesive bonds formed with inhibitor-treated panels. Our results indicate that 1) NTMP adsorbs via P-O-Al bonds; 2) water initially adsorbed onto the FPL surface is displaced by the NTMP; and 3) hydration of NTMP-treated FPL surfaces occurs in three stages: i) reversible physisorption of water, ii) slow dissolution of NTMP followed by the rapid hydration of the freshly exposed Al_2O_3 to AlOOH, and iii) further hydration of the surface to $Al(OH)_3$. Additionally, by comparing the behavior of wedge tested panels treated with different inhibitors and by determining the locus of

failure, we have identified five properties of an ideal inhibitor that can improve adhesive bond durability. The inhibitor should: 1) displace water from the surface and occupy all the active sites, 2) bond strongly to the surface, 3) form an insoluble complex with aluminum, 4) be compatible with the primer/adhesive system, and 5) chemically couple the adhesive to the oxide.

6. Acknowledgements

7. References

1. H.W. EICHNER and W.E. SCHOWALTER, Forest Products Laboratory Report No. 1813, Madison, WI, (1950).

2. G.S. KABAYASKI and D.J. DONNELLY, Boeing Corporation Report No. D6-41517, Seattle, WA, (1974).

3. J.D. VENABLES, D.K. McNAMARA, J.M. CHEN, and T.S. SUN, Appl. Surf. Sci. 3, (1979) 88.

4. D.J. PACKHAM, in "Adhesion Aspects of Polymeric Coatings," edited by K.L. Mittal (Plenum, New York, 1983) p. 19.

5. J.D. VENABLES, D.K. McNAMARA, J.M. CHEN, B.M. DITCHEK, T.I. MORGENTHALER, and T.S. SUN, in Proceedings of the 12th National SAMPE Technical Conference, Seattle, WA, 1980, p. 909.

6. G.D. DAVIS and J.D. VENABLES, in "Durability of Structural Adhesives," edited by A.J. Kinloch (Applied Science, Essex, 1983) p. 43.

7. D.A. HARDWICK, J.S. AHEARN, and J.D. VENABLES, J. Mater. Sci. 19, 223 (1984).

8. J.D. VENABLES, M.E. TADROS, and B.M. DITCHEK, US Patent 4308079, (1981).

9. J.S. AHEARN, G.D. DAVIS, T.S. SUN, and J.D. VENABLES, in "Adhesion Aspects of Polymeric Coatings," edited by K.L. Mittal (Plenum, New York, 1983) p. 281.

10. D.A. HARDWICK, J.S. AHEARN, A. DESAI, and J.D. VENABLES, Environmental Durability of Phosporic-Acid-Anodized Aluminum Adhesive Joints and Protected With Hydration Inhibitors (to be published in J. Mat. Sci., 1985).

11. A.I. PLAZA, PhD Thesis, University of Maryland, Jan. 1976.

12.   G.D. DAVIS, T.S. SUN, J.S. AHEARN, and J.D. VENABLES, J. Mater. Sci.
       17, (1982) 1807.

13.   G.D. DAVIS, S.P. BUCHNER, W.A. BECK, and N.E. BYER, Appl. Surf. Sci.
       15, (1983) 238.

14.   G.D. DAVIS, J.S. AHEARN, and J.D. VENABLES, J. Vac. Sci. Technol. A. 2,
       (1984) 763.2

15.   S.S. MOROZOVA, L.V. NIKITINA, N.M. DYATIOVA, and G.V. SEREBRYAKOVA,
       Z Anal. Khim. 30 (1975) 1712.

FACTORS AFFECTING THE PROCESSING
OF EPOXY FILM ADHESIVES

R. A. Pike

United Technologies Research Center
East Hartford, Connecticut 06108

ABSTRACT

The increasing awareness that adhesive performance is controlled not only by the condition of the adherend surface but also the condition or "state" of the adhesive and the process parameters used during fabrication is expected to result in improved reliability as well as bond performance. The critical process variables which have been found to control adhesive bond formation and ultimate bond strength in 250°F and 350°F curing epoxy adhesives will be described in terms of fabrication parameters and adhesive characteristics. These include the heat-up rate and cure temperature during processing and the adhesive moisture content and age condition (degree of advancement). The diagnostic methods used to delineate the effects of these process variables on adhesive performance will be illustrated. These are dielectric, thermomechanical (TMA) and dynamic mechanical (DMA) analyses. Correlation of test results with measured mechanical tensile lap shear strengths of bonded joints will be presented and the results briefly discussed in terms of the additives and hardeners used in the adhesive systems.

DEFECTS IN ADHESIVE BONDS

- **Porosity/internal voids**

- **Disbonds (adhesive failure)**

- **Improper cure**

- **Inclusions/foreign material**

- **Bond line variation**

Control and an understanding of how processing variables affect the adhesive and final joint properties are mandatory if high levels of reproducibility and reliability are to be achieved. Processing variables can be separated into two classes; those related to the fabrication parameters:

- Pressure/temperature control
- Part design
- Heat-up rate

and those related to the adhesive:

- Adhesive quality (lot-to-lot component variations)
- Surface primer condition
- Moisture content
- Age condition of the adhesive

Studies at UTRC have addressed the effect of aging[1], and moisture content[2] on EA-9649 performance during bond fabrication. These factors are directly related to the condition of the adhesive at time of bonding. Fabrication parameters, such as variation in cure temperature, have also been identified as critical to the ultimate performance of bonded joints[3], as has heat-up rate, one of the important fabrication variables which affect the processing of epoxy adhesives[4]. Non-optimized conditions related to any of these four variables can result in one or more of the above identified defects.

AGING EFFECTS

- Resin soluble portion of catalyst reacts with epoxy to produce:

  - Increased viscosity (decreased flow)
  - Lower level of cure
  - Decreased bond strength

399

ROOM TEMPERATURE AGING EFFECTS ON EA-9649 SUPPORTED ADHESIVE

Aging time (days)	ISA[a] (flow %)	Initial softening[b] point, °C	Major softening[b] point, °C	Gel point[b] time, min.	Gel point[c] DSC (°C)
0	73	23.5	72	66 (178°C)	194
30	54	30.5	81	64	190
66	32	48	97	62.75	188.5
100	30	61	98	61.5 (173°C)	186.5

a. ISA = Increase in surface area

b. Dielectric analysis, heating rate = 2.5°C/min

c. DSC, heating rate = 5°C/min

(From ref. 1)

The degree of room temperature shelf-aging which occurs in an adhesive between time of manufacture and actual use in a bonding application is one of the factors controlling the fabrication parameters required to achieve optimum bond strength. Ultimate bond strengths can also be affected if extended aging has taken place, regardless of the fabrication process employed. The objective of the described investigation was to determine the effect of room temperature shelf-aging on the properties of the commercially available 178°C (350°F) epoxy film adhesive, Hysol EA-9649. This adhesive, available as supported or unsupported film, is an aluminum powder-filled epoxy system cured, in part, using dicyandiamide.

The room-temperature aging of the film was studied over a three-month period. The relationship between aging time, adhesive softening and gel point, and the resulting effect on adhesive flow was determined. The changes which took place in the adhesive film during the aging period are listed above. Identifiable changes are in terms of increase in surface area (flow) during cure, initial and major softening point, and resin gel point as measured by dielectric analysis and DSC. The supported tape showed a nineteen per cent decrease in flow with a 9°C increase in the major softening point over the first thirty day aging period.

During the next aging period, 30 to 66 days, there was a marked drop in ISA (flow) in the supported tape accompanied by a slightly larger increase in both initial and major softening points. A slight decrease in gel point was also noted. Thus, during the second aging period, the time difference between the softening and gelation temperatures decreases. This could account for the decrease in flow since the time to allow flow has decreased and the viscosity of the system increased through the temperature range where movement of the resin film can occur.

After the 66-day aging period, there were minor changes in the flow and softening point of the adhesive. These results indicate the rate of resin advancement decreased sharply after the 66-day period. This is probably related to the increase in viscosity of the system resulting in a lower diffusion rate of reactive catalyst as well as a concentration effect.

DISSIPATION FACTOR vs TIME

EA 9649 film adhesive, supported

——— **As received**   — - — **66 days at room temp.**

— — — **30 days at room temp.**   ·········· **100 days at room temp.**

Time, minutes

(From ref. 1)
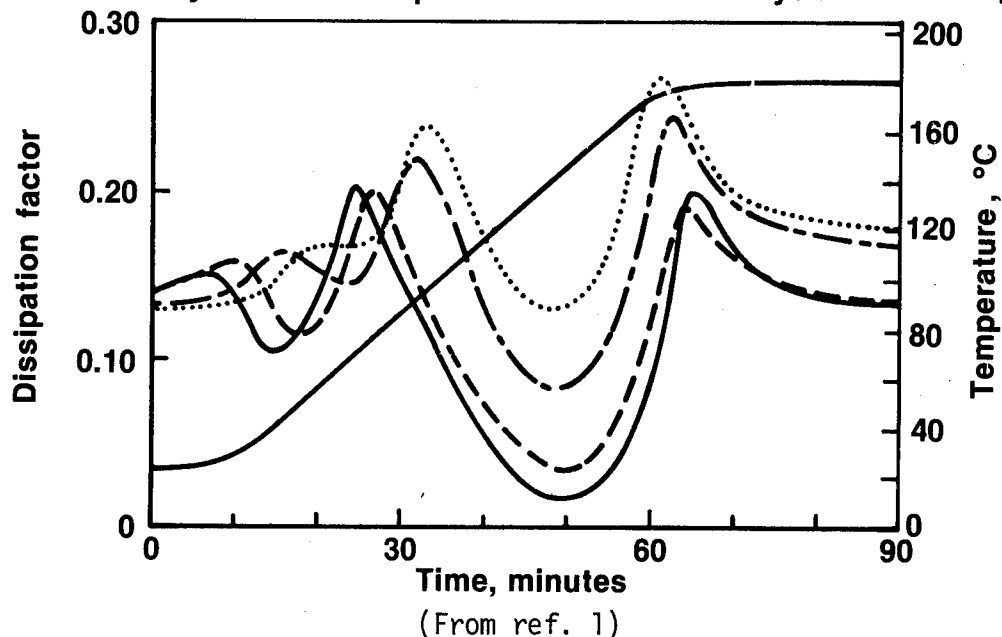
Dielectric curves obtained on the aged adhesive film simultaneously with the flow measurements are shown above. With the supported EA-9649, two resin softening temperatures are evident. The initial shallow drop in dissipation showed peak temperatures progressing from 23.5 to 61°C as aging time increased. The last two time periods resulted in less change in the dissipation factor profile, indicating less variation in the viscosity through the temperature range. In both cases after 100-day aging, there was essentially no drop in viscosity. The initial softening point is probably due to the lower molecular weight epoxy resins used in the adhesive. The major adhesive softening peak indicated by a large drop in dissipation factor varied over a range of 72° to 98°C with the largest change evident between the 30- and 66-day aging periods. As at the lower temperatures, the degree of change in dissipation factor between the softening point and the gelation peak decreased as aging time progressed. The viscosity increase shown by a decrease in dissipation factor profile between melting and gelation was also evident.

Accompanying these changes in resin behavior was the decreased time period between the major softening temperature and the gel peak. Thus, the degree of additional cross-linking or branching required to reach gelation appears to be less the longer the aging time, indicating some branching has occurred in the adhesive. The higher dissipation factor shown by the 66- and 100-day samples at the end of the heating cycle is indicative of a different final molecular structure which, because of steric considerations, would require a longer heating cycle or higher temperature to reach complete cure.

Bonded Joints prepared from the 100-day aged samples showed a 25 percent decrease in tensile lap shear strength compared to specimens fabricated from non-aged adhesive.

Determination of Tg points, using DSC analysis on the processed films at the end of each aging period, also reflected the effect of room-temperature aging. The Tg decreased from 210°C to 203°C over the aging period. In addition, the curves for the 66- and 100-day samples showed the presence of unreacted dicyandiamide catalyst having a melting point of 220°C at the 10°C/min heat-up rate used for the analysis.

The lower bonded Joint strengths and the decrease in Tg together with the higher final dissipation factor at the end of the cure cycle suggest that the principal reaction involved in room-temperature aging of the EA-9649 adhesive film is one of increasing molecular weight due to reaction of the dicyandiamide catalyst with the lower molecular weight resins used in the formulation. The structural changes which occur at room temperature affect resin flow and produce a different final resin configuration than encountered using standard cure conditions. This not only affects the ultimate bond strength but requires a modified cure cycle to achieve complete cure.

CURE TEMPERATURE EFFECTS

## Changes in reaction temperature produce

- **Flow changes**
- **Lower cure level**
- **Lower bond strengths**

Three methods were used to assess the effect of varying cure temperature on both supported and unsupported EA-9649 adhesive film in terms of flow, gel time and final Tg. These were dielectric and TMA analysis of the neat adhesive and fillet length measurements of the reticulated unsupported adhesive film in a bonded honeycomb structure.

EFFECT OF CURE TEMPERATURE
# ON DEGREE OF CURE (DSC)
EA-9649 Adhesive/6061 Al
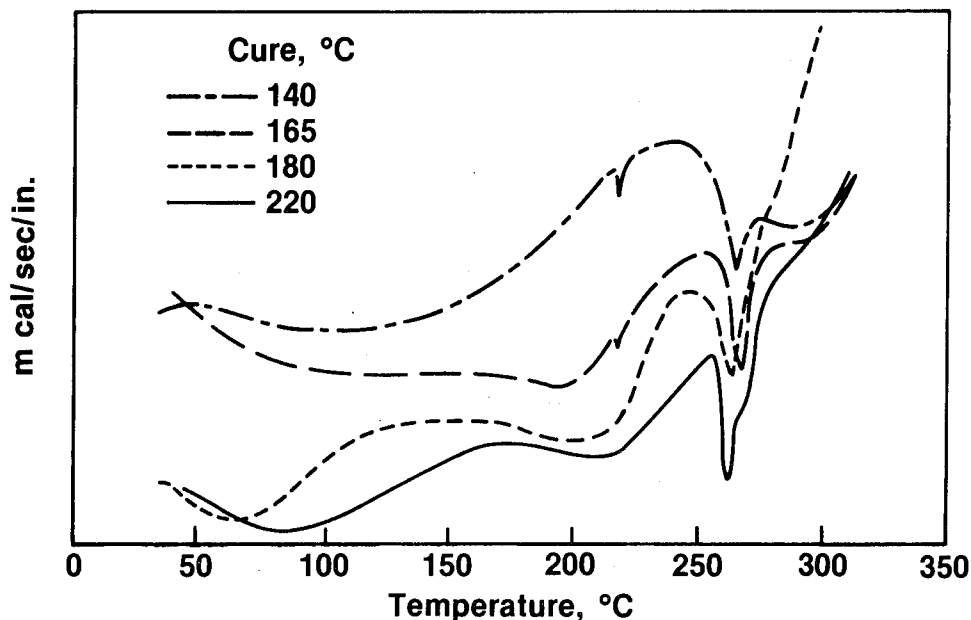
DSC analysis of the cured adhesive showed the presence of unreacted catalyst at the 140°C and 160°C temperatures. This was apparent from the slight endotherm (melting) which occurred at approximately 220°C. The melting point of dicyandiamide is 216°C at the heat-up rate used for the analysis. Thus, at temperatures below 180°C the adhesive appears to be only partially cured. The marked effect of cure temperature on flow related to resin viscosity, cure kinetics and temperature rise indicates the necessity of careful monitoring of process parameters to achieve reproducibility in bonded structures.

404

DIELECTRIC ANALYSIS-EFFECT
OF CURE TEMPERATURE

Supported EA9649 flim adhesive
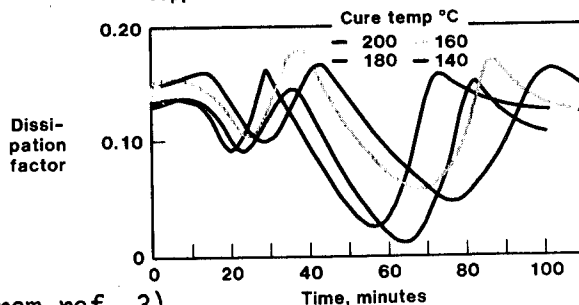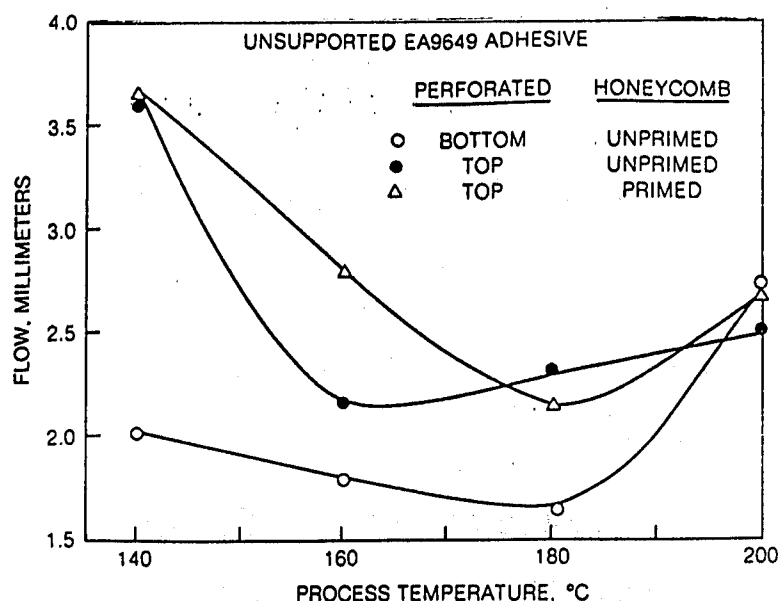

(From ref. 3)

The dissipation factor profile curve obtained on the supported adhesive film is illustrated above. The pertinent data are listed in Table I.

Table I. Cure Temperature Effects on EA-9649 Adhesive-Dielectric Analysis[a]

Cure Temp, °C	ISA[b] (%flow)	Time to gel, minutes	T_g °C[c]
Supported Adhesive			
200	97	72	246
180	70	81.5	220
160	89	86	203
140	71	101	139
Unsupported Adhesive			
200	45	70	239
180	25	81	205
160	35	90	185
145	42	102.5	142

a. Analysis run at 1000 Hz, 50 psi pressure, 2 ply lay-up.
b. ISA = Increase in surface area.
c. Measured by TMA on the cured sample.

For the unsupported adhesive, an increase in Tg point and decrease in time to gel with increasing cure temperature were observed as expected. The flow, as measured by the increase in surface area during cure, was found to be minimum at the specification 180°C level. Higher flow was experienced above and below this temperature. The supported adhesive in general gave a similar cure response with varying cure temperature. Minimum flow was again found to occur at 180°C. The low flow associated with the 140°C cure is probably due to the effect of the support scrim coupled with the higher viscosity of the adhesive. Accompanying these changes in resin behavior was the higher final dissipation factor obtained by samples cured at temperatures other than the specification 180°C. This is indicative of a different final molecular structure in either a fully or partially cured state.

(From ref. 3)

Adhesive fillet length (in terms of flow) vs processing
temperature.

In order to correlate the flow response obtained by dielectric
analysis with fillet formation in a bonded honeycomb structure,
measurements of fillet length were made on the reticulated unsupported
adhesive using specimens fabricated at the four curing temperatures with
primed and unprimed honeycomb. The results are shown graphically above.
The degree of flow obtained on the primed honeycomb with perforated plate
on top was in exact agreement with the dielectric analysis results, i.e., a
minimum flow was obtained at the 180°C cure temperature with longer fillets
being formed at cure temperatures above and below the specified cure
temperature. The flow on the unprimed honeycomb showed a slight minimum at
160°C indicative of the different response of the spreading characteristics
of the adhesive to a metal or resin surface. Reversing the honeycomb
construction so that the perforated plate was on the bottom (adhesive flows
up) gave a minimum flow condition at 180°C on the unprimed surface. Thus,
varying cure temperatures produce trends in adhesive flow and final cured
state properties which affect the mechanical properties of a bonded joint.

MOISTURE EFFECTS

- **Moisture reacts with catalysts to produce:**

  - **EA-9649**
    - **Increased flow (plasticizer)**
    - **New slower reacting catalyst**
    - **Porosity**
    - **Lower bond strengths**

EFFECT OF INITIAL MOISTURE CONTENT ON Tg OF CURED EA 9649 ADHESIVE[a]

	Tg, °C	
Moisture conditions	Unsupported	Supported
As received	200	220
1 hour soak	183	213
4 hour soak	180	205
6 hour soak	185	200

[a]Determined on cured film by TMA analysis

(From ref. 2)

The effect of initial moisture content on the Tg of the cured film samples obtained during dielectric analysis is shown above. In both cases, a decrease in Tg to a lower nearly constant value was found to occur compared to the "as-received" adhesive, particularly in the case of the unsupported film. These results would indicate that a fully cured structure of different crosslink density or chemical structure was obtained as a result of the absorption of moisture. Thus, the initial moisture content of the film not only affects the rheological properties of the curing film, but also influences the resulting structure or cure level obtained at a given set of conditions.

DISSIPATION FACTOR VS TIME – EA9649 UNSUPPORTED

Time in H$_2$O, hrs		H$_2$O retention, %
———	As rec'd	0.5%
– – –	1	1.3%
———	4	3.5%
– – – –	6	1.9%
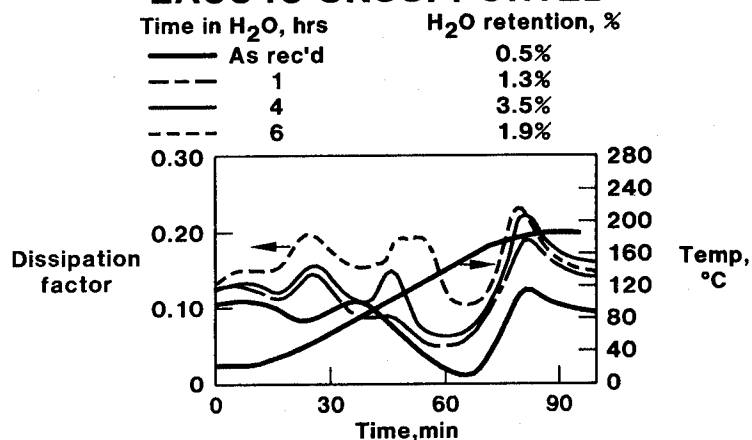
(From ref. 2)

Moisture effects on EA-9649 unsupported adhesive

Exposure Time (hr)	Moisture content (weight %)	ISA[a] (flow %)	Major softening[b] point (°C)	Moisture evolution[b] (°C)	Gel point[b] (time, min)
"as-received"	0.5	25	79	--	81
1	1.3	31	55	90	80.5
4	3.5	45	55	90	80
6	1.9	55	50	95-120	78.5

(From ref. 2)

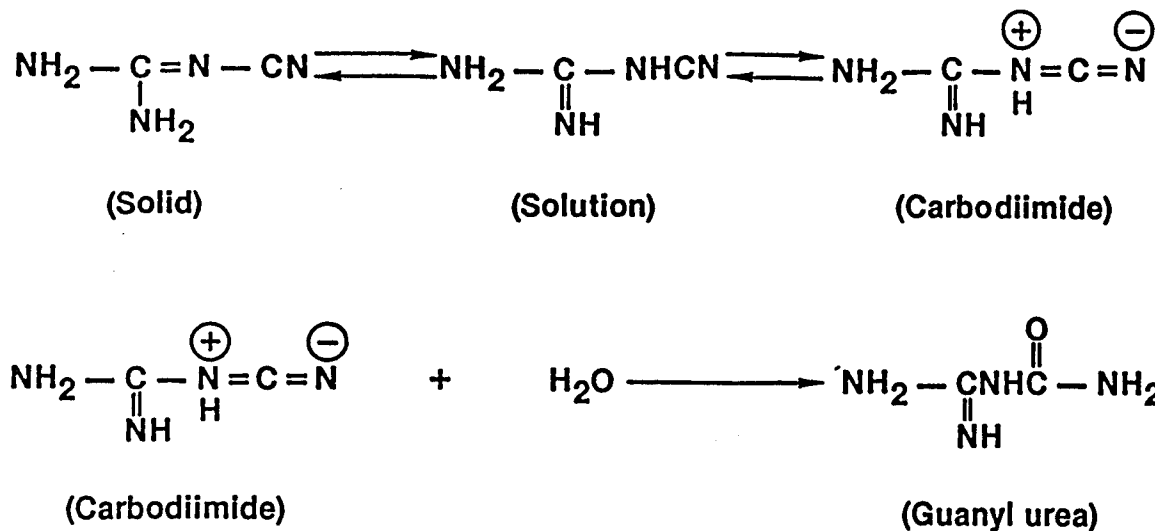a. ISA = Increase in surface area.
b. Dielectric analysis, heating rate = 2.5°C/min

A steady increase in flow was found with both types of film indicating the absorbed moisture acted as a plasticizer. This was also reflected in a lowering of the major melting point of the adhesive before cure. Thus, the time between softening and gelation was increased resulting in a longer flow period at low viscosity. The loss of absorbed moisture during heat-up was more evident with the unsupported film than the supported film at the lower moisture levels. This was probably due to the difference in film thickness as well as the absorption of water by the nylon scrim cloth used in the supported adhesive.

The unexpected change (decrease) which occurred in measured moisture level with increasing exposure in both types of film indicated the possible interaction of water with one of the active catalysts in the adhesive system. Six separate adhesive film samples produced the same result, a decrease in measured moisture level after exposure for a given time period.

Accompanying these changes in resin behavior was the higher dissipation factor shown by all samples compared to "as-received" adhesive with relatively minor changes in final gel temperature. These results are indicative of a different final molecular structure in either a fully or partially cured state.

DICYANDIAMIDE — EFFECT OF MOISTURE

$$NH_2 - \underset{\underset{NH_2}{|}}{C} = N - CN \rightleftarrows NH_2 - \underset{\underset{NH}{\|}}{C} - NHCN \rightleftarrows NH_2 - \underset{\underset{NH}{\|}}{C} - \overset{\oplus}{\underset{H}{N}} = C = \overset{\ominus}{N}$$

(Solid)	(Solution)	(Carbodiimide)

$$NH_2 - \underset{\underset{NH}{\|}}{C} - \overset{\oplus}{\underset{H}{N}} = C = \overset{\ominus}{N} \quad + \quad H_2O \longrightarrow NH_2 - \underset{\underset{NH}{\|}}{C}NH\overset{\overset{O}{\|}}{C} - NH_2$$

(Carbodiimide)	(Guanyl urea)

Water does react with dicyandiamide to produce guanyl urea as the initial reaction product in dilute acidic or basic solution. Since the adhesive film system used in our study is essentially a non-aqueous environment extremes in hydrogen ion activity can be expected which could result in greatly enhanced hydrolysis rates. Thus, there is every possibility that a reaction between dicyandiamide and water could take place at room temperature.

Based on these considerations, it is postulated that the dissolved dicyandiamide undergoes a hydrolysis reaction to produce guanyl urea. Such a reaction could proceed by two possible routes, first, via reaction of water with the carbodiimide-like resonance forms by a mechanism similar to that proposed for disubstituted carbodiimides, and second, via the direct hydrolysis of the nitrile group involving the protonated tautomer.

The rate at which the conversion of dicyandiamide to the guanyl urea occurs will depend on the concentration of solubilized dicyandiamide, moisture diffusion rate, viscosity of the medium, epoxy resin type, and the affinity of the scrim cloth (supported film) and filler for moisture. A longer time period for inversion of the cyano absorption peaks was noted in the supported adhesive.

Based on the change in the infrared spectra, the time required is approximately one hour at a moisture level greater than one weight percent for the unsupported adhesive. More exact measurements than those used in this study will be required to establish accurate reaction rates and the effect of added substituents on the interaction of dicyandiamide with water.

The suggested mechanism would account for the measured free water concentration decreasing after a given time period.

HEAT-UP RATE EFFECTS

- Resin reacts with catalysts at varying rates to produce:

    - Flow minimum at intermediate heat-up rate

    - Decreased TG with increasing rate (EA-9649)

    - Increasing TG with increasing rate (AF-163)

    - Bond strength decrease (both adhesives)

EFFECT OF HEAT·UP RATE ON
DEGREE OF CURE (Tg)

Tensile lap shear specimens
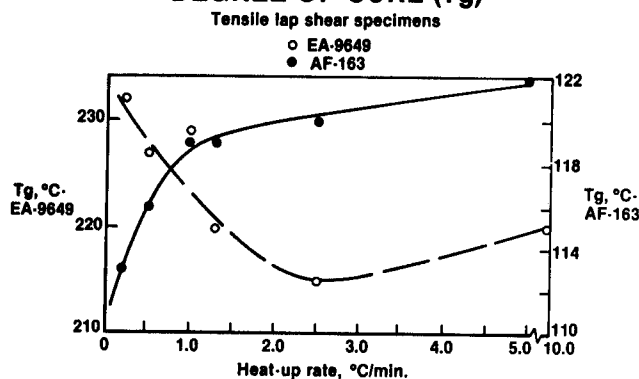
○ EA·9649
● AF·163

(From ref. 4)

Comparison of the Tg's of cured AF-163 with those obtained from EA-9649 shows the opposite effect in terms of heat-up rate. As is shown above at faster heat-up rates, the Tg of AF-163 increased while that of EA-9649 decreased.

The cause of the increasing Tg with heat-up rate could be due to several possibilities. These are: a) the precipitation of the rubber toughener may be affected by heat-up rate, thus at fast rates the effectiveness is lost producing a more brittle system, b) the exotherm generated by rapid reaction of the catalyst could lead to excessive crosslinking, producing a resin structure of low molecular weight having a high crosslink density which would yield a higher Tg. Since the gel temperature is reached more rapidly at faster heat-up rates the tendency to produce a brittle undercured system would be enhanced. Which of these factors is the major cause of increased Tg cannot be delineated at the present time.

EA-9649 is cured in part with dicyandiamide. Studies have shown that reaction with this catalyst is a two step process, an initial rapid exothermic reaction involving ring opening of the epoxy groups to produce N-alkylguanidines followed by a slower high temperature (110-200°C) reaction resulting in guanyl urea formation. Once the gel point is reached the rate of the second reaction would be considerably reduced. Thus, short gel times at fast heat-up rates could lead to incomplete crosslink formation, resulting in reduced bonded joint strength.

Reactions of aromatic amines with the diglycidyl ether of bis-phenol A have also shown a dependence of gel time on cure temperature, the gel time at a given temperature being dependent on the structure of the amine. The second catalyst in EA-9649 is one which has slower reaction kinetics. Thus, if short gel times occur at the fast heat-up rates, the cure reaction becomes diffusion controlled which, if all specimens are heated for the same total time, would lead to incomplete cure at the rapid heat-up rates, ultimately producing lower Tgs and lower strengths. In a simpler system than EA-9649 the effects noted at the rapid cure levels have been attributed to the fact that the resulting network is less highly crosslinked since competing reactions produce different networks, a characteristic which cannot be corrected by post-curing.

412

DMA

(From ref. 4)
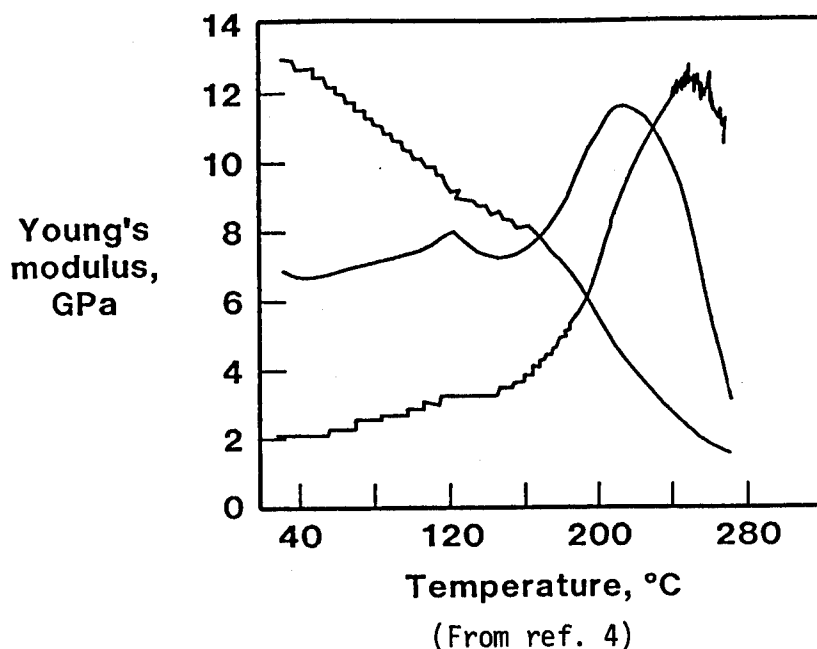
The use of DMA to measure that dynamic modulus and mechanical damping characteristics of adhesives has been reported. A typical response curve from RT to 280°C of dynamic modulus and mechanical damping (tan δ) of a specimen molded at the 1°C/minute heat-up rate is shown above. The modulus curve is in agreement with that reported for EA-9649. The mechanical damping (tan δ) of the adhesive is the corrected ratio of the viscous loss of energy to the stored elastic energy per cycle. The measurement detects molecular relaxation processes which are controlled by the structure of the adhesive's molecular network. Tan δ reaches a maximum in the glass-rubber transition region and therefore is associated with Tg. Thus, the higher the tan δ peak temperature the higher the maximum temperature at which an adhesive will maintain its structural integrity.

413

DAMPING PEAK CHANGE WITH HEAT-UP RATE*

| Heat-up rate, C/min	Sample vol mm^3	Tan δ peak area, mm^2	Peak area/ sample vol, mm^{-1}
0.2	35.4	132.3	3.74
0.5	31.0	120.6	3.89
1.0	34.1	157.4	4.62
2.5	31.7	136.8	4.32
5.0	34.8	120.0	3.45

*AF-163 supported adhesive 2-ply
sample from dielectric analysis

(From ref. 4)

As was the case with EA-9649 the maximum modulus was obtained at the 1.0°C/min heat-up rate. An indication that permanent differences in the formation of the molecular network, using varying heat-up rates, did occur was shown by comparison of the damping peak area (tan δ) normalized to constant volume. The data listed in the table shows that the maximum value was obtained at the 1.0°C/min rate. Thus, it appears that a specified heat-up rate which accommodates the cure kinetics of the reaction must be used to achieve optimum adhesive performance.

EFFECT OF HEAT-UP RATE
ON DYNAMIC MODULUS

(From ref. 4)
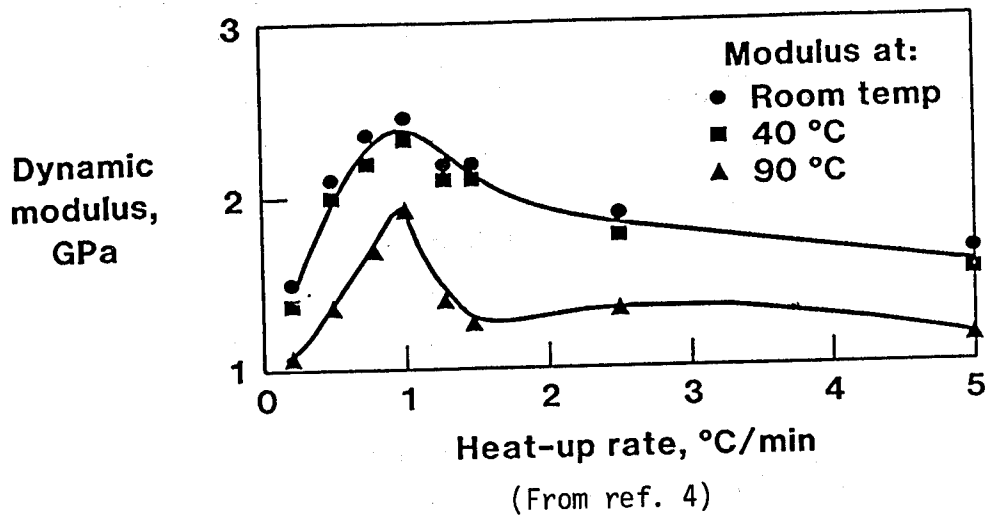
Dynamic mechanical analysis was carried out on the neat resin AF-163 specimens obtained from the dielectric analysis runs. The tan δ peak temperature which is associated with Tg showed the same general trend of high Tg with increasing heat-up rate as was shown by the Tg values obtained from fractured joint specimens. The highest initial RT modulus and modulus retention at 40° and 90°C were exhibited by the 1°C/min heat-up rate specimen as shown above.

CHANGE IN TENSILE LAP SHEAR STRENGTH WITH HEAT-UP RATE

EA 9649 supported adhesive
FPL etch, 2024 Al
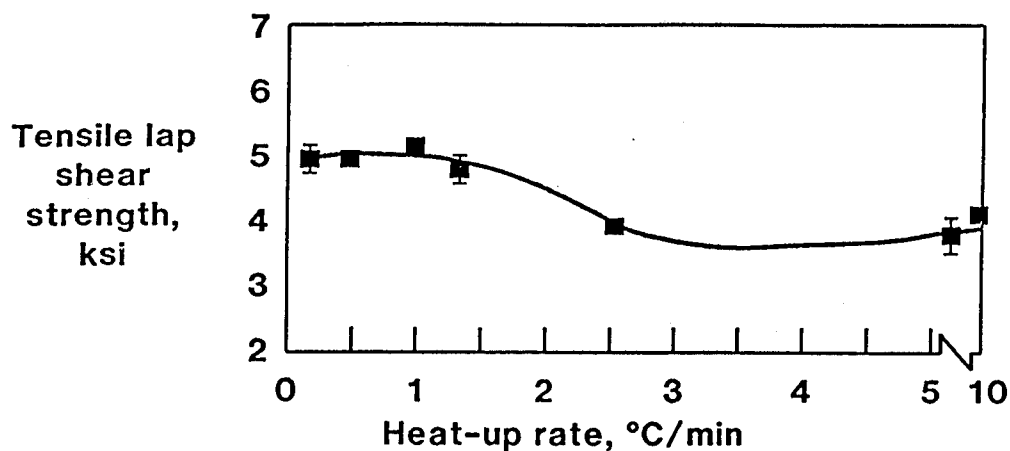
(From ref. 4)

The changes in tensile lap shear strength with heat-up rate are shown above. Each data point is an average of six specimens. These results showed that a twenty-five percent drop in tensile lap shear strength had occurred by increasing the heat-up rate from 1.3°C to 2.5°C/minute. The largest change in Tg occurred between 1° and 2.5°C/minute.

CHANGE IN TENSILE LAP SHEAR STRENGTH WITH HEAT-UP RATE

AF 163 SUPPORTED ADHESIVE
PAA ETCH, 2024 Al

(From ref. 4)
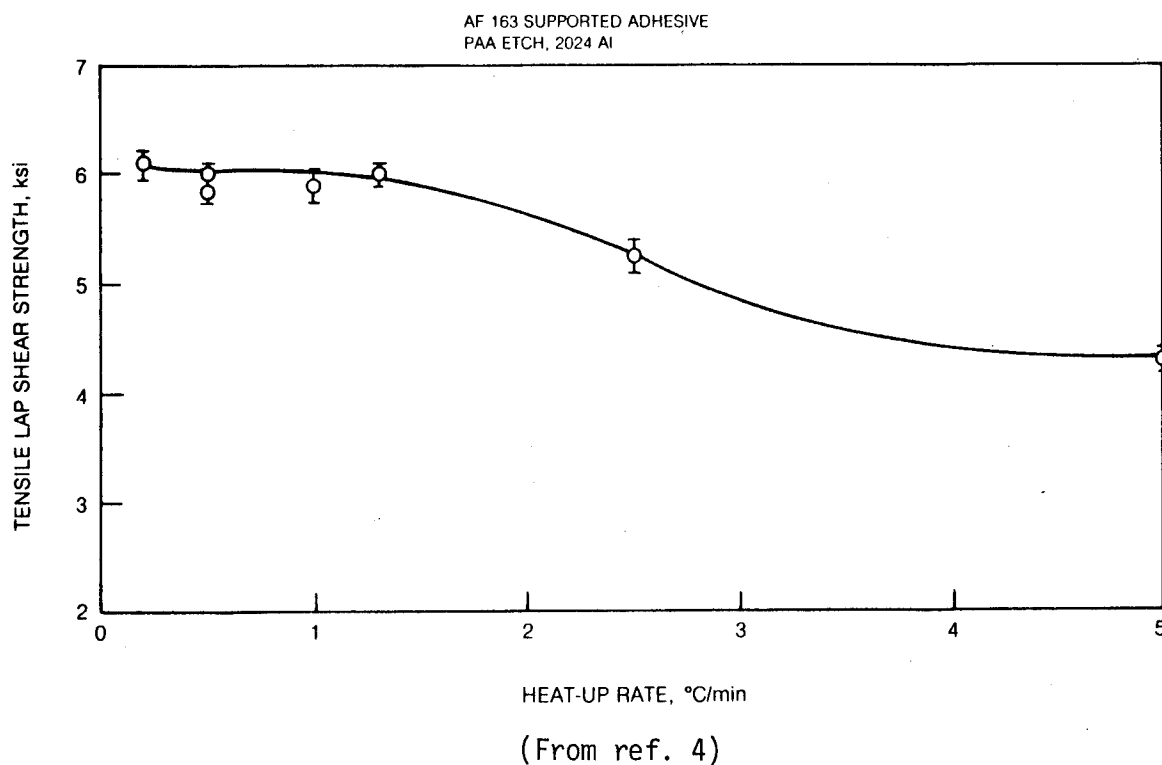
The results of heat-up rate are reflected in the tensile lap shear strength of bonded joints fabricated at varying heat-up rates. The data are shown graphically above. As was the case with EA-9649, a reduction in shear strength occurred above a heat-up rate of 1.3°C/min. The lap shear strengths obtained at the slower rates are in agreement with those reported for AF-163. The decrease in strength, as indicated, may be the result of excessive embrittlement due to poor rubber dispersion and/or excessive crosslinking due to the reaction kinetics of the catalyst system.

417

CONCLUSIONS

The marked effect of processing parameters and adhesive condition on bonded joint properties has demonstrated the necessity of "knowing" the adhesive system being employed so that optimized bond strengths can be achieved. Potential analytical techniques have been identified which can be used for QC testing as well as tools for studying adhesive compositions.

REFERENCES

1. R. A. Pike, F. P. Lamm and J. P. Pinto, J. Adhesion 12, 143 (1981).

2. R. A. Pike, F. P. Lamm and J. P. Pinto, J. Adhesion 13, 229 (1982).

3. R. A. Pike and R. S. Williams, Adhesive Joints: Formation, Characteristics, and Testing, K. L. Mittal, ed., Plenum Press, New York, 1984.

4. R. A. Pike, F. P. Lamm and J. P. Pinto, J. Adhesion 17, 51 (1984).

RAPID ADHESIVE BONDING AND FIELD REPAIR OF AEROSPACE MATERIALS

Bland A. Stein
NASA Langley Research Center
Hampton, Virginia 23665

ABSTRACT

Adhesive bonding in the aerospace industry typically utilizes autoclaves or presses which have considerable thermal mass. As a consequence, the rates of heatup and cooldown of the bonded parts are limited and the total time and cost of the bonding process are often relatively high. Many of the adhesives themselves do not inherently require long processing times. Bonding could be performed rapidly if the heat was concentrated in the bond lines or at least in the adherends.

Rapid Adhesive Bonding concepts have been developed at the NASA Langley Research Center to utilize induction heating techniques to provide heat directly to the bond line and/or adherends without heating the entire structure, supports, and fixtures of a bonding assembly. Bonding times for specimens can be cut by a factor of 10 to 100 compared to standard press or autoclave bonding. This paper reviews the development of Rapid Adhesive Bonding for lap shear specimens (per ASTM D1002 and D3163), for aerospace panel or component bonding, and for field repair needs of metallic and advanced fiber reinforced polymeric-matrix composite structures. Equipment and procedures are described for bonding and repairing thin sheets, simple geometries, and honeycomb core panels. Test results are presented for a variety of adhesives and adherends. Lap shear strengths greater than 4000 psi for titanium adherends and greater than 3000 psi for graphite/epoxy composite adherends are routinely achieved.

The promise of advanced composite and bonded metallic structures for improvements in structural efficiency and cost is limited by current processing and repair technology. Rapid Adhesive Bonding concepts can advance that technology significantly.

INTRODUCTION

RAPID ADHESIVE BONDING CONCEPTS DEVELOPMENT AT
LANGLEY RESEARCH CENTER

TECHNOLOGY NEED

RAPID, ENERGY EFFICIENT, RELIABLE ADHESIVE BONDING TECHNIQUES FOR HIGH PERFORMANCE AEROSPACE COMPOSITES AND METALS

RAB OBJECTIVES

O DEVELOP IN-HOUSE CAPABILITY FOR BONDING OF ADHESIVE SPECIMENS

O DEVELOP RAPID PRODUCTION BONDING CONCEPTS AND PROTOTYPES

O DEVELOP FIELD REPAIR BONDING CONCEPTS

APPROACH

COMBINE LaRC AND INDUSTRIAL THERMOSET AND THERMOPLASTIC ADHESIVE TECHNOLOGY WITH INDUCTION HEATED JOINING DEVELOPMENTS

Adhesive bonding of metallic and fiber reinforced plastic composite structural components and specimens using thermosetting phenolic or epoxy adhesives is a widely used technology in the aerospace industry and thermosetting materials are receiving increasing attention. Adhesive bonding is particularly important for joining composite materials because load transfer paths through mechanical fasteners (such as rivets or bolts) can cause local overloads and damage in the relatively brittle composites. Most adhesive bonding is performed in heated platen presses or autoclaves which have considerable thermal mass, limiting the heating and cooling rates of the work considerably. Thermoplastic adhesives and some thermosetting adhesives do not inherently require long processing times. A few minutes to achieve a viscosity low enough to obtain flow and wetting of the adherend surfaces (plus a short time for cure for the thermosets) are sufficient. Some research and development of adhesive bonding processes using induction heating have been reported in the literature (ref. 1). These can produce rapid bonds, but their typical frequencies of operation (in the MHz range) can limit depth of penetration and cause internal sparking in graphite fiber reinforced composites.

Recognizing the economic savings possible if adhesive bonding processes for typical aerospace components could be accomplished in minutes, concepts have been developed at the Langley Research Center (LaRC) to bond a variety of materials and geometries, using advanced induction heating technology at KHz frequencies. These concepts are designated as Rapid Adhesive Bonding (RAB) concepts for specimens, components, and field repair. The technology utilizes a combination of aerospace adhesives developed at LaRC and by the U. S. aerospace industry with induction heating developments from LaRC which produced lightweight, compact, energy efficient prototype equipment. Details of the background, and criteria for these concepts, equipment and bonding procedures, and of the test data which prove the efficacy of RAB are presented in ref. 1.

420

RAPID ADHESIVE BONDING EQUIPMENT

Toroid Induction Heater

Specimen Bonding

Production Bonding

Field Repair
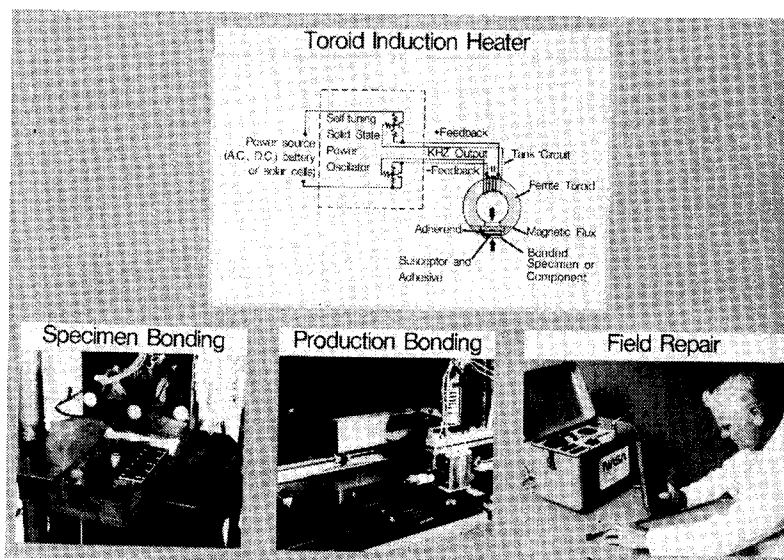
The rapid adhesive bonding equipment is based on a self-tuning solid-state power oscillator, which may be powered from a variety of sources, feeding kilohertz power to a ferrite toroid. The toroid geometry induces a uniform, concentrated magnetic flux into the specimen or component to be bonded, causing eddy currents to flow in a ferromagnetic susceptor and/or paramagnetic adherends. These currents heat only the bond line or its vicinity. Feedback circuits provide a degree of self tuning in the oscillator/toroid/specimen circuit, which usually operates at 30 to 80 kHz. The power required to heat a 1-in^2 bond area to temperatures above 800°F within approximately 1 minute is <300 watts. Maintaining the bond line temperature at 350 to 800°F typically requires less then 200 watts. Since no large fixtures are being heated, the cooling rate of the work is rapid, typically less than 2 minutes from the bonding temperature to below the glass transition temperature of the adhesive, at which time the bonded specimen/component may be removed from the RAB equipment. The specific prototype equipment for specimen bonding, production, and field repair, shown in the above photographs, is detailed subsequently.

COMPONENTS OF RAPID ADHESIVE BONDED OVERLAP SHEAR SPECIMEN
## (ASTM D1002)
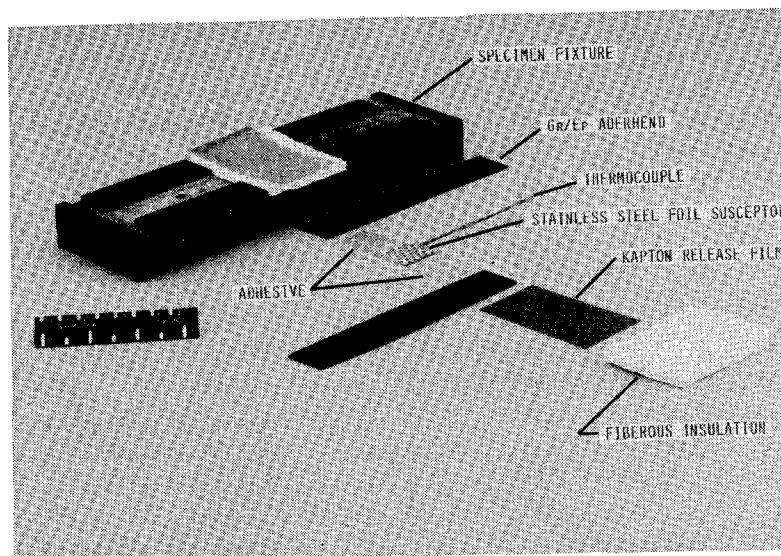
The components of an overlap shear specimen which conforms to ASTM D1002 or D3163 are shown above. In this example the adherends are high-strength fiber-reinforced polymeric composites, but similar adherends of aluminum alloy and titanium alloy have also been bonded, with excellent results (described subsequently). A perforated stainless-steel foil susceptor sandwiched between layers of adhesive is the other component of the specimen. (Flattened steel screen susceptors also work well.) Adherend surface treatments generally consist of a solvent wipe, a grit blast, and another solvent wipe for both composite and metal specimens. If long-term high-temperature exposures are to be conducted, an oxide treatment should be applied to the titanium alloy adherends.

A special fixture was devised to align the specimen components prior to bonding. The fixture is shown above. It may be fabricated from any nonconducting material. In this case the base was machined from Bakelite, with cutouts for the adherends. In the bonding region the cutout is deeper and fibrous ceramic insulation topped by a Kapton® film was used under the specimen. Another layer of Kapton®, topped by fibrous insulation, is placed atop the specimen to prevent heat conduction losses and to avoid bonding of specimen flashing to the toroid head. This fixture and the materials used in it functioned well for bonding temperatures to at least 850°F, since the heat is concentrated in the specimen bond lines, and the bonding times are relatively short.

RAB SPECIMEN BONDING EQUIPMENT
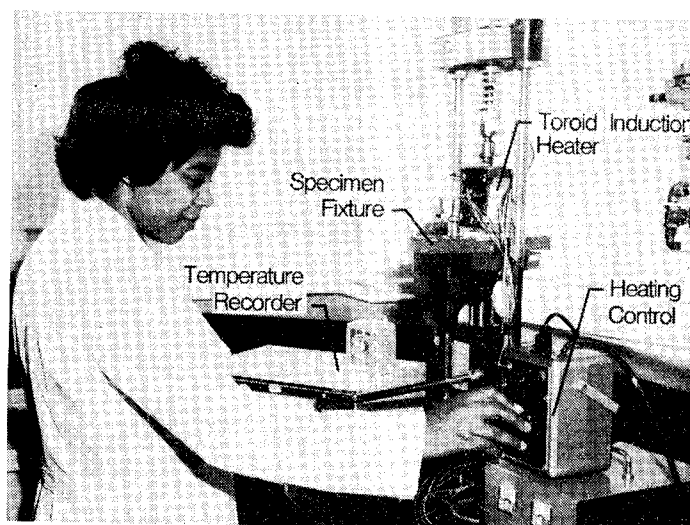
The RAB overlap shear specimen bonding equipment is shown. Much of the equipment is identical to that used for conventional bonding, including a load cell, the temperature recorder, and the laboratory press. In the laboratory press, the conventional heated platens have been replaced by a toroid induction heater. Bonding is accomplished by assembling the specimen in the specimen fixture, placing the fixture in the press under the toroid head, applying hydraulic pressure, and applying the induction field with the heating control. A thermocouple attached to the susceptor where it protrudes from the bond overlap is used to monitor bond temperature. Typical bonds are made at pressures from 10 to 200 psi, with heating rates from 100 to 1200°F/min., short holds at bonding temperature, and rapid cooling to temperatures below the adhesive Tg. The entire process is typically completed in less than 5 minutes. Both the temperature and pressure histories on the specimen could be readily automated, but they are easily controllable manually.

TYPICAL RAB OVERLAP SHEAR TEST SPECIMENS
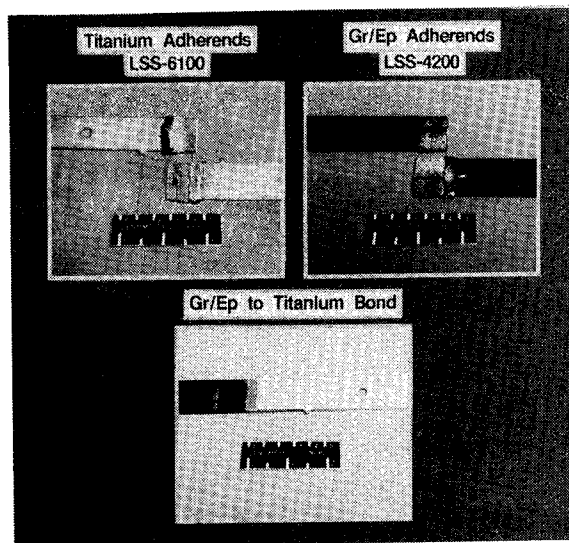
The appearance of typical overlap shear test specimens is shown. All
specimens were bonded with commercially available thermosetting adhesives,
using moderate pressures, and heating rates above 500°F to the bonding temper-
ature. Bonding temperatures were about 100°F above those suggested for auto-
clave or press bonding. Hold time at bonding temperature was 2 minutes.
Cooling times were about 2 minutes to temperatures below the Tg of the
adhesive, at which time the specimen was removed for testing.

The RT overlap shear strength of the titanium specimen at the upper left was
6100 psi; the failure mode was cohesive failure of the thermoset adhesive.
The RT overlap shear strength of the Gr/Ep specimen at the upper right was
4200 psi; the failure mode was adherend delamination. The versatility of RAB
is shown for the lower specimen, where a Gr/Ep adherend is bonded to a
titanium alloy adherend. Strengths on the order of 3000 psi were generated
for such specimens.

MATERIAL APPLICATIONS FOR RAPID ADHESIVE BONDING
THERMOPLASTIC ADHESIVES

ADHERENDS	ADHESIVES	BONDING TEMPERATURE, TIME, PRESSURE; °F, MIN, PSI	R. T. OVERLAP SHEAR STRENGTH, PSI
Ti/Ti Gr/PI//Gr/PI	P1700 (POLYSULFONE)	800, 2, 80 800, 2, 80	4600 3900
Ti/Ti	PISO$_2$ (POLYIMIDESULFONE)	650, 2, 50	4400
Ti/Ti	TPI (THERMOPLASTIC POLYIMIDE)	650, 2, 300	6500
Ti/Ti	PEEK (POLYETHERETHERKETONE)	750, 2, 50	6100
Ti/Ti	PPQ (POLYPHENYLQUINOXALINE)	800, 2, 100	3600
Gr/ULTEM// Gr/ULTEM	ULTEM (POLYETHERIMIDE)	625, 2, 5	5000
Ti/Ti	LARC-TPI (ENDCAPPED WITH SILANE)*	450, 3, 100	3500
Ti/Ti	LINEAR PI WITH SILOXANE*	450, 3, 100	4400
Ti/Ti	HOT MELT POLYIMIDE (ACETYLENE TERMINATED)*	450, 3, 100	4000

*EXPERIMENTAL

The versatility of Rapid Adhesive Bonding has been demonstrated for a number of adherend combinations with both thermoplastic and thermosetting adherends. All thermoplastic adhesives investigated to date have responded to RAB with moderate to high lap shear strengths after short bonding cycles. The data shown are for a number of commercially available and experimental high-performance aerospace adhesives, utilized in film form or on fiberglass cloth carriers with a steel screen or perforated stainless-steel foil susceptor in bond line. In obtaining this adhesive screening data, the surface treatments on the adherends usually consisted of a methyl alcohol solvent wipe, a grit blast, and another solvent wipe. It is recognized that more extensive surface treatments and possibly surface priming should be used for optimum bond strength and environmental resistance, but the lap shear strength values shown above indicate high bond strength potential. Continuing bonding studies indicate that lower bond pressures could be used than those listed above to make equally strong bonds.

## MATERIAL APPLICATIONS FOR RAPID ADHESIVE BONDING
THERMOSETTING ADHESIVES

ADHERENDS	ADHESIVES	BONDING TEMPERATURE, TIME, PRESSURE; °F, MIN, PSI	R. T. OVERLAP SHEAR STRENGTH, PSI
Ti/Ti Ti/Al Gr/Ep//Gr/Ep	HT-424 (EPOXY-PHENOLIC ON GLASS CLOTH CARRIER)	450, 2, 40 400, 5, 80 450, 2, 10	4000 3300 3500
Ti/Ti Gr/Ep//Gr/Ep	EC-1386 (EPOXY PASTE)	415, 3, 10 415, 3, 10	6200 3200
Ti/Ti Gr/Ep//Gr/Ep	AF-163 (ELASTOMER MOD.EPOXY FILM)	350, 2, 10 350, 2, 10	5600 4000
Ti/Ti	BISMALEIMIDE*	450, 3, 100	2100
Ti/Ti	GENERAL PURPOSE EPOXY	450, 3, 50	5000

*EXPERIMENTAL

A number of thermosetting adhesives have been found to make acceptable bonds between titanium and composite adherends via RAB. These bonds are achieved by heating rapidly to cure temperature and curing for short times at temperatures considerably higher than those suggested by the adhesive supplier for autoclave or press cure. (It must be noted that some thermosetting adhesives will not respond to RAB. Each potential adhesive/adherend combination must be screened.)

The above table lists the thermosetting adhesives and adherends which have responded to RAB to produce moderate-to-high-strength bonds. Bonding conditions of temperature, hold-time, and pressure are given, along with typical room temperature overlap shear strengths. The high strengths for the titanium specimens usually have accompanying cohesive failure modes. Failure modes in the composite specimens are typically adherend delamination.

## RAPID ADHESIVE PRODUCTION BONDING EQUIPMENT
-BOND IN PROGRESS-
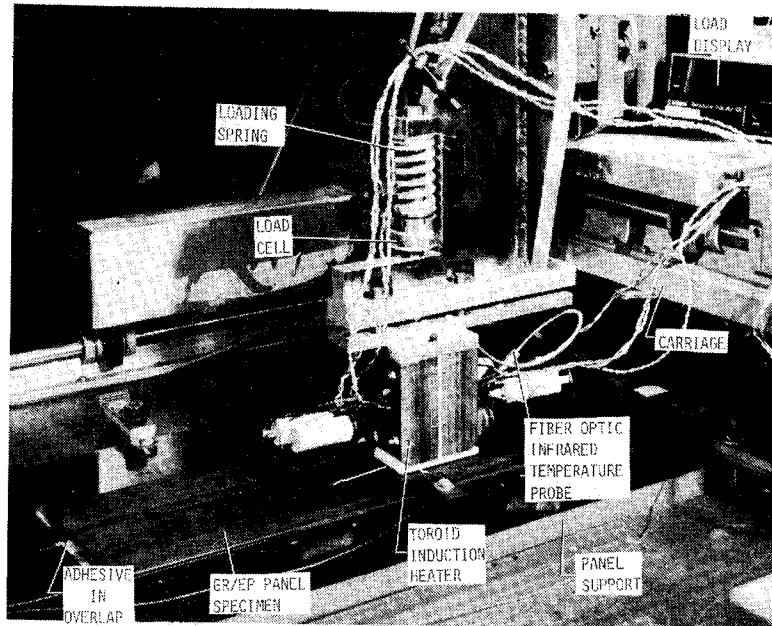
RAB equipment for continuous seam bonding of overlap panel assemblies is shown in operation. Two toroid induction heaters are mounted with a load cell on a support structure, which in turn is mounted to a transverse alignment slide. That slide is located on a longitudinal traversing carriage which travels along a standard machine bed. In this photograph, the toroids are moving at 0.5 inch per minute above the overlap between two graphite/epoxy panels and applying a bonding pressure of 20 psi while they are melting and curing the HT-424 epoxy-phenolic adhesive at 450°F as they pass. Two layers of adhesive with a flattened steel screen susceptor between them are in the bond line.

RAPID ADHESIVE PRODUCTION BONDING
T300/5208 GRAPHITE/EPOXY PANELS
HT 424 EPOXY-PHENOLIC ADHESIVE

NO SUSCEPTOR
IN BOND LINE

STEEL SCREEN SUSCEPTOR
IN BOND LINE
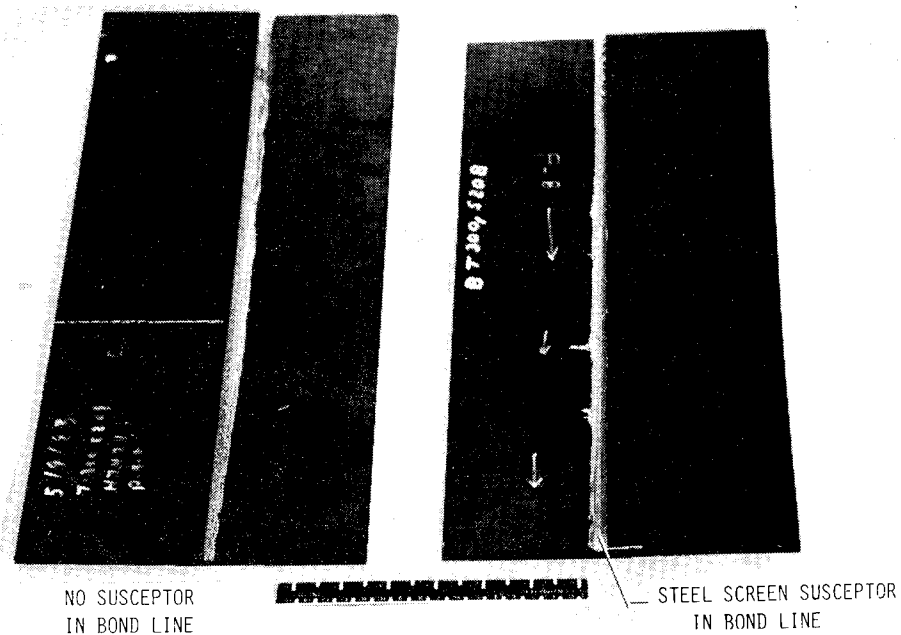
Graphite/epoxy panels bonded with the HT 424 adhesive are shown. They were made with and without susceptors in the bond line. An important finding in this application of RAB is that graphite/epoxy laminates can be heated directly in the induction field of the toroid heaters. Some lap shear specimens, cut from a graphite/epoxy panel bonded with HT-424 epoxy-phenolic adhesive and with the steel screen susceptor, were tested at room temperature and at 180°F (in accordance with ASTM D1002 or D3163). Other samples were tested at RT and 180°F after 1000 thermal cycles from -100 to +180°F, and at RT and 180°F after a 72-hour boiling water exposure. The RAB process had no degrading effect on shear strength of Gr/Ep//HT-424//Gr/Ep bonds, compared to standard bonding, and thermal cycling did not significantly degrade these properties. The water boil exposure degraded bond strengths about 35 percent at room temperature and 28 percent at 180°F. This degradation is approximately the same as that noted for the HT-424 adhesive in the adhesive supplier's literature.

RAPID ADHESIVE PRODUCTION BONDING
Ti-6A1-4V TITANIUM ALLOY PANELS
LARC-TPI ADHESIVE

STEEL SCREEN
SUSCEPTOR IN BOND LINE

NO SUSCEPTOR
IN BOND LINE
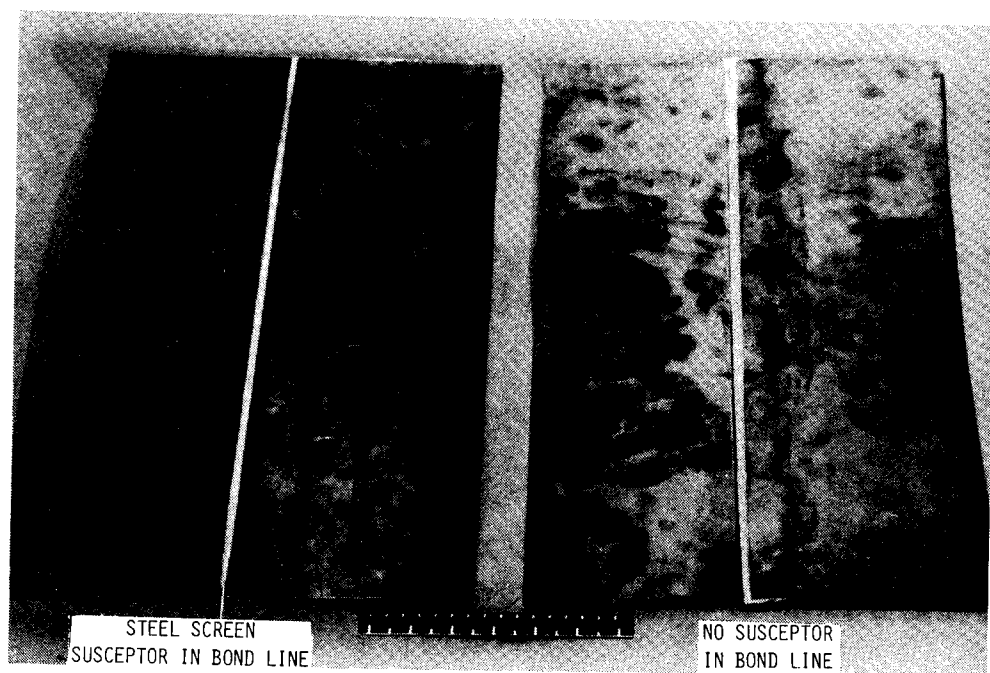
Titanium panels bonded with LaRC-TPI thermoplastic polyimide adhesive are shown. These panels were made by placing one sheet of titanium on the panel support atop several layers of fibrous insulation. The panels had previously been cleaned by simple degreasing and grit blasting. The titanium sheet was not primed before bonding. A 3/4-inch wide strip of adhesive tape the length of the panel was laid on this sheet with 1/8-inch protruding along the edge. If a susceptor was used, it was placed over the adhesive and another strip of adhesive tape placed on it. The other sheet of titanium was then laid on this assembly to produce a 1/2-inch overlap, the length of the sheets. As this photograph and the previous figure indicate, distortion in these panels was not excessive, considering that unstiffened sheets were bonded. The distortion was on the same order as that seen in similar panels bonded in a press or autoclave.

429

TYPICAL AEROSPACE SPECIMEN GEOMETRIES
FABRICATED BY RAB
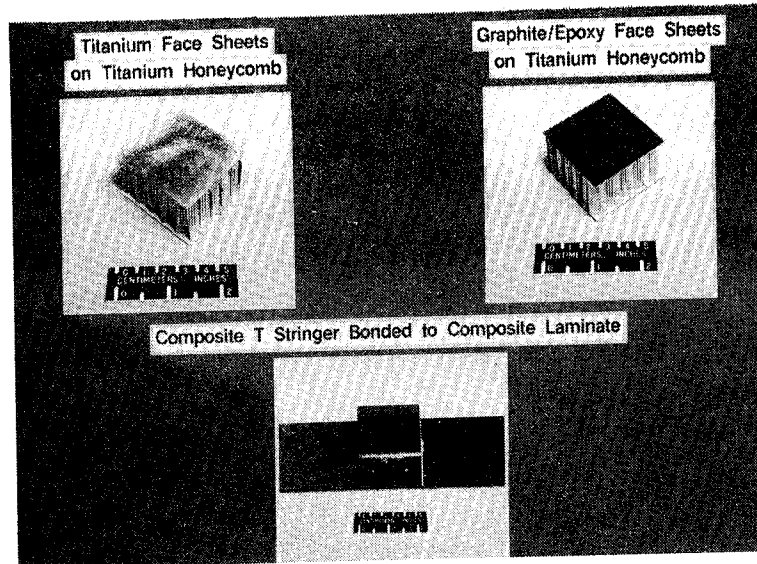
Panels or structures of many geometries can be bonded by the RAB process. Examples, shown above, are stiffeners or stringers on panels, honeycomb core panels, repair patches, etc. Simple fixtures would have to be designed to hold the specific geometries in place. The only significant geometric limitation with the current prototype equipment would be that one of the adherends must be 1/4 inch or less in thickness and the toroids must traverse and apply pressure to the outer surface of that adherend. The use of steel screen or stainless-steel foil susceptors in the bond lines of polymeric composite face sheet honeycomb core panels or stiffened panels may provide an additional advantage for aerospace applications - lightning strike protection. In a very complex structure, where autoclaving or press bonding with shaped platens is advantageous, RAB may still have an important role. RAB can be used in a "spot bonding" mode to hold parts in place before they are inserted into the autoclave or press, thus alleviating the need for a good deal of expensive fixturing.

FIELD REPAIR REQUIREMENTS

- **FAST REPAIR THAT IS STRUCTURALLY SOUND**

- **REPAIR UNDER ALL FIELD CONDITIONS**

- **LOW POWER REQUIREMENTS**

- **SIMPLE EQUIPMENT REQUIREMENTS**

- **EASY EXECUTION OF REPAIR**

- **LOW COST**

Field repair is the most challenging area of aircraft maintenance. The requirements for repair integrity and quality are difficult to meet because of the constraints of field operations. Bolted or riveted metallic panels are currently the most commonly used methods for structural field repairs in the aerospace industry. Such repairs utilize simple, readily available equipment and are usually easy to accomplish. However bolted or riveted repairs usually encompass areas much larger than the original damage, are heavy, and may have long-term durability problems. Adhesive bond repairs would be desirable but the problems of bulky, heavy equipment with high power requirements limit the applicability of current adhesive bonding techniques.

Field repairs must be executed in the shortest possible time with simple, lightweight equipment and low-power requirements. The repairs must be possible under severe weather conditions in primitive shelters. Repair materials must remain stable and handleable at temperatures from below 32°F to 120°F.

RAB FIELD REPAIR OF HELICOPTER WINDSCREEN
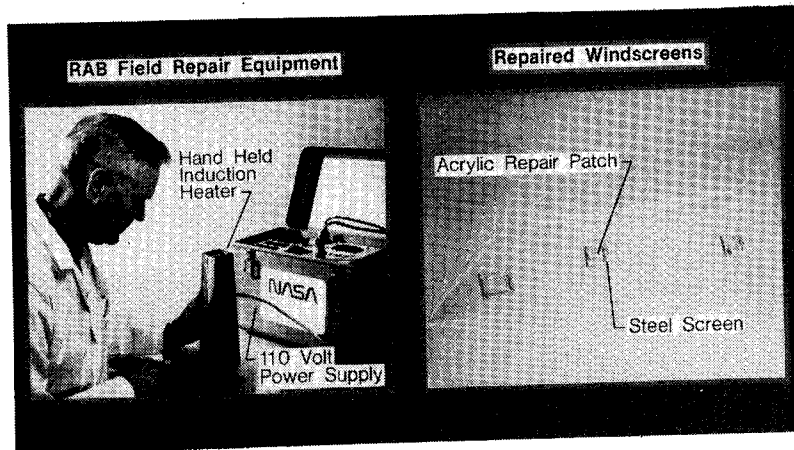
The Rapid Adhesive Bonding concepts described previously have been further developed to meet typical field repair requirements. The induction-heating power supply has been engineered into a "ruggedized" solid-state electronics unit, in a one-cubic-foot package weighing 20 pounds. A hand-held bonding gun weighing 3 pounds plugs into this power supply on a long power cord. The maximum power required for the single-toroid head is 300 watts. Adhesive bonds are attained rapidly by directly heating the susceptor and the adhesive in the bond line with minimal heating of the structure surrounding the bond line. Lightly loaded repair bonds can be made in several minutes at an average power input of 150 watts on metallic, polymeric, or polymeric-matrix composite secondary structures.

The repair of a helicopter windscreen in the field is currently achieved by "stop-drilling" the cracks emanating from the damage region. An acrylic or polycarbonate patch is drilled with matching holes and "laced" to the damaged windscreen with safety wire. This patch does not seal out the environment during operations. The above photograph illustrates the potential for RAB field repair of such a windscreen. Several "damage holes" were made in a polycarbonate windscreen with a .45 caliber service pistol to simulate battle-field damage. The polycarbonate patch and a ring of steel susceptor screen were cut from stock and laid over the holes. The hand-held induction head applied the required pressure while heating the screen to the melt temperature of the polycarbonate. The head was moved around the circumference of the patch to complete the bond in less than 10 minutes per hole. The patches formed doubler plates over the cracks emanating from the bullet holes to restrain crack propagation. The bonded patches should be effective in sealing the helicopter interior from rain and dust during operations. The RAB field repair technique provides a faster, simpler, stronger repair than the conventional field repair technique.

RAB REPAIR OF FUEL OR HYDRAULIC LINES
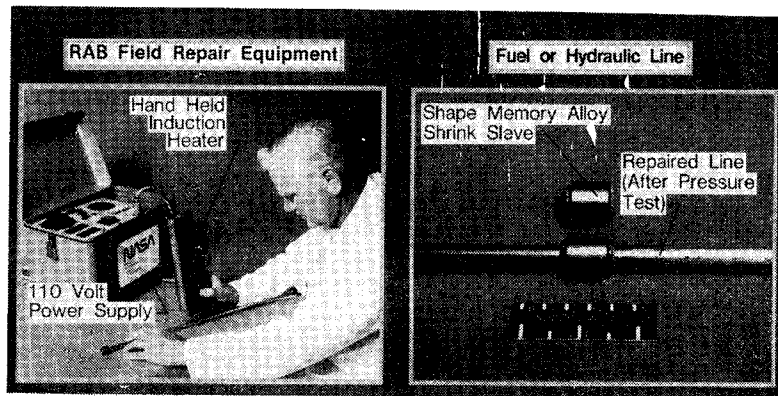
Another potential application for RAB is field repair of hydraulic fluid and fuel lines. Current fluid line repair procedures often utilize shrink sleeves (fabricated from "shape memory" alloys and an adhesive). An open flame from a torch is often used to heat the sleeves to the temperature at which they shrink (415°F) and bond to the line, effecting the repair. In the confined spaces of an airframe, fuel or hydraulic line vapors from the damaged line are often present; any open flame procedure can be hazardous. Furthermore, the uneven heating of a torching procedure can overheat the fittings. Oxidation, adhesive damage, uneven shrinkage, and warpage of the fluid line can result.

The RAB process was investigated as a simple method to heat the sleeves more uniformly and far more safely than a torch process. The results of these investigations are very promising. The RAB process heated the fittings uniformly and rapidly with minimal effect on surrounding areas. The hydraulic line repaired by RAB was tested to more than twice its rated operating pressure with no leakage. Repair of fluid lines in aerospace structures appears to be a very promising application for RAB.

RAB REPAIR OF GRAPHITE/EPOXY COMPOSITE LAMINATE
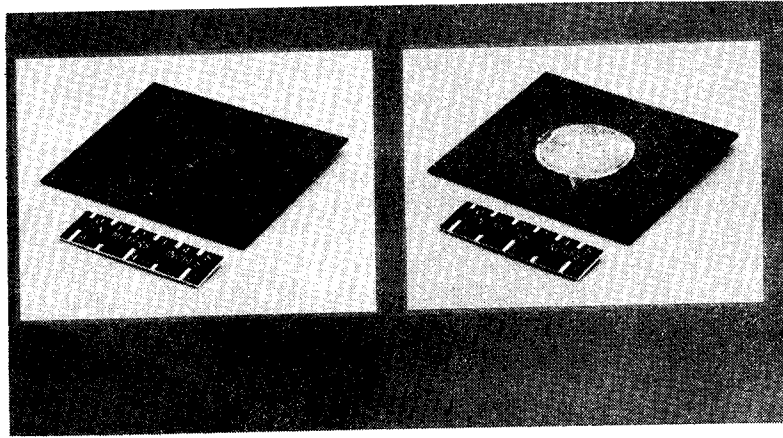
A common aircraft supportability requirement is the repair of small surface defects such as dents and gouges caused by impacts from runway debris, minor bumps, inadvertent occurrences during repair, etc. These are not structural concerns, but must be repaired to maintain surface integrity and, in many cases, aerodynamic smoothness. Rapid Adhesive Bonding techniques can be used to repair such minor defects. A patch of metallic or composite material, susceptor, and adhesive can be readily prepared with simple hand tools to fit the required repair geometry. A short bonding cycle using the hand-held unit shown previously is all that is required to wet the surfaces and cure the adhesive into a bond with adequate strength. The repaired surface can then be smoothed, if necessary, with conventional tools for this purpose. Such a patch on a graphite/epoxy composite panel surface is shown above.

RAB REPAIR MATERIALS
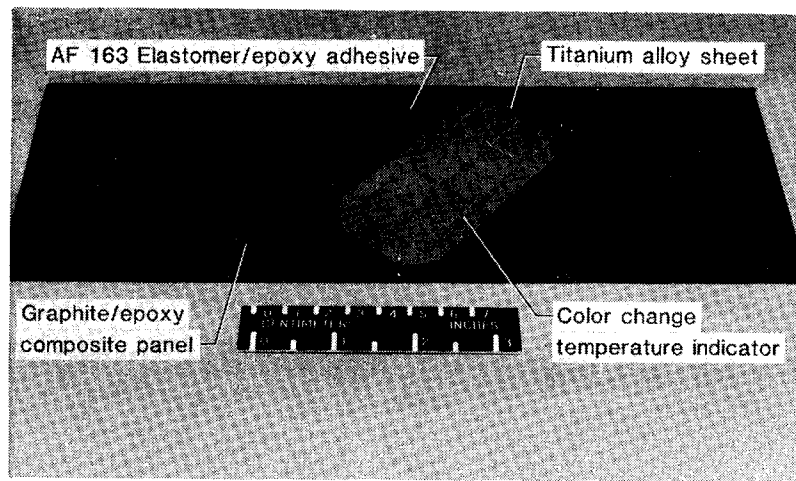
A preliminary feasibility study has begun on a structural RAB repair concept for a graphite/epoxy composite panel. The patch is composed of several laminated titanium alloy sheets, bonded sequentially using AF 163 elastomer modified epoxy adhesive. Color change indicators are used on each of the patch laminations to indicate that the bonding process has achieved the required adhesive cure temperature.

RAPID ADHESIVE BONDING REPAIR OF Gr/Ep
COMPOSITE PANEL USING LAMINATED TITANIUM SHEET
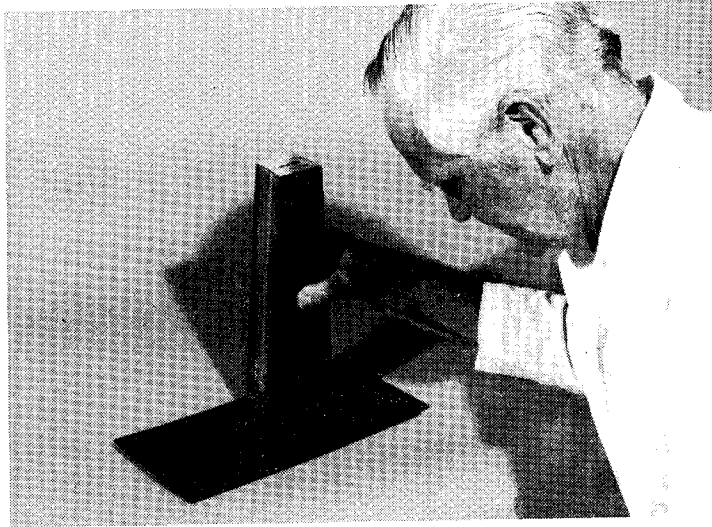
The hand-held RAB unit is again utilized in performing this laminated titanium sheet repair. Hand-induced bonding pressure is applied by the technician as he moves the bonding head in a path which traverses the entire patch. If a spot has not reached bonding temperature (as indicated by a lack of color change in the temperature indicating markings), he can return to that spot and reheat the adhesive.

RAB LAMINATED TITANIUM REPAIR
OF GRAPHITE/EPOXY PANEL
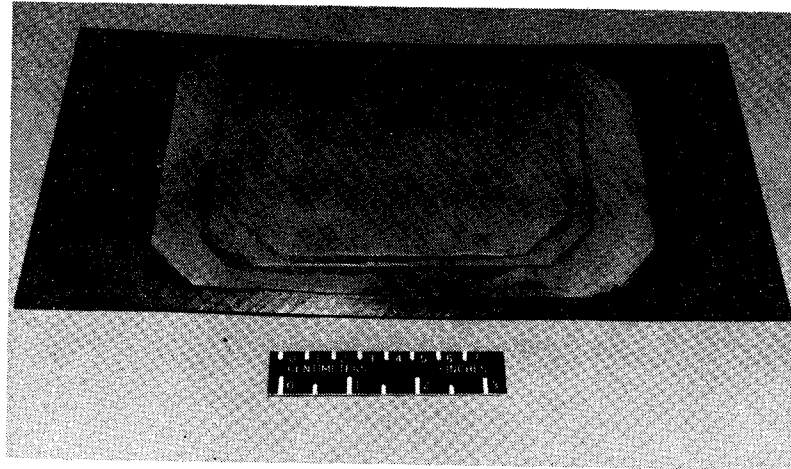
The initial feasibility specimen of a RAB laminated titanium alloy repair of a graphite fiber reinforced epoxy panel is shown. Process feasibility was demonstrated. Process enhancement studies are in progress. Structural tests on such panels have not yet been performed.

CONCLUDING REMARKS

RAPID ADHESIVE BONDING
High-Strength Bonds in Minutes
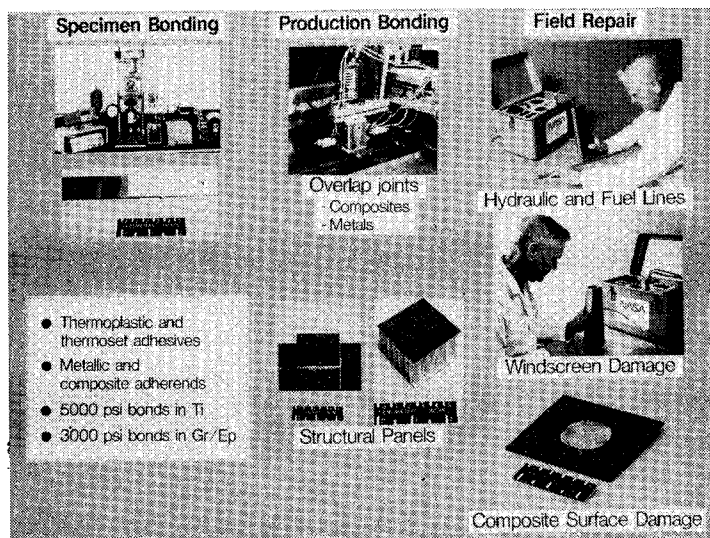
In conclusion, Rapid Adhesive Bonding (RAB) concepts and prototype equipment have been developed at Langley Research Center for specimen bonding, production bonding (including depot repair), and field repair. RAB utilizes induction heating methodology to provide heat directly to the bond line and/or adherend without heating the entire structure, supports, and fixtures of a bonding assembly. Bonding times for standard ASTM overlap shear specimens can be cut by a factor of 10 to 100 compared to standard press or autoclave bonding. High lap shear strengths can be generated with a range of adherend materials (including metals and polymer matrix composites) and adhesives (both thermoplastic and thermosetting). Short-term thermal cycling and water boil exposures have shown encouraging environmental stability for these rapid bonds, including those which contain steel screen or stainless-steel foil susceptors in the bond lines. The RAB concepts were extended to continuous seam bonding of metallic and composite panels with promising results for bonding of both like and unlike adherends. Rapid bonding of other geometries such as face sheets of fiber-reinforced polymeric-matrix composites or titanium alloy to titanium honeycomb core were proven feasible.

The inherent portability of RAB equipment suggested that field repair procedures for adhesive bonding of damaged metallic, polymeric, or composite structures are possible. Initial development of these procedures showed that patches of titanium alloy and graphite/epoxy composite materials could be bonded in the field to typical aircraft panels. Furthermore, variations of the RAB process can be used to repair polycarbonate or acrylic windscreen materials and hydraulic tubing. The promise of advanced composite and bonded metallic structures for improvements in structural efficiency and cost is limited by current processing and repair technology. Rapid Adhesive Bonding concepts show promise for significant technology advances.

REFERENCE

1. B. A. Stein, J. R. Tyeryar, and W. T. Hodges: Rapid Adhesive Bonding Concepts. NASA TM-86256, June 1984.

REDUCTION OF MOISTURE EFFECTS DURING THE CURE
OF EPOXY ADHESIVES USED IN COMPOSITE REPAIR

Joseph Augl and George T. Sivy
Naval Surface Weapons Center Detachment
White Oak, Silver Spring, Maryland

INTRODUCTION

The requirements for repair work on Naval aircraft composite wing skins that can be performed under depot conditions (or still worse, under field conditions) are quite restrictive. Equipment that can be used is rather limited as are the available repair space and time. The procedures must be simple enough so that they can be performed satisfactorily by personnel without special knowledge in composite materials technology. Repairs of small holes should not require more than perhaps a short predrying cycle (with heat guns) and a subsequent patch bonding using a heating blanket, held in place by applying a vacuum.

However, it has been observed during simulated experimental repair work that the glue lines frequently show a high content of pores and bubbles which are attributed to evaporation of moisture during the curing cycle. (Of course, other volatile materials such as residual solvent would act similarly). The purpose of this paper is to give some detailed analysis of the problem of moisture transport as a function of repair conditions, and to discuss some preliminary work to reduce the effect of moisture by removing moisture chemically with carbodiimides before it reaches a critical level for bubble formations.

DISCUSSION

MECHANISMS OF BUBBLE FORMATION, GROWTH, AND TRANSPORT

It appears that the major source of bubble (void) formation during repair of composites is moisture. When the partial vapor pressure of the dissolved moisture (or any other dissolved species), in the still liquid adhesive, exceeds the confinement pressure of its surrounding, bubbles may form, grow, and migrate.

There are probably always a large number of entrapped air bubbles present that can act as nucleating sites and there are many active interfacial sites that can lead to bubble formation, thus the probability for nucleation is high enough and therefore will not retard bubble formation due to volatilization.

The growth of voids is governed by 3 effects: 1) The entrapped air will expand according to the ideal gas law. Thus at constant pressure the relative increase in void volume (due to entrapped gas) is directly proportional to the change in temperature; 2) An additional growth is given by the added partial vapor pressures of volatile components dissolved in the adhesive (which is a function of their concentrations, governed by Henry's law, and by their temperature dependence); and 3) Void expansion will be limited by the confinement conditions. Obviously, this is a complex phenomenon that can not be easily calculated. It combines the applied external forces (for instance, the exterior pressure by the vacuum bag and the vacuum seen by the resin at its interface to air) and the integral of viscous forces that have to be overcome to move the confining liquid out of its way, which also includes surface tension effects of other voids that are pushed through narrow passages. One more and probably unimportant effect in the growth of bubbles is the coagulation of bubbles to form larger voids. This coagulation changes only the number of voids but not the void volume fraction.

To calculate effect 1 is trivial. Calculation of effect 2 is more difficult because it includes the rate of diffusion of volatiles into the bubble but can be done by numerical means. A calculation of the third effect appears to us rather hopeless. A recent discussion on that subject has been presented by Kardos et al.[1] We believe it might be possible to approach it experimentally

---

[1]Kardos, J. L., and Dudukovic, M. P., "Void Formation and Transport during Composite Laminate Processing," ACS Paper presented at Kansas City, Organic Coatings and Applied Polymer Science Proceedings, Sep 1982, p. 639.

by actually measuring the force necessary to push an adhesive at a given temperature through a model adhesive patch. (Thus, the integral forces are actually measured rather than calculated.)

Knowledge of all three effects mentioned above would probably suffice to estimate under which circumstances one reaches the critical conditions for rapid void generation and growth; i.e., <u>sufficient conditions</u> for void formation and growth.

However, it is not only considerably easier to estimate the <u>necessary</u> conditions for accelerated void growth, but also, in considering the necessary conditions only, one is automatically on the safe side which is more desirable anyway for practical applications.

NECESSARY CONDITIONS FOR RAPID VOID FORMATION

Since the increase in void volume (due to thermal expansion of entrapped air voids) is only linear with increasing temperature this effect is a simple superposition and shall not be considered here.

The necessary conditions for void growth therefore assumes that the viscosity effect is negligible compared to the pressure generated inside the void. This leaves us with the simple measurement of the equilibrium partial pressure of the volatile species (moisture, etc.) as a function of temperature and of its concentration (activity) in the adhesive, i.e., a determination of the sorption isotherm. This defines whether the vapor dissolved in the adhesive will tend to desorb into the void or not.

The concentration of moisture in the adhesive will change if moisture diffuses out of the heated composite into the adhesive or out of the adhesive into the applied vacuum.

Therefore we have, in essence, to deal simultaneously with the problem of volatility (vapor pressure of dissolved moisture) and of moisture transport as a function of applied pressure, temperature and concentration. The two important concepts to consider are therefore the sorption isotherm and a transport equation for moisture.

SORPTION ISOTHERMS

Sorption isotherms (or the equilibrium concentration between moisture dissolved and moisture in the gas phase) are usually given in the form of Figure 1, where ϕ is the weight (or volume) fraction dissolved, a = moisture activity, p = partial vapor pressure, p_0 = saturation pressure above pure water ($p*100/p_0$ is usually called relative humidity). This means that at a given relative humidity the immediate surface of the absorbent will be in equilibrium with its surrounding vapor (for all practical purposes instantaneously). The question of whether the diffusion of vapor is outward or inward is given by the concentration gradient in the interior of the sorbent and not by the average concentration. Thus, it is the boundary condition (which may change rather quickly) that will determine the net flow through the surface in a given time. The rate of flow is given by the slope, i.e., the moisture gradient.
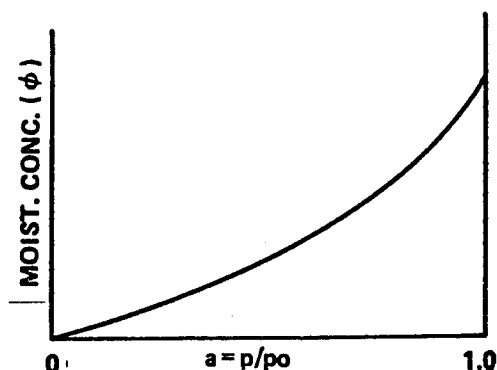
FIGURE 1. SORPTION ISOTHERM

In conjunction with the sorption isotherm one has to consider the vapor pressure curves as shown in Figure 2. The top curve of Figure 2 shows the vapor pressure curve of pure water as a function of temperature (i.e., 100 percent relative humidity). The other curves show the partial vapor pressures for the indicated relative humidities.

As an example let us say we had fully equilibrated a liquid adhesive at 60% RH and we would heat it (at 760 mm Hg=atmospheric pressure) then we would not expect to see bubbles form until the temperature has reached 115°C (not 100°C) as can be seen from Figure 2. If we had applied a vacuum of 10 mm Hg we might expect bubble formation as low as 19°C (slightly below room temperature). Note, these are only the necessary conditions; whether bubble formation really occurs depends on the total dynamics given by the sufficient conditions.

The relative humidity in the gas phase can change rapidly with temperature. For example, see Figure 2: assuming we had 60% RH at 20°C, this corresponds to 10^{-5}g H_2O/cm^3 of water in air (intersection 20°C with 60% RH curve). Heating this gas to 100°C (go horizontally to the right until intersecting the 100°C vertical) one can see that the RH is between 1 and 2.5. A reduction in pressure at constant temperature will have a similar effect (going down vertically on the same diagram). Thus, by using this diagram or an analytical representation of it one can easily determine the boundary conditions at each time step during the cure (the computer code uses a third degree polynominal subroutine to calculate the respective boundary conditions).

MODEL FOR A NUMERICAL APPROACH OF SOLVING THE DIFFUSION PROBLEM

For estimating the simultaneous transport of moisture in the composite and in the adhesive patch we believe that Fick's diffusion equation is suitable if there is a predrying step involved which removes quickly the moisture from the open pores, cracks and fiber debonds which have either existed in the virgin composite or which were caused by the normal aging in service or, more likely, which were generated as a result of the damage. A preheating step is not only beneficial in removing entrapped moisture in open pores but also will reduce the rate of moisture flux through the surface per unit time. It may not be necessary to remove all or even most of the moisture in a composite that is to be repaired. It is sufficient to reduce the rate of flux such that it will not
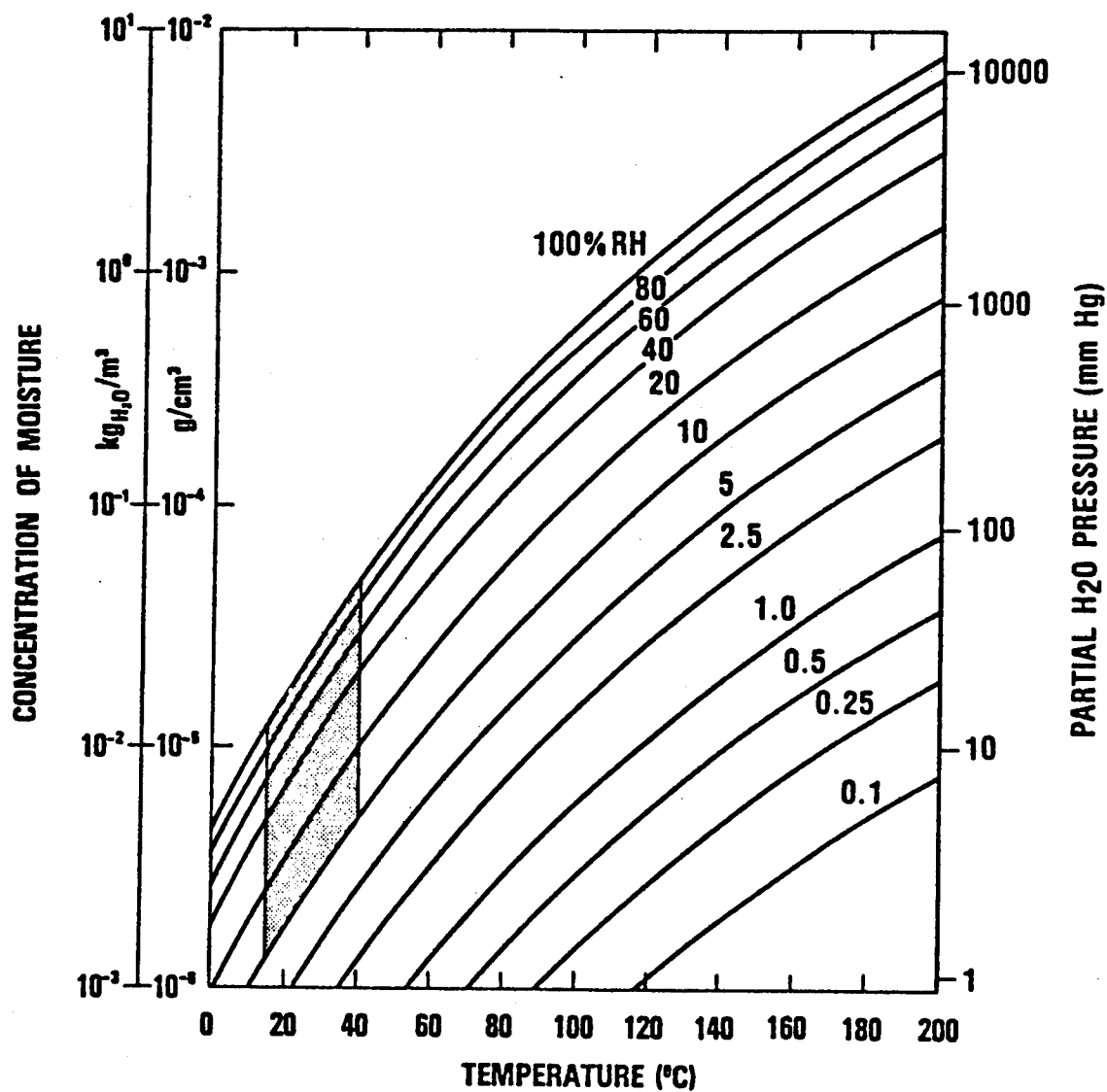
FIGURE 2. MOISTURE CONCENTRATION IN HUMID AIR AS A FUNCTION OF TEMPERATURE FOR DIFFERENT RELATIVE HUMIDITIES

exceed the critical, "necessary conditions" for bubble formation in the adhesive during the curing process or until the adhesive has reached at least the gelation point where it is no longer fluid.

For modeling the moisture transport we will use a finite difference approach, changing the Fickian equation to a finite number of linear algebraic equations that can be solved by a simple matrix inversion. In addition it is necessary to specify boundary conditions and curing conditions (which will govern the change in boundary conditions and diffusion coefficients). The following subsections will discuss some details of the modeling which include boundary conditions, curing conditions and other required input data, and finally, a specific example is considered where a metal patch is thought to be bonded to a carbon fiber composite.

FINITE DIFFERENCE EQUATIONS

Since the thickness of the composite plate to be repaired is small compared to the overlapping distance of the patch the problem of moisture transport by diffusion becomes essentially one-dimensional (away from the edges of the patch or the composite). Fick's equation (1) can be replaced by the finite difference equations (2):

$$\frac{\partial M}{\partial t} = D(T,M) \frac{\partial^2 M}{\partial X^2} \tag{1}$$

$$\frac{M_i^{n+1} - M_i^n}{\Delta_t} = \frac{2D\left(t^{n+1}\right)}{\Delta_i + \Delta_{i+1}} \left[\frac{M_{i-1}^{n+1}}{\Delta_i} - \left(\frac{1}{\Delta_i} + \frac{1}{\Delta_{i+1}}\right) M_i^{n+1} + \frac{M_{i+1}^{n+1}}{\Delta_{i+1}} \right] \tag{2}$$

In equation (1) M = Moisture concentration in ml H_2O per unit volume (ml) of composite or adhesive. (Note: For consistency the weight percent values are internally converted into volume percents via densities of adhesive and composite.) T = Temperature (°K), t = time (sec), X = distance (cm) into the composite and adhesive, D = moisture diffusion coefficient (cm^2/sec).

In equation (2) Δt = time step (sec), ΔX_{i+1} = finite distances in the x-direction, the subscripts i and i+1 in M represent the spatial points and the superscripts n and n+1 the points at the nth and $n+1^{st}$ time steps, $D(t^{n+1})$ is the diffusion coefficient at the $n+1^{st}$ time step.

Since the structure of the linear system of equations is quite similar to those we discussed previously in connection with modeling moisture diffusion in an outdoor environment we wish to refer to the respective report[2] rather than repeat the extended derivation. Suffice it here to say that the system of equations gives a tridiagonal matrix which upon decomposition into upper and lower triangular matrix is particularly easy and fast to invert with a computer.

INITIAL AND BOUNDARY CONDITIONS

To solve a general problem as indicated in Figure 3, it is necessary to consider five different boundary situations shown in Figure 4. The patch in Figure 3 can be either a composite or a neat adhesive, the bleeder cloth may be replaced by a metal sheet (thus providing a metal patch), the cover has the purpose of holding the patch in place by means of an applied vacuum. The honeycomb structure on the opposite side may be perforated to release the generated pressure, or may be closed, retaining the enclosed air and moisture which may develop a considerable internal pressure. Figure 4 shows the following boundary conditions: a. Composite/air; b. composite/closed cavity; c. composite/adhesive patch; d. adhesive/metal; e. symmetric condition (interior). Boundary condition e is actually the same as d.

Since the solubility of moisture in the composite is probably different from that of the adhesive it is necessary to introduce a distribution coefficient at this interface (boundary condition c) which governs the concentration on each side of the interface. This distribution coefficient $K_c = C_c/C_a$ is the ratio of moisture concentration in the composite to that in the adhesive (in terms of weight percent). Again, this is internally converted with respect to volume percent $K_d = K_c * \zeta_c/\zeta_a$.

In order to solve the diffusion equation one needs to know the initial distribution of the diffusant (moisture) in both the composite and the adhesive patch.

It is obviously not easy to determine the internal moisture distribution in the composite since this depends on its previous history. However, in the absence of specific data it suffices to assume the worst condition that one might find in a realistic environment; then, at least, one is on the conservative side of the prediction. (These and other assumptions will be discussed in the following subsection.) The concentration of moisture at the surface (or interface) and the diffusion coefficient (as a function of temperature) determine the rate of change of concentration in the interior. Thus, the sorption isotherms for both the adhesive and the composite have to be known as well as both diffusion coefficients and the temperature profiles of predrying and subsequent curing. If the room temperature RH is known for both the surrounding air and that in the honeycomb cavity (worst case, closed) then the RH changes with temperature and/or applied vacuum are easily calculated from the

---

[2]Augl, J. M., and Berger, A. E., The Effect of Moisture on Carbon Fiber Reinforced Composites. III Prediction of Moisture Sorption in a Real Outdoor Environment," NSWC/WOL/TR 77-13, Jun 1977, p. 13.
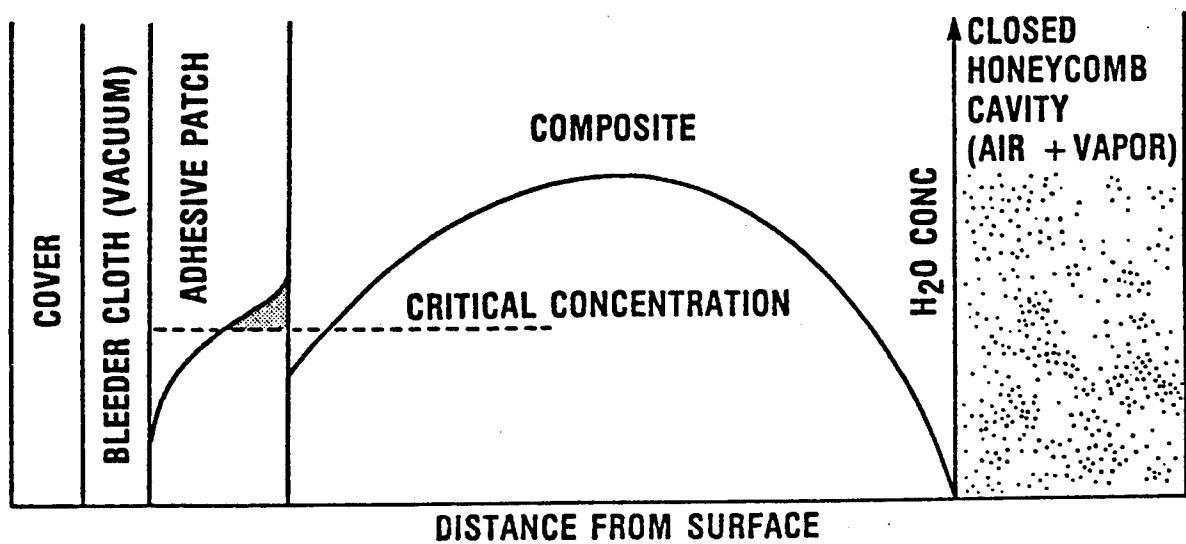
FIGURE 3. SCHEMATIC OF A MOISTURE PROFILE AT SOME TIME DURING
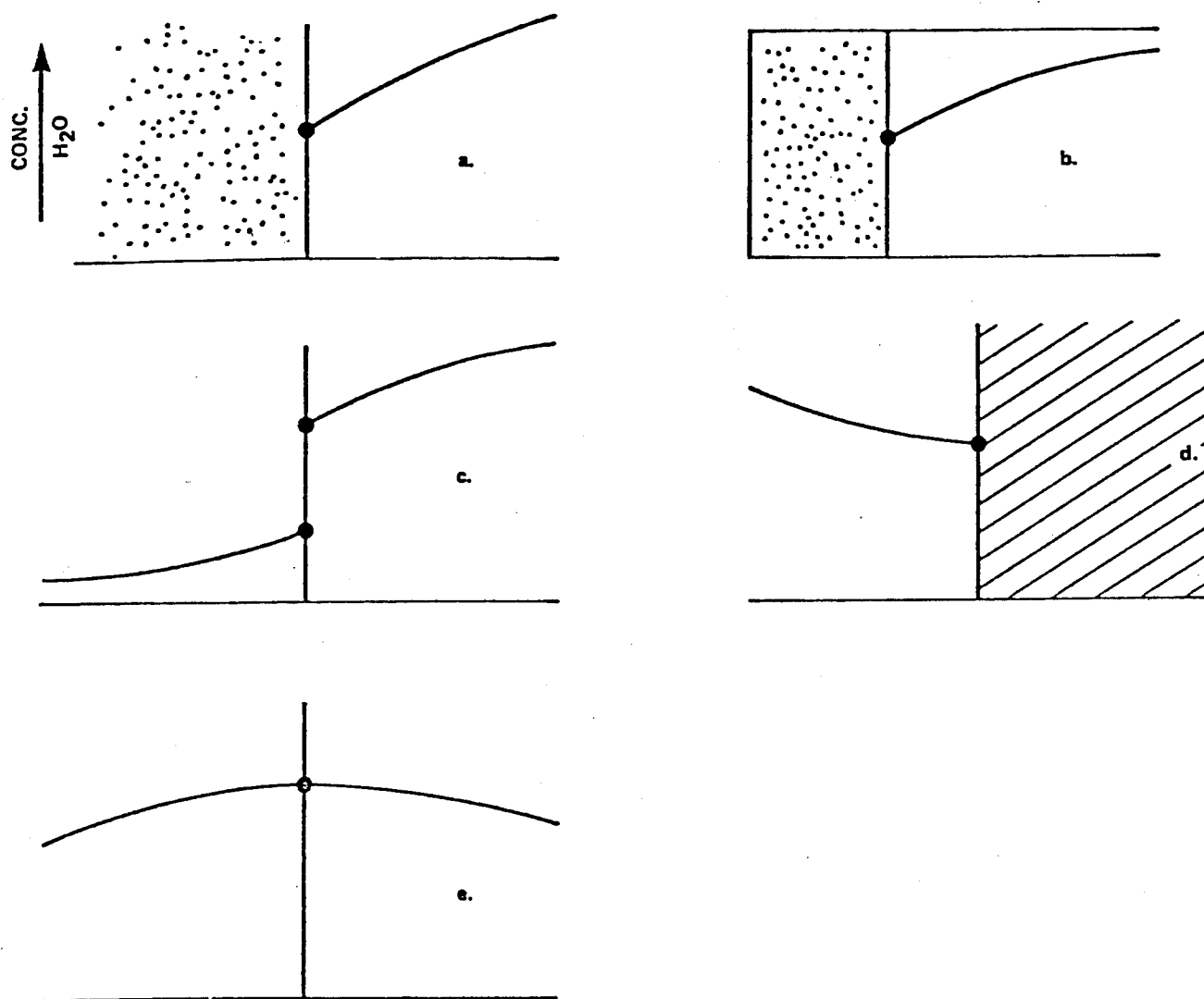THE ADHESIVE PATCH CURE

FIGURE 4. BOUNDARY CONDITIONS DURING DRYING AND CURING

steam table (given in Figure 2) which is done by a subroutine in the program. Moisture will diffuse into the adhesive and into the honeycomb cavity. The change in mass of water in the cavity and the combined pressure increase of air and vapor in the cavity are also calculated in a subroutine.

It appears that the initial condition of the moisture concentration in the adhesive should be easier to establish since it is the result of a controllable fabrication process. If the adhesive patch is prefabricated and sealed, or if the adhesive fluid is well sealed before use, one may expect that it will not exceed a preestablished maximum moisture concentration. The lower that is the better, because it then has a larger capacity to sorb additional moisture befor bubbles may form. During this time the adhesive may have gelled and will exert a much higher resistance to bubble formation, even when the necessary condition are exceeded.

REASONABLE FIRST APPROXIMATIONS FOR MATERIAL PARAMETERS

The following input data are required for solving the diffusion equation. a. Sorption isotherms of the composite and of the adhesive. (This establishes at the same time the distribution coefficient at the interface between composit and adhesive.) b. Diffusion coefficients as a function of temperature (and possibly of concentration) for both the adhesive and the composite. c. The initial moisture distributions in the adhesive and in the composite. d. The temperature profile of the predrying and curing schedule. e. The applied vacuum during the curing procedure. An accurate knowledge of all these data may be desirable but they are most likely unavailable in practical repair work. Thus, the question is: can one reasonably estimate the "necessary conditions" for bubble formation under prescribed predry and curing conditions?

The answer is that one can estimate a conservative, safe limit in time and temperature or any combination thereof by assuming "worst conditions".

In a previous investigation[3,4] we showed that it may take a very long time until the interior of a composite is in equilibrium with the average moisture level of its surroundings. Also, there are only very few places on the surface of the earth and sea where the average relative humidity exceeds 80%. Therefore, the assumption that the composite to be repaired has a uniform concer tration that is in equilibrium with a surrounding of 80% RH may, for all practical purposes, be considered as a worst case. Thus, in the absence of better information, we will take this value in order to be on the safe side.

For many polymers, rubbers and epoxy resins the sorption isotherm up to 80. RH is fairly linear so that the moisture concentration may be represented by $C = \gamma$ RH (where γ is a constant). (Of course any shape of the sorption isotherm can be approximated satisfactorily by a third or fourth degree polynominal if necessary.)

---

[3]Augl and Berger, Moisture. III, Jun 1977.

[4]Augl, J. M., and Berger, A. E., The Effect of Moisture on Carbon Fiber Reinforced Composites. I Diffusion, NSWC/WOL/TR 76-7, Sep 1976.

For instance, the moisture equilibrium in Hercules 3501-6 epoxy resin at 80% RH is 3.76% (by weight) and for the composite with 0.62 fiber volume fraction it is 1.18%. Also, it appears that the sorption isotherm is not too strongly dependent on the temperature.[5,6] Thus the temperature dependence of the sorption isotherm may in a first approximation be taken as independent or at worst linear with temperature.

For many epoxy resins the temperature coefficient of the diffusivity (i.e., the activation energy of diffusion) is about the same[5] though the absolute values may differ within an order of magnitude between 10^{-9} to 10^{-8} cm^2/sec. Using a finite difference method[5], we obtained the change in composite diffusion coefficient as a function of fiber volume fraction which was in good agreement with experimental measurements. For carbon fiber lamina of a volume fraction of 0.62 the diffusion coefficient is about 23% of that of the neat resin matrix. The temperature coefficient in composites is the same as that of the matrix (if there is no appreciable diffusivity in the fiber itself). The program uses the diffusion coefficient for Hercules 3501-6 and its temperature coefficient as default values (which can be easily changed if necessary). It also appears that, for a number of polymer systems,[6] the temperature coefficient of the moisture diffusion coefficient is the same below and above glass transition temperature. Whether this behavior also extends into the ungelled state is not explored. However, as a first approximation it was taken to be such. (Experimental measurements are planned to investigate this assumption.)

CONVERGENCE OF THE METHOD

One of the questions in using differences instead of differentials is obviously the convergence as a function of time and space differences.

Figure 5 shows the calculated interior moisture distribution through half the composite after 10 hours drying time using 1, 2, 4, 10, 20, 40 and 100 time steps. This figure shows that 10 time steps seem quite adequate for practical purposes. The same absolute time step does not give equally good convergence for different times (see Figure 6) where 360, 720, and 1500 sec were used as time steps to calculate the internal moisture distribution after 1 and 10 hours drying time. In order to obtain an equally good time step which is independent of composite thickness we used arbitrarily a 1/2000 of the time necessary to reach 97% of the equilibruim concentration. This time we call quasi equilibrium time. (Why not wait until the system is at 100% equilibrium? Because it takes infinitely long to get to that point.) The quasi equilibrium time is given by $t_{eq} \simeq 1.5 * h^2/D$ and therefore $\Delta t = 1.5 * h^2/(2000 * D)$. This time step assures good convergence for all practical time intervals of interest. (It is automatically chosen by the program and may be changed manually if so desired in order to obtain simple printout time intervals).

---

[5]Augl and Berger, _Moisture. I_, Sep 1976.

[6]Stannett, V., and Williams, J. L., "The Permeability of Poly(ethylmethacrylate) to Gases and Water Vapor," _J. Pol. Sci. Part C_, No10,45 (1965).
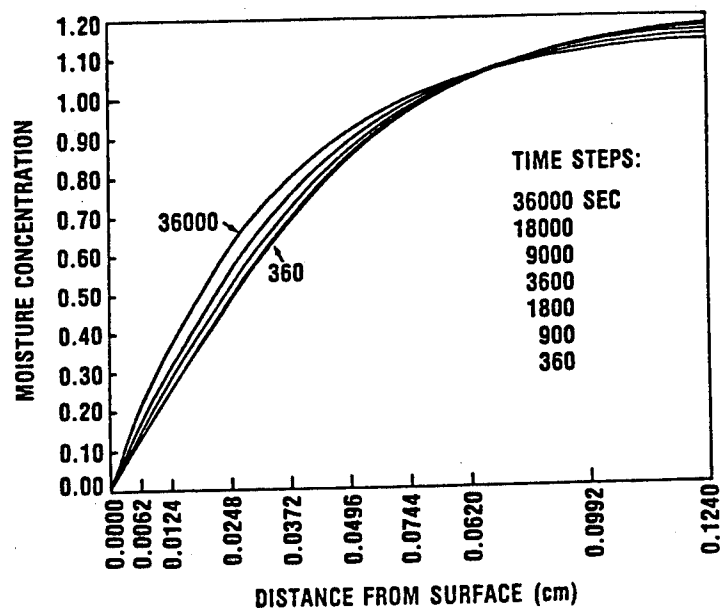
FIGURE 5. CONVERGENCE OF FINITE DIFFERENCE METHOD USING DIFFERENT Δt
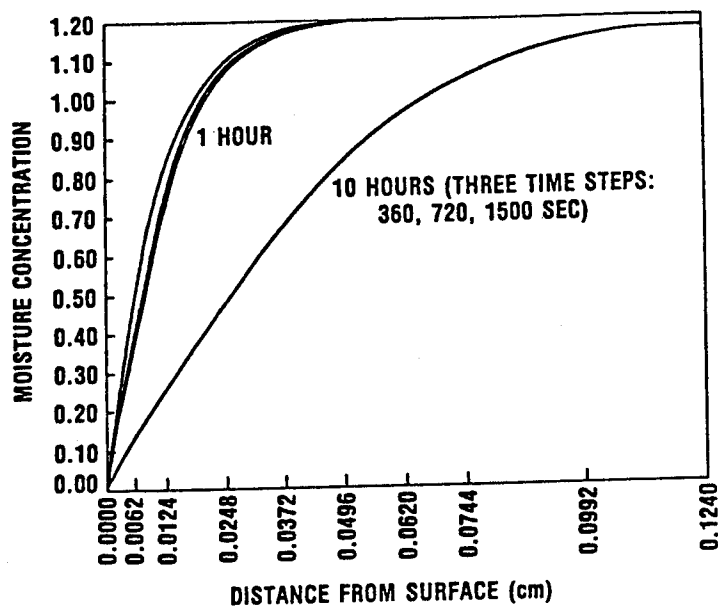

FIGURE 6. CONVERGENCE OF FDA METHOD FOR SAME Δt BUT DIFFERENT TIMES

SPECIFIC EXAMPLE

Since it may lead to a better understanding of the discussion we want to run briefly through a specific example.

We will consider a 3501-6/AS carbon fiber epoxy composite plate (since we have studied the sorption and diffusion behavior of this resin in some detail[7]). The plate is to have a thickness of .248 cm and is to be repaired with an adhesively bonded metal sheet. The glue line shall be 0.01 cm, and the initial moisture concentration in the adhesive 0.1%. The opposite side of the composite plate is a closed honeycomb structure which we assume to confine the moisture (worst case). The composite shall be predried for 2 hours at 150°C with heat guns. After this predrying step the metal/adhesive plate is bonded to the composite. The applied vacuum is 500 mm Hg. The temperature is raised to 121°C at a rate of 2°C per minute and held at this temperature for 45 minutes, then the temperature is increased to 177°C at a rate of 2° per minute. The final hold time at this temperature is 120 minutes.

The limited time for predrying can obviously not remove all the moisture in the composite. To do that would require times as long as those shown on Figure 7 where the times to remove 97% of all the absorbed moisture are shown as a function of composite thickness and drying temperature.

Another question which is frequently asked is whether it is possible to shorten the drying time significantly if, in addition to heat, vacuum is also applied to the composite. The perhaps surprising answer is no. Figure 8 shows the difference in internal moisture concentrations after 10 hours drying time for different temperatures with and without use of vacuum. Only at 70°C the graph resolves two slightly different curves. At 100°, one can barely resolve the difference and at higher temperatures it can not be seen. The reason is simple. The surface equilibrium is given by the surrounding RH which decreases rapidly with increasing temperature and therefore vacuum has little additional effect on the internal gradient.

Therefore a reasonable predrying time of two hours was chosen. The change of the internal moisture distribution after 30, 60, 90 and 120 minutes is shown in Figure 9. Figure 10 shows the moisture distribution in the adhesive and in the composite at 30 minute time intervals during the indicated curing schedule.

The corresponding critical concentrations not to be exceeded were given (in weight %) as: 4.89, 1.67, 1.67, and 0.37 up to the end. Looking at the concentration profiles in the adhesive (see Figure 10) one can see that the first 3 time steps do not exceed this critical limit but as the ultimate cure temperature is reached (between 1.5 and 2 hours) the sorbed moisture

---

[7]Augl, J. M., Moisture Sorption and Diffusion in Hercules 3501-6 Epoxy Resin, NSWC TR 79-39, Mar 1979.
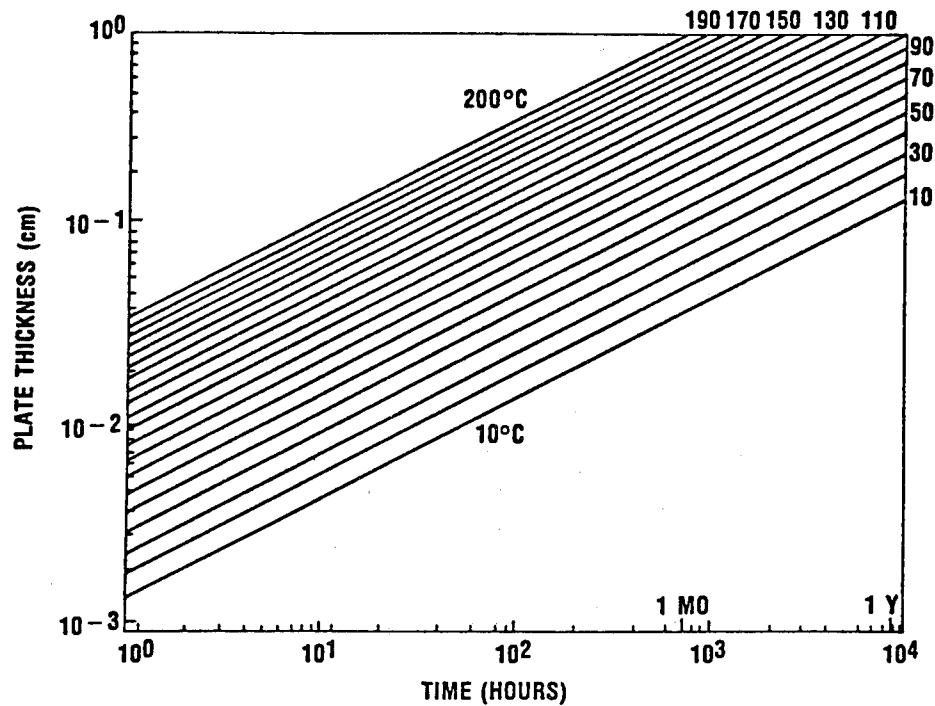
FIGURE 7. SORPTION TIMES TO 97% OF THE EQUILIBRIUM CONCENTRATION
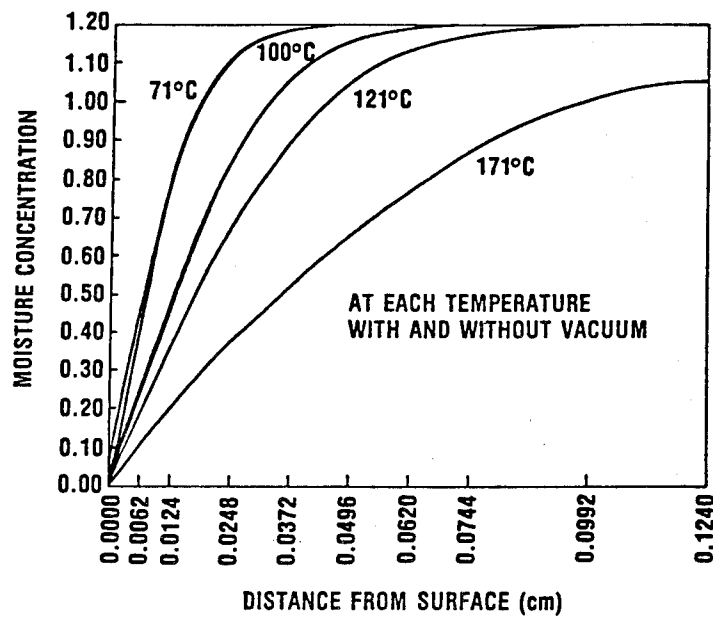FOR A COMPOSITE WITH V_f = 0.62 (3501-6 RESIN/CARBON FIBER)

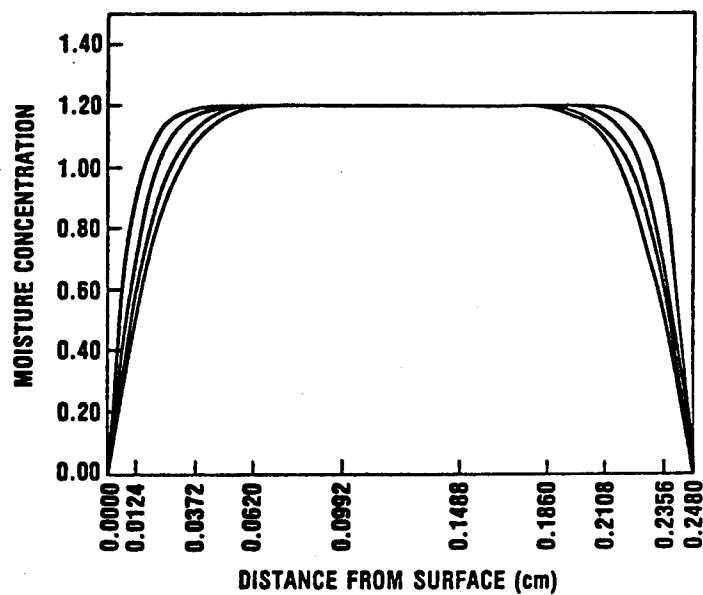FIGURE 8. EFFECT OF DRYING WITH AND WITHOUT VACUUM (10 HRS)

FIGURE 9. MOISTURE DISTRIBUTION IN THE COMPOSITE AFTER 30, 60, 90 AND 120 MINUTES (WITH A UNIFORM 1.2% DISTRIBUTION AT TIME ZERO)
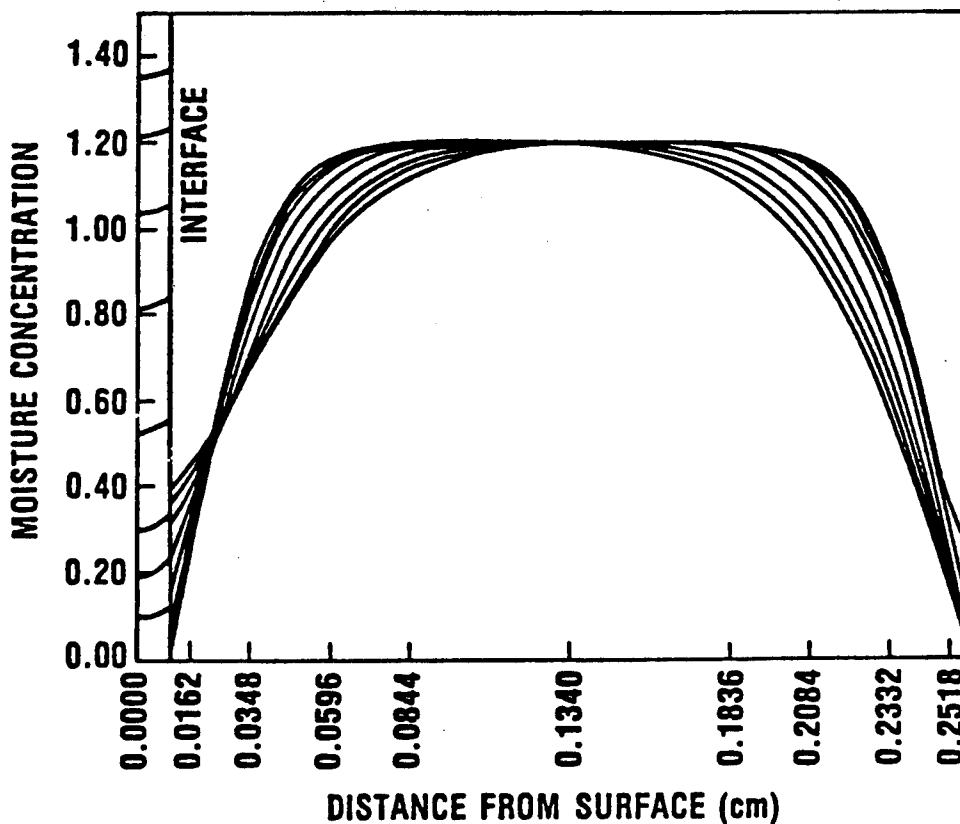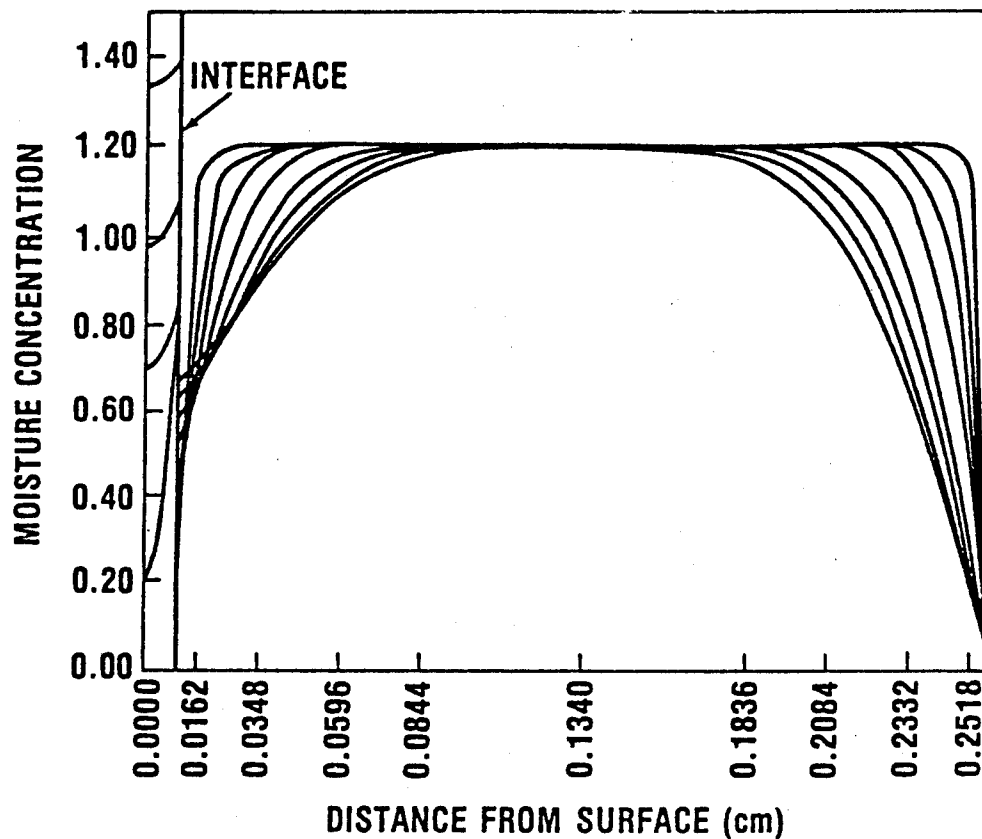

FIGURE 10. MOISTURE DISTRIBUTION (IN 30 MIN. INTERVALS) IN THE COMPOSITE AND IN THE ADHESIVE DURING THE PATCH BONDING PROCESS. (USING A PREDRIED COMPOSITE)

exceeds the critical concentration which may lead to bubble formation unless the adhesive has sufficiently gelled in the meantime to prevent void expansion and transport. If there is no predrying step, the moisture pickup in the adhesive is much higher per unit time as can be seen on Figure 11 (where the fifth moisture distribution line is already out of plotting range), although the first hold temperature (121°C) remains in the safe range (below 1.67%).

FIGURE 11. MOISTURE DISTRIBUTION (IN 30 MIN. INTERVALS) IN THE COMPOSITE AND IN THE ADHESIVE DURING THE PATCH BONDING PROCESS (WITHOUT PRIOR DRYING STEP).

USE OF CARBODIIMIDE AS MOISTURE SCAVENGER

OTHER SOURCES OF MOISTURE

Table I lists the 3 possible sources of water which need be considered during the adhesive cure. The latter two have been discussed in the preceding sections; the last source will briefly be discussed here. Amines are known to readily form hydrates upon sitting in moist air, but the number of hydrated waters is still questionable. This penchant to hydrate is facilitated by the physical mixing of the hardener with the resin to prepare the adhesive.

For example, Figure 12 shows the weight increase as a function of time for mildly predried amine being stirred at two different relative humidities. From this plot one can clearly see that after a relatively short time, stirring at 50-60% RH results in a considerable gain in moisture content.

ADDITION OF WATER TO CARBODIIMIDES

In the context of composite repair, any attempts to mitigate void formation in the adhesive as a result of the cure cycle must contend with both the composite moisture as well as the adhesive moisture. Even if the composite sufaces could be completely dried, moisture would still be present in the adhesive.

Chemical additives such as isocyanates or acid anhydrides could be incorporated in the adhesive to react with moisture but both of these groups react with the amine as well as with water. Furthermore, should the isocyanate react with water, CO_2 would be eliminated which would result in void formation.

A class of compounds which resembles the isocyanates is carbodiimides (Table II). Carbodiimides, like isocyanates, are characterized by cumulative double bonds and, therefore, undergo addition reactions similar to isocyanates. However, unlike iscoyanates, carbodiimides add water to form stable ureas.

Table III lists the types of carbodiimides examined thus far.

Intuitively, one might expect amine addition to the carbodiimide leading to formation of guanidines. This appears to be the case for the aromatic carbodiimides only. Infrared data have shown that for R=R'= aromatic, addition of amine is favored due to the increased suceptibility of the central carbon atom to nucleophilic attack by the amine. Conversely, carbodiimides containing electron donating groups (R=R'=aliphatic) will preferentially add water. Accordingly, the aliphatic carbodiimides were chosen as candidate water scavengers with the dicyclohexyl carbodiimide (DCC) receiving the most attention due to its solubility in the resin, high boiling point, and availability.

TABLE I

SOURCES OF MOISTURE

1. WATER ABSORBED IN ADHESIVE

    − WATER OF HYDRATE OF AMINE (1:1)

    − EXCESS WATER FROM MIXING

2. MOISTURE ABSORBED IN COMPOSITES
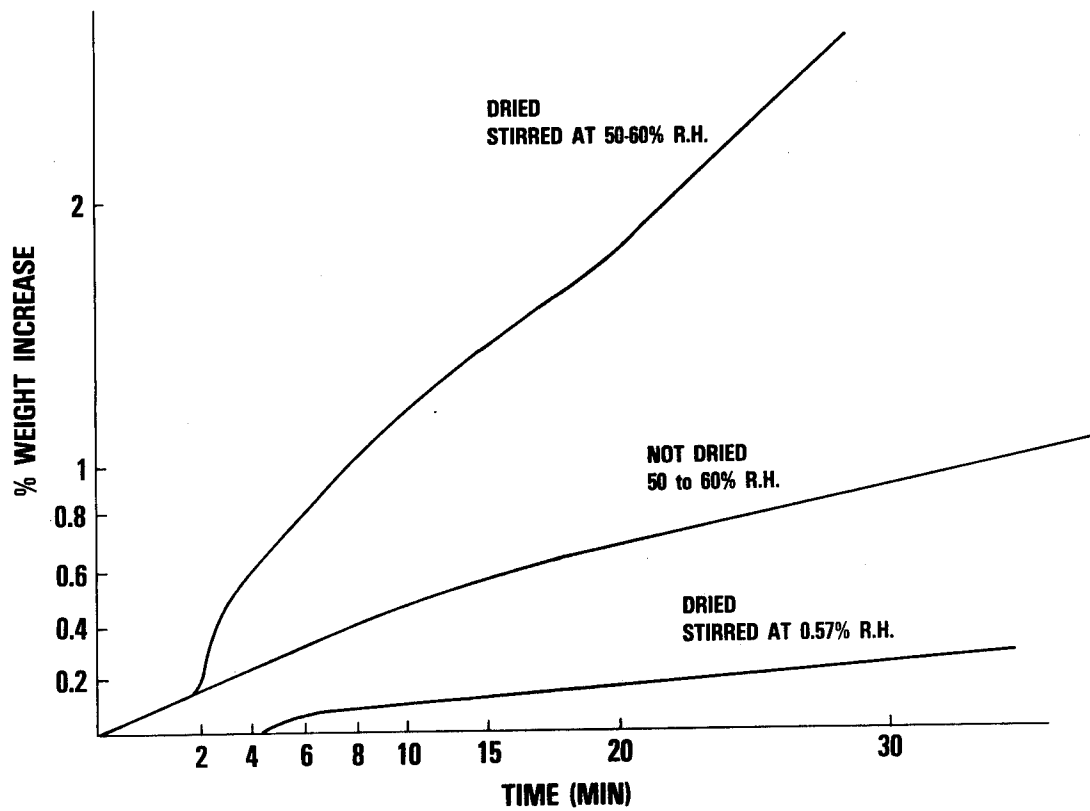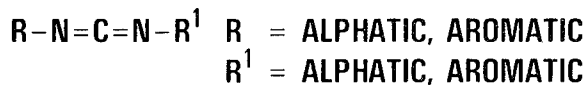
3. MOISTURE IN STRUCTURES NEAR AREA TO BE REPAIRED

FIGURE 12. WEIGHT INCREASE AS A FUNCTION OF TIME FOR PACM-20 BEING STIRRED UNDER DIFFERENT RELATIVE HUMANITIES.

TABLE II

CARBODIIMIDES

$$R-N=C=N-R^1 \quad R = \text{ALPHATIC, AROMATIC}$$
$$R^1 = \text{ALPHATIC, AROMATIC}$$

REACTIONS: ADDITION REACTIONS DUE TO DOUBLE BOND

PHYSICAL PROPERTIES:

ALPHATIC: LIQUID, OR CRYSTALLINE SOLID

AROMATIC: CRYSTALLINE SOLID

STABILITY: DEPENDS UPON R; $(R_3 C-) > (R_2 CH-) > (RCH_2^-)$

TOXICITY: UNCERTAIN. SOME ARE ANTI-TUMOR

TABLE III

MATERIALS

CARBODIIMIDES:

STABAXOL-M (M.BAY)
(STAB)
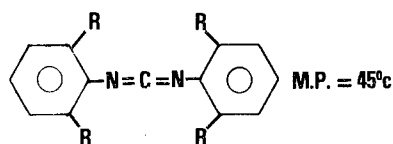
M.P. = 45°c

R = ISOPROPYL

DIISOPROPYL CARBODIIMIDE
(DIC)

B.P.=186°c
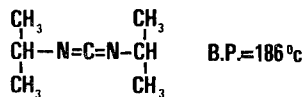
ETHYL-3 (DIMETHYLAMINO) PROPYL CARBODIIMIDE HYDROCHLORIDE
(EPC.HCL)

DICYCLOHEXYLCARBODIIMIDE
(DCC)

457
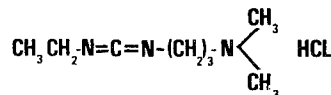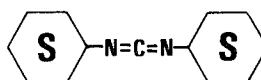
In order to demonstrate the ability of DCC to react with water in the presence of the amine, one is referred to the IR spectra shown in Figures 13, 14, and 15. Figure 13 shows the IR spectrum in the range of 4000 to 1333 cm^{-1} of a 1:1 equimolar mixture of the amine and water. In the 4000 to 3000 cm^{-1} the broad intense absorption due to water completely obscures the NH_2 absorptions of the amines. Figure 14 shows the IR spectrum of the same water/amine mixture with an equimolar amount of DCC added taken after 1 minute at 75°C. The intense absorption at approximately 2175 is due to the $-N=C=N-$ stretching of the carbodiimide; but, most importantly, in the previously water dominated 4000-3000 cm^{-1} range, bands attributable to the NH_2 stretching deformations are now discernable. After 3 minutes, at 75°C (Figure 15), the broad water absorption has been mitigated while the two NH_2 bands (and even the overtone) are now prevalent in the high frequency region. The 2175 band is also greatly reduced. Such spectral changes clearly establish DCC's ability to react with moisture.

To determine the efficacy of DCC with regard to composite repair, lap shear strengths of aluminum/aluminum and composite/composite joints bonded with epoxy-amine adhesive were measured. The specific epoxy-amine adhesive system is shown in Figure 16. Acid etched aluminum lap joints were prepared [ASTM-D3163 (ref. 1), 9 1/2" X 1", 1/2" overlap] using a predried resin and resins equilibrated at 80% RH with varying concentrations of carbodiimide or without. Similarly, lap joints were made from graphite/epoxy composites, both predried and equilibrated at 80% RH, using adhesive containing varying concentrations (0-16 wt%) of carbodiimide. For all joints a mylar scrim cloth (American Cyanamid BSC 1176/2385) was employed to ensure a uniform bond line of approximately 5 mil.

The cure schedule was as follows:

Heating Rate: 1°C/min

Vacuum: 630 mm Hg

At 65°C full vacuum was applied and the heating rate was increased to 2°C/min up to 150°C and held at 150°C for 1 hour.

Figures 17 and 18 show the lap shear strengths as a function of weight % carbodiimide of both the aluminum and composite lap joints respectively. The aluminum lap joints bonded with an 80% RH resin containing 3 to 16 weight % carbodiimide (Figure 17) show increased load at failures ($\sim$ 80-100%) as compared to similar joints without carbodiimide. Lap joints made of graphite composite material equilibrated at 80% RH and bonded with adhesive containing carbodiimide (Figure 18) also show an increased load at failure as compared to the same joints without carbodiimide. Furthermore, varying the concentrations of carbodiimide has a significant effect on strength. For both aluminum joints bonded with 80% RH resin and composite joints equilibrated at 80% RH the strength of the bond increases with increasing carbodiimide content and reaches a maximum with 2-5 weight % loading. Above the range (up to 16 weight %) the strength begins to decrease but still remains above the 80% RH cases without carbodiimide.
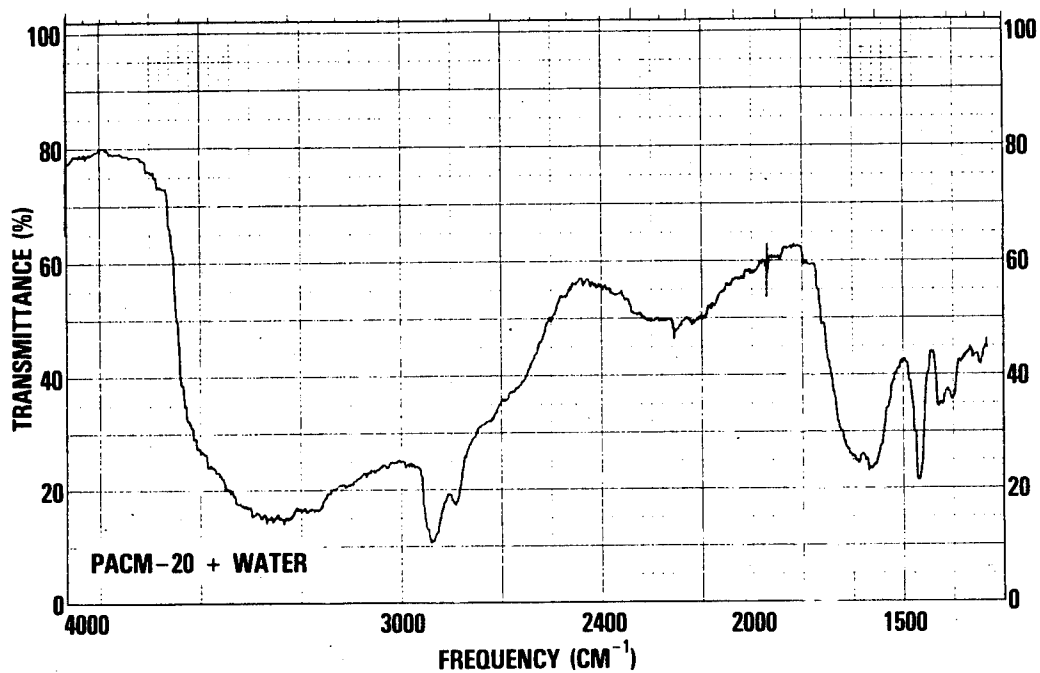
FIGURE 13.   INFRARED SPECTRUM OF AN EQUIMOLAR MIXTURE OF PACM-20 AND WATER.
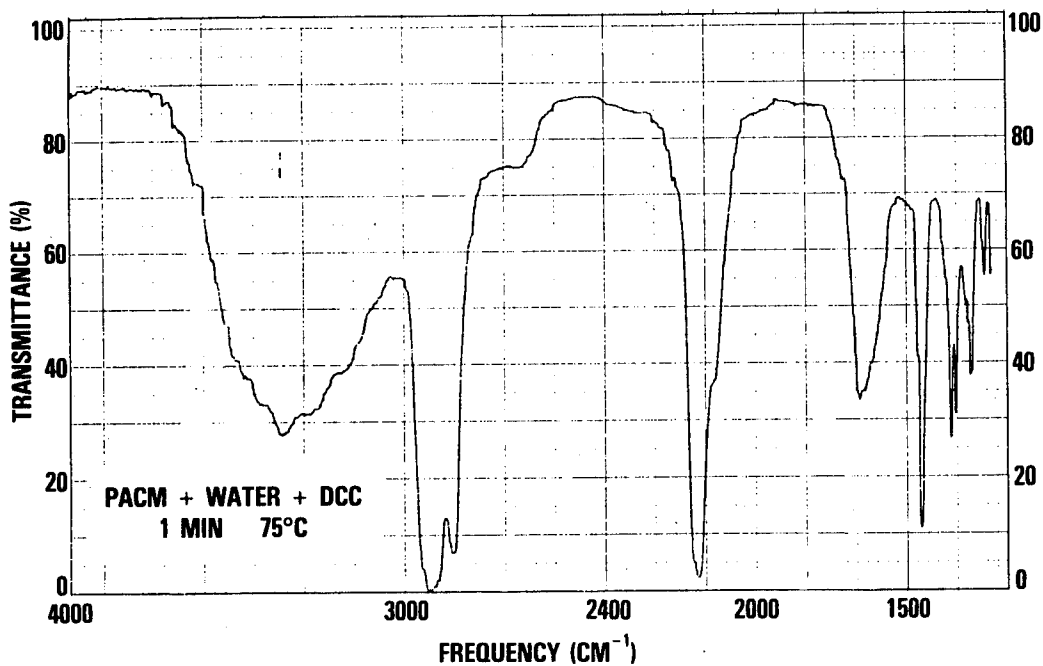

FIGURE 14.   INFRARED SPECTRUM OF AN EQUIMOLAR MIXTURE OF PACM-20,
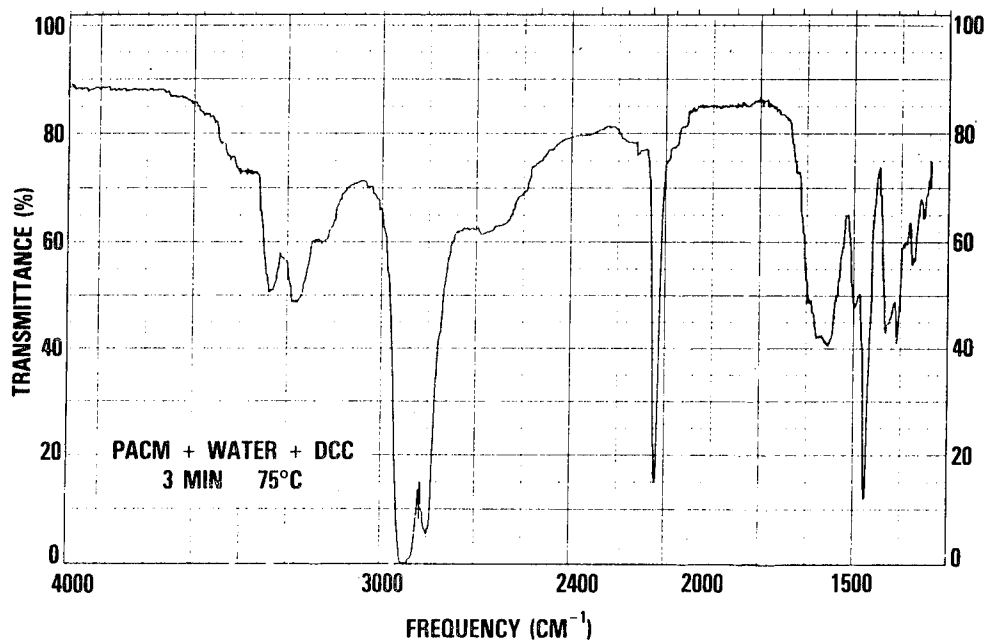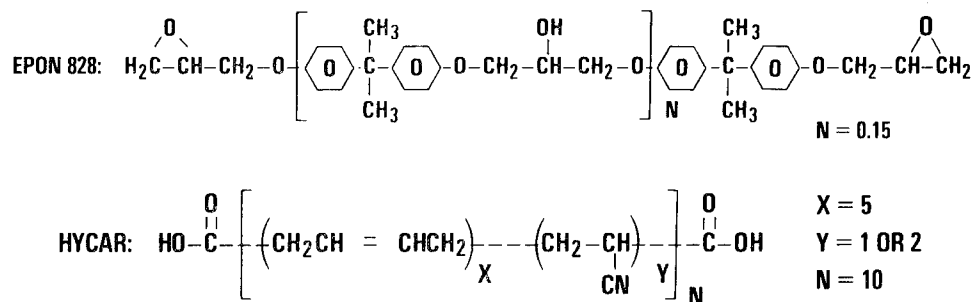   WATER, AND DCC AFTER 1 MINUTE AT 75°C.

FIGURE 15. INFRARED SPECTRUM OF AN EQUIMOLAR MIXTURE OF PACM-20, WATER, AND DDC AFTER 3 MINUTES AT 75°C.

RESIN: EPON 828 MODIFIED WITH HYCAR CTBN 1300 × 8
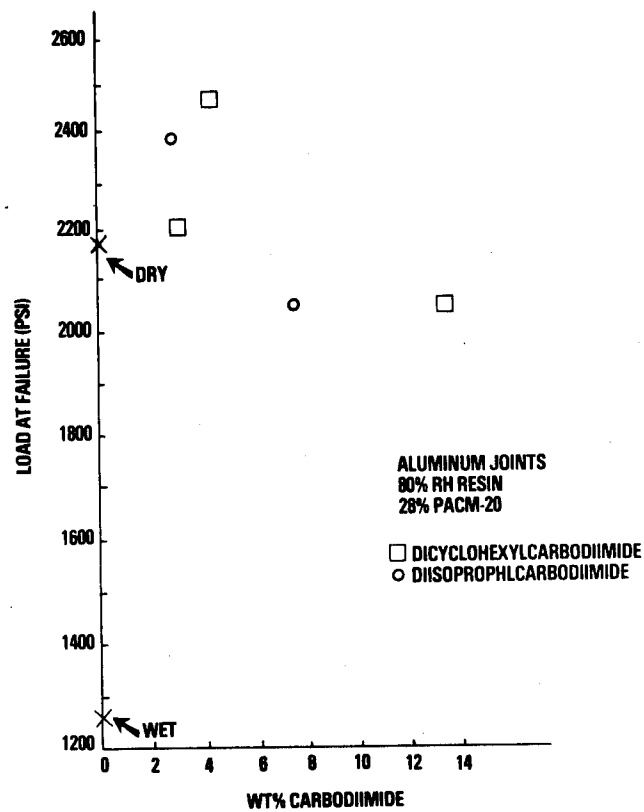

HARDNER: DUPONT PACM-20

FIGURE 16. MATERIALS

460

FIGURE 17. LOAD AT FAILURE AS A FUNCTION OF WEIGHT % CARBODIIMIDE
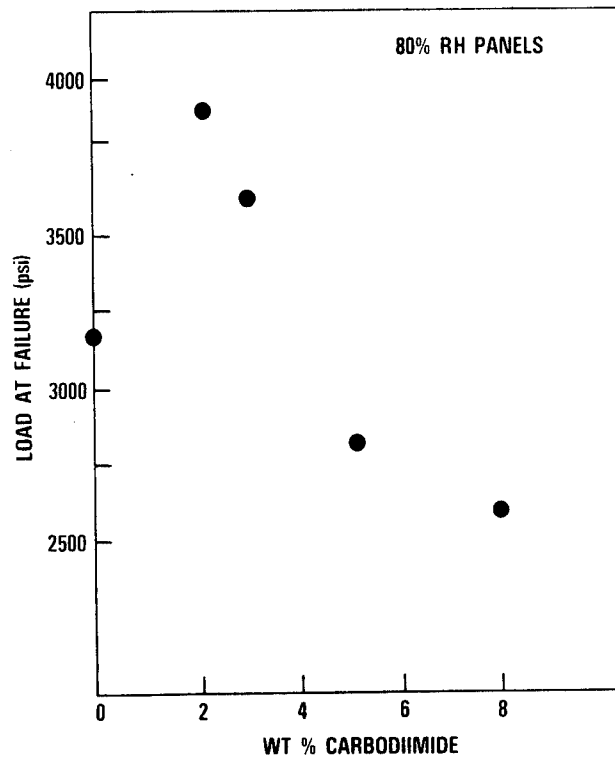(IN AN 80% RH RESIN) FOR ALUMINUM LAP JOINTS.

FIGURE 18. LOAD AT FAILURE AS A FUNCTION OF WEIGHT % DCC
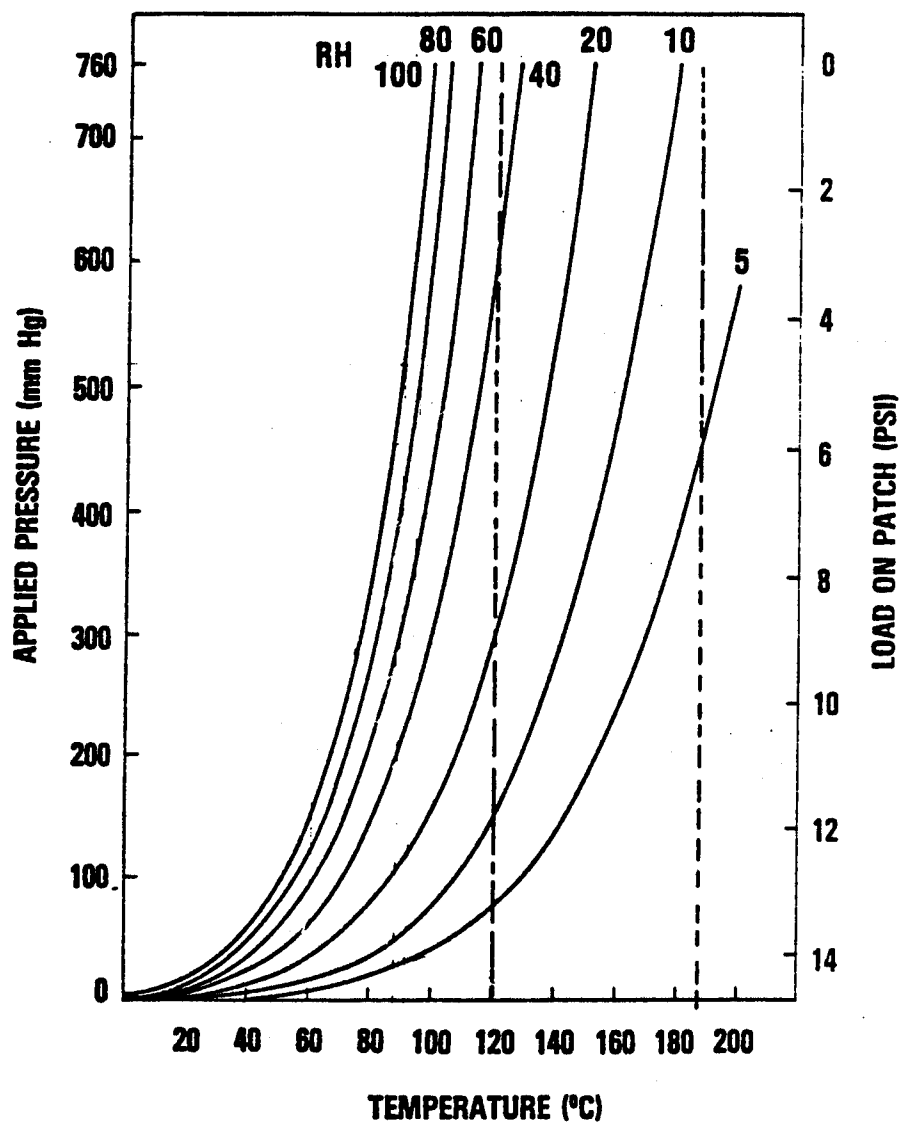FOR COMPOSITE PANELS EXPOSED TO 80% RH.

FIGURE 19. EQUILIBRIUM PRESSURE OF WATER VAPOR AS A FUNCTION OF
TEMPERATURE FOR DIFFERENT RELATIVE HUMIDITIES

CONCLUSIONS AND CONSIDERATIONS FOR OPTIMIZATION

1. The "necessary conditions" for bubble formation in an adhesive during patch cure have been discussed on the basis of sorption isotherms and vapor pressure curves. Fick's diffusion equation together with the changing boundary conditions (which are governed by the predrying and curing procedures) allow one to calculate the moisture distributions in the adhesive and in the composite at all times, and therefore to estimate the critical conditions for bubble formation.

Partial predrying of the composite is useful in two respects: it removes entrapped moisture from open cracks and it reduces the rate of flux into the adhesive.

2. It will be useful to gel the adhesive at a temperature such that the "critical concentration" of moisture (which is a function of temperature and applied pressure) is not exceeded.

3. Application of vacuum should be reduced to a minimum. Bubble formation increases strongly with the applied vacuum if the adhesive has access to the vacuum as can be readily seen in Figure 19.

4. A chemical approach to quench moisture during the curing process (such as the use of a carbodiimide) has been investigated. Aliphatic carbodiimides will react with water in the presence of the epoxy/amine adhesive.

5. Small concentrations of aliphatic carbodiimides have a beneficial effect on the lap-shear strengths of "moist" composites.

6. Further studies should be carried out to determine the optimum carbodiimide concentration.

7. Examine the possibility of incorporating carbodiimide in other adhesives.

REFERENCE

1. Determining the Strength of Adhesively Bonded Rigid Plastic Lap-Shear Joints in Shear by Tension Loading; ASTM-D3163, Annual Book of ASTM Standards, Part 22, 1980.

INITIAL INVESTIGATION OF CRYOGENIC

WIND TUNNEL MODEL FILLER MATERIALS

George C. Firth
NASA Langley Research Center
Hampton, Virginia 23665

ABSTRACT

Filler materials are commonly used to fill surface flaws, instrumentation grooves, and fastener holes in wind tunnel models. More stringent surface quality requirements and the more demanding test environment encountered in cryogenic wind tunnels eliminate usage of filler materials such as polyester resins, plaster, and waxes which are used on conventional wind tunnel models. In order to provide a material data base for cryogenic models, various filler materials have been investigated for their applicability.

Surface quality requirements and test temperature extremes require matching of coefficients of thermal expansion for interfacing materials. Microstrain versus temperature curves have been generated for several candidate filler materials for comparison with cryogenically acceptable materials. Matches have been achieved for aluminum alloys and austenitic steels.

Simulated model surfaces have been filled with candidate filler materials for determination of finishing characteristics, adhesion and stability when subjected to cryogenic cycling. Filler material systems have been identified which meet requirements for usage with aluminum model components.

INTRODUCTION

Aerodynamic research models require smooth, continuous surfaces to minimize surface-induced flow disturbances. Flaws in surfaces of conventional wind tunnel models have been satisfactorily filled with waxes, plasters, and plastic body filler. However, the National Transonic Facility (NTF), with its unique capabilities and test environment, renders such common materials unsuitable.

The NTF has high Reynolds number capabilities which require higher surface contour fidelity and finish than is required in conventional facilities. The NTF also operates at cryogenic temperatures; this causes the conventional filler materials to become brittle, lose contour fidelity because of greater thermal contraction than primary structural materials, and suffer bond failure because of thermally induced stresses.

A program was initiated at Langley Research Center to identify or develop materials which could be used to fill imperfections on cryogenic wind tunnel models. The initial phase of the program was completed with the identification of two suitable filler materials. During this phase, candidate materials were examined for structural and dimensional stability, ease of use, surface quality, and usage limitations.

466

CONVENTIONAL WIND TUNNEL MODEL
WITH FILLED INSTRUMENTATION GROOVES
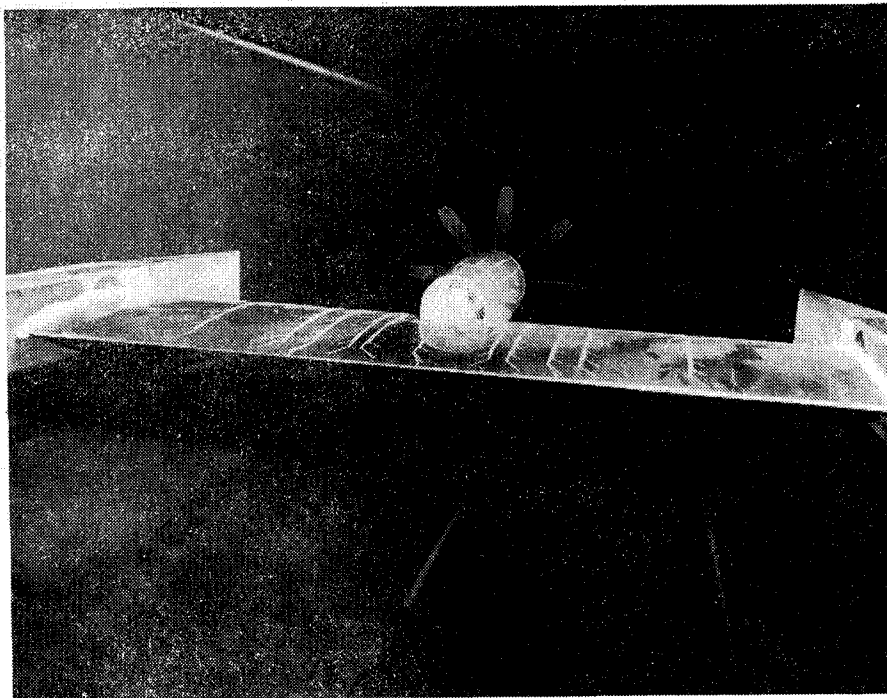
Often surface flaws are created intentionally as shown in the figure above. In this 16-Foot Transonic Tunnel model, grooves were cut in the wing and engine nacelle surfaces for routing static pressure orifice tubes from the points being monitored to the pressure trans- ducers. Other intentional flaws would include fastener and dowel holes as well as reference (fixturing) holes. This model was filled with a commercial epoxy which, unfortunately, becomes brittle at low temper- atures thus precluding its use in NTF models.

PROGRAM GOAL: IDENTIFY/DEVELOP FILLER MATERIALS SUITABLE FOR CRYOGENIC MODELS

o   ADHESION

o   STABLE SURFACE

o   HAND FINISHING

o   RAPID REMOVAL/REPLACEMENT

Realizing the necessity of filling flaws and the inadequacies of the conventional model filler materials, the current program was initiated with a simply stated goal, "Identify and/or develop materials which will be suitable for cryogenic wind tunnel models." The primary factors which need to be considered when evaluating a filler material's suitability are: 1. Adhesion throughout the test environment. 2. Dimensional stability of the filler material upon exposure to thermal and tensile cycling. 3. The difficulty of hand finishing the material at the test facility. 4. The capability of rapid removal and replacement to allow quick model configuration modifications.
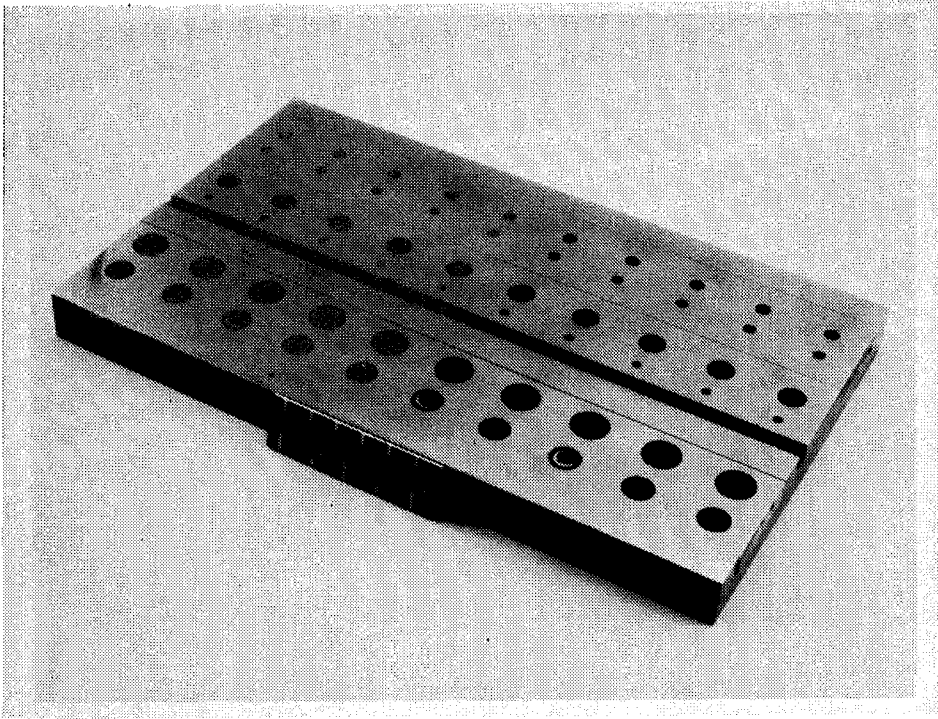
SCREENING SPECIMEN
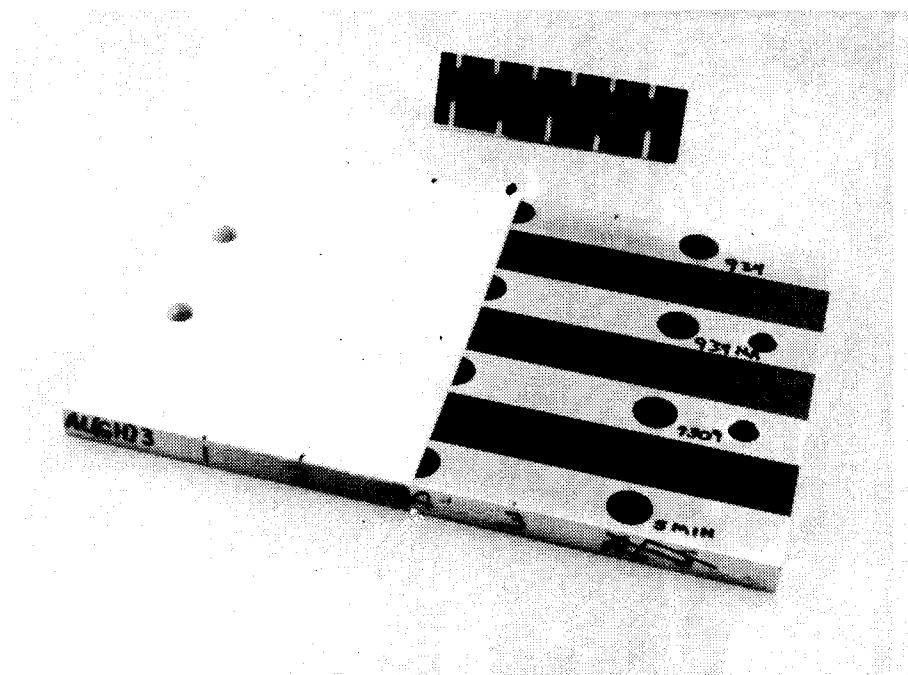
A simple specimen configuration was used to make an initial evaluation of a candidate filler material's suitability. This specimen consisted of a flat rectangular plate of an acceptable cryogenic model structural material with a series of counterbored holes and grooves. The grooves and holes were filled with the filler(s) being evaluated and are hand polished. The finished sample was measured with a profilometer which provided a recording of the contour and surface finish. The specimen was then thermally cycled between room and cryogenic temperatures several times and subsequently remeasured in the profilometer. The before and after recordings of surface contour and finish were compared for detection of filler instability.

These specimens have been utilized to test commercial metal filled epoxies, waxes, low-temperature structural adhesives and quick setting epoxies modified with additions of aluminum, steel, and talc powders as well as carbon spheres. Only one commercial product, Belzona "Super Metal"; one structural adhesive, Hysol "EA 9309", filled with carbon, steel or talc; and a fast-setting epoxy, Hardman "Extra-Fast-Setting", filled with carbon passed this screening test. The common mode of failure was fracture of the bond line.

The carbon filled adhesives did not meet the surface finish requirements due to the spheres creating a pebbled surface. The specimen shown above was one of many which was painted with an acrylic lacquer to improve the surface finish and successfully tested.

469

FLAT PLATE SPECIMEN

The flat plate specimens were used to continue testing of filler materials which survived the screening evaluation. This configuration, which is more representative of an actual model, incorporated cover-plates with deliberate gaps around the perimeter, surface grooves, and various fasteners with submerged heads. The specimen was filled, measured, thermally cycled, and remeasured in the same manner as the screening specimens.

The best performing filler material tested with this specimen configuration has been EA 9309 filled with steel or carbon. Belzona "Supe Metal" has not been tested with this specimen configuration.

FLAT PLATE SPECIMEN
WITH BOND LINE FAILURE
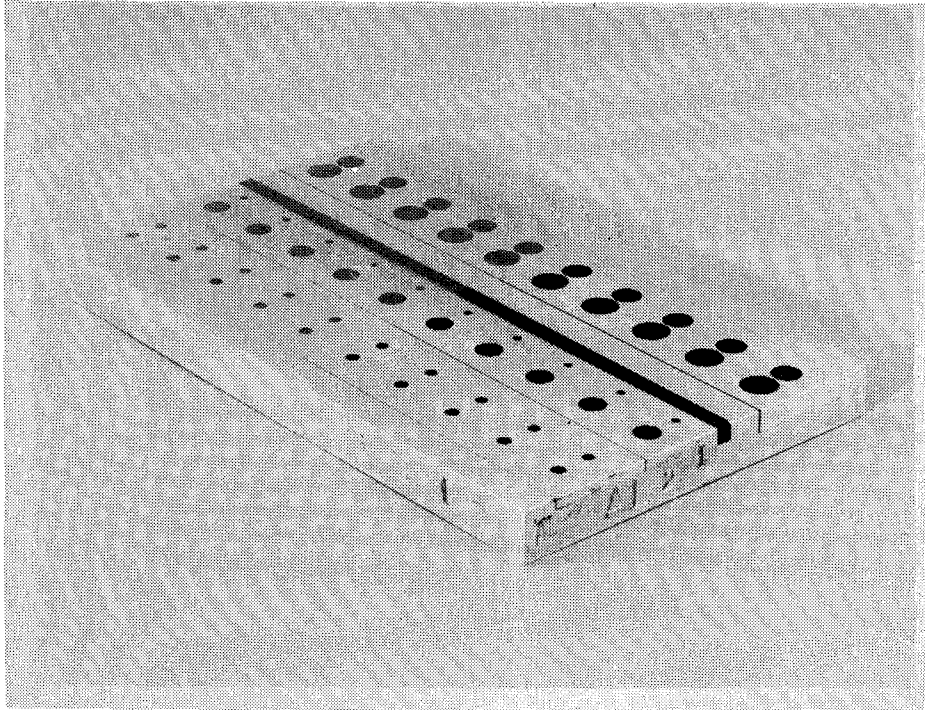
        As mentioned previously, a number of tests resulted in elimination
of several filler materials due to shrinkage, bond line fracture, and/or
instability. It is worth noting that these specimens were static speci-
mens and were only subjected to thermally induced stresses. The aluminum
specimen shown above had one side filled with an aluminum powder and
structural adhesive mixture and the other side filled with the same
structural adhesive mixed with steel powder. This particular specimen
suffered a bond line failure along the wide surface groove and movement
of the filler which can be seen easily in the close up on the next page.

CLOSE UP - FLAT PLATE
WITH BOND LINE FAILURE
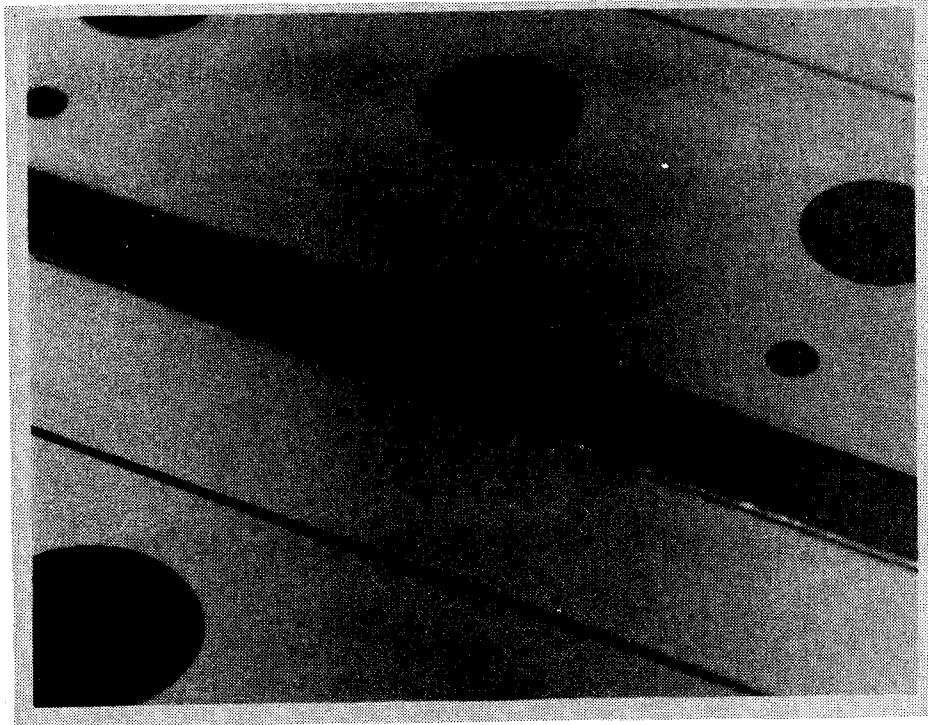
The bond line fractured and the filler material moved with respect to the metal surface during the thermal cycling. This type of failure was quite common, but seldom as dramatic as in this specimen. Failures of this type are attributed to stresses created by the mismatch of coefficients of thermal expansion between the metal plate and the filler material and the resultant relative contraction.
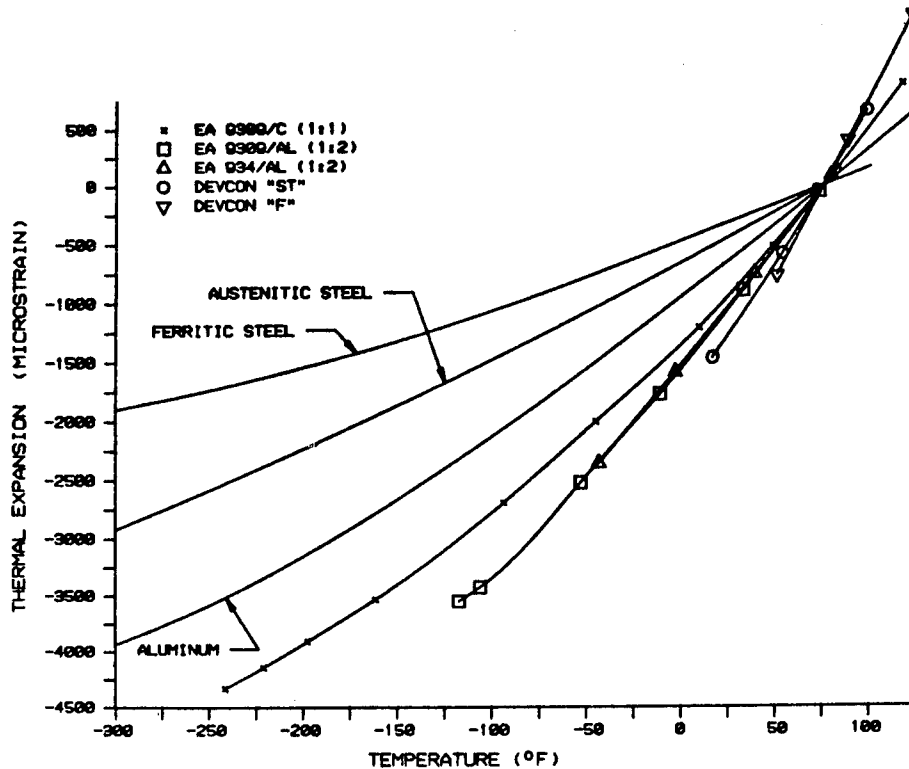
COEFFICIENTS OF THERMAL EXPANSION

PRIEST INTERFEROMETER
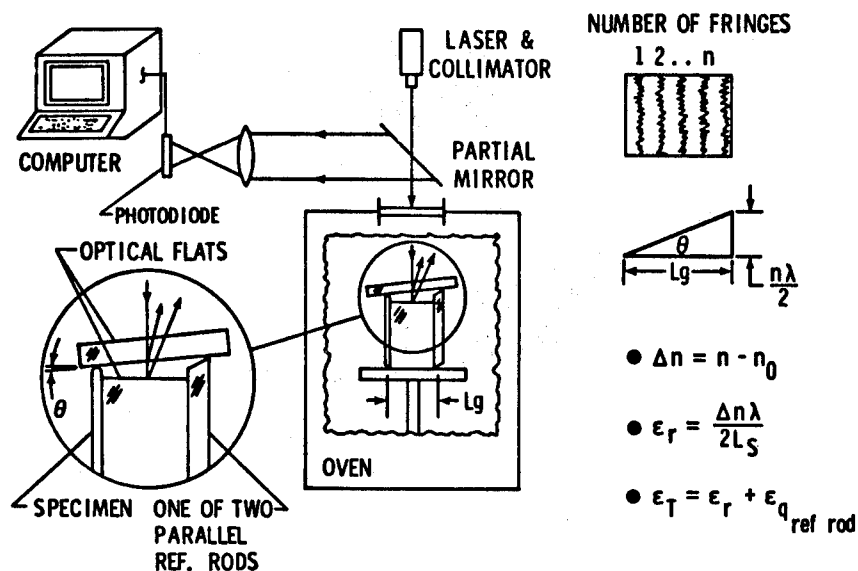
After experiencing several disappointments with the flat plate specimens which were related to mismatched coefficients of thermal expansion, it became obvious that the coefficients of the various candidate filler materials needed to be determined. The information generated would assist in matching filler materials to substrate metal, eliminating various fillers from further consideration, and determining optimum epoxy-to-filler ratios.

The device which was used to measure the coefficients of thermal expansion is shown schematically above. Briefly, an optical flat is supported on two reference rods and a specimen rod of the material being measured. As the temperature is changed the length of the specimen rod changes with respect to the reference rods, tilting the optical flat. The increasing tilt angle creates an increase in the number of interference fringes resulting from the reflected laser beam. A photodiode counts the number of fringes which is then used to calculate the relative contraction of the specimen with respect to the reference rods.

THERMAL EXPANSION VERSUS TEMPERATURE
## OF VARIOUS METAL FILLED ADHESIVES

The first candidate filler materials examined for determination of coefficient of thermal expansion were two commercial metal filled epoxies, two aluminum filled structural adhesives, and a carbon filled structural adhesive. As can be seen in the graph, the carbon filled structural adhesive performed better than any of the metal filled systems. It should be noted that the epoxy-to-filler ratios given are weight ratios. Thus, the aluminum filled structural adhesives and the carbon filled structural adhesive had about the same epoxy-to-filler volume ratio.

THERMAL EXPANSION VERSUS TEMPERATURE OF EA 9309
## WITH VARIOUS CONCENTRATIONS OF CARBON SPHERES
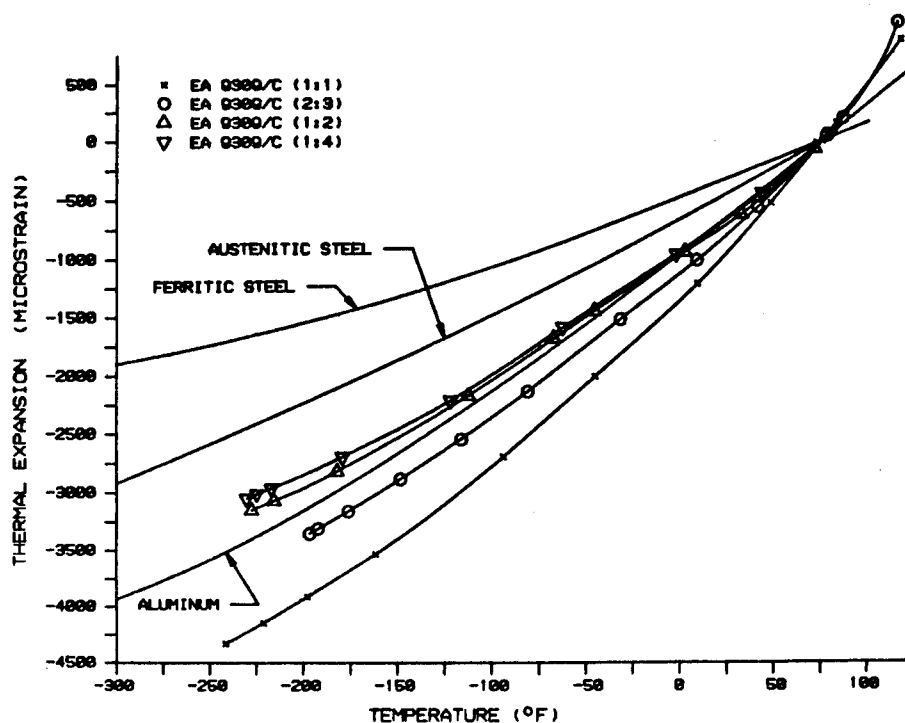
A series of tests were run on the filler material which came the closest to matching aluminum's coefficient of thermal expansion to determine the effect of varying the epoxy-to-filler ratio. As can be seen in the graph, an increase in the amount of carbon above a 1:2 epoxy-to-filler ratio resulted in no significant decrease in the rate of contraction. Shear specimen tests were conducted to determine the effect of varying the carbon concentration and revealed a significant reduction in shear strength when the carbon content was increased beyond the 1:2 epoxy-to-filler ratio. The higher ratios also proved to be difficult to mix and apply due to the dryness of the resulting mixture.

THERMAL EXPANSION VERSUS TEMPERATURE
## EFFECTIVENESS OF VARYING GRAIN SIZE
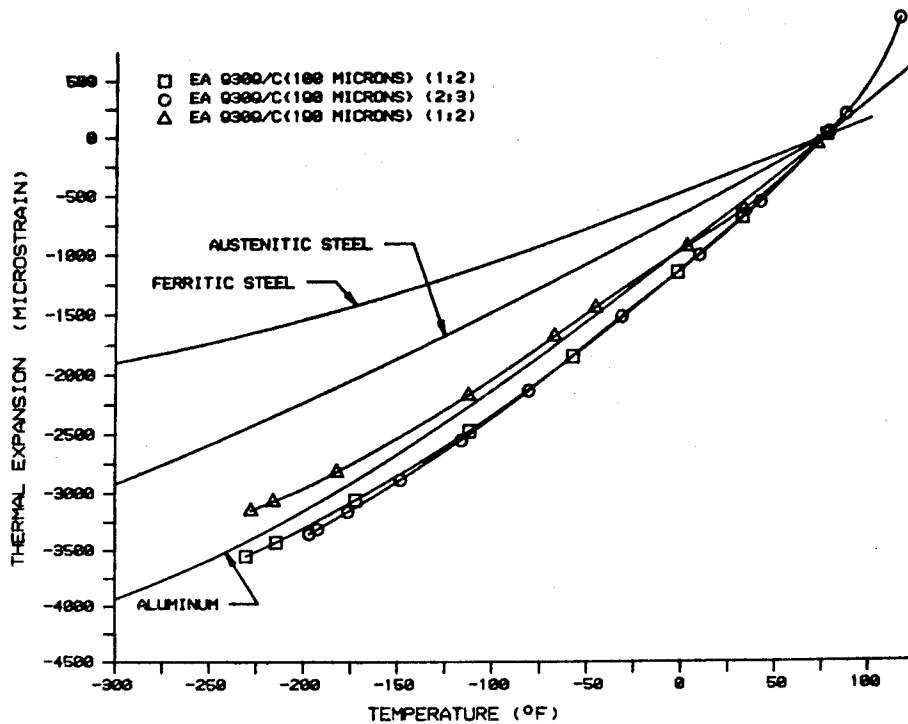
The effects of particle size were examined using 190 micron and 100 micron carbon spheres. The 190 micron size spheres were more effective than the 100 micron size spheres using the same epoxy-to-filler ratios by weight. Additionally, the smaller sphere size tended to saturate the epoxy at lower concentrations resulting in extremely dry mixtures. The smaller grain size was attractive from the stand point of offering a better surface finish, but its general ineffectiveness and dryness precluded its further evaluation.

476

THERMAL EXPANSION VERSUS TEMPERATURE
OF THREE CARBON FILLED ADHESIVES
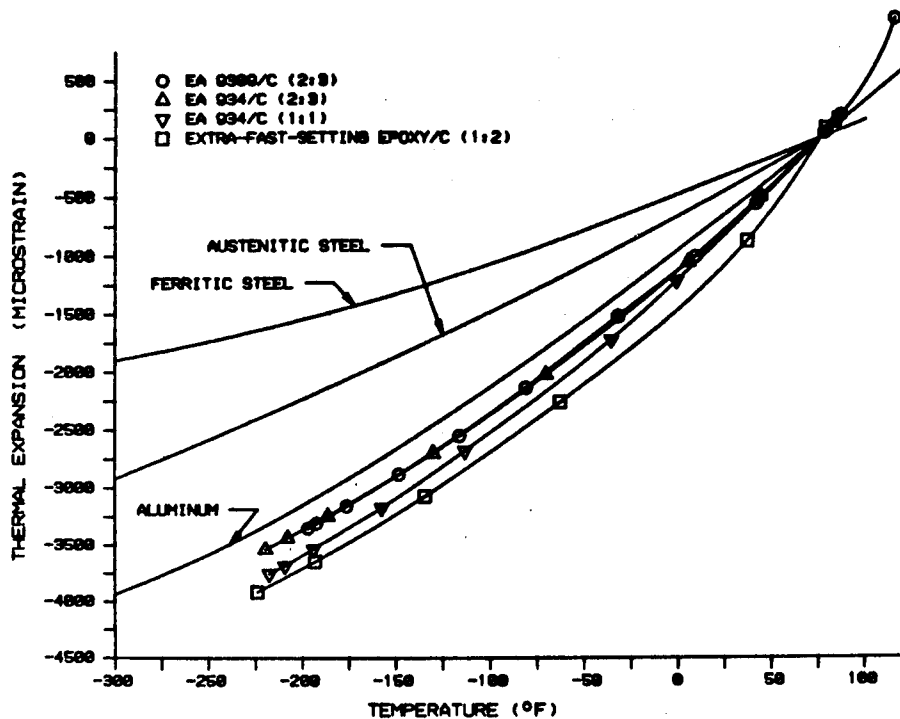
Evaluation of the effects of the addition of the 190 micron carbon spheres to three different epoxy systems revealed that the two structural adhesives' contraction rates were modified by the same amount. The third epoxy, a fast setting system, was not as effectively altered, but did perform better than the commercial products examined previously. Shear tests indicated that each of these systems had a shear strength in excess of 2 thousand pounds per square inch at both room and cryogenic temperatures. Of the systems examined here, the carbon filled EA 934 was the most difficult to use as the already thick fiber filled system became extremely dry with the addition of the carbon.

THERMAL EXPANSION VERSUS TEMPERATURE
FILLER MATERIALS OFFERING BEST MATCHES WITH BASE METALS
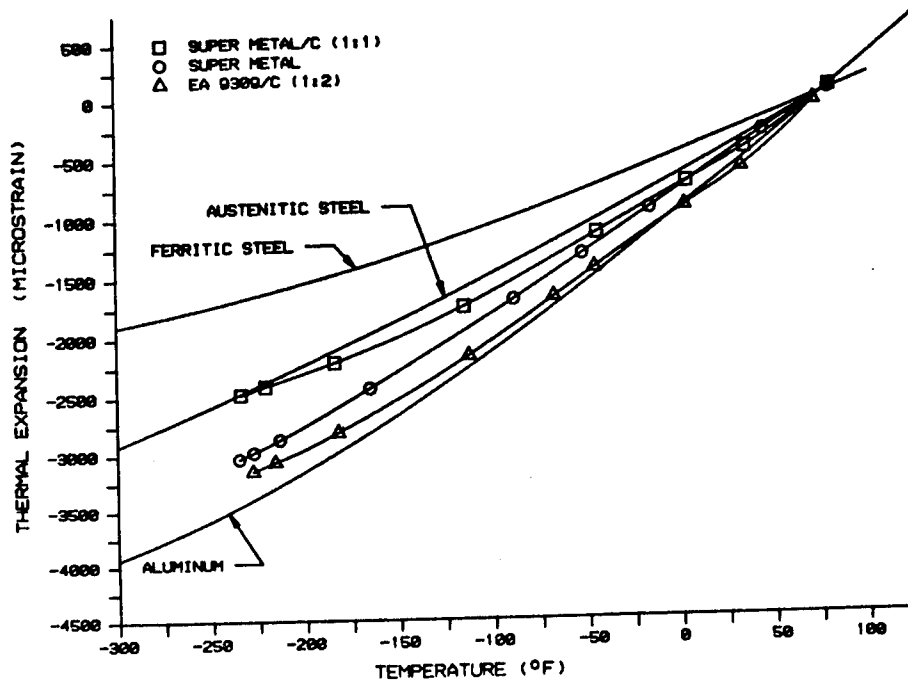
Recently a commercial product was identified which provides a near match with the coefficient of thermal expansion of aluminum and austenitic steels. The product, Belzona "Super Metal", was also modified by being filled with carbon spheres to reduce its coefficient even lower. This effort did reduce its contraction rate, but resulted in a saturated mixture which was difficult to apply and had virtually no shear strength. The unmodified product has the same shear strength as the carbon filled structural adhesive systems.

478

DYNAMIC TEST SPECIMEN
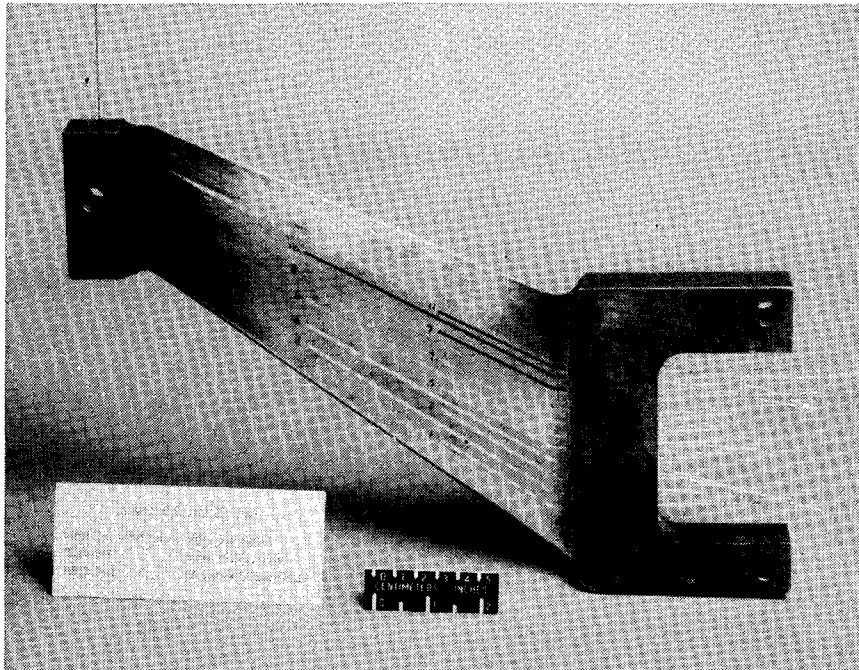
A dynamic test at cryogenic temperatures was conducted to determine suitability of the carbon filled EA 9309 for covering instrumentation grooves in a stressed wind tunnel model. A simulated model, with grooves filled with two solders (from a parallel development program) and the carbon filled EA 9309, was used for this test. The specimen was clamped at the right end in a loading fixture. The assembly was lowered into a cryostat and allowed to reach equilibrium at approximately -300 F. A load was then applied to the block of material on the left end at a rate of 12 cycles per minute for 5 thousand cycles. This sequence was repeated to give 5 thousand cycles at each of 4 levels of loading. The loading levels represented specimen surface bending stress levels of 22, 44, 66, and 88 thousand pounds per square inch. The carbon filled EA 9309 passed this extremely demanding test with no indication of any degradation.

SUMMATION

o   **EA 9309/C: ACCEPTABLE FOR**

     MOST CRYOGENIC APPLICATIONS

o   **EXTRA-FAST-SETTING EPOXY/C:**

     ACCEPTABLE FOR FILLING HOLES

o   **SUPER METAL: POTENTIAL FOR**

     WIDE CRYOGENIC APPLICATIONS

The EA 9309 modified by the addition of 190 micron carbon spheres in a 1:2 epoxy-to-carbon weight ratio has proven to be acceptable in terms of adhesion, stability, and capability to be worked by hand. Its primary drawbacks are its long curing cycle and the necessity of using a glazing compound or lacquer over the filled area to achieve the desired surface finish.

The Extra-Fast-Setting epoxy filled with carbon spheres performs adequately for filling fastener holes and small surface flaws, but because of its higher than desired coefficient of thermal expansion should not be used on critical aerodynamic surfaces.

Super Metal has the potential for wide usage on cryogenic wind tunnel models. It has the best thermal contraction rate match with cryogenic model structural materials, adequate shear strength, and can provide a good surface finish. A full endorsement is not given at this time due to incomplete evaluation.

BIBLIOGRAPHY

1. Bradshaw, James F.; and Lietzke, Donald A.: Cryogenic Technology, NASA CP-2122, Part II, Nov. 1979, pp 399-402.

2. Franches, M. F.: Aspects of Cryogenic Wind Tunnel Testing Technology at Douglas, AIAA-82-0606, March 1982, p. 8.

3. Young, Jr., C. P.; Bradshaw, J. F.; Rush, Jr., H. F.; Wallace, J. W.; and Watkins, Jr., V. E.: Cryogenic Wind-Tunnel Model Technology Development Activities at the NASA Langley Research Center, AIAA-84-0586, March 1984.

4. Griffin, S. A.; Madsen, A. P.; and McClain, A. A.: Design Study of Test Models of Maneuvering Aircraft Configurations for the National Transonic Facility (NTF); General Dynamics, GDC-CRAD-83-002, Nov. 1983.

1. Report No. NASA CP-2387	2. Government Accession No.	3. Recipient's Catalog No.
4. Title and Subtitle WELDING, BONDING, AND FASTENING - 1984		5. Report Date September 1985
		6. Performing Organization Code 505-42-23-03
7. Author(s) John D. Buckley and Bland A. Stein, Editors		8. Performing Organization Report No. L-16023
		10. Work Unit No.
9. Performing Organization Name and Address NASA Langley Research Center Hampton, Virginia 23665		11. Contract or Grant No.
		13. Type of Report and Period Covered Conference Publication
12. Sponsoring Agency Name and Address NASA, Washington, DC; American Society for Metals, Metals Park, Ohio; The George Washington University, Washington, DC; American Welding Society, New York, NY; Society of Manufacturing Engineers, Dearborn, MI		14. Sponsoring Agency Code

15. Supplementary Notes

16. Abstract

This document is a compilation of papers presented in a joint NASA, American Society for Metals, The George Washington University, American Welding Society, and Society of Manufacturing Engineers conference on Welding, Bonding, and Fastening at Langley Research Center, Hampton, VA, on October 23-25, 1984. Papers were presented on technology developed in current research programs relevant to welding, bonding, and fastening of structural materials required in fabricating structures and mechanical systems used in the aerospace, hydrospace, and automotive industries. Topics covered in the conference included equipment, hardware and materials used when welding, brazing, and soldering, mechanical fastening, explosive welding, use of unique selected joining techniques, adhesives bonding, and nondestructive evaluation. A concept of "The Factory of the Future" was presented, followed by advanced welding techniques, automated equipment for welding, welding in a cryogenic atmosphere, blind fastening, stress corrosion resistant fasteners, fastening equipment, explosive welding of different configurations and materials, solid-state bonding, electron beam welding, new adhesives, effects of cryogenics on adhesives, and new techniques and equipment for adhesive bonding.

17. Key Words (Suggested by Author(s)) Welding, bonding, and fastening Brazing Soldering explosive welding Adhesive bonding cryogenic Solid-state bonding	18. Distribution Statement Unclassified - Unlimited Subject Category 23
19. Security Classif. (of this report) Unclassified	20. Security Classif. (of this page) Unclassified	21. No. of Pages 494	22. Price A21

National Aeronautics and
Space Administration

Washington, D.C.
20546

Official Business
Penalty for Private Use, $300

SPECIAL FOURTH CLASS MAIL
BOOK

U.S.MAIL

3   1 1J,C,   850819 S00942DSR
DEPT OF THE ARMY
ARMY ARMAMENT RES & DEV COMMAND
PLASTICS TECH EVALUATION CTR
ATTN: AS MARY OLSEN   BLDG 351-N
    DRSMC-SCA-O/RDC-AMCCOM
DOVER NJ 07801

NASA